



INDIAN AGRICULTURAL  
RESEARCH INSTITUTE, NEW DELHI

I. A. R. 16

MGH C-34-10 AR-21.8 49-1,000







PROCEEDINGS  
OF THE  
ROYAL SOCIETY OF LONDON

SERIES A. MATHEMATICAL AND PHYSICAL SCIENCES

VOL 175

LONDON

Printed and published for the Royal Society  
By the Cambridge University Press  
Bentley House, N.W.1

18 July 1940

PRINTED IN GREAT BRITAIN BY  
WALTER LEWIS M A  
AT THE CAMBRIDGE UNIVERSITY PRESS

# CONTENTS

## SERIES A VOL 175

No. A 960. 28 March 1940

|  | PAGE |
|--|------|
| Further investigation of the velocity of propagation of light <i>in vacuo</i> in a transverse magnetic field. By C. J. Banwell and C. C. Farr, F.R.S. (Plate 1) . . . . .      | 1    |
| Thermal ionization of barium. By B. N. Srivastava . . . . .  | 26   |
| On the thermal conductivity of gases by a relative method with an application to deuterium. By W. G. Kannuliuk . . . . .   | 36   |
| Properties of superconducting colloids and emulsions. By D. Shoenberg . . . . .  | 49   |
| The $\beta$ -ray spectrum of radium E. By G. J. Neary . . . . .  | 71   |
| On the photon component of cosmic radiation and its absorption coefficient. By L. Jánossy and B. Rossi . . . . .   | 88   |
| Crystal boundaries in tin. By B. Chalmers . . . . .  | 100  |
| Comparison of the acceleration due to gravity at the National Laboratory, Teddington and the Bureau of Standards, Washington, D.C. By B. C. Browne and E. C. Bullard . . . . . | 110  |
| The kinetics of decarboxylation in solution. By P. Johnson and E. A. Moelwyn-Hughes . . . . .  | 118  |

No. A 961. 10 April 1940

|  |     |
|--|-----|
| The thermal decomposition of gaseous benzaldehyde. By R. E. Smith and C. N. Hinshelwood, F.R.S. . . . .  | 131 |
| The theory of reflexion of very long wireless waves from the ionosphere. By M. V. Wilkes . . . . .   | 143 |
| The reaction of atomic hydrogen with hydrazine. By E. A. B. Birse and H. W. Melville. . . . .  | 164 |
| The photolysis of ammonia. By E. A. B. Birse and H. W. Melville . . . . .  | 187 |
| Investigations of infra-red spectra. Determination of C-H frequencies ( $\sim 3000 \text{ cm.}^{-1}$ ) in paraffins and olefins, with some observations on "polythenes". By J. J. Fox and A. E. Martin . . . . . | 208 |

|   | PAGE |
|---|------|
| The dielectric capacity of electrolytes in mixed solvents: ion association in solutions of magnesium sulphate. By W. A. Mason and W. J. Shutt | 234  |
| The behaviour of polar molecules in solid paraffin wax. By D. R. Pelmore and E. L. Simons   | 253  |
| The thermal explosion of diethyl peroxide. By E. J. Harris  | 254  |

## No. A 962. 12 June 1940

|  |     |
|--|-----|
| Relaxation methods applied to engineering problems. VI. The natural frequencies of systems having restricted freedom. By A. Pellew and R. V. Southwell, F.R.S.   | 262 |
| The glide elements of body-centred cubic crystals, with special reference to the effect of temperature. By E. N. da C. Andrade, F.R.S. and Y. S. Chow. (Plates 2-4)  | 290 |
| Experiments with a velocity-spectrometer for slow neutrons. By G. E. F. Fertel, D. F. Gibbs, P. B. Moon, G. P. Thomson, F.R.S. and C. E. Wynn-Williams   | 316 |
| A magnetic study of the two-phase iron-nickel alloys. By A. T. Pickles and W. Sucksmith, F.R.S.  | 331 |
| Determination of the Rydberg constants, $c/m$ , and the fine structures of $H_\alpha$ and $D_\alpha$ by means of a reflexion echelon. By J. W. Drinkwater, Sir Owen Richardson, F.R.S. and W. Ewart Williams | 345 |
| Some cases of the steady two-dimensional percolation of water through ground. By B. Davison and L. Rosenhead   | 346 |
| Hyperfine structure in the arc spectrum of bromine. By S. Tolansky and S. A. Trivedi   | 366 |
| Orientation of nuclear spins in metals. By H. Fröhlich and F. R. N. Nabarro  | 382 |
| The determination of the lifetime of active polymeric molecules. By T. T. Jones and H. W. Melville   | 392 |

## No. A 963. 18 July 1940

|  |     |
|--|-----|
| The pressure of water waves upon a fixed obstacle. By T. H. Havelock, F.R.S.                           | 409 |
| An investigation of cold-worked polycrystalline alpha-iron. By L. Mullins and J. W. Rodgers. (Plate 5) | 422 |

## *Contents*

v

|  | PAGE |
|--|------|
| The steady two-dimensional radial flow of viscous fluid between two inclined plane walls. By L. Rosenhead . . . . .  | 436  |
| Dielectric loss in simple alkyd resins. By D. R. Pelmore and E. L. Simons . . . . .  | 468  |
| Thermal transpiration of a dissociating gas. By B. N. Srivastava . . . . .   | 474  |
| Radiative processes involving fast mesons. By F. Booth and A. H. Wilson . . . . .  | 483  |
| The strains produced by precipitation in alloys. By F. R. N. Nabarro . . . . .   | 519  |
| The combustion of aromatic and alicyclic hydrocarbons. V. The products of combustion of benzene and its monoalkyl derivatives. By J. H. Burgoyne . . . . . | 539  |
| Index . . . . .  | 565  |

---



# Further investigation of the velocity of propagation of light *in vacuo* in a transverse magnetic field

BY C. J. BANWELL, M.Sc. AND C. C. FARR, F.R.S.

*Physics Department, Canterbury University College,  
Christchurch, New Zealand*

(Received 25 January 1938—Revised 29 March 1939)

[Plate 1]

In a previous paper (1932) an attempt to measure the effect, if any, of a transverse magnetic field on the velocity of light *in vacuo* was described. No change greater than 1 part in  $2 \times 10^7$  was found in a field of 18,000 oersted. As the Jamin interferometer used had certain drawbacks for an experiment of this kind, it was decided to set up a Michelson type of interferometer, the use of which might be expected to avoid some of these difficulties and increase the sensitivity. In particular, one of the interfering rays could be made to pass twice through the magnetic field, or, by means of auxiliary mirrors, a multiple of this, while the other interfering ray, being at right angles to the first, was well away from the vicinity of the main leakage field, which would have a compensating effect as far as any change in velocity was concerned.

On setting up the Michelson interferometer it was found that the optical quality of the mirrors used, which were two optical flats silvered, was such that it was possible to find an adjustment which would cause a single interference band to fill the whole field of view almost uniformly. Also, using a mercury vapour lamp with a green line filter as source of light, the brightness of the bands was sufficient to operate a photoelectric cell-amplifier-galvanometer combination. Thus band movements would, with the interferometer suitably adjusted, result in changes in the amount of light incident on the photoelectric cell, and these movements could be observed visually as displacements of the galvanometer light spot, or the displacements could be recorded photographically. An arrangement of this type, used for another purpose, has been described by H. J. P. V. Ohain (1935), and selenium cells have been used for counting interference bands in a somewhat similar manner, by Barnard (1930), by Fournier d'Albe and Symonds (1926). It was considered that this method would be much better than the direct method of observing the bands by eye, since in observing directly the position of a band with respect to an index line, any movement



will be seen as a change of brightness in the vicinity of the index line, owing to the manner (approximately sinusoidal) in which the illumination along the band system passes from maximum to minimum. In the absence of any standard of comparison of brightness, sensitivity of observation under these circumstances will be poor. Kennedy (1926) and Illingworth (1927) have greatly increased the sensitivity of this method by dividing the field of view into two parts by using mirrors with a "step" a fraction of a wave-length in height. In this way band movements are made to appear as changes in relative brightness of two adjacent portions of the field. If, however, the changes of brightness occurring in the bands obtained with simple flat mirrors are converted into changes of electric current by means of a photoelectric cell and these changes amplified and used to actuate a galvanometer, the light spot from which may be arranged to be as sharp as required, visual observation of the movements of this spot, or of its recorded photographic trace, may be made with considerable sensitivity. By making a photographic record, using a galvanometer of relatively long period (4 sec.), and averaging the resulting curve with a planimeter, the effect of unsteadiness of the bands could be largely eliminated, whereas such unsteadiness would greatly reduce the certainty of visual observation. A disadvantage of the photoelectric method is that, since the band movement is measured in terms of change of brightness, any change in brightness of the source, or any change in the effective aperture of the optical system, will produce effects which, on any single record, will be indistinguishable from actual band movements. However, by averaging the results of a number of records, using a different band position for each, such uncertainties can be eliminated. Stray magnetic fields from the electromagnets, or electrical disturbances resulting from switching the current on or off, may affect the operation of the photoelectric cell or amplifier. Such effects did indeed occur, and the various measures taken to minimize them will be described later in this paper.

The smallest band movement that could be observed by the method described above (approximately 0.0005 band) compares favourably with the sensitivity achieved by other refinements in band measurement, such as those described by Piccard and Stahel (1926, 1927*a*, 1927*b*), Kennedy (1926), Illingworth (1927), and Kennedy and Thorndike (1932).

#### DESCRIPTION OF APPARATUS

The general arrangement of the interferometer, electromagnets, photoelectric cell and amplifier is shown in plan in figure 1.

### *Propagation of light in vacuo in a transverse magnetic field 3*

*Optical system.* Light from the mercury vapour lamp *L* is made approximately parallel by a lens and after passing through a Wratten no. 77 filter *R*, which renders it approximately monochromatic, it falls on the optical flat *N*, which is half-silvered on the side towards *M*. From *N*

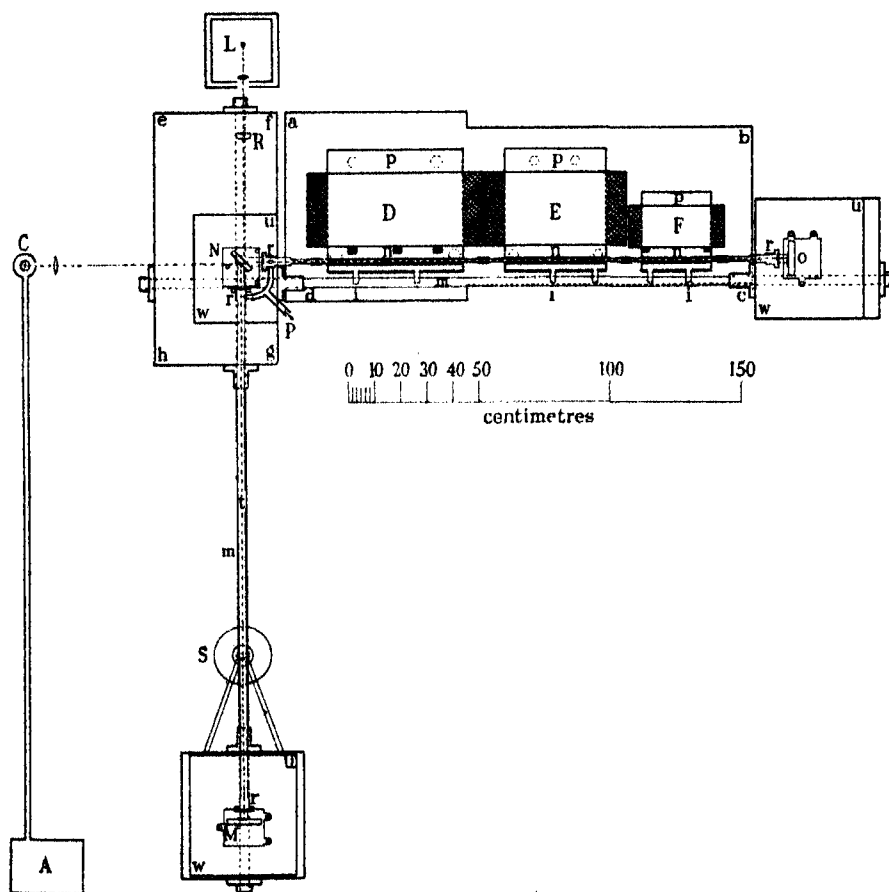


FIGURE 1

the transmitted portion passes through an airtight brass tube *t*, closed at each end by an optically flat glass window, mounted in a frame with sealing wax. The light is reflected at normal incidence from the silvered front surface of the optical flat *M*, travels back over the same path, and a portion is reflected at the half-silvered surface of *N* towards the photo-electric cell *C*. The reflected portion of the initial ray passes through the gaps *n* of the three electromagnets *D*, *E*, *F*. It is reflected normally at the

surface of a mirror  $O$ , similar to  $M$ , passes back through the gaps, and a portion is transmitted through the half-silvered surface of  $N$  towards  $C$ . The gaps of the magnets and the necessary connecting tubes form an airtight system closed at the ends by windows similar to, and as nearly as possible the same distance apart, as those closing the tube  $t$ . These two airtight systems are connected together near  $N$  by a rubber tube, of large diameter, which has a branch outlet to a pump at  $P$ . The windows closing the ends of this vacuum system are tilted slightly to divert light reflected at their surfaces out of the main optical path.

The mirror  $N$  is provided with fine adjustments about horizontal and vertical axes in its own plane, while the mirrors  $M$  and  $O$  have, in addition, linear motions perpendicular to their planes, along their respective light rays. All these adjustments are operated by means of differential screws with an effective pitch of  $\frac{1}{800}$  in. All metallic parts of these mirror supports, and all other metal parts associated with the interferometer, except the cores of the magnets, are made of brass or gunmetal. Each mirror is supported by three screws which rest in a hole, slot, and plane arrangement in the tops of three brass plugs, let into the surfaces of the marble slabs  $u, w$ , which in turn are cemented to the tops of brick and concrete pillars of such a height that the centre of the optical system was level with the magnet gaps.

When the interferometer was first set up in this way, it was found that it was much more susceptible to vibration than the former Jamin arrangement, largely owing to the fact that, since the two interfering rays were now separated, any small movement of the foundation affected their respective paths unequally and caused relatively large band movements. To reduce this as far as possible, two thick (3 cm.) brass bars  $m$  were passed horizontally through the central supporting pillar  $efgh$  at right angles near its upper surface, and each also passed through one of the pillars supporting mirrors  $M$  and  $O$ . Brass collars with flanges were screwed to the bars at the surface of each pillar and were tightened up, thus tending to join all three pillars up in a single fairly rigid system. This system has no direct contact with the brick and concrete foundation  $abcd$  carrying the magnets, except through the floor, which is of concrete 6 in. thick resting on a sandy foundation. The tube  $t$  is supported by two clamps (not shown in figure 1), attached to the rod  $m$  in such a way that the position of  $t$  may be adjusted. Two similar clamps, attached to the ends of pole-pieces of magnets  $D$  and  $F$  respectively, support the frames  $r$  carrying the windows closing the two ends of the magnet vacuum system. To minimize drifts of the bands due to temperature changes, it was found necessary to cover the

exposed parts of the bars  $m$  with thick felt lagging. Those portions of the paths of the interfering rays open to the atmosphere between the four windows at  $r$  and their respective mirrors are enclosed in brass casings, only a little larger than would be required for the passage of the ray, and reaching to within a few millimetres of the faces of the mirrors. This was found to improve the steadiness of the bands. The light finally emerging from the interferometer is focused by means of a lens on the cathode of the photoelectric cell  $C$ . Arrangements were also made for introducing a mirror into the path of the emergent ray near  $N$ , to enable a telescope placed on  $efgh$  to be used for initial band adjustments.

Since monochromatic light was used, the usual compensating plate in the path of one of the interfering rays was not required. During some preliminary experiments, an incandescent filament lamp was used in place of the mercury vapour lamp at  $L$ . A suitable compensating optical flat was introduced between  $N$  and  $M$ , near  $N$ , and by permitting the emergent light to fall on the slit of a spectroscope, it was found possible to find the adjustment of the mirrors necessary to give white-light bands, by a method similar to that described by Simon (1927). These bands were not especially sharp and the required adjustment would have been difficult to maintain, so they were not used for any of the measurements. Using the approximately monochromatic light from the mercury vapour lamp and filter, it was possible to move either  $M$  or  $N$  longitudinally several millimetres before the bands became indistinct.

*Magnets.* Figure 1 gives in plan a view of a horizontal section through the gaps  $n$  of the three electromagnets  $D$ ,  $E$ , and  $F$ , fully described in an earlier paper (1932). Only minor changes in the magnets themselves and in their electrical connexions have been made for the present work as compared with the former paper by the present authors (1932). The width of the air gap in the direction of the lines of force (i.e. perpendicular to the plane of figure 1) is 3 mm. in each case, the other dimensions being 13 mm. from back to front for each magnet, and 117 cm. for the total length of the three magnets.

The bracing between the poles to prevent any narrowing of the gap by attractive forces when the current is switched on was found to be adequate, as tests showed that no measurable dimming of the light through the gaps resulted from this cause. Since any such effects would cause spurious galvanometer deflexions with the present method of observation, it was also important to ensure that no change of alignment of the individual magnet gaps could occur, as a result of mutual forces arising from interaction of their respective fields, and to this end the three magnets are

braced together at front and back with steel bars. Since it was found necessary to place thick rubber disks under the feet of all the magnets to reduce the effect of mechanical vibration from them on the bands, the rigidity of this bracing is very important. The bracing used was effective.

In order to enable the field strength in the gaps to be measured, six tubes (two on each magnet) were provided in the brass boxing enclosing the front portion of the gap, through which the fluxmeter search coil could be inserted into the gap. A special search coil constructed to fit into the gap was made, and was used with a Grassot fluxmeter, calibration against a standard search coil being afterwards effected in the field of another electromagnet. Three of these tubes were normally closed with rubber corks, when the field was not being measured; the other three marked  $i$  were used for attaching charcoal tubes for maintaining the vacuum.

*Vacuum.* As already indicated, the greater part of the space through which the path of each of the interfering rays passes was enclosed so as to enable it to be evacuated, and these two enclosures were in communication near the central mirror  $N$ . The magnet gaps were closed at the back by a flexible brass strip, and at the front by a brass boxing. At the ends of each gap suitable brass tubes were provided to enable connexion to be made between magnets and to the window frames  $r$ . The brass strip and boxing enclosing the gap were soldered to the iron pole pieces, and the brass tubes were soldered into holes in heavy brass plates covering the ends of the gaps; the joints were given several coats of metallic paint. The various brass tubes are joined by slipping rubber sleeves over them and sealing the joints with paint. The window frames  $r$  were soldered on to their respective tubes.

The preliminary evacuation was carried out by means of a mercury condensation pump backed with a rotary oil pump, but since vibration from the backing pump greatly disturbed the bands, and makes them practically invisible while it was running, this pump was shut off during an actual measurement and the vacuum was maintained with charcoal tubes and liquid air. The pressure of the residual air in the apparatus was observed by means of a small discharge tube located at the junction of the two vacuum systems where the branch tube goes to the pump. The appearance of the discharge during a measurement was noted and subsequent calibration was carried out with a McLeod gauge.

*Current supply.* Current for the magnet windings was obtained from the 220 V D.C. city main. The windings of the three magnets were connected in series, their total resistance when cold being  $3.18 \Omega$ , and since they were connected directly to the supply without extra resistance the current should be 69 amp. Actually it was nearly always somewhat less than this, especially

as the coils warmed up. Since the iron was being worked near saturation, small changes in current did not make much difference to the strength of the field. To prevent damage to the insulation from high induced voltages when the circuit was opened, two large electrolytic rectifiers were connected across the windings in such a way as to provide a low-resistance path for the current flowing in the windings when the switch was opened. The switch itself was the same as that used before, but it was removed to the next room in order to avoid any possibility of disturbance of the photoelectric cell by light from the arc formed when the circuit was broken, the door between the two rooms being closed during a run.

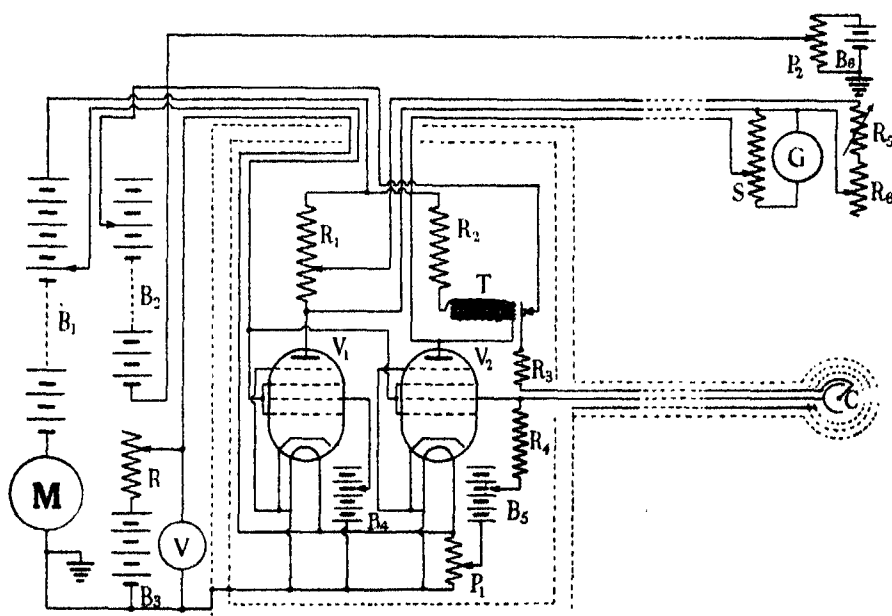
The *general photograph* of the apparatus, figure 3 (plate 1), corresponds to an elevation of the apparatus. On the extreme right the mirror *O* can be seen on its brick pillar, with one of the flanges of the bracing bar on its right-hand face. The brackets supporting the windows at each end of the magnets are bolted to the upper part of the poles. Three liquid air-flasks are in position over the charcoal tubes and an electric furnace used for baking out the charcoal is visible between the two right-hand flasks. Just to the left of the left-hand liquid-air flask is the discharge tube, and above and behind it the edge of the mirror *N* can be seen. The method of supporting the tube *t* from the rod *m* by two clamps can be clearly seen in the middle portion of the photograph. Towards the left is the mirror *M* and its supporting pillar, and beyond this, in the background, are the lead storage cells of the H.T. battery for the amplifier, which in turn is still farther back almost against the rear wall, being nearly hidden by the battery and the large bottle in the foreground. The recording camera and controls, to be described later, were in the room through this rear wall.

The wooden framework shown surrounding the magnets and part of the interferometer was originally covered with black cloth to form a nearly dark enclosure. However, since it was necessary to carry out all the present experiments at night, and since no one was in this room during a run, the wooden wall at the back was all that was required to shield the photoelectric cell from stray light from the mercury vapour lamp. The rest of the framework was retained, as it was useful for supporting the electrolytic rectifiers (which are on top), and various electrical fittings.

*Amplifier.* Since the light flux finally emerging from the interferometer with the magnets in position was rather small ( $7 \times 10^{-8}$  lumen approx.), it was necessary to amplify the resulting current from the gas-filled cell used before a galvanometer could be operated satisfactorily.

The amplifier first tried employed two ordinary triodes (type 201 A), in a bridge circuit. It was found that, unless both grids were connected to the

filament through relatively low resistances, the zero of the galvanometer became too unsteady for satisfactory operation. Modification of the socket so that an isolated lead could be attached to the grid pin, and sawing slots in the valve base so as to further isolate this pin, caused some, but not sufficient, improvement. Complete shielding of the amplifier also gave little improvement, and so it was decided to try a type of valve having better insulation of the grid connexion. The type 78 radio-frequency pentode appeared suitable, because the grid terminal is at the top of the



glass envelope, all other leads being brought out to the base pins in the normal way, the mutual conductance is fairly high (1650 micromhos), and its filament voltage (6.3) and current have convenient values. An experimental amplifier was therefore set up, using two of these valves in the usual bridge arrangement, the screens being connected directly to a suitable source of fixed voltage; the suppressor grids and cathodes were connected to the negative side of the heaters. It was at once evident that stability was much improved, even with high resistance grid leaks, and amplification was adequate.

The circuit and general arrangements of the amplifier finally used are shown in figure 2. The two valves  $V_1$  and  $V_2$ , together with their anode

resistances  $R_1$  and  $R_2$ , grid batteries  $B_4$  and  $B_5$ , high-resistance grid leak  $R_4$ , and some other apparatus, are enclosed in a double-walled iron shield, shown by the dashed lines; an extension of this shield reaches to and surrounds the photoelectric cell  $C$  and its leads. The resistances  $R_1$  and  $R_2$ , which, together with  $V_1$  and  $V_2$ , make up the Wheatstone network, are wire wound and of adequate size to prevent their heating appreciably. Their nominal value is 25,000  $\Omega$  each, and they are provided with a number of adjustable clips for taking out connexions at several points. Since the galvanometer  $G$  is located some distance from the amplifier, in an adjacent room, it is necessary to have some means of balancing the bridge from a point where the galvanometer can be seen. This is accomplished by taking an extra lead, from a tapping on  $R_1$ , out to the galvanometer location, where the variable resistances  $R_5$  and  $R_6$  are connected between this lead and the side of the galvanometer connected to the anode of  $V_1$ .

The heaters of  $V_1$  and  $V_2$  are supplied from the battery  $B_3$ , consisting of four large capacity lead storage cells, the heater voltage being kept at its rated value by means of the rheostat  $R$  and voltmeter  $V$ . The battery  $B_1$ , consisting of 120 small capacity lead storage cells, supplies screen and anode voltages for  $V_1$  and  $V_2$ , both screens being connected to a tapping at the middle of  $B_1$ . The milliammeter  $M$  (0–50 mA) indicates total of plate and screen currents for both valves. Since it was found necessary during the later stages of the work to operate the photoelectric cell near its ionizing voltage, where its output changes rapidly with applied voltage, a separate battery  $B_2$  of eighty small storage cells, and a two cell battery of larger capacity, in conjunction with the potentiometer  $P_2$ , were used to provide its anode voltage. Until this was done, slow drifts in the voltage of  $B_1$  during operation caused the sensitivity to be continually changing. To prevent damage to the photoelectric cell and changes in its characteristics, in the event of its ionizing, a resistance  $R_3$  (1 M $\Omega$ ) in the positive lead and a relay  $T$  are provided. The resistance  $R_3$  served to limit the maximum value of the ionization current, while  $T$ , adjusted to operate when the anode current of  $V_2$  rose above normal, removed anode voltage entirely from the cell, and thus prevented it from being glowed for a long period if the operator failed to notice what had happened.

The two photoelectric cells used on different occasions were of similar construction, with a hemi-cylindrical metallic cathode coated with light-sensitive material, and a rod-shaped anode along the axis of the cylinder. Anode and cathode connexions are brought out to two pins of a standard four pin valve base. The high resistance  $R_4$ , between the grid of  $V_2$  and its bias battery  $B_5$ , consisted of a small glass tube with platinum foil electrodes,



containing a mixture of pure alcohol and xylol in suitable proportions to give a resistance of 70 M $\Omega$ . The tube was sealed off and was buried in paraffin wax.

*Amplifier stability.* Although, as will be seen later, the chief causes of instability of the galvanometer light spot were not due to the amplifier, it is nevertheless desirable to have the amplifier as stable as possible, particularly with regard to quick disturbances. Causes of irregularities may be classified under the following headings: (a) batteries, (b) faulty insulation (particularly in the grid circuit of  $V_2$ ), (c) high-frequency disturbances. These were considered and effective steps taken to eliminate them.

*Spurious effects in amplifier and cell.* It is important that the stray magnetic field from the electromagnets should produce no disturbance of the bridge balance, since any such effect will appear in the final record, and its elimination from the measurements would be an undesirable added complication. The photoelectric cell was initially built into the amplifier, and the whole unit supported near *efgh* (figure 1), about 80 cm. from the nearest part of the magnets. During some preliminary trials the stray field apparently produced no effect, but suddenly an appreciable movement appeared every time the magnets were excited, even with the cell not illuminated. Magnetic shielding not being apparently completely effective, the amplifier was removed to the most distant corner of the room (shown at *A* in figure 1), where the stray field was found to be negligible. (Figure 1 is not quite to scale with respect to the distances from *N* to *C*, and from *C* to *A*, the actual distances being 243 and 275 cm. respectively.)

During preliminary runs, while the magnets were still pushed back out of the path of the ray between *N* and *O*, ample light was available, and it was not found necessary to operate the photoelectric cell very near its glow voltage. Under these circumstances there was no apparent effect of the stray field on the photoelectric current, even with the cell located in the original position of the amplifier, near the magnets. However, with the much reduced illumination resulting when the ray between *N* and *O* had to pass through the magnet gaps, it became necessary to work the cell very near its critical voltage. It was found that, with the cell illuminated by an incandescent lamp, arranged to give approximately the same intensity of illumination at the cell as the interferometer, and with the cell voltage and amplifier sensitivity such that a calculated galvanometer deflexion of 460 cm. would be obtained, switching on the magnet current gave a movement of 3 cm. in the direction corresponding to an increase in cell current. Effects of this order were found with two different types of

gas-filled cells. The action of a magnetic field on photoelectric cells has been investigated by Fourmarier (1932), who in every case found a decrease in cell current due to the field. He does not give either the field strength or the intensity of illumination employed, but it is thought that both would be considerably greater than in the present case. Since the cell current is greatly amplified by ionization of the gas filling by photoelectrons and secondary electrons, any factor which would tend to increase length of electronic path in the gas might be expected to increase the amount of ionization produced and thus the final current. Should the gas pressure in the cell be such that the mean free path of an electron is comparable with the distance between the electrodes, the curvature of the paths of the electrons in the magnetic field might produce such an effect.

To overcome this trouble, the cell was enclosed in a magnetic shield consisting of three concentric iron cylinders, each about  $\frac{1}{8}$  in. thick, and closed at each end by an iron lid. A hole  $\frac{1}{8}$  in. diameter through all three shields was necessary to admit the light, and other holes were also needed to make connexion to the cell. These latter were staggered, so as to maintain the shielding as far as possible. Despite these precautions, a small effect still remained, and the cell, with its shield, was finally placed in the position shown in figure 1, where the effect of the field was reduced to  $\frac{1}{2}$  mm. with the operating conditions previously specified. Since the light from the interferometer was nearly parallel, no serious loss resulted from the increase in distance.

The galvanometer used had a resistance of 1000  $\Omega$ , and a sensitivity of 550 mm. per  $\mu\text{A}$  at the scale distance used. The period was 4 sec., and, to prevent over-damping, a resistance of 10,000  $\Omega$ , not shown in figure 2, was included in the circuit between shunts (*S*, figure 2) and galvanometer. With the amplifier and associated apparatus in its final form, a sensitivity could be obtained such that the light from the interferometer, using both rays, but with no bands visible, would give a galvanometer deflexion of 80–100 cm. with the shunt set at unity. The deflexions produced by light from each interferometer path separately are almost equal.

*Recording camera.* The recording apparatus and control panel were located in the room previously mentioned adjacent to that containing the equipment already described. The recording apparatus consists of a drum, enclosed in a light-tight box, and driven by a small electric motor through reduction gearing at a speed of approximately one revolution in 70 sec. A strip of bromide photographic paper is held by a clip round the outer circumference of the drum, and an image of the filament of a small lamp, after reflection at the mirror of the galvanometer, is focused on the surface

of the paper through a slit in the side of the box. The slit is covered by a shutter which can be raised when required by means of a solenoid.

In order to avoid errors in measurement of the record which might arise from any irregularity in the motion of the recording drum, a base line is put on every record by means of a second lamp—an image of the filament of this lamp is focused on the slit near one edge of the record. To mark the points on the record at which the current through the magnets is switched on or off, the light from this second lamp is directed on to the photographic paper through a time marker. This contains a small vane, operated by an electromagnet, which momentarily obscures the light each time the current through the winding is turned on or off, thus causing a short break in the base line. The electromagnet is actuated by means of a cell and pair of contacts, the contacts being closed by the movement of a strip of iron pivoted so as to project, horizontally, from the upper pole piece of magnet *F* (figure 1). The iron strip is normally held up by a spring, but, when the field of *F* reaches nearly its maximum value, it is pulled down and closes the contacts. As however the breaks in the base-line were rather difficult to locate at times, a third lamp, similar to the other two, was connected across the winding of *m*, so that a dark line appeared on the record during each period when the current through the magnet windings was on. The whole camera, including lamps, galvanometer, motor, etc., was enclosed in a wooden case with a small opening in its top closed by a ground glass screen on to which the image of a portion of the galvanometer spot is directed by means of a mirror. Thus movements of the galvanometer spot can be watched by eye, the amplifier can be kept balanced, and a suitable moment can be chosen for a record.

To obtain satisfactory records, the camera must fulfil the following requirements: (a) the shutter must open just after the join in the paper has passed the slit, and must close again just before it again reaches it; (b) within the limits set by (a) the shutter must be capable of being operated whenever required; (c) since the camera is covered during operation, some indication of conditions must be given externally; (d) the camera case must be easily removable for changing paper. Arrangements for fulfilling these conditions were satisfactorily made.

*Sensitivity.* An advantage of recording methods over direct visual observation of the bands is that it is possible to measure with some certainty the actual sensitivity obtainable, a quantity entering into the final result in a definite manner in the present work, whereas with visual observation the limiting sensitivity is at best an estimate only.

To measure sensitivity, several bands are caused to move slowly across

the field of view, immediately after each actual run. The resulting changes in brightness cause the galvanometer spot to record an approximately sine trace on the record. By noting the amplitude of this curve and the phase of its starting point, any measured displacement of the record trace can at once be expressed in terms of a fraction of a band. A convenient way of imparting a smooth movement to the bands was found to be by loading the pillar supporting one of the interferometer mirrors with water run slowly from one bottle standing on a shelf into another hanging from a wire. The suspended bottle, marked *S* in figure 1, and both bottles used can be seen in figure 3 (plate 1). As will be seen in the photograph, the bottle *S* is supported by a pair of brass rods and wire in such a way as to give an increasing approximately horizontal pull to its pillar as its weight increases. This causes *M* to approach *N* very gradually, and produces the required band movement. In figure 3 the bottles are shown ready for the measurement, *S* being empty. It is only necessary to release the looped rubber tube (which can be done from the next room from a point near the control board) to start the water flow.

*Sources of irregularity in final record.* Since a smooth trace is very desirable for the final measurements, any sources of disturbance likely to cause irregular movements of the galvanometer spot had to be eliminated as far as possible. Drifts of any magnitude, particularly those due to band movement, would cause some uncertainty as to the actual sensitivity, and should be avoided.

The mercury vapour lamp used had a tendency to flicker and such a flickering caused large disturbances of the record. The flickering was avoided by carefully adjusting the operating current and directing an air blast on the part containing the arc and on the cooling fins, and by keeping the lamp switched off as much as possible between measurements. The lamp was run from a large storage battery, which was used only for this purpose and for driving the small motor actuating the drum during the course of an experiment.

Band movements due to mechanical vibration and changes of temperature were at first troublesome. Continuous slight vibration blurs the bands and causes a loss of sensitivity. Intermittent vibration should cause no displacement of the galvanometer spot provided the phase of the bands was half-way between dark and bright, since the illumination simply performed rapid excursions symmetrically about the mean value, which the galvanometer was too sluggish to follow. With the bands in any other phase, the unequal curvatures of the band position-illumination curve on either side of the mean position had a "rectifying" effect, causing

the average illumination to alter, thus giving a galvanometer displacement as long as the vibration lasted. To reduce effects from the motor driving the drum, it was mounted as freely as possible on sponge rubber, the whole camera box stood on pieces of sponge rubber, and finally the legs of the table rested on felt. Resonance occurred at certain motor speeds, and caused greater vibration, and to assist in choosing the best motor speed, a vibration indicator consisting of a dish of mercury, a small lamp and a screen, was set up on the table. This simple device was remarkably effective for quickly adjusting camera speed, since the resonances were quite sharp, and had a beautiful and characteristic appearance, and by adjusting the motor speed to fall between two selected resonance patterns the speed could be kept close to the required value.

Vibrations arising outside the building were often intense enough to be troublesome, causing continual irregular wandering of the galvanometer spot, and making it necessary to carry out the experiments between about midnight and 4 a.m. Microseisms, when moderately strong, were troublesome, and during one series of experiments, when bad drifts were experienced, two minor earthquakes were afterwards found to have occurred. Microseismic conditions could be obtained from seismographs installed about one third of a mile away.

Temperature changes were capable of causing serious band drifts by changing the dimensions of interferometer parts, particularly of the two long brass stiffening rods, unequally. Fortunately, the apparatus being situated in a basement, the temperature was found to change by only a few tenths of  $1^{\circ}\text{C}$  during the course of a night's work, and, by lagging the rods, temperature drifts were made slow and of tolerable magnitude.

#### EXPERIMENTAL PROCEDURE

Two series of records were obtained, one with the three magnets pushed back so as to be just clear of the path of the light ray, in order to discover, and, if possible, eliminate any spurious effects, and the other with the magnets pushed up so that the ray passed through their gaps, as in figure 1. The general procedure was the same in both cases. At about 11 p.m. on a suitable evening, the amplifier batteries were connected up, and electric furnaces put over the three charcoal tubes on the magnets. The rotary backing pump for the mercury condensation pump was started, and, when the pressure in the vacuum system was low enough, the condensation pump and the electric furnaces were turned on. When the charcoal temperature

had reached about 300° C, they were switched off, a fair vacuum having meanwhile been attained by the pumps. By the time the tubes had cooled again, the vacuum was usually approaching a steady condition. The mercury vapour lamp, which was then switched on, takes some minutes to reach a stable state. As soon as it was steady enough, the pumps were stopped. A telescope was set up temporarily and the bands were brought to the best adjustment by rotating the mirror *N* about its two axes, a single band being caused, as far as possible, to fill the whole field of view. The telescope was then removed, voltage was applied to the photoelectric cell, and adjustments were made until the light from the interferometer falling on the cell cathode gave a convenient deflexion. The amplifier had, by this time, reached a fairly stable state, and any drift or unsteadiness was usually found to be due to disturbances of the bands, or to lamp flickers. The latter can be easily seen. They can be stopped by changing the lamp current, or by starting the air blast, or by both. Effects due to band movements usually settled down on waiting, when the galvanometer became steady. Connexion of the auxiliary galvanometer (which can be seen when the observer is in the vicinity of *N*) across *G*—the main galvanometer—enabled any small final adjustments for greater illumination, and for maximum galvanometer displacement between “bright” and “dark” band positions, to be made. All the above operations required about an hour to complete. If the bands were sufficiently steady when the adjustments had been made, and if other conditions were satisfactory, the electric furnaces, and any other apparatus containing iron, were removed, the pumps were shut off with a clamp, and flasks containing liquid air were put over the charcoal tubes, which were by this time generally at normal temperature. All lights in the room containing the interferometer, except the mercury vapour lamp, were turned out (fluctuations in the brightness of these lights due to changes in the supply voltage caused galvanometer movements), and the two operators proceeded to the next room, one to the switch controlling the magnet current, and the other to the control board near the camera. The sensitivity was brought up to its maximum safe value by raising the voltage on the cell by means of the potentiometer *P*<sub>2</sub> (figure 2). Too high a cell voltage caused the galvanometer spot to creep badly, sometimes at a rapidly increasing rate, until the cell ionized. The observer at the camera watched the galvanometer spot, and chose a suitable moment, when the sensitivity and steadiness appeared to be satisfactory, and signalled to the operator at the switch, who closed it for a few seconds. Any movement of the spot was noted; if it was at all large, it was probably due to the appearance of magnetizable

particles in the gap. These particles appeared. They probably lay in the boxing enclosing the gap, and may have been due to flaky corrosion of the pole faces. They seemed to stand up in the gap and obstruct the light variably as the field changed. Blowing air through the gap removed the effect for a long or a short time, but eventually it reasserted itself until the gap was again blown through. Any difficulty of this kind having been overcome, preparations were made for a photographic record. The speed of the drum carrying the photographic paper was adjusted, with the aid of a stop-watch, to about 1 revolution in 70 sec., speed being finally arranged so as to avoid vibration as described above. Since sensitivity is a maximum when the band phase is half-way between "dark" and "bright", it is desirable that all records should be made, as far as possible, with the bands in this condition. As already mentioned, any vibration will, unless the band phase is as above, cause a change in the average light flux emerging from the interferometer, such change being always towards a value corresponding to mid-band phase. Thus, if the operator set up a vibration purposely, the galvanometer spot would always move towards the position it would take up (in the absence of vibration) for maximum sensitivity. By adjusting the balance of the bridge, it was possible to cause this position to be at the centre of the viewing screen. Some band drift was nearly always present, but as long as it was not too rapid, it was always possible, by waiting until the spot is in the middle of the screen, to make a record while sensitivity was near a maximum. If the galvanometer was then reasonably steady, a key on the control panel was depressed, opening the shutter, and lighting a lamp near the main switch. As soon as this occurred, the operator at the switch started a stop watch, and, after an interval of 10 sec., which was altered later to 7 sec., he closed the switch, holding it closed for an equal period. He continued in this way, alternately opening and closing the switch, until the drum had completed a revolution, when the shutter closed and the lamp went out. To obtain the sensitivity, the operator at the control board quickly set the shunt  $S$  (figure 2) at  $1/3$  (it was set at unity during the preceding period), and pressed the key again. The shutter opened again and about 10 sec. later the loop in the rubber tube between the two bottles was released. Provision had been made for doing this without any change in position of the operator. The light spot then moved back and forth across the paper, giving a trace resembling a sine curve; at the end of the revolution the shutter closed again, three or four complete bands having passed in the interval. This gave a complete record. A numbered note of any important details was made, the exposed paper strip was removed and marked with the same number and date,



FIGURE 3

(Facing p. 16)





and a fresh piece of paper was inserted for the next record. During this interval, the mercury vapour lamp had been turned off to cool, and the water that had run into the sensitivity bottle *S* (figure 1) was returned to the other bottle and the tubing was looped up for the next run. An observation of the state of the vacuum was then made, with the aid of the induction coil and discharge tube, and the appearance of the discharge noted. Usually the charcoal and liquid air quickly brought the pressure down to a low value and maintained it there during the whole series of measurements. Subsequent determinations with a McLeod gauge showed this to be about 0.05 mm. of mercury.

If everything appeared satisfactory, four or five records were generally taken in the course of a night's work, occupying three or four hours. Between records any small adjustments to the interferometer, amplifier, etc. that appeared to be necessary were made, any resulting changes in sensitivity being taken care of by including a sensitivity curve, taken immediately after the actual run with the magnet, on each record. A note was made of the current through the magnet windings during the run, and also of the temperature (by means of a thermometer on the lagging of one of the interferometer bars) and of the barometric pressure. A rapid fall in the barometer is usually associated with microseismic activity, in this locality, and so it was generally possible to decide whether any unsteadiness or bad drifting of the galvanometer was due to external causes or to some fault in the apparatus.

Altogether twenty-seven records were secured with the light passing through the magnet gaps. Of these, nine were finally selected for comparative smoothness of the record and high sensitivity, for measurement with a planimeter. Four such records are shown in figure 4, the size of the originals being 62 cm. long by 10 cm. wide. In the upper two the "On" and "Off" periods can be seen near the bottom edge of each record, and the base line just above. The sensitivity and measurement traces can be easily identified from their appearance, and it will be noticed that each sensitivity curve starts from a point lying between crest and trough. No. II, 5 July 1936, is the best example of this, the starting point being almost on the axis of the sine curve. In all four records the sensitivity curve has been obtained with the shunt set at  $1/3$  (i.e., the galvanometer movements for it must be multiplied by three), and the other trace with it set at unity. The vertical lines and the rectangle are construction lines put on afterwards to facilitate planimeter measurements. Equal intervals of either 7.5 or 5 cm., depending on whether the period is 10 or 7 sec., are marked off within each "On" and "Off" period, the smoothest part of the

period being chosen whenever possible, and vertical lines drawn between record and base line. A rectangle 6 cm. high, with one of these intervals as base, was also constructed on most of the records. The areas included as base, was also constructed on most of the records. The areas included between the main trace and the base line in each interval and the area of the rectangle were then measured with a planimeter. The distances between a number of crests and troughs of the sensitivity curve and a base-line were measured, and the average amplitude was calculated. The direction of the initial (left) part of this curve, whether towards or away from the base-line, was noted. The vertical distance between a crest and a trough on the

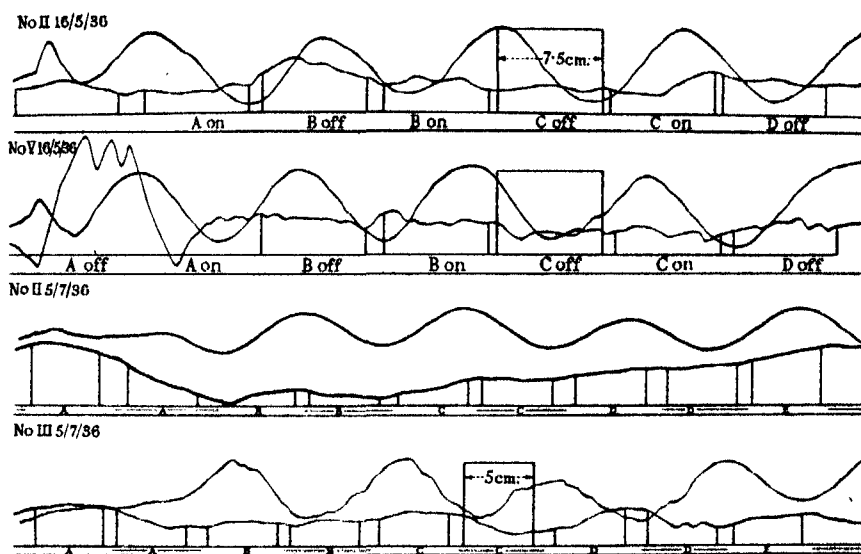


FIGURE 4

sensitivity curve evidently represents a displacement of half a band, corresponding to a path change of half a wave-length. To obtain the displacement for a path difference corresponding to a full band this distance must be multiplied by the factor 2 and also by the shunt factor (usually 3) before reducing displacements to fractions of a band interval, which was taken as the distance between successive bright or dark bands.

Since the bases of the "On" and "Off" areas, and of the standardizing rectangle are, for any record, the same (viz. 7.5 cm. or 5 cm. as the case may be), the planimeted areas, above these bases, are proportional to the average heights of these areas, and the difference between the mean of two consecutive "Off" areas and the intervening "On" area is proportional to the difference of galvanometer deflexions during these periods,

that is to say to the effect sought. This difference in heights (i.e. the difference in galvanometer readings) can be converted into centimeters by comparison with the planimeter reading for the standardizing rectangle, and this, again, into "band movements" by comparison with the sensitivity curve corrected for the amount of shunting used for it (usually 1/3). From this to the wave-lengths of the light used, and thence to the difference of velocity of the light through the two paths of the interferometer, is a matter of quite simple physics and arithmetic. The formulae used and the data for the computations are given below.

The difference of mean band displacement  $\beta$  between the "On" and the "Off" periods for each record is given by

$$\beta = \frac{hDS_1}{4PaS_2}, \quad (1)$$

where  $h$  = height of rectangle constructed on record (6 cm.),

$P$  = planimeter reading obtained by traversing rectangle, in planimeter scale divisions,

$D$  = mean of differences, in planimeter scale divisions,

$a$  = mean amplitude of sensitivity trace, in cm.,

$S_1$  = shunt setting when making sensitivity trace,

$S_2$  = shunt setting during run with magnetic field.

Whether the displacement calculated by (1) represented an increase or decrease in velocity of the ray passing through the magnetic field was decided in the following manner. Since the displacement of the trace recorded during the sensitivity run was the result of a band movement caused by a shortening of the path of the ray which did not pass through the magnetic field, the direction of the initial displacement of this trace gave the direction corresponding to a decrease in velocity of the other ray (i.e. the ray passing through the magnetic field). Hence a comparison of the sign of  $D$  with the direction of the initial part of the sensitivity trace, on each record, rendered it possible to determine, in each case, whether a decrease or an increase in velocity of the ray passing through the magnet gaps when the field was switched on was indicated.

The results of measurement of the nine records are given in the accompanying tables. The row marked "differences" gives the difference between each "On" period and the mean of the preceding and succeeding "Off" periods. A negative sign indicates that the trace has moved towards the base line during the "On" period. The predominance of negative signs

TABLE 1. MEASUREMENT OF RECORDS

Record No. V, 25 April 1936, 1 a.m.

| Switch              | ... | Off     | On     | Off    | On     | Off   | On |
|---------------------|-----|---------|--------|--------|--------|-------|----|
| Planimeter readings |     | 231.0   | 194.5  | 208.6  | 202.9  | 207.7 | —  |
|                     |     | 231.7   | 194.2  | 208.4  | 203.0  | 208.3 | —  |
| Means               |     | 231.35  | 194.35 | 208.5  | 202.95 | 208   | —  |
| Differences         |     | - 25.58 |        | - 5.30 |        |       |    |

Mean of differences - 15.44 (=  $D$ ) in planimeter divisions. Displacement for one complete band  $\left( = 4a \frac{S}{S} \right)$  10.2 cm. Planimeter reading round rectangle 6 cm. high 379.5 (=  $P$ ).

Mean displacement of trace from record for the "On" periods 0.024. Increase.

Record No. II, 16 May 1936, 2.45 a.m.

| Switch              | ... | Off     | On     | Off     | On    | Off     | On    | Off | On |
|---------------------|-----|---------|--------|---------|-------|---------|-------|-----|----|
| Planimeter readings | 130 | 102.6   | 201.2  | 135.0   | 110.4 | 120.4   | 151.0 | —   | —  |
|                     | 130 | 102.65  | 201.1  | 135.6   | 110.8 | 120.5   | 151.2 | —   | —  |
| Means               | 130 | 102.5   | 201.15 | 135.3   | 110.6 | 120.45  | 151.1 | —   | —  |
| Differences         |     | - 62.95 |        | - 20.58 |       | - 10.40 |       |     |    |

Mean of differences - 31.31. Displacement for one complete band 30 cm. Planimeter reading for 6 cm. displacement 380.4. Mean displacement of trace during On periods 0.016 band. Increase.

Record No. V, 16 May 1936, 4.10 a.m.

| Switch              | ... | Off | On    | Off     | On     | Off     | On     | Off | On |
|---------------------|-----|-----|-------|---------|--------|---------|--------|-----|----|
| Planimeter readings | —   | —   | 156.0 | 151.2   | 104.4  | 100.2   | 134.0  | —   | —  |
|                     | —   | —   | 156.0 | 151.0   | 103.9  | 100.4   | 134.1  | —   | —  |
| Means               | —   | —   | 156   | 151.1   | 104.15 | 100.3   | 134.05 | —   | —  |
| Differences         |     |     |       | + 21.03 |        | - 18.80 |        |     |    |

Mean of differences + 1.11. Displacement for one complete band 30 cm. Planimeter reading for 6 cm. displacement 377.0. Mean displacement of trace during On periods 0.00059 band. Increase.

Record No. III, 7 June 1936, 4.3 a.m.

| Switch              | ... | Off     | On     | Off     | On     | Off   | On     |
|---------------------|-----|---------|--------|---------|--------|-------|--------|
| Planimeter readings |     | 350.4   | 246.2  | 189.7   | 155.2  | 177.9 | 107.7  |
|                     |     | 351.1   | 245.7  | 189.8   | 155.3  | 177.3 | 108.0  |
| Means               |     | 350.75  | 245.95 | 189.75  | 155.25 | 177.6 | 107.85 |
| Differences         |     | - 24.30 |        | - 28.43 |        |       |        |

Means of differences - 26.37. Displacement for one complete band 20 cm. Planimeter reading for 6 cm. displacement 377.2. Mean displacement of trace during On periods 0.021 band. Increase.

Record No. IV, 7 June 1936, 4.21 a.m.

| Switch              | ...    | Off     | On     | Off     | On     | Off     | On    | Off | On |
|---------------------|--------|---------|--------|---------|--------|---------|-------|-----|----|
| Planimeter readings | 223.8  | 132.2   | 180.0  | 172.7   | 195.0  | 199.5   | 182.2 | —   | —  |
|                     | 224.3  | 132.7   | 179.5  | 172.8   | 195.1  | 199.9   | 182.2 | —   | —  |
| Means               | 224.05 | 132.45  | 179.75 | 172.75  | 195.05 | 199.7   | 182.2 | —   | —  |
| Differences         |        | - 69.45 |        | - 14.65 |        | + 11.08 |       |     |    |

Mean of differences - 24.34. Displacement for one complete band 15 cm. Planimeter reading for 6 cm. displacement 374.45. Mean displacement of trace during On periods 0.026 band. Increase.

TABLE 1 (*continued*)

Record No. II, 21 June 1936, 3.00 a.m.

| Switch ...  | Off    | On     | Off    | On    | Off     | On     | Off     | On   | Off    | On |
|-------------|--------|--------|--------|-------|---------|--------|---------|------|--------|----|
| Planimeter  | 86.0   | 131.3  | 166.7  | 184.8 | 205.6   | 107.4  | 87.2    | 52.3 | 122.2  | —  |
| readings    | 85.7   | 131.8  | 167.1  | 185.4 | 205.8   | 107.5  | 87.4    | 51.9 | 122.3  | —  |
| Means       | 85.85  | 131.55 | 166.9  | 185.1 | 205.7   | 107.45 | 87.3    | 52.1 | 122.25 | —  |
| Differences | + 5.18 |        | - 1.20 |       | - 39.05 |        | - 52.68 |      |        |    |

Mean of differences -21.94. Displacement for one complete band 30.6 cm. Planimeter reading for 6 cm. displacement 252.3. Mean displacement of trace during On periods 0.017 band. Decrease.

Record No. III, 21 June 1936, 3.30 a.m.

| Switch ...  | Off     | On     | Off     | On    | Off    | On     | Off     | On    | Off   | On    |
|-------------|---------|--------|---------|-------|--------|--------|---------|-------|-------|-------|
| Planimeter  | 146.2   | 209.2  | 236.3   | 256.7 | 244.0  | 258.3  | 254     | 212.2 | 196.0 | 125.4 |
| readings    | 145.4   | 209.5  | 236.4   | 257.1 | 244.2  | 259.2  | 254     | 211.8 | 195.8 | 125.8 |
| Means       | 145.8   | 209.35 | 236.35  | 256.9 | 244.1  | 258.75 | 254     | 212   | 195.9 | 125.6 |
| Differences | + 18.28 |        | + 16.68 |       | + 9.70 |        | - 12.95 |       |       |       |

Mean of differences +7.93. Displacement for one complete band 31.8 cm. Planimeter reading for 6 cm. displacement 252.9. Mean displacement of trace during On periods 0.0059 band. Increase.

Record No. II, 5 July 1936, 1.23 a.m.

| Switch ...  | Off    | On   | Off     | On   | Off    | On    | Off     | On     | Off    | On |
|-------------|--------|------|---------|------|--------|-------|---------|--------|--------|----|
| Planimeter  | 178.2  | 74.4 | 32.7    | 32.4 | 54.6   | 81.7  | 103.3   | 116.6  | 155.2  | —  |
| readings    | 177.8  | 74.6 | 32.5    | 32.6 | 54.8   | 81.8  | 103.3   | 116.9  | 155.3  | —  |
| Means       | 178.0  | 74.5 | 32.6    | 32.5 | 54.7   | 81.75 | 103.3   | 116.75 | 155.25 | —  |
| Differences | - 30.8 |      | - 11.15 |      | + 2.75 |       | - 12.53 |        |        |    |

Mean of differences -12.93. Displacement for one complete band 15 cm. Planimeter reading for 6 cm. displacement 254.0. Mean displacement of trace during On periods 0.0204 band. Decrease.

Record No. III, 5 July 1936, 1.54 a.m.

| Switch ...  | Off     | On    | Off     | On   | Off     | On    | Off     | On   | Off   | On |
|-------------|---------|-------|---------|------|---------|-------|---------|------|-------|----|
| Planimeter  | 123.2   | 74.4  | 69.7    | 71.8 | 96.7    | 56.4  | 83.9    | 68.9 | 82.5  | —  |
| readings    | 122.9   | 74.5  | 69.7    | 71.6 | 96.3    | 56.9  | 83.9    | 69.1 | 82.4  | —  |
| Means       | 123.05  | 74.45 | 69.7    | 71.7 | 96.5    | 56.65 | 83.9    | 69.0 | 82.45 | —  |
| Differences | - 21.93 |       | - 11.40 |      | - 33.55 |       | - 14.18 |      |       |    |

Mean of differences -20.27. Displacement for one complete band 22.8 cm. Planimeter reading for 6 cm. displacement 254.0. Mean displacement of trace during On periods 0.021 band. Increase.

TABLE 2. FINAL MEANS FROM TABLE 1, GROUPED ACCORDING TO DIRECTION OF INITIAL PART OF SENSITIVITY TRACE

| Towards base-line |              |           | Away from base-line |               |          |
|-------------------|--------------|-----------|---------------------|---------------|----------|
|                   | Record No.   | Band      |                     | Record No.    | Band     |
| V                 | 16 May 1936  | + 0.00058 | V                   | 25 April 1936 | + 0.024  |
| II                | 21 June 1936 | - 0.017   | II                  | 16 May 1936   | + 0.016  |
| III               | 21 June 1936 | + 0.0059  | III                 | 7 June 1936   | + 0.021  |
| II                | 5 July 1936  | - 0.0204  | IV                  | 7 June 1936   | + 0.026  |
|                   |              |           | III                 | 5 July 1936   | + 0.021  |
|                   | Mean         | - 0.00773 |                     | Mean          | + 0.0216 |

Mean of -0.00773 and +0.0216 = +0.0069 band.

indicates a residual spurious effect, which will tend to be eliminated in the final result as follows:

Depending on the position of the bands during a measurement, a change of velocity, in one path, of a given sign, will cause either an increase or decrease of light flux, according to whether the change tends to reduce or increase the phase difference between the oscillations in the two interfering rays. Since the loading of one pillar during a sensitivity measurement is known to shorten the path of a particular ray, it is possible by inspection of the initial part of each sensitivity curve to determine whether a given displacement of the trace secured during the run with the magnets represents an increase or decrease in velocity of the ray through the field. Spurious effects due to factors tending to change the total light flux (otherwise than by band displacement), being always in the same direction, will, therefore, be interpreted as increases in velocity in some cases and as decreases in others. The final results from the records, expressed as fractions of a band displacement, are, therefore, divided into two groups, according to whether the initial movement of the sensitivity trace is towards or away from the base-line. Each group is averaged separately, and, lastly, the means of these two values taken for the calculation of a change in velocity. This procedure will not, of course, eliminate any spurious effect resulting in actual band displacement. The magnitude of any such effect, determined in the preliminary tests already described, was, however, relatively small.

Table 2 gives the results from each record grouped in this way. When the difference has a negative sign, a decrease in the velocity of the ray in the magnetic field is indicated.

The probable error,  $R$ , of determination of band displacement was ascertained in the ordinary way from the equation

$$R = 0.6745 \sqrt{\frac{S}{n(n-1)}},$$

where  $n$  = number of observations (= 28), and  $S$  is given by

$$S = V_1^2 + V_2^2 + V_3^2 + \dots + V_n^2, \quad (2)$$

where  $V_1, V_2, \dots, V_n$  are the differences between the individual observations and the mean of all the observations. The mean referred to (= 0.0152) is that of the twenty-eight "differences" listed in Table 1, after conversion of each of these differences into band displacement by the use of equation (1). The value thus found for the probable error was 0.00265 band.

During the preliminary measurements, with the magnets pushed back just clear of the appropriate ray, a spurious effect amounting to 0.002 band, and indicating an increase in velocity, was obtained. Since the presence of even a small piece of iron, such as a screw, in any of the instruments on the pillars supporting the interferometer mirrors was found to give a marked band displacement in the same direction when the field was switched on, it was concluded that this effect would probably be due to traces of magnetic impurities in the materials of the pillars or mirror mounts. This must, therefore, be subtracted from the previous result (0.0069), giving +0.0049 band for the final value. The change in velocity of the ray in the magnetic field may now be calculated by means of the equation

$$V_h - V = V \left( \frac{\beta \lambda}{l} \right),$$

where  $V_h$  = velocity of light in the magnetic field,  
 $V$  = normal velocity of light,  $3 \times 10^{10}$ ,  
 $\beta$  = band displacement (0.0049),  
 $\lambda$  = wave-length of light used ( $5461 \times 10^{-8}$  cm.),  
 $l$  = length of path of ray in magnetic field (234 cm.).

Hence  $V_h - V = 34.31$  cm./sec.  $\pm 18.56$  cm./sec.

Looking at the figures in Table 2, which are derived from the records tabulated above, it is seen that they are divided into two parts, viz. those on the left, in which the initial movement of the sensitivity trace was towards the base line, and vice versa, those on the right-hand side of the table. Those on the right-hand side have had their signs changed, so as to take account of this difference of initial movement of sensitivity trace. If, on the other hand, this difference of initial movement be disregarded, the signs throughout remain as they are in the details above, and it will be seen that of the whole nine, all but two are negative, and the two positive ones are relatively very small. These are from Records V and III on the left-hand side. Amongst the other seven a considerable uniformity is obvious. They are all negative, they all lie between 0.016 and 0.026, with a mean of 0.0208. As against these there are the two positive values, 0.00058 and 0.0059, which, as between themselves, are not so consistent. There is thus a considerable balance of evidence, that, when a magnetic field is switched on, there is a movement of the galvanometer needle away from the base line (negative sign) which is *not* connected with the phase of the bands, and which is therefore *not* due to an effect of the magnetic field upon the velocity of light. The outside value deduced above (34.31 cm./sec.) takes in all the records and is influenced considerably by the two



least reliable positive ones on the left-hand side of Table 2. It appears therefore, that whilst the value 34.31 cm./sec. is the maximum effect which is found in the work, yet the evidence of selected records is, that the value is spurious, and is due to causes other than an effect of a transverse magnetic field upon the velocity of light.

*Field strength.* The iron of the magnets was carefully demagnetized with alternating current, and one branch of a B.H. curve was taken by means of the special search coil mentioned below. On switching off the current the residual field was found to be of the order of 5000 oersted. From the form of the curve at the maximum current used (70 amp.), it was clear that a near approach to saturation had been obtained, so that small departures from this value during actual runs would be relatively unimportant.

Obviously with the authors' objective, the change in field strength only, on switching on the current, was relevant. This was measured by introducing a specially made search coil, connected to a Grassot fluxmeter, into the gaps through the tubes provided (figure 1), and switching on the current. The fluxmeter reading thus obtained then gave the change in flux produced, and by calibrating the special search coil against a standard coil in the field of an electromagnet the value of the change of flux was obtained. The change of field strength in the gaps of each of the three magnets was practically the same, no individual value differing by more than 2% from the mean, which was found to be 19,917 oersted, with a current of 70 amp. This is a little larger than that usually obtained while recording (about 65 amp.).

*Vacuum.* Subsequent calibration of the discharge tube used with the apparatus, by means of a McLeod gauge, showed the pressure of the residual air to have been reduced to about 0.05 mm. of mercury during measurements.

*Polarization.* Observations with a Nicol prism of the light emerging from the interferometer, and (by removing the mirror *O*) of the light passing through the magnet gaps, showed no appreciable polarization.

#### DISCUSSION OF RESULT

While, as indicated in the course of this paper, every effort has been made to eliminate or minimize any spurious effects, and it is not thought that any major cause of uncertainty has been overlooked, the smallness of the final result, combined with the magnitude of the calculated probable error, make it difficult to accept the observed change in velocity as real, unless some theoretical support is forthcoming.

### SUMMARY

This paper is an account of work done to determine, to a higher degree of precision than before, the effect (if any) of a transverse magnetic field on the velocity of propagation of light in air at reduced pressure.

The experimental results indicate that there is an increase in the velocity of light of 34.31 cm./sec., in a field in which the magnetic force was 20,000 oersted, in the presence of air at a pressure of 0.05 mm. of mercury. The probable error of the observations was found to be 18.56 cm./sec. An interferometer method, using the Michelson arrangement, was employed, one interfering ray passing through the field in the gaps of three electromagnets, and the other passing through free space. A photoelectric cell and amplifier were used in conjunction with a galvanometer, to record band movement on a moving photographic strip, the resulting record being subsequently measured by means of a planimeter. The mean of the results from a number of such records was taken, and preliminary check experiments carried out. The authors consider that they have taken all precautions to eliminate causes tending to give a spurious effect greater than the probable error of observation quoted above. They would however be very hesitant in accepting the above final result as real. All that can be said definitely is that in such a field (20,000 oersted) the effect is less than 1 part in about  $5 \times 10^8$ .

### REFERENCES

- Barnard 1930 *The selenium cell*.  
Farr and Banwell 1932 *Proc. Roy. Soc. A*, **137**, 275-82.  
Fourmarier 1932 *C.R. Acad. Sci., Paris*, **195**, 1387-9.  
Fournier d'Albe and Symonds 1926 Some new applications of selenium.  
*Proc. Optical Convention*, Part 2, p. 884.  
\*Illingworth 1927 *Phys. Rev.* **30**, 692-6.  
\*Kennedy 1926 *Proc. Nat. Acad. Sci., Philadelphia*, **12**, 621-9.  
\*Kennedy and Thorndike 1932 *Phys. Rev.* **42**, 400-18.  
\*Ohain, H. J. P. V. 1935 *Ann. Phys., Lpz.*, **23**, 5, 431-41.  
Piccard and Stahel 1926 *C.R. Acad. Sci., Paris*, **183**, 420.  
— — 1927a *C.R. Acad. Sci., Paris*, **184**, 152.  
— — 1927b *C.R. Acad. Sci., Paris*, **185**, 1198-1200.  
Simon 1927 *C.R. Acad. Sci., Paris*, **185**, 1269-70.

\* Available in New Zealand in abstract form only.

---

# Thermal ionization of barium

By B. N. SRIVASTAVA, M.Sc.

*Physics Laboratory, Allahabad University*

*(Communicated by M. N. Saha, F.R.S.—Received 3 July 1939)*

The theory of thermal ionization of gases was first given by M. N. Saha in a series of papers (1920*a*, 1920*b*, 1921) and widely applied by him and others to explain the spectrum of the sun and furnish a satisfactory physical theory of stellar spectra and their classification. Saha considered the ionization of a unicomponent system, but it is evident that in actual practice electrons may generally be obtained from the ionization of other atoms or from other surfaces and must therefore be considered as an independent constituent. This was done by E. A. Milne (1921) and H. N. Russell (1922). The theory was further developed by Darwin and Fowler (1923) to include the different excited states of the atom and of the ionized atom, all of which are simultaneously in thermodynamical equilibrium. There may also be multiple ionization. At the time when the theory was first formulated the ionization potentials and the spectral characteristics of only a few elements were known and hence it could be applied only to those few elements, but thanks to the recent developments in atomic physics we are now in possession of the values of ionization potentials as well as the spectra of almost all the elements in their different stages of ionization. So a detailed comparison of the theory with experimental results can now be satisfactorily done. A full account of the theory and its applications to astrophysical problems has been given by Pannekoek (1930).

On the purely experimental side the progress has not been so marked. This is mainly due to the extremely difficult technique encountered at high temperatures which are necessary for producing a measurable ionization in the case of most substances. Even for the most easily ionizable gases, such as the alkali vapours, a temperature of about 2000° C is necessary. Saha and his co-workers (1927) performed a number of laboratory experiments in which they proved that the alkali metals can be ionized by heating their vapours to temperatures of about 2000° C which are available in the laboratory. The ionization was detected from the fact that their vapours which are non-conducting at the lowest temperature acquire increasing conductivity at higher temperatures, and elements with the lowest ionization potential showed the greatest amount of conductivity. These experi-

ments only served as a qualitative confirmation of the theory but an exact quantitative verification was yet lacking.

The quantitative verification of the theory was first achieved by I. Langmuir and K. H. Kingdon (1925) for caesium vapour. Further work in this direction was done by T. J. Killian (1926) in America with rubidium and potassium vapour, by E. Meyer (1930) in Germany with potassium and by N. Morgulis (1934) in Russia with sodium. The theory of all such experiments was first given by Langmuir and Kingdon (1925). The apparatus used by them was an ordinary thermionic valve having a central filament and a coaxial cylindrical anode. Caesium was kept in a side pocket, and thus the whole tube was filled with caesium vapour at its saturation vapour pressure. The axial filament was heated, and when the caesium atoms struck it they became ionized into caesium ion and electron. At the surface of the filament the atoms, the ions and the electrons are in thermodynamic equilibrium and their concentrations must obey the Saha formula. The concentrations of the ions and electrons are determined by measuring the respective currents between the filament and the anode when suitable potentials are applied, it being assumed that on account of absence of molecular collisions the equilibrium state is not altered when these move away from the filament. The method is very elegant in that the whole apparatus is not to be raised to the temperature at which the dissociation is to be investigated and thus very high temperatures can be conveniently employed. It is, however, complicated by the adsorption of the atoms or ions on the filament surface. The extent and thickness of this coating varies with the temperature of the filament, the pressure of the vapour, etc. The coating is also found not to be uniform all along the surface. This coating alters the effective thermionic work function for the surface and thus materially alters the electronic emission. On account of these uncertainties, the results of the different workers are not quite concordant. Another disadvantage is that on account of this coating the electron emission from the surface varies in an irregular manner, and it may so happen that at certain temperatures the electron current and the ion current may not both be quite suitable for measurement. For caesium, rubidium and potassium on tungsten or molybdenum filaments the ionization potential is less than the electronic work function of the pure metal, and the currents in these cases are quite suitable over a sufficient range of temperatures. With sodium on tungsten surface the reverse is the case, and Morgulis found that there is very little ionization at low temperatures, but at high temperatures the sodium coating evaporates and there is considerable ionization. He, however, finds for any one temperature different degrees of ionization for different pressures, a result not in

accordance with Saha's theory. There is, however, in general an increase of ionization with increase of temperature. There is thus only a qualitative agreement with the theory.

Quite a different type of apparatus has been constructed in this laboratory by M. N. Saha and A. N. Tandon (1936, 1937) and has been widely used by Tandon (1937, 1938) and the present author (Srivastava 1938, 1939) for studying the dissociation of some alkali halides. This apparatus is eminently suited for investigations on thermal ionization of vapours and has been employed in the present paper for studying the thermal ionization of barium. Barium was chosen for several reasons. First, there is very little work hitherto done on the thermal ionization of barium. The only experiments done with barium are those of J. M. Elgin (1928), H. Nelson (1931), J. A. Becker (1929) and some unpublished work of Ryde and Harris. These are all concerned with the emission from a barium-coated tungsten surface and a detailed study of the surface effects, but no attempt has been made to verify the ionization formula in detail. Secondly, unlike the alkali metals, barium is very convenient to handle and experiment with. Thirdly, the ionization of barium is very interesting in view of the well-known barium anomaly in the solar spectrum. Though barium and sodium have almost equal ionization potentials, yet it is found that while barium is almost completely ionized in the sun, sodium is only slightly ionized. In fact, it is found that barium and rubidium, in spite of their great difference in ionization potential (about 1 V), are equally ionized in the sun. We shall presently see how our experimental results fully support the usual explanation given for this phenomenon, viz. the existence of weight factors and the metastable states of barium ion.

### THEORY

According to Darwin and Fowler's modification (1923) of the ionization formula, we have

$$\ln \frac{p_{\text{Ba}}}{p_{\text{Ba}}} \frac{p_e}{p_{\text{Ba}}} = -\frac{\chi_1}{kT} + \frac{5}{2} \ln T + \ln \frac{g_e (2\pi m_e)^{3/2} k^4}{h^3} - \ln b(T) + \ln b'(T), \quad (1)$$

where  $\chi_1$  denotes the energy required to ionize the unexcited atom (i.e. the ionization potential for the fundamental state),  $g_e$  the weight factor for the electron and is equal to 2, and  $b(T)$  and  $b'(T)$  are given by the relations

$$b(T) = g_1 + g_2 e^{-(\chi_1 - \chi_2)/kT} + \dots + g_n e^{-(\chi_1 - \chi_n)/kT} + \dots, \quad (2)$$

$$\text{and} \quad b'(T) = g_{i,1} + g_{i,2} e^{-(\chi_{i,1} - \chi_{i,2})/kT} + \dots + g_{i,n} e^{-(\chi_{i,1} - \chi_{i,n})/kT} + \dots \quad (3)$$

Here  $g_{i,n}$  denotes the weight factor and  $\chi_{i,n}$  the energy of the ionized atom in the  $n$ th quantum state.

Equation (1) can be written in the form

$$\begin{aligned} \log \frac{p_{\text{Ba}^+} p_e}{p_{\text{Ba}}} &= -\frac{U}{4.573T} + \frac{5}{2} \log T + \log \frac{(2\pi m_e)^{3/2} k^3}{h^3} + \log 2 + \log b'(T) - \log b(T) \\ &= -\frac{U}{4.573T} + \frac{5}{2} \log T - 6.479 + \log 2 + \log b'(T) - \log b(T), \end{aligned} \quad (4)$$

if the pressures are expressed in atmospheres, and the values of the other quantities are substituted.  $U$  is the energy of ionization of a gram-atom of barium vapour in calories and is equal to  $NeV_i/300J$ , where  $V_i$  is the ionization potential of barium equal to 5.19 V,  $N$  the Avogadro number. Thus  $U = 119.5$  kcal. For calculating  $b(T)$  and  $b'(T)$  we must know the energy states of barium and barium ion and their quantum weights. These are given by Bacher and Goudsmit (1932, pp. 70–77), and are taken from the works of Paschen-Götze, Fowler and Russell and Saunders. For barium the term values corresponding to the configurations  $6s^2$ ,  $6s5d$ ,  $6s6p$  are considered as the contribution of the higher terms becomes less and less and is negligible. Similarly for barium ion the normal level  $5p^66s^2S_{1/2}$ , the metastable levels  $5p^65d^2D_{3/2,1}$  and the levels corresponding to the configuration  $5p^66p$  have been considered and the higher terms neglected. The detailed calculation of  $b(T)$  and  $b'(T)$  is given later and the values obtained for different temperatures are given in table 1. From equation (4) it is evident that the effect of the weight factors is, so to say, to decrease the ionization potential of the atom. We shall call this reduced value the effective ionization potential and denote it by  $U_{\text{eff}}$ . It is evidently given by

$$U_{\text{eff}} = U - 4.573T\{\log 2 + \log b'(T) - \log b(T)\}, \quad (5)$$

where  $U$  is the true heat of ionization. For purposes of comparison the values of  $U_{\text{eff}}$  obtained experimentally and that obtained from formula (5) are both given in table 1.

#### APPARATUS

The demountable vacuum graphite furnace used in these experiments has been described in detail by M. N. Saha and A. N. Tandon (1936), and the internal arrangement employed here has been described by the author (Srivastava 1938) and is shown in figure 1. High temperature is produced in the graphite tube  $F$  which is heated by a current of the order of a thousand amperes from a low-tension transformer. This tube has a fine circular hole on one side, while on the other side there is a conical cavity  $C$  in which a

hollow conical plug  $P$  of graphite fits gastight. The auxiliary furnace  $A$  which contained barium at the bottom was fitted gastight with the help of screw and collar arrangement into the main furnace near one end as shown in the figure. This furnace was thus heated simply by conduction from the graphite furnace  $F$  and by using a tube of suitable length and wall thickness the desired temperature was obtained. Further the furnace is made thicker at the bottom where the barium powder is kept so that the temperature gradient in its neighbourhood is very small and the temperature of the solid is correctly given by the nickel-nichrome thermocouple  $T$  inserted in the wall.

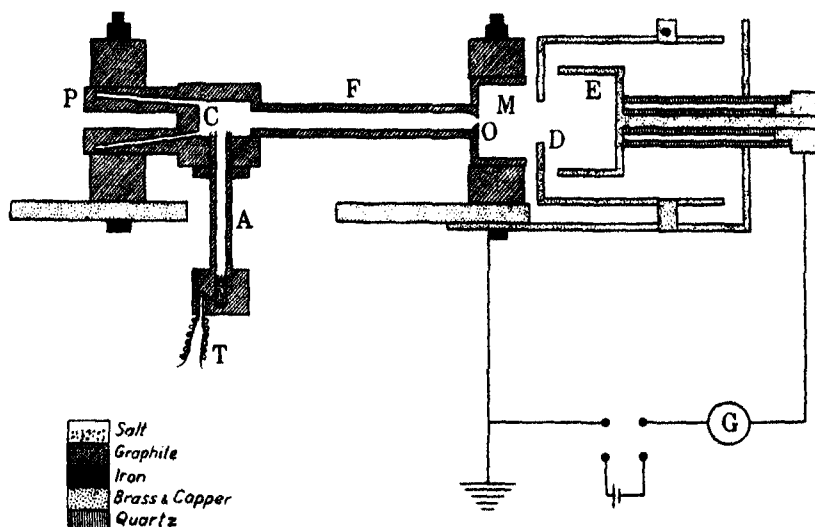


FIGURE 1

Barium vapour coming from  $A$  suffers dissociation inside  $F$  into barium ions and electrons according to equation (4) and the products of dissociation effuse out through the narrow orifice after which they traverse a magnetic field produced by two electromagnets  $M$  placed on either side. The magnetic field had no particular purpose to serve in this case. It only showed that the negative current almost wholly consists of electrons in this case while the positive particles are much heavier as is expected. The effusion beam is limited by a diaphragm  $D$  of radius  $r$  placed at a distance  $d$  from the effusion hole. Behind the diaphragm is a Faraday cylinder connected to a sensitive galvanometer and suitable positive or negative potentials were applied between the Faraday cylinder and diaphragm in order to collect the particles of the desired charge.

Under the conditions it can be shown that the galvanometer current  $i_g$  is given by the relation

$$i_g = \frac{epS}{\sqrt{(2m\pi kT)}} \frac{r^2}{r^2 + d^2},$$

where  $S$  is the area of the effusion hole,  $p$  and  $T$  denote the pressure and temperature of the ion inside the furnace. The equilibrium constant  $K$  is therefore given by the relation

$$K = \frac{p_{\text{Ba}} + p_e}{p_{\text{Ba}}} = \frac{2\pi kT}{e^2 S^2} \left( \frac{r^2 + d^2}{r^2} \right)^2 \frac{i_g^+ i_g^-}{p_{\text{Ba}}} \sqrt{(m_{\text{Ba}}, m_e)}.$$

If all the pressures are expressed in atmospheres, we have

$$K = \frac{p_{\text{Ba}} + p_e}{p_{\text{Ba}}} = \frac{2\pi kT}{e^2 S^2} \left( \frac{r^2 + d^2}{r^2} \right)^2 \frac{i_g^+ i_g^-}{p_{\text{Ba}}} \frac{\sqrt{(m_{\text{Ba}}, m_e)}}{(1.013 \times 10^6)^2}. \quad (6)$$

All the quantities occurring in this equation can be experimentally measured or are otherwise known, and hence  $K$  can be experimentally determined. This can be compared with the theoretical value given by the ionization formula (4).

There is some uncertainty regarding the quantity  $p_{\text{Ba}}$ , the pressure of atomic barium vapour in the furnace  $F$ . The vapour pressure of barium in the required range of temperatures has been measured by Rudberg and Lempert (1935) and is found to be given by the formula

$$\log_{10} p(\text{mm.}) = -\frac{8980}{T} + 6.99. \quad (7)$$

In the absence of any information to the contrary it is safe to assume that at the temperatures under consideration the vapour is almost entirely monatomic. This, however, gives the vapour pressure in the auxiliary furnace. Due to thermal transpiration the pressure in the main furnace will be somewhat different. As discussed by the author elsewhere (Srivastava 1939) this cannot be exactly determined. For our present purpose we shall assume the full Knudsen effect, i.e.  $p_1/p_2 = \sqrt{(T_1/T_2)}$ . There will be some uncertainty in the value of  $K$  due to this cause alone, but the corresponding effect on  $U_{\text{eff}}$  will be almost negligible.

#### EXPERIMENTAL PROCEDURE

First the graphite tube was thoroughly degassed by prolonged intermittent heating for several hours, after which the currents in the blank experiment diminish to a negligible value. This was particularly necessary in this case since the positive currents during the actual experiment are somewhat small. In order to ensure that the currents during the main experiment are



much greater than those in the blank experiment care was taken to first perform the blank experiment and note the currents for the different temperatures. Then without disturbing the rest of the arrangement the auxiliary tube was taken out, filled with barium and again fitted in and the currents again observed for different temperatures. In every case it was found that the currents during the experiment were much greater than those for the blank experiment. After the steady state had been attained the currents were measured at 2 V with different currents through the electromagnet and for purposes of calculation the negative current without magnetic field and the positive current with magnetic field were employed.

The temperature of the graphite furnace was measured by means of a Siemens' optical pyrometer and was correct to  $\pm 10^\circ$ . As the temperature of the furnace was not quite uniform, the mean temperature of the tube was determined and employed for the purpose of calculation. In view of these uncertainties the slight difference of temperature between the inside and outside of the graphite tube as well as the slight difference between the true temperature and the blackbody temperature of the graphite tube have been neglected.

The experiments were done with two different tubes. The barium used was supplied by Merck and the tube was freshly opened. The results obtained are recorded in table 1.

In the columns (11) and (12) the values of  $b(T)$  and  $b'(T)$  are recorded. These have been calculated from equations (2) and (3) by substituting the proper values. Thus for the normal atom the first few term values are  $(6s^2^1S_0)$  42029.4,  $(6s5d^3D_{1,2,3})$  32995.6, 32814.1, 32433.0,  $(6s5d^1D_2)$  30634.1,  $(6s6p^3P_{0,1,2})$  29763.3, 29392.8, 28514.8,  $(6s6p^1P_1)$  23969.2, ..., and the corresponding  $g$  values are 1, 3, 5, 7, 5, 1, 3, 5, 3, .... Hence  $b(T)$  is given by the relation

$$\begin{aligned} b(T) = & 1 + 3e^{-9034x/T} + 5e^{-9215x/T} + 7e^{-9596x/T} \\ & + 5e^{-11895x/T} + e^{-12266x/T} + 3e^{-12637x/T} \\ & + 5e^{-13515x/T} + 3e^{-18060x/T} + \dots, \end{aligned} \quad (8)$$

where  $x = hc/k$ . Similarly for barium ion the term values are  $(5p^66s^2S_{1/2})$  80655.5,  $(5p^65d^2D_{3/2,5/2})$  75781.4, 74980.3,  $(5p^66p^2P_{1/2,3/2})$  60393.5, 58702.5, ..., and the corresponding  $g$  values are 2, 4, 6, 2, 4, .... Hence  $b'(T)$  is given by the relation

$$b'(T) = 2 + 4e^{-4874x/T} + 6e^{-5675x/T} + 2e^{-20262x/T} + 4e^{-21953x/T} \dots \quad (9)$$

It is seen that the contribution of higher terms goes on decreasing and hence only a few terms need be considered. Only five terms in  $b(T)$  and three terms in  $b'(T)$  have been employed here in the calculations.

TABLE I

Radius of limiting diaphragm = 4.2 mm. Accelerating potential = 2 V. Current sensitivity of the galvanometer =  $1.54 \times 10^{-8}$  amp./mm.

| (1)<br>Mean<br>tempera-<br>ture of<br>graphite<br>furnace<br>in °C | (2)<br>Tempera-<br>ture of<br>auxiliary<br>furnace<br>in °K | (3)<br>Vapour<br>pressure of<br>barium in<br>auxiliary<br>furnace<br>in mm. | (4)<br>Diameter<br>of effusion<br>hole in<br>mm. | (5)<br>Distance<br>between<br>hole and<br>limiting dia-<br>phragm<br>in mm. | (6)<br>Current<br>through<br>electro-<br>magnet<br>in amp. | (7)<br>Negative<br>deflection<br>in mm. | (8)<br>Posi-<br>tive de-<br>flexion<br>in mm. | (9)<br>log K<br>in atmo-<br>spheres<br>per cm. <sup>2</sup> | (10)<br>$U_{\text{eff}}$<br>(exp.)<br>in kcal. | (11)<br>$b(T)$ | (12)<br>$b(T)$ | (13)<br>$U_{\text{eff}}$<br>(theor.)<br>from<br>equation<br>(5) | (14)<br>$U_{\text{eff}}$ (exp.)<br>- $U_{\text{eff}}$<br>(theor.) | (15)<br>log K<br>(theor.) |
|--|---|---|--|---|--|---|---|---|--|----------------|----------------|---|---|---------------------------|
| 1550   | 1003  | $1.081 \times 10^{-2}$  | 1.21   | 18  | 0  | $120 \times 30$                         | 38  | 12.119  | 113.0  | 1.010          | 2.157          | 114.2   | -1.2  | 13.973                    |
| 1500   | 1010  | $1.253 \times 10^{-2}$  | 1.21   | 18  | 7  | $100 \times 3$                          | 38  | 13.558  | 114.1  | 1.008          | 2.140          | 114.4   | -0.3  | 13.533                    |
| 1430   | 987   | $7.78 \times 10^{-3}$   | 1.21   | 18  | 7  | $176 \times 10$                         | 25  | 14.545  | 117.1  | 1.006          | 2.117          | 114.6   | +2.5  | 14.879                    |
| 1410   | 983   | $7.161 \times 10^{-3}$  | 1.21   | 18  | 7  | $42 \times 3$                           | 25  | 14.463  | 116.4  | 1.006          | 2.110          | 114.7   | +1.7  | 14.686                    |
| 1465   | 940   | $3.062 \times 10^{-3}$  | 1.21   | 18  | 7  | $152 \times 3$                          | 6   | 14.917  | 116.9  | 1.007          | 2.128          | 114.5   | +2.4  | 13.211                    |
| 1485   | 963   | $4.613 \times 10^{-3}$  | 1.22   | 19  | 0  | $140 \times 3$                          | 5   | 13.430  | 114.2  | 1.008          | 2.135          | 114.5   | -0.3  | 13.394                    |
| 1470   | 973   | $5.754 \times 10^{-3}$  | 1.22   | 19  | 7  | $122 \times 3$                          | 7   | 13.420  | 113.2  | 1.007          | 2.130          | 114.5   | -1.3  | 13.264                    |
| 1425   | 945   | $3.062 \times 10^{-3}$  | 1.22   | 19  | 7  | $15 \times 3$                           | 12  | 14.945  | 113.8  | 1.008          | 2.115          | 114.7   | -0.9  | 14.826                    |
| 1370   | 916   | $1.535 \times 10^{-3}$  | 1.22   | 19  | 7  | $235 \times 3$                          | 18  | 14.508  | 113.1  | 1.005          | 2.100          | 114.8   | -1.7  | 14.280                    |
| 1485   | 967   | $5.047 \times 10^{-3}$  | 1.22   | 19  | 7  | $155 \times 3$                          | 5   | 13.277  | 115.4  | 1.008          | 2.135          | 114.5   | +0.9  | 13.364                    |
|  |   |   |  |   | 7  | $21$                                    | 5   |   |  |                |                |   |   |                           |
|  |   |   |  |   | 7  | $220$                                   | 2   |   |  |                |                |   |   |                           |
|  |   |   |  |   | 7  | $4$                                     | 2   |   |  |                |                |   |   |                           |
|  |   |   |  |   | 7  | $205 \times 3$                          | 13  |   |  |                |                |   |   |                           |
|  |   |   |  |   | 7  | $10$                                    | 13  |   |  |                |                |   |   |                           |

## DISCUSSION OF RESULTS

It will be observed that the positive currents are much smaller than the negative currents. This is to be expected since the barium ion being  $2.5 \times 10^5$  times heavier than the electron, its rate of effusion will be about 500 times slower. The positive and negative currents will, however, not exactly follow this relation since their concentrations inside the furnace are not equal, for electrons are also given out by the graphite tube.

In view of the uncertainty in the determination of  $T$  by about 2 % as stated before, it is not safe to compare the values of  $K$  obtained experimentally, since a slight error in  $T$  produces a large error in  $K$  as  $\log K$  varies as  $1/T$ . It is, however, reasonable to compare the values of  $\log K$ , as errors in this quantity will occur to the same percentage as the experimental errors in  $T$ . A comparison of the values of  $\log K$  at different temperatures shows that in general the values of  $\log K$  at lower temperatures are smaller than those at higher temperatures as demanded by the ionization theory. For the purpose of detailed comparison with the theory we have calculated  $\log K$  theoretically for different temperatures and recorded the values in column (15). A comparison of columns (9) and (15) will show that the experimental and theoretical values of  $\log K$  agree well within the limits of experimental error. A more striking comparison is obtained by calculating a quantity  $U_{\text{eff}}$ , which we call the effective ionization energy, from the simple formula

$$\frac{U_{\text{eff}}}{4.573T} = \frac{5}{2} \log T - 6.479 - \log K, \quad (10)$$

using the values of  $\log K$  obtained above experimentally. These values are recorded in column (10). The values of  $U_{\text{eff}}$  calculated from the theoretical formula (5) are given in column (13) and the difference between the experimental and theoretical values are recorded in column (14). The figures in column (14) show that the agreement between theory and experiment is quite satisfactory, the departure being no greater than the errors of observation.

This method of comparison shows clearly that the effective ionization energy is not 119.5 kcal. corresponding to the ionization potential (5.19 V) of barium atom, but is less as required by the existence of the weight factors. The difference is also approximately equal to the amount given by the theory.  $U_{\text{eff}}$  on the whole appears to increase with decrease of temperature as required by equation (5), but the experimental evidence is, however, not quite conclusive. The expected change during the small range of temperatures of the experiment is only about 0.5 % and is so small that it is

more or less masked by the experimental errors which are greater than this amount. The contribution of higher levels and the metastable levels of barium ion at these temperatures is extremely small, amounting only to about 0.2 % in  $U_{\text{eff}}$ , and cannot therefore be demonstrated by these experiments. Our experiments, however, clearly show that at the temperature of the sun ( $6000^\circ$ )  $U_{\text{eff}}$  will be much less.

These experiments therefore verify the ionization formula completely within the limits of experimental error and also support the explanation usually given for the fact that barium is completely ionized in the sun but sodium is not, though the ionization potentials of both are nearly equal (barium = 5.19 V, sodium = 5.12 V). The weight factor terms for sodium cancel out but for barium they have a finite contribution and this brings down the effective ionization potential of barium at  $6000^\circ$  to 4.10 V nearly.

In conclusion I take this pleasant opportunity of expressing my sincere thanks and gratefulness to Professor M. N. Saha, D.Sc., F.R.S., for his valuable guidance throughout the work. Our thanks are also due to the Royal Society of London for giving a grant which enabled us to construct the furnace and buy its accessories.

#### SUMMARY

In this paper a new method has been described for experimentally studying the thermal ionization of gases. The apparatus used has already been described in detail by Saha and Tandon elsewhere. Thermal ionization of barium vapour has been investigated at various temperatures and the equilibrium constant and the effective energy of ionization have been calculated. The results obtained agree, within the limits of experimental error, with the theory of thermal ionization. The results also support the usual interpretation of the well-known barium anomaly in the solar spectrum, and yield for the effective ionization energy at  $1500^\circ\text{C}$  a value of 114.1 kcal., though the ionization potential of barium is 5.19 V corresponding to 119.5 kcal. The theoretical value for this quantity at  $1500^\circ\text{C}$  is 114.4 kcal. The agreement is therefore quite satisfactory.

#### REFERENCES

- Bacher, R. F. and Goudsmit, S. 1932 *Atomic energy states*, 1st ed. New York and London: McGraw-Hill Book Co.  
Becker, J. A. 1929 *Trans. Amer. Elect. Chem. Soc.* 55, 153.  
Darwin and Fowler 1923 *Phil. Mag.* 45, 1.  
Elgin, J. M. 1928 *Phys. Rev.* 31, 1127.

- Killian, T. J. 1926 *Phys. Rev.* **27**, 578.  
 Langmuir, I. and Kingdon, K. H. 1923 *Science*, **57**, 58.  
 — — 1925 *Proc. Roy. Soc. A*, **107**, 61.  
 Meyer, E. 1930 *Ann. Phys., Lpz.*, **4**, 357.  
 Milne, E. A. 1921 *Observatory*, **44**, 261.  
 Morgulis, N. 1934 *Z. Sowjet.* **5**, 221.  
 Nelson, H. 1931 *Physics*, **1**, 84.  
 Pannekoek, A. 1930 *Handbuch der Astrophysik*, **3** (1), 323.  
 Rudberg, E. and Lempert, J. 1935 *J. Chem. Phys.* **3**, 627.  
 Russell, H. N. 1922 *Astrophys. J.* **55**, 119.  
 Saha, M. N. 1920a *Phil. Mag.* **40**, 472.  
 — 1920b *Phil. Mag.* **40**, 809.  
 — 1921 *Proc. Roy. Soc. A*, **99**, 135.  
 Saha, Sur and Majumdar 1927 *Z. Phys.* **40**, 648.  
 Saha, M. N. and Tandon, A. N. 1936 *Proc. Nat. Acad. Sci. India*, **6**, 212.  
 — — 1937 *Proc. Nat. Inst. Sci. India*, **3**, 287.  
 Srivastava, B. N. 1938 *Proc. Nat. Inst. Sci. India*, **4**, 365.  
 — 1939 *Proc. Nat. Inst. Sci. India*, **5**, 313.  
 Tandon, A. N. 1937 *Ind. J. Phys.* **11**, 99.  
 — 1938 *Proc. Nat. Acad. Sci. India*, **7**, 102.

## On the thermal conductivity of gases by a relative method with an application to deuterium

BY W. G. KANNULUIK, D.Sc.

*Natural Philosophy Laboratory, University of Melbourne*

(Communicated by T. H. Laby, F.R.S.—Received 25 July 1939)

### INTRODUCTION

The present paper is an account of a simple relative method of obtaining the thermal conductivity of a gas or a gaseous mixture to within 1 % for the complete range of gas conductivities. This is followed by an application of the method to deuterium gas.

The principle of the apparatus to be described is similar to that upon which the so-called "conductivity meters" (e.g. the katharometer of G. A. Shakespeare, 1916–17) is based, but only in so far as both depend for their action on a transfer of heat from a heated wire through a surrounding gas. In the author's apparatus this transfer takes place by conduction only but

in the "conductivity meters" it takes place partly by conduction and partly by convection.

The term "conductivity meter", often applied to this and similar instruments, is misleading, for they do not and cannot measure the thermal conductivity of a gas or gaseous mixture. Calibrated empirically in terms of gaseous mixtures of known composition they are used industrially in the investigation of composition of other mixtures.

Generally these industrial meters employ two similar fine metal filaments of considerable resistance (often 10–20  $\Omega$ ) connected in series and placed in the adjacent arms of a Wheatstone bridge. They are mounted in some form of cell designed for working at a constant temperature and either wire can be surrounded by any selected gas or mixture.

If, while the wires are being heated by a fixed steady current, the composition of the gas surrounding one of the wires alters, then, in general, the balance of the bridge will be disturbed. The change in composition of the gas is related to the change in resistance of the wire. Various methods of using the bridge which may be rebalanced or left unbalanced are described by H. A. Daynes (1933, chap. iv).

The bridge method used with the industrial meters is excellent in principle for use with a relative method of determining the thermal conductivity, as it enables the same property of any two gases to be directly and simultaneously compared.

As already mentioned none of the existing types of industrial meter is suitable for obtaining the thermal conductivity. It would seem to be impossible to derive any simple relations connecting the change in resistance of one of the filaments with the change in the thermal conductivity of the gas surrounding it. The theory for fine filaments is complicated by the existence of troublesome and uncertain "end" corrections and also by the probable presence of convection in the cell itself. However, by the use of a pair of short thick wires instead of thin filaments the simple theory given below becomes applicable. As low-resistance wires have to be substituted for high resistance filaments it is no longer feasible to use a Wheatstone bridge. In the present work this is replaced by a simple form of the Kelvin double bridge.

### THEORY

The essential part of the theory for thick wires has already been given in several earlier papers (Kannuliik and Martin 1934) and will not be repeated here but merely the results given. It has been shown that for a wire of diameter  $2b$ , length  $2l$  and thermal conductivity  $\lambda$ , and which is mounted

axially in a tube of internal diameter  $2a$  and filled with a gas of thermal conductivity  $k$ , the following relations hold:

$$\left(\frac{1}{\beta l}\right)^2 \left(1 - \frac{\tanh \beta l}{\beta l}\right) = \frac{2\pi b^2 \lambda J (R - R_0)}{R_0^2 I^2 \alpha l}, \quad (1)$$

with

$$\beta^2 = \frac{2h}{b\lambda} - \frac{I^2 R_0 \alpha}{2\pi b^2 J \lambda l},$$

and

$$h = k/b \log_e a/b,$$

where  $R$  is the resistance of the wire heated by a steady current of  $I$  amp.;  $R_0$  is the true resistance of the wire at  $0^\circ \text{C}$ ;  $\alpha$  is the temperature coefficient of the resistance; and  $J$  is the electrical equivalent of heat.

(1) may be written in the form

$$\frac{c}{R - R_0} = \frac{\beta^3 l^3}{\beta l - \tanh \beta l},$$

where

$$c = \frac{R_0 I^2 \alpha l}{2\pi b^2 J \lambda}.$$

If  $\beta l < \frac{1}{2}\pi$ ,  $\tanh \beta l$  may be expanded as the well-known power series and we get

$$\begin{aligned} \frac{c}{R - R_0} &= \frac{\beta^3 l^3}{\beta l - (\beta l - \frac{1}{3}\beta^3 l^3 + \frac{1}{45}\beta^5 l^5 - \frac{1}{315}\beta^7 l^7 + \dots)} \\ &= 3[(1 + \frac{2}{5}\beta^2 l^2) - \beta^4 l^4/525] \quad (\text{nearly}). \end{aligned}$$

For values of  $\beta l > 1$  the error introduced in the right-hand side of the last relation by neglecting  $\beta^4 l^4/525$  is small, e.g. for  $\beta l = 1$  it is readily seen to be 1 in 300.

If this term be neglected, the last relation simplifies to

$$\frac{2k}{\lambda b^2 \log_e a/b} = \frac{R_0 I^2 \alpha}{2\pi b^2 J \lambda l} \left[ \frac{5R_0}{6(R - R_0)} + 1 \right] - \frac{5}{2l^2}. \quad (2)$$

It is evident from (2) that  $k$  is a linear function of  $1/(R - R_0)$  for a fixed value of the heating current  $I$ . Thus we may write

$$k = \frac{C}{R - R_0} + C', \quad (3)$$

where  $C$  and  $C'$  are constants, the values of which depend on the heating current  $I$  and the geometrical and electrical constants of the wire.

The existence of an appropriate linear relation of the form of (3) was first noticed by the author by plotting  $k$  against  $1/(R - R_0)$  using the data in

the paper by Kannuluik and Martin cited above. The platinum wire employed in that work was 10.6 cm. long and 1.5 mm. in diameter and the values of  $\beta l$  ranged from 3.4 for hydrogen down to 1.2 for air. Though the values of  $\beta l$  for which  $\tanh \beta l$  is convergent are exceeded,  $k$  still remained approximately a linear function of  $1/(R - R_0)$ . For example, if a straight line be drawn through the points  $(k, 1/(R - R_0))$  for hydrogen and for air respectively, the error made in using it to determine intermediate conductivities (corresponding to known values of  $1/(R - R_0)$ ) is approximately 1 %. Better approximations to (3) are obtained by using shorter and thicker wires. For a wire half as long (5.3 cm.) and of the same diameter the corresponding values of  $\beta l$  for hydrogen and air diminish to 1.7 and 0.6 respectively and any intermediate conductivity can be determined to within 0.5 % of its true value. For a relative method based on the use of (3) this accuracy is sufficient, but it should be noted that for all gases excluding only hydrogen and helium  $k$  is a linear function of  $1/(R - R_0)$  to a very much higher degree of accuracy and it is permissible to use longer wires.

The method of applying (3) to relative determinations of  $k$  consists in obtaining the specific constants  $C$  and  $C'$  experimentally. If it is desired to use (3) over the full range of gas conductivities, it is best to measure  $(R - R_0)$  for an assumed value of  $k$  for hydrogen for some convenient fixed value of the heating current. For the same current we can then measure another value of  $(R - R_0)$  for  $k = 0$  by the production of a high vacuum ( $< 10^{-5}$  mm. Hg) in the conductivity apparatus. The two equations so obtained suffice to determine  $C$  and  $C'$ . In this way we are really obtaining gas conductivities in terms of a single assumed value of  $k$ —that of hydrogen. The advantages of the method are its simplicity and the ease with which the requisite apparatus can be calibrated.

#### EXPERIMENT

In the practical applications of (3) it is preferable to use a bridge method rather than a potentiometer one to measure the resistance changes of the wire. The actual apparatus consisted of two similar nickel wires 5 cm. long and 1.5 mm. in diameter mounted in similar stainless steel tubes about 1.2 cm. in internal diameter. One of the two tubes was used as a reference tube, being left permanently filled with air, while the other was filled with the gas under investigation. As the resistance of the wires is a few thousandths of an ohm ( $0.0034 \Omega$ ), a Kelvin double bridge arrangement was used. The two tubes comprising the conductivity apparatus form the low resistance arms of the bridge which is shown schematically in figure 1.  $R$  and  $S$  are the two tubes containing the nickel wires ( $S$  being the reference (dummy) tube). The



bridge resistances  $\alpha$ ,  $\beta$ ;  $a$ ,  $b$  were each  $1\Omega$ . For sensitivity  $\alpha$ ,  $\beta$ ,  $a$ , and  $b$  should be equal and small as convenient. The shunt resistances  $r$  and  $\rho$  consisted each of a set of decade boxes  $10 \times 10$ ,  $10 \times 1$  and  $10 \times 0.1\Omega$ . The resistances  $\alpha$ ,  $\beta$ ,  $a$  and  $b$  were mounted in a single container so that the temperatures of all four should remain the same. The coils comprising them were of manganin and were annealed at  $140^\circ\text{C}$  for 24 hr. as recommended by O. Wolff. After this treatment these resistances remained extremely constant. As this bridge is designed only for measuring small changes in the

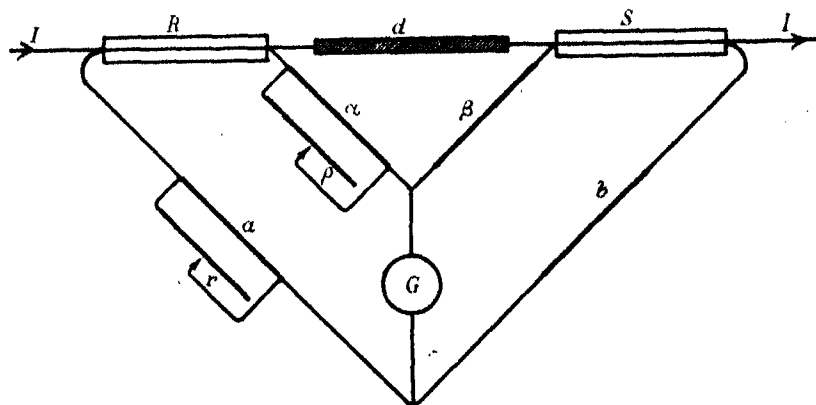


FIGURE 1

resistance of  $R$ , an exact adjustment of the coils to  $1\Omega$  is unnecessary. The measured resistances were

$$\begin{aligned}\alpha &= 0.999193\Omega; & \beta &= 1.00025\Omega; \\ a &= 0.996925\Omega; & b &= 0.995673\Omega.\end{aligned}$$

To balance the bridge the shunt resistances  $r$  and  $\rho$  were alternately adjusted with the link  $d$  in (i.e. as a double bridge) and then with  $d$  out (i.e. as a Wheatstone bridge) until the bridge remained balanced with  $d$  in or out. In practice it was found more convenient to carry out the above procedure by a simple double adjustment of  $r$  and  $\rho$  by which the necessity of removing and replacing  $d$  was avoided. The shunt resistances  $r$  and  $\rho$  consisted of suitable sets of decade boxes.

Periodic checks on the stability of the Wheatstone bridge balance are obtained by removing  $d$ .

For the balanced bridge the following relations hold:

$$\frac{R}{S} = \frac{\alpha}{\beta} \cdot \frac{\rho}{\rho + \alpha} = \frac{a}{b} \cdot \frac{r}{r + a}. \quad (4)$$

In using this bridge it is convenient to keep the reference tube  $S$  permanently filled with a standard gas (air) and then to balance the bridge with the other tube filled first with the standard gas and then with the gas under investigation, both balances being obtained for the same fixed value of the heating current. From the above bridge relations it is manifest that the difference in resistance of  $R$  for the two gases is

$$\delta R = \frac{a}{b} \left( \frac{r}{r+a} - \frac{r'}{r'+a} \right) S, \quad (5)$$

where  $r$  and  $r'$  are the values of shunt resistance on  $a$  for the two gases.

The bridge determines  $R$  quickly and accurately for any gas and so if  $R$  and  $S$  are known by independent determinations one can calculate at once the resistance of  $R$  for the given gas.

The bridge as described was sensitive enough to detect with certainty a change in resistance of 1 part in  $2 \times 10^5$  in either  $R$  or  $S$ . In terms of the conductivity the equivalent sensitivity is 1 in 1200 for  $k = 6 \times 10^{-5}$  and 1 in 2000 for  $k = 40 \times 10^{-5}$ .

From the theory of the Kelvin bridge the best resistance  $G$  for the galvanometer can be shown to be equal to  $\frac{\alpha\beta}{\alpha+\beta} + \frac{(R+a)(S+b)}{a+b+R+S}$  (Glazebrook 1922). For the bridge used here the best value of  $G$  is  $1 \Omega$ . The resistance of the galvanometer actually used was  $20 \Omega$ . Since the galvanometer deflexion is proportional to  $\sqrt{G}$  and to the current  $I$ , the substitution of a galvanometer of resistance  $1 \Omega$  for the one actually used would increase the sensitivity by a factor of 4.5 for the same current  $I$ .

#### DESCRIPTION OF THE APPARATUS

The choice of the material and dimensions of the wires for the conductivity apparatus centres round the necessity for keeping  $\beta l$  (see (1)) small and employing wire as thick as possible. The use of a thick wire greatly minimizes the magnitude of the temperature discontinuity in the gas at the surface of the wire. The most suitable metals for thick wires are platinum and nickel. In the present experiments "Vactite" nickel wire which was carefully annealed was used and proved quite satisfactory. The wires fitted into the tubes  $R$  and  $S$  were 5 cm. long and 1.5 mm. in diameter.

The details of the conductivity apparatus will be gathered from figure 2. The tubes  $R$  and  $S$  (see also figure 1) are of thin-walled stainless steel each being approximately 5 cm. long and 1.2 cm. in internal diameter.  $R$  and  $S$  are closed at both ends by copper caps, but to insulate the wire from the

tube the upper cap in each case is electrically insulated from the tube by means of the copper-glass joints  $g$ .

The two copper side tubes  $t$  and  $t'$  connect to the pumping and filling system. The low resistance link  $d$  (see figure 1) consists principally of two short lengths of copper rod  $C$  and  $C'$  and the removable copper block  $B$ . A low melting-point alloy of Wood's metal is used to solder  $B$  to the rods  $C$  and  $C'$ .

The whole apparatus was placed in a dewar flask filled with a mixture of ice and distilled water, which mixture was stirred vertically by means of a motor driven plunger.

A simpler but quite practical form of apparatus can be constructed by substituting glass tubes for the stainless steel ones used in this work. These tubes may be closed by copper caps either joined directly to the glass or else waxed on with picein or other suitable wax.

#### EXPERIMENTAL PROCEDURE

To calibrate the apparatus it is necessary to determine  $B$  and  $S$  for the fixed value of the heating current  $I$ , and also  $R_0$  the true resistance of  $R$  at  $0^\circ\text{C}$ . The fixed value of the heating current used throughout these experiments was 9.490 amp. and was obtained by the adjustment to an exact reading of 32 on a Weston millivoltmeter connected to a 15 amp. low-resistance shunt. The measurements of the resistances were obtained by means of a Wolff "thermokraftfrei" low-resistance potentiometer of the three dial pattern.

The values of  $R$  and  $S$  for  $I = 9.490$  amp. were

$$R = 0.00354396\Omega, \quad S = 0.00363795\Omega.$$

The value of  $R_0$  was

$$R_0 = 0.00341896\Omega.$$

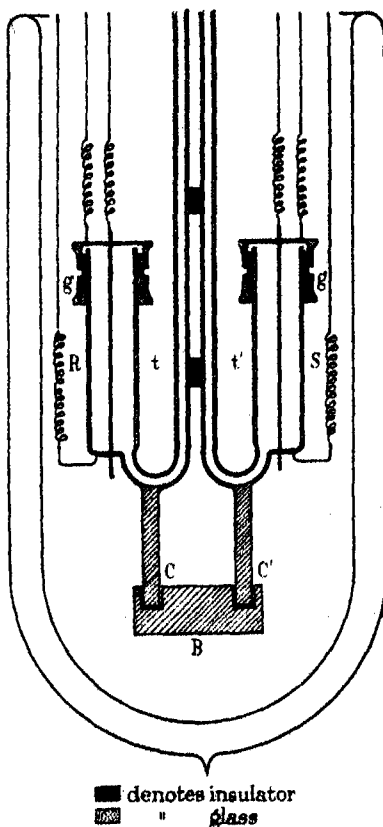


FIGURE 2

Both tubes were filled with air at atmospheric pressure. It was found that the conductivity of air is extremely constant from atmospheric pressure downwards over a wide range of pressures in the present apparatus. Further, no difference could be detected in the conductivity of dried and undried samples of air. The mean temperature of the air for  $I = 9.490$  amp. is  $5.6^\circ\text{C}$ . Assuming that  $k = 5.76 \times 10^{-5}$  c.g.s. at  $0^\circ\text{C}$  (Kannuliik and Martin 1934), we find that at  $5.6^\circ\text{C}$

$$k = 5.86 \times 10^{-5},$$

if the temperature coefficient of  $k$  is 0.003. (The temperature coefficients used in this paper are those given by Laby and Nelson 1929.)

As already indicated the constants  $C$  and  $C'$  in the formula

$$k = \frac{C}{R - R_0} + C' \quad (3)$$

are calculated by measuring  $(R - R_0)$  for hydrogen ( $k = 41.3 \times 10^{-5}$  at  $0^\circ\text{C}$ ) (Kannuliik and Martin 1934) and for  $k = 0$  by the production of a high vacuum in  $R$ . A residual pressure of less than  $10^{-5}$  mm. Hg was obtained by means of a charcoal tube immersed in liquid air. At this pressure the total transfer of heat from the wire by conduction and by radiation is negligibly small. The tube  $R$  was filled with pure hydrogen by diffusing cylinder hydrogen through a heated palladium tube into the evacuated apparatus. In effect the apparatus is calibrated for the entire range of gas conductivities in terms of the assumed value of  $k$  for hydrogen. For the heating current  $I = 9.490$  amp. the mean temperature of the gas is  $2.9^\circ\text{C}$  and the value of  $k$  given above for  $0^\circ\text{C}$  must be increased to  $41.7 \times 10^{-5}$ . The temperature coefficient of the resistance of the nickel wire for a short range  $0$ – $15^\circ\text{C}$  is 0.0033. The mean temperature of the wire can be calculated. The mean temperature of the gas is one-half the mean temperature of the wire. The method described here gives correctly the ratio of the conductivity of any gas to that of hydrogen. The corresponding absolute value of the conductivity will depend on the assumed value of the conductivity of hydrogen.

When the tube  $R$  was first filled with air and then with pure hydrogen and the bridge balanced for each gas in turn, the values of the shunt resistances were

$$\left. \begin{array}{l} r = 33.40 \, \Omega \\ \rho = 37.6 \, \Omega \end{array} \right\} \text{ for air; } \quad \left. \begin{array}{l} r' = 20.50 \, \Omega \\ \rho' = 21.8 \, \Omega \end{array} \right\} \text{ for hydrogen.}$$

The balance of the double bridge is not sensitive to changes in  $\rho$  of an ohm or two so that an approximate balance of the bridge with the link out is all that is necessary. No change in the balance of the bridge was observed when

the presence of the hydrogen was reduced by successive stages from 60 to 30 cm. of Hg.

The corresponding bridge data for  $k = 0$  (with the high vacuum in  $R$ ) is as follows:

$$\left. \begin{array}{l} r = 33.44 \, \Omega \\ \rho = 37.60 \, \Omega \end{array} \right\} \text{for air; } \left. \begin{array}{l} r' = 44.50 \, \Omega \\ \rho' = 52.8 \, \Omega \end{array} \right\} \text{for } k = 0.$$

From the above data the corresponding values of  $R$  are computed by means of (5). The values of  $(R - R_0)$  are obtained immediately by adding  $R$  algebraically to 0.00012500, which is the value of  $(R - R_0)$  for air.

The corresponding values of  $1/(R - R_0)$  for  $k = 0$  and  $41.7 \times 10^{-5}$  are respectively 6639 and 16278. Substituting these in (3), we get finally

$$C = 4.3257 \times 10^{-8}, \quad C' = -28.72 \times 10^{-5}.$$

An immediate check is obtained by calculating  $k$  for air using the value of  $R - R_0 = 0.00012500$ . The corresponding value of  $1/(R - R_0) = 8000$ . Substituting this in (3) and making use of the calculated values of  $C$  and  $C'$ , we find that

$$k = 5.88_8 \times 10^{-5} \text{ at } 5.6^\circ \text{ C.}$$

This is to be compared with the value

$$k = 5.86 \times 10^{-5} \text{ at } 5.6^\circ \text{ C,}$$

based on the absolute determination of  $k = 5.76 \times 10^{-5}$  at  $0^\circ \text{ C}$  obtained by the author and Martin.

The agreement is satisfactory and is as close as can be expected in a relative method of this kind.

Experiments were also carried out on pure carbon dioxide, the gas being prepared by Lord Rayleigh's method of inverting a  $\text{CO}_2$  cylinder. The corresponding values of  $r$  and  $r'$  when  $R$  was filled first with air and then with carbon dioxide gas were 33.10 and 36.30  $\Omega$  respectively. The range of pressures over which  $r'$  was exactly constant was 18 to 0.9 cm. Hg. The corresponding value of  $1/(R - R_0)$  is 7455. This gives a value of  $k = 3.51 \times 10^{-5}$  at  $6^\circ \text{ C}$ . The reduced value for  $0^\circ \text{ C}$  is  $k = 3.45 \times 10^{-5}$  which is in satisfactory agreement with the value of  $3.43 \times 10^{-5}$  obtained by the author and Martin (Kannuluik and Martin 1934).

#### EXPERIMENTS ON DEUTERIUM

In a letter to *Nature* (1936) the author published a value of  $k = 33 \times 10^{-5}$  at  $0^\circ \text{ C}$  for deuterium and this was obtained by the absolute method. This value is probably too high, being 7 % in excess of the recent determination of

Archer (1938). The gas used was impure, as the method used for preparing it was unsuitable. A new determination was therefore made—the gas being obtained in this instance from some 99.95 % heavy water.

The method of preparing the gas by the reduction of heavy water vapour over heated magnesium, though slow, is simple and good. This method was also used by Archer.

In figure 3 a pyrex tube ( $\frac{1}{2}$  in. diameter) is closed at one end and has a single right-angled bend. A small quantity of heavy water is placed in the closed end of the tube in a tiny glass container. The magnesium ribbon packed into the horizontal part of the tube is surrounded by a furnace winding on an alundum tube which slips on over the glass tube. To dry the

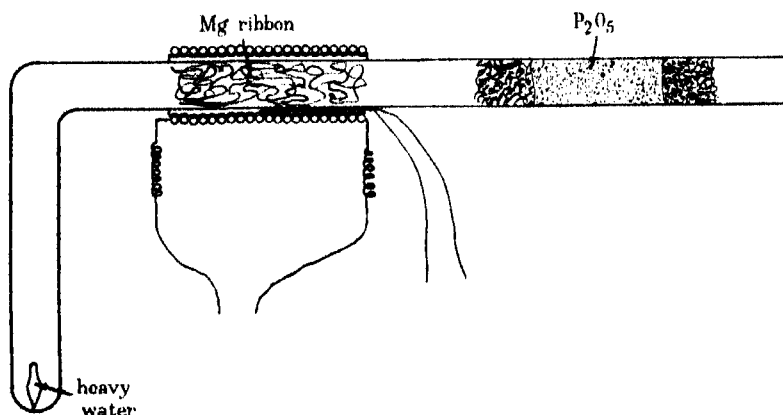


FIGURE 3

gas a quantity of phosphorus pentoxide between plugs of glass wool is placed between the magnesium and the apparatus to which the tube is directly connected. A preliminary outgassing of the magnesium is necessary with the closed end of the tube immersed in liquid air.

To effect this the apparatus was evacuated whilst the magnesium was heated to 600° C, the temperature being measured roughly by a thermojunction between the glass and alundum tubes. When the vacuum, as judged by a discharge tube, was equal to that normally obtainable in the apparatus, the pump was cut off and the liquid air removed. A slow but steady reduction of the water vapour then took place. The maximum pressure of deuterium thus obtained was a little over 30 cm. of Hg. As the effect of the temperature "sprung" in this apparatus is not very marked, it is possible to make a satisfactory determination of  $k$  without the use of a mercury lift to compress the gas still further.

The effectiveness of the reaction with magnesium was tested in quite a simple way. The above experiment was repeated using ordinary distilled water instead of heavy water and the conductivity of the hydrogen so obtained was compared with that obtained by diffusing cylinder hydrogen through a heated palladium tube. At corresponding pressures the conductivities were found to be exactly the same for both methods. It is reasonable, therefore, to assume that both deuterium and hydrogen are obtained pure by the reaction with magnesium. Though hydrogen as an impurity might have been present in the magnesium to start with, this must have been completely removed by the preliminary degassing of the metal.

The following data were obtained for deuterium:

| Pressure<br>( $p$ ) | Bridge balance |                | $R \Omega$ | $(R - R_0)$<br>$\Omega$ | $\frac{1}{R - R_0}$<br>$\Omega^{-1}$ | $k \times 10^5$ |
|---------------------|----------------|----------------|------------|-------------------------|--------------------------------------|-----------------|
|                     | $r' \Omega$    | $\rho' \Omega$ |            |                         |                                      |                 |
| 33.58 cm. Hg        | 22.05          | 23.50          | 0.00005190 | 0.00007310              | 13,680                               | 30.45           |
| 22.19               | 22.07          | 23.5           | 5176       | 7324                    | 13,654                               | 30.34           |
| 11.25               | 22.10          | 23.5           | 5156       | 7344                    | 13,617                               | 30.18           |
| 3.31                | 22.15          | 23.50          | 5121       | 7379                    | 13,552                               | 29.90           |
| 1.06                | 22.33          | 23.7           | 5001       | 7499                    | 13,335                               | 28.96           |
| 0.60                | 22.53          | 24.0           | 4869       | 7631                    | 13,105                               | 27.96           |

With air:  $r = 33.37 \Omega$ ;  $\rho = 37.60 \Omega$ .

From the above data the conductivity can be obtained by plotting  $p/k$  against  $p$  (Kannuluik and Martin 1934). A straight line is obtained and the cotangent of the angle between this line and the pressure axis is equal to  $k$ . This procedure leads to the value

$$k = 30.45 \times 10^{-5} \text{ at } 3.2^\circ \text{C.}$$

Assuming a temperature coefficient of  $k$  equal to 0.003, we get

$$k_0 = 30.25 \times 10^{-5} \text{ at } 0^\circ \text{C.}$$

This is appreciably lower than the recent value obtained by Archer:

$$k_0 = 30.8 \times 10^{-5} \text{ at } 0^\circ \text{C.}$$

It is, however, preferable to compare the ratios of the thermal conductivity of hydrogen to that of deuterium. The value of the thermal conductivity of hydrogen at  $0^\circ \text{C}$  used in this work is  $41.3 \times 10^{-5}$ . This is the absolute value obtained by Kannuluik and Martin. The author adopted this value first because he regards it as the most reliable existing value and second because the method used is a derivative of the absolute method. The corresponding value obtained for hydrogen by Archer (1938) is  $41.82 \times 10^{-5}$ . The required

ratios are 1.365 (author's data) and 1.358 (Archer's data). The agreement between the two values to within  $\frac{1}{2}\%$  is quite satisfactory.

Figure 4 is a graph of the relation  $k = \frac{C}{R - R_0} + C'$  and is obtained by drawing a straight line through the two extreme points (hydrogen and a high vacuum). The check points for air and  $\text{CO}_2$  fall upon this line, but the line fixes the point for deuterium.

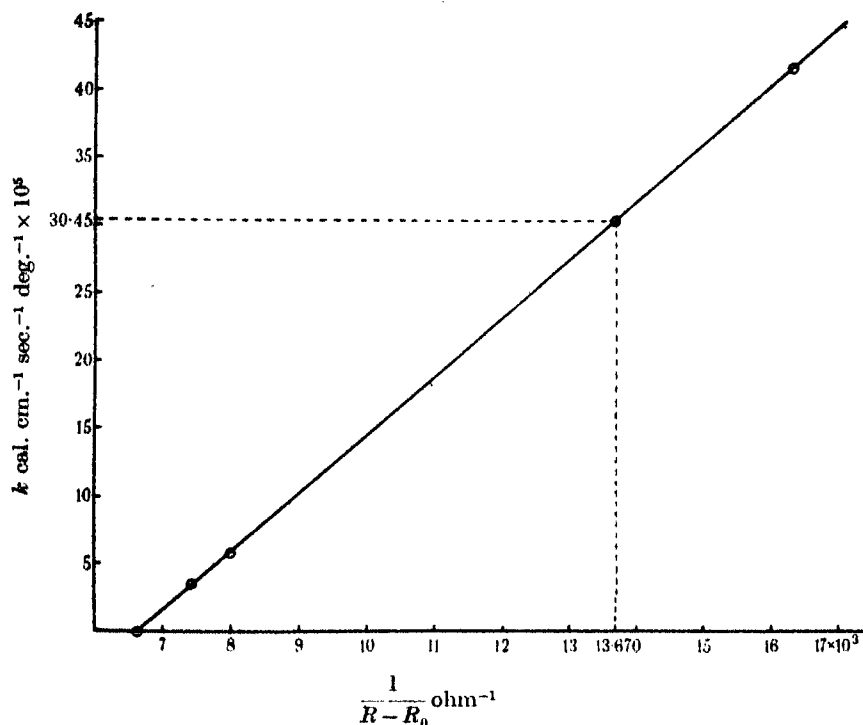


FIGURE 4. Graph of the relation  $k = \frac{C}{R - R_0} + C'$ .

#### CONCLUDING REMARKS

A comparison of the apparatus used in this investigation with the industrial meters of the katharometer type is not without interest. On a number of counts the former would appear to be superior. The following advantages may be claimed for it:

(1) A simple approximate theory has been derived for it, but for the industrial meters employing thin filaments no simple theory can be given.



In the latter the use of thin filaments introduces troublesome and uncertain end corrections.

(2) By the present method relative conductivities are measured, and the method is available for determining the composition of binary mixtures of gases if desired. The industrial meters are limited to gas analysis only.

(3) The transfer of heat from the wires by convection is inappreciable in the author's apparatus but in the industrial meters it is considerable. To minimize convection the hot wires must be vertical and their mean temperature rise kept as low as possible. This rise of  $6^{\circ}$  to  $12^{\circ}$  in the present experiments is much less than that which normally obtains in the industrial meters.

Preliminary experiments along the lines of those described in this paper were carried out during 1937 by the author and Miss Mary Shepherd, M.Sc. of the Kodak Research Laboratory, Melbourne. The apparatus was, however, reconstructed for the present work, metal tubes being substituted for the glass ones used in the earlier work.

It is a pleasure for the author to acknowledge the continued interest of Professor T. H. Laby, F.R.S. in the work and to thank him for much helpful advice and criticism. The work was made possible by a research grant by the University of Melbourne.

#### SUMMARY

The paper describes a "hot wire" method of determining the thermal conductivity of any gas relative to that of hydrogen. The use of short, thick wires enables a simple, approximate theory to be given.

The apparatus employed is of the double tube kind and consists of a pair of similar metal tubes each containing a thick nickel wire. These two wires are used as the nearly equal ratio arms of a Kelvin double bridge.

The method is applied to measure the thermal conductivity of deuterium gas. At  $0^{\circ}\text{C}$  the ratio of the conductivity of hydrogen to that of deuterium is found to be equal to 1.365.

#### REFERENCES

- Archer, C. T. 1938 *Proc. Roy. Soc. A*, **165**, 474.  
Daynes, H. A. 1933 *Gas analysis*. Camb. Univ. Press.  
Glazebrook, R. 1922 *Dict. Appl. Phys.* **2**, 720.  
Kannuluik, W. G. 1936 *Nature, Lond.*, **137**, 741.  
Kannuluik, W. G. and Martin, L. H. 1934 *Proc. Roy. Soc. A*, **144**, 496.  
Laby, T. H. and Nelson, E. A. 1929 *International critical tables*, **5**, 213.  
Shakespeare, G. A. 1916-17 *Tech. Rep. Adv. Comm. Aero.* **2**, 579.
-

# Properties of superconducting colloids and emulsions

By D. SHOENBERG

*Royal Society Mond Laboratory, Cambridge, Exhibition of 1851*

*Senior Student*

*(Communicated by J. D. Cockcroft, F.R.S.—Received 30 October 1939)*

## INTRODUCTION

The characteristic feature of a large superconductor is that it cannot be penetrated appreciably by an external magnetic field lower than the critical field; in other words, the permeability of a superconductor is practically zero and its susceptibility strongly diamagnetic. It is reasonable, however, to expect that actually there is a slight penetration of the field, and theoretical predictions as to the details of this penetration have been made by F. and H. London (1935). Judging from the accuracy with which the permeability has been found zero for large specimens, the depth of penetration cannot be greater than  $10^{-3}$  cm., and so to obtain appreciable penetration effects very small specimens must be used. One method of experiment which has been used successfully is that of resistance measurements on thin wires (Pontius 1937) and thin films (Shalnikov 1938; Appleyard and Misener 1938; Appleyard, Bristow and London 1939; Appleyard, Bristow, London and Misener 1939) of superconductors; with this method, however, all that can be learnt is the size dependence of critical field, and thermodynamic arguments (which, as will be seen, involve certain assumptions) are necessary to infer anything about the details of the field penetration. A much more direct method is to measure susceptibilities of small specimens, since if there is any appreciable penetration it must reduce the diamagnetic susceptibility characteristic of the superconductor in bulk; thus, from the size dependence of the susceptibility, information can be obtained about the penetration law. Moreover, by measuring magnetic moments, the critical field can be deduced as well as the susceptibility, so that results of the same nature as from resistance measurements can also be obtained.

Experimentally, such a method of investigation is difficult because the magnetic moment is proportional to the volume and so becomes exceedingly small if the linear dimensions are reduced sufficiently to produce penetration effects. One way of overcoming this difficulty is to measure the total magnetic moment of a colloid or emulsion, where the small

volume of each particle is compensated by the large number of particles present, and this has been the method adopted in the present investigation. Its main disadvantage is that the size of the individual particles cannot be either varied or accurately determined in any simple way, but, owing to the fortunate circumstance that the penetration depth turns out to vary considerably with temperature (Appleyard *et al.* 1939; Shoenberg 1939), this disadvantage is not so serious as it appears. Thus change of temperature with a preparation of given particle size has the same effect (through the change of penetration depth) as a change of particle size at given temperature, so that much of the information needed can be obtained with any given particle size once the temperature dependence of the penetration depth is known.

All the measurements to be described were made with mercury preparations: (a) because of the relative ease of obtaining mercury colloids and emulsions of high mercury content, (b) because the individual particles are probably spherical and thus amenable to theoretical treatment, and (c) to allow of comparison with the work of Appleyard *et al.* (1938, 1939) on thin films of mercury.

#### EXPERIMENTAL DETAILS

##### (a) *Magnetic*

A ballistic induction method was used to measure the magnetic moments of the specimens. Two exactly similar coils connected in series with each other and a ballistic galvanometer were fixed one above the other symmetrically about the centre of a large solenoid, the connexions being arranged so that the coils were in opposition, having practically no mutual inductance with the solenoid. By means of a Bowden cable arrangement the specimen, which was suspended in a Dewar vessel containing liquid helium, could be jerked rapidly from the centre of one coil to the centre of the other, thus producing a deflexion of the ballistic galvanometer proportional to the magnetic moment of the specimen. The advantage of having two coils rather than only one is that slight fluctuations of the current in the solenoid have practically no effect on the zero of the galvanometer. The solenoid used for most of the experiments gave nearly uniform fields up to 900 G over the distance of travel of the specimen (about 3 cm.), but for some special measurements up to 10,000 G a water-cooled solenoid constructed by Mr Laurmann was used, and this had a rather smaller region of uniformity.

The whole arrangement was calibrated by measuring the deflexions produced by a small superconducting lead sphere, and the sensitivity proved to be 77.5 cm. deflexion per c.g.s. unit of magnetization. The

main source of error was due to slight motions of the coil system in the solenoid which gave rise to small stray deflexions; these, together with zero drift and occasional slight induction effects from other fields in the laboratory, limited the accuracy of readings to between  $\frac{1}{10}$  mm. at fields below 100 G and 1 or 2 mm. at 900 G. The inaccuracies of measurements in the high-field solenoid were greater, but, by stiffening of the apparatus against jerks due to the working of the Bowden cable and careful balancing of the two coils, the errors were reduced to less than 5 mm. at the highest fields.

Two corrections have to be considered before the magnetic moment per unit volume of a single sphere in one of the preparations for given field can be deduced from the observed deflexion. First, if the specimen occupies an appreciable length in the measuring coil, different parts of the specimen move from different positions of the coil, while the sensitivity mentioned above refers to motion only from the centre of one coil to the centre of the other. This correction was determined experimentally by studying how the deflexion in the calibration experiment varied with the initial position and distance of travel of the lead sphere. After applying this correction (which amounted to 20 % for a specimen length of 32 mm., and 3 % for a length of 13 mm., that most often used) the observed magnetic moments were reduced to unit volume of mercury, the volume of mercury present being deduced from a chemical analysis in each case.

The second correction is that due to the mutual interactions of the colloid particles on each other: this has the effect that the field acting on each sphere is not exactly the uniform field of the solenoid. Fortunately, the volume concentration of mercury in all the preparations was not high enough (usually less than 5 %) to make this correction serious. The magnitude of the correction can be estimated\* by assuming that the field acting on each sphere is decreased by the Lorentz term  $4\pi I/3$  corresponding to a random distribution, where  $I$  is the negative magnetic moment per unit volume of the whole specimen; actually the correction never amounted to more than 1 %, and, moreover, is compensated partly by the "demagnetizing" effect of the whole specimen if this has not a long thin shape, so that it was not allowed for in reducing the observed data. Although these considerations show that the *average* field acting on a particle is just the external field, they do not allow for the possibility of large clusters of particles much closer together than the average separation; the occurrence of such clusters may be responsible for some of the details of the magnetization curves to be described, but it is very difficult to make any theory of such effects.

\* I have to thank Dr Casimir for pointing this out to me.

*(b) The specimens*

The main requirements which had to be satisfied by the specimens were a sufficient mercury content to give measurable magnetic moments, and uniformity of particle size. In the case of colloids these two requirements are difficult to reconcile, since any method of separating out one particular size involves diminution of concentration, and the colloids used were in fact not very uniform; it will be seen below to what extent this is important. Reasonable uniformity of size was obtained, however, in the case of an emulsion of mercury in chalk by a sufficiently thorough mechanical disintegration.

The specimens used are described in table 1.\* It should be emphasized that the particle sizes given are only order of magnitude estimates and may be wrong by a factor of 2 or more. Attempts to estimate  $\tau$  by the speed of settling of solutions (or in the case of Hg C4, of a mixture shaken with water) of the preparations gave rather larger sizes (between 5 and 10 times larger) than indicated in the table, probably due to clustering of the particles into larger aggregates. The specimens as used for measurement were contained in open quartz or pyrex tubes. In the case of Hg A the susceptibilities were so small that the paramagnetism of pyrex produced a serious correction, and the temperature variation of this correction was not properly allowed for in the earlier measurements (Shoenberg 1939); the use of quartz, which is practically non-magnetic, removed the necessity for this correction and thus improved the accuracy of the results.

## THE EXPERIMENTAL RESULTS

To avoid confusion of the diagrams, the results for each specimen are given first only for increasing fields, and the hysteresis features of the curves are discussed separately.

Hg A. In this case the particle size is so small that the penetration of the field is almost complete, and the diamagnetic moment per unit volume very small ( $< 1\%$  of the value for a large sphere). Figure 1† shows the magnetization curves up to 900 G at various temperatures and figure 2 the curves less accurately measured up to 9,000 G for a few temperatures.

\* Some measurements were made with other preparations, but these will not be described since they were less uniform as regards size than those in table 1, and gave no new information.

† In all the magnetization curves (figures 1, 2, 4, 5, 7 and 8) the ordinates have been left as galvanometer deflexions. The reduction to absolute values of magnetization per unit volume is made only in the values of the initial slope  $\chi$  (figures 3, 6 and 11).

TABLE 1. DESCRIPTION OF SPECIMENS.

| Name of specimen | Description   | Supplied by              | Order of magnitude of radius of particles $r$  | Weight percentage of mercury  | Remarks on uniformity   |
|------------------|---|--------------------------|--|---|---|
| Hg A             | A colloid in albumen prepared by reducing a mercurous nitrate solution in hydrolysed albumen with hydrazine hydrate and drying the precipitate after washing with water | British Colloids Ltd.    | From a study of polarization of scattered light* $r$ was estimated as $5 \times 10^{-6}$ cm.   | 78.1 %  | Judging by the settling of a solution in caustic soda, a wide range of sizes present  |
| Hg B             | A colloid in gelatine prepared by reducing a jelly of mercurous nitrate in gelatine with hydrazine hydrate solution, washing the jelly, drying and powdering            | Do.                      | Direct microscopic examination of a solution in water showed $r \sim 10^{-6}$ cm. Counts in a cell gave $r \sim 5 \times 10^{-6}$ cm.          | Not very uniform: two analyses of different samples gave 38 and 49.5 %; mean 44 % | Under the microscope many particles much smaller than average size could be seen  |
| Hg C1            | Commercial "mercury in chalk" used for medicinal purposes. Prepared by grinding a mixture of chalk in mercury under an edge-roller mill                                 | Boots Pure Drug Co. Ltd. | Microscopic examination showed that most of the particles had $r \sim 10^{-4}$ cm. The presence of the chalk confused the observations however | 33 %  | As will be seen from the results of the magnetic measurements these products are successively more uniform, but this could not be detected directly |
| Hg C2            | The commercial product Hg C1 was passed once through a disintegrator  | Do.                      |  | No analysis made but probably about 32 %  |   |
| Hg C3            | The product Hg C2 was passed 3 times through the disintegrator  | Do.                      |  | 30.3 %  |   |
| Hg C4            | The product Hg C3 was passed 10 times through the disintegrator   | Do.                      |  | 24.9 %  |   |

\* I have to thank Mr R. S. Krishnan for carrying out this measurement.

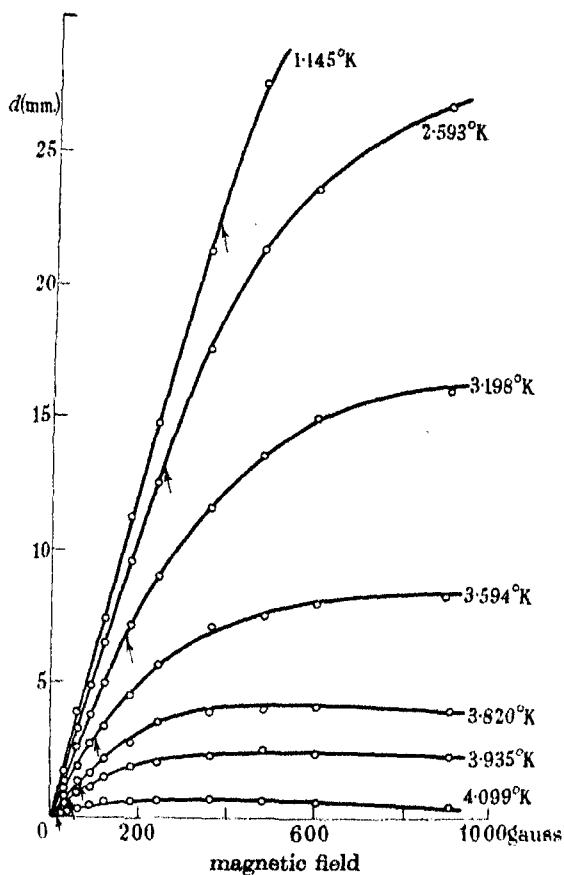


FIGURE 1. Magnetization curves of Hg A.  $d$  is the galvanometer deflection in mm. The arrows indicate the values of  $H_c$  for bulk mercury at the various temperatures.

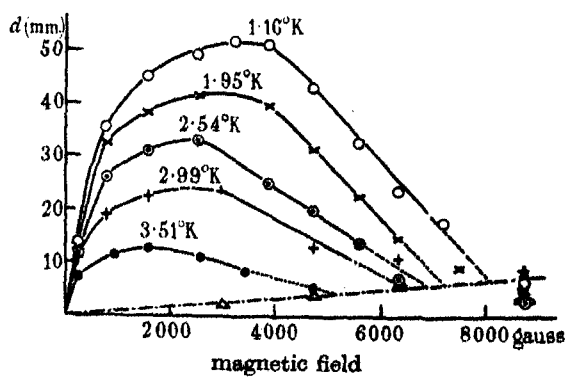


FIGURE 2. Magnetization curves of Hg A at high fields.

In figure 2 the dot-dash line represents the deflexions obtained when the specimen was absent, due to jerking of the apparatus by the Bowden cable; the magnetizations should be measured from this line, and the fields  $h$  at which the magnetization disappears are given by the intersections of the curves with it. Figure 3 shows the temperature dependence of the initial slopes  $\chi$  per unit volume of the magnetization curves (from figure 1) as compared with  $\chi_0 = 3/8\pi$ , the value for a large sphere, and also the temperature dependence of  $h/H_c$  obtained from figure 2, where  $H_c$  is the critical field of bulk mercury. It should be noticed that owing to lack of particle size uniformity,  $\chi/\chi_0$  and  $h/H_c$  do not refer to the same size of particle, since  $\chi$  evidently refers to the average slope over *all* the particle

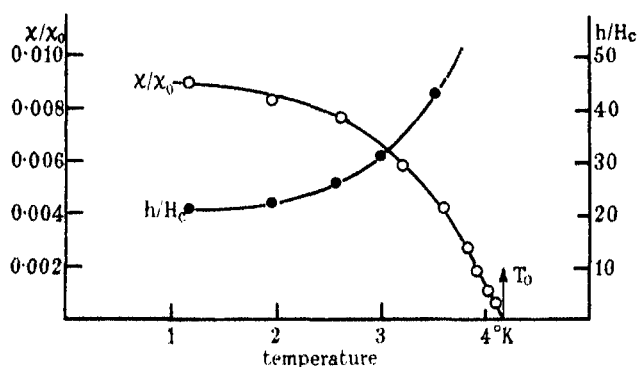


FIGURE 3. Temperature variation of  $\chi/\chi_0$  and  $h/H_c$  for Hg A.

sizes in the specimen, while  $h$  refers to the size with the highest critical field, which we shall see is the smallest size.

Hg B. The results with this preparation have already been published (Shoenberg 1939), and since similar results are described in detail below for the more uniform product Hg C4, the experimental curves will not be reproduced here. Some of the quantitative data obtained from Hg B will, however, be introduced in the discussion (see figure 11).

Hg C 1, 2, 3 and 4. In figure 4 are reproduced the magnetization curves of Hg C 1, 2, 3 and 4 at one particular temperature ( $4.00^\circ$  K) in order to show how the mechanical disintegration has improved the size uniformity. Since, as has been mentioned in the introduction, reduction of particle size (when it is comparable with the penetration depth) should decrease the diamagnetism, it is evident that the reduction of initial slope with increased mechanical treatment represents removal of the larger particles present in the original Hg C1. It will be seen that the end-point of all the curves is



approximately the same, and, since this corresponds to the smallest size present, this means that the mechanical treatment does not appreciably reduce the minimum size. From the sharpness of the descent of the curve (representing the transition from super to normal conductivity) for Hg C4 as compared with the others, it may be concluded that it is very nearly

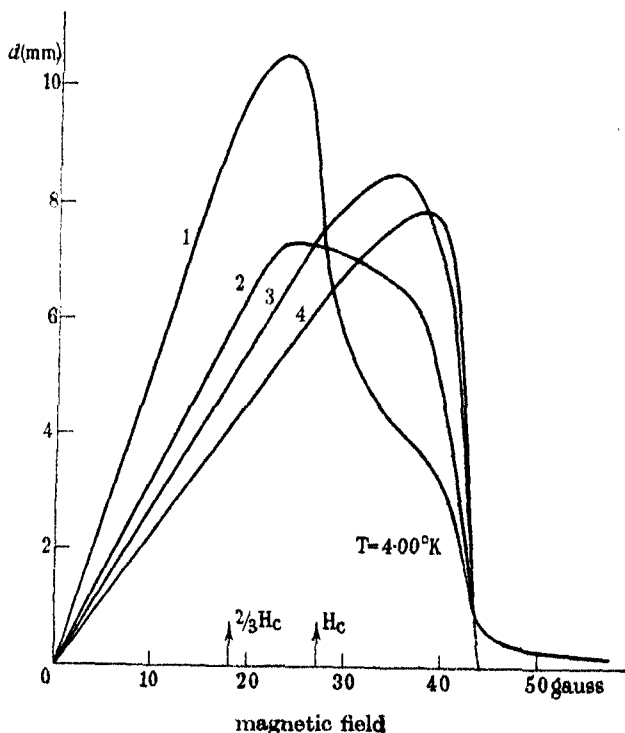


FIGURE 4. Comparison of magnetization curves of Hg C1 to 4 at 4° K. The deflexions  $d$  for Hg C1 to 3 have been reduced to refer to the same mass of mercury as in Hg C4.

uniform, i.e. nearly all the particles have the smallest size. Finally, it should be pointed out that the slight "tail" common to all the magnetization curves is probably due to the presence of a small volume percentage (not much changed by the mechanical treatment) of extremely small particles, i.e. smaller than what has been loosely called the "smallest" size above.

In figure 5 are reproduced a few of the measured magnetization curves for Hg C4 at different temperatures (some of the quantitative data for the other Hg C products will be used in the discussion, but the shapes of the individual magnetization curves are of no special interest since they

are evidently conditioned by the size distributions). Figure 6 gives the curves of  $\chi/\chi_0$  and  $h/H_c$  against temperature for Hg C4, deduced from the magnetization curves.\*

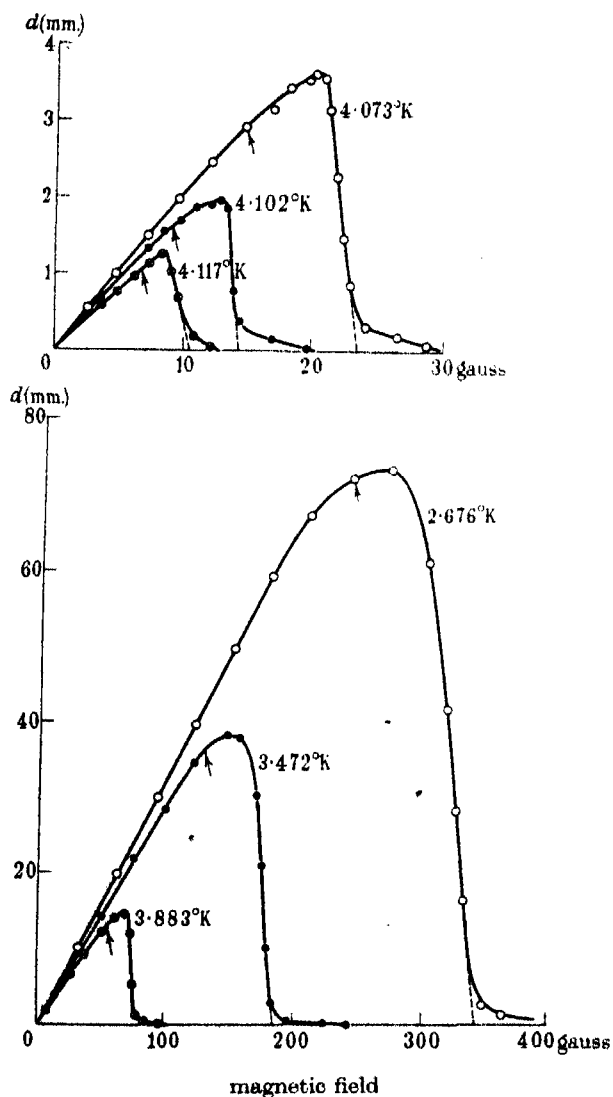


FIGURE 5. Magnetization curves of Hg C4. The arrows have the same meaning as in figure 1.

\* The values of  $h$  were obtained by extrapolating the rapid part of the descent of the curves to meet the field axis, i.e. disregarding the "tails".

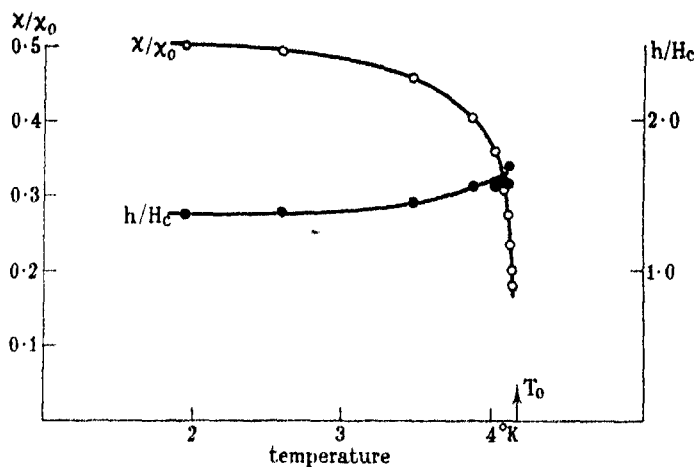
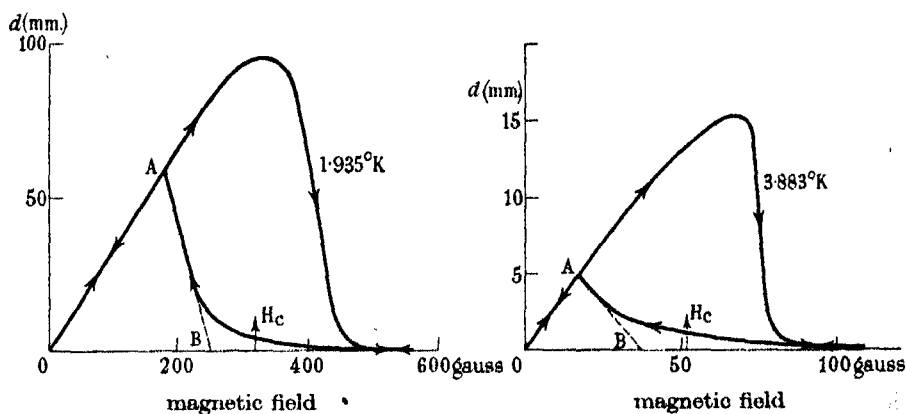
FIGURE 6. Temperature variation of  $\chi/\chi_0$  and  $h/H_c$  for Hg C4.

FIGURE 7. Hysteresis loops of Hg C4 for decrease of field from above critical field.

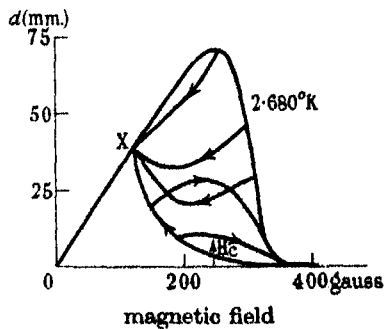


FIGURE 8. Details of hysteresis loops of Hg C4 for various cycles.

### HYSTERESIS FEATURES

The magnetization curves described so far have been for increasing fields only, and I shall now describe how far these curves are reversible when the field is decreased.

For Hg A there was practically no hysteresis when the field was reduced from the high field at which the magnetization disappeared or from any other field value. For Hg B and C, however, the return curve always lay below the increasing field curve; some typical hysteresis curves for Hg C4 are shown in figures 7 and 8. For Hg B the hysteresis becomes less marked at higher temperatures,\* while for Hg C4 (and the other Hg C specimens) the reverse occurs. In each case the "tail" is retraced without hysteresis. All these apparently conflicting results can be reconciled by the simple hypothesis that the hysteresis is marked for a particular range of ratios of the size  $r$  to the penetration depth  $\lambda$ , while for much smaller or much larger ratios there is no hysteresis. As was mentioned in the introduction, and will be elaborated later, the penetration depth increases with increasing temperature, and  $r$  for Hg B is smaller than for Hg C (see table 1), so it may be supposed that increase of temperature brings  $r/\lambda$  for Hg B *out* of the range in which hysteresis is marked by increasing  $\lambda$ , while it brings  $r/\lambda$  for Hg C *into* this range from the side of large  $r/\lambda$ . On this hypothesis, moreover, the absence of hysteresis in the "tails" and for Hg A is explained as due to the small values of  $r/\lambda$  for the particles responsible for the tails.

The general appearance of the hysteresis (the fact that there is no appreciable frozen-in moment and that the return curve is always diamagnetic) distinguishes it definitely from the sort of hysteresis found in impure superconductors. In order to see whether it resembles at all the hysteresis due to shape in a pure superconductor (Shoenberg 1937) I investigated at one particular temperature (2.68° K) how the magnetization varied when the field was decreased and increased from a variety of values. The results of this experiment are shown in figure 8, and are quite different from the corresponding effects due to shape, in as far as the curves inside the main hysteresis loop are not even roughly parallel to the initial rise of the increasing field curve. An interpretation consistent with figure 8 is that the hysteresis is due to a kind of "supercooling" in the sense that a particle does not become superconducting until the field is reduced some way below the critical value†. On this view it appears that the not quite sharp descent

\* In the sense that the area under the decreasing field curve becomes more nearly equal to that under the increasing field curve.

† [Footnote added in proof, February 1940. A marked supercooling effect of this kind has recently been found in superconducting aluminium (Shoenberg 1940).]

of the main magnetization curve is partly due to the slight lack of size uniformity, and that at each point of the descent some of the particles (the smaller ones) are still superconducting, while the larger ones are in the normal phase. On reducing the field from such a point the moment of the superconducting particles decreases linearly (notice that the beginning of each return curve points to the origin in figure 8), while the normal particles are "supercooled" (i.e. remain normal below their critical fields). With further decrease of field more and more particles become superconducting, thus eventually outweighing the decrease of moment of those that are already superconducting and causing an *increase* of the total diamagnetism. Eventually at  $X$  all the particles have become superconducting, and the original magnetization curve is retraced. Thus the field at  $X$  (or  $A$  in figure 7) should be that at which the *largest* particles present return to the superconducting phases, and this is consistent with the fact that *all* the return curves meet there.

This interpretation, which assumes that the "degree" of supercooling is very size sensitive, is put forward only tentatively, and can be confirmed only by working with still more uniform specimens, but since the hysteresis phenomena may prove to be of theoretical importance, some of the relevant data have been collected in table 2.\* The field  $h_1$  is that at which hysteresis

TABLE 2. SUMMARY OF HYSTERESIS DATA.  $h_1$ ,  $h_2$ ,  $h$  AND  $H_c$  IN GAUSS

| Specimen | $T^\circ \text{K}$ | $h_1$ | $h_2$      | $h$ | $H_c$ |
|----------|--------------------|-------|------------|-----|-------|
| Hg C1    | 1.98               | 220   | 300        | 440 | 322   |
|          | 4.060              | 10    | 18         | 28  | 17    |
| Hg C2    | 1.96               | 210   | 280        | 449 | 324   |
|          | 4.003              | 11    | 30         | 45  | 28    |
| Hg C3    | 1.94               | 195   | 280        | 455 | 326   |
|          | 3.88               | 20    | 45         | 80  | 51    |
|          | 4.103              | 3.5   | Indefinite | 14  | 9.3   |
| Hg C4    | 1.94               | 180   | 260        | 449 | 326   |
|          | 2.68               | 124   | 180        | 346 | 245   |
|          | 3.88               | 19    | 40         | 79  | 51    |
|          | 4.073              | 6.1   | Indefinite | 24  | 15    |

ceases (e.g. corresponding to  $A$  in figure 7), and is quite definite for Hg C4 but less so for the other Hg C specimens, and very vague for Hg B, on account of a rounding of the return curve where it approaches the increasing field curve; when this rounding occurs,  $h_1$  is obtained by extrapolation of the straight part of the return curve. The field  $h_2$  is that obtained

\* The data for Hg B is omitted as it is too rough to be of any use (partly because the hysteresis measurements on Hg B were made with a more primitive technique).

by extrapolating backwards the rising part of the return curve to meet the field axis (e.g. corresponding to  $B$  in figure 7); it is much less definite than  $h_1$  especially at higher temperatures. For comparison the critical field  $h$  of the specimen, and the bulk critical field  $H_c$ , are also included for each temperature.

#### DISCUSSION OF THE RESULTS

##### *Evidence that the results are due to smallness of size*

It is important to be sure that the differences between the results described and the properties of large spheres are genuinely due to the small size of the particles in the specimens, rather than to some secondary cause. There are several indications that this is so.

(1) It can be seen from figure 7 that no appreciable frozen-in moments, typical of impure superconductors, are left in our preparations when the field is reduced from above the critical value.

(2) In the case of several of the preparations, the mercury was extracted in bulk form by dissolving away the dispersing medium, and this mercury was found to behave just like pure mercury.

(3) The transition temperatures of all the preparations are very close to that of pure mercury in bulk ( $4.17^\circ\text{K}$ ). The slight differences that occur (e.g.  $4.15^\circ\text{K}$  for Hg C 4 as deduced from its  $h$ - $T$  curve) can, perhaps, be ascribed to the effect of mechanical strains.

(4) It will be shown (p. 68) that the results for Hg A, B and C are all consistent with each other in spite of the different dispersing media, so that it is very unlikely that the results are due to some contamination effect by the dispersing medium.

Since, moreover, the work of Appleyard *et al.* (1939) suggests that the penetration depth varies from  $10^{-5}$  to  $10^{-4}$  cm. over the temperature range of these experiments, it is reasonable to expect that the preparations are of particle sizes small enough to show size effects. It will therefore be assumed that the differences between these results and those for a large sphere are entirely due to the small size of the spheres in the preparations.

##### *The shape of the magnetization curves*

In all cases the initial part of the magnetization curve is a straight line, and this must mean that at low fields the penetration of field into a small sphere is the same at all fields, or, in other words, that the penetration depth is independent of field strength (this is assumed implicitly in the Londons' theory).

The rest of the magnetization curve will evidently be seriously affected by lack of size uniformity, and here the experiments on the series of successively more uniform preparations Hg C1 to 4 are very useful in indicating what is the shape of the magnetization curve for an ideally uniform specimen, i.e. for a single small sphere. On the basis of figure 4 it is a fairly safe conclusion that this "ideal" curve for a small sphere is as sketched in figure 9a (the return curve as inferred provisionally from the considerations of the observed hysteresis—see p. 59, is also shown, and for comparison, the curve for a large sphere—figure 9b). Whether the transition is quite discontinuous, as shown, or spread over a small range of fields, is not quite certain, since (judging by the rounding of the

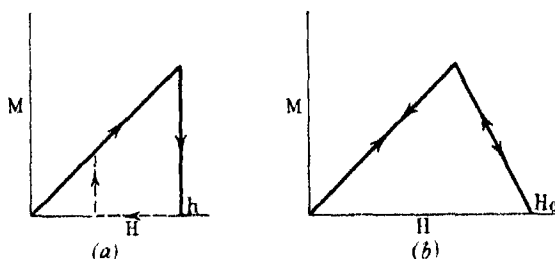


FIGURE 9. (a) Idealized magnetization curve of a very small sphere. (b) Magnetization curve of a large sphere. The scales of  $M$  (magnetization) and  $H$  (field) are arbitrary, and not the same in (a) and (b).

tops of the magnetization curves, which decreases with increasing uniformity) Hg C4 is not yet ideally uniform, and so one cannot distinguish a genuine spread-out transition region from a spread due to size distribution.

On the view that figure 9a gives the shape of the magnetization curve of a sufficiently small sphere,\* the large transition region of Hg A (figure 2) is to be ascribed entirely to lack of size uniformity, i.e. to the superposition of a large number of curves of the type of figure 9a with different slopes and end-points, corresponding to the different particle sizes present. The spread of size required for this interpretation would be over a range of something like a factor of 10 in radius, and this is not at all improbable.

The fact deduced from Hg C4 that the magnetization curve of a very small superconductor drops almost discontinuously at the critical field, instead of dropping linearly over a range from  $2/3$  of the critical field as for

\* It has been shown on p. 59, however, that the hysteresis disappears when the sphere is small enough; if the sphere is so small that  $r \ll \lambda$ , these remarks apply only to the increasing field curve of figure 9a.

a large sphere (Shoenberg 1936), is an entirely new feature, and can be interpreted very simply as due to an appreciable penetration of the field. Thus for a large sphere the  $2/3$  factor arises merely because the sphere has zero permeability, thus increasing the local field at the equator of the sphere to  $3/2$  of the applied field value, but if the permeability is appreciably different from zero due to penetration, as it is for Hg C4 ( $\chi/\chi_0 \leq 0.5$ ), there will no longer be such a large difference between the highest field at the surface of the sphere and the applied field.

To make a rough estimate it can be assumed that even when there is penetration, the sphere is homogeneously magnetized (though actually of course the diamagnetic magnetization increases from the surface inwards). The field at the equator of the sphere is then  $(1 + 4\pi\chi/3)$  times the applied field, where  $\chi$  is the average diamagnetic moment per unit applied field per unit volume. This factor can be written as  $1 + \frac{1}{2}\chi/\chi_0$ , where  $\chi_0 = 3/8\pi$ , and consequently the field at the equator reaches the critical value for an applied field  $h/(1 + \frac{1}{2}\chi/\chi_0)$  if  $h$  is the critical field.

According to this calculation (which probably gives too low a field for the commencement of the transition) the transition for Hg C4 should commence at  $0.8h$  for the lowest temperature and at something like  $0.9h$  for the highest temperature used. Overlooking the rounding at the top of the experimental curves (probably due to a few larger particles), these rough estimates are supported by the experiments. There is indeed a sharpening of the transition as the temperature rises,\* but the existence of a slight spread of particle sizes makes it difficult to be certain that this sharpening would occur for an ideally uniform preparation; thus it may be mentioned that the sharpening of the transition at  $4.07^\circ \text{K}$ , as compared with  $1.93^\circ \text{K}$ , was much more pronounced for the less uniform Hg C3 than for Hg C4.

This explanation of why the shapes of the magnetization curves change with reduction of size is only rough when the size is still comparable with the penetration depth as in Hg C4, and a detailed theory requires an understanding of the transition mechanism for this case. When the size is much smaller (as in Hg A), however, it is evident without any calculation that the transition of a sphere must be quite sharp, as in figure 9a, since if the field penetrates the sphere almost completely, it cannot be appreciably distorted by the superconductivity of the sphere, and all parts of the sphere are very nearly equivalent.

\* Except very close to the transition temperature, where the transition is again more spread out. This is probably due to the main descent of the curve becoming confused with the "tail", which is the more important the higher the temperature.



*The initial slopes*

As can be seen from figure 6, and even more strikingly from figure 3, the initial slope  $\chi$  per unit volume of the magnetization curve of a small sphere is less than for a large sphere, and decreases with increase of temperature, in contrast to that of a large sphere which is independent of temperature. The fact that  $\chi < \chi_0$  can be immediately interpreted as due to appreciable penetration of the field, and, describing the penetration by a characteristic length  $\lambda$ , the "penetration depth", it is evident that  $\chi/\chi_0$  for a sphere of radius  $r$  can depend only on the ratio  $r/\lambda$ . Since  $\chi/\chi_0$  varies with temperature for given  $r$ , it can be concluded that the penetration depth is itself temperature dependent, and evidently  $\lambda$  increases with  $T$  (as deduced also by Appleyard *et al.* (1939) from the temperature dependence of  $h/H_c$  for thin mercury films). To deduce how  $\lambda$  varies with  $T$  from the experiments, one must first find out something about the dependence of  $\chi/\chi_0$  on  $r/\lambda$ . This can be done if the law of penetration of field into a superconductor is known; thus for the only penetration law so far proposed, namely,

$$\nabla^2 H = H/\lambda^2, \quad (1)$$

put forward by F. and H. London (1935), F. London (1936) has calculated the size dependence of the magnetic moment per unit volume of a small sphere. In the present notation, his result can be expressed as

$$\frac{\chi}{\chi_0} = 1 - \frac{3\lambda}{r} \coth \frac{r}{\lambda} + \frac{3\lambda^2}{r^2}, \quad (2)$$

which for  $r \ll \lambda$  reduces to 
$$\frac{\chi}{\chi_0} = \frac{1}{15} \frac{r^2}{\lambda^2}. \quad (3)$$

Fortunately, the result  $\chi/\chi_0 \propto r^2/\lambda^2$  for  $r \ll \lambda$  can be shown to be more general than the penetration law (1), so that, apart from the numerical value of the proportionality factor, equation (3) can be used without assuming any particular penetration law. Since the formal proof of this for a sphere is rather lengthy, the argument will be given only for the simpler, but essentially similar, one-dimensional case of a plate of thickness  $2r$  in a longitudinal field. If  $r$  is much smaller than the penetration depth, the field  $H$  inside the plate is only slightly less than the field  $H_0$  at the surface, so the difference  $H_0 - H$  can be expanded in powers of  $x$ , the distance from the centre of the plate. Since the curve of  $H$  against  $x$  must be symmetrical about  $x = 0$  and have no kink there, the first term in the expansion, apart from a normalizing constant term, must be proportional to  $x^2$ , and to be

dimensionally correct, the constant of proportionality must itself be proportional to  $\lambda$ , where  $\lambda$  is a length characteristic of the phenomenon, i.e. the penetration depth, which will be assumed to be independent of  $r$ . Thus

$$H_0 - H = \alpha H_0 (r^2 - x^2) / \lambda^2, \quad (4)$$

where  $\alpha$  is some numerical constant. It should be noticed that the definition of  $\lambda$  is arbitrary to the extent of a numerical factor, and can be made precise only from a knowledge of the actual penetration law or by assigning some numerical value to  $\alpha$  and using (4) as a definition (with the Londons' definition of  $\lambda$  by equation (1), for instance,  $\alpha = \frac{1}{2}$ ). From (4) it follows at once that the diamagnetic moment per unit volume per unit field is

$$\chi = \frac{1}{8\pi H_0 r} \int_{-r}^r (H_0 - H) dx = \frac{\alpha}{6\pi} \frac{r^2}{\lambda^2}.$$

Therefore the result for  $r \ll \lambda$ ,

$$\frac{\chi}{\chi_0} \propto \frac{r^2}{\lambda^2}, \quad (5)$$

is independent of any particular penetration law provided only that the characteristic length of the penetration is not size dependent (this is of course implied in the Londons' penetration law (1), since it is in the form of a differential equation, and does not depend on the position of the boundary of the superconductor).

Judging by the smallness of the  $\chi/\chi_0$  values for Hg A, the particle size is well in the region where (5) applies, and consequently the temperature variation of  $\chi/\chi_0$  (figure 3) gives immediately that of  $1/\lambda^2$ .\* Figure 10 shows the temperature dependence of  $\lambda/\lambda_0$  ( $\lambda_0$  is the penetration depth at 1° K, where  $\lambda$  is practically independent of temperature) obtained in this way. Since  $\chi/\chi_0$  is proportional to  $T_0 - T$  close to the transition temperature  $T_0$ ,  $\lambda$  becomes infinite at  $T_0$  as  $(T_0 - T)^{-\frac{1}{2}}$ . The curve for the temperature dependence of  $\lambda$  may be compared with that of Appleyard *et al.* (1939) and the agreement is reasonably satisfactory except that the curve in figure 10 rises rather more rapidly near  $T_0$ . This discrepancy cannot be explained by the presence of a small volume of larger particles with  $r > \lambda$  in Hg A, since this would mean that the true curve should rise even more rapidly than in figure 10. Since the curve involves only square

\* It should be noticed that the lack of particle size uniformity in Hg A is irrelevant here, provided that there is not an appreciable volume percentage of particles with  $r \geq \lambda$  present. Also (5) is probably valid for any shape, and so it is immaterial whether the particles in Hg A are spherical or not.

roots of the experimental data, the discrepancy is probably to be ascribed to the experimental errors in the experiments of Appleyard *et al.*, especially since the method of reduction of their data tends to exaggerate such errors. Assuming that the discrepancy is not significant, the agreement of figure 10 with the thin film results is a confirmation of the correctness of (5) and so of the assumption that the penetration depth is independent of size.

Knowing  $\lambda$  as a function of  $T$  the curve of  $\chi/\chi_0$  against  $T$  for the nearly uniform product Hg C4 can be interpreted as a curve of  $\chi/\chi_0$  against  $\lambda/r$ , thus testing the validity of equation (2) which directly involves the validity of the Londons' penetration law (1). In figure 11 is shown the

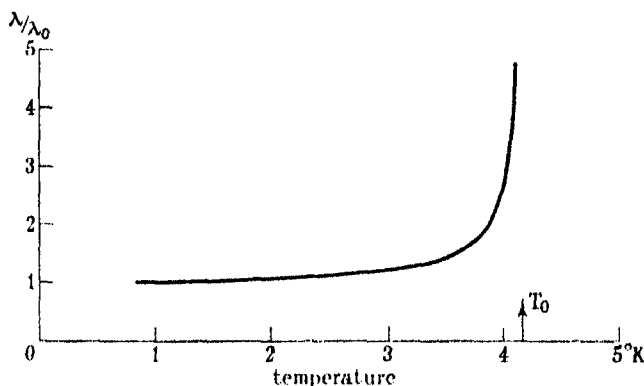


FIGURE 10. Temperature variation of the penetration depth.

experimental curve of  $\chi/\chi_0$  against  $\lambda/r$  obtained in this way from figures 6 and 10, together with the curve of equation (2) corresponding to the Londons' theory. Although the scale of abscissae of the experimental curve is arbitrary, it is evident that it cannot be adjusted to fit the Londons' theory; actually a scale has been chosen which corresponds reasonably to Appleyard's estimate of the absolute value of  $\lambda_0$ , and which allows the experimental curve to go over into an  $r^2/\lambda^2$  law for not too high values of  $\lambda/r$ .

There is good evidence that the discrepancy between the curves of figure 11 is not due to lack of size uniformity. First, it was found that if equation (2) was averaged over various size distributions involving very considerable spread of size, the shape of the resulting curve of  $\bar{\chi}/\chi_0$  against  $\lambda/\bar{r}$  differed only very slightly (over the range of values of  $\lambda/r$  in figure 11) from that shown in figure 11 (although of course the scale of  $\lambda/\bar{r}$  was changed). Secondly, it turns out that the results for the various preparations, of very different size uniformities, can all be fitted reasonably

well on the same experimental curve of figure 11 by merely adjusting the scale of  $\lambda/r$  for each case. Thus drastic change of uniformity (as between Hg B and Hg C1 to C4) has very little effect on the shape of the experimental curve.

It can be seen also that the discrepancy cannot be due to any reasonable systematic error in the absolute values of  $\chi/\chi_0$ , such as might be due to incorrect estimation of the metallic mercury present in the preparations

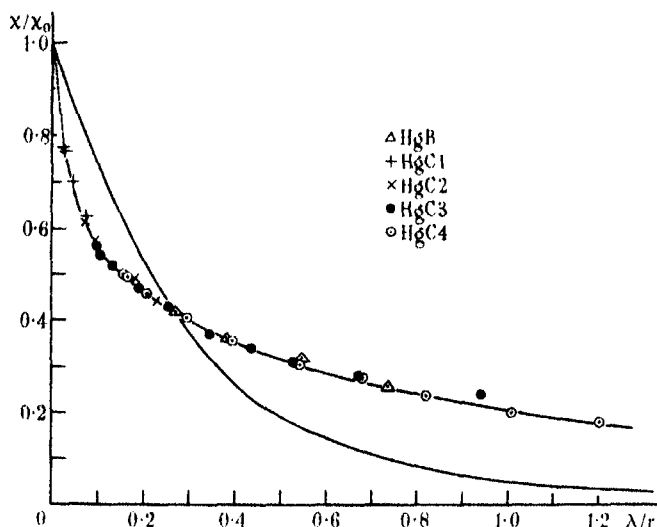


FIGURE 11. Variation of  $\chi/\chi_0$  with  $\lambda/r$ . The curve without points is calculated from the Londons' theory (equation (2)).

(an error of this sort is possible for Hg B, but very unlikely for Hg C). Thus, even assuming that the  $\chi/\chi_0$  values for Hg C4 are only 75% of the true values, the experimental curve could still not be fitted to equation (2).

Finally, there remains the possibility that the discrepancy is due to the particles in the preparations not being spherical. The influence of non-sphericity is very difficult to predict, but on the whole one might expect that if a large variety of shapes occurred (due to mechanical stresses produced by the solid dispersing medium) the effects would average out to those for a sphere. Actually, it is rather improbable that the shapes should be very different from spheres, on account of the large effect of surface tension in small particles of mercury, and indeed direct microscopic examination of the Hg C specimens showed no departure from sphericity.\* It cannot be

\* In the case of Hg B, the gelatine had to be dissolved in water before examination was possible, and so nothing can be said of the shapes in the actual dry specimen.

excluded, however, that the particles change shape on solidification, though it is unlikely.

These experiments suggest then that the London penetration law (1) is not in fact quantitatively valid, although it is, of course, very useful for a qualitative description of the penetration. The question of replacing it by a different one is a difficult one, since it is hardly possible to work back from the variation of  $\chi/\chi_0$  with  $\lambda/r$  for spheres to the general law of penetration (this might, however, be possible in the one dimensional case of a plate in a longitudinal field, and experiments in this direction would be valuable) but the experimental curve of figure 11 should be useful in providing a check on any other penetration law that may be proposed.

To conclude this section it is of interest to verify that the values of  $\lambda/r$  for Hg C4 and Hg A are consistent with what is known about the relative particle sizes. Thus, assuming that the  $r^2/\lambda^2$  law is already valid for  $\lambda/r = 1$  (on our arbitrary scale), then to get  $\chi/\chi_0 = 8.4 \times 10^{-3}$  (the value for Hg A at about 2° K) one must have  $\lambda/r \approx 5$ . Now the scale of  $\lambda/r$  has been chosen so that  $\lambda/r = 0.16$  for Hg C4 at 2° K, and thus the average particle size of Hg C4 must be about 30 times that of Hg A. Taking  $r = 5 \times 10^{-6}$  cm. for Hg A, this gives  $r = 1.5 \times 10^{-4}$  cm. for Hg C4, which is of just the right order of magnitude (see table 1). Similarly the results for Hg B are consistent with a particle size about half that of Hg C4.

### *The critical fields*

As can be seen from figures 3 and 6 the critical fields  $h$  of the specimens, particularly for small particle size, are appreciably higher than those ( $H_c$ ) for bulk mercury at the same temperature, and the ratio  $h/H_c$  increases with temperature (i.e. with increasing  $\lambda$ ) as already found by Appleyard *et al.* (1939).

On account of the spread of sizes in the specimens and other circumstances explained below, no detailed quantitative interpretation of the data on critical fields is worth while, but with a view to interpretation of any future data on more uniform specimens, I shall show how the increase of critical field can be connected thermodynamically with the field penetration.

In the case of a large sphere the treatment is complicated by the spreading of the transition between  $2/3 H_c$  and  $H_c$ , but it has been seen that already for the sizes in Hg C4 this spreading of the transition has almost disappeared (figure 4), and so the usual thermodynamics of sharp transitions may be applied to determine the critical fields of the spheres in the specimens.\*

\* The transition for the sizes in Hg C4 is not, however, perfectly sharp, and so the application of the theory in this case is not very certain.

Let  $G_n$  and  $G_s$  be the free energies per unit volume of the normal and superconducting phases per unit volume in the absence of a field, then in a field  $H$  the free energy of the superconducting phase is increased by the energy of magnetization  $\frac{1}{2}\chi H^2$ , where  $\chi$  is the diamagnetic volume susceptibility. Thus the free energies of the two phases become equal for a field  $h$  given by

$$G_n - G_s = \frac{1}{2}\chi h^2. \quad (6)$$

For the metal in bulk  $G_n - G_s$  is just  $H_c^2/8\pi$ , and so to allow for any possible size dependence of  $G_n - G_s$  I shall write

$$G_n - G_s = fH_c^2/8\pi, \quad (7)$$

where  $f$  is a dimensionless factor which may be constant, equal to unity, or may depend on size and temperature in some way which cannot be predicted by thermodynamical arguments.

Combining (6) and (7) and introducing  $\chi_0 = 3/8\pi$ ,

$$\frac{h}{H_c} = \left( \frac{f}{\chi/\chi_0} \right)^{\frac{1}{2}}. \quad (8)$$

Thus, provided that the factor  $f$  does not vary too much, equation (8) explains why  $h/H_c$  increases as  $\chi/\chi_0$  decreases, and in principle any variation of  $f$  should be deducible from the experimental data by means of equation (8). Owing however to the lack of particle size uniformity, no detailed application of equation (8) to the experimental data is possible; thus, as already pointed out,  $\chi/\chi_0$  as determined experimentally is an average over all the sizes present, while  $h/H_c$  refers to the smallest size present, and, moreover, in the case of Hg A, the determinations of  $h$  were rather rough, and could not easily be improved without changing the method of measurement.

If the spread of sizes is disregarded, then at 2° K,  $f$  for Hg C4 is 1.4 and for Hg A about 6.3. Taking into account that the observed  $\chi/\chi_0$  value for Hg A must be appreciably greater than the value appropriate to the particles to which  $h$  refers, it can be concluded that these figures are not inconsistent with the assumption that  $f = 1$  and size independent, though an increase of  $f$  from 1 to 2 or 3 as the size  $r$  is reduced to  $5 \times 10^{-8}$  cm. cannot be excluded. In other words these experimental data suggest that the free energy difference per unit volume does not change much with reduction of size.

In conclusion I should like to thank the various people whose help has been invaluable in this research: Mr Haynes of British Colloids Ltd., and Mr Powell of Boots Pure Drug Co., Ltd., for their co-operation in preparing the colloids and emulsions, Mr Barkla and Mr Laurmann for occasional help with the measurements, and the late Dr Appleyard, Dr Heitler and Dr H. London for many theoretical discussions.

#### SUMMARY

Magnetization curves of colloids and emulsions of mercury are described which provide direct evidence for an appreciable penetration, increasing with temperature, of magnetic fields into small superconductors. From the temperature variation of  $\chi/\chi_0$  (the susceptibility ratio of a small to a large sphere) for a very fine colloid, the temperature dependence of the penetration depth  $\lambda$  is deduced, in fair agreement with the results of Appleyard *et al.* This is used to transform the temperature dependence of  $\chi/\chi_0$ , for an emulsion with  $r > \lambda$ , into a curve of  $\chi/\chi_0$  against  $\lambda/r$ , which is compared with a theoretical curve based on the Londons' penetration law, suggesting that the latter is only qualitatively valid. The critical fields  $h$  of the colloids and emulsions were larger than for bulk mercury, and it is shown how, together with the susceptibility data, they can be used to calculate the free energy difference per unit volume between superconducting and normal phases for a small sphere. The results suggest that this difference increases (if at all) by a factor of at most 2 or 3, when the size is reduced from macroscopic dimensions to  $5 \times 10^{-6}$  cm. The shape of the magnetization curves and various hysteresis features are found to differ between a small and a large sphere, and these differences are discussed.

#### REFERENCES

- Appleyard and Misener 1938 *Nature, Lond.*, **142**, 474.  
Appleyard, Bristow and London 1939 *Nature, Lond.*, **143**, 433.  
Appleyard, Bristow, London and Misener 1939 *Proc. Roy. Soc. A*, **172**, 540.  
F. London 1936 *Physica*, **3**, 450.  
F. and H. London 1935 *Proc. Roy. Soc. A*, **149**, 71.  
Pontius 1937 *Phil. Mag.* **24**, 787.  
Shalnikov 1938 *Nature, Lond.*, **142**, 74.  
Shoenberg 1936 *Proc. Roy. Soc. A*, **155**, 712.  
— 1937 *Proc. Camb. Phil. Soc.* **33**, 260.  
— 1939 *Nature, Lond.*, **143**, 434.  
— 1940 *Proc. Camb. Phil. Soc.* **36**, 84.
-

# The $\beta$ -ray spectrum of radium F

By G. J. NEARY, M.A.

*Gonville and Caius College, Cambridge*

*(Communicated by J. D. Cockcroft, F.R.S.—Received 2 November 1939)*

## INTRODUCTION

The problem of the  $\beta$ -ray spectrum of RaE is too familiar now to require more than brief introduction. Owing to the eminent experimental suitability of this substance, its  $\beta$ -ray spectrum has been investigated widely, and various workers have given summaries of the results up to date, e.g. O'Connor (1937) and Martin and Townsend (1939). Most work has been done on the upper limit or on the form of the intermediate part of the spectrum, with fairly concordant results. Only a scanty amount of work has been done on an accurate investigation of the lower regions of the spectrum, where the experimental difficulties are much greater on account of the necessity of avoiding scattering in the source and along the track of the particles in the spectrograph, and of reducing the absorption in the window of the counter. Richardson (1934) first demonstrated by cloud chamber measurements, using a satisfactorily thin source mounting, that there is a considerable intensity of slow electrons between 15 and 60 ekV, and that the ordinate of the energy distribution curve is about as high in this region as at the previously estimated maximum. However, on account of straggling and other causes, it would be extremely difficult to determine exactly the form of the energy spectrum below 100 ekV by cloud chamber methods, and most other work has been done by semicircular magnetic deflexion with Geiger counters for registration of the particles. The results of chief importance are those of Alichanian and Zavel'sky (1937) and of Flammersfeld (1937, 1939). In the discussion below the conclusion is reached that in both these sets of investigations the source mountings were quite satisfactory even down to 30 or 20 ekV, but that in the former the thickness of the counter window ( $1\mu$  cellulose acetate) can scarcely be regarded as small enough for measurements below 50 ekV, whilst in the latter absorption effects in the  $0.3\mu$  Zaponlak window must begin to enter between 30 and 20 ekV.\* Moreover, in both cases the spectrographs are not sensibly free from scattering.

\* According to Flammersfeld, no effect above 25 ekV.



The experiments to be described below were made in an attempt at a precise and direct observation of the undistorted spectrum, especially below 100 ekV, and it is believed that the results do represent a practical realization of this ideal, down to the region of 20 ekV at least, without the need for the application of corrections of any kind.

## APPARATUS

### *Spectrograph*

In magnetic spectrographs for  $\beta$ -ray work employing semicircular focusing, it has hitherto been the custom to have a defining slit close to the source, the separation being usually of the order of 1 cm. It appeared that

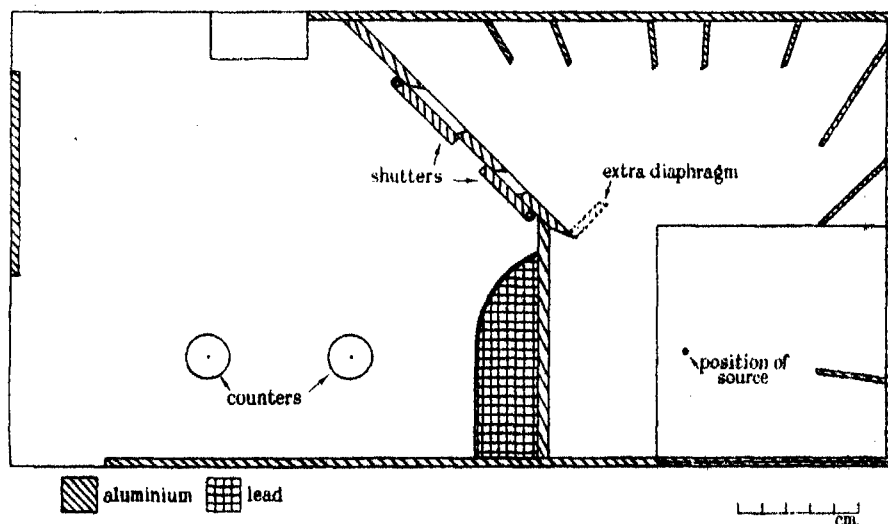


FIGURE 1.  $\beta$ -ray spectrograph.

this was undesirable if the slow disintegration electrons were to be observed, because of the possibility of considerable scattering of all the primary electrons at the slit edges, thereby vitiating the precautions taken to have a thin source mounting, for such an arrangement is qualitatively analogous to a source on a thick mounting. It was therefore decided to have the source in a free space as isolated as possible from other matter (figure 1 and figure 2). The focusing or defining slit was situated half-way round the semicircular path of the particles, where obviously the spatial density of particles traversing the semicircular path is a minimum, and the density of other particles is greatly reduced merely by the increased

distance from the source. This slit is situated in the surface which separates the object or source space from the image or counter space. The form of the essential part of this surface was a plane sloping towards the source at an angle of  $45^\circ$  to the line joining source and counters. This form was chosen because, when the slow electrons are deflected through a semicircle, the majority of the other primary particles travel in nearly straight lines

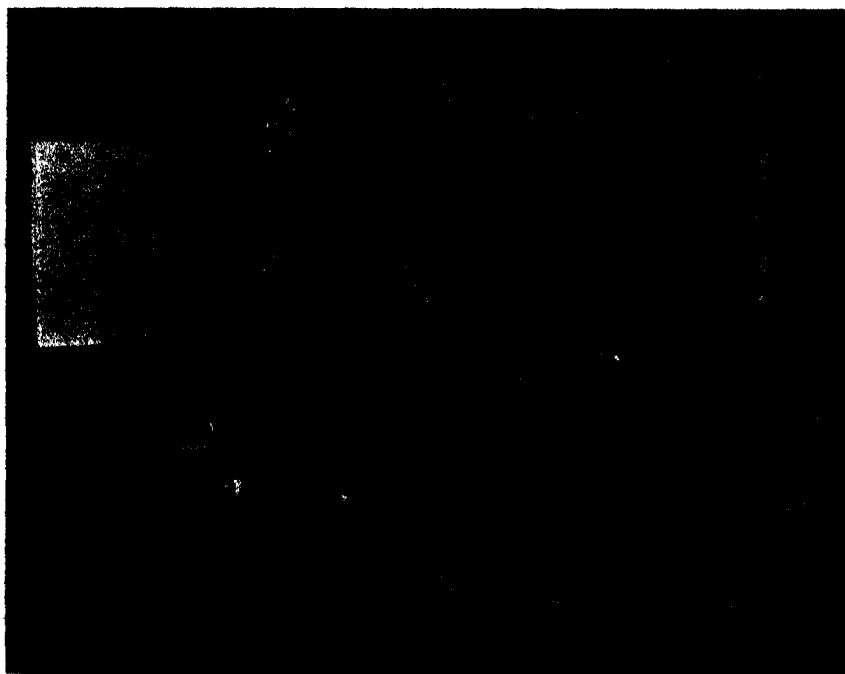


FIGURE 2

radiating from the source, and so merely graze the slit surface. The area of slit edge thus presented for scattering effects is very small; it might have been reduced to zero by tilting the slit surface, so that it pointed slightly above the source. However, little extra advantage was to be gained in this way, and as it was desired for some purposes to have two slits for two different radii of curvature, each being at the top of the relevant semi-circular trajectory, it was simplest to have one plane surface pointing to the source with slits in the appropriate positions. The question of whether any appreciable scattering of the main distribution of particles took place at the slit edges was investigated by inserting a diaphragm in the position

marked in figure 1 and again observing the spectrum. In these circumstances all particles of momentum slightly greater than those which it is intended to observe are prevented from striking the slit at all. The results confirmed that negligible scattering took place at the slit (see below). The scattering at the slits themselves has been mentioned in detail because particles scattered there have a very large chance of entering the image space, whereas particles scattered at other places in the object space have only a small chance of passing through a slit into the image space. The possibility of scattering at the edge walls in the object space of the spectrograph was circumvented by arranging short, straight diaphragms pointing to the source, in such positions that the edge walls were completely screened off from the counters. This construction is based on the same assumption as before, namely, that when small fields are employed nearly all the particles radiate in straight lines from the source. This screening is, in fact, almost equally efficient if all particles are of the same sign, whatever the magnetic field, i.e. virtually no edge walls are present. The optimum length and number of the diaphragms was obtained by simple calculation. In the case of the side walls, glancing angle scattering would be the principal effect, and so the coating of colloidal graphite which covered the whole of the interior of the spectrograph was considered an adequate precaution. One further feature minimizing the effects of scattering may be mentioned; the counter "slits" consisted of several small holes drilled in a brass plate, the diameter being  $\frac{1}{8}$  mm. and the length 1 mm. Particles incident obliquely could therefore enter the counter only by scattering in these holes, while normally incident particles could enter quite freely. Tests showed that this selective effect of the counter slits was, in fact, important.

The spectrograph was constructed so that observations could be made at two radii of curvature,  $\rho = 7$  cm. and  $\rho = 10$  cm. This necessitated the use of two defining slits and two counters. However, each slit gives a complete "spectrum" along the horizontal axis and so, if both slits are open together, a counter receives particles from two slits. For simultaneous counting to be possible, clearly a diaphragm must be placed so as to run from a point between the focusing slits to a point between the counters. Since this was undesirable for the special purpose of the present investigation, because of the increased scattering effects, only one slit was opened at a time and only the appropriate counter observed. With Ra E, which has a lifetime of 5 days, no disadvantage was incurred. In most of the experiments, in fact, only one counter was used throughout a run, because of the rather elaborate counter circuit employed (see below).

The form of the spectrum produced with a source emitting a continuous distribution of particles from a plane rectangular area was calculated completely for the spectrograph, the details being too long to give here. From the calculation it was possible to choose the various dimensions so that the nominal resolving power  $H\rho/\Delta(H\rho)$  was 100, on the assumption that the source would be 1 cm. square, suitably tilted.

It was a very useful feature of the design that owing to the large distance between source and defining slit an extended source could be used while retaining a high resolving power, for it would be very difficult to deposit a strong source of Ra E ( $\sim 1$  millicurie) on a very thin film of small area. The length parallel to the magnetic field of all slits was 1 cm.; the other dimensions were:

|    | Radius of curvature<br>cm. | Effective counter slit width<br>mm. | Defining slit width<br>cm. |
|----|----------------------------|-------------------------------------|----------------------------|
| I  | 7.0 <sub>0</sub>           | 1.4                                 | 1.1 <sub>3</sub>           |
| II | 10.0 <sub>0</sub>          | 2.0                                 | 2.2 <sub>0</sub>           |

while the tilt of the source was  $82\frac{1}{2}^\circ$  to the diameter of focusing. These dimensions were chosen so that a group of electrons of a given  $H\rho$  would be counted with equal intensity when recorded in either counter. An excellent check on the performance of the spectrograph was thereby afforded, and it was found that the ratio of intensities of the spectra in the two counters agreed with the calculated value to 1%.

The spectrograph was constructed of aluminium of thickness 4 mm. ( $\sim$  range of 2 MeV electron) coated with colloidal graphite. A lead block,  $2\frac{1}{2}$  cm. thick, cased in aluminium, was situated between source and counters so that the weak  $\gamma$ -radiation of Ra E was of no influence. The side walls of the spectrograph were 3.6 cm. apart and the least distance from the source to the edge wall was 4.4 cm. (the average distance was  $\sim 10$  cm.). Shutters were arranged behind the defining slits and were controlled from outside by a ground joint. The same zero count was obtained with the shutter closed as with the shutter open and the magnetic field reversed. The spectrograph was contained in a brass box evacuated by a two-stage oil diffusion pump. A very low pressure was thus maintained; it was checked from time to time on a Pirani gauge.

### Counters

The counters were Geiger-Müller tube counters arranged with their axes parallel to the magnetic field. In this arrangement particles entering normally approached the central wire and were therefore counted with

maximum efficiency. The internal diameter of the counters (and so the path length for the particles) was 1 cm., and the gas pressure was  $11\frac{1}{2}$  cm. (air + trace of alcohol). Under these conditions, according to the results of Ornstein and others (1938), particles of all energies should be recorded with uniform efficiency. The length of the counters was 4.0 cm.; the length of the slits 1 cm. The counter walls were of brass thicker than 1 mm. ( $\sim$  range of 2 MeV electron). A flat polished brass surface, supported over a slit in the counter wall, carried the window, which faced inwards. In one experiment this window was of mica 1.0 mg./cm.<sup>2</sup>; in a second of "Zaponlak", showing first order red by reflected light and therefore about  $0.2\mu$  thick and  $\sim 0.04$  mg./cm.<sup>2</sup>, and in a third of "Zaponlak" which was black by reflected light and was of the order of  $0.05\mu$  thick and  $\sim 0.01$  mg./cm.<sup>2</sup>. (A second order blue film by direct weighing was  $\sim 0.05$  mg./cm.<sup>2</sup>.) When using these exceedingly thin windows of "Zaponlak" it was not possible to admit sufficient alcohol to the counters to make them self-extinguishing. They were therefore controlled by the Wynn-Williams circuit using a thyatron. Since the counters had a small volume, only a small impulse was obtained from them—in many cases too small an impulse to operate a thyatron directly. For this reason the pulses were first amplified in two high-frequency pentode stages and then passed to a thyatron. The *entire* circuit was direct current coupled, so as to avoid the various disadvantages of condenser coupling. Owing to these precautions a very satisfactory characteristic was obtained with the counters; voltage changes and small pressure changes were without detectable influence on the counting rate. It was found that if the thyatron recovery was rapid, multiple kicks would appear. This was probably due to the fact that de-ionization of the counter was then incomplete. The effect was avoided, without increasing the resolving time too much, by employing quite small quantities of alcohol with the air in the counters. Small quantities of alcohol leaked only slowly through the 0.01 mg./cm.<sup>2</sup> window of "Zaponlak", and a large reservoir was attached. Observations with a source of Ra (D + E) in equilibrium showed that the efficiency of the counters remained constant from day to day. A direct test with two sources showed that there was no appreciable loss of counts at a counting rate of 1000 per min., which was about twice the maximum rate effective during the main observations.

#### *Magnetic field*

The magnet used was the permanent magnet described by Cockcroft, Ellis and Kershaw (1932). The uniformity and constancy of a given field have been checked by Ellis (1932) and by other workers. The method of measuring

the field was that described by Ellis, in which the throw from a search coil rotated in the field is balanced against the throw from a Duddell standard inductometer. Since the field strength was altered many times during a run and it was obviously very inconvenient to have to open the vacuum box during counting, for admission of a search coil to measure each field, a coil was rotated outside the box in the stray field. This coil was held rigidly in a fixed position with respect to the pole pieces and the throws were calibrated against the throws at the same field from a standard search coil in the gap. The calibration so obtained was constant to 1 part in a 1000 and the accuracy in the measurement of the field was more than adequate for the purpose required.

#### Source

The source of Ra (D + E) or of Ra E was deposited by rapid evaporation *in vacuo* of a drop of solution on a  $\frac{1}{2}\mu$  aluminium foil. The area of the drop was considerably less than 1 cm.<sup>2</sup>, while the area of the foil was about 15 cm.<sup>2</sup>. The foil was attached at its four corners to a thin, three-sided mica frame ( $\sim 6$  cm. stopping power) which rested lightly in the appropriate position in the spectrograph. Thus the radioactive material was well isolated from heavy matter. It is shown below that, in conformity with theoretical expectation, such a thin foil of aluminium introduces negligible reflexion effects even down to the lowest energies ( $\sim 13$  ekV). The Ra (D + E) source was in equilibrium but contained impurities giving some absorption in the source at lower energies, equivalent to about 0.17 mg./cm.<sup>2</sup> normal thickness. The Ra E was perfectly pure and free from Ra D, being separated by a cathodic deposition on platinum at a current density even below that at which Ra D appeared on the anode. In this way much stronger sources were obtainable than by deposition on platinum cathodically polarized with hydrogen. The source strength was  $\sim 2$  millicuries, enabling rapid counting at small magnetic fields. The statistical error of a point was  $1 \sim 2\%$ .

#### EXPERIMENTS AND RESULTS

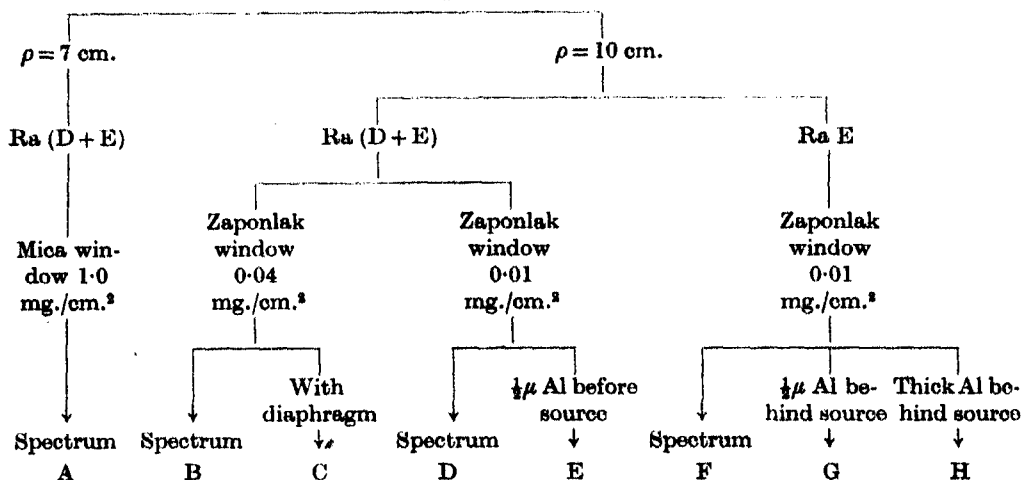
Of the sets of results the most important are A, B and D, and F; these together give directly the undistorted spectrum throughout its whole range. The other results are secondary in character and are included as providing a check, in various ways, on the primary results:

Set A is valid from the region of the upper limit to 300 ekV without appreciable absorption.

Sets B and D extend from 300 to 50 ekV; absorption in the source is appreciable only below 100 ekV.

Set F extends from 200 to 13 ekV and is valid throughout the range without appreciable absorption (or reflexion).

### Plan of experiments



The same source was used in A, B and D, and the relative intensities at the two radii of curvature agreed with calculation to 1%, showing that scattering was negligible. A different source was used in F and the curve was normalized to fit those in A, B and D. Hence the complete distribution curves in figures 3 and 4 on energy and on momentum bases were obtained. These curves are discussed in detail below.

### Secondary results

Some of the results A to H are exhibited in figure 5.

*Set A, absorption in 1 mg./cm.² mica at counter.* It has sometimes been the practice to make allowance for counter window absorption on the basis of Schonland's (1925) results for transmission of cathode rays through aluminium foil. Such a comparison would, however, seem to be erroneous, and evidence is not lacking that this is the case. The transmission ratio of Schonland's data relates to all particles transmitted into the forward hemisphere, and this gives rise to the well-known initial flat portion on the transmission curve. With a Geiger counter as recording instrument, however, only a comparatively narrow cone of particles is detected with full

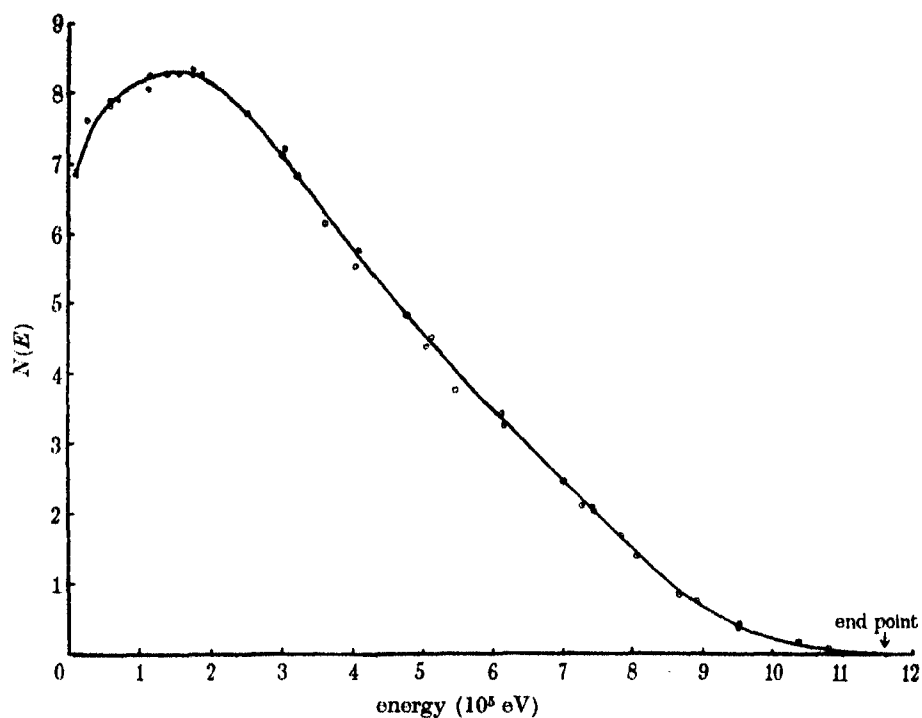


FIGURE 3. Energy distribution curve for Ra E.

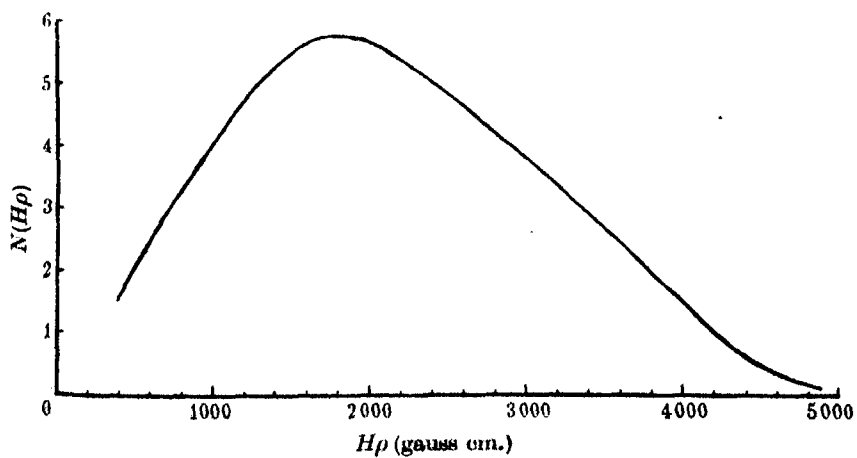


FIGURE 4. Momentum distribution curve for Ra E.



efficiency and all the particles in the forward hemisphere could not possibly be detected. Accordingly, an approximately exponential form of transmission curve would be expected in this case—certainly a curve already falling with full gradient initially. An example from the work of Flammersfeld, and of Martin and Townsend makes this clear. From Flammersfeld's

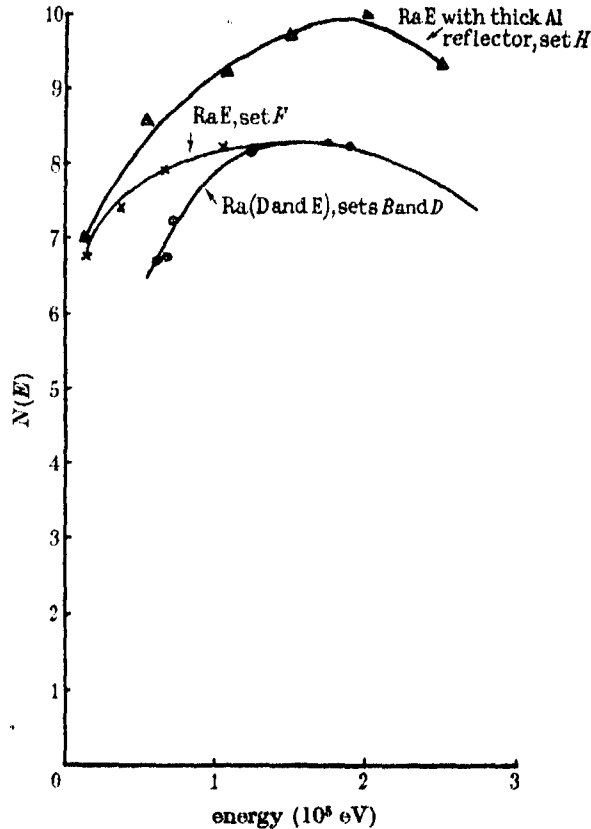


FIGURE 5. Secondary results. Distribution curves.

×, points with Ra E and  $\frac{1}{2}\mu$  Al reflector, set G.

⊙, points with Ra (D + E) and extra diaphragm, set C.

curve with  $5\mu$  aluminium before the counter the absorption per  $1\text{ mg./cm.}^2$  is 10% at 173 ekV, while Martin and Townsend find about 7% per  $1\text{ mg./cm.}^2$  mica. At 81 ekV the corresponding figures are 24 and 20%. If the absorption were linear from the start to the end of range, the absorption of 81 ekV electrons in  $1\text{ mg./cm.}^2$  would be 10%, while an actual observation of Schonland (1925) gave 3% absorption of 81 ekV electrons

in 1.5 mg./cm.<sup>2</sup> aluminium. Thus Schonland's data are quite inapplicable to most cases of counter absorption. The effect is even more marked with coincidence counters. In this case Langer and Whittaker (1937) found about 59 % transmission through 6.85 mg./cm.<sup>2</sup> of aluminium for 335 ekV electrons, where Martin and Townsend's figure would be 80 % transmission. Lastly, Ference and Stephenson (1938) have made observations of transmission through thin collodion films using a Faraday cylinder collector, so that only a cone of transmitted particles of small solid angle entered, in an attempt to reproduce conditions which obtained in a previous experiment with a counter. Here the absorption is enormously greater than in the Schonland type of experiment and the curves are roughly exponential. The writer's results for absorption in 1 mg./cm.<sup>2</sup> mica were in fair agreement with those of Martin and Townsend, and of Flammersfeld, viz. 9½ % at 173 ekV and 24 % at 81 ekV.

Sets B and D, absorption in  $\left( \begin{smallmatrix} 0.2\mu \\ 0.04 \text{ mg./cm.}^2 \end{smallmatrix} \right)$  "Zaponlak". This film was used down to 50 ekV, and by comparison with 0.01 mg./cm.<sup>2</sup> film showed no absorption at all, as would be expected from the results of Ference and Stephenson.

Set C, effect of extra diaphragm. As may be seen in figure 5, points from sets B and D and set C lie on the same curve, showing scattering at the defining slit to be negligible.

Sets B, C, D and E, absorptions in source and in ½  $\mu$  aluminium before source. By viewing the source of Ra (D + E) and other foils by transmitted light, it appeared that the thickness of the source was of the order of 0.1 mg./cm.<sup>2</sup>. Accordingly, a foil of aluminium ½  $\mu$  thick was placed in front of this source and observations taken at 50.5 and 83.0 ekV. It is evident that absorption in or near the source corresponds as regards order of magnitude with the Schonland type, since particles are incident at all angles on the absorber and a narrow emergent beam is observed. The tilt of the foil (which was approximately parallel to the source) was about 7°; the effective thickness was therefore cosec 7°  $\times$  ½  $\mu$  of aluminium = 1.1 mg./cm.<sup>2</sup>. This would give, on Schonland's data, about 87 % transmission at 50.5 ekV and 97 % at 83 ekV; the experimental figures were 87 and 95 % respectively.

Passing next to absorption in the source of Ra (D + E), the experimental absorption at 50.5 ekV relative to a pure Ra E source was 16 %, which would require ~ 1.36 mg./cm.<sup>2</sup>, or 0.16 mg./cm.<sup>2</sup> normal thickness (the Ra D contributed a considerable part of this mass). Such a thickness would give about 4 % absorption at 83 ekV, while the experimental value was 3.7 %.

*Set G, reflexion from extra  $\frac{1}{2}\mu$  aluminium behind source of Ra E.* As may be seen from figure 5, there is no distinguishable difference between points with and without the extra  $\frac{1}{2}\mu$  aluminium behind the source, even down to 13 ekV. There are no reflexion data covering precisely the case of isotropic incident radiation and grazing emergence, but existing data would suggest that with such a foil the reflexion would be at most a few per cent even at very low energies (20 to 13 ekV); the experimental result is taken to indicate that no appreciable reflexion was present with the pure Ra E source on  $\frac{1}{2}\mu$  aluminium down to 20 ekV at least.

*Set H, reflexion from thick aluminium foil.* The aluminium foil was several millimetres thick; reflexion was at grazing emergence and there appear to be no data for comparison. No interpretation of the curve is offered and it is shown chiefly by way of contrast to the result with an isolated thin source. It has a definite maximum at about 188 ekV, whereas the curve of Flammersfeld for Ra E on diamond had no maximum, while Martin and Townsend found for normal emergence from platinum that the ordinates were increased in a constant ratio. It seems probable that in some at least of the many curves for Ra E with thick sources, the maximum was partly due to a reflexion effect and not solely to absorption of particles of the lower energies in the window of the counter or ionization chamber.

The photoelectric lines of Ra D were not investigated in the present experiment because with a permanent magnet and fixed counters this would have been a very lengthy operation.

## DISCUSSION

As shown in the previous section, the curves of figures 2 and 3 represent directly the undistorted  $\beta$ -ray spectrum of Ra E in respect of energy and momentum. It may be stated at the outset that there is very close agreement in nearly every detail between these distributions and those published recently by Flammersfeld. The most conspicuous feature of the energy curve is the well-defined maximum at about 150 ekV. The end-point, which was not investigated for a precision determination in view of already existing concordant results, is 1.17 MeV, in complete agreement with these. Perhaps the most interesting single feature of the curve is that the mean energy is 340 ekV, which is in remarkable agreement with the calorimetric determinations, viz.  $344 \pm 34$  ekV, by Ellis and Wooster (1927) and  $337 \pm 20$  ekV by Meitner and Orthmann (1930). This again provides strong evidence that distortion of the spectrum has been completely eliminated. The number of electrons of energies between 15 and 60 ekV, given as about 8%

by Richardson, is 7.3 %. The momentum ( $H\rho$ ) distribution curve has a maximum at  $H\rho = 1800$  G-cm. compared with Flammersfeld's 1750 G-cm.

A strict comparison with theory is hardly possible since the case of a forbidden transition in a heavy nucleus has not been treated satisfactorily and the results are uncertain especially at the low energy end of the spectrum. However, the usual method of exhibiting Fermi and K.U. plots affords at least a useful comparison of experimental results.

For  $Z = 83$  and neutrino mass = 0

$$\left[ \frac{N(\eta)}{\eta + 0.355\eta^2} \right]^{\frac{1}{2}} \propto [\sqrt{(1 + \eta_0^2)} - \sqrt{(1 + \eta^2)}], \quad (\text{Fermi})$$

$$\left[ \frac{N(\eta)}{\eta + 0.355\eta^2} \right]^{\frac{1}{2}} \propto [\sqrt{(1 + \eta_0^2)} - \sqrt{(1 + \eta^2)}], \quad (\text{K.U.})$$

where  $\eta$  = momentum of  $\beta$  particle in  $m_0C$  units,  $\eta_0 = \eta$  at upper limit.

The two plots are given in figure 6 and show the usual features, the K.U. plot being straight for a considerable portion of the energy range and then falling rapidly as the upper limit is approached, while the Fermi plot is concave upwards through most of the energy range but has a smoother approach to the observed upper limit. This limit occurs at 3.30 in  $m_0C^2$  units, while the extrapolated K.U. end-point is 3.85  $m_0C^2$ . The difference, 0.55  $m_0C^2$ , is the so-called neutrino mass. Corresponding figures, according to other workers, are:

|                              | Extrapolated<br>end-point | Extrapolated<br>end-point—<br>experimental<br>end-point |
|------------------------------|---------------------------|---|
| Flammersfeld (1939)          | 3.79                      | 0.50  |
| Martin and Townsend (1939)   | 3.80                      | 0.47  |
| Alichanian and others (1938) | 3.69                      | 0.37  |
| O'Connor (1937)              | 3.52                      | 0.22  |
| Langer and Whittaker (1937)  | 3.82                      | 0.52  |
| Lyman (1937)                 | 3.68                      | 0.45  |

The explanation of the difference between observed and extrapolated end-points in terms of a finite neutrino mass seems of doubtful validity. Although Alichanian and others, and O'Connor, find that the introduction of this quantity brings about agreement between experiment and the predictions of the K.U. theory, Lyman, Flammersfeld and the writer find that agreement is quite impossible by this means, nor apparently can the results of Martin and Townsend be reconciled. Alichanian and others found that the required neutrino mass for the Th C spectrum was 0.8, while Zavel'sky states that agreement is not possible for the Th C' and Th B spectra

unless an intermediate energy is taken as the limiting energy, lying between the observed and extrapolated K.U. limits. Thus it seems that the simple hypothesis of attributing the discrepancy between observed and

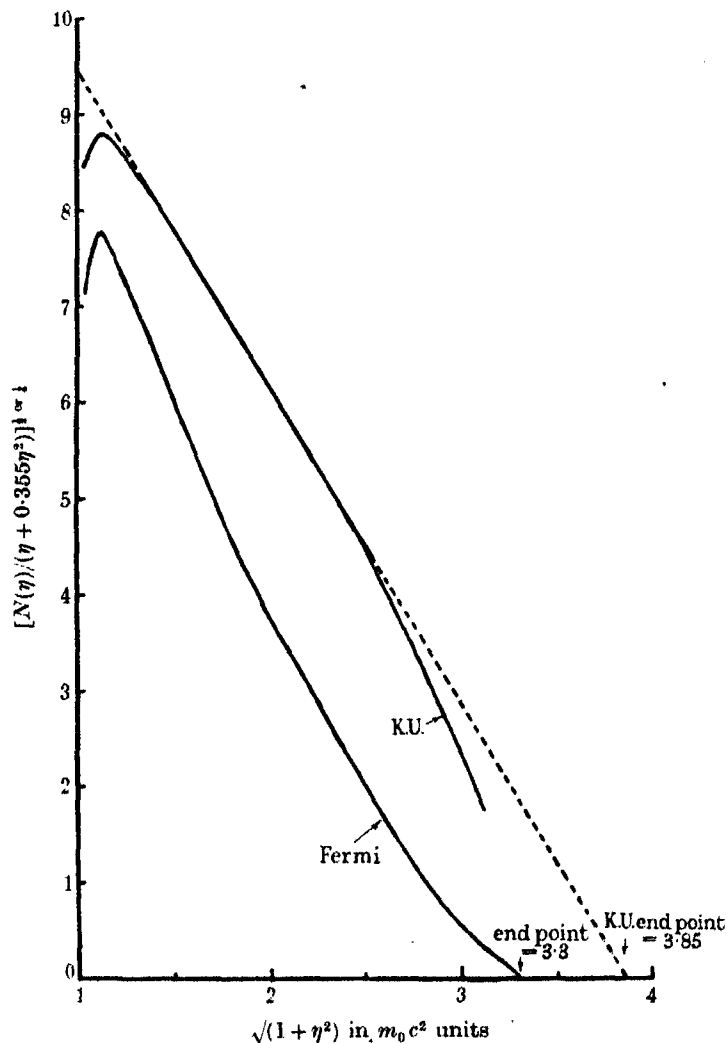


FIGURE 6. Fermi and K.U. plots for Ra E.

extrapolated K.U. limits to the effect of a finite neutrino mass is not generally tenable. As was pointed out by Richardson, an improved agreement with the Ra E experimental curve may be obtained by taking a linear combination of Fermi and K.U. terms, but even then the agreement is not wholly satisfactory. Likewise, the modifications to the distribution

introduced by the  $\beta$ -decay theory of Yukawa (1938) do not result in appreciable improvement in this matter.

Turning next to the low energy part of the distribution, the writer's curve lies below the K.U. curve after 150 ekV, the reduction being 6 % at 100 ekV, 13 % at 50 ekV, and 32 % at 13 ekV, as deduced from the non-linearity of the K.U. plot. This cannot be due to any kind of absorption in the counter window or in the source. Flammersfeld (1939), on the other hand, finds practical agreement with the K.U. distribution down to the lowest energies, while Alichanian and Zavel'sky (1937) find the experimental curve above the K.U. curve to the extent of 10 % at 50 ekV. It appears to the writer that Flammersfeld's explanation of the latter result as due to scattering, etc. in an aged source is definitely untenable. The writer encountered no such effect with a source similar to that of Alichanian and Zavel'sky ( $\frac{1}{2}\mu$  aluminium) and in any case the effect of an impure source is always to reduce the apparent number of slow particles, "absorption" being more important than back scattering, cf. preceding section, sets B, C, D, E.\* The writer therefore considers that extraneous scattering must have played some part in the spectrograph of Alichanian and Zavel'sky and to a lesser extent in that of Flammersfeld also, and the following considerations appear to favour this conclusion. Although it is not possible to say precisely what effect absorption by scattering had in the counter window of  $1\mu$  cellulose acetate used by Alichanian and Zavel'sky, yet it seems very likely that this absorption was greater than the authors considered. On the basis of the type of absorption which obtained in the counters of Martin and Townsend, of Flammersfeld and of the writer, the "absorption" in  $1\mu$  cellulose acetate would be about 18 % at 30 ekV and 22 % at 20 ekV. Hence the properly "corrected" curve would be expected to be even higher than that given by Alichanian and Zavel'sky since they assumed an absorption of only 4 % at 40 ekV. However, such a curve could hardly be regarded as correct and the excess at low energies must be attributed to scattered particles. The spectrograph had a defining slit close to the source and several limiting slits round the semicircular trajectory, and edge effects may well have been present. If this were in fact the case, the complete agreement with the K.U. distribution found by these authors using the same apparatus for Th C" and Th B requires further consideration.† In the experiments of Flammersfeld the mean energy of the distribution is

\* Apart from the effect of back scattering, "absorption" in the source (for small thicknesses) removes completely more particles from the lowest energy range than it reintroduces into this range by the retardation of particles of higher energy.

† The excess of particles at low energies (300 ekV downwards), found by Martin and Townsend, may almost certainly be attributed to the inadequate gas pressure of 5 cm. air in the counter, giving a higher efficiency of detection for particles of lower energy.

330 ekV, which is slightly but appreciably lower than the calorimetric values. This fact alone suggests that the low energy part of his curve may be slightly too high. The radius of curvature employed in Flammersfeld's spectrograph was 4 cm., while the writer used 10 cm. for the low-energy region. The defining slit was not immediately in front of the source but it was not, on the other hand, as far away as possible and, most important of all, the slit presented practically the same solid angle or aperture for admission into the "image" or counter space of particles of all energies. In the spectrograph used by the writer, the effective aperture at small fields was smaller the higher the energy of the particle, so that practically only the relevant low energy particles entered the image space at small magnetic fields, and a stray electronic "atmosphere" was avoided, cf. preceding section, set C. Although certain low energy photoelectron lines appeared perfectly sharply in Flammersfeld's experiments, this is no proof that a contribution of scattered particles from the whole of the distribution was not present as well. The absorptions of a line and of the neighbouring continuous background in  $2\mu$  "Zaponlak" were found to be the same, but this hardly rules out the possibility that the background should contain 5 ~ 10 % of scattered radiation, and indeed the latter might appear nearly homogeneous if most scattered particles were produced at the slit edges, because of the mode of observing the zero count.\* Thus the final conclusion would seem to be that the slight disagreement between the curves of Flammersfeld and the writer below 150 ekV may probably be attributed to the effects of scattering in the former case. The writer's curve showing fewer slow electrons than corresponds to the K.U. distribution for an allowed transition might conceivably exhibit just that reduction in the number of these electrons which appears to be generally expected in a forbidden transition, but at present this interpretation is entirely speculative in character. On the other hand, the K.U. plot obtained here, with the marked fall at each end, is similar to some of the possibilities described by Hoyle (1937, 1938).

It is a pleasure to thank Dr N. Feather for his continued interest in the work and to acknowledge the valuable assistance of Mr E. Wild of Trinity College with the observations in the latter stages of the experiment.

#### SUMMARY

The  $\beta$ -ray spectrum of Ra E has been investigated with a magnetic spectrograph of special design with a source on  $\frac{1}{2}\mu$  aluminium and a counter window of  $10^{-5}$  g./cm.<sup>2</sup> Zaponlak.

\* This zero count in fact varied somewhat with the magnetic field.

It is considered that the experimental results represent directly the distribution of particles from about 20 ekV upwards without distortion from any cause. The energy curve has a maximum at 150 ekV and an end-point at 1.17 MeV, with a mean energy of 340 ekV in complete agreement with calorimetric determinations. The momentum curve has a maximum at  $H\rho = 1800$  G-cm. in satisfactory agreement with Flammersfeld,  $H\rho = 1750$  G-cm. The intermediate part of the K.U. plot is straight, the energy difference between experimental and extrapolated end-points being  $0.55 m_0 C^2$ ; on the other hand, the introduction of a finite neutrino mass does not bring about agreement with theory. The K.U. plot also falls below the straight line below 150 ekV, and resembles some of the possible distributions for "forbidden" transitions, as given by Hoyle.

## REFERENCES

- Alichanian, Alichanow and Ozelopov 1938 *C.R. Acad. Sci. U.R.S.S.* **19**, 375.  
Alichanian and Nikitin 1938 *C.R. Acad. Sci. U.R.S.S.* **19**, 377.  
Alichanian and Zavelsky 1937 *C.R. Acad. Sci. U.R.S.S.* **17**, 467.  
Cockcroft, Ellis and Kershaw 1932 *Proc. Roy. Soc. A*, **135**, 628.  
Ellis 1932 *Proc. Roy. Soc. A*, **138**, 318.  
Ellis and Wooster 1927 *Proc. Roy. Soc. A*, **117**, 109.  
FERENCE and Stephenson 1938 *Rev. Sci. Instrum.* **9**, 246.  
Flammersfeld 1937 *Phys. Z.* **38**, 973.  
— 1939 *Z. Phys.* **112**, 727.  
Hoyle 1937 *Proc. Camb. Phil. Soc.* **33**, 277.  
— 1938 *Proc. Roy. Soc. A*, **166**, 249.  
Langer and Whittaker 1937 *Phys. Rev.* **51**, 713.  
Li 1937 *Proc. Roy. Soc. A*, **158**, 571.  
Lyman 1937 *Phys. Rev.* **51**, 1.  
Martin and Townsend 1939 *Proc. Roy. Soc. A*, **170**, 190.  
Meitner and Orthmann 1930 *Z. Phys.* **60**, 143.  
O'Connor 1937 *Phys. Rev.* **52**, 303.  
Ornstein, Milatz, ten Kate and Miesowicz. 1938 *Proc. Acad. Sci. Amst.* **41**, 1055.  
Richardson 1934 *Proc. Roy. Soc. A*, **147**, 442.  
Schonland 1925 *Proc. Roy. Soc. A*, **108**, 187.  
Yukawa, Sakata, Kobayasi and Taketani 1938 *Proc. Phys. Math. Soc. Japan*, **20**, 720.  
Zavelsky 1939 *Phys. Rev.* **55**, 317.
-



# On the photon component of cosmic radiation and its absorption coefficient

BY L. JÁNOSSY\* AND B. ROSSI†

(Communicated by P. M. S. Blackett, F.R.S.—Received 17 November 1939)

## 1. INTRODUCTION

It has been established that the soft component of the cosmic radiation consists of electrons and photons. Much experimental data on the electrons forming the soft component are available and they are known to form a fraction of about 25–30 % of the whole beam of ionizing particles at sea level, excluding particles below  $10^7$  eV (e.g. Rossi 1933; Nielsen and Morgan 1938). The energy spectrum of the electrons is known roughly from the work of Blackett (1938), Wilson (1939) and others. The energy loss of electrons in metal plates has been investigated by Anderson and Neddermeyer (1934), Blackett and Wilson (1937), Williams (1939), Wilson (1938, 1939), showing that the experimental values of the energy loss are in agreement with the prediction of the quantum theory (Bethe and Heitler 1934).

Much less is known about the photon component of cosmic radiation, as comparatively few experiments have been carried out to investigate their properties. Further the results of the investigations available are partly contradictory.

The theory of the absorption of high energy photons has been worked out to the same extent as for electrons (Bethe and Heitler). Owing to the lack of experimental material, the theory could be tested only up to energies of about five million volts (McMillan 1934; Gentner 1935). The success of the theory of cascade showers due to Bhabha and Heitler (1937) and Carlson and Oppenheimer (1937), based on the Bethe-Heitler theory of electrons and photons, provides however an indirect test for the validity of the absorption formula for high energy photons.

The lack of experimental data on high energy photons is due to the difficulties in the method of observation; photons unlike electrons cannot be observed directly.

\* John Harling Fellow in Physics at the University of Manchester.

† Fellow of the Society for the Protection of Science and Learning, now at the University of Chicago.

In the present paper a simple method for investigating cosmic-ray photons is described. Using this method, data about the number, energy distribution and absorption of cosmic-ray photons have been obtained.

## 2. THE EXPERIMENTAL ARRANGEMENT

The experimental arrangement is shown schematically in figure 1 and the dimensions of the counters and of the screens are given in table 1.

The counters were made of pyrex glass, with a copper foil 0.1 mm. thick as cathode and a 0.1 mm. tungsten wire as anode, and were filled with a mixture of argon and alcohol vapour.

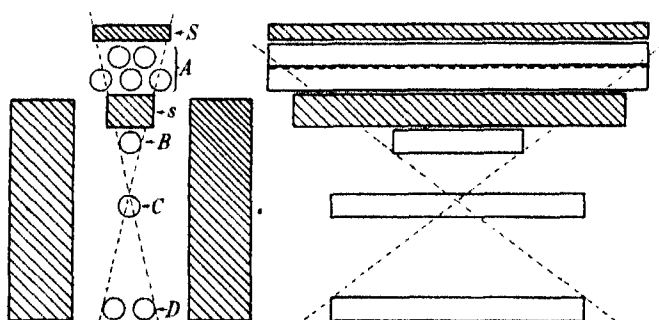


FIGURE 1. The experimental arrangement.

TABLE 1

|                                  |                                |
|----------------------------------|--------------------------------|
| Counters <i>A</i> :              | 60 cm. long, 3.0 cm. diameter. |
| Counter <i>B</i> :               | 20 cm. long, 3.0 cm. diameter. |
| Counters <i>C</i> and <i>D</i> : | 40 cm. long, 3.0 cm. diameter. |
| Screen <i>s</i> :                | 60 × 7 sq. cm.                 |
| Screen <i>S</i> :                | 60 × 7 sq. cm.                 |

Threefold coincidences between *B*, *C*, *D*, and fourfold coincidences between *A*, *B*, *C*, *D*, were recorded simultaneously as described in detail by one of us (Rossi 1930). Each of the counters or counter batteries *A*, *B*, *C* and *D* were coupled respectively to the valves *a*, *b*, *c* and *d*. The anodes of the valves *b*, *c*, *d* were connected in the usual way and received the anode potential through a common 200,000  $\Omega$  resistance  $R_1$ . The anode of the valve *a* was connected through an extra resistance  $R_2$  of 70,000  $\Omega$  to the anodes of the other valves. The pulses occurring at that end of  $R_2$  which was connected to  $R_1$  were large whenever *A*, *B*, *C* and *D* discharged simultaneously, whilst a simultaneous discharge of *B*, *C* and *D*, not accompanied by a discharge

of  $A$ , produced a smaller pulse at this point. By means of two thyratrons with different grid biases the large and the small pulses could easily be separated.

Since the resolving power of the arrangement was about  $10^{-5}$  sec., the number of threefold or fourfold chance coincidences was less than 1 in 10 hr. and was therefore negligible. The efficiency of the counter battery  $A$ , as shown by control experiments, was at least 99 %.

### 3. THE EXPERIMENTAL METHOD

The principle of the experiment was to detect the electrons generated by photons in a metal plate. The experiments will be discussed assuming that no non-ionizing agent other than photons occurs to an appreciable extent. It will be seen that the results are consistent with this assumption although the existence of a small fraction of other non-ionizing rays cannot be excluded.

As can be seen from figure 1, the counter battery  $A$  covers the whole solid angle subtended by the counters  $B, C, D$ . Thus each single ionizing particle passing through  $B, C$  and  $D$  must have passed through  $A$  as well unless (a) it is produced by some non-ionizing agent between  $A$  and  $B$ , or (b) it is scattered by  $s$ . Process (b) seems in our arrangement not to be of great importance. In the present experiments we are therefore mainly concerned with threefold coincidences  $B, C, D$  which were not accompanied by a fourfold coincidence  $A, B, C, D$ . For brevity threefold coincidences not accompanied by fourfold coincidences are to be termed "anti-coincidences". In an experiment of this kind it is essential to count simultaneously the number  $N_3$  of threefold coincidences and the number  $N_4$  of fourfold coincidences, since the average fluctuation of the small difference  $N_3 - N_4$  is  $\sqrt{(N_3 - N_4)}$  for the case of simultaneous recording, whereas it is  $\sqrt{(N_3 + N_4)}$  when  $N_3$  and  $N_4$  are measured by separate observations. The disturbing effect due to variations of the cosmic-ray intensity is also greatly reduced by simultaneous recording.

### 4. THE TRANSITION CURVE FOR THE SHOWERS PRODUCED BY PHOTONS

#### (a) *The experimental results*

Measurements were carried out with no absorber above the counters  $A$  and an absorber of variable thickness between  $A$  and  $B$  in position  $s$ . The various thicknesses of absorber  $s$  were placed so that the upper surface was always as close as possible to  $A$ .

The experimental results are collected in table 2 and the observed rates of anti-coincidences together with the statistical fluctuations are plotted against the thickness of the absorber  $s$  in figure 2. A zero rate of 11.4 anti-coincidences per hour has been subtracted from each value (see § 5a).

TABLE 2. TRANSITION CURVE OF PHOTON INITIATED SHOWERS

| $s$<br>cm. Pb | Threefold coincidences |               | Anti-coincidences |                |
|---------------|------------------------|---------------|-------------------|----------------|
|               | Total                  | Rate per hour | Total             | Rate per hour  |
| 0.1           | 10665                  | $441 \pm 4$   | 443               | $6.9 \pm 0.9$  |
| 0.45          | 10616                  | $444 \pm 4$   | 1064              | $33.1 \pm 1.0$ |
| 0.8           | 11369                  | $451 \pm 4$   | 1334              | $41.6 \pm 1.5$ |
| 1.1           | 20344                  | $446 \pm 3$   | 2394              | $41.0 \pm 1.1$ |
| 1.45          | 20915                  | $441 \pm 3$   | 2218              | $35.4 \pm 1.0$ |
| 2.15          | 12405                  | $414 \pm 3$   | 1143              | $26.9 \pm 1.1$ |
| 2.8           | 19045                  | $418 \pm 3$   | 1411              | $18.4 \pm 0.8$ |
| 5.1           | 16703                  | $366 \pm 3$   | 770               | $5.4 \pm 0.6$  |

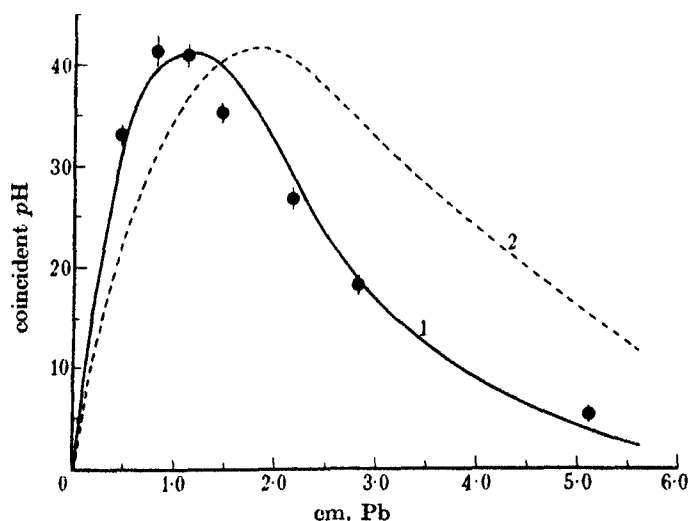


FIGURE 2. The transition effect for showers initiated by photons. ● observed. .... calculated for  $E_c/E^2$  spectrum. — calculated for  $E_c/E^3$  spectrum ( $E > E_c$ );  $1/E$  spectrum ( $E < E_c$ ).

Without any lead at  $s$ , 18.3 anti-coincidences per hour were recorded. The lead screen  $s$  increased the number of anti-coincidences considerably. This increase was obviously due to photons generating Compton or pair electrons in the screen  $s$  and so starting showers hitting the three counters underneath. The points given in figure 2 represent therefore the transition effect of showers generated by photons.

The anti-coincidences observed with no lead do not represent the "true zero effect" because some amount of matter was always present between the counters *A* and *B* (the walls of the counters themselves plus 6 mm. wood and 0.5 mm. iron of the framework of the apparatus). We estimated this amount of matter to be roughly equivalent to 0.1 cm. Pb and added, therefore, in the first column of table 2, 0.1 cm. to the actual thickness of the lead screen *s*. The assumed zero rate of 11.4 anti-coincidences per hour will be justified by experiments to be described later. The zero rate was due mainly to showers coming from the side, i.e. to air showers not completely cut off by the lead walls (see figure 1) and to knock-on showers generated in the lead itself by penetrating particles. As already mentioned the lack of efficiency of the counters could not account for more than 1 % of the anti-coincidences, i.e. four anti-coincidences per hour.

As it is unlikely that the zero effect can be altered appreciably by varying the lead screen *s*, it can be regarded as a constant background of the transition curve.

(b) *Discussion of the observed transition effect*

The transition curve obtained with the arrangement described above is very suitable for comparison with the theoretical transition curve. This is so, since a fairly accurate estimate can be obtained for the probability that a shower of a given size emerging out of *s* will give rise to a coincidence. The expected transition curve was calculated from the cascade theory on the following assumptions:

(1) The showers recorded are due to *single* photons hitting the absorber *s*. Photons accompanied by electrons do not give rise to anti-coincidences and the probability of two or more photons coming together without being accompanied by electrons is small (see § 5 (b)).

(2) Electrons of energy less than  $10^7$  eV (i.e. the critical energy for lead) are neglected. This assumption is justified since most of these electrons are stopped by the material between the counters and the counter walls (total quantity 2 g./cm.<sup>2</sup>).

We will work out the probability that a photon of energy *E* hitting *s* will produce an anti-coincidence. For simplicity we assume that the average angular spread of a shower produced by a photon in *s* is  $\Omega$  and that the shower particles are distributed at random inside  $\Omega$ . The solid angle covered by the counters *D* as seen from a point inside *B* we call  $\omega$  and we suppose  $\omega \ll \Omega$ . The probability that a photon of a given direction produces an anti-coincidence is, according to the above assumptions,

$$p = (1 - e^{-\omega/\Omega \bar{N}(E_1 x)}) \\ \approx \omega/\Omega \bar{N}(E_1 x) \quad \text{for } \omega/\Omega \bar{N} \ll 1.$$

The number of showers per unit time is therefore

$$J_s = J\Omega Fp,$$

where  $F$  is the average effective area of the absorber from which particles crossing the counters  $B$ ,  $C$  and  $D$  may arise and  $J$  is the number of photons per unit time, unit area and unit solid angle. It is useful to compare  $J_s$  with the number  $J_p = J\omega F$  of photons travelling along lines crossing the counters  $B$ ,  $C$ ,  $D$ . We find

$$J_s/J_p \equiv P(E, x) = \Omega/\omega(1 - e^{-\omega/\Omega \bar{N}(E, x)}), \quad (1)$$

$$\approx \bar{N}(E, x) \quad \text{for } \bar{N}\omega/\Omega \ll 1. \quad (2)$$

We see from (2) that for small showers  $P(E, x)$  is independent of the value of  $\Omega$ . For large showers we can put, as a rough approximation,  $\Omega = 2\pi$ . Showers containing many particles however are produced by very energetic photons only and are very rare. Our results therefore cannot be affected appreciably by the above assumptions concerning big showers. The effect of big showers is especially small for the first part of the transition curve. Putting  $\omega/2\pi = 0.035$  (obtained from the dimensions of the counters arrangement) we have  $\omega/2\pi \bar{N} < 0.1$  up to light quanta of  $4 \times 10^9$  eV, according to the numerical values given by Arley.

From (1) we get for the number of anti-coincidences at the thickness

$$T(x) = \int_{10^9 \text{ eV}}^{\infty} \rho(E) P(E, x) dE. \quad (3)$$

The function  $\bar{N}(E, x)$  for photons has been recently calculated by Arley.\* Therefore  $P$  can be regarded as a known function of  $E$ . Theoretical considerations seem to indicate that the differential spectrum of photons is roughly of the following form (see Heitler 1937, Nordheim 1939)

$$\left. \begin{aligned} \rho(E) &\sim E_c^\alpha/E^{\alpha+1}, & E > E_c & \quad (a) \\ \rho(E) &\sim 1/E, & E < E_c & \quad (b) \end{aligned} \right\} \quad (4)$$

We evaluated (3) by numerical integration, using the spectrum given in (4) and taking  $E_c = 1.5 \times 10^8$  eV. The values obtained for  $T(x)$  are plotted in figure 2. The full line corresponds to the spectrum with  $\alpha = 2$ , while the broken line corresponds to the spectrum with  $\alpha = 1$ .

The intensity factors have been chosen so as to give the observed intensities for the maximum, i.e. 41.5 anti-coincidences per hour.

The agreement of the calculated curve for the spectrum given in (3) for  $\alpha = 2$  is as good as it can be expected. Hence it is concluded that both the

\* We are indebted to Dr N. Arley for having kindly communicated the unpublished numerical results.

assumptions about the shape of the energy spectrum and the results deduced by Arley from the Bethe-Heitler theory are a good approximation to the facts. On the other hand, the transition curve calculated for the  $1/E^2$  spectrum (i.e. for  $\alpha = 1$ ) differs markedly from the observations.

(c) *The total intensity of photons*

The total number of incoming photons can be estimated from our observations. The initial rise of the transition curve is only slightly affected by the shape of the energy spectrum, since, for small values of  $x$ ,  $\bar{N}$  varies very slowly with  $E$ . Thus the factor required to fit the first slope of the calculated transition curve to the observations gives the total photon flux. According to equations (1) and (3) the average number of anti-coincidences recorded per photon with an energy greater than  $10^7$  eV is given by

$$t(x) = T(x) \int_{10^7 \text{ eV}}^{\infty} \rho(E) dE.$$

Assuming the spectrum has the form given in (4) and  $\alpha = 2$ , one finds for  $x = 0.8$  cm. Pb

$$t(0.8) = 0.89.$$

Since from table 2 the observed number of anti-coincidences per hour is

$$T(0.8) = 41.6,$$

we find 
$$\int_{10^7 \text{ eV}}^{\infty} \rho(E) dE = \frac{T(0.8)}{t(0.8)} = 47 \text{ per hour.}$$

This is the number of photons with energy greater than  $10^7$  eV travelling along straight lines passing through the counters *B*, *C* and *D*. The corresponding number of ionizing particles is 450 per hour (table 2). Thus the number of photons with energy greater than  $10^7$  eV is  $47/450 = 10.5\%$  of the number of single particles. Using the spectrum (4),  $\alpha = 2$ , we get table 3.

TABLE 3

| Energy interval in eV                     | $1-5 \times 10^7$ | $5-15 \times 10^7$ | $> 15 \times 10^7$ | $> 10^7$ |
|---|-------------------|--------------------|--------------------|----------|
| No. of photons per 100 ionizing particles | 5.3               | 3.6                | 1.6                | 10.5     |

The above estimate represents a lower limit for the actual number of photons for it does not include those photons which are accompanied by at least one electron within an area of  $600 \text{ cm.}^2$ , i.e. photons occurring in

the denser parts of the extensive air showers. Moreover, some photons are certainly missed because of shower particles scattered back from the lead screen  $s$ , towards the counters  $A$ .

## 5. THE ABSORPTION OF HIGH-ENERGY PHOTONS

### (a) *Experimental results*

In order to determine the absorption curve of cosmic-ray photons, measurements were made with a constant amount of lead in position  $s$  (figure 1) and different screens above the counters  $A$  (position  $S$ ). The measurements were carried out with 0.35 and 2.0 cm. of lead at  $s$ .

A photon hitting the screen  $S$  can (a) traverse the screen unabsorbed, (b) produce a Compton electron or an electron pair. Case (a) is exactly the same as if the absorber  $S$  had not been there at all, and the chance of recording the photon as an anti-coincidence is the same as it was without the absorber  $S$ . In case (b), however, a shower is started in the screen  $S$ . This shower may or may not emerge from  $S$ , but if it does it is very improbable that the counters  $B$ ,  $C$ ,  $D$  are discharged without one of the counters  $A$  being discharged as well. Thus the decrease of the number of anti-coincidences due to  $S$  is a direct measure of the probability that a photon is removed by pair production or Compton scattering.

As the probability of a photon traversing 5 cm. of lead with no encounter is extremely small, the frequency of the anti-coincidences observed with 5 cm. of lead in  $S$  is to be considered as the zero effect due to showers coming from the side and similar disturbing effects. The zero effects amount to 10.3 coincidences per hour for the observations with 0.34 cm. Pb at  $s$  and to 12.0 for the measurements with 2.0 cm. Pb at  $s$ . The difference of the two zero effects is not outside the statistical fluctuations. Nevertheless, since the possibility of a systematic difference cannot be excluded, the individual values for the two sets of measurements were preferred. The zero effect used in the discussion of the transition curve was the mean of the two values.

The results of the two sets of measurements are given in tables 4 and 5. The results of the absorption measurements in lead are given graphically in figures 3 and 4, where the logarithms of the observed quantities (after the subtraction of the zero effect) are plotted against the thickness of  $S$  in cm. of lead. The full lines represent straight lines fitted with the method of the least squares to the observations. The broken lines give the slopes expected according to the theory of Bethe and Heitler. Observations were also made with 1.0 cm. Fe and 6.3 cm. Al to compare the effect of different elements.



TABLE 4. ABSORPTION CURVE FOR  $s = 0.35$  cm. Pb

| X cm. | Material | Threefold coincidences |               | Anti-coincidences |                |
|-------|----------|------------------------|---------------|-------------------|----------------|
|       |          | Total                  | Rate per hour | Total             | Rate per hour  |
| 0.00  | Pb       | 13297                  | $437 \pm 4$   | 1341              | $44.2 \pm 1.2$ |
| 0.35  |          | 10620                  | $442 \pm 5$   | 826               | $34.4 \pm 1.2$ |
| 0.70  |          | 10737                  | $446 \pm 5$   | 715               | $29.6 \pm 1.1$ |
| 1.40  |          | 9161                   | $417 \pm 4$   | 456               | $20.7 \pm 1.0$ |
| 5.0   |          | 8972                   | $374 \pm 4$   | 248               | $10.3 \pm 0.6$ |

TABLE 5. ABSORPTION CURVE FOR  $s = 2.0$  cm. Pb

| X cm. | Material | Threefold coincidences |               | Anti-coincidences |                |
|-------|----------|------------------------|---------------|-------------------|----------------|
|       |          | Total                  | Rate per hour | Total             | Rate per hour  |
| 0.00  | Pb       | 21858                  | $430 \pm 3$   | 1932              | $37.9 \pm 0.9$ |
| 0.35  |          | 19801                  | $417 \pm 3$   | 1326              | $28.0 \pm 0.8$ |
| 0.70  |          | 19389                  | $410 \pm 3$   | 1118              | $23.6 \pm 0.7$ |
| 1.40  |          | 17119                  | $402 \pm 3$   | 768               | $18.1 \pm 0.7$ |
| 5.0   |          | 16938                  | $372 \pm 3$   | 547               | $12.0 \pm 0.5$ |
| 1.0   | Fe       | 16504                  | $408 \pm 3$   | 1089              | $27.0 \pm 0.8$ |
| 6.3   | Al       | 16097                  | $409 \pm 3$   | 1056              | $16.9 \pm 0.8$ |

(b) *Discussion of the results*

The interpretation of the above results is affected by two possible sources of error namely:

(1) *Multiple photons striking S.* Let us suppose the absorption coefficient of a single photon to be  $\mu$ . When  $n$  photons hit  $S$  simultaneously the variation of the number of anti-coincidences with  $S$  corresponds to an absorption coefficient  $n\mu$ . This is due to the fact that anyone of the photons has independently a certain chance of producing an electron which can pass through  $A$  and prevent the anti-coincidences. An estimate of the density of air showers however suggests that this effect cannot give rise to an appreciable correction to our result. This can easily be understood since photons accompanied by electrons cannot give rise to anti-coincidences. Thus the denser parts of air showers where there are more than one photon in an area comparable with the surface of  $S$  will also contain electrons and so will not be recorded.

The following experimental test showed too that the effect of multiple rays could not be appreciable. A lead absorber of 1.4 cm. thickness covering only *half* the area of  $S$  was brought above the counters  $A$ . In case of single photons such an absorber ought to reduce the intensity by a factor

$$\frac{1}{2}(e^{-\mu X 1.4} + 1) = 0.63,$$

where  $\mu$  is the observed absorption coefficient. Since the observed reduction was  $(64 \pm 5)\%$  the photons must be nearly all single. If multiple photons were present the observed reduction would be larger.

(2) *A single electron is stopped in  $S$  by the emission of an energetic light quantum.* This light quantum may escape out of  $S$  without producing a secondary effect and so may give rise to an anti-coincidence by absorption in  $s$ . It seems very difficult to evaluate theoretically the correction due to this effect, but it is unlikely to be important for the absorption curve with 2.0 cm. of lead at  $s$  although it may have some effect on the absorption curve with 0.35 cm. Pb at  $s$ . We intend to carry out at a later date an experiment to investigate the correction arising from this effect.

(c) *Comparison of the observed absorption curve with the theory*

The absorption curve is given theoretically by the following expression

$$A(X) = \int \rho(E) P(E_1 x) e^{-\mu(E) X} dE,$$

the functions  $P(E_1 x)$  and  $\rho(E)$  having been defined in the previous section ( $x$  is the thickness of the lead screen where the showers are produced and  $X$

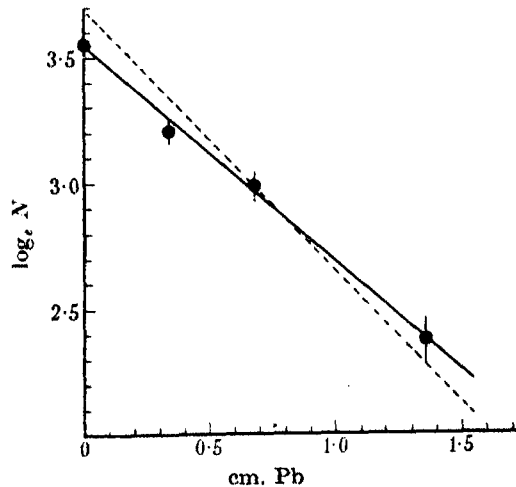


FIGURE 3. The absorption curve of cosmic-ray photons.  $s = 0.35$  cm. Pb.  
● observed, ---- calculated.

the thickness of the absorbing screen  $S$ ). We have evaluated the expression (5) numerically for  $x = 0.35$  cm. Pb and  $x = 2.0$  cm. Pb using the values for  $\rho(E)$  given by Bethe and Heitler (see Heitler 1936). The results for lead are represented graphically in figures 3 and 4 by the dotted curves.

It appears from the calculations that the theoretical absorption curve  $A(x)$  is almost exactly exponential. The reasons for this are that the absorption coefficient of photons in the high-energy region varies only very slowly with the energy and that most of the observed anti-coincidences arise from a rather narrow band of the photon spectrum. As it can be seen from figures 3 and 4 the observed absorption curves are also closely exponential in form. The theoretical and experimental absorption coefficients are compared in table 5.

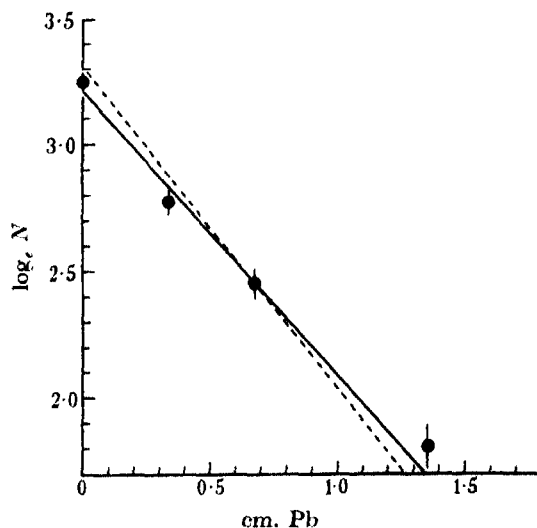


FIGURE 4. The absorption curve of cosmic-ray photons.  $s = 2.0$  cm. Pb.  
● observed, ---- calculated.

The absorption coefficient in lead found with  $s = 2.0$  cm. of lead is in good agreement with the theory, while the absorption coefficient with  $s = 0.35$  is rather smaller than the calculated one. This deviation may be partly due to the effect of electrons stopping in  $S$  as discussed above.

TABLE 6. ABSORPTION COEFFICIENTS OF COSMIC-RAY PHOTONS

| Material | $x$ cm. | $\mu$ cm. <sup>-1</sup> |                   |
|----------|---------|-------------------------|-------------------|
|          |         | Calc.                   | Obs.              |
| Pb       | 0.35    | 1.12                    | 0.85 $\pm$ 0.07   |
| Pb       | 2.00    | 1.19                    | 1.02 $\pm$ 0.07   |
| Fe       | 2.00    | 0.35                    | 0.54 $\pm$ 0.07   |
| Al       | 2.00    | 0.068                   | 0.085 $\pm$ 0.010 |

The observed absorption coefficients in Fe and Al seem to be both somewhat larger than calculated. On the whole, however, the agreement of observed and calculated values is satisfactory.

## 6. CONCLUSION

The cross-section for pair production by high energy photons has been measured and was found to be in agreement with that predicted by the theory of Bethe and Heitler for energies of about  $1.5 \times 10^8$  eV. The dependence of the absorption coefficient on the atomic number was found to be in fair agreement with theory for lead iron and aluminium absorbers.

The shower transition curve has been obtained for photon-initiated showers in lead. The result indicates a photon spectrum as given in equation (4), and confirms the conclusions of the cascade theory as extended by Arley.

The present experiments do not suggest the existence of non-ionizing particles other than photons. We estimate that if such non-ionizing particles occur at all in the cosmic-ray beam they did not produce more than about 10 % of the anti-coincidences at the maximum of the transition curve.

One of us (B. R.) has pleasure in expressing his thanks to the Society for the Protection of Science and Learning for financial support and to Professor P. M. S. Blackett for his hospitality in the laboratory at Manchester.

## SUMMARY

Photons unlike ionizing particles cannot be observed directly with counters. Owing to this difficulty very few investigations dealing with the photon component of cosmic radiation have been carried out. In the present paper a simple method is described which is suitable for the observations of cosmic-ray photons. The transition effect of photon-initiated showers in lead has been measured. The result is in agreement with the prediction of the cascade theory of Bhabha and Heitler as extended by Arley. The absorption coefficients of cosmic-ray photons have been measured in lead, iron and aluminium, and they agree with the theoretical values as given by Bethe and Heitler. The lower limit for the total flux of cosmic-ray photons above  $10^7$  eV has been found to be 10 % of the ionizing component of the cosmic-ray beam.

## REFERENCES

- Anderson, C. D. and Neddermeyer, J. H. 1934 *Phys. Rev.* **46**, 325.  
 Bethe, H. and Heitler, W. 1934 *Proc. Roy. Soc. A*, **146**, 83.  
 Bhabha, H. J. and Heitler, W. 1937 *Proc. Roy. Soc. A*, **159**, 432.  
 Blackett, P. M. S. 1938 *Proc. Roy. Soc. A*, **165**, 11.  
 Blackett, P. M. S. and Wilson, J. G. 1937 *Proc. Roy. Soc. A*, **160**, 304.  
 Carlson, J. F. and Oppenheimer, J. H. 1937 *Phys. Rev.* **51**, 220.  
 Gentner, W. 1935 *J. Phys. Radium*, **6**, 274, 340.  
 Heitler W. 1936 *Quantum theory of radiation*. Oxford.  
 — 1937 *Proc. Roy. Soc. A*, **161**, 261.  
 McMillan, E. 1934 *Phys. Rev.* **46**, 325.  
 Nielsen, W. M. and Morgan, K. Z. 1938 *Phys. Rev.* **53**, 915.  
 Nordheim, L. W. and Hobb, M. H. 1939 *Phys. Rev.* **56**, 494.  
 Rossi, B. 1930 *R.C. Accad. Lincei*, **11**, 831.  
 — 1933 *Z. Phys.* **82**, 151.  
 Williams, E. J. 1939 *Proc. Roy. Soc. A*, **172**, 194.  
 Wilson, J. G. 1938 *Proc. Roy. Soc. A*, **166**, 482.  
 — 1939 *Proc. Roy. Soc. A*, **174**, 72.

## Crystal boundaries in tin

BY BRUCE CHALMERS, PH.D.

(Communicated by E. N. da C. Andrade, F.R.S.—Received 2 December 1939)

## INTRODUCTION

When an ingot of tin is melted, it can be seen that the crystals break off as if the material forming the crystal boundaries melts at a lower temperature than the crystals themselves. It is impossible, however, to draw any quantitative conclusions from observations of this kind, although such results would yield much wanted evidence as to the nature of the crystal boundary. In particular, it would be of interest to evaluate the temperature difference referred to, and to determine to what extent it varies with the amount of impurities present and with the angle between the crystallographic axes of the two crystals between which the boundary occurs. The present paper describes a series of experiments in which specimens consisting of two crystals with a single boundary between them were examined from this point of view.

## EXPERIMENTAL METHOD

The experimental procedure consisted of the preparation of the specimens and the measurement of the temperatures at which the boundary melted and at which the crystals melted.

*(a) Preparation of specimens*

It was necessary to evolve a technique for the preparation of "bicrystal" specimens in which the angle between the axes is under control, and which are of such a shape that a tension can be applied normally to the boundary. Previous work (Chalmers 1937) has shown that it is possible to prepare cylindrical bicrystal specimens, with the boundary forming a plane containing the axis of the cylinder. Such a shape is not suitable for the present purpose, but the general method, i.e. the growth of the bicrystal from two seed crystals of known orientations, was taken as the starting point for the

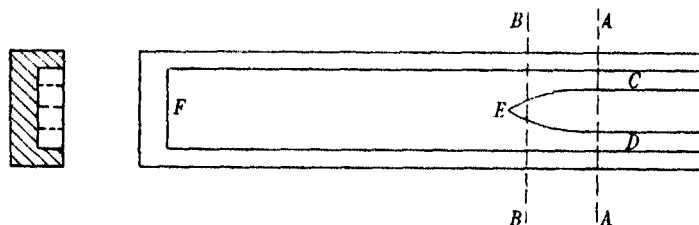


FIGURE 1

development of a new technique. The following procedure was finally adopted. Plaster of Paris "boats" were made of the shape shown in the diagram (figure 1). The boats were painted with an aqueous suspension of colloidal graphite in order to avoid the possibility of contamination of the metal by the material of the boat. In order to prepare a bicrystal specimen, the boat was supported horizontally on a carriage so that it was inside an electric tube furnace from the left-hand end as far as *AA* (figure 1). The carriage was so arranged that it could be drawn to the right at a speed of 0.4 cm./min. The boat was heated up to about 250°C and molten tin at the same temperature was poured into it so that it was filled from the left-hand end to the line *BB*, the depth being sufficient to fill the boat. The surface tension of the tin was sufficient to prevent it flowing beyond the line *BB*. Single crystals were then inserted in the grooves *C* and *D* and set to the required orientations. The boat was then moved a short distance further into the furnace, so that the ends of the "seed" crystals in *C* and *D* were melted and formed a continuous liquid with that already there. It was sometimes found useful to heat the junction of the seed crystals and the main

liquid with a small flame in order to encourage coalescence. As soon as this stage was reached, the mechanism was started for withdrawing the boat from the furnace. As the metal cooled, freezing progressed from right to left, and the metal solidified as two crystals with one boundary running the entire length of the specimen, i.e. from *E* to *F*. This did not occur unless the two seed crystals were symmetrically oriented with respect to a plane perpendicular to the diagram and containing the line *EF*. In other cases the boundary started at *E* and followed a line inclined to *EF*. This appears to be due, at any rate in part, to the fact that the boundary tends to travel perpendicularly to the freezing isothermal and that the differing thermal conductivities of the crystals in different crystallographic directions prevent the temperature gradient from following its normal course which is perpendicular to *EF*. It is possible that a factor connected with the speed of crystal growth in various crystallographic directions may also be concerned.



FIGURE 2

The tendency of the crystal boundary to remain perpendicular to the freezing isothermal was well illustrated in the following experiment in which an attempt was made to grow crystals in such a way that the material near the boundary was not disturbed when the specimen was cut transversely in order to obtain specimens of the required size. Boats were prepared as shown in figure 2, the islands *A*, *B*, *C*, etc., consisting of small blocks of plaster of Paris that penetrated the specimen. It was hoped that the boundary would follow a straight line from *E* to *F*, in which case cutting could be carried out at *A*, *B*, *C*, etc., with no danger of disturbing the part of the specimen near the boundary. Instead, however, the boundary always followed a line like the dotted line in figure 2. This is explained by the fact that the island *A*, for example, has no latent heat and a much smaller heat capacity than the tin, and so it cools very much more rapidly than the tin; the isothermals are accordingly modified, e.g. *PQ*. At *RS*, however, the cooling is greatest at the edges, and so the isothermal is curved; this accounts for the curious form of the boundary. It also accounts for the striking way in which the boundary keeps to the centre in a specimen in which there are no "islands" to disturb the isothermals. In such cases, the isothermals are all of the form *RS*, and any deviation from the centre will result in the boundary being turned back towards the centre owing to the curvature of the isothermal.

Although it should be possible to overcome the ineffectiveness of the "islands" by supplying them with heat in some other way, it was decided to abandon this method and to minimize the severity of the cutting operation by providing grooves penetrating half way through the specimen by means of suitable ridges on the bottom of the boat. This was found to be quite satisfactory, the final separating cut being made by means of a fairly fine saw. The specimens as cut were roughly 2 cm. by 5 mm., each crystal being  $1 \times 1 \times 0.5$  cm. and the boundary about  $1 \times 0.5$  cm. in area.

After some preliminary experiments it was found necessary to prepare the specimens with thermocouples embedded in them, so that the actual thermojunction was as close to the boundary as possible. This was accomplished by making small thermocouples of 47 s.w.g. eureka and copper wires, the junction being fused into the end of a very fine glass tube that served to insulate the couple from the specimen. The wires were insulated from each other inside this tube by inserting one of them in a still thinner capillary tube. The external diameter of the outer tube was usually under 0.5 mm. These thermocouples were fixed into the boats so that the junctions were very close to the eventual position of the boundary, and so that each couple was in the centre of a specimen as determined by the cutting grooves.

#### (b) *Measurement of melting-points*

The experiments consisted in measuring, for each specimen, the temperature at which the two crystals separated under a given tension, and the temperature at which one of the crystals melted.

The specimen was set up so that the half containing the thermocouple was held in a clip that was just sufficiently tight to prevent slipping, while the other end, previously drilled with a thin drill, was pulled upward by means of a wire fixed through the hole in the specimen. The wire was attached to a lever to which any required force could be applied by dead loading. By this method a force was applied normally to the boundary, i.e. tending to pull the crystals apart. The specimen was heated in a bath of oil that was heated slowly and stirred vigorously. The temperatures were measured by means of a Tinsley potentiometer using the following procedure. The potentiometer was set so that no deflexion was obtained at a temperature approximating to the melting-point, and the deflexion was observed when the crystals separated. The deflexion was again observed when it became steady, indicating that melting had commenced. The deflexion per microvolt was determined for each couple by observing the change of deflexion when the potentiometer setting was altered by a definite amount during the period of steady deflexion. A typical thermocouple was also calibrated for microvolts



per degree by comparison with a thermometer over a range of temperature near the melting-point. The indicating system was a galvanometer with a sensitivity of 185 mm./ $\mu$ A at 1 m. and a resistance of 11 ohms. The scale distance was 2 m. The sensitivity was such that a deflexion of 1 mm. corresponded to a change of temperature of about 0.01° C. Although the setting of the potentiometer could not be read to this accuracy, the difference between two temperatures, both of which are measured without altering the setting, depends upon the accuracy with which the galvanometer deflexion can be read, and the error of such a reading should not exceed 0.005° C.

#### EXPERIMENTAL RESULTS

The results of the boundary fusion experiments show that the temperature at which the two crystals separate is independent of the tension between the limits 1000 g. wt./cm.<sup>2</sup>, and 3000 g. wt./cm.<sup>2</sup> and is also independent of the rate of heating within quite wide limits.

In these experiments seed crystals were always prepared with the *c* axis perpendicular to the length of the specimen. The following table contains the results of experiments on the effect of the angle *A* between the *c* axes of the two crystals, and the difference between the melting-point of the boundary and that of the crystals for Chempur tin (purity 99.986%).

|                                 |               |               |               |               |
|---------------------------------|---------------|---------------|---------------|---------------|
| Angle <i>A</i>                  | 85°           | 80°           | 72°           | 52°           |
| Temperature difference<br>(° C) | 0.148 ± 0.005 | 0.143 ± 0.005 | 0.139 ± 0.005 | 0.137 ± 0.005 |
| Angle <i>A</i>                  | 45°           | 26°           | 14°           |               |
| Temperature difference<br>(° C) | 0.137 ± 0.005 | 0.137 ± 0.005 | 0.143 ± 0.005 |               |

The experiment was also performed on tin of the following degrees of purity: (a) 99.998 %, (b) 99.996 %, (c) 99.986 % (Chempur), (d) Chempur + 0.05 % lead, (e) Chempur + 0.2 % lead, the angle *A* in each case being about 45°. The temperature differences obtained were

$$(a) 0.14^{\circ}, \quad (b) 0.14^{\circ}, \quad (c) 0.14^{\circ}, \quad (d) 0.24^{\circ}, \quad (e) 0.70^{\circ},$$

showing that the amount of impurity must be increased considerably before it has any appreciable effect on the temperature difference. A further observation was that in one case, with Chempur tin, the boundary moved from its original position before fracture took place; fracture occurred at the site of the new boundary.

The macro-mosaic effect, sometimes observed in large single crystals, was found to be present in certain single crystals grown by the method adopted.

When such specimens are heated, there is some evidence of fusion of the boundaries of the structure, but no fracture was obtained. This is taken to indicate that the macro-mosaic structure does not extend through the whole thickness of the crystal.

#### DISCUSSION OF RESULTS

The first step in considering the relation of the results detailed above to the theory of the crystal boundary is to form a clear picture of the process by which a boundary is formed. It is necessary at the outset to distinguish between two kinds of boundary, differing in their mode of formation and probably also in their properties. The first type of boundary is that which forms between two crystals while they are both growing, and consequently comes into being simultaneously with considerable parts of the two crystals. This type of boundary grows in a direction at right angles to the isothermal at the freezing-point. This is the type of boundary that accompanies the production of a columnar structure, in which the crystals grow in a direction perpendicular to the surface from which cooling takes place, and for brevity it will be referred to as a columnar boundary. The second type of boundary arises as a result of a different process, the details of which are as follows. When a crystal grows from the melt, the solid that separates is generally purer than the liquid that remains. This depends, of course, on the lowering of melting-point by impurities, and the fact that the solidus at a given temperature represents a purer material than the liquidus at the same temperature. This process, which is continually being counteracted by the process of diffusion in the liquid, must result in a redistribution of impurities so that they are more concentrated in the liquid near the liquid-solid interface than elsewhere.

If the liquid is cooled uniformly from one end, the distribution of temperature will take the form shown in figure 3, curve *A*, in which  $x$  represents the distance from the hotter end. The "hump" at *P* is due to the evolution of the latent heat. On account of the redistribution of impurities mentioned above, the melting-point of the material will vary with  $x$  in the manner shown in figure 3, curve *B*. The third curve, figure 3, curve *C*, indicates how far the material at any point is above its own melting-point, the point *Q* representing the position of the solid-liquid interface. The effect of further cooling of the liquid may be either to even out the melting-point curve as a result of the diffusion of impurities in the liquid, or else, if the cooling is more rapid, the lowering of the general temperature may result in the metal at the point *R*, figure 3, reaching its freezing-point before the material to the

right of it. This will cause the formation of solidification nuclei at *R* and these will grow in all directions, including to the right. The boundary formed between *C* and the existing crystal will be formed parallel to the isothermal, and will necessarily contain an excessive amount of impurities. It may be noted that columnar type boundaries may form between crystals of the type just described, but not between such crystals and the already existing solid. The chief difference between the columnar boundaries and the second or

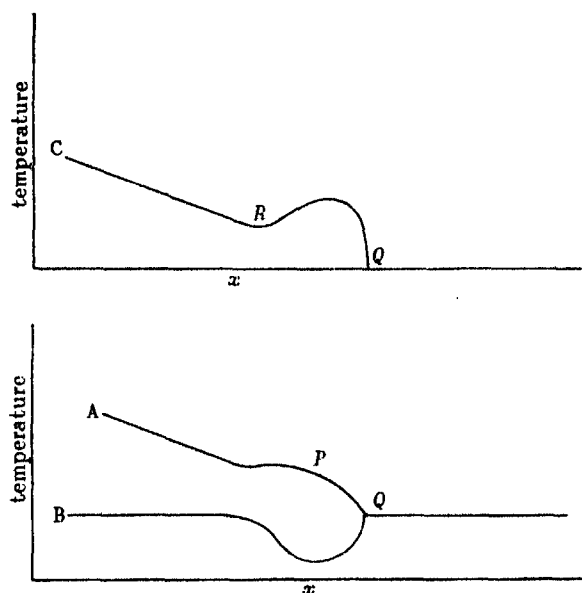


FIGURE 3

segregation type is the mechanism by which impurities are caused to segregate or concentrate at the boundaries. It will be realized that the familiar "ingot" structure, in which the outer crystals are columnar and the inner ones equiaxed, illustrates the difference between the two types of boundary growth. The columnar structure, due to growth of crystals from nuclei formed at the surface, persists until the increasing concentration of impurities in the melt causes fresh nuclei to be formed in the liquid as a result of the process described above. These nuclei, which are surrounded by liquid, grow outwards in all directions, the result being an equiaxed structure. It has been pointed out by Andrade and Roscoe (1937) that fresh nuclei may form in the liquid as a result of the cooling conditions in the absence of impurities. In such cases, the melting-point curve (figure 3 B) will be a straight

line and the effect is entirely due to the evolution of latent heat. A more thorough analysis of this case will be found in the paper referred to.

The conclusion reached above, that the segregation type of boundary grows parallel to the freezing isothermal, is probably only true in connexion with the general direction of the isothermal. The boundary must always grow in a direction perpendicular to the isothermal in its immediate neighbourhood, but owing to the irregularities set up by the evolution of latent heat, the local direction of an isothermal may be quite different from its general direction. It is evident that the present series of experiments is concerned with boundaries of the columnar type.

The most obvious explanation of the observation that the boundary fuses at a lower temperature than the crystalline material is that it is due to impurities, but this cannot be accepted for the following reasons. In the first place, the measured temperature difference is independent of the amount of impurity present if this does not exceed about 0.02 %, whereas the influence of 0.05 % is quite pronounced. It is known, however, that the impurities present in "Chempur" tin (0.02 %) cause a definite lowering of the melting-point of the order of 1° C (Homer and Plummer 1939). This shows that an amount of impurity which causes a considerable change of melting-point does not cause a measurable difference in the boundary fusion effect and that it requires a greater concentration of impurity to increase the difference of melting-points.

A second reason that leads to the same conclusion is that there would be no tendency for the impurities to segregate on a columnar boundary unless this in itself had a lower freezing-point than the normally crystalline material. A third justification for this point of view follows from the observation that when the crystal boundary moves, owing to some action connected with the process of grain growth, the fracture takes place at the new position of the boundary and not at its original site.

It is concluded, therefore, that the same material may have different melting-points according to whether it is crystalline or forms a crystal boundary. This must be due to the differing atomic arrangement of the atoms at the boundary, and the alternative explanations that have been offered are that the boundary material forms a separate phase in which the atoms are disposed at random about their normal atomic spacing, i.e. as in a liquid, or that the atoms are in their geometrically determined positions on the lattices of the two crystals as distorted by their mutual proximity. These two views can be referred to as the "amorphous layer" theory, and the "transitional lattice" theory. The amorphous layer theory does not explain the experimental results because an amorphous material should not possess

a sharp melting-point but should pass from solid to liquid by a continuous change of viscosity, whereas it has been shown in the present experiments that a sharp melting-point does, in fact, exist.

The other explanation, that the atoms occupy a transitional lattice, postulates that each atom in the boundary region is held in place by a system of forces similar to that which would act if the atom were in the normal crystal lattice. Since the boundary is, according to this view, a compromise between two mutually incompatible lattices, the atomic positions and the interatomic forces must differ from the values pertaining to the undistorted lattice. Some or all of the atomic distances will be in excess of the usual lattice values, and this can only be due to the action of tensional forces. These tensions are the resultants of the distorted lattice forces, and must be counterbalanced by compressive forces on other atoms. It is suggested that the observed depression of the melting-point of the boundary material below that of the crystalline material is due to these tensions. The effect of the compression can be disregarded as fusion will depend on the lowest melting-point constituent.

It is possible to calculate the value of the tension that will result in the observed lowering of the melting-point as follows, using the thermodynamic relation

$$\frac{L}{T} = (v_2 - v_1) \frac{dp}{dT},$$

where  $L$  is the latent heat,  $T$  is the absolute temperature,  $v_1$  and  $v_2$  the specific volumes of the liquid and solid, and  $p$  the pressure.

Using the following values for tin:

$$L = 14 \text{ cal./g.}, \quad T = 505^\circ \text{K}, \quad v_2 = 0.143 \text{ c.c./g.}, \quad v_1 = 0.139 \text{ c.c./g.},$$

it follows that 
$$-\frac{dp}{dT} = 3.1 \times 10^2 \text{ kg./cm.}^2/\text{°C},$$

then the tension required to produce a lowering of melting-point of  $0.14^\circ \text{C}$  is equal to  $43 \text{ kg./cm.}^2$ .

It is interesting to consider the elastic energy that a tin crystal would possess if it could be stretched by a force of this magnitude. Using Cuthbertson's value (1939) for the Young's modulus of tin at its melting-point, i.e.  $1.2 \times 10^5 \text{ kg./cm.}^2$ , the energy stored is found to be of the order of  $10^5 \text{ ergs/cm.}^3$ , or  $0.01 \text{ Joules/cm.}^3$ . This is less than, but comparable with, the values of energy stored in cold-worked aluminium ( $0.47 \text{ Joules/g.}$ ) and copper ( $0.12 \text{ Joules/g.}$ ) found by Rosenhain and Stott (1933). It is also

comparable with the figures given by Farren and Taylor (1925) for experiments of a similar type.

It appears reasonable to suppose, therefore, that the boundary material consists of, or contains, atoms that are displaced from their equilibrium lattice positions so that they possess this amount of strain energy, and that this is the maximum strain energy that the material can retain. It does not appear from these experiments whether the amount of material with this added strain energy is dependent on the difference of orientation of the two crystals, but it seems probable that this is the case. It is clear, however, that boundaries in which the values of this angle vary between  $14^\circ$  and  $85^\circ$  contain material with the same maximum strain energy. It is perhaps significant that the boundary between twinned and untwinned parts of a crystal, prepared in the way described in a previous publication (Chalmers 1935), does not melt at a lower temperature, within the limits of the experiments, than the crystals themselves.

The macro-mosaic effect, referred to in the second section of the paper, appears to correspond to a case where a boundary between crystals, whose orientations differ by less than  $2^\circ$ , only penetrates part of the thickness of the specimen. The two surface crystals are both continuous with the same crystal, the difference of angle between them resulting from the "tolerance" which a crystal displays to slight variations in orientation of the material that grows on to it. This may happen when the small angles that normally occur between the mosaic blocks happen to be oriented favourably, so that their effects accumulate. This effect may be conditioned by the relative directions of the crystal axes and the direction of growth. It is often observed, for example, that the lines of separation of the macro-mosaic elements are parallel to the boundary of the bicrystal. This effect is receiving further attention.

In conclusion, the author wishes to record his appreciation of the encouraging interest taken in this investigation by Professor E. N. da C. Andrade, F.R.S. This work forms part of a programme of research carried out in the laboratories of the International Tin Research and Development Council. The author is indebted to the Council for permission to publish.

#### SUMMARY

A new technique is described for preparing specimens of tin consisting of two crystals of controlled orientation of such a size and shape that a tension can be applied transversely to the boundary. It is found that the temperature

at which the crystals separate under tension is below the melting-point of the crystalline material, and that the difference is independent of the angle between the crystal axes of the two crystals and of impurity providing this does not exceed about 0.02 %. The mechanism of boundary formation is considered, a distinction being drawn between two types of boundary described as "columnar" and "segregational". The structure of the boundary is discussed in the light of the new experimental evidence, which favours a "transitional lattice" rather than an "amorphous layer" theory.

## REFERENCES

- Andrade, E. N. da C. and Roscoe, R. 1937 *Proc. Phys. Soc.* **49**, 152.  
 Chalmers, B. 1935 *Proc. Phys. Soc.* **47**, 733.  
 — 1937 *Proc. Roy. Soc. A*, **162**, 120  
 Cuthbertson, J. W. 1939 *J. Inst. Met.* **64**, 209.  
 Farren, W. S. and Taylor, G. I. 1925 *Proc. Roy. Soc. A*, **107**, 422.  
 Homer, C. E. and Plumner, H. 1939 *J. Inst. Met.* **64**, 169.  
 Rosenhain, W. and Stott, V. H. 1933 *Proc. Roy. Soc. A*, **47**, 733.

---

## Comparison of the acceleration due to gravity at the National Laboratory, Teddington and the Bureau of Standards, Washington, D.C.

BY B. C. BROWNE AND E. C. BULLARD

*Department of Geodesy and Geophysics, Cambridge*

(Communicated by Sir Gerald P. Lenox-Conyngham, F.R.S.—

Received 20 December 1939)

For many years values of gravity all over the world have been obtained relative to that at Potsdam by observations with invariable pendulums. The value at Potsdam was determined by Kühnen and Furtwängler (1906) by Kater's method and a standard error of 0.003 cm./sec.<sup>2</sup> was claimed for the result. Any error in the Potsdam value would involve an equal error in the related values all over the world. As the acceleration of gravity is involved in all measurements of force with the balance and thus in the unit of electric current and in such quantities as the velocity of an  $\alpha$ -particle, it is important to know whether the accepted value at Potsdam has the accuracy claimed for it. A recent absolute determination by Heyl and

Cook (1936) at the National Bureau of Standards, Washington, D.C., gave a result  $0.020 \text{ cm./sec.}^2$  less than that obtained by comparison with Potsdam, whilst one by Clark at the National Physical Laboratory, Teddington gave  $0.013_8 \text{ cm./sec.}^2$  less. The relative gravity connexion between Potsdam and Washington is strong, but those between Teddington and Washington and between Teddington and Potsdam are weak and indirect. Advantage has therefore been taken of the visit of the authors to Washington to attend the recent meeting of the International Union of Geodesy and Geophysics to make a comparison of the values of  $g$  at the places used for the absolute determinations at the National Physical Laboratory and at the National Bureau of Standards. It had been intended also to connect the National Physical Laboratory directly with Potsdam, but the outbreak of war has made it necessary for this to be postponed.

The two-pendulum apparatus belonging to the Department of Geodesy and Geophysics of Cambridge University was used with six half-seconds invar pendulums numbered 1A, 1B, 1C, 6A, 6B, and 6C. A photograph of this apparatus has been given by Bullard (1936, plate 28, lower figure). As the manometer generally used to measure the pressure inside this apparatus has shown a tendency to stick, a new one with a 3 mm. bore was provided and was connected externally so that it could be tapped before reading. The pendulums were timed against seconds signals derived from the quartz oscillator frequency standards of the laboratories. At the National Physical Laboratory the 100,000 cycle frequency derived from the crystal is demultiplied to 1000 cycles and used to drive a phonic motor which closes a switch for a few thousandths of a second every second. Current controlled by this switch was fed to a moving iron oscillograph and recorded on moving bromide paper. The transits of the pendulums through their equilibrium positions were also recorded on this paper. The recording arrangements and chronograph were those described by Bullard (1933). At the National Bureau of Standards the arrangement was similar except that the seconds signal consisted of five cycles of a thousand cycle current every second, the five cycles being selected by a multivibrator and the timing being thus independent of any mechanical contact. The rate of the crystal at the National Physical Laboratory was determined by daily comparisons with the 10 a.m. signal from Rugby, the corrections given by Greenwich in the Admiralty Notices to Mariners being applied. At the National Bureau of Standards signals and corrections from the Naval Observatory were used. In both cases the rate is derived from smooth curves drawn through the time signal observations for some days before and after the gravity measurements. The comparisons of the clocks with



the signals and the computations of the rates were done by the staffs of the laboratories.

The pendulums were swung in pairs in opposite phase to eliminate sway of the support. Four one-hour observations were made with each pair and the same four pairs (1A and 1C, 1A and 1B, 6A and 6C, 6A and 6B) were observed on the same agate blocks at both stations. The opening observations were made at the National Physical Laboratory from 27 July to 3 August 1939, 1A and 1C were first observed followed by 1A and 1B. After the latter measurements a few cu.mm. of oil were found on the bob of 1A. This oil had presumably been blown on to the pendulums from the bore of one of the taps when letting air into the apparatus. It was unfortunately impossible to say whether this had happened before the start of the measurements, between those on the two pairs, or after those on the latter pair; it was therefore thought desirable to repeat the measurements on 1A and 1C and to reject the measurements on 1A obtained previously. When the results were worked out it was found that the mean of the eight rejected values of the period only differed by  $0.5 \times 10^{-7}$  sec. from the mean of the four repeat measurements. This small difference is of no practical importance, and means that either the oil got on the pendulum after the swings or that its centre of gravity happened to coincide with that of the pendulum.

The measurements at the National Bureau of Standards were made between 7 and 12 September 1939 and the closing measurements at the National Physical Laboratory between 1 and 4 October 1939. The individual swings were satisfactorily concordant, the probable errors of a single swing deduced from the deviations of the individual pendulums from the mean being:

| Single<br>pendulum | Mean<br>of a pair | Difference<br>of a pair   |
|--------------------|-------------------|---------------------------|
| 1.1                | 0.73              | $1.5 \times 10^{-7}$ sec. |

It is noteworthy that the difference in the periods of a pair of pendulums is more variable than their mean period. This is probably due to the effect of small ground motions being eliminated from the mean whilst it is doubled in the difference. Previously this effect has been obscured by errors from other sources (see Bullard 1936, p. 467). The probable error of the mean can be accounted for by the known errors of measurement.

As the scatter of the measured periods is so small ( $1 \times 10^{-7}$  sec. is equivalent to four parts in ten million in  $g$ ) it is not thought necessary to reproduce the 104 individual periods. The mean periods for the pairs reduced to zero

pressure, 0° C and zero arc are given in table 1, each entry is the mean of four observations. The means for each pendulum are summarized in table 2. The changes in period between the first and last sets at the National Physical Laboratory are rather larger than has been usual in recent years with these pendulums. This may be due to the pendulums having travelled in their boxes in a large packing case packed all round with a foot of wood wool instead of being carried by hand as is usual. In order to determine whether any pendulum had suffered a large change on the way to or from Washington the differences of the period of each from the mean of the six were found, the changes in these differences (table 3) do not indicate any striking change. The mean of the initial and final sets has therefore been used for each pendulum and the ratio of the values of  $g$  at the two stations calculated. Then, using Clark's value at Teddington, the value at Washington was found. The results are given in the last line of table 2. Rounded off to the nearest 0.001 five pendulums give 981.085 and one gives 981.083, the mean is 981.0848. At the National Physical Laboratory the instrument rested at floor-level on the pillar used by Clark, the mean height of the centre of gravity of his pendulum was 1.0 m. above the floor. At the National Bureau of Standards our instrument was on the floor 4 m. to the north of the position of Heyl and Cook's pendulum and 2 m. to the north-east and at the same level as the point used by E. J. Brown (1936) for his relative measurements.\* As the mean centre of gravity of Heyl and Cook's pendulums was 1.5 m. above the floor a correction of  $-0.0002 \text{ cm./sec.}^2$  is required and the final result is

$$\text{National Bureau of Standards (Heyl and Cook's station)} = 980.0846 \text{ cm./sec.}^2,$$

based on Clark's result

$$g \text{ (National Physical Laboratory)} = 981.1815 \text{ cm./sec.}^2.$$

Heyl and Cook's result is

$$g \text{ (Bureau of Standards)} = 980.080 \text{ cm./sec.}^2,$$

which is  $0.0046 \text{ cm./sec.}^2$  lower. Clark ascribes a "possible range of about 1.5 mgal." to his result. Heyl and Cook round their result off to " $980.08 \pm 0.003$  (average deviation)"; their result is probably also uncertain by 1 or 2 mgal. The uncertainty of the relative determination depends almost entirely on the changes in the pendulums. From the differences between the results with the different pendulums a probable error of 0.51 mgal. is

\* Brown allows for his pendulums being below Kühnen and Furtwängler's but not for their being below Heyl and Cook's.

TABLE 1

| Date<br>1939 | Periods $\times 10^7$ sec.               |           |           |
|--------------|--|-----------|-----------|
|              | National Physical Laboratory (1st visit) |           |           |
|              | 1A                                       | 1B        | 1C        |
| 27 July      | 5062486.9*                               | —         | 5062479.4 |
| 28 „         | 5062487.1*                               | 5062491.8 | —         |
| 2 and 3 Aug. | 5062486.5                                | —         | 5062478.3 |
|              | 6A                                       | 6B        | 6C        |
| 31 July      | 5054602.7                                | —         | 5054609.2 |
| 1 Aug.       | 5054600.4                                | 5054643.4 | —         |
|              | National Bureau of Standards             |           |           |
|              | 1A                                       | 1B        | 1C        |
| 7 Sept.      | 5065318.3                                | —         | 5065312.7 |
| 8 „          | 5065320.5                                | 5065326.6 | —         |
|              | 6A                                       | 6B        | 6C        |
| 9 „          | 5057429.0                                | —         | 5057434.8 |
| 12 „         | 5057429.2                                | 5057477.2 | —         |
|              | National Physical Laboratory (2nd visit) |           |           |
|              | 1A                                       | 1B        | 1C        |
| 3 Oct.       | 5062491.7                                | —         | 5062486.5 |
| 4 „          | 5062491.4                                | 5062498.6 | —         |
|              | 6A                                       | 6B        | 6C        |
| 1 Oct.       | 5054604.1                                | —         | 5054604.5 |
| 2 „          | 5054603.8                                | 5054648.2 | —         |

\* Oil on pendulum 1A?

TABLE 2. MEAN PERIODS

|                    | 1A        | 1B        | 1C        | 6A        | 6B        | 6C                              |
|--------------------|-----------|-----------|-----------|-----------|-----------|---------------------------------|
| N.P.L. (1st visit) | 5062486.5 | 5062491.8 | 5062478.8 | 5054601.6 | 5054643.4 | 5054609.2 $\times 10^{-7}$ sec. |
| N.P.L. (2nd visit) | 5062491.6 | 5062498.6 | 5062486.5 | 5054604.0 | 5054648.2 | 5054604.5 „                     |
| Difference         | + 5.1     | + 6.8     | + 7.7     | + 2.4     | + 4.8     | - 4.7 „                         |
| Mean N.P.L.        | 5062489.0 | 5062495.2 | 5062482.6 | 5054602.8 | 5054645.8 | 5054606.8 „                     |
| N.B.S.             | 5065319.4 | 5065326.6 | 5065312.7 | 5057429.1 | 5057477.2 | 5057434.8 „                     |
| $g$                | 980.0853  | 980.0849  | 980.0854  | 980.0852  | 980.0833  | 980.0845 cm./sec. <sup>2</sup>  |

Mean  $g$  at National Bureau of Standards = 980.0848 cm./sec.<sup>2</sup>.

TABLE 3. DIFFERENCES OF INDIVIDUAL PENDULUMS FROM MEAN

|                                | 1A     | 1B     | 1C     | 6A       | 6B       | 6C                             |
|--------------------------------|--------|--------|--------|----------|----------|--------------------------------|
| N.P.L. (1st visit)             | 3934.6 | 3939.9 | 3926.9 | - 3950.3 | - 3908.5 | - 3942.7 $\times 10^{-7}$ sec. |
| N.B.S.                         | 3936.1 | 3943.3 | 3929.4 | - 3954.1 | - 3905.9 | - 3948.6 „                     |
| N.P.L. (2nd visit)             | 3936.0 | 3943.0 | 3930.9 | - 3951.6 | - 3907.4 | - 3951.1 „                     |
| Change on way<br>to Washington | + 1.5  | + 3.4  | + 2.5  | - 3.8    | + 2.6    | - 5.9 „                        |
| Change on way<br>back          | - 0.1  | - 0.3  | + 1.5  | + 2.5    | - 1.5    | - 2.5 „                        |

obtained for the result from a single pendulum and 0.21 mgal. for that from the mean. If the changes in period found on returning to the National Physical Laboratory are regarded as a measure of the uncertainty in the Washington-Teddington difference a probable error of 1.5 mgal. is found for a single pendulum and 0.63 mgal. for the mean of the six. The latter is likely to be an overestimate of the uncertainty as the changes are partially eliminated by taking the mean of the initial and final measurements. Systematic errors might be caused by uncertainties in the constants used to reduce the periods to 0° C, vacuum and zero arc, but the differences in pressure, temperature and arc are so small (table 4) that the error produced cannot exceed a few tenths of a milligal (Bullard and Jolly 1936, p. 468; Mace and Bullard 1939). The uncertainty in the clock rates certainly does not exceed 0.01 sec./day and cannot contribute more than a few parts in  $10^7$  to the uncertainty in  $g$ . On the whole a probable error of 0.001 cm./sec.<sup>2</sup> for the relative connexion and 0.002 for each absolute measurement seems a conservative estimate. This gives a probable error of 0.003 cm./sec.<sup>2</sup> for the comparison of Clark's and Heyl's results. The observed discrepancy of 0.0046 is therefore satisfactory, and both absolute determinations can be regarded with considerable confidence.

TABLE 4. MEAN PRESSURES, TEMPERATURES AND AMPLITUDES

|                    | Pressure<br>mm. Hg | Temperature<br>° C | Double<br>amplitude<br>radians |
|--------------------|--------------------|--------------------|--------------------------------|
| N.P.L. (1st visit) | 30.6               | 19.8               | 0.0192                         |
| „ (2nd visit)      | 29.8               | 18.7               | 0.0183                         |
| „ mean             | 30.2               | 18.2               | 0.0187                         |
| N.B.S.             | 31.8               | 22.8               | 0.0179                         |

The observed difference between Washington and Teddington may also be compared with that obtained from previous relative determinations. The relevant connexions are indicated in figure 1, those between the English stations and Potsdam and De Bilt were subjected to a least squares adjustment by Bullard and Jolly (1936, see also a correction, 1937) with the result\*

$$g \text{ (National Physical Laboratory)} = 981.1953,$$

\* Clark gives the value at Potsdam, derived from his absolute determination and this connexion, as 981.2612; this should be 981.2602, the error has arisen through a confusion between the *Pendelsaal* where the absolute measurement was made and the *Ost Keller* which is generally used for relative determinations and where  $g$  is greater by 0.001.

relative to Kühnen and Furtwängler's absolute measurement at Potsdam. E. J. Brown's connexion of Potsdam and the Bureau of Standards gave

$$g \text{ (National Bureau of Standards)} = 980.1000$$

relative to Potsdam. The difference is 1.0953 compared to our observed difference of 1.0969. This agreement is better than might have been anticipated from the number of links in the chain. A least squares adjustment of the net is not worth while at present as it will be considerably strengthened when the National Physical Laboratory, Cambridge and Potsdam have been connected.

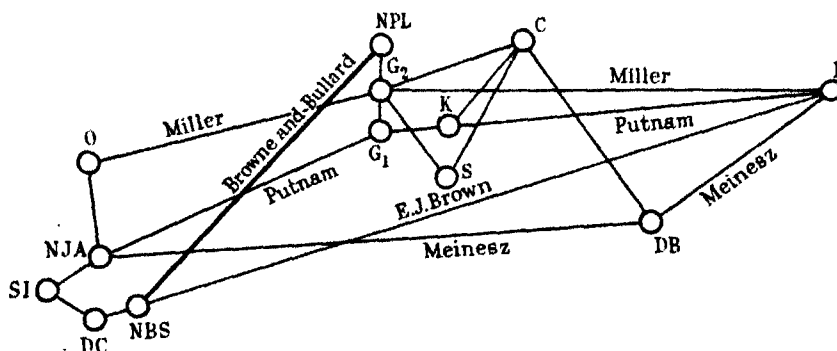


FIGURE 1. Relative gravity connexions. P = Potsdam, DB = De Bilt, C = Cambridge, S = Southampton, K = Kew,  $G_1$  = Greenwich (Record Room),  $G_2$  = Greenwich (National Station), NPL = National Physical Laboratory, O = Ottawa, NBS = National Bureau of Standards, DC = Department of Commerce, Washington, SI = Smithsonian Institution, Washington, NJA = 205 New Jersey Avenue, Washington.

The agreement of the two recent absolute determinations leaves little doubt that the Potsdam value is considerably in error. According to Heyl and Cook's absolute determination and E. J. Brown's Washington-Potsdam connexion it is 0.020 cm./sec.<sup>2</sup> too high, according to Clark's absolute determination and Bullard and Jolly's (1936) reduction of the relative connexions it is 0.0138 too high. Using Clark's absolute determination and the Teddington-Washington-Potsdam relative connexions it is 0.0154 too high. Considering the uncertainties of the various measurements we regard -0.017 as the best correction and as being consistent with all the data. This correction should be applied to values in the Potsdam system when values of  $g$  are to be used in connexion with other physical quantities (for example in the determination of the electrical units), but it should not be applied in calculating gravity anomalies for geophysical purposes. A gravity anomaly is the difference between observed gravity and that calculated from an expression representing "normal

gravity", the latter is itself derived from a large number of observations scattered all over the earth, and a correction applied to the observed values would therefore involve a correction to the "theoretical" values and would leave the anomalies unchanged. The correction should therefore not be applied to values of  $g$  for geophysical purposes unless the normal gravity formula is also changed and it is undesirable that this should be done without international agreement.

We are indebted to the Directors and Staffs of the National Physical Laboratory and of the National Bureau of Standards for providing facilities for this work and for assisting us in many ways. A large part of the computations were performed by Mr T. F. Gaskell of the Department of Geodesy and Geophysics to whom we wish to express our thanks. The expenses were met by a grant from the Government Grant Committee of the Royal Society.

#### SUMMARY

The values of the acceleration due to gravity at the points used for the recent absolute determinations at the National Physical Laboratory, Teddington, and at the National Bureau of Standards, Washington, D.C., have been compared. The difference found is  $1.096_g$  cm./sec.<sup>2</sup>. The difference between the two absolute determinations is  $1.101_g$  cm./sec.<sup>2</sup> whilst that deduced from previous indirect relative connexions is  $1.095_g$  cm./sec.<sup>2</sup>. The agreement is within the uncertainties of the measurements, and leaves little doubt that the hitherto accepted value at Potsdam is some seventeen parts in a million too great.

#### REFERENCES

- Brown, E. J. 1936 *Spec. Publ. U.S. Cst Geod. Surv.* no. 204.  
Bullard, E. C. 1933 *Proc. Roy. Soc. A*, **141**, 233-258.  
— 1936 *Phil. Trans. A*, **235**, 445-531.  
Bullard, E. C. and Jolly, H. L. P. 1936 *Mon. Not. R. Astr. Soc. Geophys. Suppl.* **3**, 443-477.  
— — 1937 *Mon. Not. R. Astr. Soc. Geophys. Suppl.* **4**, 132.  
Clark, J. S. 1939 *Phil. Trans. A*, **238**, 65-123.  
Heyl, P. R. and Cook, G. S. 1936 *Bur. Stand. J. Res., Wash.*, **17**, 804-839.  
Kühnen, F. and Furtwängler, P. 1906 *Veröff. preuss. geodät. Inst.*, N.F. no. 27.  
Mace, C. and Bullard, E. C. 1939 *Mon. Not. R. Astr. Soc. Geophys. Suppl.* **4**, 476.

# The kinetics of decarboxylation in solution

By P. JOHNSON AND E. A. MOELWYN-HUGHES

*The University Chemical Laboratory, Cambridge*

(Communicated by R. G. W. Norrish, F.R.S.—Received 21 December 1939)

In the study of chemical kinetics, great importance attaches to the manner in which the velocity coefficient,  $k$ , varies with the temperature,  $T$ . Their relation is generally expressed by the differential equation

$$\frac{d \ln k}{dT} = \frac{E_A}{RT^2}, \quad (1)$$

where  $E_A$  is now by common consent referred to as the apparent energy of activation. Integrating on the assumption that  $E_A$  is a constant, independent of temperature, we obtain the well-known equation of Arrhenius,

$$\ln k = B - \frac{E_A}{RT}. \quad (2)$$

Having regard to the accuracy usually ascribable to experimental velocity coefficients, the assumption is a valid one. In recent years, however, precise work on certain selected reactions has shown that the supposition is ill founded. The newer data are in better agreement with the differential equation

$$\frac{d \ln k}{dT} = \frac{E}{RT^2} + \frac{J}{RT}. \quad (3)$$

Integrating on the assumption that  $E$  and  $J$  are independent of temperature, we have the more general relation

$$\ln k = C + \frac{J}{R} \ln T - \frac{E}{RT}, \quad (4)$$

which reduces to the simpler formula when  $J$  is zero. This equation, though not wholly satisfactory, is to be regarded as an improvement on equation (2) because (1) it is in better accordance with experiment, and (2) it is not restricted to systems wherein the average energy of reactive molecules and the average energy of normal molecules respond identically to temperature.

Very few reactions have been examined with sufficient precision to allow of an evaluation of the constants in equation (4), and it is with the object of increasing their number that the present investigation was undertaken.

For the inversion of cane sugar, catalysed by hydrochloric acid in aqueous solution,  $J$  has been found by experiment to be  $-89 \pm 5$  cal./g. mol.-deg. (Moelwyn-Hughes 1934), in satisfactory agreement with a theoretical prediction of  $-89.4$  (Moelwyn-Hughes 1929). The experimental work has been independently confirmed (Leininger and Kilpatrick 1938). The uncatalysed hydrolysis of the methyl halides is consistent with an experimental value of  $J = -67$  (Moelwyn-Hughes 1938), which in the most favourable case is probably accurate to within  $\pm 7$ . In so far as these reactions may be regarded as representative, we see that catalysed and uncatalysed hydrolyses in aqueous solution contradict the law of Arrhenius. The true and apparent energies of activation in these cases differ considerably; and the determination of their numerical relationship, which is given by the equation

$$E_A = E + JT, \quad (5)$$

is an essential step in the elucidation of the mechanism of reaction.

The present paper contains the results of our experimental investigation into a set of reactions differing from ordinary hydrolysis, namely, the elimination of carbon dioxide from carboxylic acids in aqueous solution. The chemical changes are represented by the equation



We had intended to study the decomposition of three of the fully halogenated derivatives of acetic acid, but the scheme failed on account of the extreme instability of tri-iodoacetic acid. We consequently followed our work on trichloroacetic and tribromoacetic acids by examining a highly symmetrical acid from the aromatic group—2:4:6-trinitrobenzoic acid. The kinetics of the decarboxylation of two of these acids have already been fairly extensively investigated, the first by Kappanna (1932), and the last by Moelwyn-Hughes and Hinshelwood (1931). In the latter work (p. 189), which dealt with the solvent effect, a real departure from the equation of Arrhenius was noted but not pursued. The result of the present investigation is to show that equation (2) is inapplicable to the kinetics of the three decompositions, and that yet another set of chemical reactions has been found with a considerably more complicated mechanism of activation than had been previously imagined. A summary of the experimental figures is given in table 1. The unit of  $k$  is the reciprocal second, and of  $E$  the calorie per gram-molecule. In view of experimental difficulties and other limitations, it is not possible to assess the value of  $J$  more closely than is indicated here.



TABLE I

|                 | $\text{CCl}_3\text{COOH}$ | $\text{CBr}_3\text{COOH}$ | $\text{C}_6\text{H}_5(\text{NO}_2)_2\text{COOH}$ |
|-----------------|---------------------------|---------------------------|--|
| $k$ (298.1°)    | $4.97 \times 10^{-9}$     | $5.08 \times 10^{-7}$     | $2.41 \times 10^{-9}$                            |
| $k$ (373.1°)    | $1.11 \times 10^{-2}$     | $3.69 \times 10^{-2}$     | $7.70 \times 10^{-4}$                            |
| $E_a$ (298.1°)  | 36,950                    | 33,650                    | 38,875   |
| $E_a$ (373.1°)  | 35,450                    | 32,150                    | 35,500   |
| $J$ ( $\pm 5$ ) | -20                       | -20                       | -45  |

## PREPARATION OF MATERIALS

Pure trichloroacetic acid was prepared from the commercial product by repeated crystallizations from solution in benzene, which had been successively treated with sulphuric acid and with lime before being distilled. The solution was prepared by adding to the solid acid, in an all-glass reflux condenser, just sufficient benzene to dissolve it at 343°. Water was excluded by means of calcium chloride tubes. The solution was cooled in a freezing mixture, and the solvent pumped off in a vacuum desiccator. The product melted without decomposition at  $331.6^\circ \text{K} \pm 1^\circ$ .

Pure tribromoacetic acid was made by oxidizing bromal (Schaeffer 1871) which was itself prepared by brominating paraldehyde (*Organic Synthesis*, 1937). The crystals obtained after heating 58 c.c. of bromal with 100 c.c. of fuming nitric acid for 2 hr. at  $320^\circ \text{K}$  were filtered off on sintered glass, and freed from nitrogen oxides by drawing air through them. The acid was stored in a vacuum desiccator over sticks of potash. The crystals were colourless, slightly hygroscopic, and sublimed readily. When thoroughly dried, they melted at  $403^\circ \text{K} \pm 2^\circ$ , but not sharply.

The prescribed method of preparation of tri-iodoacetic acid (Angeli 1893) proved unsatisfactory, and we were unable to improve upon it. When malonic and iodic acids are allowed to react in solution, a yellow colour develops during effervescence, sometimes with and sometimes without the appearance of iodine vapour. On cooling, an unstable solid appears which decomposes on contact with the Buchner funnel at room temperatures. Filtration was next carried out in an apparatus completely immersed in a freezing mixture. The solid, after being dissolved in the cold, gave an unstable solution, for which we were able to measure accurately the rate of evolution of gas at several temperatures, using a sensitive differential manometer. Our experience with the other acids, however, which were examined by chemical analysis, indicates that the rate of elimination of carbon dioxide in this case is a complicated process, probably involving hydroxy acids, and the work was abandoned.

Trinitrobenzoic acid, prepared in the ordinary way by the oxidation of trinitrotoluene, gave a melting-point of  $498^{\circ}\text{K} \pm 1^{\circ}$ , which lies between the extreme values of  $483^{\circ}$  and  $511^{\circ}$  found in the literature.

#### EXPERIMENTAL METHOD

On account of the slowness with which carbon dioxide is eliminated from these stable acids, the sealed tube technique was employed, in preference to the manometric method used with the unstable acid. 20 c.c. samples of reaction solution, which was prepared by weighing the solute into a known volume of solvent, were placed in reaction vessels which were sealed off and kept in electrically heated thermostats for measured time intervals. The tubes were chilled in ice before their contents were titrated. At the higher temperatures, the thermostat liquid was changed from water to oil, and the regulator liquid from toluene to xylene. For a few experiments with trinitrobenzoic acids, boiling vapour baths were employed. The temperature control varies with the extent of reaction and with the temperature itself; on an average,  $T$  is considered correct to  $\pm 0.07^{\circ}$ . The initial concentration of the aliphatic acids was usually 0.1 M, and of the aromatic acid 0.025 M. The amount of unchanged trihalogen acid was estimated by titration against standard alkali, using bromocresol green as indicator. In the case of the less soluble trinitrobenzoic acid, however, the apparent constants were found to drift until we decarboxylated each sample with fresh air. Bromthymol blue was found to be the most suitable indicator. The decomposition of the substituted acetic acids is accompanied by some hydrolysis, the exact extent of which was determined by titrating the ionic halogen in each reaction sample, using silver nitrate and potassium chromate. The difference between the concentrations of total acid and halogen ion is taken to be the true concentration of the decomposing acid. Although never exceeding 0.45 %, the difference introduces an important correction into the value of the constant. For trichloroacetic acid at  $333.0^{\circ}$ , the correction is nearly 9.1 %. The titration values published here are the corrected ones.

#### EXPERIMENTAL RESULTS

In aqueous solution, the rate of elimination of carbon dioxide from each of the acids obeys the unimolecular law

$$c_t = c_0 e^{-kt}, \quad (7)$$

where  $c_t$  is the concentration of acid remaining after a lapse of  $t$  sec. Some representative figures are shown in tables 2-4, where the experimental titration,  $T_t$  (column 2), is compared with  $T_0 e^{-kt}$ , and the observed percentage of the total change with  $100(1 - e^{-kt})$ .

TABLE 2. TRICHLORACETIC ACID IN WATER

$$T = 332.78; k = 3.23 \times 10^{-4}$$

| $t$ (min.) | c.c. of standard reagent |       | Percentage change |       |
|------------|--------------------------|-------|-------------------|-------|
|            | Obs.                     | Calc. | Obs.              | Calc. |
| 300        | 39.86                    | 40.04 | 6.1               | 5.6   |
| 600        | 37.62                    | 37.71 | 11.4              | 11.0  |
| 1020       | 34.79                    | 34.79 | 18.1              | 17.9  |
| 1500       | 31.88                    | 31.74 | 24.9              | 25.2  |
| 2140       | 28.32                    | 28.02 | 33.3              | 33.9  |
| 2700       | 25.05                    | 25.15 | 41.0              | 40.8  |
| 3624       | 21.34                    | 21.01 | 49.7              | 50.5  |
| 4536       | 17.65                    | 17.60 | 58.4              | 58.5  |
| 5985       | 13.20                    | 13.32 | 68.9              | 68.6  |
| 8061       | 8.66                     | 8.90  | 79.6              | 79.0  |

TABLE 3. TRIBROMACETIC ACID IN WATER

$$T = 317.87; k = 1.77 \times 10^{-5}$$

| $t$ (min.) | c.c. of standard reagent |       | Percentage change |       |
|------------|--------------------------|-------|-------------------|-------|
|            | Obs.                     | Calc. | Obs.              | Calc. |
| 45         | 32.08                    | 32.14 | 4.9               | 4.7   |
| 120        | 29.73                    | 29.72 | 11.9              | 12.0  |
| 240        | 26.05                    | 26.12 | 22.8              | 22.5  |
| 420        | 21.44                    | 21.58 | 36.4              | 36.0  |
| 600        | 17.87                    | 17.82 | 47.0              | 47.1  |
| 840        | 13.87                    | 13.80 | 58.9              | 59.0  |
| 1080       | 12.06                    | 10.72 | 64.3              | 68.2  |
| 1380       | 8.25                     | 7.80  | 75.6              | 76.9  |
| 1680       | 6.06                     | 5.66  | 82.0              | 83.2  |

In the concentration range to which this work is confined, the velocity coefficient is but slightly influenced by the initial concentration of the reactant. The results obtained in the case of the least soluble acid are given in summarized form in table 5. Both the constancy of  $k$  for a given experiment and its independence on the initial concentration are consistent with equation (7). Apparent departures from it are due to the influence of dissolved carbon dioxide in the case of trinitrobenzoic acid, and to partial hydrolysis in the other cases.

TABLE 4. TRINITROBENZOIC ACID IN WATER

$$T = 368.29; k = 4.11 \times 10^{-4}$$

| (min.) | c.c. of standard reagent |       | Percentage change |       |
|--------|--------------------------|-------|-------------------|-------|
|        | Obs.                     | Calc. | Obs.              | Calc. |
| 10     | 43.15                    | 43.24 | 21.5              | 21.9  |
| 15     | 38.35                    | 38.26 | 30.7              | 30.9  |
| 20     | 33.75                    | 33.80 | 39.0              | 38.9  |
| 25     | 30.00                    | 29.88 | 45.8              | 46.0  |
| 30     | 26.75                    | 26.41 | 51.7              | 52.3  |
| 35     | 23.80                    | 23.35 | 57.0              | 57.8  |
| 40     | 20.40                    | 20.64 | 63.1              | 62.7  |
| 51     | 15.85                    | 15.74 | 71.4              | 71.6  |
| 61     | 11.75                    | 12.30 | 78.8              | 77.8  |
| 96     | 5.25                     | 5.19  | 90.5              | 90.6  |

TABLE 5. THE DILUTION EFFECT IN THE CASE OF TRINITROBENZOIC ACID IN WATER

| $T^{\circ}$       | Initial concentration (mM./l.) | $k \times 10^4$ |
|-------------------|--------------------------------|-----------------|
| $373.13 \pm 0.03$ | 5                              | $7.28 \pm 0.86$ |
| $373.35 \pm 0.00$ | 10                             | $7.47 \pm 0.21$ |
| $373.38 \pm 0.08$ | 25                             | $7.44 \pm 0.13$ |
| $373.33 \pm 0.07$ | 50                             | $7.88 \pm 0.13$ |

## THE INFLUENCE OF TEMPERATURE ON THE VELOCITY COEFFICIENTS

The observed velocity coefficients at various temperatures, and at the concentrations referred to above, are more satisfactorily reproduced by equation (4) than by the Arrhenius equation. Subject to the limitation on the accuracy with which  $J$  can be determined, we arrive at the following empirical expressions:

for trichloroacetic acid:  $\ln k = 110,824 - 42,910/RT - (20/R) \ln T$ ,

for tribromoacetic acid:  $\ln k = 109,862 - 39,610/RT - (20/R) \ln T$ ,

for trinitrobenzoic acid:  $\ln k = 197,728 - 52,300/RT - (45/R) \ln T$ .

Comparison with experiment is shown in tables 6-8. Clearly, in the case of the aliphatic acids, the difference in rates of decomposition is due chiefly to a difference of some 3000 cal. in the energy of activation, whereas in the case of the aromatic acid the mechanism of reaction seems altogether more complicated. Similar observations have been made in the case of oxalic acid (Dinglinger and Schröer 1937), for which  $E_a$  falls as  $T$  is raised,

though not as simply as in equation (5). The decomposition of malonic acid in water has also been extensively studied. Combining the data of Bernouilli and Wege (1919) with those of Knaus (1928), we obtain, as a first approximation holding in the range 348–423° K,  $E = 79,000$  cal., and  $J = -128$  cal./deg. The present results give an apparent energy of activation of

TABLE 6. TRICHLORACETIC ACID IN WATER

| $T$    | $k$ (obs.)            | $k$ (formula)         |
|--------|-----------------------|-----------------------|
| 323.15 | $6.03 \times 10^{-7}$ | $6.13 \times 10^{-7}$ |
| 328.11 | $1.42 \times 10^{-6}$ | $1.44 \times 10^{-6}$ |
| 332.78 | $3.23 \times 10^{-6}$ | $3.16 \times 10^{-6}$ |
| 338.25 | $7.75 \times 10^{-6}$ | $7.67 \times 10^{-6}$ |
| 343.11 | $1.63 \times 10^{-5}$ | $1.63 \times 10^{-5}$ |
| 348.30 | $3.56 \times 10^{-5}$ | $3.61 \times 10^{-5}$ |
| 353.07 | $7.19 \times 10^{-5}$ | $7.29 \times 10^{-5}$ |
| 358.03 | $1.47 \times 10^{-4}$ | $1.48 \times 10^{-4}$ |
| 363.14 | $2.96 \times 10^{-4}$ | $2.97 \times 10^{-4}$ |
| 368.02 | $5.96 \times 10^{-4}$ | $5.76 \times 10^{-4}$ |
| 373.13 | $1.10 \times 10^{-3}$ | $1.12 \times 10^{-3}$ |

TABLE 7. TRIBROMACETIC ACID IN WATER

| $T$    | $k$ (obs.)            | $k$ (formula)         |
|--------|-----------------------|-----------------------|
| 297.91 | $4.89 \times 10^{-7}$ | $4.97 \times 10^{-7}$ |
| 302.98 | $1.28 \times 10^{-6}$ | $1.29 \times 10^{-6}$ |
| 308.10 | $3.25 \times 10^{-6}$ | $3.25 \times 10^{-6}$ |
| 313.10 | $7.65 \times 10^{-6}$ | $7.77 \times 10^{-6}$ |
| 317.87 | $1.77 \times 10^{-5}$ | $1.74 \times 10^{-5}$ |
| 322.82 | $4.06 \times 10^{-5}$ | $3.89 \times 10^{-5}$ |
| 327.97 | $8.44 \times 10^{-5}$ | $8.75 \times 10^{-5}$ |
| 333.03 | $1.86 \times 10^{-4}$ | $1.89 \times 10^{-4}$ |
| 338.12 | $4.12 \times 10^{-4}$ | $4.00 \times 10^{-4}$ |
| 343.12 | $8.17 \times 10^{-4}$ | $8.15 \times 10^{-4}$ |

TABLE 8. TRINITROBENZOIC ACID IN WATER

| $T$    | $k$ (obs.)            | $k$ (formula)         |
|--------|-----------------------|-----------------------|
| 328.05 | $8.95 \times 10^{-7}$ | $8.75 \times 10^{-7}$ |
| 333.13 | $2.09 \times 10^{-6}$ | $2.12 \times 10^{-6}$ |
| 338.10 | $4.94 \times 10^{-6}$ | $4.81 \times 10^{-6}$ |
| 343.10 | $1.01 \times 10^{-5}$ | $1.07 \times 10^{-5}$ |
| 346.12 | $1.73 \times 10^{-5}$ | $1.73 \times 10^{-5}$ |
| 349.91 | $3.03 \times 10^{-5}$ | $3.10 \times 10^{-5}$ |
| 357.98 | $1.03 \times 10^{-4}$ | $9.68 \times 10^{-5}$ |
| 363.10 | $2.12 \times 10^{-4}$ | $2.06 \times 10^{-4}$ |
| 368.29 | $4.05 \times 10^{-4}$ | $4.11 \times 10^{-4}$ |
| 373.27 | $7.44 \times 10^{-4}$ | $7.91 \times 10^{-4}$ |

35,850 in the case of trichloroacetic acid at  $353.1^{\circ}$ , which is about 1400 cal. less than that found by Kappanna (1932). For trinitrobenzoic acid at the same temperature we have a value of 36,410, which is greater by about 2500 cal. than that found by taking the extreme constants in the work of Moelwyn-Hughes and Hinshelwood (1931).

#### SUPPLEMENTARY EXPERIMENTS

The decomposition of acetonedicarboxylic acid is catalysed by weak bases (Wiig 1928), and the kinetics of the catalysis have found a simple interpretation (Moelwyn-Hughes 1933). Trinitrobenzoic acid, however, does not appear to respond to the bases which we used, namely, redistilled pyridine and aniline. The titration method does not give accurate results in the presence of much added alkali. Using thymol blue as indicator, and working at  $349.52^{\circ}$ , we obtained the results of table 9. Clearly the catalytic effect is extremely small.

TABLE 9

| Base         | Concentration<br>(mM./l.) | $k \times 10^5$ |
|--------------|---------------------------|-----------------|
| None         | —                         | 2.95            |
| KOH          | 5.6                       | 3.0             |
| $C_6H_5N$    | { 4.8                     | 3.2             |
|              | { 9.6                     | 3.2             |
|              | { 38.5                    | 3.0             |
| $C_6H_5NH_2$ | { 23.7                    | 3.4             |
|              | { 154.3                   | 3.4             |

There has been considerable discussion as to whether the anion or the undissociated acid is responsible for the rate of elimination of carbon dioxide from aqueous solutions of carboxylic acids. No general conclusion can be reached. With the appearance of more accurate and extensive data, cases will doubtless come to light where both decompose with comparable rates and where one mechanism is relatively so facile as to exclude the other. The point at issue is not easy to settle in the case of the three acids at present under discussion, because they behave in water as strong electrolytes, and therefore the addition of salts, including those with a common ion, influences primarily the ionic environment rather than the extent of dissociation. If, however, the decomposition occurs mainly by an ionic mechanism, we may anticipate that (1) salts formed from the acid with strong bases will decompose at rates and with apparent energies

of activation which lie near to the figures holding for the acid solutions, and (2) the rate in non-ionizing solvents will be considerably slower than in water.

(1) We have examined the rate at which carbon dioxide is evolved from solutions of sodium tribromacetate at various temperatures. On account of hydrolysis of the anion, which takes place concurrently, the analysis of the data is not easy. By measuring the extent of hydrolysis in each case, however, we have found the extrapolated constants shown in table 10. They yield an apparent energy of activation of 34,000 cal.  $\pm$  2000, which, within the limits of error, agrees with the value 32,950 found for the acid solution at this temperature. The former figure differs from that obtained by Fairclough (1938) by 10,000 cal. In the case of trichloroacetic acid there is much better agreement. Thus for the ion at 345°, he finds  $E_A$  to be 36,600, and for the acid at the same temperature we obtain 36,000 cal. These results are not inconsistent with the hypothesis that it is the ion which decomposes. On account, however, of the smallness of the free energy change attending ionization, the ionic and non-ionic mechanisms may be experimentally indistinguishable.

TABLE 10

| $T$   | $k_0 \times 10^4$ |
|-------|-------------------|
| 327.9 | 1.34              |
| 333.2 | 3.2               |
| 338.1 | 6.8               |

(2) At temperatures where the rate of decomposition in water is extremely rapid, no detectable change could be found after several days with solutions of tribromoacetic acid in toluene fractionated with care at 382.9° from metallic sodium. The solvent was stored, and as far as possible handled, in the absence of atmospheric moisture. At 403.0°, however, a slow decomposition was detected. It was attended by the development of a yellow coloration, and persisted when the experiments were repeated in sealed tubes from which the air had been removed. Analysis of the contents of 20 c.c. samples of oxygen-free solutions kept at this temperature for long intervals gave the results of Table 11. The brown coloration reduced the accuracy of the estimations. If the figures in the last column are a reliable measure of the total organic acidity, the rate of decomposition of the acid in this solvent is seen to be less than the rate in water by a factor of about  $10^7$ . This strikingly large solvent effect would be accountable by a change of some 13,000 cal. in the apparent energy of activation. It is

probable, however, that the splitting off of carbon dioxide from tribrom-acetic acid does not occur by such a simple mechanism. A fairly strong solution was refluxed on a sand-bath for about a fortnight. The product, which contained carbonaceous matter and was a powerful lachrymatory,

TABLE 11. TRIBROMACETIC ACID IN TOLUENE AT 403.0°,  
IN THE ABSENCE OF OXYGEN

| Time<br>hr. | c.c. of<br>0.0592N<br>KOH | c.c. of<br>0.0592N<br>AgNO <sub>3</sub> | Difference |
|-------------|---------------------------|---|------------|
| 50          | 34.3                      | 3.0                                     | 31.3       |
| 71          | 35.7                      | 4.7                                     | 31.0       |
| 145         | 34.9                      | 4.4                                     | 30.6       |
| 168         | 36.4                      | 5.7                                     | 30.7       |
| 212         | 35.8                      | 5.5                                     | 30.3       |
| 259         | 36.4                      | 6.2                                     | 30.2       |

was neutralized by dilute sodium carbonate, separated and fractionated after removal of the solvent. We obtained constant boiling fractions at 456–457° and at 472°, which correspond so nearly to the boiling points of *o*-, *m*-, and *p*-bromtoluene (454.9, 456.8, 456.6) and benzyl bromide (472) that the substitution of bromine in the benzene nucleus and side chain may be regarded as established.

#### DISCUSSION

The principal feature of these results is that they bring the decarboxylation reactions into line with catalysed and uncatalysed hydrolyses in solution. For all these cases it may now be stated that the equation of Arrhenius is inadequate as an empirical summary of their kinetics, and must be replaced by more satisfactory formulae towards which equation (5) is an approximation.

The object of the following brief discussion is less to seek illumination from statistical theory than to indicate the direction in which we consider that theory should advance while retaining close contact with the facts.

For a solute molecule composed of *N* atoms in a solution so dilute that the mutual interaction of solute molecules may be neglected, we may propose the use of the partition function

$$f = \frac{g(2\pi mkT)^{3/2} v_f}{h^3} \frac{1}{\pi\sigma} \left( \frac{8\pi^3(I_A I_B \dots I_G)^{1/n} kT}{h^2} \right)^{1/n} \prod_{i=1}^{3N-3-n} (1 - e^{-h\nu_i/kT})^{-1} e^{-\phi/kT}, \quad (8)$$



where  $g$  is the degeneracy of the electronic level, and  $m$  is the mass of the solute molecule. The term  $v_f$  is the average free volume available to the solute molecule, and is to be determined for the two-component system by an extension of the methods developed by Lennard-Jones and Devonshire (1937).  $\sigma$  is a symmetry factor, and  $n$  the number of degrees of freedom of rotation of the solute molecule and its parts, to which the moments of inertia,  $I_A, I_B, \dots, I_G$  refer (Halford 1934; Eidenhoff and Aston 1935).  $\nu_i$  is the frequency of the  $i$ th of the internal vibrations, all of which are assumed to be simple harmonic. Finally,  $\phi$  is the average energy of interaction of the solute molecules with the solvent molecules which enclose it. Special forms of  $\phi$  have been considered by us in some of the previous papers of this series. A similar expression, adjusted to a common reference level for the energy, obtains for the active molecule. Denoting the variables pertaining to the active molecule of solute by an asterisk, we then obtain for the ratio of the concentration,  $n^*$ , of active molecules to the concentration,  $n$ , of normal molecules, the equilibrium expression:

$$\frac{n^*}{n} = \frac{V_f^* \left( \frac{I_A^* I_B^* \dots I_G^*}{I_A I_B \dots I_G} \right)^{\frac{1}{2}} \prod_{j=1}^{3N-3-n} (1 - e^{-h\nu_j/kT})^{-1}}{\prod_{i=1}^{3N-3-n} (1 - e^{-h\nu_i/kT})^{-1}} e^{-(\phi^* - \phi)/kT} e^{-\epsilon/kT}. \quad (9)$$

The terms  $V_f$  and  $V_f^*$  are total free volumes, and the expression holds for equilibrium established at constant total volume. The multiplicity of the electronic states have been assumed equal, and the number of modes of vibration not to change during activation.  $\epsilon + (\phi^* - \phi)$  is the energy of activation in a solution supercooled to the absolute zero of temperature.

The experimental magnitudes for the frequency terms,  $\nu_i$ , with reference to the normal solute molecule—as distinct from the gaseous molecule—are forthcoming from a study of the Raman spectra of solutions; and it is not difficult to compute reasonable values for the five moments of inertia required to specify the rotations of a trihalogenoacetate ion in solution. Unfortunately, however, data for activated solute molecules are mostly lacking, and the advances in the kinetics of reactions in solution await comparable advances in the statics of solutions. Not before the latter have been made, can one hope to derive from equation (9) the expression holding for equilibria at constant pressure and to take the further trivial step of thermodynamic annotation.

In the meanwhile, general statistical expressions have to be abbreviated by the cancellation or suppression of terms so as to make comparison with

experiment possible. Before doing so in the present case, we recall that, in accordance with the general hypothesis of activation, the fate of most of the active molecules is reversion to the normal type. A small number of the active molecules, insufficient to destroy the equilibrium ratio, suffer chemical change. The frequency with which such transformation of an active molecule occurs in the gas phase has been assumed by Herzfeld (1919) and by Eyring (1935) to be that of slowest internal motion of which the active molecule is capable. In the case of an active solute molecule, however, it may well happen that the rate of destruction is governed by one of the frequencies of vibration of the molecule in its cage. This is thought to be especially relevant to reactive solutes in polar solvents, for which, as we have shown, one has to consider the activation of the whole cluster of molecules. If the forces exerted between solute molecule and solvent molecules are spherically symmetrical, we have the following approximate expression for the frequency of the intracellular vibration:

$$\nu = \frac{1}{2\pi} \left\{ \frac{2cBm}{3! \mu r^{m+2}} \left[ (n-1) \left( \frac{r_0}{r} \right)^{n-m} - (m-1) \right] \right\}^{\frac{1}{2}}. \quad (10)$$

Here  $c$  is the number of solvent molecules,  $\mu$  the reduced mass of the cluster (virtually equal to the mass of the solute),  $r$  the average solute-solvent separation, and  $B$ ,  $m$  and  $n$  are constants of the equation

$$\phi(r) = c\{Ar^{-n} - Br^{-m}\}. \quad (11)$$

A more exact form is available in the papers of Lennard-Jones and Devonshire (1937), and of Corner (1939). In the present equation, of course,  $B$  is the attractive energy constant for an isolated pair of unlike molecules. The product of the right-hand expressions in equations (9) and (10) gives us the unimolecular constant.

It is to be noted that the dependence of  $\nu$  on  $r$  is of the form necessary to explain the abrupt changes in reaction velocity in solution observed by Sutherland and Maas (1931) in the neighbourhood of the critical temperature.

The assumptions which must be made in order to compare these relations with the experimental results under discussion are the following: (1) The difference between the observed velocity coefficient and that which would hold at constant volume must not be so great as to invert the sign of  $J$ . (2) The product of the intracellular vibration frequency and the first and fourth terms of equation (9) must be independent of temperature. The pre-exponential terms in the equilibrium expression thus reduces to a ratio of the products of the vibrational partition functions of the active

and normal molecules. (3) In the normal molecule, let a number,  $p$ , of the vibrational motions be quantal, and a number,  $q$ , classical. The corresponding numbers for the active molecule may be denoted by the letters  $r$  and  $s$ . Then

$$k_{\text{uni.}} = \text{constant} \times \frac{\prod_r (1 - e^{-h\nu_r/kT})^{-1} \prod_s (kT/h\nu_s)}{\prod_p (1 - e^{-h\nu_p/kT})^{-1} \prod_q (kT/h\nu_q)} e^{-\epsilon/kT}, \quad (12)$$

and consequently, if  $\epsilon_m$  stands for the difference in internal energy of the active and normal molecules considered statically at the absolute zero of temperature, we have

$$E_A/N_0 = \epsilon_m - (q - s)kT - \frac{1}{2} \sum_p h\nu_p \coth(h\nu_p/kT) + \frac{1}{2} \sum_r h\nu_r \coth(h\nu_r/kT). \quad (13)$$

This expression conforms with equation (5) provided  $q > s$ . The conclusion is that it is impossible to loosen the carbon-carbon bond in the solute molecule without tightening the other bonds. In polar solvents, where the long range electrostatic forces have a co-ordinating influence on the mechanism of activation, it is not likely that the rate of activation is in any real sense a problem. The structural difference between normal and active molecules, and the rate at which the latter break up, seem to be more relevant.

One of the authors desires to thank the Department of Scientific and Industrial Research for a maintenance grant.

#### SUMMARY

The kinetics of the decomposition of trichloroacetic acid, tribromoacetic acid and 2:4:6-trinitrobenzoic acid in aqueous solution have been investigated experimentally over wide temperature ranges. The results do not conform to the equation of Arrhenius, but are moderately well reproduced by the empirical formula:  $\ln k = c + \frac{J}{R} \ln T - E/RT$ .

Certain general conclusions concerning the kinetics of reactions in solution have been drawn.

#### REFERENCES

- Angeli 1893 *Ber. deutsch. chem. Ges.* 26, 596.  
 Bernouilli and Wege 1919 *Helv. Chim. Acta*, 2, 511.  
 Corner 1939 *Trans. Faraday Soc.* 35, 711.  
 Dinglinger and Schröder 1937 *Z. phys. Chem. A*, 179, 401.

- Eidenhoff and Aston 1935 *J. Chem. Phys.* **3**, 379.  
Eyring 1935 *J. Chem. Phys.* **3**, 107.  
Fairclough 1938 *J. Chem. Soc.* p. 1186.  
Halford 1934 *J. Chem. Phys.* **2**, 694.  
Herzfeld 1919 *Ann. Phys., Lpz.*, **59**, 635.  
Kappanna 1932 *Z. phys. Chem. A*, **158**, 355.  
Knaus 1928 *Tables Annuelles* **6**, 1031.  
Leininger and Kilpatrick 1938 *J. Amer. Chem. Soc.* **60**, 2891.  
Lennard-Jones and Devonshire 1937 *Proc. Roy. Soc. A*, **163**, 53.  
Moelwyn-Hughes 1929 *Trans. Faraday Soc.* **25**, 516.  
— 1933 *The kinetics of reactions in solution*, p. 224. Oxford Univ Press.  
— 1934 *Z. phys. Chem. B*, **26**, 281.  
Moelwyn-Hughes and Hinshelwood 1931 *Proc. Roy. Soc. A*, **131**, 186.  
*Organic Synthesis* 1937 **17**, 18.  
Schaeffer 1871 *Ber. dtach. chem. Ges.* **4**, 370.  
Sutherland and Maas 1931 *Canadian J. Res.* **5**, 48.  
Verhoek 1939 *J. Amer. Chem. Soc.* **61**, 186.  
Wiig 1928 *J. Phys. Chem.* **32**, 961.
-



- Eidenhoff and Aston 1935 *J. Chem. Phys.* **3**, 379.  
 Eyring 1935 *J. Chem. Phys.* **3**, 107.  
 Fairclough 1938 *J. Chem. Soc.* p. 1186.  
 Halford 1934 *J. Chem. Phys.* **2**, 694.  
 Herzfeld 1919 *Ann. Phys., Lpz.*, **59**, 635.  
 Kappanna 1932 *Z. phys. Chem. A*, **158**, 355.  
 Knaus 1928 *Tables Annuelles* **6**, 1031.  
 Leininger and Kilpatrick 1938 *J. Amer. Chem. Soc.* **60**, 2891.  
 Lennard-Jones and Devonshire 1937 *Proc. Roy. Soc. A*, **163**, 53.  
 Moelwyn-Hughes 1929 *Trans. Faraday Soc.* **25**, 516.  
 — 1933 *The kinetics of reactions in solution*, p. 224. Oxford Univ Press.  
 — 1934 *Z. phys. Chem. B*, **26**, 281.  
 Moelwyn-Hughes and Hinshelwood 1931 *Proc. Roy. Soc. A*, **131**, 186.  
*Organic Synthesis* 1937 **17**, 18.  
 Schaeffer 1871 *Ber. dtsh. chem. Ges.* **4**, 370.  
 Sutherland and Maas 1931 *Canadian J. Res.* **5**, 48.  
 Verhoek 1939 *J. Amer. Chem. Soc.* **61**, 186.  
 Wiig 1928 *J. Phys. Chem.* **32**, 961.

## The thermal decomposition of gaseous benzaldehyde

BY R. E. SMITH AND C. N. HINSHELWOOD, F.R.S.

(Received 27 January 1940)

### INTRODUCTION

The thermal decompositions of the lower aliphatic aldehydes, including chloral, are in general of no definite integral or half integral order except with formaldehyde. The order of the reaction changes from the second with formaldehyde to nearer the first with the more complex aldehydes (Hinshelwood, Fletcher, Verhoek and Winkler 1934). To explain this, one theory postulates the existence of several simultaneously operating activation mechanisms. The more complex mechanisms predominating with larger molecules would have a longer time lag between activation and decomposition since they involve the transfer of energy from the more distant parts of the molecule. Hence they would be more nearly of the first order at moderate pressures. The superposition of different mechanisms accounts for some of the complex behaviour observed.

The acetaldehyde decomposition is not inhibited by small amounts of nitric oxide and responds negatively to other tests for chains (Staveley

and Hinshelwood 1936; Smith 1939). With propaldehyde and butaldehyde, nitric oxide shows both a chain reaction and one insensitive to nitric oxide (Staveley and Hinshelwood 1937). Over a limited range of pressures the acetaldehyde decomposition is nearly of the  $3/2$  order, and attempts have been made to explain this by a chain mechanism, the chains being supposed immune to the action of nitric oxide (Letort 1937; Rice 1934). Experiments have definitely shown the presence of chains in the photochemical decomposition (which is inhibited by nitric oxide), and free radicals can be detected in a stream of decomposing aldehyde at temperatures of  $1000^{\circ}\text{C}$ . But direct evidence for the existence of chains in the range of measurably slow thermal decomposition is lacking.

A study of the thermal decomposition of benzaldehyde has made possible further investigation into the properties of two parts of the reaction mechanism; namely, (*a*) that which is inhibited by nitric oxide and is by general consent a chain reaction, and (*b*) that which is not inhibited by nitric oxide. According to one view (*b*) should be a non-chain reaction, and according to another view a chain reaction insensitive to the inhibition.

It will be clearest to state first the principal results of the investigation, and to tabulate separately the evidence supporting the various statements:

(*a*) The predominant reaction is a homogeneous decomposition according to the equation  $\text{C}_6\text{H}_5\text{CHO} = \text{C}_6\text{H}_6 + \text{CO}$ . There is a certain proportion of side reaction giving diphenyl (§ 5).

(*b*) The rate is lowered to a definite limit (not a transitory minimum) by the addition of a few millimetres of nitric oxide (§ 2).

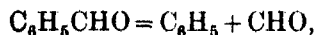
(*c*) The uninhibited reaction is very nearly of the first order with respect to the benzaldehyde concentration from 100 mm. to 300 mm.; below 100 mm. the first order velocity constant falls off (§ 1). This behaviour is in sharp contrast with that of acetaldehyde.

(*d*) The inhibited reaction is of a different order, variable and between one and two. The curve of  $1/(\text{half-life})$  against initial pressure closely resembles that given by the nitric oxide-insensitive acetaldehyde reaction (§ 3).

(*e*) If  $\rho$  is the rate for a given amount of nitric oxide,  $\rho_0$  that for none and  $\rho_{\infty}$  the limiting rate, then  $(\rho - \rho_{\infty})/(\rho_0 - \rho_{\infty})$  plotted against the pressure of nitric oxide, the "inhibition curve", is found to be identical for different initial benzaldehyde pressures (§ 2).

That a substantial part of the normal reaction takes place by a chain mechanism is shown by (*b*). As its characteristics are unlike those of the acetaldehyde reaction, doubt arises about the validity of arguments which make the latter depend on a chain mechanism.

The order of a chain reaction depends upon the mechanism by which the chains are ended. If the primary process is



and if the chains end by the combination of two similar radicals, then the reaction order would be 3/2. To account for the first order one must assume either (1) that the two radicals combine in a termolecular collision, or (2) that the mechanism involves two radicals, one of which can only propagate the chain after itself suffering a thermal decomposition to give a smaller radical. Chains are broken by the recombination of the two kinds of radical. This is similar to the mechanism invoked to explain the chain part of the ether decomposition (Hobbs 1938). Alternatives (1) and (2) can be distinguished by determining the curves of  $(\rho - \rho_\infty)/(\rho_0 - \rho_\infty)$  against nitric oxide pressure for a series of initial benzaldehyde pressures. According to (2) they would be superimposable while according to (1) they would be widely different. The result (e) indicates that alternative (2) is the correct one.

A hypothetical scheme which fulfils the conditions imposed by the various results is:

- (1)  $\text{C}_6\text{H}_5\text{CHO} \rightarrow \text{C}_6\text{H}_5 + \text{CHO},$
- (2)  $\text{CHO} \rightarrow \text{CO} + \text{H},$
- (3)  $\text{H} + \text{C}_6\text{H}_5\text{CHO} \rightarrow \text{C}_6\text{H}_6 + \text{CHO},$
- (4)  $\text{CHO} + \text{H} \rightarrow \text{CO} + \text{H}_2,$
- (5)  $\text{CHO} + \text{NO} \rightarrow \text{inactive products}.$

From the equations  $d[\text{CHO}]/dt = 0$  and  $d[\text{H}]/dt = 0$ ,

$$[\text{H}]^2(2k_3k_4) + [\text{H}](k_1k_4 + k_3k_5[\text{NO}]) - k_1k_2 = 0.$$

Thus  $[\text{H}]$  is independent of the benzaldehyde concentration and a function of the nitric oxide concentration only:  $[\text{H}] = f([\text{NO}])$ . The rate of the chain reaction is very nearly  $k_3[\text{C}_6\text{H}_5\text{CHO}][\text{H}]$  which equals  $k_3[\text{C}_6\text{H}_5\text{CHO}]f([\text{NO}])$ , i.e. the reaction is of the first order. To this must be added any non-chain reaction. Similarly  $(\rho - \rho_\infty)/(\rho_0 - \rho_\infty)$  is a function of  $[\text{NO}]$  only.

If on the other hand it were assumed:

- (1)  $\text{C}_6\text{H}_5\text{CHO} \rightarrow R + \text{intermediate products},$
- (2)  $\text{C}_6\text{H}_5\text{CHO} + R \rightarrow R + \text{products},$
- (3)  $R + R + \text{C}_6\text{H}_5\text{CHO} \rightarrow R_2 + \text{C}_6\text{H}_5\text{CHO},$
- (4)  $R + \text{NO} \rightarrow \text{inactive products},$



then the rate of the chain reaction would be

$$k_2[\text{C}_6\text{H}_5\text{CHO}]/\{[\text{NO}]/[\text{C}_6\text{H}_5\text{CHO}]\},$$

and the inhibition curves would be by no means superimposable for different benzaldehyde pressures.

#### EXPERIMENTAL DETAILS

The methods were similar to those used in previous work from this laboratory, except for extensions of technique necessitated by the high boiling-point of benzaldehyde. Pyrex reaction vessels were used and attached by graded seals so that no lubricated ground joints were necessary. The stopcocks were heated by a constant-temperature oil bath, and greased with a mixture of aluminium soaps found to be suitable in the range 150°–170° C.

As the vapour pressure of mercury in the manometer column is approximately 4 mm. at 160° C, precautions were taken to prevent distillation of the mercury into the apparatus. However, heating of the manometer to a considerably higher temperature did not affect the reproducibility of the reaction rates.

#### (1) ORDER OF THE UNINHIBITED REACTION

$t_4$  is the time necessary for a pressure increase of half that corresponding to the end-point (which was observed in all cases). The results at 550° C are given in table 1.

TABLE 1

| Unpacked reaction vessel |                     | Packed reaction vessel |                     |
|--------------------------|---------------------|------------------------|---------------------|
| Initial pressure         |                     | Initial pressure       |                     |
| mm.                      | $1/t_4 \times 10^3$ | mm.                    | $1/t_4 \times 10^3$ |
| 14                       | 0.33                | 22                     | 0.22                |
| 37                       | 0.55                | 41                     | 0.32                |
| 58                       | 0.66                | 69                     | 0.59                |
| 70                       | 0.63                | 93                     | 0.68                |
| 77                       | 0.88                | 132                    | 0.90                |
| 81                       | 0.81                | 152                    | 0.95                |
| 117                      | 0.83                | 159                    | 0.89                |
| 153                      | 0.97                | 219                    | 0.89                |
| 216                      | 0.96                | 275                    | 0.94                |
| 249                      | 0.93                | 339                    | 1.00                |
| 336                      | 0.95                |                        |                     |

Values of the first-order constant determined over the course of a run of 245 mm. initial pressure are given in table 2.

TABLE 2

|                            |      |      |      |      |      |      |      |
|----------------------------|------|------|------|------|------|------|------|
| Percentage decomposed, $x$ | 20   | 30   | 40   | 50   | 60   | 70   | 80   |
| $1/t \log 100/(100 - x)$   | 3.34 | 3.30 | 3.32 | 3.10 | 2.84 | 2.50 | 2.32 |

The reaction velocities in an ordinary vessel, and in a vessel packed with small lengths of fire-polished pyrex tubing, were compared. The results, as given in table 1 and figure 1, show the decomposition to be practically

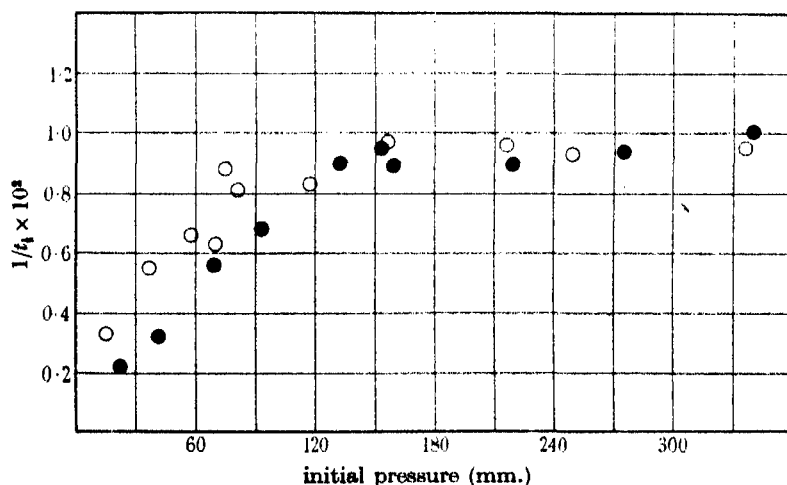


FIGURE 1. The rate of the uninhibited reaction.

○ Unpacked reaction vessel; ● packed reaction vessel.

homogeneous above 100 mm. At lower pressures the increased surface causes a slight retardation. The change in the surface to volume ratio was sevenfold.

## (2) INHIBITION BY NITRIC OXIDE

The decomposition of benzaldehyde is subject to inhibition by nitric oxide. The apparent chain length at 100 mm. pressure and 550° C is 3.8. Catalysis of the reaction is caused by concentrations of nitric oxide greater than 15 mm. The minimum in the inhibition curve is, however, by no means due to the counterbalancing of the inhibition and the catalysis, but is a definite limiting rate, constant within experimental error for partial

pressures of nitric oxide between 3 and 15 mm. This can be seen from the data in table 3 for 200 mm. initial pressure. The end-point is not affected by 5 mm. of nitric oxide.

TABLE 3

| Pressure of<br>nitric oxide<br>mm. | $1/t_1 \times 10^3$ |
|------------------------------------|---------------------|
| 0                                  | 10.4                |
| 1.9                                | 4.53                |
| 3.9                                | 3.00                |
| 6.5                                | 3.28                |
| 10.0                               | 3.40                |
| 10.8                               | 3.47                |
| 12.5                               | 3.44                |
| 15                                 | 4.14                |
| 17.5                               | 5.15                |
| 20                                 | 10.7                |

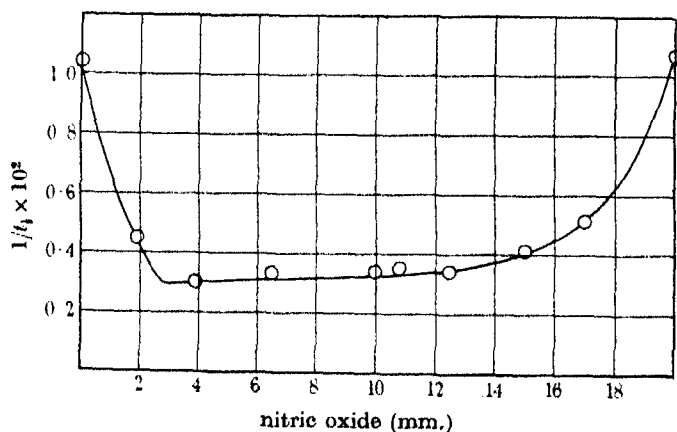


FIGURE 2. The effect of nitric oxide.

The variation of  $(\rho - \rho_\infty)/(\rho_0 - \rho_\infty)$  with pressure of nitric oxide was determined for initial pressures of benzaldehyde of 50 mm. and 150 mm. in an ordinary vessel, and for an initial pressure of 100 mm. in a vessel packed with pyrex tubing. The results at 550° C are given in table 4 and plotted in figure 3.

In spite of a threefold increase in the pressure of the benzaldehyde, these curves coincide. That is, the inhibition is independent of the pressure of benzaldehyde. As the packed reaction vessel gave the same result the possibility of a surface effect is ruled out.

TABLE 4

| Pressure of<br>nitric oxide<br>mm. | $(\rho - \rho_{\infty})/(\rho_0 - \rho_{\infty})$ |               |               |
|------------------------------------|---|---------------|---------------|
|                                    | $P_0$ 50 mm.                                      | $P_0$ 100 mm. | $P_0$ 150 mm. |
| 0                                  | 1.00  | 1.00          | 1.00          |
| 0.5                                | 0.87  | 0.86          | 0.54          |
| 1.0                                | 0.46  | 0.33          | 0.34          |
| 1.5                                | 0.21  | —             | 0.19          |
| 2.0                                | 0.06  | 0.06          | 0.07          |
| 2.5                                | 0.03  | —             | 0.03          |
| 3.0                                | —   | —             | 0.05          |

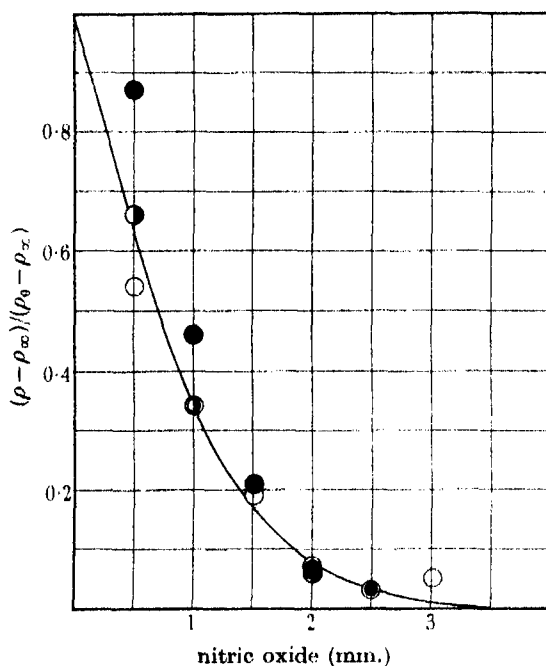


FIGURE 3. Inhibition curves.

● 50 mm.; ◐ 100 mm. and packed reaction vessel; ○ 150 mm.

According to the mechanism given above, the CHO radical decomposes at a rate proportional to its own concentration only. A mechanism which requires that it decompose at a rate proportional to the frequency of its collisions with other molecules, that is with the benzaldehyde molecules, is not so simple mathematically. However, it will give inhibition curves varying only slightly with pressure of benzaldehyde and an order of between 1.0 and 1.5. It is possible that this difference is so small as to be unimportant.

## (3) THE INHIBITED REACTION

The order of the inhibited reaction was obtained by determining the reaction velocities of a series of runs with two constant pressures (5 and 10 mm.) of nitric oxide but various initial pressures of benzaldehyde. The

TABLE 5

| Initial pressure<br>mm. | $1/t_i \times 10^3$ |
|-------------------------|---------------------|
| 23                      | 0.84                |
| 45                      | 1.34                |
| 58                      | 1.54                |
| 80                      | 2.10                |
| 110                     | 2.41                |
| 144                     | 2.78                |
| 170                     | 3.08                |
| 213                     | 3.62                |
| 250                     | 4.05                |
| 303                     | 4.54                |

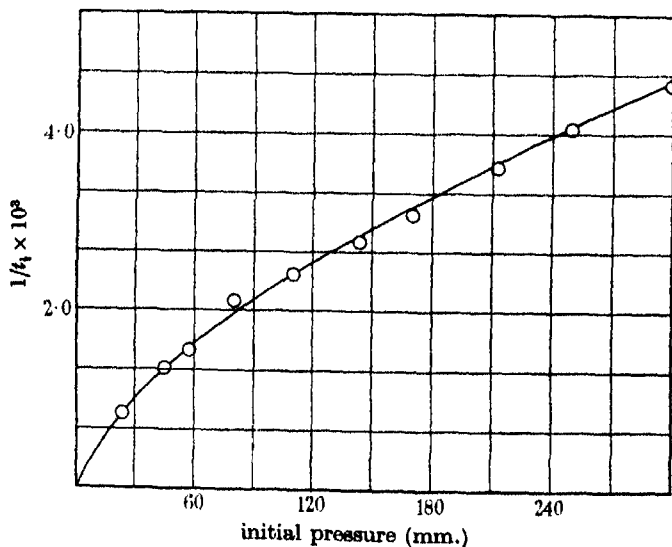


FIGURE 4. The rate of the inhibited reaction.

two sets gave curves identical within experimental error. Table 5 and figure 4 show the inhibited reaction to be of an order intermediate between one and two. In shape and absolute magnitude this curve is very similar to the curve for acetaldehyde without nitric oxide (Fletcher and Hinshelwood 1933).

(4) ACTIVATION ENERGIES

The temperature coefficient of the inhibited reaction was determined for initial pressures of 30, 150 and 250 mm. The objective method of least squares was used in calculating slopes. The values are corrected for the variation of the actual number of molecule per c.c. as the temperature is varied at constant pressure. No regular variation of the percentage pressure change at the end-point could be detected within the ranges of temperature and initial pressure used. For this reason end-points were not taken for all the runs but a fixed percentage of the initial pressure (45 %) was assumed as the standard for determining the half life. Detailed results are given in table 6 and the activation energies in table 7. There is a variation in the activation energy of the benzaldehyde with pressure similar to that observed with acet-aldehyde (Smith 1939).

TABLE 6

| Temperature<br>°C           | Half life<br>sec. |
|-----------------------------|-------------------|
| Initial pressure of 30 mm.  |                   |
| 535.5                       | 2180              |
| 550                         | 1000              |
| 563                         | 471               |
| 580                         | 235               |
| 593                         | 155               |
| Initial pressure of 150 mm. |                   |
| 520                         | 1305              |
| 528                         | 1060              |
| 535                         | 751               |
| 550                         | 349               |
| 565                         | 204               |
| 573                         | 163               |
| 580                         | 98                |
| Initial pressure of 250 mm. |                   |
| 520                         | 1060              |
| 535                         | 526               |
| 550                         | 246               |
| 565                         | 146               |
| 574                         | 112               |

TABLE 7

| Initial pressure<br>mm. | Activation energy<br>cal. |
|-------------------------|---------------------------|
| 30                      | 63,400                    |
| 150                     | 58,000                    |
| 250                     | 57,100                    |

## (5) DECOMPOSITION PRODUCTS

The pressure increase during the reaction followed a smooth curve to a steady end-point corresponding to about 90 % of the initial pressure. No regular variation of the end-point with initial pressure or temperature was detected.

Hurd (1929) found that the products of the decomposition of benzaldehyde by a streaming method in a pyrex tube at 690° C consisted chiefly of benzene and carbon monoxide. He detected as well the presence of about 5 % by moles of diphenyl and 6 % by moles of hydrogen. This requires a 100 % pressure increase. Of the 10 % defect in the experimental result 4 % is due to the "dead-space" in the apparatus. The rest is probably due to a condensation or polymerization. At 350° C in a sealed tube benzaldehyde is known to react with itself by the Cannizzaro reaction to give benzyl benzoate.

To see if the products were different under our conditions two quantities were determined: (1) the percentage of non-condensable gas; (2) the percentage of products which condense in various temperature ranges during cooling. The first was obtained by condensing in a trap surrounded by a carbon dioxide-acetone mixture. The percentage by moles of non-condensable gas was 57.5. As it is probable that 50 % of the products is carbon monoxide, the remaining 7.5 % is accordingly due to hydrogen. On cooling the products, the pressure obeyed Charles's Law from 550° to 250° C. Below this range condensation produced an apparent deviation. At 120° C this condensation was complete and the gas once more obeyed Charles's Law. Unchanged benzaldehyde in the dead space will account for a condensation of about 4 %. The remaining 5 % is due to diphenyl or benzyl benzoate. The products of the nitric oxide inhibited reaction gave slightly more condensation, 7 %.

The diphenyl and hydrogen may have been formed in the primary reaction or may be due to a secondary reaction of the benzene, either with the benzaldehyde or with more benzene. However, benzene heated to 550° C for 2 hr. by itself gave no condensation of diphenyl. When benzaldehyde was decomposed in the presence of an excess of benzene the amount of product condensable above 120° C increased, which suggests a secondary reaction.

Radical chains yielding diphenyl can easily be devised. In the observed reaction they play, if any, so small a part that the kinetic results are not accurate enough to give any information about them. If the diphenyl is formed mainly from benzaldehyde and benzene, then in the early stages of

the reaction when the concentration of the benzene is small the deviation from the reaction  $\text{C}_6\text{H}_5\text{CHO} \rightarrow \text{C}_6\text{H}_6 + \text{CO}$  must be small and the influence on the kinetics unimportant.

#### GENERAL CONCLUSIONS

From the above results two striking things may be noted:

(1) The similarity in properties between the acetaldehyde decomposition and the inhibited benzaldehyde decomposition.

(2) The existence of a chain mechanism with benzaldehyde not found with acetaldehyde.

We conclude that the acetaldehyde decomposition is certainly not a chain reaction similar to that postulated for the benzaldehyde. That it, and also the inhibited benzaldehyde decomposition itself, should be chain reactions with a different mechanism uninfluenced by nitric oxide might seem possible. For example, they might involve a mechanism in which the chains are broken by the bimolecular union of two radicals which are insensitive to nitric oxide. In this way the nearly  $3/2$  order could be explained. This, however, is unlikely for the following reasons: (1) It is difficult to devise a mechanism during no step of which a radical is formed which is sensitive to nitric oxide. (2) The previous arguments in favour of a molecular rearrangement process still stand (Fletcher and Hinshelwood 1933; Smith 1939).

A general picture of the aldehyde decompositions can now be given. The alternative processes of break-up to give stable products and break-up to give free radicals are in close competition. In the measurable thermal decomposition of acetaldehyde the former is easier. As the size of the aldehyde molecule increases, the chain reaction becomes of increasing importance. The apparent chain lengths in the cases of the acetaldehyde, propaldehyde, butaldehyde and benzaldehyde at  $550^\circ\text{C}$  and 100 mm. pressure are approximately 1.0, 3.1, 3.5, 3.8, respectively. The rates of the non-chain reactions of the aldehydes vary little. The increased number of degrees of freedom is counterbalanced by the increase in activation energy, except with chloral where there is a greater reaction rate principally due to a lowered activation energy.

#### SUMMARY

The thermal decomposition of benzaldehyde, which takes place predominantly according to the equation  $\text{C}_6\text{H}_5\text{CHO} \rightarrow \text{C}_6\text{H}_6 + \text{CO}$  is homogeneous, and differs from the corresponding reaction of acetaldehyde in



that it is of the first order above 100 mm., and is subject to partial inhibition by nitric oxide. The residual inhibited reaction shows a pressure dependence very like that of the normal acetaldehyde reaction. The activation energy increases as the pressure decreases.

The results can be explained by assuming the superposition of a chain reaction and of a molecular reaction. The order of the uninhibited reaction and the influence of nitric oxide at different initial pressures of benzaldehyde indicate the probable mechanism of the chain part of the decomposition, which appears to involve the decomposition of the radical CHO as an essential step.

#### REFERENCES

- Fletcher, C. J. M. and Hinshelwood, C. N. 1933 *Proc. Roy. Soc. A*, **141**, 41.  
Hinshelwood, C. N., Fletcher, C. J. M., Verhoek, F. H. and Winkler, C. A. 1934 *Proc. Roy. Soc. A*, **146**, 327.  
Hinshelwood, C. N. and Hobbs, J. E. 1938 *Proc. Roy. Soc. A*, **167**, 439.  
Hobbs, J. E. 1938 *Proc. Roy. Soc. A*, **167**, 456.  
Hurd, C. D. 1929 *The Pyrolysis of Carbon Compounds*. New York: The Chemical Catalog Co.  
Letort, M. 1937 *J. Chim. phys.* **34**, 355.  
Rice, F. O. 1934 *J. Amer. Chem. Soc.* **56**, 284.  
Smith, R. E. 1939 *Trans. Faraday Soc.* **35**, 1328.  
Staveley, L. A. K. and Hinshelwood, C. N. 1936 *J. Chem. Soc.* p. 812.  
— — 1937 *J. Chem. Soc.* p. 1568.
-

# The theory of reflexion of very long wireless waves from the ionosphere

BY M. V. WILKES, M.A., PH.D.

*The Mathematical Laboratory, Cambridge*

*(Communicated by E. V. Appleton, F.R.S.—Received 1 June 1939.—  
Revised 31 January 1940.)*

## 1. INTRODUCTION

In two previous papers (which will be referred to as I and II) Best, Ratcliffe and Wilkes (1936), and Budden, Ratcliffe and Wilkes (1939) have given an account of some experiments on the nature of the downcoming wave received at Cambridge from the British Post Office transmitter at Rugby (GBR wave-length 18·8 km.; distance 90 km.). Data are there given concerning the polarization of the wave, and the height of reflexion and the daily and seasonal changes of these quantities. Reflexion of very long waves takes place low down in the ionosphere where the density of ionization is only a few hundred electrons per c.c. The purpose of this paper is to discuss the theoretical implications of the data given in I and II, and to make such deductions as are possible from them concerning physical conditions in the lowest part of the ionosphere.

In § 2 the changes in reflexion height at sunset, and in following sections the polarization and amplitude of the reflected wave will be discussed. Use will be made of Chapman's well-known theory of the production of ions in a rotating atmosphere illuminated by ultra-violet light from the sun (Chapman 1931). It will be assumed that electrons tend to disappear sufficiently rapidly for the ionization to be always in quasi-equilibrium with changes in the rate of production of ions. It has been possible to interpret short-wave absorption and critical frequency results on this basis (Appleton 1937; Best, Farmer and Ratcliffe 1938) and we are consequently encouraged to try it for long waves.

Finally, in § 7 the relation of this paper to previous theoretical work on the reflexion of very long waves will be discussed.

## 2. CHANGES IN EFFECTIVE REFLEXION HEIGHT

The notation to be used is that introduced by Chapman, and is summarized below.

$h$  = height in km.

$I$  = number of electrons produced per c.c. per second at height  $h$ .

$N$  = number of ions per c.c. at height  $h$ .

$m$  = mean molecular mass of gas.

$H = \frac{kT}{mg}$  = scale height of atmosphere.

$h_0$  = height at which  $I$  is maximum when the sun is overhead.

$Z = \frac{h - h_0}{H}$ .

$I_0$  = max. value of  $I$ .

$N_0$  = max. value of  $N$ .

$f(\chi)$  = a function depending on the zenith angle of the sun ( $\chi$ ) and tabulated by Chapman; when  $\chi$  is small it is approximately equal to  $\sec \chi$ .

Chapman's theory then gives for the rate of production of ions

$$I = I_0 \exp [1 - Z - e^{-Z} f(\chi)].$$

It will be assumed that reflexion takes place low down in the region where  $e^{-Z} \gg 1$  ( $Z$  is negative for low levels). The term  $e^{-Z} f$  in the exponent then varies much more rapidly than the term  $1 - Z$  in the reflecting region (which is only a few km. thick—see figure 6). We may therefore treat  $1 - Z$  as approximately constant, writing

$$I'_0 = I_0 \times \text{mean value of } e^{1-Z},$$

we have

$$\begin{aligned} I &= I'_0 \exp [-f \exp (-Z)] \\ &= I'_0 \exp [-\exp (-Z + \log f)]. \end{aligned}$$

If there is quasi-equilibrium between the rate of production of ions and their disappearance by recombination or attachment, we shall have

$$N = F(I),$$

where the function  $F$  depends on the exact manner of disappearance. For simple recombination alone

$$N = N_0(I/I'_0)^{\frac{1}{2}}.$$

The above approximation will then be sufficiently accurate if the layer is such that

$$N'_0 > 10^4.$$

The ionization varies so rapidly with height, like  $\exp[-\frac{1}{2}\exp(-Z)]$  that it increases from a negligible value to one amply sufficient to reflect the waves in a distance of a few km. Since the wave-length is 18.8 km., reflexion may therefore be thought of as taking place at a sharp boundary, in contrast to the reflexion of short waves which are gradually bent round.

From the expression for  $I$  it will be seen that as  $\log f$  increases at sunset the bottom of the layer moves upwards without any change of shape. The equivalent reflexion height (as measured by the phase of the reflected wave relative to the ground wave) will therefore increase, its change being proportional to  $\log f$ . This will be true whatever the actual mechanism of reflexion since the region always presents the same aspect to the wave, but at different heights.

The argument is not strictly true if collisional friction is present in a varying degree at different heights, since more ionization is required to reflect the waves in a region where there is considerable collisional friction than in a region where there is only a little. For reasons given in § 5 I do not consider that collisional friction is important anywhere in the reflecting region, but in any case differences of a few hundred per cent in the amount of ionization required for reflexion would not appreciably affect the height of reflexion as such a change corresponds to only a small difference in height. For the same reason, a variation with height of the recombination coefficient would not be expected to show up unless it were very great.

The variation of the observed phase lag with  $\log f$  is discussed in II, and it is shown that the above relation does hold quite accurately. It is there shown how a value for  $H$  can be calculated from the slope of the straight line obtained by plotting phase lag against  $\log f$ , and this is found to be  $6 \pm 0.5$  km. For further details see II, § 4.

### 3. POLARIZATION AND AMPLITUDE OF REFLECTED WAVE

In making theoretical calculations about the propagation of short waves it is possible to assume that the medium is slowly varying, i.e. that its constants vary by only a small fraction of themselves in a distance comparable with the wave-length. This is the same as using a ray theory in optics. For waves whose length is 18.8 km., it is no longer obvious that this assumption is justified, and the problem has to be approached by way of wave theory. I shall, however, in this section discuss the type of reflected wave to be expected if the "slowly-varying" theory applicable to short waves continued to hold, and later discuss the modifications to be expected on using a wave theory. It will be shown that these modifications are less

than might be expected. Two cases will be considered, one with, and the other without the Lorentz term.

We use the following notation:

- $c$  = velocity of electromagnetic waves *in vacuo*.
- $m$  = mass of an electron.
- $e$  = charge of an electron (e.s.u.).
- $N$  = electron density.
- $H_e$  = the earth's magnetic field in gauss.
- $H_L$  = component of the earth's magnetic field along the positive direction of propagation.
- $H_T$  = component of the earth's magnetic field perpendicular to the direction of propagation.
- $p = 2\pi \times$  frequency of waves ( $\doteq 10^5$  for 16 kc./sec.).
- $k = p/c$ .
- $\nu$  = the frequency of electronic collisions (which determines the effective damping).
- $x = \frac{4\pi Ne^2}{mp^2}$  ( $\doteq 0.3 N$  on 16 kc./sec.).
- $y = \frac{eH_e}{mcp}$  ( $\doteq 80$  on 16 kc./sec.).
- $y_L = \frac{eH_L}{mcp}$ .
- $y_T = \frac{eH_T}{mcp}$ .
- $z = \frac{\nu}{p}$ .
- $l$  = a parameter which is taken equal to zero if the Lorentz term is to be omitted, and equal to  $\frac{1}{2}$  if it is to be included.

In discussing the magneto-ionic equations it is usual to consider two separate cases, known respectively as quasi-longitudinal and quasi-transverse propagation, the conditions for which are respectively

$$\frac{y_T^4}{4y_L^2} \ll \quad \text{or} \quad \gg [1 - (1-l)x]^2 + z^2.$$

It is found that these cover most of the cases required in practice (Appleton and Builder 1933; Booker 1935).

In the experiments described in I and II,  $p = 10^5$  and the angle of incidence on the ionosphere was about  $30^\circ$  in a south-east direction, the latitude being  $52^\circ$ . This makes the left-hand side of the inequality about 10.

It will be seen that the condition for quasi-longitudinal propagation can

be satisfied either on account of a high value of ionization density or of collisional frequency. The critical region is where  $x$  is of the same order as  $1/(1-l)$ . This implies an electron density of about 3 or 4 per c.c., and the value of  $z$  here may be expected to be sufficiently large to make conditions quasi-longitudinal. Once the waves have passed this region they will not be reflected until they have reached the place where  $x$  is of the order of  $y$ , and consequently large enough for the quasi-longitudinal condition to hold. In all that follows, therefore, the quasi-longitudinal formulae will be used.

The incident plane polarized wave gives rise to two waves in the medium—the magneto-ionic components—which are propagated independently (Booker 1936). The refractive index as a function of the intensity of ionization for the two waves is, according to Appleton's theory, given by (quasi-longitudinal conditions)

$$q^2 = (\mu - i\chi)^2 = 1 - \frac{x}{1 + lx - iz \pm y_L}. \quad (1)$$

Both waves are circularly polarized, one left-handedly and the other right-handedly about the downward vertical. In the northern hemisphere these correspond respectively to the upper and lower signs. Reflexion takes place at the lowest level where  $\mu = 0$ ; if no such level exists the wave passes right through the region.

Curves showing the variation of  $\mu$  with  $x$  are plotted in figure 1*a* for each component in the case  $z = 0$  (no Lorentz term). It will be seen that for the left-handed component  $\mu$  becomes zero for  $x = 1 + y$ . This wave is therefore reflected. For the right-handed component  $\mu$  increases without limit, and never becomes zero and this wave is not reflected. An incident plane polarized wave therefore gives rise to a left-handed circularly polarized reflected wave. The resultant reflexion coefficient is  $\frac{1}{2}$ . If  $z$  is not zero, absorption takes place. The effect of this will be considered later when discussing the wave theory.

The corresponding curves  $l = \frac{1}{3}$  are given in figure 1*b*. The refractive index for the left-handed component decreases in much the same way as when  $l = 0$ , and this component is totally reflected. For the right-handed component  $\mu$  also becomes zero for large values of  $x$ , but before doing so it passes through an infinity when  $x = 3(1-y)$ . The fact that  $\mu$  is zero for large values of  $x$  means that no energy can be propagated right through the medium, and therefore if  $z = 0$  there must be total reflexion. If, however,  $z$  is appreciable it may be expected that strong absorption will take place where  $\mu$  is large. The amount of such absorption can be estimated only roughly on a ray theory, and the question of determining the minimum value

of  $z$  which gives appreciable absorption will be discussed later using a wave theory.

It follows that when  $l = \frac{1}{3}$  and  $z$  is sufficiently small, both components are totally reflected, and the resultant downcoming wave is plane polarized (not necessarily in plane of incidence) and the resultant reflexion coefficient is unity.

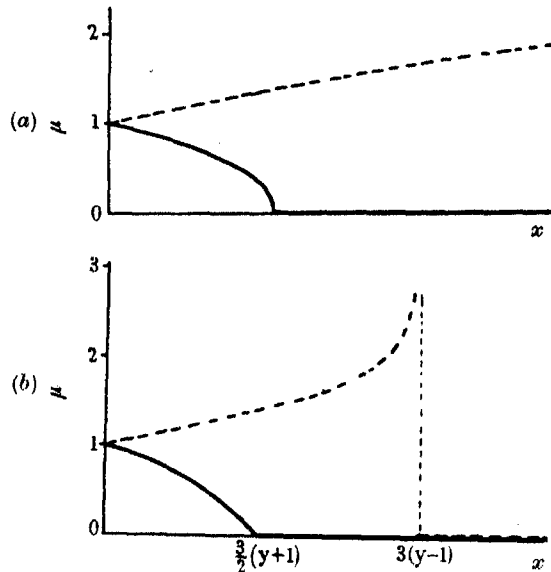


FIGURE 1. Variation of  $\mu$  with  $x$ , upper figure (a), without Lorentz term; lower figure (b), with Lorentz term.

#### 4. WAVE THEORY

##### (a) *Reflection from idealized regions*

It has already been pointed out that for waves 18.8 km. long the use of a theory in which it is assumed that the constants of the medium vary by only a small fraction of themselves in a distance equal to the wave-length is not really justifiable. The alternative and correct way of proceeding is to obtain a solution of the set of differential equations comprising the field equations and the equations of motion of the electrons. If this is attempted it is found that in general the magneto-ionic components do not exist, and the problem depends on the solution of a fourth-order differential equation governing the propagation of waves in the medium. This being so, it is not possible to make any progress with the general problem, except perhaps by numerical methods.

However, in the special case of normal incidence on a stratified medium, with the magnetic field parallel to the direction of propagation, the magneto-ionic components exist even in the case of a rapidly varying medium. The fourth-order differential equation splits into two second-order equations, one for each component. As this case corresponds roughly to the conditions of the experiments it will be adopted, and solutions given for certain assumed distributions of ionization. The results will not be found to differ greatly from those to be expected on "slowly varying" theory, and since the quasi-longitudinal condition holds, we should not expect the results at slight inclination to the field, and at slightly oblique incidence to be appreciably different from the purely longitudinal case.

As we go up in the atmosphere, the ionization increases and the collisional frequency decreases. In order to solve the differential equation it is necessary to assume some definite law of variation for each of these, and in general the equation will have to be solved numerically. However, in two special cases, which represent extreme idealizations of the ionosphere, it has been possible to obtain solutions in terms of standard functions, and these are treated in detail below. It is shown later that one of them can be used to deduce the wave reflected from a Chapman region.

The two cases are

(1) Collisional frequency constant, and ionization increasing according to a square law with height.

(2) Ionization constant, and collisional frequency decreasing inversely as the increase of height.

It can be shown that the differential equations to be solved for the two components are

$$\frac{d^2 L}{ds^2} + k^2 \left( 1 - \frac{x}{1 - iz \pm y} \right) L = 0, \quad (2)$$

where  $s$  is a linear coordinate in the direction of propagation,  $L$  is the amplitude of the component in question, the  $+$  sign refers to the left-handed component, and the  $-$  sign to the right-handed component.

Suppose we find a solution of equation (2), say  $F(\zeta)$ , where  $(\zeta)$  is a function of  $s$ , which satisfies suitable conditions as  $s$  tends to infinity. Then if the complex reflexion coefficient for the component\* in question is  $R$ , the complete solution of the problem is

$$\begin{aligned} L &= F(\zeta) & s > 0, \\ &= Re^{iks} + e^{-iks}, & s < 0. \end{aligned}$$

\* Care should be taken to distinguish between the reflexion coefficients for the separate components, and that for the whole incident wave.



The boundary conditions at  $s = 0$  ( $\zeta = \zeta_0$ ) are that  $L$  and  $\partial L/\partial s$  should be continuous. Expressing these we finally obtain

$$R = \frac{1 + i\sigma}{1 - i\sigma},$$

where

$$\sigma = -\frac{1}{k} \frac{d\zeta}{ds} \frac{F'(\zeta_0)}{F(\zeta_0)}. \quad (3)$$

*Case 1. Ionization increasing according to square law.*

$$z = \text{constant},$$

$$x = Ks^2, \quad s > 0,$$

$$= 0, \quad s < 0.$$

From equation (2), taking  $z = 0$  for the present, and omitting the Lorentz term,\*

$$\frac{d^2 L}{ds^2} + k^2 \left( 1 \pm \frac{ks^2}{y} \right) L = 0. \quad (4)$$

Consider first the wave whose polarization is left-handed, i.e. the one corresponding to the lower sign. Following Hartree† we put

$$\zeta = 2^{\frac{1}{2}} \frac{k}{\alpha} s,$$

$$n = \frac{1}{2}(\alpha^2 - 1),$$

where  $\alpha^2 = k\sqrt{(y/K)}$ , giving

$$\frac{d^2 L}{d\zeta^2} + \left( n + \frac{1}{2} - \frac{1}{4}\zeta^2 \right) L = 0, \quad (5)$$

which is the form of the equation which Whittaker and Watson (1927, p. 347) take as standard. Two independent solutions of it are, in their notation,  $D_n(\zeta)$  and  $D_{-n-1}(-i\zeta)$ . For large  $|\zeta|$

$$D_n(\zeta) \sim e^{-i\zeta^2} \zeta^n$$

provided  $|\arg \zeta| < \frac{3\pi}{4}$ . Thus  $D_n(\zeta)$  and  $\frac{\partial}{\partial \zeta} D_n(\zeta)$  both tend to zero as  $s$  tends to infinity.

$F = D_n(\zeta)$  is therefore the solution in this case. Using results given by Whittaker and Watson, we obtain from (3)

$$\sigma = \frac{2 I' \left\{ \frac{1}{2}(3 - \alpha^2) \right\}}{\alpha I' \left\{ \frac{1}{2}(1 - \alpha^2) \right\}}.$$

\* As a slight simplification  $\pm y$  has been written for  $1 \pm y$ , since  $y \gg 1$ .

† Hartree (1931) discusses equation (4) with the minus sign in relation to slowly varying media.

Since  $\alpha$  is real

$$|R| = \left| \frac{1+i\sigma}{1-i\sigma} \right| = 1,$$

and the wave is totally reflected whatever  $\alpha$ .

For the other wave we make the substitution

$$\zeta = (2i)^{\frac{1}{2}} \frac{k}{\alpha} s; \quad n = -\frac{1}{2}(i\alpha^2 + 1),$$

giving as before equation (5). The two linearly independent solutions are, with their asymptotic expansions for large  $|\zeta|$

$$D_n(\zeta) \sim Ce^{-i\zeta^2} \zeta^{-i(1+i\alpha^2)},$$

$$D_{-n-1}(-i\zeta) \sim Ce^{i\zeta^2} \zeta^{-i(1-i\alpha^2)}.$$

Each of these tends to zero like  $\zeta^{-i}$  as  $s \rightarrow \infty$ , i.e. as  $\zeta \rightarrow i^{\frac{1}{2}}\infty$ , but it is not possible to find a linear combination of them such that its derivative tends to zero at infinity. This corresponds physically to the fact that energy is flowing to infinity, so that the Poynting vector (which is numerically proportional to the product of the real parts of  $F$  and  $\partial F/\partial s$ ) must be finite.

Clearly  $D_n(\zeta)$  represents a flow of energy in the direction of  $s$  increasing, while  $D_{-n-1}(-i\zeta)$  represents a flow in the opposite direction. The former is therefore the appropriate solution. Equation (3) then gives

$$\sigma = \frac{2}{\alpha} e^{i\pi i} \frac{\Gamma\{\frac{1}{4}(3+i\alpha^2)\}}{\Gamma\{\frac{1}{4}(1+i\alpha^2)\}}.$$

Using Stirling's theorem  $\sigma$  can be computed from this formula.

The curves marked  $z = 0$  in figures 2 and 3 show how the reflexion coefficient depends on the sharpness of the boundary as measured by  $\alpha^2$ . For large values of  $\alpha^2$ , the right-handed wave is scarcely reflected at all, while the left-handed wave is totally reflected. This is what is to be expected from the "slowly varying" theory in §3. For smaller values of  $\alpha^2$  this theory breaks down, and reflexion of the right-handed wave takes place.

If  $z$  is not zero the differential equation for  $L$  is

$$\frac{d^2 L}{ds^2} + k^2 \left( 1 - \frac{Ks^2}{\pm y - iz} \right) L = 0.$$

As before this can be reduced to the standard form (5). The appropriate substitution is

$$\zeta = 2^{\frac{1}{2}} (\cos \beta)^{\frac{1}{2}} \frac{k}{\alpha} e^{i\phi} s,$$

$$n = \frac{1}{2} [\alpha (\sec \beta)^{\frac{1}{2}} e^{-i\phi} - 1],$$

where  $\beta = \tan^{-1}(z/y)$  (the acute angle), and the right- and left-handed components are respectively given by

$$\phi = \pi - \beta \quad \text{and} \quad \phi = \beta.$$

Two independent solutions are  $D_n(\zeta)$ ,  $D_{-n-1}(-i\zeta)$ .

Using the asymptotic expansion given by Whittaker and Watson it can be seen that the first of these tends to zero as  $s \rightarrow \infty$ . It is therefore the solution required.

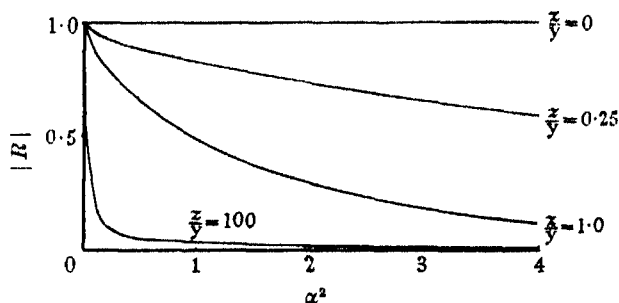


FIGURE 2. Reflexion coefficient for the left-handed component ( $x \propto s^2$ ).

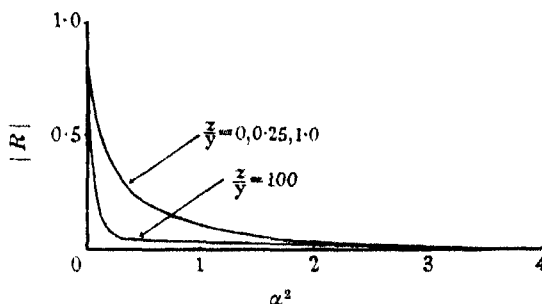


FIGURE 3. Reflexion coefficient for the right-handed component ( $x \propto s^2$ ).

We have now for  $\sigma$ :

$$\sigma = \frac{2}{\alpha} e^{i\phi} \frac{I\left\{\frac{1}{4}[3 - \alpha^2(\sec \beta)^{\frac{1}{2}} e^{-i\phi}]\right\}}{I\left\{\frac{1}{4}[1 - \alpha^2(\sec \beta)^{\frac{1}{2}} e^{-i\phi}]\right\}}.$$

Figures 3 and 4 show curves plotted from this formula for different values of  $z/y$ . It will be seen that for values of  $z/y$  of about unity the amplitude of the left-handed component is reduced, while that of the right-handed component is not affected appreciably. For large values of  $z/y$  the curves for the two components become identical.

We have taken  $x = Ks^2$  for all  $s > 0$ . The ionization in the ionosphere does not actually become infinite, and a more accurate representation of it would be

$$\begin{aligned} x &= Ks^2, & 0 < s < s, \\ &= Ks_1^2, & s > s, \end{aligned}$$

and the solution can be worked out in this case. However, the value of  $x$  actually attained in the  $E$  region (about 3000 at night and  $10^5$  in the day time) is so large that it is sufficiently accurate to take it as infinite.

*Case 2. Ionization constant and friction decreasing inversely as the distance.*

The reflecting region is defined by

$$\begin{aligned} x &= \text{constant}, \\ z &= \beta/s, \quad s > 0, \\ z &\text{ infinite, } s < 0. \end{aligned}$$

The wave equation is

$$\frac{d^2 L}{ds^2} + k^2 \left( 1 - \frac{sx}{-i\beta \pm sy} \right) L = 0.$$

It will be assumed that  $y/x < 1$ . This can be reduced to the following standard form:

$$\frac{d^2 L}{d\zeta^2} + \left( -\frac{1}{4} + \frac{K}{\zeta} \right) L = 0, \quad (6)$$

which is a special case of Whittaker's equation (1927, p. 335), by making the transformation

$$\begin{aligned} \zeta &= -2ikq_0 \left( s \mp \frac{i\beta}{y} \right), \\ K &= \frac{k\beta}{2xyq_0}, \end{aligned}$$

where  $q_0 = \sqrt{(1 \mp x/y)}$ , when

$$s = 0, \quad \zeta = \zeta_0 = \mp \frac{2kq_0\beta}{y}.$$

The two solutions with their asymptotic forms for large  $\zeta$  are

$$\begin{aligned} W_{K, \frac{1}{2}}(\zeta) &\sim \zeta^K e^{-i\zeta} \propto s^K e^{ikq_0 s} \quad \text{provided } |\arg \zeta| < \pi, \\ W_{-K, \frac{1}{2}}(\zeta) &\sim \zeta^{-K} e^{i\zeta} \propto s^{-K} e^{-ikq_0 s} \quad \text{provided } |\arg -\zeta| < \pi. \end{aligned}$$

For the right-handed wave (lower sign)  $q_0$  is real: take the positive value of the square roots so that  $q_0 > 0$ . Then  $K$  and  $\zeta_0$  are real and positive. The appropriate solution (for outgoing waves) is  $W_{-K, \frac{1}{2}}(-\zeta)$ .

For the left-handed wave (upper sign)  $q_0$  is a pure imaginary; take  $iq_0$  real and positive. Then  $iK$  and  $i\zeta_0$  are real and negative, so that the solution which tends to zero as  $s$  tends to infinity is  $W_{-K, \frac{1}{2}}(-\zeta)$ .

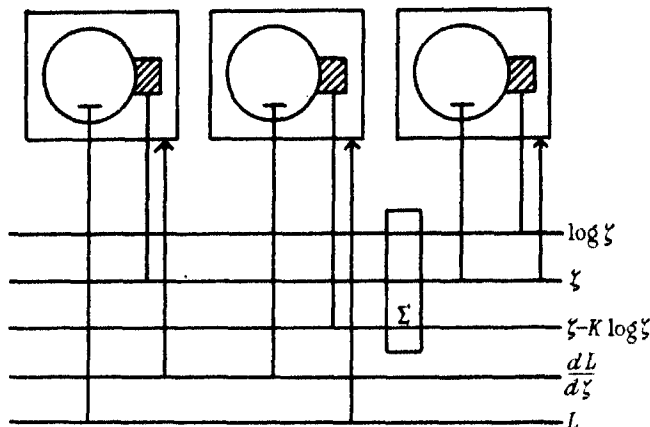


FIGURE 4. Set up of the differential analyser for the equation

$$\frac{d^2 L}{d\zeta^2} + \left(1 - \frac{K}{\zeta}\right)L = 0 \quad \text{or} \quad \frac{dL}{d\zeta} + \int L d(\zeta - K \log \zeta) = 0.$$

(Scale and sign factors are omitted.)

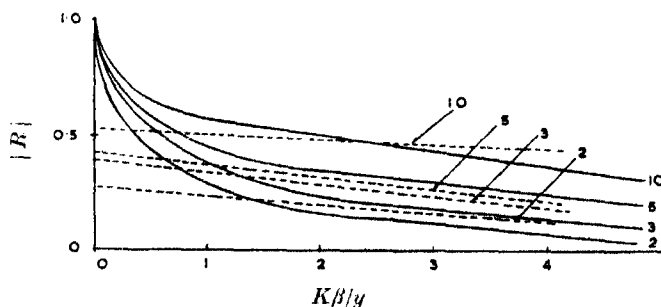


FIGURE 5.  $z \propto 1/s$ . The continuous curves refer to the left-handed component, and the dotted curves to the right-handed component. The number against each curve is the corresponding value of  $x/y$ .

Thus in each case the reflexion coefficient is obtained by taking

$$\sigma = 2iq_0 \frac{\frac{d}{d\zeta} W_{-K, \frac{1}{2}}(-\zeta_0)}{W_{-K, \frac{1}{2}}(-\zeta_0)}.$$

Unfortunately no suitable tables of the Whittaker functions have been published. Using the methods given in Whittaker and Watson, a power

series (involving a logarithmic term) valid for small  $\zeta$ , and an asymptotic expansion valid for large  $\zeta$ , can be obtained. The function was, however, required for intermediate values, and it was actually evaluated by direct solution of the differential equation (6) using the model of the Bush Differential Analyser belonging to the Mathematical Laboratory, Cambridge (Lennard-Jones, Wilkes and Bratt 1939). The set up is given in figure 4. Integral values of  $K$  from 1 to 5 were taken.

Curves showing how the reflexion coefficient varies with the sharpness of the transition as measured by  $\beta$  are given in figure 5. This case will not be discussed in greater detail because, as will be seen in the next subsection, case 1 is likely to be a much better approximation to the actual structure of the ionosphere.

#### (b) Reflexion from a Chapman region

We have already seen how the changes of reflexion height which occur at sunset can be explained by supposing that reflexion takes place from the bottom of a Chapman region. It is therefore interesting to calculate the reflexion coefficient of such a region for the two components. In this subsection I shall show how this can be done using the results of case 1 above. Direct solution of equation (2) for a Chapman region is not possible except by numerical methods.

The ionization at the base of a Chapman region (assuming recombination to take place) increases very rapidly like  $\exp \frac{1}{2}(-\exp -Z)$ , while the collisional friction decreases much more slowly, like  $\exp(-Z)$ . This can be represented approximately by case 1 above, in which the friction is constant and the ionization increases according to a square law. The value of  $\alpha^2$  is to be chosen to give as good a fit as possible between the actual ionization curve, and the parabola in the region where  $x$  is of the same order of magnitude as  $|-iz \pm y|$ .

The parabola may either be fitted to the ionization curve graphically, or, in the case of a Chapman region, an analytical formula may be obtained for  $\alpha^2$  in terms of the constants of the region by equating the slopes of the two curves at the point  $Z_1$  where  $x = x_1$  given by  $x_1 = |-iz \pm y|$ . This gives

$$\alpha^2 = \frac{2kH}{\log \frac{x_1}{x_0} - \frac{1}{2}Z_1} \sqrt{\frac{y}{x_1}}.$$

In order to test the accuracy of the method, a numerical wave solution has been worked out for one representative case, that of a Chapman region in which  $N_0$  was  $10^5$  electrons per c.c., and the scale height 10 km. Figure 6

shows ionization and collisional friction plotted against height, and also the amplitude of the disturbance propagated in the medium. On the left-hand side of the curve where the wave is travelling in free space standing waves formed by interference between the reflected and incident waves are shown. In the ionized medium the disturbance is rapidly attenuated when it reaches the region where  $x = x_1$ , falling to a small value in the distance

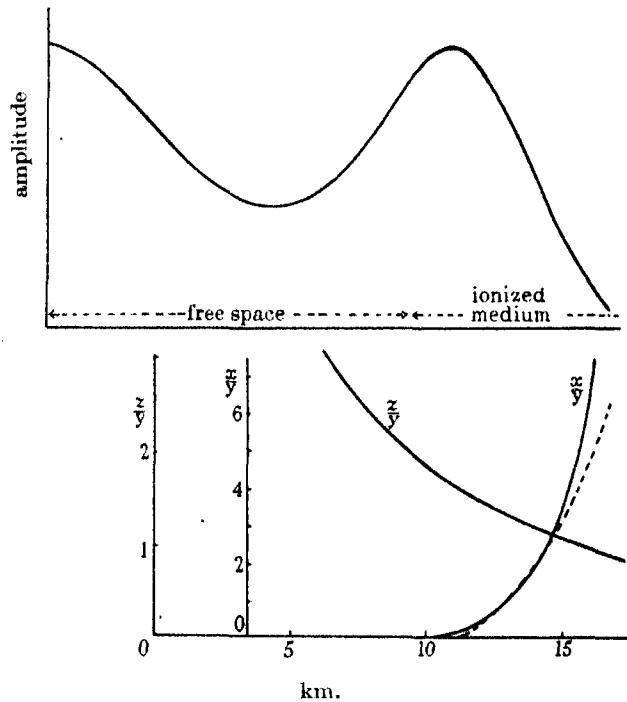


FIGURE 6. Wave incident on a Chapman region. The lowest curves give the variation of ionization and collisional frequency in the region, and the upper curve the amplitude of the propagated wave.

of a few km. The collisional frequency is nearly constant over this distance, and a parabola, shown dotted, can be fitted to the ionization curve with fair accuracy in this region.

The value of  $\alpha^2$  corresponding to the parabola shown is 0.9 and the value of  $z$  about 1.2. Referring to the curves in figure 2 (the numerical wave solution is for the left-handed wave) the reflexion coefficient is found to be 0.4. Its actual value from the numerical wave solution is 0.44. This is sufficient accuracy for the purpose in view.

Some curves are given in figure 7 showing how the reflexion coefficient depends on the collisional frequency in the reflecting region for two different values of  $N_0$  in the region. If the whole  $E$  region may be regarded as a single Chapman region this will be about  $5 \times 10^5$ , but it may be that long waves

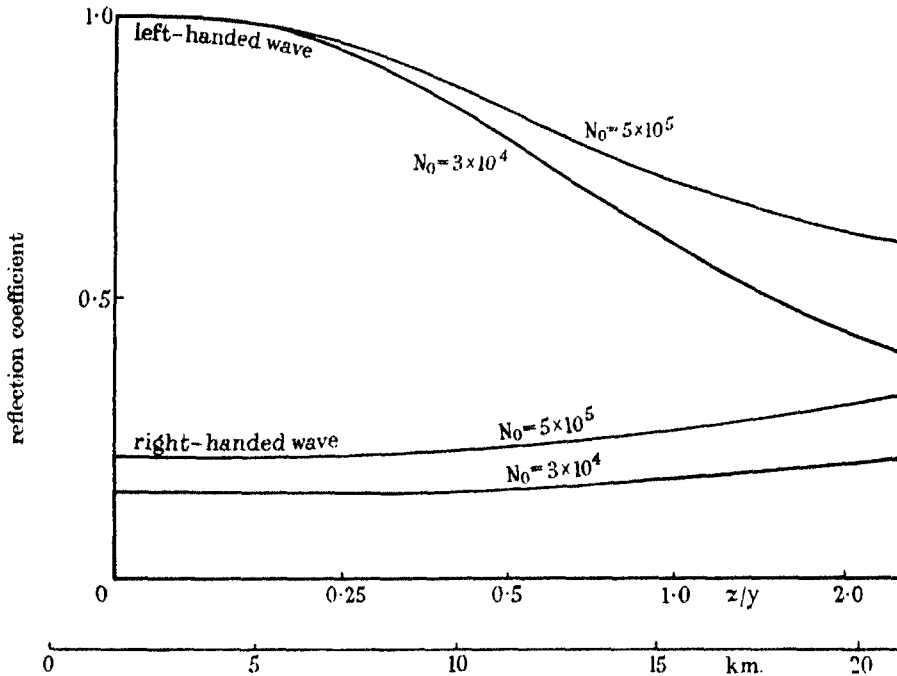


FIGURE 7. Reflexion coefficients for a Chapman region.

are reflected from a subsidiary region just below the main region. The scale height is taken as 6 km., the value which fits the phase variations. It will be noticed that though the values of  $N_0$  taken differ widely, there is little difference between the two curves. For convenience a scale of height is also given.

## 5. CONSIDERATION OF EXPERIMENTAL RESULTS

### (a) Amplitude

It has already been shown that the variations in the phase of the down-coming wave which are observed to take place at sunset can be explained on the basis of reflexion from the bottom of a Chapman region. The variations of amplitude, on the other hand, are not so simple, and depend not



only on the zenith angle of the sun but on the time of the year. For example, at noon on 21 December and at about 17.00 hr. local time on 21 June (at Cambridge) the zenith angles of the sun are the same, but the amplitude on the former occasion is about five times as great as on the latter. It would appear therefore that there must be some physical difference in the ionosphere between winter and summer. We are not able to put forward any rational explanation of this.

The deductions are based as far as possible on the summer daytime results, since at this time of the year conditions are very steady and repeat well from day to day. There are three main facts which emerge:

- (1) The amplitude is very constant during the day, until the sunset phase cycle is nearly over when it increases rapidly.
- (2) The steady daytime reflexion coefficient is about 0.12.
- (3) The polarization of the wave is roughly circular (left-handedly). More accurately, it is an ellipse with its major axis on the vertical plane, and 1.5 times the minor axis.

To simplify the discussion the theory in which the Lorentz term is omitted is used in this section. The question of including it will be discussed in § 6.

Fact (2) shows at once that some collisional absorption must take place, because otherwise the reflexion coefficient is never less than 0.5. There are two possibilities:

- ( $\alpha$ ) absorption in the reflecting region;
- ( $\beta$ ) absorption in a region situated below the reflecting region.

Referring to figure 7 in which reflexion coefficient for each component is plotted against  $z/y$  it will be seen that possibility ( $\alpha$ ) requires that  $z/y$  should be of the order of unity. The reflexion coefficient is very sensitive to changes in  $z/y$  and for it to remain constant during the sunset period it is necessary for  $z/y$  to be constant to within about 25 %. On the other hand, we know that as the sun sets the level at which reflexion takes place moves upwards and so passes into regions where the air pressure is lower. The total change in reflexion height is about 18 km.—three times the scale height—corresponding to a decrease by a factor of 20:1 in the air pressure. It is difficult to see how the collisional frequency could be unaffected by this change in pressure. It would be more reasonable to suppose that it were proportional to air pressure, in which case it would likewise decrease by a factor of 20:1. Such a large percentage change in  $z$  could only be without effect on the amplitude of the reflected wave if  $z/y$  were everywhere negligibly small in the reflecting region. I therefore consider that there can be no appreciable friction in the reflecting region. This is so if  $z/y < 0.25$

(say) at the lowest reflecting level which is estimated in II to be 65 km., i.e.  $\nu < 2 \times 10^6$  at 65 km. At the highest level  $z/y$  will then be less than 0.01.

Consideration will now be given to possibility ( $\beta$ ) in which there is a separate absorbing region situated below the reflecting region. This raises several interesting questions. In the first case it is not obvious that such a region can exist for very long waves, since the change from free space to absorbing conditions must take place in a distance which is of the same order as the wave-length, and this might be expected to result in reflexion of most of the energy. In order for it to be a true absorbing region, the amount so reflected has to be small compared with the wave reflected higher up, which has suffered absorption twice, once in passing through the region on the way up, and once on the way down. To investigate this point, some numerical solutions\* of the field equations have been made for one or two hypothetical regions in which the ionization was assumed to be constant, and  $z$  to decrease exponentially with a scale height of 10 km. Such a region, with an ionization density of 60 to 120 electrons per c.c. absorbs 60–80 % of the wave, and reflects less than 3 %. The existence of a purely absorbing region for long waves would therefore appear to be quite possible. It should be noted that for this amount of ionization the absorption coefficient  $\chi$  given by equation (1) has the same value for each component.

Moreover, it is interesting to see that a Chapman region† depending on ultra-violet light from the sun, and situated very low down in the atmosphere, would give a diurnal variation of the right kind. The absorption of a wave traversing such a region has been considered by Appleton who gives an expression from which it can be calculated (Bakerian lecture 1937). If  $\nu$  at the maximum of the region,  $\nu_0$ , is small compared with  $p$ , the absorption takes place mainly at the bottom of the region, and is proportional to  $[f(\chi)]^\dagger$ ; this is the case applicable to short waves absorbed in a "D" region. If, however,  $\nu_0 \gg p$ , as it would be in the case of low-frequency waves and a region extremely low down, like the one we are considering, the absorption takes place at the top. The ionization here depends very little on the zenith angle of the sun until it has nearly set, and the absorption is therefore nearly constant until near sunset. Two curves calculated from Appleton's formula, contrasting the two cases, are shown in figure 8. One is for  $\nu_0 \ll p$

\* These numerical solutions have been obtained using the method described by Hartree (1933), extended to deal with equations involving complex numbers. It was found possible to avoid a good deal of the numerical labour by making use of the Mallock Linear Equation machine in the Mathematical Laboratory, Cambridge (Mallock 1933), and it is hoped to publish a note describing this method elsewhere.

† This region is supposed to be situated below, and to be independent of, the region responsible for reflexion.

and the other for  $\nu_0 = 500p$ . The latter gives a constant amplitude during the day with a sudden increase at sunset, which is the type of variation observed.

In the winter there is not so much daytime absorption as in the summer (see II), so we must suppose that there is a seasonal change in the constants of the absorbing region. This need not be large since absorption is very sensitive to changes in ionization or collisional friction in the region. The effect is probably connected with the slight general depression of reflexion heights in the winter mentioned in II.

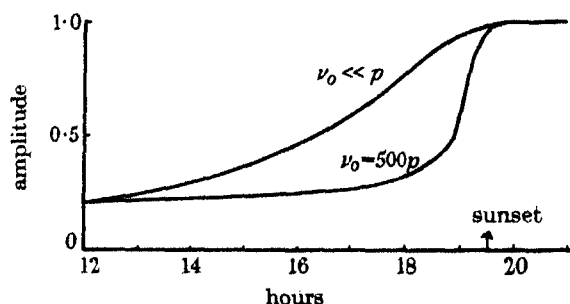


FIGURE 8. Diurnal variation of absorption in a Chapman region.

### (b) Polarization

The fact that the polarization remains as constant as can be determined during the greater part of the sunset period agrees with the conclusion arrived at above that  $z/y$  is negligible in the reflecting region. Knowing this we can read off from figure 7 the relative amplitude of the left- and right-handed components after reflexion. It will be noticed that these depend very little (within wide limits) on the maximum ionization in the region ( $N_0$ ). The left-handed wave is reflected totally, and the right-handed wave to the extent of about 20%. Adding the components together we obtain a polarization ellipse in which the axes are in the ratio 3:2. This is in agreement with the experimental results.

## 6. THE LORENTZ TERM

It is not possible to obtain solutions in analytical form of the equation corresponding to equation (2) when the Lorentz term is included, either in the case of a Chapman region or a parabolic region. Consequently, in order to investigate the effect of the Lorentz term a number of solutions have been obtained numerically (see § 5, footnote).

It has already been pointed out that when the Lorentz term is included both waves are totally reflected if  $z = 0$ , but that if  $z$  is appreciable considerable absorption may be expected to take place. The object of the numerical wave solutions is to determine for what values of  $z$  this absorption becomes important. In the case of a Chapman region ( $N_0$  about  $10^5$ ,  $H = 6$  km.) it is found that the reflexion coefficient for the right-handed wave is about 70 % when  $z = 0.1$ , and this may be taken as the critical value of  $z$ . For smaller values the reflexion is total, and for larger values the reflexion coefficient may be expected to be nearly the same as with the Lorentz term omitted, since all the energy will be either absorbed or reflected before the region where the Lorentz term is important is reached. This is confirmed by actual solutions for  $z = 0.25$ , and  $1.0$ . It follows from the fact that the reflexion coefficient is the same with or without the Lorentz term when  $z/y > 0.1$ , that the reasons given above for believing that  $z/y < 0.25$  at the lowest reflexion level (65 km.) still hold if the Lorentz term is included. Since  $z/y$  decreases exponentially with height, it will be less than 0.1 above 70 km., and consequently the polarization of the reflected wave when reflexion takes place above this level will depend on whether the Lorentz term is included or omitted.

When it is omitted the downcoming wave is elliptically polarized with axes in the ratio 3 : 2. With it included the wave is plane polarized, though not necessarily in the plane of incidence. These two polarizations are so different that there is no doubt that the experiments are sufficiently good to discriminate between them. The first agrees with the experimental results, the second does not.

The long-wave evidence therefore appears to be against the inclusion of the Lorentz term. It cannot be regarded as conclusive, however, since the analysis used has been entirely one-dimensional. This means that the possibility that the right-handed wave may be deflected by the action of the magnetic field and escape horizontally has not been taken into account. Dr H. G. Booker has pointed out to the writer that this might well take place if conditions were slowly varying. An analysis of what would take place under rapidly varying conditions would be difficult since the magneto-ionic components are not then propagated independently.

## 7. PREVIOUS WORK

Some theoretical work on the reflexion of very long waves has been published by Green and Builder (1934). They sought to explain the experimental results of Hollingsworth (1928), who performed a series

of experiments under similar conditions to ours. As explained in Paper I, § 3, we do not agree with Hollingsworth and Naismith's conclusions.

Builder and Green regard the incident wave as split up into two magneto-ionic components, as is done in this paper, and they consider that each of these waves is totally reflected at some point in the ionosphere. Any difference in amplitude of the two waves on returning to the earth is then due to a different degree of absorption suffered by the waves when traversing the region below the actual place of reflexion. If I have understood them correctly, it will be seen that my point of view is quite different. I concentrate attention on the mechanism of reflexion, and show that unless the ionization gradient is very steep, only one of the waves is reflected, and it is this fact which determines the polarization of the resultant reflected wave. If any absorption takes place below the reflecting region, both waves will be equally affected.

Mention should also be made of a paper by Yokoyama and Shogo (1932) discussing the reflexion of waves from an ionized gas bounded by a sharp discontinuity in the absence of a magnetic field.

I wish to express my thanks to Mr J. A. Ratcliffe for his help in this work, and to Professor J. E. Lennard-Jones, F.R.S., Director of the Mathematical Laboratory, in connexion with the use of the calculating machines.

#### SUMMARY

This paper is concerned with the theoretical interpretation of the experimental data already published by Best, Ratcliffe and Wilkes and by Budden, Ratcliffe and Wilkes on the reflected wave received via the ionosphere at short distances (about 90 km.) from the British Post Office transmitter at Rugby (wave-length 18,800 m.; 16 kc./sec.). It is shown that the diurnal changes in reflexion height are in agreement with what would be expected if reflexion took place from the bottom of a region of the type described by Chapman, in which the ionization is in quasi-equilibrium with the changes in zenith angle of the sun. The polarization and amplitude of the wave reflected from a layer of ionized gas in a magnetic field when a plane polarized wave of wave-length comparable with the dimensions of the layer is incident on it are discussed, and in particular the type of wave reflected from a Chapman region is deduced. It is shown that the observed constancy of the amplitude of the downcoming wave until near the end of the sunset period leads to the conclusion that in the reflecting region the frequency of electronic collisions is not greater than about  $2 \times 10^6$  per sec.,

and the possibility of collisional absorption taking place below the reflecting level is discussed. The question of whether or not the "Lorentz term" is to be included in the magneto-ionic equations is considered, and it is shown that the long-wave evidence, though not conclusive, appears to be against including it.

#### REFERENCES

- Appleton 1937 *Proc. Roy. Soc. A*, **162**, 451.  
 Appleton and Builder 1933 *Proc. Phys. Soc.* **45**, 208, 673.  
 Best, Farmer and Ratcliffe 1938 *Proc. Roy. Soc. A*, **164**, 96.  
 Best, Ratcliffe and Wilkes (I) 1936 *Proc. Roy. Soc. A*, **156**, 614.  
 Booker 1935 *Proc. Roy. Soc. A*, **150**, 267.  
 — 1936 *Proc. Roy. Soc. A*, **155**, 235.  
 Budden, Ratcliffe and Wilkes (II) 1939 *Proc. Roy. Soc. A*, **171**, 188.  
 Chapman 1931 *Proc. Phys. Soc.* **43**, 26, 483.  
 Green and Builder 1934 *Proc. Roy. Soc. A*, **145**, 145.  
 Hartree 1931 *Proc. Roy. Soc. A*, **131**, 428.  
 — 1933 *Proc. Manchr Litt. Phil. Soc.* **77**, 91.  
 Hollingsworth 1928 *Proc. Roy. Soc. A*, **119**, 444.  
 Lennard-Jones, Wilkes and Bratt 1939 *Proc. Camb. Phil. Soc.* **35**, 485.  
 Mallock 1933 *Proc. Roy. Soc. A*, **140**, 457.  
 Whittaker and Watson 1927 *Modern Analysis*. Camb. Univ. Press.  
 Yokoyama and Shogo 1932 *Rep. Radio Res. Japan*, **2**, 145.
-

# The reaction of atomic hydrogen with hydrazine

BY E. A. B. BIRSE

*Chemistry Department, University of Edinburgh*

AND H. W. MELVILLE

*Colloid Science Department, University of Cambridge*

*(Communicated by J. Kendall, F.R.S.—Received 15 December 1939)*

The reason for studying the reaction of hydrogen atoms with hydrazine is that a controversy has arisen in attempting to elucidate the mechanism of the photochemical decomposition of ammonia. It has been generally agreed that the ammonia molecule is decomposed to a hydrogen atom and an amine radical when it absorbs light around  $2000^{\circ}\text{A}$ . Presuming that the atomic hydrogen combines on the walls or in the gas phase it is possible to calculate what its stationary concentration ought to be under any given set of conditions. If, however, the stationary concentration is actually measured by using para-hydrogen as a detector, as was done by Farkas and Harteck (1934), it is found that the measured value is lower than the value calculated from the above assumptions. A number of suggestions, discussed in detail in the following paper, were made to explain this discrepancy, and among the most reasonable was that of Mund and van Tiggelen (1937) who suggested that the hydrazine known to be formed in the system removed such atoms more rapidly than would occur in the ordinary course of events. The result of their suggestion was the invention of elaborate schemes to explain the mechanism of the ammonia photolysis. As a further essential step in the ammonia problem it therefore seemed necessary to measure the efficiency of the reaction between hydrogen atoms and hydrazine. At the same time further information was also desirable about the photochemistry of hydrazine itself. This paper will therefore be concerned with this aspect of the subject. The results will then be discussed in the following paper together with a number of new experiments on ammonia in order that the mechanism of the ammonia reaction may be more fully established.

Experiments by Dixon (1932), using electrically produced atomic hydrogen in a flow system, have shown that atomic hydrogen readily interacts with hydrazine, producing ammonia, nitrogen and hydrogen. Unfortunately, it is not possible to deduce even approximately the velocity coefficient of this

reaction. The only satisfactory method is to compare the reaction with one in which the velocity coefficient is known accurately. The ideal reaction for the purpose is the conversion of para-hydrogen. One disadvantage of this method is that the velocity of the reaction under study should be comparable with that of the para-conversion itself. If it is much faster certain modifications to the technique are necessary. This happens in the present instance.

#### APPARATUS

A schematic diagram of the essential parts of the apparatus is given in figure 1. A variety of reaction vessels to be described below may be attached at *R* by means of a waxed ground-joint. Hydrazine is readily absorbed

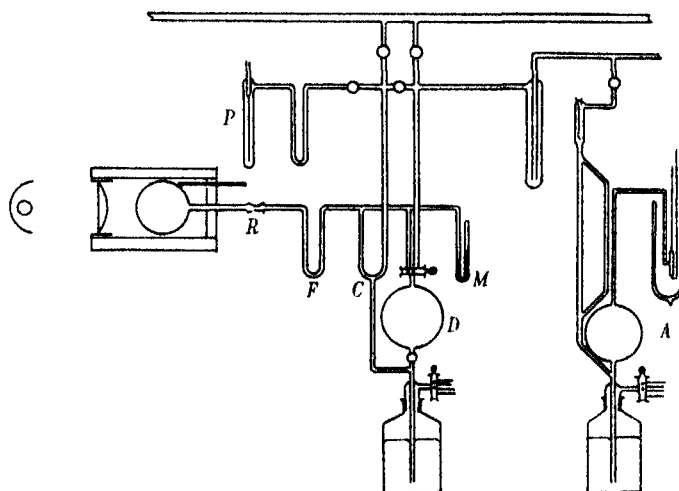


FIGURE 1. General diagram of apparatus.

even by Apiezon grease, and hence the reaction system is shut off from the remainder of the apparatus by a mercury cut-off *C*. The U-tube *F* was used for condensing out hydrazine and ammonia. Pressures are normally measured by a mercury manometer *M*. *D* is a combined Töpler pump and gas pipette arranged so that a convenient volume of gas could be withdrawn from the reaction system for delivery to the analytical devices. This is absolutely essential in view of the fact that hydrogen and nitrogen are easily separated in being transferred along many centimetres of relatively narrow-bore glass tubing. If a number of small doses are removed from the reaction system this partial separation is much accentuated, with the



result that the hydrogen percentage of a hydrogen-nitrogen mixture is always much too high. A further advantage of this arrangement is that hydrazine may rapidly be removed from the reaction mixture at high pressures by flowing the gases a few times through *F*. It is a curious fact that hydrazine, when mixed with high concentrations of say nitrogen and hydrogen, often escapes removal when passed through a liquid-air trap. This system is also employed to measure the pressure of gases, non-condensable in liquid air, present during the reaction. This is necessary since even with the above-mentioned precautions hydrazine is strongly adsorbed on the walls of the reaction vessel, so that it vitiates the readings on the manometer *M*. However, by freezing out the hydrazine, withdrawing small doses by the Töpler pump and expanding into a McLeod gauge the pressure of non-condensable gas can easily be measured with reasonable accuracy. Two Pirani gauges *P* and a micro-thermal conductivity analyser *A* of a type described previously (Bolland and Melville 1937) are also attached to the apparatus. Another precaution which enables the speed of the operation of the Pirani gauges to be increased consists in protecting each from hydrazine vapour by a U-tube cooled in liquid air. Without such traps the zero of the Pirani is variable, and the time required to get a steady reading may be as much as 30 min.

A simplified type of micro-thermal conductivity gauge is employed, consisting of a tungsten spiral 0.1 mm. diameter, the gauge of the wire being 0.01 mm. with a resistance of 25 ohms at 20° C. Since the gauge is required for measuring para-hydrogen mixtures it is maintained at a constant temperature of 200° K while immersed in liquid oxygen. The potential required to maintain these conditions when the spiral is surrounded with gas at 50 mm. pressure is measured to 0.03 % by a high-voltage potentiometer (the voltage across the wire is about 4). For normal hydrogen-nitrogen mixtures the gauge is calibrated with known mixtures made up with the aid of the ordinary Pirani gauges, care being taken to prevent separation in manipulation. An unexpected effect arises during such calibrations. When samples of different volume but of exactly the same composition are used it is found that *different* voltages are required for balance. This effect is only appreciable with mixtures of about 25–75 % hydrogen. Its magnitude can be seen in figure 2 where the voltage difference is plotted against the volume of the gas in the analyser. With a little practice the volume of the dose during the reaction can be kept within reasonable limits so that this correction is small. It would appear that the phenomenon is due to some separation of the mixture by effusion effects, for the comparison capillary of the gauge is at room temperature while the gauge

itself is  $-183^{\circ}\text{C}$ , the two being connected by a capillary tube 0.05 mm. in diameter. Although the mean free path is of the order  $10^{-3}$  mm. the effect is just noticeable with a fairly sensitive potentiometer. With mixtures of  $\text{H}_2$  and  $\text{D}_2$  the effect is absolutely negligible. This correction is always applied when nitrogen-hydrogen mixtures are being analysed.

The para-hydrogen-normal hydrogen mixtures obtained during these experiments always contain a large percentage of nitrogen. A method of

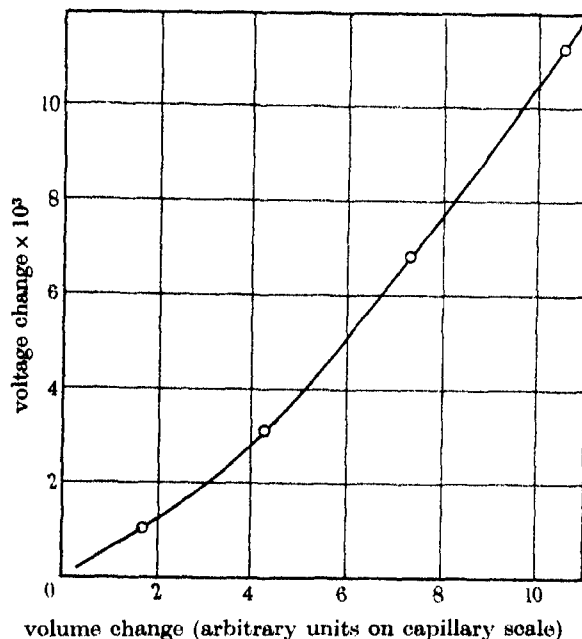


FIGURE 2. Change in analysis voltage with volume of sample.

analysing such ternary mixtures has already been worked out (Bolland and Melville 1937). This, however, necessarily involves rather a lengthy calibration, and the gauge must be absolutely constant in its behaviour. With para-hydrogen the method may be much simplified in the following way. First the voltage ( $V_{p-\text{H}_2}$ ) is read for the mixture as received from the reaction system. The mercury in the micro-gauge is then lowered so as to bring the mixture into contact with a glowing platinum wire for about 5 min. when the para-hydrogen is completely converted. Another voltage reading ( $V_{\text{equil}}$ ) is taken. These two figures alone will not provide sufficient data for computing the composition of the gas, since  $V_{p-\text{H}_2} - V_{\text{equil}}$  is not a true measure of the para-hydrogen content on account of the presence of nitrogen.

In the absence of nitrogen the heat loss by the wire may be expressed by the equation

$$kV^2 = bK_{p-H_2} + (1-b)K_{o-H_2},$$

where  $V$  is the voltage applied across the spiral,  $b$  is the fraction of para-hydrogen and  $K_{p-H_2}$  and  $K_{o-H_2}$  are the thermal conductivities of para- and ortho-hydrogen respectively. The change in applied voltage with change in para-hydrogen fraction is

$$\frac{dV}{db} = \frac{2kV}{K_{p-H_2} - K_{o-H_2}}.$$

Similarly in the presence of nitrogen the heat lost from the spiral is given by

$$kV_{N_2}^2 = dK_{N_2} + bK_{p-H_2} + (1-b)K_{o-H_2}$$

and

$$\frac{dV}{db} = \frac{2kV_{N_2}}{K_{p-H_2} - K_{o-H_2}}.$$

If  $db$  is the same in both cases, then

$$dV = \frac{V}{V_{N_2}} dV_{N_2}.$$

Thus it is easy to calculate from the nitrogen percentage of the mixture what percentage of para-hydrogen is present in any mixture. As the nitrogen percentage increases, the accuracy of the estimation of the para-hydrogen becomes less, but in these experiments the majority of the mixtures are low in nitrogen content. That the above simple theory is sufficient to account for the facts to a first approximation is shown by the figures in table 1.

TABLE 1. ANALYSIS OF PARA-HYDROGEN IN PRESENCE OF NITROGEN

| Nitrogen<br>% | Analysis<br>voltage | Voltage after<br>equilibration | $\Delta V$ obs. | $\Delta V$ calc. |
|---------------|---------------------|--------------------------------|-----------------|------------------|
| 0.0           | 1.7750              | 1.7151                         | 0.0599          | 0.0599           |
| 2.0           | 1.7485              | 1.6858                         | 0.0594          | 0.0604           |
| 5.0           | 1.7131              | 1.6563                         | 0.0568          | 0.0588           |
| 8.0           | 1.6652              | 1.6093                         | 0.0559          | 0.0595           |
| 12.0          | 1.6246              | 1.5701                         | 0.0513          | 0.0560           |

The fourth and fifth columns show the observed and calculated values of the change in voltage on converting para-hydrogen to normal hydrogen. Particular care is taken with the platinum wire used for the para-conversion to ensure that no contamination of the mixture arises from gases evolved from the wire.

Para-hydrogen is prepared in the usual way by adsorption of normal hydrogen on charcoal maintained at about 60° K. The para-content is measured in the following way. Even at 50 mm. pressure with a spiral micro-gauge the conductivity of hydrogen is dependent on pressure according to the simple formula

$$1/V_{\infty}^2 = 1/V^2 - C/p,$$

where  $V$  is the voltage across the spiral at pressure  $p$  and  $C$  a constant. From measurements at a few values of  $p$ ,  $V_{\infty}$  is easily calculated for normal and for the given sample of para-hydrogen. From data given in a previous paper (Bolland and Melville 1937) it is then easy to calculate the para-content.

Hydrazine was prepared by repeatedly distilling 33 % hydrazine solution *in vacuo* over potassium hydroxide in an all-glass apparatus. The liquid was stored over potassium hydroxide. The purity of the sample was checked by decomposition on a nickel wire at 900° C followed by analysis of the gas produced. Before use the hydrazine was frozen in liquid air and any non-condensable gas pumped off. Synthetic ammonia was purified by fractionation. Cylinder nitrogen was freed from oxygen by passage over active copper and through a liquid-air trap.

#### QUANTUM EFFICIENCY OF THE REACTION BETWEEN ATOMIC HYDROGEN AND HYDRAZINE

Although the experiments of Dixon have shown that hydrogen atoms react with hydrazine rapidly, it was first of all necessary in this work to obtain some idea about the overall efficiency of the reaction by determination of the quantum efficiency of the mercury-sensitized reaction. As only a vertical low-pressure mercury lamp was available the reaction system was arranged as shown in figure 3. The reaction cell was cylindrical, 6 cm. diameter and 2 cm. thick, the light from the arc being brought to a focus below the lower window of the cell; suitable diaphragms limited the size of the beam. Liquid mercury was present in the cell.  $P$  is a fused silica prism. A weak solution of uranium oxalate (0.005 M in oxalic acid 0.0025 M) was used as actinometric liquid, the precautions recommended by Forbes and Heidt (1934) being employed.

In order to avoid unduly long exposures of the actinometer solutions the following procedure was adopted. The total number of quanta up to 4000 Å entering the cell was determined by filling the cell completely with actinometer solution. Immediately before and after exposing this solution 2 ml. portions of the actinometer solution were exposed for 5 min. in small

crystallizing dishes above the lens *L*. A comparison of the rates of decomposition in the dishes and in the reaction vessel was thus established for any particular set-up, and thus the accuracy of measuring the quantum yields was increased although the lamp conditions were maintained as constant as is possible. The proportion of the total radiation at 2537 Å was determined by interposing first a filter of acetic acid to cut off wave-lengths shorter than about 2500 Å, and second a carbon tetrachloride filter to cut out effectively any wave-length shorter than 2600 Å (Melville and

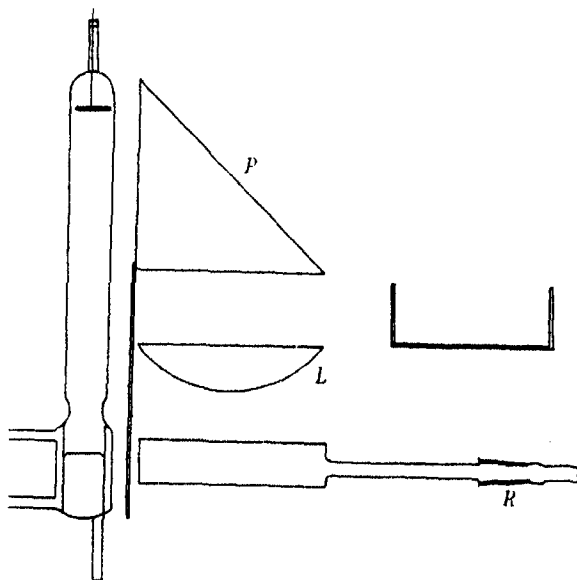


FIGURE 3. Arrangement for actinometric measurements.

Walls 1933). In the 2 cm. thick cell the uranyl oxalate solution absorbs all the light at 2537 Å, and hence it is necessary to measure what fraction of the light is absorbed by the mercury vapour. For this purpose the actinometer solution was placed beneath the reaction vessel. An exposure with a carbon tetrachloride filter was made, next a similar exposure with the cell filled with mercury vapour at 0.0012 mm. and hydrogen at 50 mm. to simulate actual reaction conditions, and thirdly an exposure with an acetic acid filter. As table 2 shows, there is not more than 5 % increase in the number of oxalic acid molecules decomposed in the third exposure, and hence it may be concluded that at least 95 % of the 2537 Å radiation is absorbed by the mercury vapour. In absence of mercury vapour the rate of decomposition is increased by 40 %.

Owing to the strong adsorption of the hydrazine on the reaction vessel walls the decomposition could not be measured by the increase in pressure. Previous experiments (Dixon 1932) have shown that the decomposition can be represented by  $\text{H} + \text{N}_2\text{H}_4 = \text{NH}_3 + \frac{1}{2}\text{N}_2 + \text{H}_2$ . The pressure of

TABLE 2

| Filter                   | Contents of cell         | Molecules decomposed  |
|--------------------------|--------------------------|-----------------------|
| $\text{CCl}_4$           | Hg                       | $1.45 \times 10^{18}$ |
| $\text{CCl}_4$           | Hg + 50 mm. $\text{H}_2$ | $1.45 \times 10^{18}$ |
| $\text{CH}_3\text{COOH}$ | Hg                       | $1.52 \times 10^{18}$ |

hydrogen and nitrogen can therefore be used as a measure of the amount of decomposition. In the experiments given in table 3 a small fraction of the mixture was withdrawn by the gas pipette, freed from hydrazine and ammonia and its pressure measured on a McLeod gauge. At the end of the run the hydrazine and ammonia were frozen out by liquid air, the hydrogen pumped out and finally the ammonia vaporized by replacing the liquid air with a  $\text{CO}_2$ -ether bath. At  $-80^\circ\text{C}$  the vapour pressure of hydrazine is only  $10^{-3}$  mm.

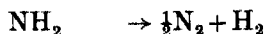
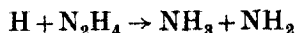
TABLE 3. QUANTUM EFFICIENCY OF THE H-ATOM SENSITIZED DECOMPOSITION OF HYDRAZINE ( $20^\circ\text{C}$ ; VOL. OF SYSTEM 61 C.C.)

| Pressure<br>$\text{N}_2\text{H}_4$<br>mm. | Pressure<br>$\text{H}_2$<br>mm. | Exp.<br>min. | Molecules<br>$\text{N}_2 + \text{H}_2 \times 10^{18}$ | Pressure<br>$\text{NH}_3$<br>mm. | $\text{NH}_3/\text{N}_2\text{H}_4$ | $h\nu$ abs.<br>$\times 10^{18}$ | $\gamma$ |
|---|---------------------------------|--------------|---|----------------------------------|------------------------------------|---------------------------------|----------|
| 10.7                                      | 47.6                            | 15           | 3.35  | 3.6                              | 0.66                               | 7.60                            | 0.44     |
| 12.7                                      | 50.0                            | 40           | 9.90  | 2.0                              | 0.42                               | 1.93                            | 0.51     |
| 12.1                                      | 51.1                            | 50           | 10.1  | 2.3                              | 0.46                               | 25.5                            | 0.40     |
| 12.1                                      | 50.7                            | 60           | 11.0  | 3.0                              | 0.56                               | 31.2                            | 0.35     |

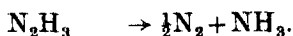
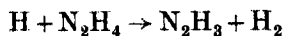
Hydrazine pressures below 10 mm. cannot be usefully employed, and the hydrogen pressure was so chosen that the majority of the excited mercury atoms were deactivated by hydrogen. The quenching radius of hydrazine has not been determined, but its square is unlikely to exceed  $25 \times 10^{-16} \text{ cm.}^2$  (Mitchell and Zemansky 1934). Under the conditions employed in these experiments 82% of the atoms are deactivated by hydrogen. In spite of this high percentage it will be seen that the quantum yield of the reaction does not have the expected value of 2. As will be shown later this low value is not due to the hydrogen atoms recombining before they react with hydrazine. There are two probable explanations: (1) that if  $\text{NH}_2$

radicals are produced they may recombine to form hydrazine, (2) that not every mercury atom deactivated produces two hydrogen atoms. Together these factors could easily be sufficient to account for the observations.

There are two possible mechanisms for the reaction, namely,



and



Both give rise to the same end-products in the same proportions, and thus no discrimination can be made in this way. Some facts favour the first mechanism. When hydrogen atoms attack ammonia they do not dehydrogenate it but exchange positions if the energy of activation during the collisions exceeds 10 kcal. (Farkas and Melville 1936). It is not unlikely that the H atoms in hydrazine possess a similar reactivity and since, as will be shown later, the energy of activation of the reaction is only 5.3 kcal. it would seem that the —N—N— bond is the more easily attacked. The analogy with hydrocarbons also supports this viewpoint. Methane is attacked by atomic hydrogen, dehydrogenation occurring thus:  $\text{H} + \text{CH}_4 \rightarrow \text{CH}_3 + \text{H}_2$ . Ethane, on the other hand, instead of being dehydrogenated is split up thus,  $\text{H} + \text{C}_2\text{H}_6 \rightarrow \text{CH}_4 + \text{CH}_3$ , the —C—C— bond being more easily attacked than the CH bond (cf., e.g., Steacie and Phillips 1938).

#### COLLISION EFFICIENCY OF THE REACTION $\text{H} + \text{N}_2\text{H}_4 \rightarrow \text{NH}_3 + \text{NH}_2$

In order to compute the velocity coefficient of this reaction the following factors require to be known: concentration of H-atoms and of hydrazine and the rate of disappearance of hydrazine. The most difficult factor to measure is the H-atom concentration. The method of measuring the rate of reaction with hydrazine has been detailed in the preceding section. As has already been mentioned, the only satisfactory method of measuring the H-atom concentration is to use para-hydrogen, since the rate of removal of the atoms by reaction with hydrazine is comparable with their rate of removal by combination. If this method is to be satisfactory then the rate of removal must be made comparable with the rate of conversion of para-hydrogen. The conversion of para-hydrogen is a first-order reaction, that is

$$u_t = u_0 \exp(-kt),$$

where  $u_0$  and  $u_t$  are respectively the excess concentrations of para-hydrogen above the normal value at times 0 and  $t$ , and  $k$  a constant.  $k$  is further defined by

$$k = k^*(H),$$

where  $k^*$  is the sum of the partial velocity constants  $k_1$  and  $k_2$ , i.e.  $k = 4k_2(H)$ .  $k_2$  is the velocity constant for the reaction  $H + p\text{-}H_2 \rightarrow o\text{-}H_2 + H$ . Hence

$$\begin{aligned} (H) &= \frac{\ln(u_0/u_t)}{k^*t} \\ &= \frac{2.303 \log_{10} 2}{t_1 k^*}, \end{aligned}$$

where  $t_1$  is the half-life for the conversion.  $k^*$  has been determined by separate experiments, and therefore the concentration of  $(H)$  may be computed. Matters are, however, complicated by a number of factors which are peculiar to the reaction.

Arrangements were made so that the temperature of the water bath surrounding the reaction vessel could be maintained at any value up to 90° C. At higher temperatures an electrically heated furnace was employed. The mercury lamp was placed outside these thermostats and the light focused on the reaction vessel by a silica lens. The mercury pressure in the vessel was maintained at 0.001 mm., the gases being saturated with mercury vapour before entering the reaction cell.

An upper limit to the temperature at which the reaction could be studied was fixed by the thermal decomposition of hydrazine. This reaction, which is probably heterogeneous, was simply investigated by freezing out the hydrazine and measuring the pressure of residual hydrogen and nitrogen. A similar experiment with para-hydrogen was carried out to measure the rate of its conversion. As tables 4 and 5 show, decomposition becomes marked at 200° C and appreciable conversion of para-hydrogen occurs. This latter is of course partly due to the hydrogen produced in the decomposition. Conditions were so arranged that such interfering factors were negligible in the actual experiments.

The procedure and methods of applying the various corrections may be briefly described in the following typical run. The requisite mixture of para-hydrogen and hydrazine was introduced into the reaction vessel, a sample withdrawn and analysed in the micro-thermal conductivity gauge. This sample of para-hydrogen was equilibrated to check the normal hydrogen voltage of the gauge. Next followed a period of illumination after which another sample of gas was withdrawn. First the voltage on the



micro-gauge was determined, the mixture brought to equilibrium and the voltage redetermined. From previously constructed calibration curves the nitrogen and para-hydrogen percentages of the mixture were immediately obtained. Another precaution which enabled more reproducible results to be obtained consisted in freezing out the hydrazine in the U-tube

TABLE 4. THERMAL DECOMPOSITION OF HYDRAZINE

| Temp.<br>° C | Pressure                             | Time<br>min. | N <sub>2</sub> + H <sub>2</sub><br>mm. | % decom. |
|--------------|--------------------------------------|--------------|--|----------|
|              | N <sub>2</sub> H <sub>4</sub><br>mm. |              |  |          |
| 75           | 8.0                                  | 15.0         | 0.002                                  | 0.03     |
| 100          | 8.0                                  | 15.0         | 0.006                                  | 0.09     |
| 218          | 9.0                                  | 15.0         | 0.500                                  | 5.6      |

TABLE 5. APPARENT CONVERSION OF PARA-HYDROGEN BY HYDRAZINE

| Temp.<br>° C | Pressure                             | Pressure                        | Time<br>min. | % <i>p</i> -H <sub>2</sub> |
|--------------|--------------------------------------|---------------------------------|--------------|----------------------------|
|              | N <sub>2</sub> H <sub>4</sub><br>mm. | <i>p</i> -H <sub>2</sub><br>mm. |              |                            |
| 100          | 12.0                                 | 53.0                            | 0.0          | 62.1                       |
|              |                                      |                                 | 15.0         | 62.0                       |
| 200          | 9.0                                  | 50.0                            | 0.0          | 62.1                       |
|              |                                      |                                 | 15.0         | 61.1                       |

(*F*) attached to the reaction system. If this were not done, any hydrazine which passed through the liquid oxygen trap decomposed on the hot wire used to equilibrate the para-hydrogen. Simultaneously with the withdrawal of the gas for analysis a portion of the sample was admitted to a McLeod gauge and the pressure measured. By previous calibration experiments the pressure of hydrogen and nitrogen in the reaction vessel could be determined.

In table 6 typical analyses of the nitrogen percentage of the non-condensable gas produced in the reaction are given. The percentage of nitrogen shows a tendency to increase with increasing decomposition and is much larger than the 33.3 % of the mechanism above. No theoretical significance has been taken from these results, since there is necessarily uncertainty in the absolute values. The tendency to increase is in all probability due to errors in the corrections applied for gas withdrawn for analysis. Such errors are cumulative. Further, the values are in effect percentages of percentages. Their importance is qualitative rather than quantitative, in that they clearly show the formation of nitrogen in the reaction.

TABLE 6. PERCENTAGE NITROGEN PRODUCED IN THE REACTION  $\text{H} + \text{N}_2\text{H}_4$ 

| Time<br>min. | Pressure                      | Obs. total                       | Obs. %<br>$\text{N}_2$ | Pressure            | Pressure*                          | % $\text{N}_2$ in<br>$n\text{-H}_2 + \text{N}_2$ |
|--------------|-------------------------------|----------------------------------|------------------------|---------------------|------------------------------------|--|
|              | $\text{N}_2\text{H}_4$<br>mm. | $\text{H}_2 + \text{N}_2$<br>mm. |                        | $\text{N}_2$<br>mm. | $n\text{-H}_2 + \text{N}_2$<br>mm. |  |
| 0.0          | 6.0                           | 51.1                             | —                      | —                   | —                                  | —  |
| 2.0          | —                             | 51.6                             | 1.0                    | 0.5                 | 2.0                                | 25   |
| 4.0          | —                             | 52.0                             | 2.5                    | 1.3                 | 3.9                                | 33   |
| 6.0          | —                             | 51.6                             | 4.5                    | 2.3                 | 4.7                                | 49   |
| 8.0          | —                             | 51.7                             | 5.8                    | 3.0                 | 6.1                                | 50   |
| 10.0         | —                             | 50.5                             | 6.5                    | 3.3                 | 5.9                                | 56   |
| 0.0          | 3.0                           | 51.1                             | —                      | —                   | —                                  | —  |
| 2.0          | —                             | 51.8                             | 1.5                    | 0.8                 | 2.7                                | 30   |
| 4.0          | —                             | 51.3                             | 3.0                    | 1.6                 | 3.7                                | 43   |
| 6.0          | —                             | 50.4                             | 3.5                    | 1.8                 | 4.3                                | 42   |
| 8.0          | —                             | 48.3                             | 3.5                    | 1.7                 | 3.2                                | 53   |
| 10.0         | —                             | 47.2                             | 3.5                    | 1.7                 | 3.5                                | 50   |

\* Corrected for loss by pipetting samples (1.0 and 1.3 mm. respectively per sample) and by hydrogen disappearing in the reaction (multiplied by 4/3).

The collision efficiency was computed from the ratio of effective collisions to total collisions, that is to say from

$$\text{Collision efficiency} = \frac{d(\text{N}_2\text{H}_4)/dt}{(\text{H})(\text{N}_2\text{H}_4)(r_{\text{H}} + r_{\text{N}_2\text{H}_4})^2 \{8\pi RT(1/M_{\text{H}} + 1/M_{\text{N}_2\text{H}_4})^{1/2} V'}$$

where  $r_{\text{H}}$  and  $r_{\text{N}_2\text{H}_4}$  are the molecular radii and  $M_{\text{H}}$  and  $M_{\text{N}_2\text{H}_4}$  are the molecular weights of atomic hydrogen and hydrazine respectively.  $V$  is the volume of the reaction system. The rate of hydrazine decomposition is calculated from the increase in non-condensable gas pressure during the reaction on the assumption of the reaction mechanism above. Corrections have been applied for loss of gas by withdrawal of analysis samples and for hydrogen being used up in reacting with hydrazine. Table 7 gives the values of this term in several runs at different temperatures. The concentration of hydrazine was measured by direct manometric observation of the pressure introduced.

The stationary hydrogen atom concentration has been computed from the rate of para-hydrogen conversion in the manner outlined above. Two corrections had to be applied, one for the nitrogen accumulating in the course of the reaction and the other for the normal hydrogen produced. The first correction has been discussed above and the second is given simply by

$$\text{True \% } p\text{-H}_2 = \frac{np + 25\Delta p}{100(p + \Delta p)},$$

TABLE 7. RATE OF HYDRAZINE DECOMPOSITION

| Run | Temp.<br>° C | Pressure<br>N <sub>2</sub> H <sub>4</sub><br>mm. | Pressure<br>p-H <sub>2</sub><br>mm. | Exp.<br>time<br>min. | Pressure<br>H <sub>2</sub> +N <sub>2</sub><br>mm. | $\Delta p$<br>n-H <sub>2</sub> +N <sub>2</sub><br>mm. | $-d(N_2H_4)/dt$<br>mm./min. |
|-----|--------------|--|-------------------------------------|----------------------|---|---|-----------------------------|
| 1   | 208          | 8.8  | 53.6                                | 0.0                  | 53.6  | —   | —                           |
|     |              |  |                                     | 2.0                  | 55.2  | 2.4   | 1.20                        |
|     |              |  |                                     | 4.0                  | 54.8  | 3.6   | 0.90                        |
|     |              |  |                                     | 6.0                  | 54.6  | 5.0   | 0.83                        |
|     |              |  |                                     |                      |   | (0.8)   | 0.98 Mean                   |
| 2   | 203          | 8.5  | 53.3                                | 0.0                  | 53.3  | —   | —                           |
|     |              |  |                                     | 2.0                  | 54.2  | 1.9   | 0.95                        |
|     |              |  |                                     | 4.0                  | 53.8  | 3.5   | 0.88                        |
|     |              |  |                                     | 6.0                  | 54.3  | 6.0   | 1.00                        |
|     |              |  |                                     |                      |   | (1.0)   | 0.94 Mean                   |
| 3   | 199          | 8.5  | 53.3                                | 0.0                  | 53.3  | —   | —                           |
|     |              |  |                                     | 2.0                  | 54.4  | 2.1   | 1.05                        |
|     |              |  |                                     | 4.0                  | 54.9  | 4.6   | 1.15                        |
|     |              |  |                                     | 6.0                  | 55.2  | 6.9   | 1.15                        |
|     |              |  |                                     |                      |   | (1.0)   | 1.12 Mean                   |
| 4   | 209          | 8.6  | 54.1                                | 0.0                  | 54.1  | —   | —                           |
|     |              |  |                                     | 2.0                  | 55.5  | 2.4   | 1.20                        |
|     |              |  |                                     | 4.0                  | 56.2  | 5.1   | 1.27                        |
|     |              |  |                                     | 6.0                  | 56.6  | 7.5   | 1.25                        |
|     |              |  |                                     |                      |   | (1.0)   | 1.24 Mean                   |
| 5   | 90           | 5.2  | 50.1                                | 0.0                  | 50.1  | —   | —                           |
|     |              |  |                                     | 2.0                  | 50.9  | 1.7   | 0.85                        |
|     |              |  |                                     | 4.0                  | 50.7  | 3.3   | 0.83                        |
|     |              |  |                                     | 6.0                  | 50.2  | 4.6   | 0.78                        |
|     |              |  |                                     |                      |   | (0.9)   | 0.82 Mean                   |
| 6   | 92           | 5.2  | 52.1                                | 0.0                  | 52.1  | —   | —                           |
|     |              |  |                                     | 2.0                  | 52.9  | 1.7   | 0.85                        |
|     |              |  |                                     | 4.0                  | 52.4  | 3.0   | 0.75                        |
|     |              |  |                                     | 7.0                  | 52.9  | 5.3   | 0.76                        |
|     |              |  |                                     |                      |   | (0.9)   | 0.79 Mean                   |
| 7   | 93           | 5.3  | 52.7                                | 0.0                  | 52.7  | —   | —                           |
|     |              |  |                                     | 2.0                  | 53.0  | 1.2   | 0.60                        |
|     |              |  |                                     | 6.0                  | 51.3  | 3.1   | 0.50                        |
|     |              |  |                                     | 8.0                  | 50.3  | 4.8   | 0.60                        |
|     |              |  |                                     |                      |   | (0.9)   | 0.57 Mean                   |
| 8   | 91           | 5.3  | 53.7                                | 0.0                  | 53.7  | —   | —                           |
|     |              |  |                                     | 2.0                  | 54.2  | 1.4   | 0.70                        |
|     |              |  |                                     | 4.0                  | 53.6  | 2.0   | 0.50                        |
|     |              |  |                                     | 6.0                  | 53.2  | 4.0   | 0.67                        |
|     |              |  |                                     |                      |   | (0.9)   | 0.62 Mean                   |
| 9   | 23           | 4.0  | 53.1                                | 0.0                  | 53.1  | —   | —                           |
|     |              |  |                                     | 2.0                  | 53.6  | 1.2   | 0.60                        |
|     |              |  |                                     | 4.0                  | 53.7  | 2.2   | 0.55                        |
|     |              |  |                                     | 7.0                  | 53.5  | 3.9   | 0.56                        |
|     |              |  |                                     |                      |   | (0.7)   | 0.57 Mean                   |

TABLE 7 (continued)

| Run | Temp.<br>°C | Pressure<br>$N_2H_4$<br>mm. | Pressure<br>$p-H_2$<br>mm. | Exp.<br>time<br>min. | Pressure<br>$H_2 + N_2$<br>mm. | $\Delta p$<br>$n \cdot H_2 + N_2$<br>mm. | $-d(N_2H_4)/dt$<br>mm./min |
|-----|-------------|-----------------------------|----------------------------|----------------------|--------------------------------|--|----------------------------|
| 10  | 22          | 1.9                         | 53.9                       | 0.0                  | 53.9                           | —  | —                          |
|     |             |                             |                            | 2.0                  | 54.5                           | 1.3                                      | 0.65                       |
|     |             |                             |                            | 4.0                  | 54.1                           | 2.3                                      | 0.57                       |
|     |             |                             |                            | 6.0                  | 51.9                           | 2.2                                      | 0.37                       |
|     |             |                             |                            |                      |                                | (0.7)                                    | 0.53 Mean                  |
| 11  | 23          | 4.6                         | 53.3                       | 0.0                  | 53.3                           | —  | —                          |
|     |             |                             |                            | 2.0                  | 54.1                           | 1.5                                      | 0.75                       |
|     |             |                             |                            | 4.0                  | 53.8                           | 2.6                                      | 0.65                       |
|     |             |                             |                            | 6.0                  | 54.0                           | 4.2                                      | 0.70                       |
|     |             |                             |                            |                      |                                | (0.7)                                    | 0.70 Mean                  |
| 12  | 23          | 4.2                         | 53.4                       | 0.0                  | 53.4                           | —  | —                          |
|     |             |                             |                            | 2.0                  | 54.3                           | 1.6                                      | 0.80                       |
|     |             |                             |                            | 4.0                  | 54.1                           | 2.8                                      | 0.70                       |
|     |             |                             |                            | 6.0                  | 54.1                           | 4.2                                      | 0.70                       |
|     |             |                             |                            | 8.0                  | 53.7                           | 5.2                                      | 0.67                       |
|     |             |                             |                            |                      |                                | (0.7)                                    | 0.72 Mean                  |
| 13  | 23          | 5.0                         | 52.4                       | 0.0                  | 52.4                           | —  | —                          |
|     |             |                             |                            | 2.0                  | 52.9                           | 1.2                                      | 0.60                       |
|     |             |                             |                            | 5.0                  | 52.4                           | 2.1                                      | 0.42                       |
|     |             |                             |                            | 8.0                  | 52.3                           | 3.4                                      | 0.43                       |
|     |             |                             |                            | 11.0                 | 52.1                           | 4.6                                      | 0.42                       |
|     |             |                             |                            | 14.0                 | 51.9                           | 5.4                                      | 0.36                       |
|     |             |                             |                            |                      |                                | (0.7)                                    | 0.45 Mean                  |

The bracketed figures in column 7 are independently measured corrections for loss of pressure by sampling; one dose was removed initially in all runs and either one or two after each exposure.

where  $n$  is the observed percentage,  $p$  and  $\Delta p$  are the respective pressures of para-hydrogen and normal hydrogen. From the data in table 7 the values of  $\Delta p$  have been computed, correction being made for hydrogen lost in the reaction. In table 8 are given the corresponding stationary atom concentrations for the runs in table 7. Since the absolute values depend on the values of  $k^*$ , they have been calculated for the data both of Farkas (1935) and of Geib and Harteck (1931). The radius of the hydrazine molecule has not been experimentally determined. On analogy with the hydrogen peroxide molecule Penney and Sutherland (1934) have suggested a skew double Y structure which strictly cannot be treated as spherical. But for the present purposes we have taken the N-N link as 1.5° A, the N-H link as 1.02° A and the effective radius as the distance from the midpoint of the N-N link to the extension of the N-H link by the radius of the sphere of

TABLE 8. RATE OF PARA-HYDROGEN CONVERSION

| Run | Exp.<br>time<br>min. | Obs.<br>% $p\text{-H}_2$ | Pressure<br>$n\text{-H}_2$<br>mm. | Corr.<br>% $p\text{-H}_2$ | $-du/dt$  |
|-----|----------------------|--------------------------|-----------------------------------|---------------------------|-----------|
| 1   | 0.0                  | 68.6                     | —                                 | 68.6                      | —         |
|     | 2.0                  | 68.3                     | 1.7                               | 69.6                      | +ve       |
|     | 4.0                  | 65.3                     | 1.7                               | 68.0                      | 0.15      |
|     | 6.0                  | 63.9                     | 1.7                               | 67.8                      | 0.13      |
|     |                      |                          |                                   |                           | 0.14 Mean |
| 2   | 0.0                  | 68.6                     | —                                 | 68.6                      | —         |
|     | 2.0                  | 66.3                     | 1.7                               | 67.7                      | 0.45      |
|     | 4.0                  | 64.1                     | 1.7                               | 66.8                      | 0.45      |
|     | 6.0                  | 61.4                     | 1.7                               | 65.4                      | 0.53      |
|     |                      |                          |                                   |                           | 0.48 Mean |
| 3   | 0.0                  | 68.6                     | —                                 | 68.6                      | —         |
|     | 2.0                  | 67.0                     | 2.0                               | 68.5                      | 0.05      |
|     | 4.0                  | 65.1                     | 2.0                               | 68.1                      | 0.13      |
|     | 6.0                  | 62.9                     | 2.0                               | 67.3                      | 0.22      |
|     |                      |                          |                                   |                           | 0.13 Mean |
| 4   | 0.0                  | 68.6                     | —                                 | 68.6                      | —         |
|     | 2.0                  | 66.5                     | 2.2                               | 68.4                      | 0.10      |
|     | 4.0                  | 64.2                     | 2.2                               | 67.8                      | 0.20      |
|     |                      |                          |                                   |                           | 0.15 Mean |
| 5   | 0.0                  | 68.3                     | —                                 | 68.3                      | —         |
|     | 2.0                  | 66.6                     | 1.4                               | 68.1                      | 0.10      |
|     | 4.0                  | 65.0                     | 1.4                               | 67.7                      | 0.15      |
|     |                      |                          |                                   |                           | 0.13 Mean |
| 6   | 0.0                  | 68.3                     | —                                 | 68.3                      | —         |
|     | 2.0                  | 66.6                     | 1.4                               | 67.8                      | 0.25      |
|     | 4.0                  | 65.1                     | 1.4                               | 67.6                      | 0.18      |
|     | 7.0                  | 63.4                     | 2.1                               | 67.5                      | 0.11      |
|     |                      |                          |                                   |                           | 0.18 Mean |
| 7   | 0.0                  | 63.3                     | —                                 | 63.3                      | —         |
|     | 2.0                  | 61.7                     | 1.0                               | 62.4                      | 0.45      |
|     | 4.0                  | 60.8                     | 1.0                               | 62.2                      | 0.23      |
|     | 6.0                  | 60.3                     | 1.0                               | 62.3                      | 0.16      |
|     | 8.0                  | 58.6                     | 1.0                               | 61.3                      | 0.25      |
|     |                      |                          |                                   |                           | 0.27 Mean |
| 8   | 0.0                  | 63.3                     | —                                 | 63.3                      | —         |
|     | 2.0                  | 61.8                     | 1.1                               | 62.5                      | 0.40      |
|     | 4.0                  | 61.0                     | 1.1                               | 62.3                      | 0.25      |
|     | 6.0                  | 57.2                     | 1.1                               | 60.2                      | 0.50      |
|     |                      |                          |                                   |                           | 0.38 Mean |
| 9   | 0.0                  | 64.8                     | —                                 | 64.8                      | —         |
|     | 2.0                  | 63.8                     | 1.0                               | 64.6                      | 0.10      |
|     | 4.0                  | 62.4                     | 1.0                               | 63.9                      | 0.23      |
|     | 7.0                  | 60.5                     | 1.5                               | 63.0                      | 0.30      |
|     |                      |                          |                                   |                           | 0.21 Mean |

TABLE 8 (continued)

| Run | Exp.<br>time<br>min. | Obs.<br>% $p\text{-H}_4$ | Pressure<br>$n\text{-H}_2$<br>mm. | Corr.<br>% $p\text{-H}_4$ | $-du/dt$  |
|-----|----------------------|--------------------------|-----------------------------------|---------------------------|-----------|
| 10  | 0.0                  | 68.3                     | —                                 | 68.3                      | —         |
|     | 2.0                  | 66.8                     | 1.1                               | 67.7                      | 0.30      |
|     | 4.0                  | 65.8                     | 1.1                               | 66.5                      | 0.18      |
|     |                      |                          |                                   |                           | 0.24 Mean |
| 11  | 0.0                  | 68.3                     | —                                 | 68.3                      | —         |
|     | 2.0                  | 68.1                     | 1.2                               | 69.1                      | +ve       |
|     | 4.0                  | 65.9                     | 1.2                               | 67.8                      | 0.13      |
|     | 6.0                  | 63.8                     | 1.2                               | 66.6                      | 0.27      |
|     |                      |                          |                                   |                           | 0.20 Mean |
| 12  | 0.0                  | 68.3                     | —                                 | 68.3                      | —         |
|     | 2.0                  | 66.9                     | 1.3                               | 68.0                      | 0.15      |
|     | 4.0                  | 65.2                     | 1.3                               | 67.3                      | 0.25      |
|     | 6.0                  | 63.8                     | 1.3                               | 66.9                      | 0.23      |
|     | 8.0                  | 63.0                     | 1.3                               | 67.0                      | 0.16      |
|     |                      |                          |                                   |                           | 0.19 Mean |
| 13  | 0.0                  | 68.3                     | —                                 | 68.3                      | —         |
|     | 2.0                  | 65.4                     | 0.8                               | 66.1                      | (1.1)     |
|     | 5.0                  | 65.2                     | 1.2                               | 66.8                      | 0.30      |
|     | 8.0                  | 64.0                     | 1.2                               | 66.5                      | 0.23      |
|     | 11.0                 | 62.0                     | 1.2                               | 65.4                      | 0.26      |
|     | 14.0                 | 60.4                     | 1.2                               | 64.7                      | 0.25      |
|     |                      |                          |                                   |                           | 0.26 Mean |

influence of the hydrogen atom, which has been arbitrarily taken as the difference of the N-N and N-H links. The value so computed is 2.65 A.

The collision efficiency of the reaction has been calculated from the data in tables 7 and 8 in the following manner:

$$\text{Collision efficiency} = \frac{d(\text{N}_2\text{H}_4)/dt k^* u}{du/dt(\text{N}_2\text{H}_4) (r_{\text{H}} + r_{\text{N}_2\text{H}_4})^2 \{8\pi RT(1/M_{\text{H}} + 1/M_{\text{N}_2\text{H}_4})\}^{1/2} V}$$

substituting data for run (1),

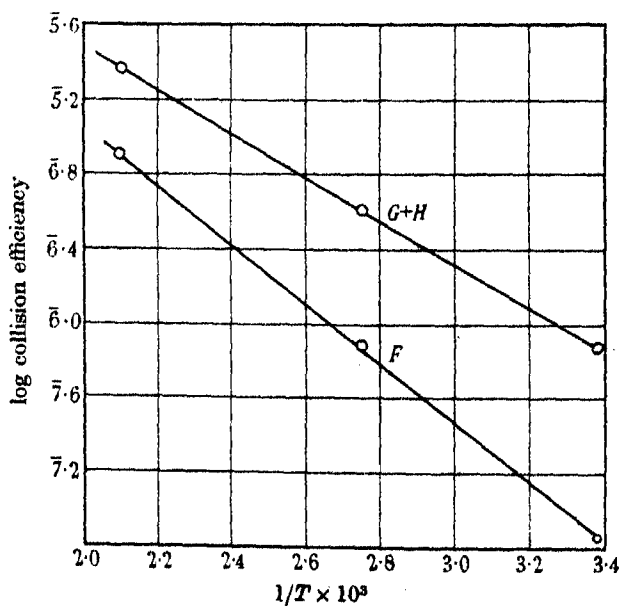
$$\begin{aligned}
 &= \frac{0.98 \times 7.96 \cdot 10^7 \times 43.6}{0.14 \times 8.8 \times 1.7 \cdot 10^{-9} \times 6.06 \cdot 10^{20} \times 110} \\
 &= 2.44 \cdot 10^{-5}.
 \end{aligned}$$

In table 9 are tabulated the other runs together with the stationary hydrogen atom concentration for reference.

The activation energy of the reaction has been computed by plotting the logarithm of the collision efficiency against the reciprocal of the temperature. From the slopes of the graphs in figure 4 the activation energy is

TABLE 9. COLLISION EFFICIENCY OF THE REACTION  $\text{H} + \text{N}_2\text{H}_4$ 

| Run | Temp.<br>° C | $k^*$                   |                                      | (H)                                |   | Collision efficiency              |  |
|-----|--------------|-------------------------|--------------------------------------|------------------------------------|---|-----------------------------------|--|
|     |              | Farkas<br>$\times 10^6$ | Geib and<br>Harteck<br>$\times 10^6$ | $k^*$<br>(F.)<br>$\times 10^{-13}$ | $k^*$<br>(G. and H.)<br>$\times 10^{-13}$ | $k^*$<br>(F.)<br>$\times 10^{-7}$ | $k^*$<br>(G. and H.)<br>$\times 10^{-8}$ |
| 1   | 208          | 79.6                    | 28.8                                 | 6.82                               | 1.88                                      | 244                               | 882                                      |
| 2   | 203          | 75.7                    | 26.9                                 | 24.3                               | 6.82                                      | 67.1                              | 238                                      |
| 3   | 199          | 71.9                    | 25.1                                 | 6.91                               | 1.98                                      | 280                               | 878                                      |
| 4   | 209          | 79.8                    | 28.8                                 | 7.23                               | 2.60                                      | 294                               | 1060                                     |
|     |              |                         |                                      |                                    |   | 221                               | 765 Mean                                 |
| 5   | 90           | 11.0                    | 1.99                                 | 45.5                               | 25.2                                      | 72.2                              | 131                                      |
| 6   | 92           | 11.5                    | 2.19                                 | 60.3                               | 31.7                                      | 52.5                              | 102                                      |
| 7   | 93           | 11.8                    | 2.29                                 | 99.5                               | 51.4                                      | 22.5                              | 43.7                                     |
| 8   | 91           | 11.2                    | 2.09                                 | 147                                | 79.0                                      | 16.7                              | 31.2                                     |
|     |              |                         |                                      |                                    |   | 41.0                              | 77.0 Mean                                |
| 9   | 23           | 1.80                    | 0.170                                | 488                                | 517                                       | 6.29                              | 5.94                                     |
| 10  | 22           | 1.76                    | 0.162                                | 525                                | 570                                       | 11.5                              | 10.6                                     |
| 11  | 23           | 1.80                    | 0.170                                | 439                                | 459                                       | 7.67                              | 7.24                                     |
| 12  | 23           | 1.80                    | 0.170                                | 406                                | 430                                       | 9.09                              | 8.58                                     |
| 13  | 23           | 1.80                    | 0.170                                | 557                                | 590                                       | 3.49                              | 3.30                                     |
|     |              |                         |                                      |                                    |   | 7.61                              | 7.13 Mean                                |

FIGURE 4. Activation energy of  $\text{H} + \text{N}_2\text{H}_4 \rightarrow \text{NH}_3 + \text{NH}_3$ .

5300 and 7220 cal. respective to the data for  $k^*$  of Farkas and of Geib and Harteck. Since the activation energy is practically the same as that for the exchange in the para-hydrogen conversion, the relative rates of these two reactions will be temperature independent. The data in table 8 bear out this expectation.

The steric factor has been calculated from the relation

$$\epsilon = \sigma e^{-E/RT},$$

where  $\epsilon$  is the collision efficiency and  $\sigma$  the steric factor. In table 10 are given the values for the different  $k^*$  values. The only other bimolecular reactions in which the steric factors have been calculated are exchange processes with para-hydrogen (0.07), ammonia (0.1), phosphine (0.25) and methane (0.4). These are all somewhat higher than that of the reaction with hydrazine.

TABLE 10. STERIC FACTOR OF THE REACTION  $H + N_2H_4$

| Temp.<br>° C | Steric factor                               |   |
|--------------|---|---|
|              | $E = 5300 \text{ cal.}$<br>$\times 10^{-3}$ | $E = 7220 \text{ cal.}$<br>$\times 10^{-3}$ |
| 23           | 5.91  | 1.42  |
| 91           | 5.98  | 1.56  |
| 205          | 4.62  | 1.11  |

The relatively low value of the collision efficiency for the reaction actually rules out the possibility of hydrazine playing any important part in determining the stationary concentration of hydrogen atoms in the ammonia photolysis. This can be shown most directly by the following simple considerations. Suppose there is a mixture of say 10 mm. ammonia and 10 mm. hydrazine, then the problem is to calculate the effect of the hydrazine on the fate of the hydrogen atoms produced during the decomposition of the ammonia. The diffusion coefficient of the H-atoms in such a mixture is about 30 cm.<sup>2</sup>/sec. calculated from the ordinary diffusion formula. From Einstein's displacement equation  $x^2 = 2Dt$  the time for diffusion to the walls 1 cm. away is thus  $1.7 \times 10^{-2}$  sec. In this time the atom will have made  $10^{10} \times \frac{10}{760} \times 1.7 \times 10^{-2} = 2.2 \times 10^6$  collisions with hydrazine molecules. Since at room temperature the collision efficiency is of the order of  $10^{-7}$ , even with 10 mm. hydrazine, there is a much larger probability of the hydrogen reaching the walls than reacting with hydrazine. But when the quantum efficiency of the ammonia photolysis is being determined the total amount decomposed is usually around 0.1 mm. and therefore the amount of hydrazine produced during the whole run cannot exceed 0.05 mm. In actual



practice such a high figure for the concentration of hydrazine is not reached in a static system and therefore hydrazine is definitely not responsible for the observed low stationary hydrogen atom concentration. In the following paper an unambiguous experiment is described which conclusively confirms the calculation made above.

QUANTUM EFFICIENCY OF MERCURY-SENSITIZED  
PHOTODECOMPOSITION OF HYDRAZINE

The decomposition of hydrazine by activated mercury atoms has been investigated by Elgin and Taylor (1929), who compared this reaction with that of hydrogen and oxygen in order to determine the quantum efficiency. Taking 6.5 as the quantum efficiency of the latter reaction they obtain a value of at least 13 and suggest a chain reaction involving the production of atomic hydrogen. It can easily be shown that in a mixture of 10 mm. hydrazine and 50 mm. hydrogen the fraction of mercury atoms deactivated by hydrazine is small. But the atomic hydrogen produced in such a chain reaction would seriously interfere with the determination of the stationary atom concentration by the para-hydrogen conversion method in the reaction of the previous section. Although the value of 6.5 for the photosensitized reaction of hydrogen and oxygen is now known to be too large it seemed desirable to redetermine the quantum efficiency of the sensitized hydrazine decomposition.

The reaction system was the same as that shown in figure 3 and the uranyl oxalate actinometer was again used to measure the quantum input. The decomposition was observed on a Pirani gauge protected by a liquid oxygen U-tube as described above. The composition of the non-condensable gas was determined by a separate series of experiments. Typical analyses carried out with a thermal conductivity micro-gauge are given in table 11.

TABLE 11. COMPOSITION OF NON-CONDENSABLE GASES

| Pressure<br>$\text{N}_2\text{H}_4$<br>mm. | %<br>decomposition | %<br>nitrogen |
|---|--------------------|---------------|
| 5.6                                       | 11.9               | 49.1          |
| 6.2                                       | 24.2               | 50.8          |
| 4.6                                       | 24.7               | 51.2          |
| 5.6                                       | 33.3               | 51.2          |

It will be observed that the ratio of hydrogen to nitrogen is close to unity in agreement with the results of Elgin and Taylor. The quantum

efficiency has therefore been computed from the stoichiometric equation  $2\text{N}_2\text{H}_4 = 2\text{NH}_3 + \text{N}_2 + \text{H}_2$ . Extended decomposition runs showed the same rapid increase in total pressure to twice the initial pressure followed by a much slower increase as observed by the above authors. In table 12 are summarized the quantum efficiency determinations. The runs in tables 11 and 12 are all in the initial fast stage of the decomposition.

TABLE 12. QUANTUM EFFICIENCY OF THE PHOTOSENSITIZED DECOMPOSITION OF HYDRAZINE (20° C; REACTION VOLUME 140 C.C.)

| Pressure<br>$\text{N}_2\text{H}_4$<br>mm. | $-d(\text{N}_2\text{H}_4)/dt$<br>mol./min.<br>$\times 10^{17}$ | 2537° A<br>quanta<br>$h\nu/\text{min.}$<br>$\times 10^{17}$ | $\gamma$  |
|---|--|---|-----------|
| 11.0                                      | 2.0  | 5.1   | 0.39      |
| 8.0                                       | 1.8  | 5.1   | 0.35      |
| 2.7                                       | 1.6  | 5.1   | 0.31      |
| 10.0                                      | 2.2  | 5.5   | 0.40      |
| 10.0                                      | 2.0  | 5.1   | 0.39      |
|   |  |   | 0.37 Mean |

A quantum efficiency of 0.37 would indicate that this reaction is not a chain reaction. The most probable primary dissociations are disruption at the N-N link or at a N-H link.



or



Since ammonia has been shown to be a product of the decomposition by Elgin and Taylor the second reaction is to be preferred. It is improbable that the amine radicals will interact in any other way than to produce nitrogen and hydrogen or to regenerate hydrazine. Ammonia is more likely to be formed by the interaction of  $\text{N}_2\text{H}_3$  radicals or by atomic hydrogen reacting with hydrazine. The latter reaction would imply a quantum efficiency of more than unity but it is to be noted that the quantum efficiency of this reaction was found to be 0.2 (per H-atom). The low overall quantum efficiency observed is in all probability due to inefficiency of the primary mode of decomposition. This inefficiency may be due either to hydrazine deactivating the mercury atoms without necessarily dissociating or to an efficient reversal of the primary mode. But the latter would require to be more than usually efficient since the probability of collision between the primary products and further molecules of hydrazine is large and, in the case of atomic hydrogen at least, such collisions are fruitful. Lacking

definite evidence of a back reaction we prefer to explain the low overall quantum efficiency by inefficiency of the primary process, whatever it may be. At the moment there is no known technique of distinguishing the probable modes of dissociation. The method of Bolland and Melville (1937) of determining the fraction of the exchange of atomic deuterium with hydrides due to reversal of the primary process of dissociation is not applicable here since the energy of activation for decomposition is less than that for exchange.

#### PRIMARY PROCESS IN DIRECT HYDRAZINE PHOTOLYSIS

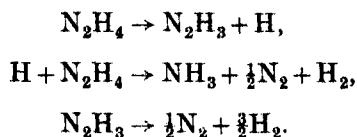
As in the mercury-sensitized decomposition of hydrazine the most probable modes of primary dissociation are disruption at the N-N link or at a N-H link. Here, however, a distinction is possible since the production of atomic hydrogen is detectable with the para-hydrogen conversion technique. But there is a serious difficulty in the fact that hydrazine is an efficient inhibitor of the conversion. Since the energy of activation of the interaction of hydrogen atoms with hydrazine is comparable with that of their exchange with para-hydrogen, it is of little advantage working at high temperatures where the chain length of the exchange increases. It was observed above that the addition of 10 mm. of hydrazine to 50 mm. of para-hydrogen reduced the stationary hydrogen atom concentration by a factor of 20. Even if the primary process of the direct photolysis has an efficiency of unity a high intensity of radiation from a spark source is necessary. For these experiments only a zinc spark generated by a 10,000 V, 4 kW transformer was available. In table 13 are tabulated para-hydrogen conversion runs in which hydrazine was the sensitizing agent.

TABLE 13

| Pressure<br>$\text{N}_2\text{H}_4$<br>mm. | Exp. time<br>min. | % $p\text{-H}_2$<br>converted | Intensity<br>$h\nu/\text{sec.}$<br>$\times 10^{10}$ |
|---|-------------------|-------------------------------|---|
| 7.0                                       | 30.0              | 9.1                           | 1.32  |
| 10.0                                      | 30.0              | 12.7                          | 3.11  |
| 9.6                                       | 30.0              | 14.2                          | 3.55  |
| 8.0                                       | 10.0              | 5.0                           | 6.63  |
| 10.2                                      | 4.0               | 0.7                           | 10.7  |

These conversion runs are corrected as before for the nitrogen and normal hydrogen produced in the reaction. The spark intensity was computed from the amount of non-condensable gas produced on the basis of a quantum efficiency of 1.2 (Wenner and Beckmann 1932) for the photolysis. The

conversions observed are rather small but qualitatively they indicate a primary process involving the breakage of a N-H link rather than the fission of the molecule into two amine radicals. This is again what would be expected by analogy with ammonia. Hence, qualitatively, the mechanism of this reaction may be written thus,



The problem is to account for the overall quantum efficiency of the reaction which is 1.2. From the hydrogen atom-sensitized decomposition of hydrazine it would appear that for every H-atom which reacts only 0.2 of the hydrazine molecules ultimately produce nitrogen and hydrogen. Assuming therefore that the primary process is here 100 % efficient then the total quantum efficiency would be 1.2 in agreement with experiment. This would mean that the  $\text{N}_2\text{H}_3$  radical wholly decomposes (by what mechanism is unknown) into nitrogen and hydrogen.

The experiments described above were carried out in the Chemistry Department of the University of Edinburgh. The authors are much indebted to Dr E. B. Ludlam for his help throughout the research. One of them (E. A. B. B.) is grateful to the Carnegie Trust for a Research Scholarship and to the Trustees of the Moray Fund for a grant for apparatus.

#### SUMMARY

The efficiency of the reaction of atomic hydrogen with hydrazine has been measured in the temperature range 20–200° C by comparison with that of the hydrogen atom-sensitized conversion of para-hydrogen. A static system is employed, the hydrogen atoms being produced by excited mercury atoms. The energy of activation is nearly the same as that of the para-hydrogen conversion, namely *ca.* 7 kcal., and the steric factor is *ca.*  $10^{-2}$ . From these results it is shown that hydrazine is not responsible for the low stationary hydrogen-atom concentration in the photolysis of ammonia as has hitherto been supposed.

Although the hydrogen atoms react very efficiently with hydrazine the quantum efficiency of this reaction is only 0.4 instead of the expected value of 2. An explanation of this result is suggested.

It is also shown that photodecomposing hydrazine converts para-hydrogen. This is taken to mean that the primary decomposition is represented by  $\text{N}_2\text{H}_4 + h\nu = \text{N}_2\text{H}_3 + \text{H}$ .

The quantum efficiency of the mercury-sensitized decomposition of hydrazine has been found to be 0.37. An explanation of this unexpectedly low value is given.

A new simplified method of analysing the ternary mixture  $p\text{-H}_2\text{—}n\text{-H}_2\text{—N}_2$  is described.

#### REFERENCES

- Bolland, J. L. and Melville, H. W. 1937 *Trans. Faraday Soc.* **33**, 1316–1329.  
Dixon, J. K. 1932 *J. Amer. Chem. Soc.* **54**, 4262–4271.  
Elgin, J. C. and Taylor, H. S. 1929 *J. Amer. Chem. Soc.* **51**, 2059–2082.  
Farkas, A. 1935 *Light and Heavy Hydrogen*, chap. v.  
Farkas, L. and Hartcock, P. 1934 *Z. phys. Chem. B*, **25**, 257–272.  
Farkas, A. and Melville, H. W. 1936 *Proc. Roy. Soc. A*, **157**, 625–651.  
Forbes, G. S. and Heidt, J. H. 1934 *J. Amer. Chem. Soc.* **56**, 2363–2368.  
Geib, K. H. and Hartcock, P. 1931 *Z. phys. Chem. Bodenstein festband*, pp. 849–862.  
Melville, H. W. and Walls, H. J. 1933 *Trans. Faraday Soc.* **29**, 1255–1259.  
Mitchell, A. G. G. and Zemansky, M. 1934 *Resonance Radiation*. Cambridge.  
Mund, W. and Tiggelen, A. van 1937 *Bull. Soc. chim. Belg.* **46**, 104–128.  
Penney, W. G. and Sutherland, G. B. B. M. 1934 *J. Chem. Phys.* **2**, 492–498.  
Steacie, E. W. R. and Phillips, N. W. F. 1938 *J. Chem. Phys.* **6**, 179–187.  
Wenner, R. R. and Beckmann, A. O. 1932 *J. Amer. Chem. Soc.* **54**, 2787–2797.  
Zemansky, M. 1930 *Phys. Rev.* **36**, 919–934.
-

# The photolysis of ammonia

By E. A. B. BIRSE

*Chemistry Department, University of Edinburgh*

AND H. W. MELVILLE

*Colloid Science Department, University of Cambridge*

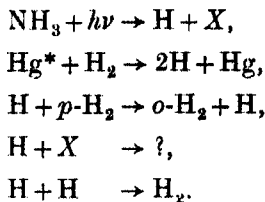
(Communicated by J. Kendall, F.R.S.—Received 15 December 1939)

It has been shown in the preceding paper that the hypothesis that hydrazine is responsible for the anomalously low hydrogen atom concentration in the decomposition of ammonia must be abandoned. In order to explain this important discrepancy some new experimental techniques require to be developed which will settle the matter without appeal to further hypotheses. There are two general explanations of the discrepancy: (1) the hydrogen atoms are not produced as fast as that calculated on the assumption that every ammonia molecule absorbing a quantum necessarily decomposes, (2) that some entity not yet recognized removes hydrogen atoms at a rate faster than that at which they normally recombine. In this paper methods will be described in which these two problems are solved, and finally there is a discussion of the photochemistry of ammonia in the light of the new results obtained during these experiments.

## EFFECT OF PHOTODECOMPOSING AMMONIA ON THE MERCURY SENSITIZED CONVERSION OF PARA-HYDROGEN

In view of the prominence given to the possibility of the removal of hydrogen atoms it is necessary first to make a decisive test which does not depend on making any assumption with regard to the nature of the interacting substance. In principle all that requires to be done is to decompose ammonia photochemically in presence of atomic hydrogen and observe whether the concentration of atomic hydrogen is reduced. Certain precautions have, however, to be taken. The para-hydrogen conversion is again employed to measure the concentration of free atoms. The arc and spark technique is employed; the first to generate the atoms and the second to decompose the ammonia and thereby produce substance X which interacts with hydrogen atoms. The experimental arrangement thus consists

in disposing the mercury arc and zinc spark at suitable distances from the reaction vessel placed in a furnace. The scheme of reactions is therefore



The question arises as to the relative intensities of the arc and spark, for the hydrogen atoms from the ammonia will also convert the para-hydrogen. The rate of decomposition of ammonia cannot be made so small as to convert the para-hydrogen at a rate much smaller than that due to excited mercury atoms, since the amount of product, which removes the hydrogen atoms, would be too small appreciably to affect the hydrogen atom concentration. On the other hand, if the rate of decomposition of ammonia is very much larger than the rate of production of excited mercury atoms, the ammonia-sensitized conversion of para-hydrogen will overshadow the mercury-sensitized conversion. The effect of  $\text{X}$  will therefore not be detectable. The best compromise is approximate equality of intensities. This introduces a further difficulty. Assuming for the moment that the hydrogen atoms are not removed by the products of the ammonia reaction, then the rate of para-hydrogen conversion will be given by the following equations:

$$\text{Rate (arc)} = \text{const. } (I_A)^x,$$

$$\text{Rate (spark)} = \text{const. } (I_S)^x,$$

$$\text{Rate (spark and arc)} = \text{const. } (I_{SA})^x,$$

where  $I$  is the intensity of the respective sources and  $x$  the intensity exponent. In order to calculate the rate of para-hydrogen conversion by the arc in presence of the spark  $A_S$ , it is necessary to correct the rate with spark and arc operating together for the contribution made by the spark itself. From the above three equations the following relationship is therefore obtained:

$$\begin{aligned}\frac{\text{Rate } A}{\text{Rate } A_S} &= \frac{\text{Const. } (I_A)^x}{\text{Rate } (S+A)} \left( \frac{I_S + I_A}{I_A} \right)^{1-x} \\ &= \left( 1 + \frac{I_A}{I_S} \right)^x \frac{\text{Rate } (S)}{\text{Rate } (S+A)}.\end{aligned}\quad \dagger$$

† This formula is deduced on the assumption that  $x$  remains constant in the range of rates ca. 2 : 1 used in the experiments. The justification for this assumption is that the intensity exponent varies comparatively slowly with intensity.

If the products of the decomposition of ammonia remove hydrogen atoms more effectively than by the normal process of combination in the gas phase and on the walls, the magnitude of the above quantity will be greater than unity. The value of  $x$  has been determined by separate experiments and found to be equal to unity under these conditions. The results in table 1 are therefore calculated on this basis.

TABLE 1

| Temp.<br>° C | Press.<br>NH <sub>3</sub><br>mm. | Press.<br>p-H <sub>2</sub><br>mm. | Exp.<br>time<br>min. | log % p-H <sub>2</sub> converted |       |       | $\frac{S+A}{SA}$ | $h\nu/\text{sec.}$ |                    |
|--------------|----------------------------------|-----------------------------------|----------------------|----------------------------------|-------|-------|------------------|--------------------|--------------------|
|              |                                  |                                   |                      | A                                | SA    | S     |                  | $A \times 10^{15}$ | $S \times 10^{15}$ |
| 100          | 50                               | 50                                | 12.0                 | 0.276                            | 0.320 | 0.082 | 1.12             | 12.0               | 4.3                |
| 100          | 50                               | 50                                | 10.0                 | 0.792                            | 0.700 | 0.193 | 1.37             | 9.4                | 4.6                |
| 100          | 50                               | 50                                | 7.0                  | 0.477                            | 0.589 | 0.063 | 0.92             | 9.4                | 3.9                |
| 100          | 30                               | 50                                | 5.5                  | 0.281                            | 0.356 | 0.074 | 1.00             | —                  | 22.0               |
| 100          | 30                               | 50                                | 5.5                  | 0.553                            | 0.528 | 0.089 | 1.22             | —                  | 22.0               |
| 100          | 30                               | 50                                | 7.0                  | 0.449                            | 0.526 | 0.100 | 1.04             | 15.0               | 8.0                |
| 100          | 30                               | 50                                | 10.0                 | 0.399                            | 0.496 | 0.086 | 0.98             | 8.0                | 4.8                |
| 100          | 30                               | 50                                | 15.0                 | 0.163                            | 0.297 | 0.107 | 0.91             | 4.0                | 9.0                |
| 100          | 30                               | 50                                | 10.0                 | 0.307                            | 0.397 | 0.091 | 1.00             | 12.0               | 4.0                |
| 100          | 5.0                              | 6.5                               | 7.0                  | 0.215                            | 0.238 | 0.037 | 1.06             | 3.4                | 3.4                |
| 100          | 2.0                              | 3.0                               | 12.0                 | 0.341                            | 0.338 | 0.029 | 1.10             | 2.1                | 0.9                |
| 50           | 32                               | 53                                | 20.0                 | 0.070                            | 0.087 | 0.016 | 0.99             | 0.7                | —                  |
| 50           | 30                               | 53                                | 15.0                 | 0.031                            | 0.053 | 0.024 | 1.04             | —                  | 1.9                |
| 50           | 30                               | 52                                | 14.0                 | 0.281                            | 0.346 | 0.013 | 0.85             | 3.8                | 2.1                |
| 50           | 15                               | 26                                | 12.0                 | 0.181                            | 0.207 | 0.016 | 0.95             | 3.8                | 2.1                |

It can be seen that in every case the value of the above expression is substantially equal to unity, from which it may be concluded that photo-decomposing ammonia has no appreciable effect in removing hydrogen atoms at an abnormally fast rate.

Since the conclusion drawn from these experiments is negative, it is desirable to furnish some positive evidence that the conditions were such that a removal of hydrogen atoms was to be expected. For this purpose a repetition of the experiments (Melville 1932) in which the ammonia photolysis was inhibited by atomic hydrogen, was most suitable. In table 2 are tabulated the results of inhibition experiments under the same conditions as employed in the conversion runs.

It will be observed that inhibition is marked at 50° C though less appreciable at 100° C. This is in accordance with expectations, since the quantum efficiency increases from 50 to 100° C which, of course, means the back reaction is of increasing importance at lower temperatures. At the low pressures of these experiments diffusion to the walls of the hydrogen atoms



would tend to overshadow any process whereby removal is effected in the gas phase. Consequently, the fact that inhibition, which is partly a gas-phase phenomenon, could be detected, is evidence that conditions at the high pressures were such that a removal of hydrogen atoms by a gas-phase process could also have been detected.

TABLE 2

| Temp.<br>° C | Press.<br>NH <sub>3</sub><br>mm. | Press.<br>p-H <sub>2</sub><br>mm. | Exp.<br>time<br>min. | Amounts of decomposition |           |          |                  |
|--------------|----------------------------------|-----------------------------------|----------------------|--------------------------|-----------|----------|------------------|
|              |                                  |                                   |                      | A<br>mm.                 | SA<br>mm. | S<br>mm. | $\frac{S}{SA-A}$ |
| 100          | 3.0                              | 0.090                             | 6.0                  | 0.008                    | 0.014     | 0.007    | 1.17             |
| 100          | 3.2                              | 0.117                             | 10.0                 | 0.012                    | 0.017     | 0.010    | 2.00             |
| 100          | 3.2                              | 0.128                             | 10.0                 | 0.002                    | 0.013     | 0.012    | 1.09             |
| 100          | 3.2                              | 0.151                             | 10.0                 | 0.007                    | 0.018     | 0.013    | 1.18             |
| 50           | 3.5                              | 0.152                             | 10.0                 | 0.007                    | 0.013     | 0.011    | 1.83             |
| 50           | 1.8                              | 0.178                             | 10.0                 | 0.004                    | 0.012     | 0.015    | 1.88             |
| 50           | 3.6                              | 0.175                             | 10.0                 | 0.007                    | 0.009     | 0.005    | 2.50             |

Spark intensity =  $2.0 \times 10^{15}$   $h\nu$ /sec. Arc intensity =  $8.5 \times 10^{15}$   $h\nu$ /sec.

#### QUANTUM EFFICIENCY OF THE PRIMARY PROCESS IN THE AMMONIA PHOTOLYSIS

Since proof has now been given that hydrogen atoms are not removed abnormally quickly the conclusion must be drawn that the primary dissociation is not as efficient as has hitherto been supposed. In considering the invention of methods suitable for measuring the primary efficiency some comparative technique is obviously the most accurate way of carrying out the experiments provided the standard for comparison can be accurately reproduced and readily compared with the unknown factor. The mercury-sensitized production of hydrogen atoms is the best method of making atomic hydrogen in a static system, and again the para-hydrogen conversion may be used as a detector. The rate of production of hydrogen atoms may be computed from the number of quanta absorbed, making the assumption that every excited mercury atom produces two hydrogen atoms. This method introduces the inaccuracy of photometry and presumes an exact knowledge of the reaction which is not yet available. While practicable, the method could be improved. A knowledge of the lifetime of the atoms combined with a measurement of their concentration by means of para-hydrogen would also give the rate of production, but here there are comparatively big uncertainties introduced by the fact that the velocity constant for the para-hydrogen conversion is not known at all exactly.

The difficulty may be overcome in the following way. The rate of conversion of para-hydrogen is given by the equations

$$-\frac{d(p-H_2)}{dt} = k_1(H)(p-H_2) + \frac{K(H)}{(H_2)} + k_2(H)^2(H_2). \quad (1)$$

The first term refers to the conversion brought about by the atomic exchange reaction, while the second two terms represent the rate of conversion due to dissociation of the para-hydrogen molecule. This latter quantity is, of course, equal to the sum of the rates of combination by diffusion to the walls  $K(H)/(H_2)$  and in the gas phase  $k_2(H)^2(H_2)$ . The hydrogen atom concentration is in turn controlled by that of the excited mercury atoms and is given by the equation

$$\frac{I_{in} k_2(H_2)}{k_3(H_2)(Hg^*) + \tau^{-1}} = \frac{K(H)}{(H_2)} + k_2(H)^2(H_2), \quad (2)$$

where  $I_{in}$  is the incident intensity,  $k_3(H_2)(Hg')$  the rate of deactivation of excited mercury atoms and  $\tau$  is the lifetime of the excited Hg atom. At high pressures of the order of several hundred millimetres the first term is much larger than the second and third terms in equation (1); further,  $k_3(H_2)$  is very much larger than  $\tau^{-1}$  and  $k_2(H)^2(H_2)$  very much larger than  $K(H)/(H_2)$ . Therefore

$$-\frac{d(p-H_2)}{dt} = k_1 \sqrt{\left(\frac{I_{in}}{k_2}\right)} (H_2)^{1/2}. \quad (3)$$

At somewhat lower pressures the term  $K(H)/(H_2)$  is more important than  $k_2(H)^2(H_2)$ , that is to say gas-phase combination gives place to wall combination. Under these conditions

$$(H) = \frac{I_{in}(H_2)}{K},$$

$$\text{and} \quad -\frac{d(p-H_2)}{dt} = \frac{k I_{in}}{K} (p-H_2)^2 + I_{in}. \quad (4)$$

$$\text{The two extremes are} \quad k I_{in} (p-H_2)^2 K^{-1} \quad (4a)$$

$$\text{and} \quad I_{in}. \quad (4b)$$

At lower pressures still when  $\tau^{-1}$  is comparable with  $k_3(Hg^*)$

$$-\frac{d(p-H_2)}{dt} = \frac{k_1}{K} (p-H_2)^2 \frac{I_{in} k_2(Hg)}{k_3(Hg^*) + \tau^{-1}} + \frac{I_{in} k_3(Hg)}{k_3(Hg^*) + \tau^{-1}}. \quad (5)$$

The extreme condition is realized when the first term in equation (5) is negligible compared with the second, i.e.

$$-\frac{d(p-H_2)}{dt} = I_{\text{in}} k_3(p-H_2)\tau. \quad (6)$$

Thus, starting at very low pressures, the *absolute* rate of para-hydrogen conversion increases linearly with pressure (equation (6)), becomes independent of pressure (equation (4*b*)) for a certain pressure range, increases again (equation (4*a*)) as the square of the pressure, and then finally increases as the square root of the pressure (equation (3)). The important part of the pressure region is that in which the absolute rate of conversion is numerically equal to the number of quanta absorbed by the system. Fortunately, this region may be extended considerably on the low-pressure side so as to increase the accuracy of measurement, since  $\tau$  is not constant. In systems of the dimensions used in these experiments and at a mercury pressure of  $10^{-3}$  mm.,  $\tau$  varies at high pressures of hydrogen from  $10^{-7}$  sec. up to as much as  $10^{-6}$  sec. at low hydrogen pressures. Thus equation (5) becomes valid at lower pressures of para-hydrogen than would have been the case if  $\tau$  had remained constant at  $10^{-7}$  sec.

In figure 1 the absolute rate of para-hydrogen conversion is plotted against the logarithm of the pressure, and as will be seen there is a considerable range of pressures in which the rate is constant in accordance with the above expectations. A pressure of about 1 mm. would appear to be the most suitable for such photometric measurements. The data from which figure 1 is drawn are given in table 3.

Having now got a method of directly measuring the rate of hydrogen atom production, the principle of the method for obtaining the efficiency of the primary process in the ammonia reaction is simply to note the number of quanta absorbed by the ammonia  $I_{\text{NH}_3}$  and observe the rate of conversion of para-hydrogen. The intensity of the mercury lamp is adjusted so that the rate of para-hydrogen conversion is the same as that produced by ammonia. With this intensity the rate of dissociation of hydrogen molecules  $I_{\text{H}_2^*}$  is obtained. The primary efficiency in the ammonia reaction is therefore  $2I_{\text{H}_2^*}/I_{\text{NH}_3}$ , since ammonia yields only one hydrogen atom. It might be argued that in so doing the unjustifiable assumption has been made that the rate of mercury-sensitized production of hydrogen atoms will be altered in presence of ammonia and para-hydrogen at high pressures owing (a) to competitive quenching and (b) pressure broadening of the absorption lines of the mercury vapour. The first point has already been discussed elsewhere (Melville 1935) and it has been shown that hydrogen certainly quenches

**TABLE 3. PRESSURE DEPENDENCE OF THE PARA-HYDROGEN CONVERSION (20° C)**

| Pressure<br>$p\text{-H}_2$<br>mm. | Log<br>pressure | Exp. time<br>min. | $-\Delta\% p\text{-H}_2$ | Absolute<br>conversion<br>mm.<br>$\times 10^{-2}$ | Absolute<br>conversion<br>rate<br>mm./min.<br>$\times 10^{-2}$ |
|-----------------------------------|-----------------|-------------------|--------------------------|---|--|
| 0.25                              | 1.398           | 6.0               | 17.2                     | 4.30  | 0.72   |
| 0.26                              | 1.415           | 5.0               | 15.2                     | 3.95  | 0.79   |
| 0.34                              | 1.532           | 7.0               | 18.4                     | 6.25  | 0.89   |
| 0.44                              | 1.644           | 9.0               | 17.7                     | 7.78  | 0.86   |
| 0.48                              | 1.681           | 8.0               | 17.9                     | 8.59  | 1.07   |
| 0.51                              | 1.708           | 4.0               | 9.0                      | 4.59  | 1.15   |
| 0.69                              | 1.839           | 12.0              | 17.7                     | 12.2  | 1.01   |
| 0.78                              | 1.892           | 4.0               | 5.3                      | 4.13  | 1.04   |
| 0.92                              | 1.964           | 12.0              | 12.8                     | 11.8  | 0.98   |
| 0.92                              | 1.964           | 10.0              | 11.3                     | 10.4  | 1.04   |
| 0.90                              | 1.959           | 5.0               | 6.1                      | 5.49  | 1.10   |
| 1.90                              | 0.279           | 10.0              | 6.0                      | 11.4  | 1.14   |
| 1.95                              | 0.290           | 8.0               | 6.1                      | 11.9  | 1.49   |
| 2.90                              | 0.462           | 15.0              | 7.5                      | 21.8  | 1.45   |
| 3.20                              | 0.508           | 14.0              | 5.3                      | 17.0  | 1.21   |
| 3.30                              | 0.519           | 13.0              | 6.7                      | 22.1  | 1.70   |
| 9.90                              | 0.996           | 11.0              | 3.5                      | 34.7  | 3.15   |
| 10.4                              | 1.017           | 11.0              | 2.7                      | 28.1  | 2.56   |
| 30.0                              | 1.477           | 10.0              | 1.7                      | 51.0  | 5.10   |
| 30.3                              | 1.481           | 11.0              | 2.9                      | 87.9  | 8.00   |
| 44.5                              | 1.648           | 10.0              | 3.6                      | 160   | 16.0   |
| 49.5                              | 1.695           | 9.0               | 2.7                      | 134   | 15.0   |

Volume of reaction system 97 c.c.

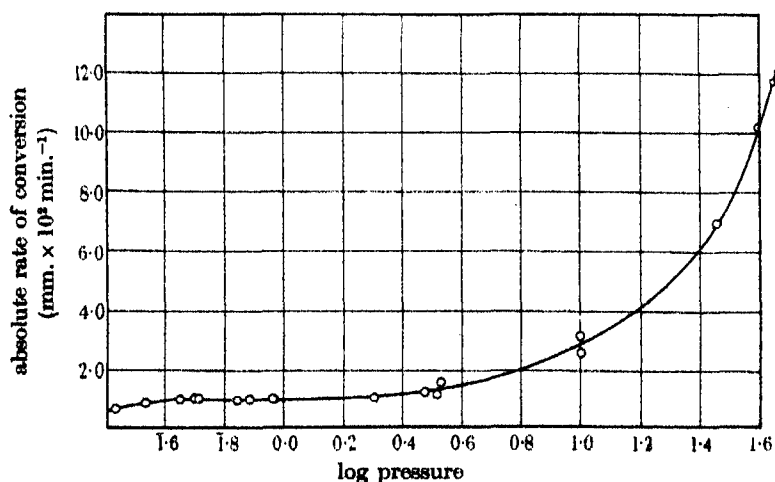


**FIGURE 1. Pressure dependence of the para-hydrogen conversion.**

at least 95 % of the mercury atoms under the conditions described below. The second objection is also ruled out by the fact that (a) the lines are certainly narrower than the absorption lines, since the argon pressure in the lamp is of the order of 1 mm. and also directly by the fact that all the light at  $2537^{\circ}\text{A}$  is absorbed by the mercury vapour (see preceding paper).

Experimentally, the actual procedure is slightly more complicated than that described above. Two similar reaction vessels are disposed on either side of a zinc spark. An argon discharge mercury lamp is set on the other side of the lower reaction cell (figure 2). The upper cell is filled with pure

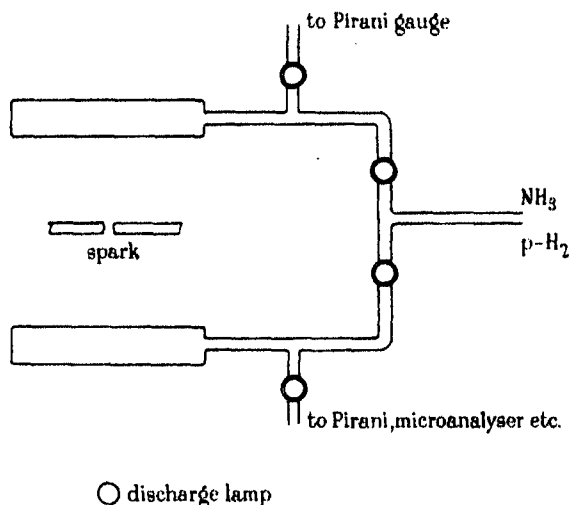


FIGURE 2. Reaction system for measuring primary efficiency.

ammonia simply to act as a photometer in view of the irregularity of the spark output. Any variation in the latter's output can thus be readily corrected. First a mixture of about 50 mm. para-hydrogen and 30 mm. ammonia is irradiated with the spark for such a time as to give a measurable para-hydrogen conversion. A similar exposure with the mercury lamp is also given. The distance is not of course adjusted so that the rates are exactly equal, since the correction is easily applied. This is then followed with a para-conversion with the mercury lamp, the para-hydrogen pressure being 1 mm. in order to get the rate of hydrogen-atom production. The final stage is the determination of the number of quanta absorbed by the ammonia. This was obtained by measuring the rate of decomposition and computing from the known value of the quantum efficiency at 50 mm. pressure in a reaction vessel of similar dimensions.

In order to correct for inequality in the para-hydrogen conversion rates, experiments were made to find how the rate of the mercury-sensitized conversion of para-hydrogen varied with intensity of the absorbed light. For these pressures the intensity exponent was found to be 0.8.  $\gamma_p$ , the primary quantum efficiency of the ammonia photolysis, is thus given by

$$\gamma_p = \frac{d(\text{H}_{\text{Hg}})/dt}{h\nu_{\text{NH}_3}(R_{\text{H}}/R_{\text{NH}_3})^{1/0.8}},$$

where  $d(\text{H}_{\text{Hg}})/dt$  is the rate of production of hydrogen atoms,  $h\nu_{\text{NH}_3}$  is the rate of absorption of quanta by ammonia per second and  $R_{\text{H}}$  and  $R_{\text{NH}_3}$  are respectively the rates of conversion of para-hydrogen by mercury sensitization and by ammonia. Table 4 gives a series of results obtained with this method.

TABLE 4. QUANTUM EFFICIENCY OF THE PRIMARY PROCESS  
OF THE AMMONIA PHOTOLYSIS

| Pressure<br>NH <sub>3</sub><br>mm. | Pressure<br>p-H <sub>2</sub><br>mm. | $R_{\text{H}}$<br>$d(\log u)/dt$ | $R_{\text{NH}_3}$<br>$d(\log u)/dt$ | Spark<br>quanta<br>$h\nu \text{ sec.}^{-1}$<br>c.c. <sup>-1</sup><br>$\times 10^{16}$ | $d(\text{H}_{\text{Hg}})/dt$<br>atoms sec. <sup>-1</sup><br>c.c. <sup>-1</sup><br>$\times 10^{15}$ | $\gamma$  |
|------------------------------------|-------------------------------------|----------------------------------|-------------------------------------|---|--|-----------|
| 30                                 | 50                                  | 0.0437                           | 0.1521                              | 17.9  | 1.99   | 0.53      |
| 29                                 | 52                                  | 0.0253                           | 0.0548                              | 7.97  | 1.99   | 0.66      |
| 29                                 | 51                                  | 0.0253                           | 0.0478                              | 6.08  | 1.99   | 0.68      |
| 29                                 | 52                                  | 0.0285                           | 0.0343                              | 5.01  | 1.99   | 0.50      |
| 31                                 | 50                                  | 0.0427                           | 0.0577                              | 5.76  | 1.99   | 0.48      |
| 30                                 | 52                                  | 0.0343                           | 0.0352                              | 3.17  | 1.99   | 0.65      |
|                                    |                                     |                                  |                                     |   |  | 0.58 Mean |

The most surprising thing is that the quantum efficiency is somewhat less than unity, thus directly confirming the expectations made at the beginning of this paper. The bearing of this result on the ammonia problem will be discussed later.

#### THE FATE OF AMINE RADICALS

In the full elucidation of the ammonia photolysis a knowledge of the reaction of the amine radicals is of no less importance than that of the hydrogen atoms. But here the difficulty arises that no way of measuring their concentration exists. None the less, an attempt has been made to obtain some idea of their lifetime. This is important, since such a determination throws some light on the mode of interaction of hydrogen atoms

and amine radicals which is partly responsible for limiting the quantum efficiency of the reaction.

The lifetime of the hydrogen atoms has also been determined. The data for computing this quantity have been given in the previous section. This lifetime is simply given by  $\tau = (H)/(d(H)/dt)$ . The concentration of atomic hydrogen is further defined by

$$(H) = \frac{du/dt}{k^*u}.$$

From the experiments quoted in the preceding section this rate of para-hydrogen conversion at 15 mm. pressure is  $3.7 \times 10^{-2}$  mm.  $p\text{-H}_2$ /min., and since the rate of conversion by dissociation is  $1.05 \times 10^{-2}$  mm./min., the rate of conversion by exchange at 15 mm. is  $2.65 \times 10^{-2}$  mm.  $p\text{-H}_2$ /min. Hence

$$(H) = 5.59 \times 10^{-11} \text{ mol. litre}^{-1} \text{ if } k^* = 9.33 \times 10^5 \text{ (Farkas),}$$

$$\text{or} \quad = 3.70 \times 10^{-10} \text{ mol. litre}^{-1} \text{ if } k^* = 1.41 \times 10^5 \text{ (Geib and Harteck).}$$

The respective lives are therefore  $1.65 \times 10^{-3}$  and  $1.09 \times 10^{-2}$  sec. This is the sort of value obtained in previous investigations using light intensities of the same order of magnitude.

It has already been shown that the ammonia photolysis is inhibited by atomic hydrogen due to the reaction  $H + NH_2 = NH_3$ . Instead of generating the amine radicals and the hydrogen atoms simultaneously, as in this type of experiment, the basis of the method of obtaining the lifetime of amine radicals is to generate these two entities separated by a known time interval. At sufficiently small intervals amine radicals, if generated first, will be removed by the subsequently generated hydrogen atoms. At larger intervals the amine radicals will have decomposed and no inhibition will be observed. Thus at some intermediate interval inhibition will just be observed and this gives an indication of the lifetime of the amine radical.

Instead of employing a disk type of sector for this purpose a rotating cylinder surrounding a cylindrical reaction vessel served to intercept the beams of light from the two sources. This has some important advantages; for instance, the sources of light may be brought close to a small reaction vessel and the interval between the two kinds of illumination may be made small by keeping their distance apart down to a small value. The apparatus finally used is shown in figure 3. The sources of light were as usual a zinc spark and an argon-mercury cold-cathode discharge lamp, the first producing amine radicals and the second hydrogen atoms by mercury sensitization. On the other side of the zinc spark was an ammonia photometer, so

that a continuous record could, if necessary, be taken of the output of the spark during any prolonged experiment. In addition to the rotating brass cylinder there were shields set around the reaction system to limit the size of the beams of light from the two sources of illumination. The silica reaction vessel just fitted into the brass cylinder with 2 mm. clearance. The cylinder itself was supported in two sets of ball bearings, the housings of which were supported on a rigid framework made of Meccano angle pieces. This permitted the cylinder to run at a speed up to 2000 r.p.m. The drive

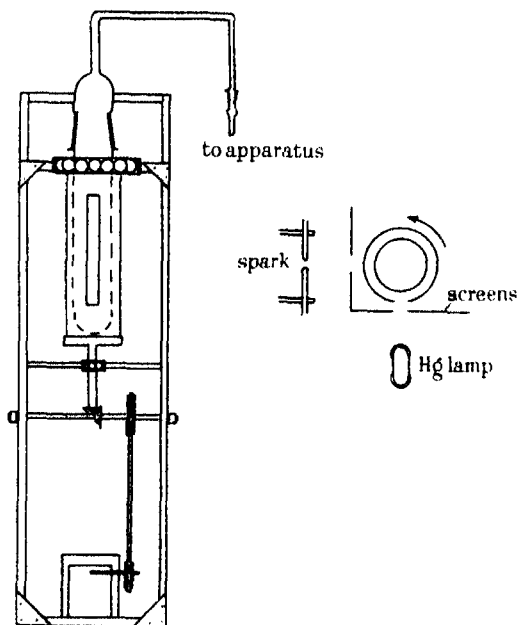


FIGURE 3. Rotating cylindrical sector.

was taken from an electric motor through a suitable reduction gearing, the lowest speed of rotation attainable being less than 1 r.p.m.

The experimental procedure consisted in introducing about 3 mm. of ammonia and about 0.25 mm. of hydrogen into the reaction vessel. With the sector rotating at the desired speed the reactants were exposed to the radiation from the mercury lamp and the increase ( $A$ ) in pressure of the non-condensable gas ( $N_2 + H_2$ ) measured on the Pirani gauge. The exposure was repeated with the spark alone and the decomposition ( $S$ ) once more determined. Finally, another exposure was made with the lamp and spark operating together ( $SA$ ). The output from the spark was checked for constancy by the photometer and any correction necessary applied. Two



methods were adopted to time the speed of rotation. At high speeds, greater than 100 r.p.m., the revolutions were counted with a revolution counter in contact with the motor armature shaft and timed with a stop-watch. At slow speeds, less than 100 r.p.m., revolutions were counted at

TABLE 5

|               |                  | Pressure    |       |       |       |       |       |            |      | Ratio<br>$S/(SA - A)$ |
|---------------|------------------|-------------|-------|-------|-------|-------|-------|------------|------|-----------------------|
| Slot          |                  | $H_2 + N_2$ |       |       |       |       |       | Photometer |      |                       |
| Exp. interval |                  | $NH_3$      | $H_2$ | $A$   | $S$   | $SA$  |       |            |      |                       |
| time          | sec.             | mm.         | mm.   | mm.   | mm.   | mm.   | $S$   | $SA$       |      |                       |
| min.          | $\times 10^{-1}$ |             |       |       |       |       |       |            |      |                       |
| 10            | 7.5              | 4.0         | 0.386 | 0.006 | 0.031 | 0.023 | —     | —          | 1.82 |                       |
| 10            | 7.5              | 4.0         | 0.372 | 0.002 | 0.028 | 0.020 | —     | —          | 1.56 |                       |
| 10            | 1.6              | 4.6         | 0.296 | 0.001 | 0.019 | 0.014 | —     | —          | 1.46 |                       |
| 10            | 3.8              | 5.5         | 0.273 | 0.003 | 0.028 | 0.025 | —     | —          | 1.27 |                       |
| 15            | 4.6              | 3.3         | 0.239 | 0.003 | 0.026 | 0.018 | 0.119 | 0.089      | 1.30 |                       |
| 15            | 4.5              | 3.8         | 0.234 | 0.006 | 0.040 | 0.036 | 0.221 | 0.246      | 1.48 |                       |
| 15            | 4.5              | 3.8         | 0.234 | 0.003 | 0.045 | 0.028 | 0.370 | 0.266      | 1.30 |                       |
| 10            | 5.0              | 3.1         | 0.307 | 0.003 | 0.015 | 0.011 | —     | —          | 1.89 |                       |
| 15            | 10.0             | 3.9         | 0.240 | 0.006 | 0.086 | 0.110 | 0.592 | 0.726      | 1.02 |                       |
| 15            | 10.0             | 3.9         | 0.240 | 0.006 | 0.036 | 0.043 | 0.216 | 0.358      | 1.61 |                       |
| 15            | 10.0             | 4.0         | 0.240 | 0.006 | 0.035 | 0.030 | 0.166 | 0.158      | 1.39 |                       |
| 15            | 10.0             | 3.7         | 0.240 | 0.001 | 0.023 | 0.014 | 0.077 | 0.076      | 1.47 |                       |
| 20            | 10.3             | 3.5         | 0.299 | 0.005 | 0.050 | 0.048 | —     | —          | 1.16 |                       |
| 20            | 14.9             | 3.7         | 0.295 | 0.010 | 0.056 | 0.053 | —     | —          | 1.30 |                       |
| 15            | 14.9             | 4.0         | 0.240 | 0.005 | 0.024 | 0.017 | 0.067 | 0.067      | 2.00 |                       |
| 15            | 20.0             | 4.0         | 0.240 | 0.004 | 0.034 | 0.037 | 0.148 | 0.148      | 1.03 |                       |
| 20            | 19.7             | 4.0         | 0.289 | 0.007 | 0.064 | 0.063 | —     | —          | 1.16 |                       |
| 16            | 27.0             | 4.3         | 0.272 | 0.009 | 0.055 | 0.048 | —     | —          | 1.40 |                       |
| 18            | 30.0             | 4.0         | 0.275 | 0.007 | 0.025 | 0.022 | —     | —          | 1.66 |                       |
| 20            | 30.0             | 4.0         | 0.296 | 0.005 | 0.018 | 0.031 | —     | —          | 0.69 |                       |
| 20            | 29.7             | 4.0         | 0.313 | 0.007 | 0.032 | 0.036 | —     | —          | 1.10 |                       |
| 16            | 30.0             | 3.7         | 0.240 | 0.006 | 0.024 | 0.030 | 0.109 | 0.124      | 1.18 |                       |
| 16            | 30.0             | 3.7         | 0.240 | 0.005 | 0.031 | 0.028 | 0.118 | 0.110      | 1.26 |                       |
| 16            | 30.0             | 3.3         | 0.240 | 0.008 | 0.022 | 0.023 | 0.102 | 0.088      | 1.26 |                       |
| 16            | 50.0             | 3.9         | 0.240 | 0.005 | 0.024 | 0.017 | 0.108 | 0.090      | 1.67 |                       |
| 20            | 75.0             | 4.0         | 0.240 | 0.005 | 0.032 | 0.027 | 0.148 | 0.164      | 1.41 |                       |
| 20            | 72.0             | 4.0         | 0.240 | 0.007 | 0.030 | 0.024 | 0.133 | 0.130      | 1.74 |                       |
| 20            | 72.0             | 3.4         | 0.240 | 0.008 | 0.042 | 0.037 | 0.144 | 0.142      | 1.59 |                       |

Reaction volume = 100 c.c. Temp.  $20^\circ C$ ,  $2537^\circ A = ca. 3.38 \times 10^{13} \text{ } h\nu/\text{sec.}$

Spark =  $ca. 9.68 \times 10^{12} \text{ } h\nu/\text{sec.}$

intervals during the exposure by direct observation and timed with a stop-watch. At very low speeds, about 1 r.p.m., every revolution during the timed exposure was counted and every other revolution timed as an intermediate check on the constancy. Reference marks were made on the cylinder and frame to facilitate counting. The results are given in table 5.

As will be observed, inhibition of the ammonia decomposition is very marked, since the quantity  $S/(S-A)$  is greater than unity not only at small intervals but also at the extraordinarily large interval of 70 sec. It may also be noted that although there is some random variation in the degree of inhibition, the value of  $S/(S-A)$  never exceeds 2.0, even although the number of hydrogen atoms produced by mercury sensitization is more than ten times that produced by the dissociation of ammonia.

There is one comment to be made on these results on account of the fact that a Pirani gauge is used to measure decomposition rates. For this particular gauge the calibration curve for hydrogen is linear up to 0.4 mm. At most the pressure increase due to non-condensable gas is 0.160 mm. Of this, only 0.040 mm. is nitrogen, and since the total pressure of nitrogen and hydrogen is about 0.4 mm., the percentage of nitrogen never exceeds 10 % and, in fact, it generally amounts to less than 5 %. The heat loss by the wire can be expressed by

$$V_{N_2}^2 = kK_{N_2}f \quad \text{and} \quad V_{H_2}^2 = kK_{H_2}(1-f),$$

where  $V$  are the voltages applied across the Pirani bridge,  $K_{N_2}$  and  $K_{H_2}$  are the thermal conductivity coefficients for nitrogen and hydrogen, and  $f$  is the fraction of nitrogen present. The fractional heat loss due to nitrogen is thus given by

$$\frac{V_{N_2}^2}{V_{N_2}^2 + V_{H_2}^2} = \frac{K_{N_2}f}{K_{N_2}f + K_{H_2}(1-f)} = 1.9 \times 10^{-2}.$$

#### DEUTEROAMMONIA

The overall quantum efficiency of the direct deuterioammonia photolysis has been found to be 0.2 at 100 mm. pressure, rather less than that of ammonia (Wiig 1937). The question naturally arises whether this low efficiency is also due to a primary efficiency of less than unity. The same technique as that employed with ammonia has been applied to determine this primary efficiency. No serious error is introduced by taking the exchange conversion of para-hydrogen initiated by D-atoms as kinetically identical with that initiated by H-atoms, since the activation energy of the reactions  $H + H_2 = H_2 + H$  and  $D + H_2 = HD + H$  are nearly the same.

Trideuterioammonia was prepared by distilling powdered 99 % deuterioammonium chloride, supplied by Imperial Chemical Industries, with deuterized soda lime which had been thoroughly dried *in vacuo* at 300° C. The heavy ammonia was freely liberated at 200° C from the chloride. The gas was purified by repeated fractional distillation with liquid oxygen. In

table 6 are given the data for the primary quantum efficiency of the direct photolysis, the reaction system being exactly the same as that used for the corresponding ammonia determination (figure 2).

TABLE 6

| Pressure |         | $R_H$          | $R_{ND_2}$     | Spark                    | $d(H_{H_2^*})/dt$        | $\gamma_p$ |
|----------|---------|----------------|----------------|--------------------------|--------------------------|------------|
| $ND_3$   | $p-H_2$ |                |                | $h\nu \text{ min.}^{-1}$ | atoms $\text{min.}^{-1}$ |            |
| mm.      | mm.     | $d(\log u)/dt$ | $d(\log u)/dt$ | c.c. $^{-1}$             | c.c. $^{-1}$             |            |
| 31       | 53      | 0.039          | 0.049          | 1.33                     | 2.81                     | 0.28       |
| 32       | 51      | 0.052          | 0.043          | 1.14                     | 4.31                     | 0.30       |
| 32       | 52      | 0.038          | 0.038          | 1.19                     | 2.64                     | 0.31       |
| 32       | 52      | 0.050          | 0.039          | 1.17                     | 3.57                     | 0.22       |

As the value of the primary efficiency is relatively nearer the overall efficiency than in the case of ammonia, the overall efficiency has been redetermined in the same conditions. For this purpose it is convenient to use a comparison method with the well-established quantum efficiency of ammonia as the standard. The reaction system is the same as that above.

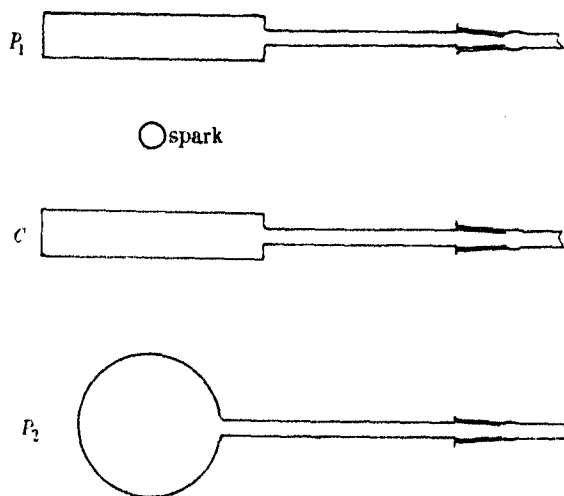


FIGURE 4. Reaction system for absorption measurements.

Ammonia and deuterioammonia are alternately introduced into the reaction system and exposed to the radiation of a zinc spark. Decomposition is measured on a Pirani gauge calibrated for 25 %  $N_2-H_2$  and 25 %  $N_2-D_2$  mixtures. Any variation in the spark intensity is corrected by the ammonia photometer placed behind the spark. Since ammonia and deuterioammonia

have different absorption coefficients, these have been determined in comparable conditions. The reaction system is shown in figure 4. The absorption cell *C* is a plane-ended cylinder, 6 cm. in diameter and 2 cm. wide.  $P_2$  is a photometer containing ammonia at 100 mm. pressure which absorbs the transmitted light.  $P_1$  is the usual ammonia photometer to check the constancy of the spark intensity. The results are given in table 7.

The value of 84.5 % for deuteroammonia is approximately twice that obtained by Wiig. In the present determination, however, monochromatic light has not been used. These absorption coefficients are employed in computing the overall quantum efficiency which is given in table 8. Since this fraction is only 20 %, the effect of nitrogen on the linear calibration of the gauge may be considered to be negligible.

TABLE 7

| Pressure<br>mm. | Absorption<br>by $\text{NH}_3$<br>% | Absorption<br>by $\text{ND}_3$<br>% |
|-----------------|-------------------------------------|-------------------------------------|
| 100             | 93.2                                | 84.5                                |
| 30              | 74.4                                | 59.3                                |

TABLE 8. OVERALL QUANTUM EFFICIENCY OF THE  $\text{ND}_3$  PHOTOLYSIS

| Pressure<br>$\text{NH}_3$<br>mm. | Pressure<br>$\text{ND}_3$<br>mm. | Ratio<br>$\frac{d(\text{N}_2 + \text{D}_2)/dt}{d(\text{N}_2 + \text{H}_2)/dt}$ | $\gamma_{\text{ND}_3}$<br>( $\gamma_{\text{NH}_3} = 0.3$ ) |
|----------------------------------|----------------------------------|--|--|
| 100                              | 100                              | 0.625  | 0.21   |
| 100                              | 100                              | 0.714  | 0.22   |
| 100                              | 100                              | 0.641  | 0.21   |

## GENERAL DISCUSSION

Before discussing the results contained in the above experiments it is worth while briefly summarizing the present position regarding the mechanism of the photodissociation of ammonia. Two detailed discussions of the question have already been published in which attempts have been made to arrive at a rational scheme of reactions to explain the greater part of the data available (Leighton 1938; Taylor 1938; cf. also Luyckx 1935).

The predissociation spectrum and absence of fluorescence with ammonia have been taken to mean that the molecule dissociates in some  $10^{-13}$  sec. after absorbing a quantum of radiation (Bonhoeffer and Farkas 1927). Several facts favour the disruption of the molecule into  $\text{NH}_2$  and H rather

than  $\text{NH}$  and  $\text{H}_2$ . The most convincing is that admixed para-hydrogen is converted to normal hydrogen on illuminating ammonia. The outstanding difficulty was, however, the explanation of the low quantum efficiency. In view of the spectroscopic evidence this was attributed to the operation of some secondary reaction producing ammonia. It is this part of the question about which there has been so much controversy. Since the decomposition of ammonia may be repressed by the addition of atomic hydrogen and not by molecular hydrogen, it was at first assumed that the reformation of ammonia is due to the reverse reaction  $\text{H} + \text{NH}_2 = \text{NH}_3$ , taking place in the gas phase or on the walls depending on the pressure of ammonia. This, too, was supported by even more direct evidence in that if deuterium atoms were used deuterated ammonia was found during the reaction. The competing reactions were supposed to be  $\text{H} + \text{H} = \text{H}_2$  and  $2\text{NH}_2 = \text{N}_2 + 2\text{H}_2$ . Moreover, since the quantum efficiency does not markedly depend on pressure of ammonia it was supposed that these reactions effectively competed with  $\text{H} + \text{NH}_2 = \text{NH}_3$ , and then it was difficult to see why the hydrogen atom concentration was exceptionally low. Under certain conditions and especially in a flow system it was observed that hydrazine was produced in considerable quantity (Gedye and Rideal 1932). In addition, experiments had shown that hydrazine is quickly decomposed by hydrogen atoms, forming ammonia together with nitrogen and hydrogen. Hence it was next suggested that hydrazine, formed in the decomposition of ammonia by the combination of the  $\text{NH}_2$  radicals, might be responsible for the low concentration of hydrogen atoms and also explain the atomic inhibition experiments in which ammonia is regenerated. The result of this suggestion was the elaboration of comprehensive and much more complicated reaction schemes for explaining the ammonia photolysis. The elaboration was such that it was relatively easy to explain such matters as the pressure dependence of the quantum efficiency, but this was compensated by the fact that it became increasingly difficult to find out anything about the kinetics of the individual reactions.

The experiments described in the preceding paper and also those in the first section of the present paper prove that the low stationary hydrogen atom concentration is certainly not due to any process involving the rapid removal of these atoms, and thus the reason for introducing hydrazine into the scheme of reactions must be dropped. This does not mean, of course, that hydrazine is not formed at all. It merely implies that any small concentration that is undoubtedly built up does not play any part in limiting the rate of the overall decomposition of ammonia. Nor do these results conflict with the observation of Ogg, Leighton and Bergstrom (1934) that

photo-dissociating ammonia can effect decomposition of hydrazine. In these latter experiments the hydrazine pressure was high enough to ensure that the hydrogen atoms from the ammonia would indeed react with the hydrazine before combining in the ordinary way. This result too is in agreement with the experiments in the preceding paper.

The experiments on the determination of the efficiency of the primary process not only confirm the above observations but prove directly that this process is not efficient, as has hitherto been supposed. The efficiency, 0.68, is, however, appreciably greater than that of the overall efficiency, *ca.* 0.2–0.3. Thus it must be concluded that a fraction of the hydrogen atoms and amine radicals recombine. The rates of these two reactions must be of comparable velocity in order effectively to compete with each other. This also means that the greater part of the ammonia re-formed is produced in the back reaction. Whether these reactions occur at the walls or in the gas phase will depend on such factors as light intensity and total pressure.

In some experiments on the decomposition of ammonia by light of 1990 Å, Welge and Beckmann (1936) found that for very small amounts of decomposition the product was exclusively hydrogen, nitrogen only gradually making its appearance as the amount of decomposition increased. Further, when hydrogen is present in large quantities, the quantum efficiency has a much higher value than the overall value of 0.3. The results are variable, 0.74–0.95. They are, however, certainly less than unity, and in fact again show that the primary efficiency is less than unity. Unfortunately, measurements were not made at 2100 Å, and thus the present experiments and those of Welge and Beckmann cannot be directly compared. The disagreement is, however, probably not serious, as it is known that the overall quantum efficiency increases with decreasing wave-length. Such an increase can only be due to an effect on the primary process (Koenig and Brings 1931).

Since the primary efficiency is less than unity the energy absorbed by the molecule must be dissipated in some way. No fluorescence has been detected even at low pressures, about 0.007 mm., and the quantum efficiency is less dependent on pressure than would have been the case had the energy been removed by any collisional process. The only manner in which it can be dissipated is by some process of internal degradation in the first place. The fact that the spectrum is diffuse shows that such a possibility is not too remote. On the other hand, with deuterioammonia in which the absorption bands are sharp the primary efficiency is even less than that for ammonia.

The next question is the behaviour of the amine radicals. It might have been anticipated that, since the two reactions responsible for the removal of hydrogen atoms compete on more or less equal terms there should also

be another reaction involving only amine radicals such as  $2\text{NH}_2 = \text{N}_2 + 2\text{H}_2$  occurring at the same speed. But it has already been shown that although the lifetime of the hydrogen atom is of the order of  $10^{-3}$  sec., that of the amine radicals is at least several seconds. This might be taken at once to imply that the product of the reaction must be hydrazine, since no free radical could possibly have such a long lifetime, at any rate in the gas phase. Another consideration altogether rules out this possibility. There is no doubt that, whatever be the product of the reaction, it does eventually decompose into nitrogen and hydrogen in absence of radiation and therefore of hydrogen atoms. It cannot therefore be hydrazine because separate experiments have shown that in the present reaction system decomposition becomes measurable only at  $200^\circ\text{C}$ . Further, it may be noted that in the flow system (Gedye and Rideal 1932) the yield of hydrazine is much reduced on raising the temperature of the system to a value which has no measurable effect on the stability of hydrazine itself. It must be added that in the flow system the gases are rapidly condensed in a liquid-air trap, and thus hydrazine formation is facilitated. At any rate the nitrogen-containing product of ammonia, with which we have to deal, is certainly not hydrazine.

The real difficulty here is to explain the long lifetime of the amine radical, since it cannot exist in the gas phase for this long period; it must therefore diffuse to the walls and remain there. At high ammonia pressures it might be thought that the probability of amine radicals would be absolutely negligible and therefore any surface reaction could be eliminated. But, owing to the increase in ammonia extinction coefficient with increasing pressure, the zone of reaction moves closer to the walls. The probability of amine radicals getting to the walls is thus unaffected by ammonia pressure. The argument may best be illustrated by considering hydrogen atoms again. At 2144 Å and 40 mm. pressure 50 % of the radiation of this wave-length is absorbed in a layer 8 mm. thick of ammonia. At  $6 \times 10^3$  mm. 50 % of the radiation will be absorbed in a layer  $6 \times 10^{-3}$  cm. thick. Now in diffusing  $6 \times 10^{-3}$  cm. such an atom will take  $10^{-4}$  sec. and make  $8 \times 10^8$  collisions with ammonia molecules. The probability of even colliding, without making a ternary collision, with another hydrogen atom is only about unity when the pressure is, say,  $10^{-3}$  mm. At 40 mm. ammonia pressure the time taken for diffusion is  $1.5 \times 10^{-2}$  and the number of collisions  $3.3 \times 10^8$ . The probability is again of the order of unity. A similar argument may be applied to amine radicals.

Thus the fate of the amine radicals may be visualized in the following way. The hydrogen atoms and amine radicals diffuse to the walls where they are absorbed to form, say, a monolayer. When further hydrogen atoms

strike the walls they either combine with the hydrogen atoms or the amine radicals with about the same probability. The exact ratio probably depends on the nature and state of the walls, since the value of the overall quantum efficiency does vary to some slight extent depending on the conditions. The hydrogen atoms are thereby soon used up, and the less reaction (i.e. the less reactive towards each other) the more amine radicals remain. These decompose at a much slower rate indicated approximately by the rotating cylinder experiments. If, however, the hydrogen atom concentration is augmented, as in the inhibition experiments, a fraction of the amine radicals will be removed rapidly. Thus the amine radicals have, as it were, a dual lifetime. If they react with atomic hydrogen their life is short; if they react with themselves their lifetime is long. In so reacting in the ordinary static system, however, the great majority form nitrogen and hydrogen and not hydrazine. It may be noted that the above explanation will also account for the sole production of hydrogen during the early stages of the ammonia photolysis.

It is now possible to write down a simple scheme for the photolysis of ammonia together with a few relevant figures relating to the various steps in the reaction. If the quantum efficiency of the whole reaction is 0.25 and the efficiency of the primary reaction is 0.58, then the efficiency of the secondary reactions is 0.43. Hence we may write for the absorption of 100 quanta:

|     |   | In terms of<br>NH <sub>3</sub> molecules |
|-----|---|--|
| (1) | NH <sub>3</sub> + hν  | 42                                       |
|     | $\begin{cases} \nearrow \text{NH}_3^* \rightarrow \text{NH}_3 \\ \searrow \text{NH}_2 + \text{H} \end{cases}$ | 58                                       |
| (2) | H + H → H <sub>2</sub>  | 25                                       |
| (3) | NH <sub>2</sub> + NH <sub>2</sub> → N <sub>2</sub> + 2H <sub>2</sub>  | 33                                       |
| (4) | H + NH <sub>2</sub> → NH <sub>3</sub>   |  |

Since the sector experiments have shown that the lifetime of NH<sub>2</sub> radicals on the walls is comparatively long, reaction (3) cannot effectively compete with (2). Hence the relative probabilities of (2) and (4) will be in the ratio of 25 to 33.

#### *The efficiency of the primary process in other reactions*

Having thus developed a method of measuring the primary photochemical efficiency or quantum yield  $\gamma_P$ , the following relationship will then exist between the overall yield  $\gamma_T$  and the yield of the secondary reactions  $\gamma_S$ , namely,

$$\gamma_T = \gamma_P \cdot \gamma_S.$$



In a previous paper (Bolland and Melville 1937) a method was described for measuring the quantum yield of the photodecomposition of phosphine by measuring the ratio of the rate of decomposition to the rate of exchange when the reaction is carried out in the presence of deuterium. This yield will be equal to  $\gamma_T$  only if it so happens that all molecules absorbing light dissociate, i.e.  $\gamma_P = 1$ . In fact, this so-called back reaction technique gives the value of  $\gamma_S$  because the secondary reactions come into operation only when the molecule is dissociated. For the direct photodecomposition of phosphine the value of  $\gamma_T$  (0.50) is practically identical with  $\gamma_S$  employing the exchange technique, and thus in the case of phosphine  $\gamma_P = 1$ . On the other hand, in the mercury-sensitized decomposition  $\gamma_T = 0.27$ , whereas  $\gamma_S = 0.50$ , and therefore we may calculate the value of  $\gamma_P$  for a mercury-sensitized reaction. For phosphine  $\gamma_P = 0.27/0.50 = 0.54$ . Hence every excited mercury atom which is deactivated does not necessarily lead to decomposition of the molecule causing the deactivation. This has often been suspected but has not hitherto been capable of exact measurement. It is significant, but not unexpected, that the values of  $\gamma_S$  for both direct and sensitized decomposition are identical. Presumably a similar state of affairs exists in the ammonia reaction. For the mercury-sensitized decomposition of ammonia  $\gamma_T \approx 0.05$  (Melville 1936), and hence  $\gamma_P = 0.05/0.43 = 0.12$ . In many of the mercury-sensitized reactions, such as the decomposition of hydrazine and deuterioammonia, the overall quantum yields are much lower than those in the direct reaction. With hydrazine, for example,  $\gamma_T$  of the direct reaction is 1.2, whereas for the sensitized reaction it is 0.4. Assuming therefore that  $\gamma_P$  of the direct reaction is 1.0, then  $\gamma_P$  for the sensitized is  $0.4/1.2 = 0.33$ . Similarly for trideuteroammonia, if the assumption is made that  $\gamma_S$  is the same for this reaction as for that of ammonia,  $\gamma_P$  for the direct decomposition is 0.47. In the case of the sensitized decomposition  $\gamma_T$  is *ca.* 0.05/7 (cf. Jungers and Taylor 1934) and thus  $\gamma_P$  is 0.02. It is not unlikely, therefore, that in a large number of mercury-sensitized reactions the efficiency of the primary decomposition may turn out to be much smaller than has hitherto been thought.

The experiments described above were carried out in the Chemistry Department of the University of Edinburgh. The authors are grateful to Dr E. B. Ludlam for his help throughout the research. One of them (E. A. B. B.) is grateful to the Carnegie Trust for a Research Scholarship and to the Trustees of the Moray Fund for a grant for apparatus.

## SUMMARY

The anomalously low stationary hydrogen atom concentration during the photodecomposition of ammonia is due either to the fact that the primary photochemical efficiency is not unity or that the hydrogen atoms are removed at an abnormally fast rate. It is shown by utilizing the para-hydrogen conversion that photodecomposing ammonia has no effect on the stationary hydrogen atom concentration of the conversion, and therefore the low concentration of the ammonia photolysis must be due to inefficiency of the primary process. The primary efficiency is determined by a careful comparison of the mercury-sensitized and the ammonia-sensitized conversion of para-hydrogen. A method is developed for measuring accurately the rate of production of hydrogen atoms, which method is essential to the foregoing determination. This primary efficiency is found to be 0.58.

A method is also developed for measuring the lifetime of amine radicals.

Similar experiments with trideuteroammonia are also described. The primary efficiency is 0.28.

A revised and simplified scheme for the ammonia photolysis is given as a result of these new experiments.

## REFERENCES

- Bolland, J. L. and Melville, H. W. 1937 *Proc. Roy. Soc. A*, **160**, 384-406.  
Bonhoeffer, K. F. and Farkas, L. 1927 *Z. phys. Chem. A*, **134**, 337-344.  
Dickinson, R. G. and Mitchell, A. C. G. 1926 *Proc. Nat. Acad. Sci., Wash.*, **12**, 692-696.  
Gedye, G. R. and Rideal, E. K. 1932 *J. Chem. Soc.* pp. 1160-1169.  
Jungers, J. C. and Taylor, H. S. 1934 *J. Chem. Phys.* **2**, 373-380.  
Koenig, A. and Brings, T. 1931 *Z. phys. Chem. Bodenstein Festband*, pp. 541-552.  
Leighton 1938 *Exposés de Photochimie*. Paris: Hermann et Cie.  
Luyckx, A. 1935 (Nov.) and 1936 (May). *Questions Scien.*  
Melville, H. W. 1932 *Trans. Faraday Soc.* **28**, 885-889.  
— 1932 *Proc. Roy. Soc. A*, **138**, 374-395.  
— 1935 *Proc. Roy. Soc. A*, **152**, 325-341.  
— 1936 *Proc. Roy. Soc. A*, **157**, 621-624.  
Ogg, R. A., Leighton, P. A. and Bergstrom, A. O. 1934 *J. Amer. Chem. Soc.* **56**, 318-323.  
Taylor, H. S. 1938 *J. Phys. Chem.* **42**, 789-794.  
Welge, H. J. and Beckmann, A. O. 1936 *J. Amer. Chem. Soc.* **58**, 2462-2467.  
Wiig, E. O. 1935 *J. Amer. Chem. Soc.* **57**, 1559-1562.  
— 1937 *J. Amer. Chem. Soc.* **59**, 827-830.
-

# Investigations of infra-red spectra. Determination of C-H frequencies ( $\sim 3000$ cm. $^{-1}$ ) in paraffins and olefins, with some observations on "polythenes"

BY J. J. FOX AND A. E. MARTIN

(Communicated by Sir Robert Robertson, F.R.S.—Received 3 January 1940)

## INTRODUCTION

In a previous communication (1938) we described the results of an investigation into the infra-red absorption in the region of  $3\mu$  of a number of hydrocarbons dissolved in carbon tetrachloride, with special reference to the absorption of  $\text{>CH}_2$  groups in different molecules. It was found that in many simple compounds the  $\text{CH}_2$  group gave rise to two frequencies, essentially C-H valency vibrations, about  $2857$  and  $2927$  cm. $^{-1}$ , and that from one compound to another these frequencies varied by only a few wave numbers. The lower frequency was identified with the mode of vibration in which the hydrogen atoms move in phase, while the other frequency was taken as the unsymmetrical mode of vibration. This assignment was substantiated by calculations with potential functions for molecules of the general type  $\text{CH}_2\text{—}X$ , where  $X$  represents the rest of the molecule and is attached to the  $\text{CH}_2$  group by single bonds. It was found that the CH frequencies of a  $\text{CH}_2$  group are but little affected by the nature of  $X$  in saturated compounds, but that when the  $\text{CH}_2$  group is attached to  $X$  by a double bond the CH frequencies are some  $150$  cm. $^{-1}$  higher. In ethylene each  $\text{CH}_2$  group has two CH valency modes of vibration, and since the  $\text{CH}_2$  groups themselves can vibrate in or out of phase with one another, four CH frequency modes are possible for the  $\text{C}_2\text{H}_4$  molecule, two being Raman active and two infra-red active. In many molecules containing several  $\text{CH}_2$  groups, similar coupling effects are important, and frequently four infra-red CH frequencies are observed.

$\text{CH}_3$  groups to some extent behave in a similar manner to the  $\text{CH}_2$  groups, since in a molecule  $\text{CH}_3\text{—}X$  two CH frequencies can be obtained. In one, the three hydrogen atoms vibrate in phase, while in the other case one atom is in opposite phase to the other two. These frequencies can be compared with the symmetrical and unsymmetrical  $\text{CH}_3$  vibrations, respectively. Methyl halides (Bennett and Meyer 1928; Sutherland 1935) and

methyl deuteride (Ginsburg and Barker 1935) are found to have these two frequencies, and from the rotational structure it has been established that the symmetrical frequency ( $\parallel$  band) is somewhat lower ( $\sim 100 \text{ cm.}^{-1}$ ) than the unsymmetrical frequency ( $\perp$  band). We have accumulated a considerable number of data on the absorption of  $\text{CH}_3$  groups in complex molecules and have already briefly described our results for  $\alpha$ - and  $\beta$ -methylnaphthalenes (1939). The spectra of a number of compounds containing methyl groups will be described in the present communication.

In aromatic compounds the CH groups give bands close to  $3.27 \mu$ , generally one, two, or three in number, and we have studied these bands for many substances including polycyclic compounds such as naphthalene and quinoline (1939). Mono-substituted benzene derivatives and benzene itself in carbon tetrachloride solution give a characteristic triple aromatic CH band about  $3.27 \mu$ , but as more groups are substituted in the ring the bands become less distinctive. CH bands in unsaturated compounds of the type  $\begin{matrix} R_1 \\ \diagup \\ \text{C} \\ \diagdown \\ \text{H} \end{matrix} = \text{C} \begin{matrix} R_2 \\ \diagdown \\ \text{H} \\ \diagup \end{matrix}$  or  $\begin{matrix} R_1 \\ \diagup \\ \text{C} \\ \diagdown \\ R_2 \end{matrix} = \text{C} \begin{matrix} R_3 \\ \diagdown \\ \text{H} \\ \diagup \end{matrix}$  have received little attention. Sherrill and Mollet (1936) have examined a few such compounds in the  $3 \mu$  region but with insufficient resolution to give any detailed information. The present communication deals with a number of compounds of this type. Bands arising from the  $\text{>CH}$  group in saturated hydrocarbons have hitherto not been recorded in the  $3 \mu$  region, although a single  $\text{>CH}$  band has been found for triphenylmethane by Wall and McMillan (1939), and independently by ourselves. In the present work a few hydrocarbons of the type  $\text{CH}_3-(\text{CH}_2\text{CH})_n-\text{CH}_3$  have been examined and a small band at  $\sim 2890 \text{ cm.}^{-1}$ , attributable to the  $\text{>CH}$  group, was detected in each case.

Many investigations on hydrocarbons in the region of  $3 \mu$  are on record, but owing to the use of apparatus of insufficient resolution by the majority of workers, the finer significant differences in the various CH bands in the  $3 \mu$  region have been rarely found. All the various types of CH valency vibrations in paraffins, olefins, and aromatic compounds are found in the range  $3.2-3.55 \mu$ , and since as many as eight distinct bands may be found in some cases within a space of  $0.15 \mu$  (e.g. naphthalene), the need for sufficient resolution in this region is apparent. Fundamental work with low resolution was carried out by Coblenz (1905), and "aromatic" and "aliphatic" CH frequencies were distinguished by Bonino (1929). A promising start in the  $3 \mu$  region with good resolution was made by Barnes (1930), and work of a similar standard has been carried out by Lambert and Lecomte (1936), but the latter investigator has mainly concentrated attention on the region

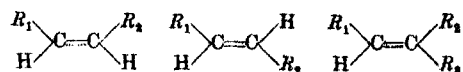
6–20 $\mu$ , where the absorption bands arise mostly from C to C vibrations and various deformation frequencies.

Most of the knowledge regarding the various types of CH vibrations has been derived from Raman observations, especially by Kohlrausch (1931, 1938) and his school. It is our purpose to show that the information derived from Raman measurements in the region of 3000 cm.<sup>-1</sup>, although of great value, is meagre and frequently of poor accuracy compared with the data obtainable with an infra-red spectrometer of comparatively high resolution.

A systematic investigation of hydrocarbons has recently been made by Rose (1938) between 1.2 and 1.8 $\mu$  in which region the first and higher harmonics of the CH vibrations occur. The compounds studied were regarded by Rose as being made up of the structural units —CH<sub>3</sub>, >CH<sub>2</sub>, >CH, and >CH (aromatic). It is known that these structural units have their maximum absorption at different wave-lengths, and if it is assumed that at a given wave-length each group has a constant unit value of absorption, then the absorption of the entire molecule will be the value of absorption for each group, multiplied by the number of similar groups and summed for all the different groups in the molecule. A method of analysis was worked out by Rose on this basis, and such a method should be equally applicable to the region of the CH fundamentals about 3 $\mu$ . It must be pointed out, however, that this method of analysis should be used with great caution, and absorption spectra of compounds having similar composition to the unknown must be available. Even with simple paraffins there are variations in the group absorption on passing from one compound to another, as the present work will show, and in the aromatic series the changes from one compound to another are very marked (cf., for example, the difference in absorption of the methyl group in  $\alpha$ - and  $\beta$ -methylnaphthalenes (Fox and Martin 1939)).

The molecular structural units studied by us in the present work can be classified as follows:

- (1) >C-H group in unsaturated hydrocarbons of the types:



- (2) =CH<sub>2</sub> group in unsaturated hydrocarbons.  
 (3) >CH<sub>2</sub> group in long-chain paraffins and other compounds.  
 (4) —CH<sub>3</sub> group in saturated and unsaturated hydrocarbons.  
 (5) >C—H group in saturated hydrocarbons.

We have also investigated some "polythenes" (resinoids from polymerized ethylene), which from X-ray evidence have been supposed to consist of very long chains of  $\text{>CH}_2$  groups, and we have compared them with some long-chain paraffins of known constitution.

#### EXPERIMENTAL

The apparatus and general technique have been described previously (Fox and Martin 1937, 1938). All the compounds were examined in solution in carbon tetrachloride at room temperature (20–24° C), but owing to low solubility some measurements with the polythenes were made at temperatures up to 50° C. The apparatus used for these measurements was that constructed by us for investigations on water at different temperatures, and an account of this work is in the Press.\* Absorption cells 1.74, 10 and 50 mm. in length, with end-plates of fused silica 0.5 mm. thick, were used. The solution was compared with pure carbon tetrachloride in a second similar absorption cell, so that reflexion losses and absorption in the carbon tetrachloride were allowed for. From the transmission of the solution  $I$ , and of the solvent  $I_0$ , the molecular extinction coefficient of the solute was calculated by the relation  $\kappa = \frac{1}{cl} \log \frac{I_0}{I}$ , where  $c$  is the molar concentration and  $l$  the cell length in cm. In many cases the final absorption curves obtained by plotting  $\kappa$  against the wave-length or frequency were rather complex, and to assess fairly the bands, as regards position and intensity, it was necessary to resort to graphical separation (e.g. Fox and Martin 1938, 1939). The integrated area of a band is approximately  $1.4f\kappa_{\max}$ , where  $f$  is the half-width of the band in  $\text{cm.}^{-1}$ , as shown previously (1938). Graphical separation of bands is advisable, in our opinion, even when only band positions are required, since we have found in unfavourable cases that the apparent position of a band may differ from the true position by as much as  $5 \text{ cm.}^{-1}$ .

Details of all the compounds examined are given at the end of this paper.

#### RESULTS

The absorption curves of all the hydrocarbons studied are given in figures 1–10; positions of bands are set out in tables 1–3; band intensities and values of  $f$ , the band half-width, in table 4. In figure 1,  $\text{CH}_2$  and  $\text{CH}_3$  bands in the range  $3.34\text{--}3.54 \mu$  are displayed for some long-chain  $n$ -paraffins

\* 1940 *Proc. Roy. Soc. A*, 174, 234.

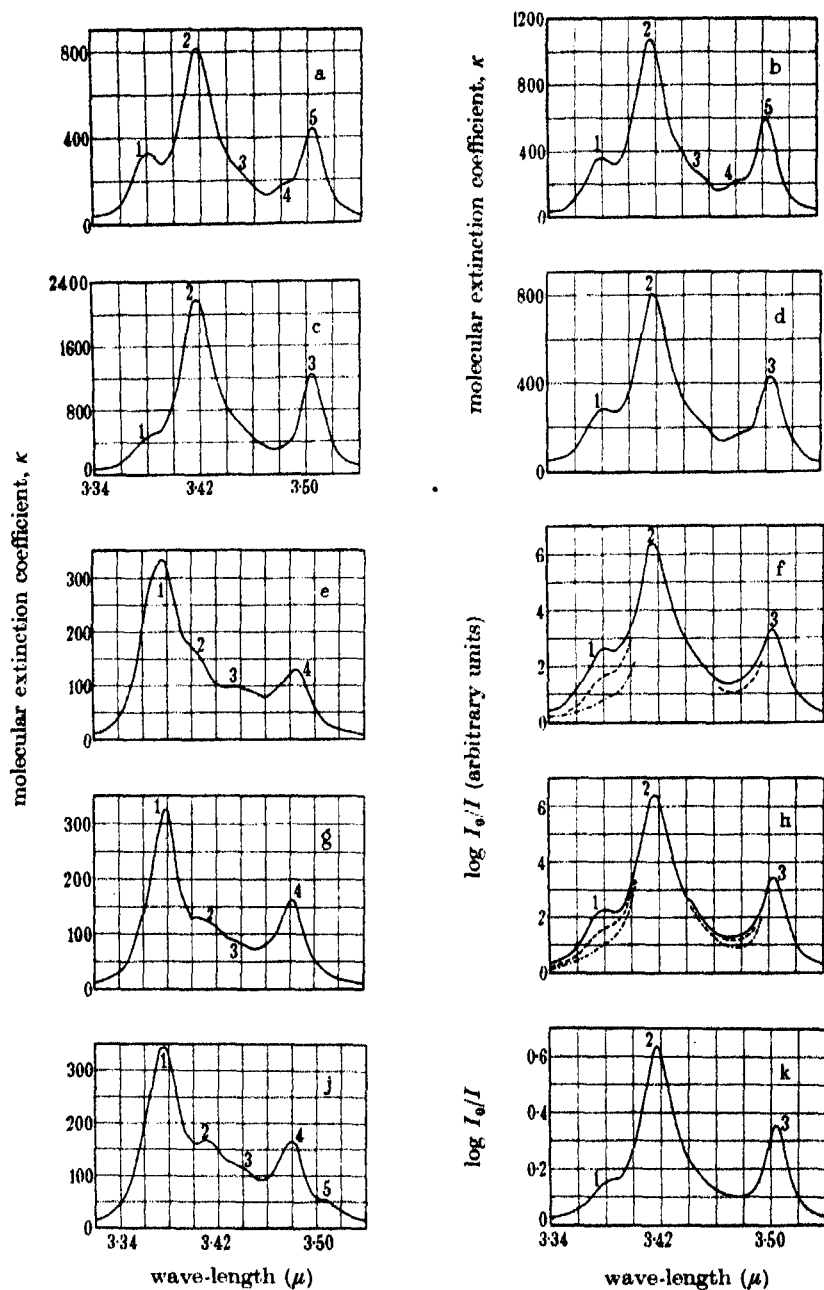


FIGURE 1. Absorption of hydrocarbons dissolved in carbon tetrachloride.

- |  |   |
|--|---|
| a, tetradecane, $\text{CH}_3(\text{CH}_2)_{12}\text{CH}_3$ ;                                       | b, heptadecane, $\text{CH}_3(\text{CH}_2)_{15}\text{CH}_3$ ;      |
| c, tetratriacontane, $\text{CH}_3(\text{CH}_2)_{32}\text{CH}_3$ ;                                  | d, cetene, $\text{CH}_3(\text{CH}_2)_{18}\text{CH}=\text{CH}_2$ ; |
| e, 2:2:3-trimethylbutane, $\text{CH}_3\text{C}(\text{CH}_3)_2\cdot\text{CHCH}_3\cdot\text{CH}_3$ ; | f, polythene "AXX";   |
| g, 2:3-dimethylbutane, $\text{CH}_3(\text{CHCH}_3)_2\text{CH}_3$ ;                                 | h, polythene "B59";   |
| i, 2:3:4-trimethylpentane, $\text{CH}_3(\text{CH}\cdot\text{CH}_3)_3\text{CH}_3$ ;                 | k, paraffin wax, 0.134 g./l.,                                     |
|  | cell length 1 cm.   |

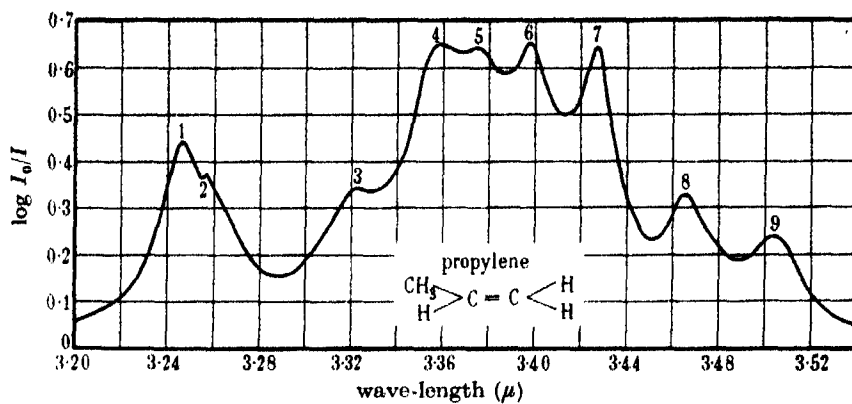


FIGURE 2

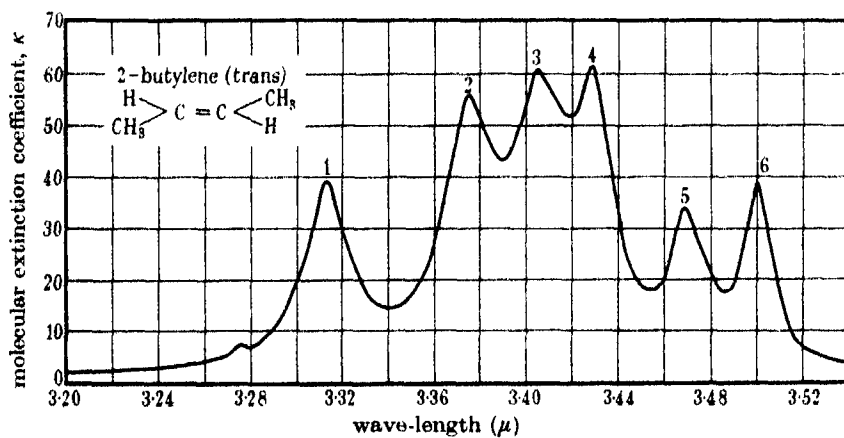


FIGURE 3

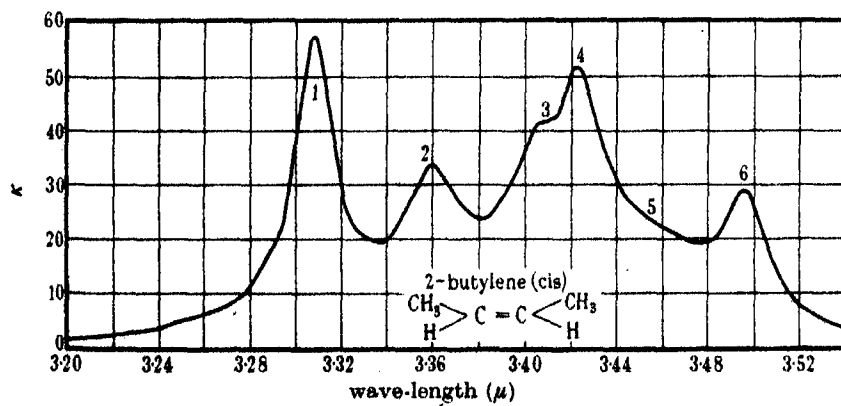


FIGURE 4



and other saturated compounds (also cetene), while in figures 2-9 the various C-H bands occurring in unsaturated substances in the region  $3.20\text{--}3.54\mu$  are shown. In table 5 are given the values of  $\kappa_{\text{max}}$  per group for the main  $\text{CH}_2$  and  $\text{CH}_3$  frequencies in saturated hydrocarbons.

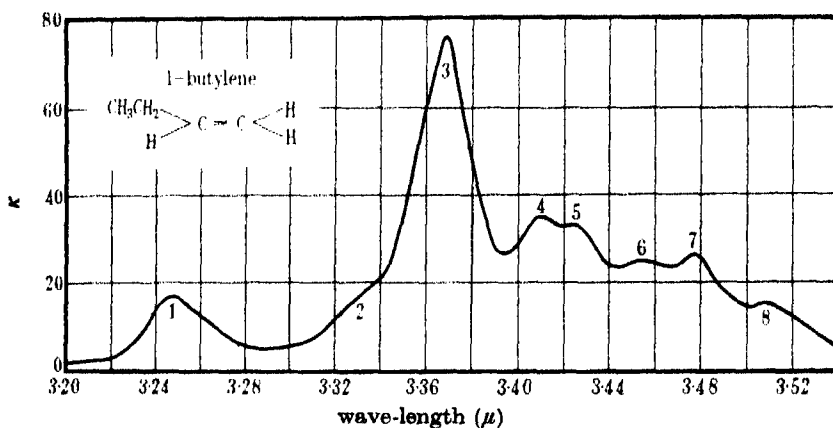


FIGURE 5

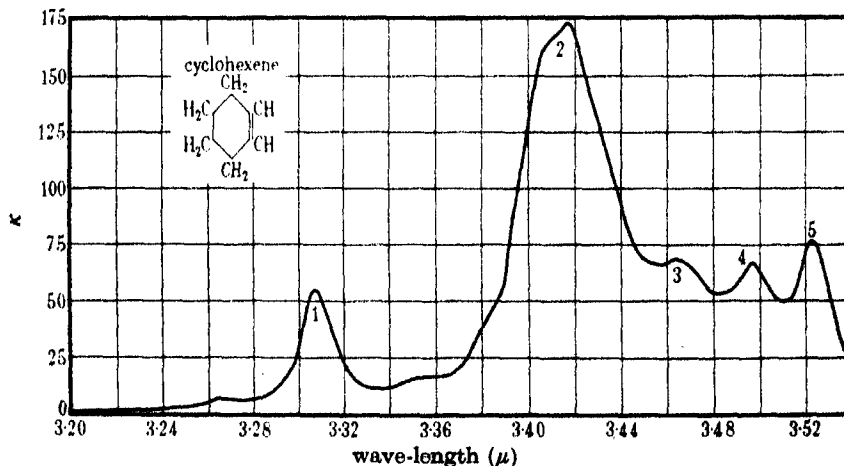


FIGURE 6

Both saturated and unsaturated hydrocarbons have a number of small bands in the region  $3.55\text{--}3.8\mu$ , and these will be found in figure 10. The origin of these bands is not known with any certainty, but on account of their low intensity they are not likely to include any CH valency vibrations and are not dealt with in detail in this communication. It may be pointed

out that the long-chain paraffins all give two bands close to  $3.66$  and  $3.74\mu$ ; the former appears to be due in some way to  $\text{CH}_3$  groups since it is weak in  $\text{C}_{34}\text{H}_{70}$ , where the proportion of  $\text{CH}_3$  is small, and absent in cyclohexene which has no  $\text{CH}_3$  groups. The band near  $3.74\mu$  seems to be associated with

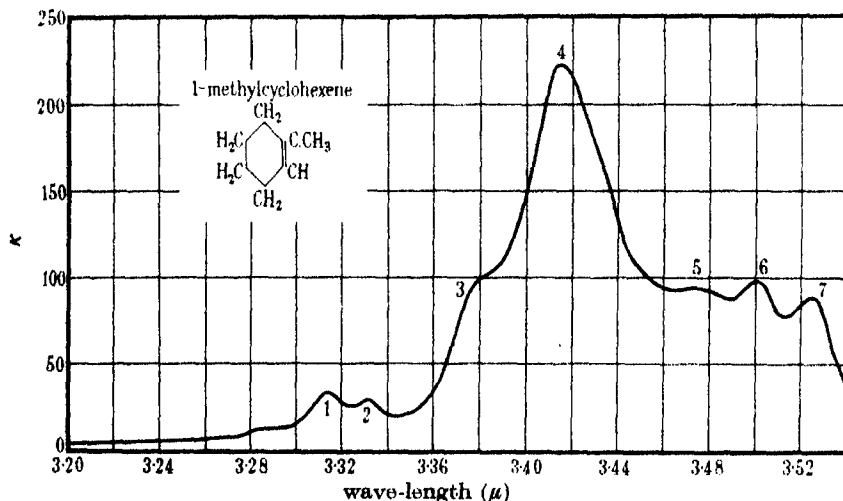


FIGURE 7

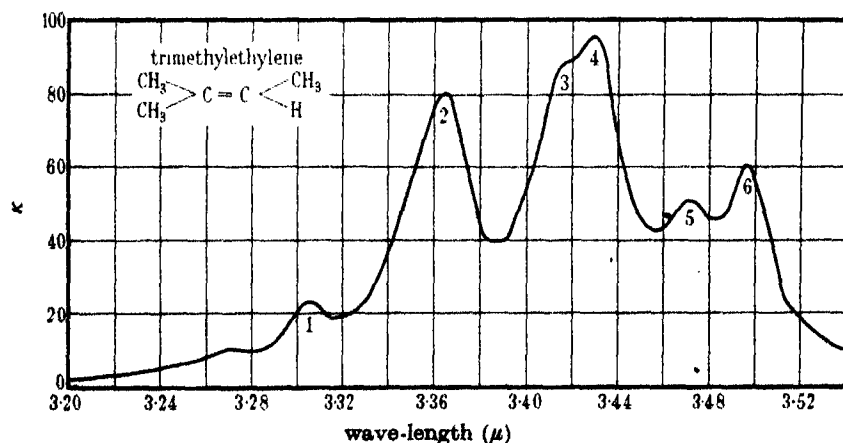


FIGURE 8

$\text{CH}_2$  groups and is generally absent in compounds not containing  $\text{CH}_2$ , although 2:3-dimethylbutane is a notable exception in this respect.

The region  $2.6\text{--}3.2\mu$  has been explored for the compounds under investigation, but only slight absorption was found.

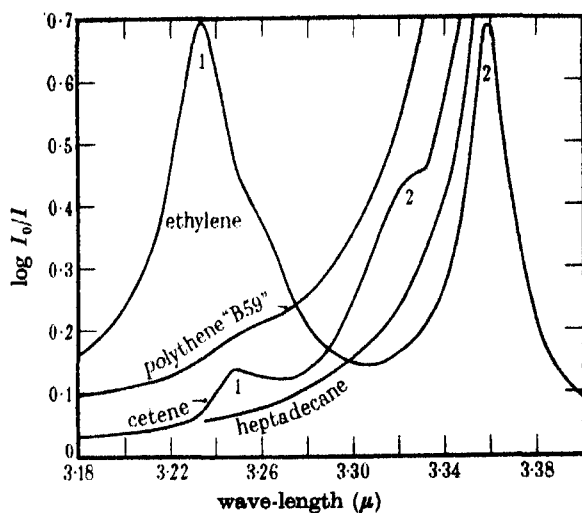


FIGURE 9. Ethylene: concentration undetermined; 1 cm. cell. Polythene: concentration  $\sim 1.8$  g./l.; 5 cm. cell;  $40^\circ$  C. Cetene and heptadecane: concentration 0.0025 mol./l.; 5 cm. cell.

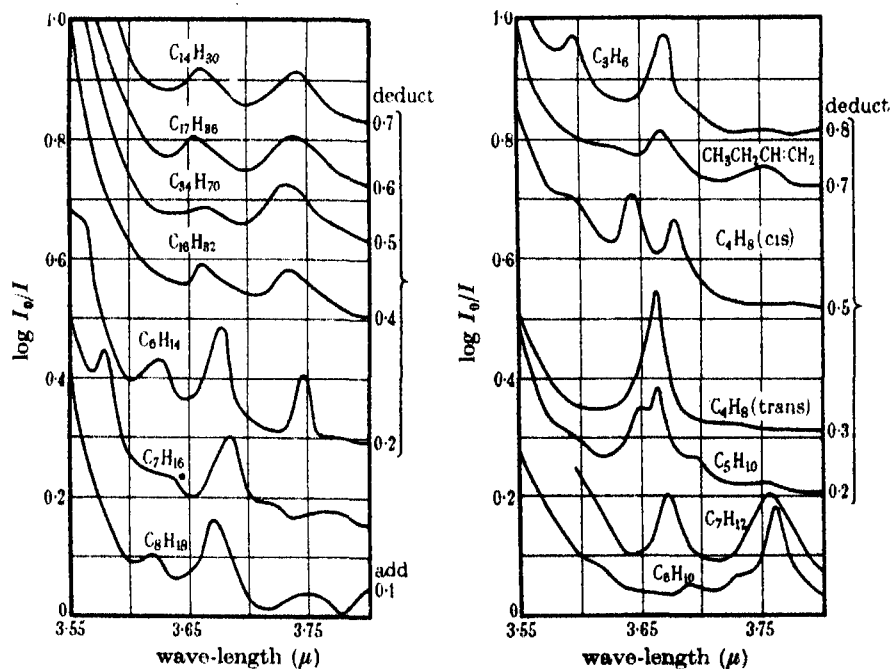


FIGURE 10. Absorption of some hydrocarbons in the region  $3.55\text{--}3.80\mu$ . Concentration 1 g./l. in all cases except propylene (concentration undetermined) and 2-butylene (*trans*), trimethylethylene and cyclohexene (0.5 g./l. for these three). Cell length 5 cm. in all cases.

TABLE 1. INFRA-RED FREQUENCIES ( $\sim 3000 \text{ cm.}^{-1}$ ) OF  $\text{=CH}_2$  AND  $\text{>CH}$  GROUPS IN HYDROCARBONS

| $\text{=C} \begin{array}{l} \text{H} \\ \diagup \\ \text{H} \end{array} \text{ group}$ |                        |                   |                        |                   |                        |                   |
|--|------------------------|-------------------|------------------------|-------------------|------------------------|-------------------|
| Substance and<br>fig. no.  | Band<br>no.<br>in fig. | cm. <sup>-1</sup> | Band<br>no.<br>in fig. | cm. <sup>-1</sup> | Band<br>no.<br>in fig. | cm. <sup>-1</sup> |
| Ethylene, fig. 9   | 1                      | (3092)            |                        |                   | 2                      | 2977              |
| Cetene, fig. 9   | 1                      | 3077              |                        |                   |                        |                   |
| 1-Butylene, fig. 5   | 1                      | 3080              |                        |                   | 3                      | (2968)            |
| Propylene, fig. 2  | 1                      | 3081              | 2                      | (3067)            | 4                      | 2979              |
| Mean frequency   |                        | 3079              |                        |                   |                        | 2978              |

| $\text{>C-H group}$                 |                        |                   |                        |                   |  |
|-------------------------------------|------------------------|-------------------|------------------------|-------------------|--|
| Substance and<br>fig. no.           | Band<br>no.<br>in fig. | cm. <sup>-1</sup> | Band<br>no.<br>in fig. | cm. <sup>-1</sup> |  |
| 1-Methylcyclohexene, fig. 7         | 1                      | (3019)            | 2                      | (3002)            |  |
| Cyclohexene, fig. 6                 | 1                      | 3023              |                        |                   |  |
| Trimethylethylene, fig. 8           | 1                      | 3025              |                        |                   |  |
| 2-Butylene ( <i>cis</i> ), fig. 4   | 1                      | 3022              |                        |                   |  |
| 2-Butylene ( <i>trans</i> ), fig. 3 | 1                      | 3018              |                        |                   |  |
| 1-Butylene, fig. 5                  | 2                      | (3001)            |                        |                   |  |
| Propylene, fig. 2                   | 3                      | 3012              |                        |                   |  |
| Cetene, fig. 9                      | 2                      | 3012              |                        |                   |  |
| Mean frequency                      |                        | 3019              |                        |                   |  |

Frequencies in brackets have not been used for determining mean values.

TABLE 2. INFRA-RED FREQUENCIES ( $\sim 3000 \text{ cm.}^{-1}$ ) OF  $\text{>CH}_2$  GROUPS IN HYDROCARBONS

| Substance and<br>fig. no.             | Band<br>no.<br>in<br>fig. | cm. <sup>-1</sup>  | Band<br>no.<br>in<br>fig. | cm. <sup>-1</sup> | Band<br>no.<br>in<br>fig. | cm. <sup>-1</sup> | Band<br>no.<br>in<br>fig. | cm. <sup>-1</sup> |
|---------------------------------------|---------------------------|--------------------|---------------------------|-------------------|---------------------------|-------------------|---------------------------|-------------------|
| $\text{C}_{14}\text{H}_{30}$ , fig. 1 | 2                         | 2925               |                           |                   | 5                         | 2853              |                           |                   |
| $\text{C}_{17}\text{H}_{36}$ , fig. 1 | 2                         | 2926               |                           |                   | 5                         | 2854              |                           |                   |
| $\text{C}_{24}\text{H}_{50}$ , fig. 1 | 2                         | 2925               |                           |                   | 3                         | 2853              |                           |                   |
| Cetene, fig. 1                        | 2                         | 2925               |                           |                   | 3                         | 2854              |                           |                   |
| Paraffin wax, fig. 1                  | 2                         | 2926               |                           |                   | 3                         | 2853              |                           |                   |
| Polythene "B 59", fig. 1              | 2                         | 2925               |                           |                   | 3                         | 2853              |                           |                   |
| Polythene "AXX", fig. 1               | 2                         | 2925               |                           |                   | 3                         | 2853              |                           |                   |
| 1-Butylene, fig. 5                    | { 4<br>5                  | { (2931)<br>(2915) | 6                         | 2894              | 8                         | 2848              |                           |                   |
| Cyclohexene, fig. 6                   | 2                         | 2928               | 3                         | 2883              | 4                         | (2859)            | 5                         | 2837              |
|                                       |                           |                    |                           |                   |                           | Mean (2848)       |                           |                   |
| 1-Methylcyclohexene, fig. 7           | 4                         | 2926               | 5                         | 2875              | 6                         | (2856)            | 7                         | 2835              |
|                                       |                           |                    |                           |                   |                           | Mean (2846)       |                           |                   |
| Mean frequency                        |                           | 2926               |                           |                   |                           | 2853              |                           |                   |

Frequencies in brackets have not been used for determining mean values. The assignments for 1-butylene are somewhat uncertain.

TABLE 3. INFRA-RED FREQUENCIES ( $\sim 3000 \text{ cm.}^{-1}$ ) OF  $\text{CH}_3$  GROUPS  
IN HYDROCARBONS

| Substance and<br>fig. no.             | Band              |                   | Band              |                   | Band              |                   | Band              |                   | Band              |                   |
|---------------------------------------|-------------------|-------------------|-------------------|-------------------|-------------------|-------------------|-------------------|-------------------|-------------------|-------------------|
|                                       | no.<br>in<br>fig. | cm. <sup>-1</sup> | no.<br>in<br>fig. | cm. <sup>-1</sup> | no.<br>in<br>fig. | cm. <sup>-1</sup> | no.<br>in<br>fig. | cm. <sup>-1</sup> | no.<br>in<br>fig. | cm. <sup>-1</sup> |
| Propylene, fig. 2                     | 5                 | 2960              | 6                 | 2942              | 7                 | 2916              | 8                 | 2884              | 9                 | 2852              |
|                                       |                   |                   |                   |                   |                   |                   |                   | Mean (2868)       |                   |                   |
| 2-Butylene ( <i>cis</i> ), fig. 4     | 2                 | 2976              | 3                 | 2940              | 4                 | 2919              | 5                 | 2891              | 6                 | 2860              |
|                                       |                   |                   |                   |                   |                   |                   |                   | Mean (2875)       |                   |                   |
| 2-Butylene ( <i>trans</i> ), fig. 3   | 2                 | 2963              | 3                 | 2936              | 4                 | 2915              | 5                 | 2883              | 6                 | 2857              |
|                                       |                   |                   |                   |                   |                   |                   |                   | Mean (2870)       |                   |                   |
| Trimethylethylene, fig. 8             | 2                 | 2973              | 3                 | 2928              | 4                 | 2913              | 5                 | 2879              | 6                 | 2858              |
|                                       |                   |                   |                   |                   |                   |                   |                   | Mean (2868)       |                   |                   |
| 2:3-Dimethylbutane, fig. 1            | 1                 | 2959              | 2                 | 2931              | 3                 | 2909              | 4                 |                   |                   | 2872              |
| 2:2:3-Trimethylbutane,<br>fig. 1      | 1                 | 2961              | 2                 | 2933              | 3                 | 2905              | 4                 |                   |                   | 2870              |
| 2:3:4-Trimethylpentane,<br>fig. 1     | 1                 | 2962              | 2                 | 2928              | 3                 | 2904              | 4                 |                   |                   | 2873              |
| 1-Methylcyclohexene,<br>fig. 7        | 3                 | 2960              |                   |                   |                   |                   |                   |                   |                   |                   |
| 1-Butylene, fig. 5                    | 3                 | (2968)            | 4                 | (2931)            | 5                 | (2915)            | 7                 |                   |                   | 2874              |
|                                       |                   |                   |                   |                   | 6                 | (2894)            |                   |                   |                   |                   |
| $\text{C}_{14}\text{H}_{30}$ , fig. 1 | 1                 | 2959              |                   |                   | 3                 | (2893)            | 4                 |                   |                   | 2871              |
| $\text{C}_{17}\text{H}_{36}$ , fig. 1 | 1                 | 2960              |                   |                   | 3                 | (2901)            | 4                 |                   |                   | 2874              |
| $\text{C}_{26}\text{H}_{54}$ , fig. 1 | 1                 | 2960              |                   |                   |                   |                   |                   |                   |                   |                   |
| Cetene, fig. 1                        | 1                 | 2960              |                   |                   |                   |                   |                   |                   |                   |                   |
| Paraffin wax, fig. 1                  | 1                 | 2959              |                   |                   |                   |                   |                   |                   |                   |                   |
| Polythene "B 59", fig. 1              | 1                 | 2960              |                   |                   |                   |                   |                   |                   |                   |                   |
| Polythene "AXX", fig. 1               | 1                 | 2959              |                   |                   |                   |                   |                   |                   |                   |                   |
| Mean frequency                        |                   | 2962              |                   | 2934              |                   | 2912              |                   |                   |                   | 2872              |

Frequencies in brackets have not been used for determining mean values. The assignments for 1-butylene are somewhat uncertain.

TABLE 4. VALUES OF  $\kappa_{\text{max}}$  AND  $f$  ( $\text{cm.}^{-1}$ ) FOR THE ABSORPTION BANDS  
OF HYDROCARBONS IN THE REGION OF  $3000 \text{ cm.}^{-1}$ 

| Band no. ...<br>Substance                             | 1                          | 2     | 3    | 4    | 5    | 6     | 7     | 8    | 9    |
|---|----------------------------|-------|------|------|------|-------|-------|------|------|
| $\text{C}_2\text{H}_2$ , fig. 2                       | $d_{\text{max}}$ 0.295     | 0.205 | 0.26 | 0.51 | 0.34 | 0.425 | 0.545 | 0.29 | 0.24 |
|   | $f$ 25.5                   | 36.5  | 34.5 | 28   | 24.5 | 21.5  | 19.5  | 23   | 26   |
| 1- $\text{C}_4\text{H}_8$ , fig. 5                    | $\kappa_{\text{max}}$ 17   | 6.4   | 76   | 23.5 | 23.5 | 22.5  | 24    | 15   |      |
|   | $f$ 32.5                   | 23    | 30.5 | 19.5 | 17.5 | 21.5  | 20    | 31.5 |      |
| 2- $\text{C}_4\text{H}_8$ ( <i>trans</i> ),<br>fig. 3 | $\kappa_{\text{max}}$ 39   | 51    | 40   | 50   | 28.5 | 38    |       |      |      |
|   | $f$ 21.5                   | 27    | 20   | 19.5 | 15   | 14.7  |       |      |      |
| 2- $\text{C}_4\text{H}_8$ ( <i>cis</i> ), fig. 4      | $\kappa_{\text{max}}$ 56.5 | 30    | 24   | 44.5 | 15   | 29    |       |      |      |
|   | $f$ 21.5                   | 29    | 26   | 27   | 31.5 | 24    |       |      |      |

TABLE 4 (continued)

| Band no. ...                             | 1                     | 2     | 3     | 4    | 5    | 6    | 7    |
|--|-----------------------|-------|-------|------|------|------|------|
| Substance                                |                       |       |       |      |      |      |      |
| C <sub>6</sub> H <sub>10</sub> , fig. 6  | $\kappa_{\max.}$ 55   | 170   | 49    | 61   | 77   |      |      |
|  | $f$ 16.5              | 41    | 26    | 19   | 16.5 |      |      |
| C <sub>7</sub> H <sub>12</sub> , fig. 7  | $\kappa_{\max.}$ 28   | 17    | 44    | 220  | 66.5 | 88.5 | 81.5 |
|  | $f$ 19.5              | 13.5  | 20.5  | 39   | 19   | 20.5 | 18.5 |
| C <sub>8</sub> H <sub>16</sub> , fig. 8  | $\kappa_{\max.}$ 12.2 | 77    | 55    | 68.5 | 30   | 53   |      |
|  | $f$ 20.5              | 33.5  | 29    | 23.5 | 22.5 | 22.5 |      |
| C <sub>2</sub> H <sub>4</sub> , fig. 9   | $d_{\max.}$ 0.695     | 0.685 |       |      |      |      |      |
|  | $f$ 42.5              | 24    |       |      |      |      |      |
| C <sub>10</sub> H <sub>20</sub> , fig. 1 | $\kappa_{\max.}$ 170  | 805   | 430   |      |      |      |      |
|  | $f$ 20.5              | 27    | 19    |      |      |      |      |
| C <sub>10</sub> H <sub>20</sub> , fig. 9 | $\kappa_{\max.}$ 5.4  | 6.9   |       |      |      |      |      |
|  | $f$ 23.5              | 16.5  |       |      |      |      |      |
| C <sub>14</sub> H <sub>30</sub> , fig. 1 | $\kappa_{\max.}$ 230  | 820   | 69    | 70   | 450  |      |      |
|  | $f$ 20                | 26.5  | 16.7  | 15.7 | 17   |      |      |
| C <sub>17</sub> H <sub>34</sub> , fig. 1 | $\kappa_{\max.}$ 255  | 1080  | 167   | 117  | 590  |      |      |
|  | $f$ 21.5              | 24.5  | 23.5  | 20   | 15.5 |      |      |
| C <sub>24</sub> H <sub>50</sub> , fig. 1 | $\kappa_{\max.}$ 230  | 2180  | 1240  |      |      |      |      |
|  | $f$ 22.5              | 27    | 18    |      |      |      |      |
| Paraffin wax,<br>fig. 1                  | $d_{\max.}$ 0.088     | 0.640 | 0.360 |      |      |      |      |
|  | $f$ 23                | 26.5  | 17.5  |      |      |      |      |
| C <sub>8</sub> H <sub>14</sub> , fig. 1  | $\kappa_{\max.}$ 330  | 90    | 72    | 165  |      |      |      |
|  | $f$ 26                | 21.5  | 29    | 23.5 |      |      |      |
| C <sub>7</sub> H <sub>14</sub> , fig. 1  | $\kappa_{\max.}$ 335  | 79    | 85    | 130  |      |      |      |
|  | $f$ 31                | 24.5  | 33    | 25.5 |      |      |      |
| C <sub>8</sub> H <sub>16</sub> , fig. 1  | $\kappa_{\max.}$ 345  | 112   | 70    | 165  | 19   |      |      |
|  | $f$ 31                | 25    | 28.5  | 22.5 | 23   |      |      |

Where  $d_{\max.}$  is given instead of  $\kappa_{\max.}$ , the necessary conversion factor from  $d$  to  $\kappa$  is not known, either because the concentration was not determined, or the molecular weight is not known accurately. Band no. 5 of C<sub>8</sub>H<sub>18</sub> occurs at 2847 cm.<sup>-1</sup>.

TABLE 5. INTENSITY OF ABSORPTION OF CH<sub>2</sub> AND CH<sub>3</sub> GROUPS IN SATURATED HYDROCARBONS AND IN CETENE

| Substance                       | No. of CH <sub>2</sub><br>groups, $n$ | $\kappa_{\max.}$<br>(~ 2926 cm. <sup>-1</sup> ) | $\kappa_{\max.}/n$ | $\kappa_{\max.}$<br>(~ 2853 cm. <sup>-1</sup> ) | $\kappa_{\max.}/n$ |
|---------------------------------|---------------------------------------|---|--------------------|---|--------------------|
| C <sub>14</sub> H <sub>30</sub> | 12                                    | 819   | 68.3               | 448   | 37.4               |
| C <sub>17</sub> H <sub>36</sub> | 15                                    | 1080  | 72.0               | 590   | 39.4               |
| C <sub>24</sub> H <sub>50</sub> | 32                                    | 2180  | 68.1               | 1238  | 38.6               |
| C <sub>18</sub> H <sub>38</sub> | 13                                    | 804   | 61.9               | 430   | 33.1               |

The low values of  $\kappa_{\max.}/n$  for cetene may be due to abnormally low absorption of one or more  $\text{>CH}_2$  groups adjacent to the double bond. This is likely since the  $\text{>CH}_2$  group in 1-butylene has only about half the normal absorption.

TABLE 5 (continued)

| Substance                       | No. of<br>CH <sub>3</sub><br>groups, <i>n</i> | $\kappa_{\max.}$<br>( $\sim 2962 \text{ cm.}^{-1}$ ) | $\kappa_{\max.}/n$ | $\kappa_{\max.}$<br>( $\sim 2872 \text{ cm.}^{-1}$ ) | $\kappa_{\max.}/n$ |
|---------------------------------|---|--|--------------------|--|--------------------|
| 2:3-Dimethylbutane              | 4   | 328  | 82.0               | 164  | 41                 |
| 2:2:3-Trimethylbutane           | 5   | 334  | 66.8               | 130  | 26                 |
| 2:3:4-Trimethylpentane          | 5   | 346  | 69.2               | 166  | 33.2               |
| C <sub>14</sub> H <sub>30</sub> | 2   | 229  | 114.5              |  |                    |
| C <sub>17</sub> H <sub>36</sub> | 2   | 255  | 127.5              |  |                    |
| C <sub>34</sub> H <sub>70</sub> | 2   | 232  | 116                |  |                    |
| C <sub>16</sub> H <sub>32</sub> | 1   | 171  | 171                |  |                    |

The value of  $\kappa_{\max.}/n$  for cotene is much too high since the absorption is partly due to the  $=\text{CH}_2$  group, cf. 1-butylene.

## DISCUSSION

## (1) CH frequencies

$\text{>CH}$  and  $=\text{CH}_2$  groups. The CH valency frequencies arising from  $\text{>CH}$  and  $=\text{CH}_2$  groups are found at wave-lengths below  $3.37 \mu$ , and are easily distinguished from  $\text{>CH}_2$  and  $\text{CH}_3$  frequencies, since these occur at longer wave-lengths.

The nature of the absorption bands of  $=\text{CH}_2$  is disclosed by an examination of the spectrum of ethylene (in carbon tetrachloride) (figure 9). Two CH frequencies are found at  $3092$  and  $2977 \text{ cm.}^{-1}$ , due to the unsymmetrical and symmetrical modes of vibration, respectively (cf. Fox and Martin 1938), while the single CH frequency of the group  $\text{>CH}$  occurs about mid-way between these, e.g.  $3023 \text{ cm.}^{-1}$  in cyclohexene (band 1, figure 6). The  $=\text{CH}_2$  group in propylene has essentially two bands (1 and 4, figure 2) as in ethylene, but in the higher olefins only one of the  $=\text{CH}_2$  frequencies can be identified ( $\sim 3080 \text{ cm.}^{-1}$ ), since the other is masked by a  $\text{CH}_3$  band. In tables 1 and 4 are given collected data relating to  $\text{>CH}$  and  $=\text{CH}_2$  absorption bands.

$\text{>CH}_2$  and  $\text{CH}_3$  groups. In a previous communication (1938) we showed that  $\text{>CH}_2$  groups gave generally two strong absorption bands near  $2927$  (unsymmetrical vibration) and  $2857 \text{ cm.}^{-1}$  (symmetrical vibration), but in some cases as many as four bands might be obtained. The present work confirms these conclusions, the mean  $\text{>CH}_2$  frequencies in the present series being  $2926$  and  $2853 \text{ cm.}^{-1}$  (table 2). Cyclohexene and 1-methylcyclohexene give four bands attributable to  $\text{>CH}_2$ . The highest frequency

is in good agreement in both cases with the value  $2926\text{ cm.}^{-1}$  found for normal  $\text{>CH}_2$  groups, but the  $2853\text{ cm.}^{-1}$  frequency is split in the cyclohexenes. The mean of the two components in the split band is  $2848$  for cyclohexene and  $2846$  for 1-methylcyclohexene, close to the normal value  $2853\text{ cm.}^{-1}$ .

Recently Ellis and Bath (1939), examining the absorption of polarized light by crystals of substances containing  $\text{>CH}_2$  groups, e.g. pentaerythritol, in the region of the first overtone of the CH vibrations, concluded that, contrary to our finding for  $\text{CH}_2$  fundamentals in general, the symmetrical frequency ( $\nu_s$ ) is higher than the unsymmetrical frequency ( $\nu_a$ ). It is possible that the crystalline substances examined by Ellis and Bath have special properties, but it is by no means clear that our results on dilute solutions are directly comparable with the crystal measurements; further work would have to be undertaken to settle this point. We consider that the correctness of our assignment is supported by consideration of the behaviour of many groups of the type  $\begin{smallmatrix} X \\ X \end{smallmatrix} \text{>Y}$ , whether actual molecules or

parts of a larger molecule. In ethylene gas (1938) the two symmetrical frequencies ( $2988, 3019\text{ cm.}^{-1}$ ) are lower than the two unsymmetrical vibrations ( $3107, 3086\text{ cm.}^{-1}$ ); also in cyclohexane (1938) there is a strong Raman frequency  $2853\text{ cm.}^{-1}$ , corresponding to a mode of vibration in which all the  $\text{CH}_2$  units execute symmetrical vibrations, while in the infra-red (in carbon tetrachloride solution) a frequency of moderate intensity arising from a rather similar mode of vibration (essentially the same as regards the  $\text{CH}_2$  groups) is found at  $2851\text{ cm.}^{-1}$ . It is usual to associate strong Raman frequencies with highly symmetrical modes of vibration; conversely, the much stronger infra-red frequency at  $2927\text{ cm.}^{-1}$  in cyclohexane has a comparatively weak counterpart in the Raman spectrum. Another example is provided by the water molecule, for which the symmetrical frequency, active in the Raman effect, is  $3654\text{ cm.}^{-1}$ , while the unsymmetrical, infra-red active, frequency is  $3756\text{ cm.}^{-1}$ .

Figure 1 and table 3 show that  $\text{CH}_3$  groups have two main frequencies near  $2962$  and  $2872\text{ cm.}^{-1}$ , but that in addition two weaker intermediate frequencies may occur. In the unsaturated compounds, when a methyl group is adjacent to a double bond, five CH frequencies are obtained with relative intensities varying greatly from one compound to another (figures 2-5, 8). In these compounds the lowest  $\text{CH}_3$  frequency, normally  $2872\text{ cm.}^{-1}$ , is split into two, the mean of the two components in each case being within a few wave numbers of  $2872$  (table 3). This behaviour, presumably resonance



splitting, is very similar to that noticed for the  $\text{>CH}_2$  group in the cyclohexenes; in both cases it is the lowest frequency (symmetrical mode) which is split.

Molecules of general type  $\text{CH}_3\text{---X}$ , such as methyl deuteride and methyl halides, have two CH valency frequencies close to  $2970$  and  $3060\text{ cm.}^{-1}$ , the mass of X in accordance with theoretical expectation having little effect on these. It may be noted here that the fundamental CH frequencies of the methyl halides, derived from the observations of Bennett and Meyer (1928), have been given rather differently by Sutherland (1935), and Slawsky and Dennison (1939). In view of these discrepancies (e.g.  $\nu_1$  for methyl bromide is given as  $2972\text{ cm.}^{-1}$  by Sutherland and  $2917\text{ cm.}^{-1}$  by Slawsky and Dennison) we have made measurements on methyl bromide in carbon tetrachloride and found three frequencies,  $3049$ ,  $2958$  and  $2840\text{ cm.}^{-1}$  in the " $\text{CH}_3$  region". The third frequency has been explained as the first overtone of one of the  $\text{CH}_3$  angular deformation frequencies ( $1451\text{ cm.}^{-1}$  in the gas), while the first two frequencies are CH valency vibrations, unsymmetrical (perpendicular) and symmetrical (parallel), respectively, as shown by their rotational structure in the gas. In carbon tetrachloride solution these frequencies are reduced by about  $13\text{ cm.}^{-1}$  from the gas values as given by Sutherland; this shift is about that usually found by us for CH vibrations. We have then the two  $\text{CH}_3$  frequencies  $2962$  and  $2872\text{ cm.}^{-1}$  in hydrocarbons, and  $3049$  and  $2958\text{ cm.}^{-1}$  in methyl bromide. The considerable frequency differences between corresponding bands,  $87$  and  $86\text{ cm.}^{-1}$ , respectively, do not appear to have been observed previously, and show that the constants of  $\text{CH}_3$  groups in hydrocarbons, where they are attached to other carbon atoms, are distinctly different from the values in methyl halides and  $\text{CH}_3\text{D}$ .

$\text{>CH group}$ . The frequency to be attributed to the CH group in saturated hydrocarbons is difficult to obtain directly, since in none of the compounds examined was such a CH band identified. The best chance of determining this frequency was thought to exist in 2:3:4-trimethylpentane (figure 1), since this molecule contains only CH and  $\text{CH}_3$  groups, but even in this case the CH band could not immediately be found. We can, however, determine where this band would come in two ways as follows: (1) in the case of  $\text{>CH}$  and  $=\text{CH}_2$  groups the  $\text{>CH}$  frequency occurs about midway between the two  $=\text{CH}_2$  frequencies, and applying a similar rule to saturated compounds the  $\text{>CH}$  frequency should be  $\frac{1}{2}(2926 + 2853) = 2890\text{ cm.}^{-1}$ ; (2) in triphenylmethane the frequency of the  $\text{>CH}$  group was found by us to be

2878  $\text{cm}^{-1}$  (Wall and McMillan 1939 found 2881  $\text{cm}^{-1}$ ), but here the presence of three phenyl groups may well modify the frequency from 2890 in saturated hydrocarbons, since in diphenylmethane (1938) we found frequencies for the  $\text{>CH}_2$  group about 12  $\text{cm}^{-1}$  lower than for completely saturated hydrocarbons. The value 2890  $\text{cm}^{-1}$  is further justified by the fact that the  $\text{>CH}$  frequency in triphenylmethane is exactly half-way between the  $\text{>CH}_2$  frequencies of diphenylmethane. A band at 2890  $\text{cm}^{-1}$  is not immediately obvious for the methyl-butanes and -pentane of figure 1 because it is obscured by  $\text{CH}_3$  frequencies, but a graphical separation of the absorption bands indicates the presence of a small band close to 2890  $\text{cm}^{-1}$  for each compound.

## (2) Intensities of CH bands

The work of Wulf and Liddel (1933, 1935) on OH and NH absorption, and of Rose (1938) on CH absorption in the region of the first and higher overtones of the valency vibrations, suggests that for the CH fundamentals a considerable degree of constancy in absorption of various molecular units should be found. In assessing band intensities Wulf and Liddel used integrated absorption areas, while Rose worked with the value of  $\kappa_{\text{max}}$  at an arbitrary wave-length which he regarded as characteristic of the group in question. We have shown (1938) that for the bands encountered in our work the integrated absorption area can be estimated from the relation  $\text{area} = cf\kappa_{\text{max}}$ , where  $f$  is the half-width of the band, and  $c$  is a constant, close to 1.4; when comparing areas  $c$  can be ignored and values of  $f\kappa_{\text{max}}$  taken. Rose has made two assumptions in his work: (1)  $f$  remains constant from one compound to another, so that the area is proportional to  $\kappa_{\text{max}}$ , and (2) that the maximum of the band always comes at the same wave-length. From our results we can now show that these assumptions are justified for long-chain paraffins, less well justified for branched-chain hydrocarbons (figure 1), and are untenable for the methyl groups in unsaturated hydrocarbons (figures 2-5, 8). In table 5 the values of  $\kappa_{\text{max}}$  of the two main  $\text{>CH}_2$  bands in the long-chain paraffins (figure 1, tables 2 and 4) have been divided by the number of  $\text{>CH}_2$  groups in the molecule, and also in table 5 the same procedure has been followed for the two main bands (when available) of the  $\text{CH}_3$  group in the compounds of figure 1. It is shown that on passing from one compound to another the absorption of  $\text{>CH}_2$  and  $\text{CH}_3$  groups does remain more or less constant. In the case of 2:3-dimethylbutane,

2:2:3-trimethylbutane and 2:3:4-trimethylpentane, a comparison of the integrated absorption areas, including all  $\text{CH}_3$  bands, is more satisfactory. These areas calculated from  $\Sigma f\kappa_{\text{max}}$  are in the ratios 4.42 : 5 : 5.21, respectively, as compared with 4 : 5 : 5 for the number of methyl groups.

For 1-butylene, *cis*- and *trans*-2-butylene, and trimethyl-ethylene, the method of Rose discussed above would fail completely, as inspection of the absorption curves (figures 5, 4, 3 and 8) shows. The integrated area, however, still provides a measure of the methyl groups and estimating  $\Sigma f\kappa_{\text{max}}$  for the methyl bands in these compounds we obtain respectively the ratios 1 : 1.76 : 1.89 : 3.50 as compared with 1 : 2 : 2 : 3 for the number of methyl groups in the molecule. It will be noticed that in 1-butylene, band no. 3 ( $2968 \text{ cm.}^{-1}$ ) is not only due to  $\text{CH}_3$  but also to some extent due to  $=\text{CH}_2$ . An allowance for the  $=\text{CH}_2$  absorption is possible by comparison with propylene (figure 2) in which the two bands are clearly separated (bands 4 and 5).

The absorption of  $>\text{CH}$  and  $=\text{CH}_2$  groups in different compounds can similarly be compared and a fair constancy of absorption is indicated. On passing from ethylene to propylene, 1-butylene, and cetene, it is found that the relative intensity of the two  $=\text{CH}_2$  bands gradually changes, the band of higher frequency becoming weaker as the length of chain increases while the other band becomes more intense. Approximate absorption values, i.e. average integrated absorption areas, of all the groups studied in the present work have been calculated and the results in units of  $\kappa$  (per group) multiplied by  $f$  ( $\text{cm.}^{-1}$ ), summed for all bands associated with a group, are as follows:  $>\text{CH}$  410,  $=\text{CH}_2$  1800,  $>\text{CH}$  120,  $>\text{CH}_2$  2400,  $>\text{C}-\text{CH}_3$  2230,  $>\text{C}-\text{CH}_3$  3800. It is of interest to note the reduction of intensity of absorption of  $>\text{CH}_2$  and  $\text{CH}_3$  groups when adjacent to a double bond. Further, it appears that as the number of hydrogen atoms attached to a carbon atom is reduced, the intensity of C-H absorption falls and for  $>\text{CH}$  is extremely low in comparison with the other groups. A similar result was found by Rose (1938) for  $>\text{CH}$  bands in the region of  $1.5\mu$ .

### (3) *Cis- and trans-2-butylene*

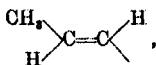
The identification of the *cis* and *trans* modifications of 2-butylene as the high and low boiling isomers, respectively, depends on five sets of observations: (1) The method of synthesis of Young, Dillon and Lucas (1929). (2) A comparison by Kistiakowsky, Ruhoff, Smith and Vaughan (1936) of the heat of hydrogenation of each compound with that of cyclohexene,

which as regards the part of the molecule containing the double bond,  $\begin{smallmatrix} \text{C} & \text{C} \\ | & | \\ \text{H} & \text{H} \end{smallmatrix}$ , is very similar to the *cis* isomer. (3) Electron diffraction measurements of Brockway and Cross (1936). (4) Ultra-violet measurements of Carr and Stücklen (1937). (5) A comparison of Raman and infra-red frequencies of the *cis* and *trans* forms by Gershinowitz and Wilson (1938). No one of these methods alone is completely satisfactory, but taken together there is little doubt that the assignment given is correct.

The infra-red spectra of Gershinowitz and Wilson were obtained with low dispersion, especially at the lower wave-lengths, so that while their results for the C to C vibrations and angular deformation frequencies (all less than  $2000\text{ cm.}^{-1}$ ) may be considered reliable, little detail was given in the region of  $3000\text{ cm.}^{-1}$ . Our results (figures 3 and 4, and tables 1 and 3) show that the absorption curves of the 2-butylenes in this region contain 6 or more bands, and these must all be considered in any theoretical discussion on the modes of vibration of these molecules. According to the above workers more coincidences between Raman and infra-red frequencies were found for the *cis* than for the *trans* isomer, as is to be expected if the latter can be regarded approximately as a molecule with a centre of symmetry. However, a difficulty arises here in judging how closely two frequencies should approach to be regarded as coincident. In a molecule such as 2-butylene, having many frequencies, it is very likely that there will exist slightly different modes of vibration, essentially the same as regards the inner vibration of a  $\text{CH}_3$  group, with frequencies almost the same, but with very different Raman and infra-red activities. The small frequency difference in this case might easily be confused with the experimental error, especially as Gershinowitz and Wilson compared infra-red results on the vapour with Raman frequencies of the liquid. The frequency shift between vapour and liquid in the region of  $3000\text{ cm.}^{-1}$  is  $\sim 10\text{ cm.}^{-1}$ , but the difference between carbon tetrachloride solution and liquid is only  $\sim 3\text{ cm.}^{-1}$  (cf. Fox and Martin 1938). A comparison of our infra-red frequencies with the Raman data shows that there are four "coincidences" in the region of  $3000\text{ cm.}^{-1}$  for each isomer, the agreement being slightly better for the *trans* (maximum difference  $10\text{ cm.}^{-1}$ ) than for the *cis* isomer (maximum difference  $14\text{ cm.}^{-1}$ ). For both isomers Raman lines are found within  $3\text{ cm.}^{-1}$  or less of the two main  $\text{CH}_3$  frequencies (table 3), but the lower frequency which is split in the infra-red is single in the Raman spectra.

Inspection of figures 3 and 4 shows that the infra-red spectra of *cis*- and *trans*-2-butylene are quite different, especially in the  $\text{CH}_3$  region ( $2820$ – $2970\text{ cm.}^{-1}$ ), and a comparison with spectra of other simple hydrocarbons

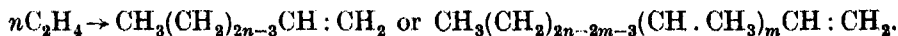
of known constitution provides, in our opinion, the most trustworthy means of deciding which isomer has the *cis* (or *trans*) configuration. For example, the  $\text{>CH}$  frequency of the *cis* compound is only  $1\text{ cm.}^{-1}$  different from that of cyclohexene but the *trans*-2-butylene differs by as much as  $5\text{ cm.}^{-1}$ ; the intensities of the bands are also similar for the first two substances. Further, in 1-methylcyclohexene the methyl group is very similarly placed to those in *trans*-2-butylene and propylene. The frequency  $\sim 2960\text{ cm.}^{-1}$  is common to all three compounds, but in *cis*-2-butylene the mutual interference of the two methyl groups shifts this frequency to  $2976\text{ cm.}^{-1}$  (cf. trimethylethylene, table 3). The striking similarity of the " $\text{CH}_3$  region" of the spectra of propylene and *trans*-2-butylene (figures 2 and 3) shows that the  $\text{CH}_3$  groups must be similarly situated in both, i.e.



while the spectrum of the *cis* compound resembles rather that of trimethylethylene, which also has two *cis*-methyl groups.

#### (4) Constitution of the polythenes

Polythenes are long-chain hydrocarbons ( $\sim 1000$  C-atom chains) obtained by condensation of ethylene (Brit. Pat. 471,590) according to some such scheme as



Whether this double bond remains in the product or is reduced by hydrogen is not clear. Bunn (1939), in making an X-ray analysis of these substances, appears to have assumed that they are normal straight chain paraffins, and to have ignored the possibility of there being branches containing methyl groups. Our results (figure 1) show that for samples B 59 and AXX,  $\text{CH}_2$  bands are obtained having intensities compatible with molecules composed of long chains of  $\text{CH}_2$  groups. An additional band is, however, observed in all cases near  $2960\text{ cm.}^{-1}$  and can only be attributed to the presence of methyl groups. The greatest proportion of methyl was found in extractions of the polythenes at room temperature with carbon tetrachloride, in which the more soluble part of the polythene, presumably the shorter chains, together with any soluble impurities would be dissolved. The absorption curves obtained for these solutions are the unbroken curves in figure 1 and by comparison with the normal paraffins  $\text{C}_{14}\text{H}_{30}$ ,  $\text{C}_{17}\text{H}_{36}$  and  $\text{C}_{34}\text{H}_{70}$  in figure 1, the proportion of methyl can be estimated as  $1\text{CH}_3:8\text{CH}_2$ . To reduce the possible effect of easily soluble impurities, some of each poly-

the sample was dissolved completely in boiling carbon tetrachloride; the solution was filtered and the polythene precipitated by cooling, filtered and dried. These products were again extracted with carbon tetrachloride at room temperature and the results are shown by the broken curves (---) of figure 1. A Rast molecular weight determination gave 4700 for the material extracted. The proportion of methyl is considerably smaller,  $1\text{CH}_3:13\text{CH}_2$ . Finally, the material purified as described was completely dissolved in carbon tetrachloride and the broken curves (— · — ·) of figure 1 were obtained. The average proportion of methyl for the whole sample is much less than for the extracted portions, about  $1\text{CH}_3:35\text{CH}_2$  for sample B 59 and  $1\text{CH}_3:70\text{CH}_2$  for AXX. These results indicate that the polythenes are mixtures of compounds containing  $\text{CH}_2$  chains of lengths varying from  $\sim 300$  to 1000 or more  $\text{CH}_2$  units, with a proportion of methyl groups varying from  $1\text{CH}_3:8\text{CH}_2$  for the shorter chains to about  $1\text{CH}_3:100\text{CH}_2$  for the long chains. The presence of these methyl groups may confer special properties on the polythenes, e.g. the ability to form thin transparent sheets; and in relation to this it is interesting to recall the fact that of the lower paraffins, while the normal compounds crystallize readily without supercooling, many branch-chained members such as 2- and 3-methylpentanes solidify to glasses (Smittenberg, Hoog and Henkes 1938; cf. Baker and Smyth 1939). The presence of an appreciable proportion of methyl in the polythenes was not considered by Bunn (1939) in his X-ray work, and it is conceivable that the serious discrepancies noticed by him may be traced to this.

A search was made for  $=\text{CH}_2$  groups in the polythenes but only a slight indication ( $\sim 3080\text{ cm.}^{-1}$ ) was found (cf. cetene and B 59 in figure 9) in that portion of the product obtained by a  $\text{CCl}_4$  extraction at  $40^\circ\text{C}$  of the unpurified material. The proportion of  $=\text{CH}_2$  can be estimated as 1 group to 200  $>\text{CH}_2$  groups and this is about what would be required if the lowest polythenes are composed of 200–300 C-atom chains with a  $=\text{CH}_2$  group at the end of the molecule.

In figure 1 a curve is given for a sample of paraffin wax and it will be seen that it is very similar to that for  $\text{C}_{34}\text{H}_{70}$ , but with a rather higher proportion of methyl than this compound. The mean composition of the paraffin wax is probably close to  $\text{CH}_3(\text{CH}_2)_{24}\text{CH}_3$ .

#### (5) Calculation of C-H force constants

From the measurement of CH frequencies in hydrocarbons many attempts have been made to determine the various CH force constants involved, e.g. Sutherland and Dennison (1935). However, to make these

calculations with accuracy not only must the CH frequencies be known with sufficient exactness, but reliable potential functions must be available for the molecules under consideration. The force constant depends on the frequency of vibration and the masses of the atoms concerned, and hence on Avogadro's number. We have taken for this the value  $6.025 \times 10^{23}$  on the physical scale, and the corresponding masses of  $^1\text{H}$  and  $^{12}\text{C}$  are 1.6729 and  $19.924 \times 10^{-24}$  g., respectively. These masses have been used for calculating all the force constants given in this communication, and small differences from the values given by other workers are in some cases due to their having used slightly different masses.

The CH force constant in methane can be arrived at quite easily following Sutherland and Dennison (1935), making use of the fact that in the totally symmetrical Raman frequency (gas) at  $2915 \text{ cm.}^{-1}$ , the carbon atom remains at rest and the hydrogen atoms move in phase to and from it. The force constant is 5.04 in the usual units ( $10^5$  dynes per cm.). We have dealt already with the  $\text{>CH}_2$  group (1938) and the force constant recalculated to the gas state is 4.56. As pointed out in an earlier section of this discussion, two sets of data are available for  $\text{CH}_3$  groups and two different values of the force constant are therefore obtained. Recently, from a consideration of the data for ethane, Stitt (1939) developed a potential function (called by him III) for this molecule, and also for  $\text{C}_2\text{D}_6$ , which we find quite satisfactory, since, besides giving good agreement between calculated and observed frequencies, it leads to a reasonable value for the C-C force constant. The CH force constant found by Stitt was 4.79 and the calculated infra-red CH valency frequencies were 3010 and  $2895 \text{ cm.}^{-1}$ . The infra-red data used by Stitt were rather uncertain, and we have therefore investigated ethane in carbon tetrachloride solution. We hope to discuss this and other hydrocarbons at a future date, but may now point out that the ethane spectrum obtained by us is very similar to that given by dimethylbutane and other compounds in figure 1. The two main frequencies in ethane in the  $3\mu$  region are 2974 and  $2880 \text{ cm.}^{-1}$ , quite close to those found for methyl compounds generally (table 3). To fit these frequencies, using the masses given above for  $^1\text{H}$  and  $^{12}\text{C}$ , the CH force constant used by Stitt must be reduced from 4.79 to 4.75 ( $\text{CCl}_4$  solution). The calculated frequencies are then 2984 and  $2870 \text{ cm.}^{-1}$ , in good agreement with our values. Knowing the CH force constant in ethane, we can readily calculate the corresponding value in methyl halides, since it may be taken with very little error that the frequency is proportional to  $\sqrt{k}$ , where  $k$  is the CH force constant. Thus for methyl bromide in carbon tetrachloride solution (see p. 222)  $k = 4.75 \times \left(\frac{3049}{2974}\right)^2$  or  $4.75 \times \left(\frac{2958}{2880}\right)^2$ .

The mean value of  $k$  is found to be 5.00 ( $= 5.04$  for methyl bromide gas) and is in exact agreement with the value 5.04 found above for methane. This result shows that the  $\text{CH}_3$  constants are almost exactly the same in methyl bromide as in methane (and  $\text{CH}_3\text{D}$ ). The CH distance in methane and  $\text{CH}_3\text{D}$  is stated to be 1.093 Å (Ginsburg and Barker 1935; Childs and Jahn 1939), and bearing in mind the Morse-Clark rule,  $kr^6 = \text{const.}$ , where  $r$  is the internuclear distance, it follows that the CH distance in methyl bromide (and probably the other halides) should be within 0.001 Å of the methane value. We hope to be able to discuss the various CH distances in organic molecules elsewhere, and then the relation between force constant and internuclear distance can be considered in more detail.

In ethylene the CH force constant has been calculated by many workers including ourselves (1938), and the value now obtained is 5.05 for the gas. The frequencies of  $=\text{CH}_2$  groups (table 1) in other olefins are close to those of ethylene, but tend to be a little lower so that 5.03 is a reasonable value for the CH force constant (corrected to the gaseous state) in olefins generally. The mean  $>\text{CH}$  frequency (table 1) is  $3019 \text{ cm.}^{-1}$  as compared with  $3062 \text{ cm.}^{-1}$  for the symmetrical Raman CH vibration in benzene, and the corresponding force constant is 4.98, derived from that of benzene (5.12 for gas state, cf. Kohlrausch 1935) by multiplying by  $\left(\frac{3019}{3062}\right)^2$ . As already explained the  $>\text{CH}$  frequency in saturated compounds is difficult to determine directly, but a probable value is  $2890 \text{ cm.}^{-1}$  for carbon tetrachloride solutions. The force constant (4.56) can be obtained in a similar manner to that for the  $>\text{CH}$  group.

We can summarize the force constants for the normal types of CH bond as follows, including our own recalculated force constants for benzene and acetylene. All force constants are calculated to the gas state by allowing for the small frequency increase ( $\sim 10 \text{ cm.}^{-1}$ ) on passing from liquid or carbon tetrachloride solution to the gas state.

| Group or molecule                            | $\text{CH}_4$ | $\text{CH}_3\text{Br}$ | $\text{H}_3\text{C}-\text{CH}_3$ | $\text{C}-\text{CH}_3$ in<br>higher<br>paraffins | $>\text{CH}_2$ | $>\text{CH}$ |
|--|---------------|------------------------|----------------------------------|--|----------------|--------------|
| CH force constant<br>( $10^8$ dynes per cm.) | 5.04          | 5.04                   | 4.78                             | 4.75   | 4.56           | 4.56         |

| Group or molecule                            | $\text{HC}\equiv\text{CH}$ | $\text{H}_2\text{C}=\text{CH}_2$ | $=\text{CH}_2$ in<br>higher<br>olefins | CH in<br>benzene | $>\text{CH}$ |
|--|----------------------------|----------------------------------|--|------------------|--------------|
| CH force constant<br>( $10^8$ dynes per cm.) | 5.92                       | 5.05                             | 5.03                                   | 5.12             | 4.98         |



## DETAILS OF THE COMPOUNDS EXAMINED

*Tetradecane*,  $C_{14}H_{30}$ , *heptadecane*,  $C_{17}H_{34}$ , and *tetratriacontane*,  $C_{34}H_{70}$ , were known to be of quite high purity, but small amounts of the closest homologues were possibly present. The melting points were 5.5, 23.5 and 72.5° C, respectively, as compared with 5.5, 22° C (Heilbron), and 76.5° C (I.C.T.).

*Cetene*,  $C_{16}H_{32}$ , was purified by vacuum distillation, a middle fraction boiling at 155° C, 15 mm., being finally retained. The position of the double bond in cetene obtained by distillation of cetyl palmitate was shown by Langedijk and Stedehouder (1937), and by Schoorl (1938) to be at the end of the molecule, and since the properties of our sample of cetene agree closely with theirs, we shall assume that our cetene is also 1-hexadecene. The infra-red spectrum justifies this assumption since a  $=CH_2$  group gives quite different absorption from the alternative arrangement— $\begin{array}{c} C & C \\ | & | \\ H & = & H \end{array}$ .

2:3-Dimethylbutane and 2:2:3-trimethylbutane were probably better than 98 % pure, whilst 2:3:4-trimethylpentane may have contained a little of the 2:3:3-isomer, which, however, in small amount would have little effect on the absorption spectrum.

*Ethylene* was prepared by the method of Newth (1901) from ethyl alcohol and phosphoric acid. After purification the gas was directly absorbed in carbon tetrachloride until a suitable concentration was reached.

*Propylene* was also prepared by the method of Newth (1901) from isopropyl alcohol, and after purification was liquefied. A middle fraction of the liquid was allowed to evaporate (−48° C) and the gas absorbed in carbon tetrachloride.

1-Butylene was prepared from pure *n*-butyl iodide and alcoholic caustic potash, the method of preparation and purification being described by Coffin and Maass (1928). The liquid was fractionated at about −6° C, and was weighed in a glass capsule which was afterwards broken under a known quantity of cold carbon tetrachloride.

2-Butylene (*cis* and *trans*). The preparation of these compounds in a very high state of purity has been described by Kistiakowsky *et al.* (1935). The compounds were weighed into glass capsules and dealt with as described for 1-butylene.

Trimethylethylene was obtained by dehydrating carefully purified *tert*-amyl alcohol with sulphuric acid in a manner similar to that described in *Organic Syntheses* (1932), vol. 1. The product was fractionated and a middle portion boiling at 38.5° C, 760 mm., was used.

1-*Methylcyclohexene* was prepared by dehydrating 2-methylcyclohexanol in a manner similar to that described for trimethylethylene. The product was fractionated and a middle portion boiling at 108° C, 760 mm., was used.

*Cyclohexene* was purified by fractionation, the final product boiling at 82.8° C, 760 mm. Absence of benzene in the sample was shown by an examination of the ultra-violet absorption spectrum.

*Paraffin wax* was a B.D.H. sample with melting point 54° C.

*Polythenes*, "B 59" and "AXX", were obtained from Imperial Chemical Industries. These compounds had been obtained by the condensation of ethylene under high pressure, and had very high molecular weights, approximately 10,000 and 35,000, respectively. Both grades melted at 100–120° C to liquids having extremely high viscosities, and could be converted into thin films of considerable strength by evaporating a solution of the polythene in xylene on a glass plate at 130° C.

We are indebted to Dr A. R. Ubbelohde of the Royal Institution for supplying us with specimens of long-chain paraffins; to Dr F. H. Garner for a sample of cetene; to Dr S. F. Birch of the Anglo-Iranian Oil Company for 2:3-dimethylbutane, 2:2:3-trimethylbutane and 2:3:4-trimethylpentane; to Prof. G. B. Kistiakowsky for *cis*- and *trans*-2-butylene; and to Mr F. S. Bengé of the Government Laboratory for his valuable assistance throughout this investigation.

#### SUMMARY

The infra-red absorption spectra of some twenty hydrocarbons in carbon tetrachloride solution have been studied in the region 2.6–3.8  $\mu$  with the following results.

1.  $=CH_2$  groups in ethylene and higher olefins give rise to two CH frequencies with mean values 3079 and 2978  $cm.^{-1}$ , corresponding, respectively, to unsymmetrical and symmetrical valency vibrations of the  $CH_2$  group.

2.  $>CH$  groups in olefins have usually a single CH valency frequency close to 3019  $cm.^{-1}$ , i.e. almost half-way between the two bands of the  $=CH_2$  group. The  $>CH$  frequency in saturated compounds is 2890  $cm.^{-1}$ .

3.  $>CH_2$  groups have normally two CH valency vibrations with mean values 2926 and 2853  $cm.^{-1}$ , corresponding, respectively, to the unsymmetrical and symmetrical vibrations within the  $CH_2$  group. In long-chain paraffins the position of these bands and their intensity per  $CH_2$  group

remain remarkably constant from one compound to another. As found previously, bands additional to these two may occur in some cases.

4.  $\text{CH}_3$  groups also have two main CH valency frequencies, corresponding to unsymmetrical and symmetrical vibrations within the  $\text{CH}_3$  group. These frequencies are close to  $2962$  and  $2872\text{ cm.}^{-1}$ , respectively, when the methyl group is attached to another carbon atom, but in methyl bromide the frequencies are  $3049$  and  $2958\text{ cm.}^{-1}$ , i.e.  $87$  and  $86\text{ cm.}^{-1}$  higher. The CH force constant in methyl bromide is almost exactly the same as in methane, and this indicates that the CH internuclear distance does not differ from that in methane by as much as  $0.001\text{ \AA}$ . The CH force constant in a  $\text{CH}_3$  group attached to a carbon atom is nearly  $6\%$  lower than in methane and methyl bromide. In saturated hydrocarbons the position of the methyl bands and their intensity per  $\text{CH}_3$  group remain fairly constant, but when a methyl group is adjacent to a double bond, as in propylene, the positions and intensities of the bands vary greatly from one compound to another for comparatively small changes in the molecule. The band near  $2872\text{ cm.}^{-1}$  is split in these compounds, the mean position of the two components being close to  $2872\text{ cm.}^{-1}$ . The total area of all the bands attributable to  $\text{CH}_3$  groups in the unsaturated molecules, although somewhat lower than in saturated compounds, is still, however, approximately proportional to the number of  $\text{CH}_3$  groups present.

5. Identification of the *cis* and *trans* forms of 2-butylene is readily carried out by examination of the infra-red spectra. A striking resemblance exists between the spectrum of the *trans* form and that of propylene.

6. Two samples of a polythene (condensed ethylene resinoid) have been examined and have spectra similar to those of long-chain normal paraffins. A band at  $2960\text{ cm.}^{-1}$  characteristic of the methyl group is found in all cases and the proportion varies from  $1\text{CH}_3:8\text{CH}_2$  for the most soluble part of the polythenes to  $1\text{CH}_3:70\text{CH}_2$  for the whole sample. The significance of these results in relation to X-ray examination is briefly discussed.

7. CH force constants are given for eleven varieties of CH bond, and mean integrated absorption areas are given for  $\text{>CH}$ ,  $\text{>CH}$ ,  $=\text{CH}_2$ ,  $\text{>CH}_2$  and  $\text{CH}_3$  groups.

#### REFERENCES

- Baker, W. O. and Smyth, C. P. 1939 *J. Amer. Chem. Soc.* **61**, 2063.  
 Barnes, R. B. 1930 *Phys. Rev.* **36**, 296.  
 Bennett, W. H. and Meyer, C. F. 1928 *Phys. Rev.* **32**, 888.  
 Bonino, G. B. 1929 *Faraday Soc. General Discussion*, p. 879.  
 Brockway, L. O. and Cross, P. C. 1936 *J. Amer. Chem. Soc.* **58**, 2407.  
 Bunn, C. W. 1939 *Trans. Faraday Soc.* **35**, 482.

- Carr, E. P. and Stücklen, H. 1937 *J. Amer. Chem. Soc.* **59**, 2138.  
Childs, W. H. J. and Jahn, H. A. 1939 *Proc. Roy. Soc. A*, **169**, 428.  
Coblentz, W. W. 1905 *Investigations of Infra-red Spectra*, part 1.  
Coffin, C. C. and Maass, O. 1928 *J. Amer. Chem. Soc.* **50**, 1427.  
Ellis, J. W. and Bath, J. 1939 *Phys. Rev.* **55**, 1098.  
— — 1939 *J. Chem. Phys.* **7**, 862.  
Fox, J. J. and Martin, A. E. 1937 *Proc. Roy. Soc. A*, **162**, 419.  
— — 1938 *Proc. Roy. Soc. A*, **167**, 257.  
— — 1939 *J. Chem. Soc.* 318.  
Gershinowitz, H. and Wilson, E. B. 1938 *J. Chem. Phys.* **6**, 247.  
Ginsburg, N. and Barker, E. F. 1935 *J. Chem. Phys.* **3**, 688.  
Kistiakowsky, G. B., Ruhoff, J. R., Smith, H. A. and Vaughan, W. E. 1935 *J. Amer. Chem. Soc.* **57**, 876.  
— — — — 1936 *J. Amer. Chem. Soc.* **58**, 137.  
Kohlrusch, K. W. F. 1931, 1938 *Der Smekal-Raman Effekt*.  
— 1935 *Z. phys. Chem. B*, **30**, 305.  
Lambert, P. and Lecomte, J. 1936 *C.R. Acad. Sci., Paris*, **203**, 164.  
Langedijk, S. L. and Stedehouder, P. L. 1937 *Rec. Trav. chim. Pays-Bas*, **56**, 526.  
Liddel, U. and Wulf, O. R. 1933 *J. Amer. Chem. Soc.* **55**, 3574.  
Newth, G. S. 1901 *J. Chem. Soc.* **79**, 915.  
Rose, F. W. 1938 *Bur. Stand. J. Res., Wash.*, **20**, 129.  
Schoorl, N. 1938 *Rec. Trav. chim. Pays-Bas*, **57**, 719.  
Sherrill, M. L. and Mollet, P. 1936 *J. Chim. phys.* **33**, 701.  
Slawsky, Z. I. and Dennison, D. M. 1939 *J. Chem. Phys.* **7**, 522.  
Smittenberg, J., Hoog, H. and Henkes, R. A. 1938 *J. Amer. Chem. Soc.* **60**, 17.  
Stitt, F. 1939 *J. Chem. Phys.* **7**, 297.  
Sutherland, G. B. B. M. 1935 *Infra-red and Raman Spectra*.  
Sutherland, G. B. B. M. and Dennison, D. M. 1935 *Proc. Roy. Soc. A*, **148**, 250.  
Wall, F. T. and McMillan, G. W. 1939 *J. Amer. Chem. Soc.* **61**, 1053.  
Wulf, O. R. and Liddel, U. 1935 *J. Amer. Chem. Soc.* **57**, 1464.  
Young, W. G., Dillon, R. T. and Lucas, H. J. 1929 *J. Amer. Chem. Soc.* **51**, 2528.
-

# The dielectric capacity of electrolytes in mixed solvents: ion association in solutions of magnesium sulphate

BY W. A. MASON, PH.D., AND W. J. SHUTT, D.Sc.

*Department of Inorganic and Physical Chemistry, University of Liverpool*

*(Communicated by W. C. M. Lewis, F.R.S.—Received 16 January 1940)*

The remarkable achievements of Debye and Hückel, Onsager, and their colleagues in explaining and rationalizing the experimental data upon the behaviour of strong electrolytes in dilute solution have naturally led to much intensive research directed towards the extension of their theories to ranges of greater ionic concentration. From this work the theory of ion association, sponsored by Niels Bjerrum, has emerged with marked success. Assuming that the forces between oppositely charged ions obey the simple Coulomb law, Bjerrum has calculated the probability of such ions being within a distance,  $q_0$ , at which the thermal energy per degree of freedom is but one-quarter of the electrostatic energy holding the ions together. Oppositely charged ions at less than this distance from one another are termed short-range pairs. The true degree of association ( $1 - \alpha^*$ ) of an electrolyte, as distinguished from the classical conception of undissociated molecules, is a measure of the number of short-range pairs, and Bjerrum has shown that the law of mass action may be applied to this association to develop a relation which reproduces the activities of electrolytes in more concentrated solution with remarkable fidelity. Onsager (1927) has calculated some approximate values of the true degree of association by consideration of the discrepancies between experimental conductivity data for aqueous solutions and the figures derived from his equation. Similar, and more extensive and more accurate measurements have been made by Davies (1927). In solvents of lower dielectric constant, the increased inter-ionic forces lead to still wider discrepancies, and many workers have shown that electrolytes which are almost completely non-associated in water are appreciably associated in solvents of reduced dielectric capacity. Martin (1928) has shown that the alkali metal halides are incompletely dissociated in benzonitrile and that the association obeys a generalized law of mass action. Fuoss and Kraus (1933*a*) have observed the same effects with the alkali metal nitrates dissolved in ammonia and other solvents of low

dielectric constant. The mass-action constants derived from their results are in complete agreement with those predicted by the Bjerrum ion-association theory and, using measurements of the conductivity of tetraiso-amylammonium nitrate in dioxan-water mixtures, the same workers (1933*b*) have succeeded in extending the theory to include higher forms of association. Swift (1938) has confirmed the views of Fuoss and Kraus for ions of small radii by an investigation of the conductivities of solutions of the alkali metal halides in dimethylamine.

Interpretation of conductivity data, from which all of the above support for the Bjerrum theory has been derived, is complicated by several factors. The evaluation of  $\Lambda_\infty$  is difficult and, at best, must ultimately depend upon extrapolation methods of doubtful validity; the solvent correction is frequently rendered abortive through lack of data upon solvolysis for solvents other than water; the transport of solvent, both by solvation of the ions and by the transfer of momentum from the moving ions, must play its part in the determination of mobility, and yet precise data on such effects are meagre or non-existent. It was felt, therefore, that the dielectric properties of electrolytes presented an entirely different mode of attack well worthy of investigation.

Ion pairs differ fundamentally from the neutral molecules envisaged by Arrhenius in his undissociated salt. They should be strongly polar in nature, and their capacity of orientation polarization should manifest itself as an enhancement of the dielectric constant of the solvent. Such an effect was postulated by Walden in 1925. Here, again, interpretation of experimental values is beset with conflicting factors; they are, however, of a different nature from those which arise in conductivity work. Account has to be taken of the creation of virtual dipoles by the relative displacement of ion and ion-atmosphere (the Debye-Falkenhagen effect) and also of the fall in dielectric constant brought about by the orientation of solvent dipoles in the strong electrostatic fields of the ions—a phenomenon investigated mathematically by Sack (1926, 1927).

The dielectric constants of aqueous solutions of salts of various valency types have been determined, relative to water, in this laboratory (Dunning and Shutt 1938), and, for each solution, the results were found to conform to an equation of the form

$$D_s - D_0 = A \sqrt{\gamma^*} - D_0 k \gamma^* + D_0 K \gamma^{*2}. \quad (1)$$

$D_s$  is the dielectric constant of the salt solution relative to that of water ( $D_0$ ).  $\gamma^*$  is the equivalence of the solution defined by  $\nu_1 Z_1 \gamma = \nu_2 Z_2 \gamma = \gamma^*$ , where  $\nu_1$  and  $\nu_2$  are the number of ions of valence types  $Z_1$  and  $Z_2$  formed by

the dissociation of one molecule of salt and  $\gamma$  is the molar concentration.  $A$  is the Debye-Falkenhagen term, given by the limiting equation

$$D_{\omega=0} - D_0 = A \sqrt{\gamma^*},$$

where  $D_{\omega=0}$  is the dielectric constant of the solution at very low or zero frequency of alternating electric field and  $A$  is given by

$$A = \frac{1.97 \times 10^6 |Z_1 Z_2| (|Z_1| + |Z_2|)^{\frac{1}{2}}}{2D_0^{\frac{1}{2}} T^{\frac{1}{2}} \left(1 + \frac{1}{q^{\frac{1}{2}}}\right)^2} q^{\frac{1}{2}}, \quad (2)$$

and

$$q = \frac{Z_1 Z_2}{Z_1 + Z_2} \frac{l_1 + l_2}{Z_1 l_2 + Z_2 l_1}. \quad (2a)$$

$l_1$  and  $l_2$  are the mobilities of the ions. The term  $k$  was interpreted in terms of the Sack effect of saturation of solvent dipoles. It was suggested that the factor  $K\gamma^{*2}$  might be explained either through the Bjerrum theory of ion association or by an effect of desaturation of the water dipoles brought about by the overlapping of the individual ionic fields in the more concentrated solutions.

It follows from Sack's calculations of solvent saturation that the radius of the sphere in which orientation of solvent occurs as a result of a central, singly charged ion is of the order of 15 Å. At the maximum concentration used in this work (0.02 M), the ions are separated by a mean distance of 45 Å. It is felt therefore that any desaturation effect of the type suggested above must be very small, and recourse must be had to the other possible explanation of the term  $K\gamma^{*2}$ , and  $K$  may be given the significance of a mass-action constant of ion association. Now  $D_0 K\gamma^{*2}$  is of the dimensions of a dielectric constant multiplied by a concentration. Some modification is required, therefore, in equation (1).  $D_0 K\gamma^{*2}$  should be replaced by  $\chi K\gamma^{*2}$ , where  $\chi$  may be termed the "equivalent rise of dielectric constant" and is numerically equal to the rise in dielectric constant which would result from the addition of one equivalent per litre of ion pairs to the solvent. In solvents of lower dielectric constant than that of water the degree of association of electrolytes might be expected to be of considerable magnitude, and the ionic concentration can no longer with accuracy be put equal to the equivalence of the salt;  $\gamma^*$  must be replaced by  $\gamma^* \alpha^*$ , where  $\alpha^*$  is the true degree of dissociation of the electrolyte. Thus a more rigorous form of equation (1) is given by

$$A \sqrt{(\gamma^* \alpha^*)} - (D_s - D_0) = D_0 k \gamma^* \alpha^* - \chi K \gamma^{*2} \alpha^{*2}. \quad (3)$$

To evaluate the true, thermodynamic association constant, it is necessary to take account of the long range interaction between free ions. This constant is given, for a symmetrical electrolyte, by

$$K_a = \frac{\nu_1 Z_1 (1 - \alpha^*) f^*}{\alpha^{*2} \gamma^{*2} f_+ f_-}, \quad (4)$$

where  $f^*$ ,  $f_+$  and  $f_-$  are the activity coefficients of the ion pairs and the positive and negative ions respectively.

To avoid the almost insuperable difficulty of finding a series of pure, non-reactive solvents of graded dielectric constant, it was decided to obtain the desired variation in dielectric constant by diluting water with dioxan. This liquid is almost inert chemically, is non-polar, and is miscible with water in all proportions, the resultant mixtures differing but little in viscosity and density from water itself. The linearity between dielectric constant and dioxan content (*vide infra*) supported this view that dioxan could be used as a pure diluent. To extend the research to ranges of dielectric constant higher than that of water, a somewhat similar principle was employed. Mixtures of urea and water were adopted as solvents.

To facilitate interpretation of results it was necessary that the electrolyte should be symmetrical as regards valency. For other than binary electrolytes, evaluation of the Debye-Falkenhagen factor  $A$  necessitates a knowledge of the mobilities of the ions in each solvent. As shown by equation (2a) for symmetrical electrolytes  $q$  degenerates to  $\frac{1}{2}$ . Uni-univalent salts affect the dielectric constant of the solvent but little and for them the method proves insensitive; for valencies beyond two, solvolysis becomes considerable. For these reasons the di-divalent salt magnesium sulphate was chosen for extensive investigation and all the figures quoted in this paper refer to that electrolyte.

#### EXPERIMENTAL

The method used for the measurement of dielectric constant was essentially the modification of the Fürth "force" method previously described (Shutt 1934; Shutt and Rogan 1936; Dunning and Shutt 1938). Some improvement has been effected both in the general form of the cell and in the structure of the suspended system.

In the earlier form of apparatus the alternating field was applied through two parallel, platinum plates clamped to the open ends of a quartz cylindrical vessel and, to maintain insulation between the contents of the cell and the surrounding thermostat, all had to be coated with wax. This wax insulation,



however carefully blended and applied, was not long-lived. The inconvenience and delay occasioned by the periodic dismantling, resetting and standardization of the instrument sharply emphasized the need for a totally enclosed glass cell. The solution of the problem of obtaining satisfactory seals between heavy electric leads and pyrex glass or quartz, which materials alone could be fitted with the necessary large plane window, was not at first apparent. One partially successful apparatus was described by Carr

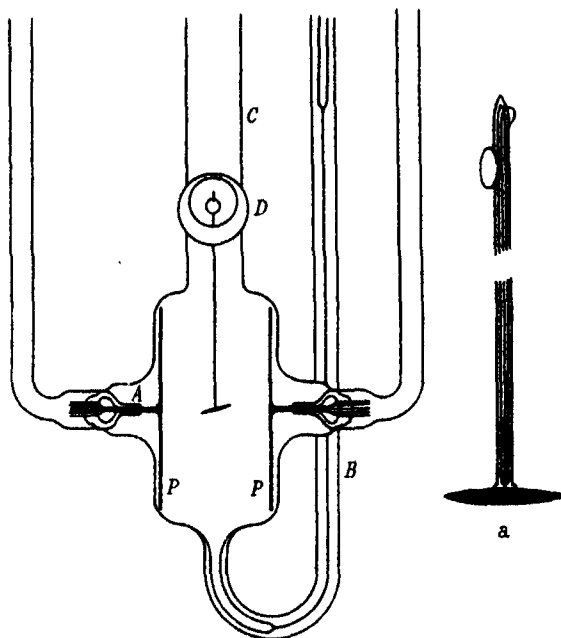


FIGURE 1

and Shutt (1939). Pyrex glass was used and through this were sealed heavy tungsten rods, which were gold-soldered to platinum rods carrying the field plates. The slow attack of the gold joint by the chlorine liberated during each platinization of the plates was a serious disadvantage in this type of cell. The most successful form of apparatus, and the one used for the bulk of this research, is shown diagrammatically in figure 1. The significant parts of this vessel lay in the pinch seal, in pyrex, closing on several fine platinum wires, and the glass bridge between these wires and the rough tubular seal supporting the heavy platinum rods which carried, at one end, the platinum plates and, at the other, the brush of fine wires. These details are shown at A. A pyrex tube, sealed over this assembly, permitted good

electrical contact with the fine wires through the usual mercury column. Other details—the filling tube *B*, the vertical chimney *C*, carrying the torsion head, and the plane window *D*—were essentially the same as in the quartz apparatus previously described (Shutt 1934; Shutt and Rogan 1936). A series of coarse teeth, cut in the edge of the plates *PP*, permitted a certain amount of support by the cell walls, and, at the same time, allowed free drainage of the space behind the plates.

In previous publications constant emphasis has been laid upon the necessity for a particular type of platinization upon the surface of the suspended ellipsoid. Satisfaction in this respect has been difficult to attain and the frequency of failure was disconcerting. It was felt that the main cause of the poor reproducibility of surface lay in an inherent uncertainty as to the precise current density at which the platinum black had been laid down. It was decided therefore to redesign the suspension, so that electrical contact with the ellipsoid could be made outside the platinizing solution, and to make a more detailed study of the conditions for depositing the platinum black.

The suspended system adopted is shown in figure 1*a*. A platinum-iridium wire, gold-soldered through a minor axis of the ellipsoid, was welded to a fine platinum wire which was threaded through a fine glass capillary tube. This tube was sealed, at its lower end, to the platinum-iridium wire in such a way as to involve the surface of the ellipsoid, as indicated in the diagram. The upper end of the fine platinum wire was sealed through the top of the capillary and bent into the form of a hook, with which good electrical contact could be made on moistening with potassium chloride solution. The stainless steel mirror and quartz fibre suspension were as previously described.

The method of platinization finally adopted was based on the work of Grinnell Jones and Bollinger (1935). The first desideratum was that the basic platinum surface should be brought, as far as possible, to a standard state. Old platinum black was removed by stirring in wet sand; the ellipsoid was then polished by brisk agitation in dry sand until all visual irregularities had been removed; a thorough cleaning with concentrated nitric acid and distilled water was followed by immediate platinization. The electrolyte was 0.025*N* hydrochloric acid containing 0.3 % platinic chloride and 0.025 % lead acetate. The quality of the deposit was found to be very sensitive to the concentration of lead ion and this tended to vary somewhat, with time, possibly owing to a slow hydrolysis; it was therefore desirable to use freshly prepared solutions. The first layers seem to be the main determinant of the quality of the final deposit and it was found advisable

to use a very low current density for the initial stage of platinization. For an ellipsoid 8 mm. in length and about 0.9 mm. in maximum thickness, a current of 0.4 mA was applied for 15 min., with reversal of the current every 10 sec. After that time the current could be raised to 1.0 mA and the deposition continued for a further 15–30 min. During the whole process of platinization, the ellipsoid was rotated from time to time and, between rotations, was kept symmetrical to the other electrode to ensure uniform treatment of the whole surface. To remove occluded platinizing solution, the ellipsoid was cleaned by electrolysis in 2.0 N sulphuric acid, using 5 mA for 10 min., again with reversal of the current every 10 sec. The commutator controlling the reversal of the current was finally stopped whilst the ellipsoid was evolving oxygen, and this evolution was allowed to continue for 30 sec. before opening the electrolysis circuit. This procedure was adopted, since the presence of hydrogen or reducing agents had been found fatal to the behaviour of the ellipsoid. The platinized surface prepared in this manner had the appearance of smooth black velvet.

Although it has been established that the success of the apparatus depends mainly upon the condition of the ellipsoid surface, the plates (*PP*) play a minor but definite part. These were platinized in the same solution with a current of 0.5 amp. reversed every 10 sec. and continued for 10 min. Subsequent cleaning was by electrolysis in 2 N sulphuric acid, at the same current density for 5 min.

Finally, both plates and ellipsoid were thoroughly washed with water for 2 or 3 days before the apparatus was tested.

The smallness of the differences in dielectric constant to be measured necessitated very stringent tests of the apparatus. These were normally three in number. The first involved proof that, when the cell was repeatedly filled with water, a constant displacement of the ellipsoid was obtained on application of a fixed field. It had already been observed (Dunning and Shutt 1938) that these "water throws" were always much too high, relative to the throws obtained in very dilute electrolyte, and this effect had tentatively been ascribed to a change in effective dimensions of the platinized surface when electrolytes were added to the pure water.\* This effect eluded Shutt and Rogan (1936) in their earlier work, and may go far towards explaining the difference between their results and those since obtained with the improved methods. Throughout the work which follows the value

\* The authors have been able to show by work (as yet unpublished) at high frequencies with a polished ellipsoid that this effect is dependent upon the properties of platinum black. Under these conditions the water throw is identical with that of an extremely dilute electrolyte.

obtained by extrapolation to infinite dilution of the results obtained in electrolyte is taken as the true throw for pure water. Nevertheless, the constancy of the water throws, both with time and with repeated refilling of the cell, was an essential criterion for accurate operation, since experience had shown that poisoning of the ellipsoid was always first manifested by erratic water throws.

The second test was for absence of polarization, as previously described. Finally, the dielectric constant curve (against concentration) for KCl was reproduced in its entirety. Uni-univalent salts have little effect upon the dielectric constant of water, and the reproduction of the form of the curve was an extremely delicate test of the apparatus.

In some experiments the solvent action of dioxan upon the anchorages of the quartz fibre and the mirror was overcome by coating the Golaz and shellac cements with the mechanically weaker, but chemically more resistant, paraffin wax. For the majority of the experiments, however, the apparatus was filled by displacing water, from below, by the slightly denser dioxan solution to a level below the shellac attachment of the mirror. To avoid mixture of the two liquids the rate of ingress of the solution was limited by the insertion of a loose glass plug at the top of the filling tube (*B* of figure 1). An added advantage of this mode of working lay in the decreased volume of dioxan required for each measurement.

As previously observed, measurements upon comparatively well-conducting electrolytes necessitate the use of the ballistic method of taking readings. To correct for the variation in viscosity, from one solvent to another, the following procedure was adopted: The dielectric constant of each dioxan-water mixture and each urea solution was determined relative to water (or  $N/10,000$  KCl), using the static displacement method, then the dielectric constant of each solution of electrolyte was compared with that of the respective solvent by the ballistic throw method. This amounts to the assumption that the viscosity of the dioxan-water mixture or urea solution was unaltered by the addition of small quantities of electrolyte.

The solubility of air in dioxan is much greater than in water and, in making the mixture, supersaturated solutions of air were formed. These tended to produce bubbles of gas on the active surface of platinum. Evacuation of the mixture proved unsatisfactory: it spoilt the electrolytic reversibility of the platinum black. The fault was entirely eliminated by equilibrating the solution with air by continued shaking of the liquid at  $20^{\circ}\text{C}$  until all signs of evolution of bubbles of gas had ceased.

All the values of dielectric constant recorded in this paper were measured at  $20 \pm 0.02^{\circ}\text{C}$  and at an alternating-current frequency of 1000 cyc./sec.

The field strength was adjusted to give a throw of about 10 cm., measured optically on a scale about 1.5 m. from the apparatus. Although the required voltage varied with the dimensions of the ellipsoid and the torsional elasticity of the quartz fibre in use, these magnitudes were adjusted to keep the voltage across the cell within the limits of 15–20 r.m.s. V.

#### PURIFICATION OF MATERIALS

The high cost of pure dioxan necessitated its recovery from the mixed liquid used in previous measurements. Electrolyte was eliminated by distillation. The water, amounting to about 50 % of the distillate, was removed by adding solid caustic soda, which is practically insoluble in dioxan, until the liquid separated into two layers. The upper layer contained so little water that it could be separated off and treated immediately with metallic sodium. After two fractionations the purified dioxan, amounting to about 80 % of that originally present in the dilute electrolyte solution, possessed the following physical characteristics: b.p. 101–101.5° C; m.p. 11.1° C;  $d_{20} = 1.0343$ ; refractive index ( $n_D^{20}$ ) = 1.4224.

Commercial urea, which has a comparatively high conductivity, was recrystallized from aqueous solution, saturated at 60° C, and dried over concentrated sulphuric acid, *in vacuo*, for several days. The product exhibited the necessary low conductivity, and samples prepared from various commercial batches yielded solutions possessing satisfactorily reproducible dielectric constants.

#### EXPERIMENTAL RESULTS

##### *Dielectric constants of the solvents*

These were determined under the same conditions as those to be used for the electrolyte solutions. The results, shown in figure 2, were determined, some with the quartz apparatus (circles) and a few others (dots) with the pyrex apparatus.

As previously observed by several workers, the dielectric constants of urea solutions vary linearly with the concentration of urea. The slope of the straight line,  $\Delta D/\Delta C$  is 3.2 units of dielectric constant per gram-molecule per litre—a figure identical with that obtained by Harrington (1916).

The dielectric constant of a dioxan-water mixture is also a linear function of concentration, but the line, followed experimentally as far as 75 % (by volume) of dioxan, does not extrapolate to the dielectric constant of pure dioxan ( $D = 2.35$ ). This graph is practically identical with that obtained by

Akerlöf and Short (1936) using a resonance method at 150 m., when allowance is made for their having plotted percentage by weight of dioxan and used 80.37, instead of 80.0, as the dielectric constant of water at 20° C. The fact that the linear, experimental part of the line does not extrapolate to 2.35, might be ascribed to some slight water-dioxan interaction. Geddes

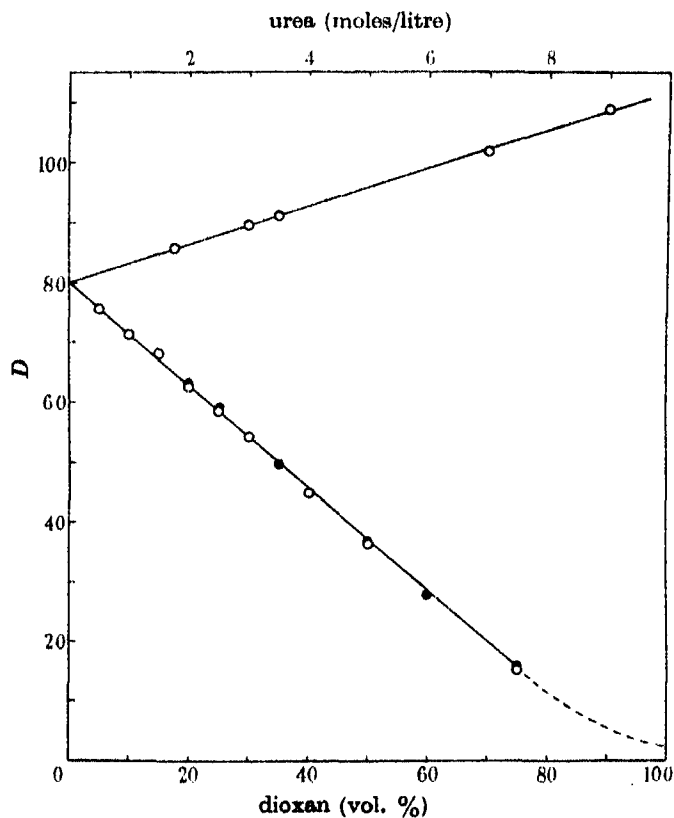


FIGURE 2

(1933) has deduced the occurrence of such interaction from viscosity data. This effect, however, is so slight as not to affect the linearity of most of the line and may be ignored over the range of concentration used in this work.

Although not the total possible range of dielectric constant obtainable with the system urea-water-dioxan, considerations of convenience and accuracy of measurement limited the work to solvents between 9 M urea and 50 % dioxan.

*Dielectric constants of magnesium sulphate solutions*

The pertinent experimental results are given in table 1. These figures are chosen from the large number of experimental results which had to be measured to construct a curve of  $D_s$  against concentration of electrolyte for each solvent used. One such curve, that for 50 % dioxan, is given in figure 3. In this figure, the symbols  $Q$  and  $P$  refer to measurements made with the quartz and pyrex glass apparatus, and  $F$  and  $D$  to the method of

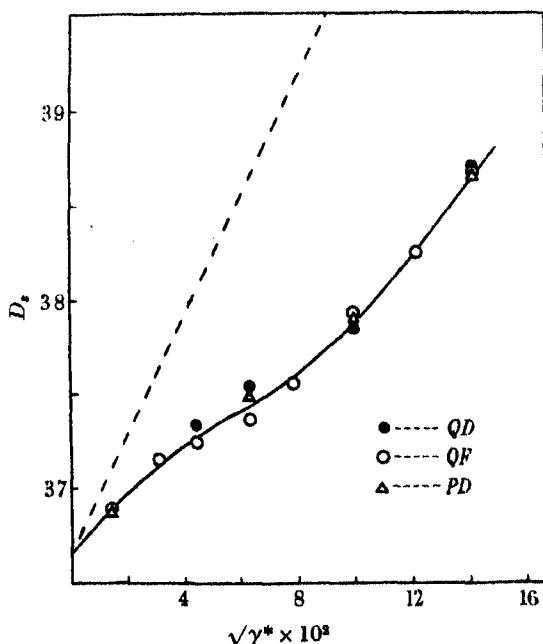


FIGURE 3

completely filling the cells and of filling by displacement of water, respectively. The general order of reproducibility of the dielectric constants and the freedom of the results from any idiosyncrasy of apparatus are indicated by the deviation of individual points from the smoothed curve. The dotted line represents the theoretical Debye-Falkenhagen slope. In table 2 are given the values of the Debye-Falkenhagen term  $A$  for a bi-bivalent salt ( $\text{MgSO}_4$ ) in each of the solvents, calculated according to equation (2).

All the dielectric constant results gave curves of the same characteristic shape. This is indicated in figure 4, where they are plotted together as percentage rise of dielectric constant against the square root of equivalent

TABLE 1

| Solvent     | $D_s$               |        |        |        |        |        |
|-------------|---------------------|--------|--------|--------|--------|--------|
|             | $\gamma^* = 0.0002$ | 0.002  | 0.004  | 0.006  | 0.01   | 0.02   |
| Water       | 80.22               | 80.57  | 80.72  | 80.85  | 80.97  | 81.46  |
| 25 % dioxan | 58.70               | 59.03  | 59.16  | 59.32  | 59.53  | 60.23  |
| 35 % dioxan | 49.82               | 50.16  | 50.31  | —      | 50.70  | 51.38  |
| 50 % dioxan | 36.88               | 37.30  | 37.45  | 37.55  | 37.89  | 38.66  |
| 3M urea     | 89.85               | 90.20  | 90.33  | 90.50† | 90.61  | 91.05  |
| 9M urea     | 109.1               | 109.45 | 109.51 | 109.59 | 109.79 | 110.20 |

†  $\gamma^* = 0.0075$ .

TABLE 2

| Solvent | 50 %<br>dioxan | 35 %<br>dioxan | 25 %<br>dioxan | Water | 3M urea | 9M urea |
|---------|----------------|----------------|----------------|-------|---------|---------|
| $D_0$   | 36.65          | 49.60          | 58.53          | 80.00 | 89.65   | 108.84  |
| $A$     | 31.49          | 27.06          | 24.92          | 21.31 | 20.13   | 18.27   |

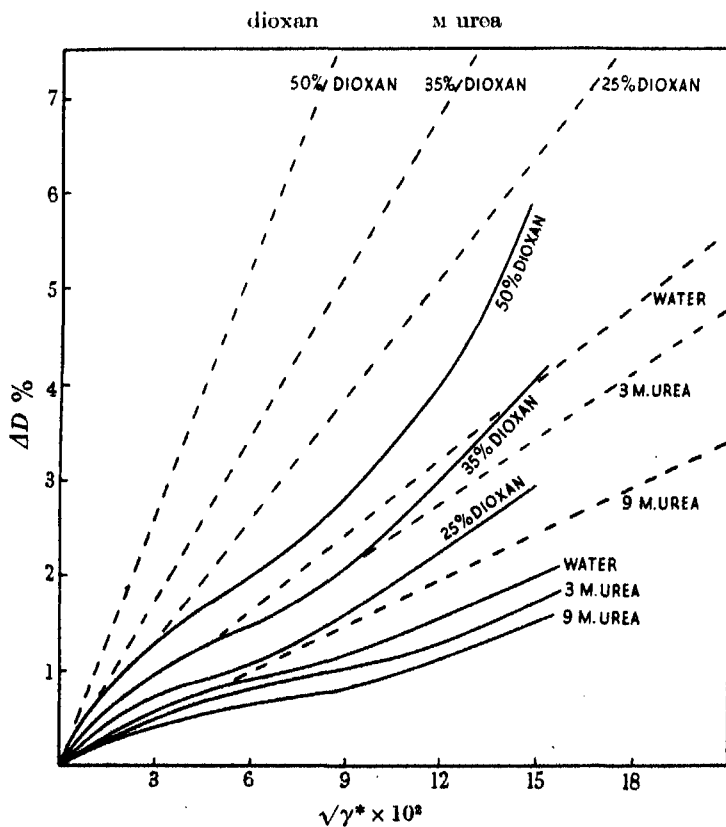


FIGURE 4



concentration of electrolyte. It will be noted that the effects due to added electrolyte increase progressively as the dielectric constants of the solvents fall.

*Calculation of  $K_a$  and  $k$ .* From equations (3) and (4), for a bi-bivalent electrolyte,

$$A \left\{ \frac{\left(1 + 2K_a \frac{f_+ f_-}{f^*} \gamma^*\right)^{\frac{1}{2}} - 1}{K_a \frac{f_+ f_-}{f^*}} \right\} - (D_s - D_0) \\ = \frac{\left(1 + 2K_a \frac{f_+ f_-}{f^*} \gamma^*\right)^{\frac{1}{2}} - 1}{2K_a \frac{f_+ f_-}{f^*}} \left[ 2D_0 k - \chi \left\{ \left(1 + 2K_a \frac{f_+ f_-}{f^*} \gamma^*\right)^{\frac{1}{2}} - 1 \right\} \right]. \quad (5)$$

As shown by Randall and Failey (1927),  $f^*$ , the activity coefficient of the associated ion pairs, may be assumed to be unity, and, for the binary electrolyte employed,  $f_+ f_- = f_{\pm}^2$ . For more concentrated solutions, Debye gives,

$$-\log f_{\pm}^2 = \frac{e^2}{D_0 k T} \frac{\Sigma \nu_1 Z_1^2}{\Sigma \nu_1} \left( \frac{4\pi e^2 \Sigma n_1 Z_1^2}{D_0 k T} \right)^{\frac{1}{2}} - 4\pi a \left( \frac{e^2 \Sigma \nu_1 Z_1^2}{D_0 k T \Sigma \nu_1} \right)^2 \Sigma n_1 Z_1^2. \quad (6)$$

From activity data for magnesium sulphate solutions, Bjerrum (1926) has calculated a value of  $4.2 \text{ \AA}$  for the mean ionic diameter  $a$ . Interpolation of this value in equation (6) permits of evaluation of  $f_{\pm}$ .

The unknowns  $\chi$ ,  $K$  and  $k$  of equation (5) could be calculated from the shape of the curves, but laborious mathematical treatment would be required. It seemed preferable, therefore, to evaluate one of the terms from external evidence.

The most reliable values for association constants are probably those obtained from conductivity measurements in aqueous solvent, where much experimental work has been carried out and due allowance for solvolysis and other complicating effects has been possible. Davies (1927) obtained the value of 0.0061 for  $1/K_a$  for aqueous magnesium sulphate at  $18^\circ \text{C}$ . For the purpose of this work  $K_a = 160$  was taken as a sufficiently accurate value of the association constant. Substitution of this figure for  $K_a$  and the experimental values of  $D_s$ , for aqueous solution, and  $\gamma^*$  in equation (5) led to the mean values of 150 and 1.9 for  $\chi$  and  $k$  respectively.

$\chi$  has been defined as the rise in dielectric constant per gram-equivalent of associated ion pairs. As such it should be a direct function of the distance apart of the centres of the two ions. Fuoss and Kraus (1934) point out that ion pairs do not consist of ions at any distance up to the Bjerrum critical

distance,  $q_0$ , from one another, but are either in "contact" or at distances much greater than  $q_0$ , save for a negligible number in transition states. Thus the distance between the opposite charges in ion pairs may be put as the ionic diameter ( $a = 4.2$  Å). There is much experimental evidence that  $a$  is independent of the dielectric constant of the solvent. For instance, Fuoss and Krauss (1933*b*) found that the degrees of association of tetraisoamylammonium nitrate, in dioxan-water mixtures, of dielectric constants ranging from 2.38 to 38, were in agreement with those calculated from the Bjerrum theory, using a practically constant value of  $a$  (6.01–6.70 Å); Linch and La Mer (1938), studying the thermodynamics of acetic acid in dioxan-water mixtures, found that  $a$  remained constant at 2.6 Å over a dielectric constant range of 21–78; Harned and his co-workers (1939) obtained a value of 5.0–5.6 Å for hydrochloric acid in dioxan-water mixtures varying in concentration of dioxan from 20 to 70 %, whilst Shedlovsky and MacInnes (1936), applying the Debye-Hückel activity theory to the aqueous acid, found a value of 5.6 Å for  $a$ .

Associated ion pairs are zwitterionic in character, and Carr and Shutt (1939) have shown, in confirmation of a hypothesis of Wyman (1939), that for simple zwitterions, the equivalent rise in dielectric constant, as a close first approximation, is directly proportional to the dipole length of the zwitterion. On this basis,  $\chi$  should be independent of the solvent.

Perhaps one further piece of evidence for the constancy of  $\chi$  may be quoted. It has been shown (Carr and Shutt 1939) that for glycine (an undoubted zwitterion) the molecular rise of dielectric constant is the same in water, in dioxan-water mixtures and in an aqueous solvent whose dielectric constant had already been raised by the presence of another zwitterion, alanine.

Accepting, then, the constancy of  $\chi$ , the values of  $K_a f_{\pm}^2$  and  $k$  were calculated, for any one solvent, by substituting the various experimental values of  $(D_s - D_0)$  for different values of  $\gamma^*$ , in equation (5), and solving simultaneously. The results for  $K_a f_{\pm}^2$  showed, in each solvent, a definite trend with concentration. This was to be expected since  $f_{\pm}^2$  varies with changing concentration,  $\gamma^*$ . If, however, it could be assumed that the diameter of the free ions remained constant in all solvents, then the Debye equation (6) might be used to calculate  $f_{\pm}$  for each concentration and  $K_a$  could be evaluated. The values of  $K_a$  and  $k$  obtained by this method were constant to within about 10 % over the whole range of concentration studied in each solvent. They are given in table 3.

## DISCUSSION OF RESULTS

*Variation of  $K_a$  with  $D_0$* 

The values of  $K_a$  presented in table 3 show that the degree of association into ion pairs decreases as the dielectric constant rises and qualitatively conforms to the physical picture involved by the Bjerrum hypothesis. Quantitatively, however, there are certain anomalies.

TABLE 3

| $D_0$  | $k$  | $K_a$ | $\log K_a$ | $\log K_a$ (calc.) | $a \times 10^8$ | $D_0 k$ |
|--------|------|-------|------------|--------------------|-----------------|---------|
| 36.65  | 10.9 | 7100  | 3.85       | 4.05               | 5.8             | 400     |
| 49.60  | 7.2  | 2700  | 3.43       | 3.25               | 5.45            | 357     |
| 58.53  | 4.7  | 1100  | 3.04       | 2.85               | 5.2             | 275     |
| 80.00  | 1.9  | 160   | 2.20       | 2.32               | 4.55            | 157     |
| 89.65  | 1.6  | 170   | 2.23       | 2.13               | 4.35            | 143     |
| 108.84 | 1.3  | 135   | 2.13       | 2.02               | 3.7             | 141     |

The values of  $K_a$  seem rather high in the urea solutions; they do not fall off so rapidly with dielectric constants rising above that of water as is to be expected from the behaviour of the electrolyte in solvents having dielectric constants below 80. This effect may tentatively be explained in terms of an essential change in the permanent hydration sheath of the ions in passing from dioxan-water mixtures to urea solutions. In dioxan-water mixtures, the dipolar water alone is attracted to the ions and forms the permanent hydration sheath, but in urea solutions there are stronger dipoles than water, the urea molecules, and these are more strongly attracted to the ions. This increased solvent attraction tends to drive the ions apart and the value of  $a$ , satisfactory in dioxan-water mixtures, may be too low in urea solutions. Thus the value of  $\chi$  used in the calculation of  $K_a$  for urea solutions may be too small and therefore give falsely high values of  $K_a$ . Furthermore, if the salting out in the higher concentrations of the dioxan-water mixtures is not 100 % efficient, the electrostatic forces between the oppositely charged ions will be increased and the  $\chi$  values given will be too large and the calculated values of  $K_a$  too low.

The Bjerrum equation for the degree of association of a bi-bivalent electrolyte may be written in the form

$$K_a = \frac{4\pi N}{1000} \left( \frac{4e^2}{D_0 kT} \right) Q(b), \quad (7)$$

where  $N$  is the Avogadro number and  $Q(b)$  is given by

$$Q(b) = \int_2^b e^{uy} y^{-4} dy,$$

where  $y = \frac{4e^2}{rD_0kT}$  and  $b = \frac{4e^2}{aD_0kT}$ .  $r$  is the distance between the two ions considered and  $a$  is the diameter of the ion pair. With the values of  $Q(b)$  tabulated by Bjerrum for  $b = 1$  to  $b = 15$ ,  $K_a$  can be calculated for values of  $D_0$ . No single value of  $a$ , substituted in equation (7), gives values of  $K_a$  identical with those obtained experimentally. If, however, the values of the ion pair diameter be assumed to fall linearly from  $a = 5.8$  Å at  $D_0 = 36.65$  to  $a = 3.7$  Å at  $D_0 = 108.85$ , the calculated values of the association constant fall on the continuous line shown in figure 5. The experimental values

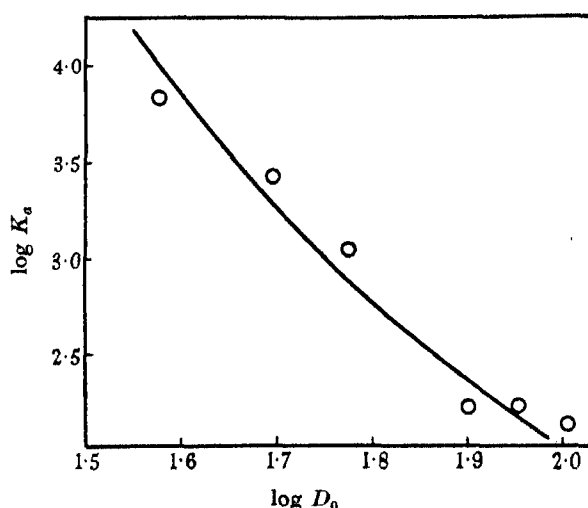


FIGURE 5

of  $\log K_a$  are shown as circles on this graph, and, within experimental error, may be considered as identical with the calculated values.

In view of the relative smallness of the experimental  $(D_s - D_0)$  and the possible inaccuracies in the equations used to calculate  $K_a$  from these results, the agreement between the constant  $a = 4.2$  Å, obtained by Bjerrum, and the range  $a = 3.7$  to  $5.8$  Å, demanded by the dielectric constants, is considered, on the whole, both a satisfactory confirmation of the Bjerrum hypothesis and a proof of the inherent soundness of the F  rth low-frequency method for measuring the dielectric constants of solutions of electrolytes.

If data were available for applying a correction for the two possible effects mentioned above—the change in the nature of the hydration sheath in the

urea solutions, and a lack of complete salting out in the dioxan-water mixtures—the application of such a correction would tend to diminish the discrepancy in the  $a$  values; a more constant value of  $a$  would reproduce all the experimental results.

*Variation of  $k$  with  $D_0$*

As regards the degree of the dipole saturation postulated by Sack, the figures presented in table 3 indicate a marked rise in the value of  $k$  with diminishing dielectric constant of the solvent. Before these values can be accepted as a true measure of the degree of saturation by single ions, two effects—disregarded in the above calculations—must be considered as possible sources of decrease in dielectric constant.

There is, first, the possible formation of associated ion triplets. Fuoss (1935) has shown that the potential energy of a single ion in contact with an ion pair is, in the ideal case, one-half the potential energy of the ion pair. Hence, in solvents of low dielectric constant, and in solutions of higher concentration, triple ions of the form  $\begin{pmatrix} + & - & + \\ + & - & + \end{pmatrix}$  and  $\begin{pmatrix} - & + & - \\ - & + & - \end{pmatrix}$  may arise.

Kraus (1934) points out that, if the electrolyte is present largely as ion pairs, the triple ions will be formed at the expense of the ion pairs, while the concentration of free ions will remain practically unchanged. Thus the nett effect of formation of triple ions will be to increase the number of free charges in solution and therefore to increase the dipole saturation. By a treatment similar to that used by Bjerrum for the formation of ion pairs, Fuoss and Kraus (1933*b*) have derived an expression for evaluation of the mass action constant for triple ion formation. This expression has been applied to the most favourable condition used in this work for the formation of ion triplets. Putting  $a'$ , the diameter of the triple ion, as 6 Å and using the Debye expression for evaluation of the activity coefficient, it was found that, for 0.02 M magnesium sulphate, in 50 % dioxan-water mixture, the equivalent concentration of triple ion was only  $4 \times 10^{-5}$ , a vanishingly small value. It may therefore be concluded that dipole saturation due to triple ions is negligible for all the solutions examined in this work.

A second question is the possibility of dipole saturation by ion pairs. The distribution of the field around the pair would seem to preclude any appreciable saturation; in even the most favourable direction, along the line of the centres of the charges, the field strength must decay as the cube of the distance. Moreover, it has been shown experimentally (Carr and Shutt 1939) that, for zwitterions of a length comparable with that of the ion pairs, there is no nett electrical effect set up by interaction between doublet and

solvent dipoles. It is considered therefore that the observed saturation phenomena are due, almost entirely, to the free ions present in the solution.

In view of the extremely low dielectric constant of dioxan, the dielectric constant of each of the solvents may be said to be due solely to the water dipoles present (ignoring the difference in moment between the urea and water dipoles).  $D_0$  may be considered directly proportional to the number of water dipoles capable of rotation in an external field. Thus the fall in dielectric constant,  $D_0 - D_s$ , on the addition of ions, becomes a direct measure of the number of water molecules immobilized by the ionic fields.

If, as a first approximation, each ion be pictured as surrounded by a water solvation sphere of constant size, in each solvent, then the water immobilized for the same concentration of ion, should be the same in every solvent, i.e.  $(D_0 - D_s)/\gamma^*$  should be a constant. According to Sack's theory

$$k = \frac{D_0 - D_s}{D_0 \gamma^*}.$$

Therefore  $kD_0$  should be a constant, independent of  $D_0$ . The values of  $kD_0$  given in table 3 are by no means constant, but rise with decreasing value of  $D_0$ . This first approximation must, therefore, be abandoned.

Sack does not regard the solvate shell as a rigid structure of orientated dipoles sharply defined from the rest of the solvent, but points out that the influence of the ion must extend radially over a considerable distance, approaching zero effect asymptotically (at about 15 Å for a univalent ion in water). The dielectric constant decreases from the macroscopic value of the electrolyte to the optical value of the solvent as the distance,  $r$ , from the ion decreases. Integration below the curve of dielectric constant against  $r$  leads to the conclusion that, although the change in dielectric constant, in regions remote from the ion, is small, the volumes of these regions are so much larger than those near the ion that they give the principal part of the saturation effect. In these outer parts of the solvation sheath, where the water dipoles are loosely held, the salting-out effect may well be imperfect and dioxan molecules may be present to an extent governed by their concentration in the bulk electrolyte. The resultant local lowering of dielectric constant would lead to a further extension of the field of influence of the ion. On this basis  $kD_0$  may well increase with increasing dioxan content of the mixture. It is, however, impossible to give any quantitative estimate of this effect.

## GENERAL CONCLUSION

It is felt that the final conclusion to be drawn from the results of these experiments upon the dielectric properties of solutions of salts is that the general behaviour of electrolytes in solution can best be described by consideration of the simple coulombic forces involved. It cannot be said that there is any evidence of need for invoking a specific influence due to the chemical nature of the solvents.

## SUMMARY

The orientation (saturation) of solvent dipoles around ionic charges and the phenomena of ion association are considered in relation to their bearings upon the dielectric constants of solutions of electrolytes.

A modified "force" method for the determination, at low frequency, of the dielectric constants of conducting liquids is described.

Figures are given for the dielectric constants of dioxan-water mixtures (from 0 to 75 % dioxan) and of aqueous solutions of urea (to 9 M urea).

The dielectric constants of solutions of magnesium sulphate in these aqueous solvents have been determined. The Bjerrum association constants ( $K_a$ ) and the Sack saturation constants ( $k$ ) have been calculated from the results.

The variation of  $K_a$  and  $k$ , with dielectric constant of solvent, is discussed.

## REFERENCES

- Akerlöf and Short 1936 *J. Amer. Chem. Soc.* **58**, 1241.  
Bjerrum 1926 *D. Kgl. Danske Videnskab. Selskab. Math-fys. Medd.* **7**, no. 9.  
Carr and Shutt 1939 *Trans. Faraday Soc.* **35**, 579.  
Davies 1927 *Trans. Faraday Soc.* **23**, 351.  
Debye 1923 *Phys. Z.* **24**, 185.  
Dunning and Shutt 1938 *Trans. Faraday Soc.* **34**, 468.  
Fuoss 1935 *Chem. Rev.* **17**, 27.  
Fuoss and Kraus 1933a *J. Amer. Chem. Soc.* **55**, 476, 1019.  
— — 1933b *J. Amer. Chem. Soc.* **55**, 2387.  
— — 1934 *J. Chem. Phys.* **2**, 386.  
Geddes 1933 *J. Amer. Chem. Soc.* **55**, 4832.  
Harned and co-workers 1939 *J. Amer. Chem. Soc.* **61**, 51.  
Harrington 1916 *Phys. Rev.* **8**, 581.  
Jones and Bollinger 1935 *J. Amer. Chem. Soc.* **57**, 281.  
Kraus 1934 *Trans. Amer. Elect. Soc.* **66**, 183.  
Linch and La Mer 1938 *J. Amer. Chem. Soc.* **60**, 1259.  
Martin 1928 *J. Chem. Soc.* p. 3270.  
Onsager 1927 *Phys. Z.* **28**, 277.  
Randall and Failey 1927 *Chem. Rev.* **4**, 271.

- Sack 1926 *Phys. Z.* **27**, 206.  
 — 1927 *Phys. Z.* **28**, 199.  
 Shedlovsky and MacInnes 1936 *J. Amer. Chem. Soc.* **58**, 1970.  
 Shutt 1934 *Trans. Faraday Soc.* **30**, 893.  
 Shutt and Rogan 1936 *Proc. Roy. Soc. A*, **157**, 359.  
 Swift 1938 *J. Amer. Chem. Soc.* **60**, 2611.  
 Walden 1925 *Z. Phys. Chem. A*, **116**, 228.  
 Wyman 1939 *J. Phys. Chem.* **43**, 143.

## The behaviour of polar molecules in solid paraffin wax

BY D. R. PELMORE AND E. L. SIMONS  
*National Physical Laboratory*

(Communicated by E. V. Appleton, F.R.S.—Received 1 February 1940)

A paper by R. W. Sillars of the National Physical Laboratory was published under the above title in 1938. Sillars showed how the relaxation time of long-chain esters embedded in a paraffin wax medium depended upon the chain length of the ester. It is well known that many properties of long-chain compounds alternate according as the number of carbon atoms is odd or even. Accordingly, Sillars was careful to use only esters with an even number of carbon atoms in order to reduce the number of possible variables affecting his investigations. He hoped the esters with an odd number would be examined later, and accordingly the work described in this paper was undertaken for the purpose of filling in an obvious gap in Sillars's experiments and to be complementary to them.

The ester amyl stearate (containing 23 carbon atoms) was mixed with the same paraffin wax (setting point 57, 60° C) used by Sillars, the concentration being 4.9 %. The loss angle,  $\tan \delta$ , was measured as a function of temperature at two frequencies (3.12 and 0.513 Mc./sec.) by the same method and in the same apparatus that Sillars used (1938). The results of the experiments may be summarized by the following table:

| Frequency<br>Mc./sec. | $\log_{10} f$ | $(\tan \delta)_{\max.}$<br>% | Temp. for<br>max. $\tan \delta$<br>( $T_{\max.}$ )<br>°C | $T_{\max.}$<br>interpolated<br>from Sillars<br>(figures 6, 9)<br>°C |
|-----------------------|---------------|------------------------------|--|---|
| 3.12                  | 6.5           | 0.695                        | +7.5   | +10   |
| 0.512                 | 5.71          | 0.75                         | -8   | -8  |



It may be seen from this that the observed values of  $T_{\max.}$  are very close to those interpolated from the series of even esters and, at least for amyl stearate, there is no contrast between the behaviour of an odd ester and its two even neighbours. Amyl stearate was chosen because its length was in the range where Sillars had shown that  $T_{\max.}$  was sensitive to chain length, and accordingly any marked alternation effect was likely to be pronounced. Since no unusual behaviour was observed, it was felt that the time and labour involved in further experiments with other odd esters was scarcely justifiable at present.

The authors are indebted to Dr E. B. Moullin for his help and interest in the work which was carried out in the Engineering Laboratory, Oxford, under his direction; and to the Department of Scientific and Industrial Research for grants.

#### REFERENCE

Sillars, R. W. 1938 *Proc. Roy. Soc. A*, **169**, 66.

---

## The thermal explosion of diethyl peroxide

BY E. J. HARRIS

*Beit Scientific Research Fellow, Department of Chemical Technology,  
Imperial College, London*

*(Communicated by A. C. G. Egerton, Sec.R.S.—*

*Received 12 February 1940)*

In a previous paper (Harris and Egerton 1938), the explosion of diethyl peroxide has been studied, and the limit of pressure at various temperatures at which the transition from unimolecular to explosive reaction takes place has been determined in various vessels. In the former work the influence of gases of high conductivity such as helium was not found to be as great in raising the critical pressure as might be expected, but apart from this it has been possible to fit both the older and a fresh series of results to the equations derived for a purely thermal explosion. The behaviour of the peroxide is compared with that of other compounds which show a similar transition to the explosive mode of decomposition, e.g. azomethane and ethyl azide.

# EXPERIMENTAL

The apparatus, consisting of a filling reservoir, fitted with a manometer, and a decomposition vessel heated in a vapour bath, has been illustrated previously (Harris and Egerton 1938, figure 1). The explosion was observed visually, when necessary in a darkened room.

## RESULTS

### *Cylindrical vessels*

| Temp. °C      | mm. Hg     | Temp. °C       | mm. Hg    | Temp. °C       | mm. Hg    |
|---------------|------------|----------------|-----------|----------------|-----------|
| Diam. 4.2 cm. |            | Diam. 3.11 cm. |           | Diam. 1.11 cm. |           |
| 172.5         | 39.7-39.3  | 182            | 42.2-42.0 | 204            | 57.4-56.7 |
| 183           | 21.9-21.6  | 189            | 26.8-26.4 | 216            | 32.3-31.8 |
| 184.5         | 20.0-19.8  | 190.7          | 23.5-23.1 | 234            | 14.1-13.7 |
| 187           | 16.9-16.85 | 202.5          | 12.3-12.0 |                |           |
| 193           | 11.9-11.7  |                |           | Diam. 0.84 cm. |           |
| 200           | 7.9- 7.5   | Diam. 2.0 cm.  |           | 204            | 84.6-83.7 |
| 201.8         | 7.6- 7.5   | 189.6          | 47.8-47.0 | 207.2          | 69.5-69.0 |
| 205           | 5.8- 5.8   | 195.5          | 35.1-34.7 | 229.4          | 26.4-26.0 |
| 210           | 5.4- 4.9   | 200.9          | 24.5-24.3 |                |           |
| 227           | 2.5- 2.4   | 201.8          | 24.0-23.8 |                |           |
|               |            | 206.3          | 17.2-17.0 |                |           |

### *Spherical vessels*

| Temp. °C       | mm. Hg     | Temp. °C       | mm. Hg      |
|----------------|------------|----------------|-------------|
| Diam. 4.32 cm. |            | Diam. 2.26 cm. |             |
| 178.4          | 43.6-43.0  | 184            | 103.5-102.5 |
| 184            | 29.8-29.5  | 194.8          | 56.2- 55.3  |
| 190.5          | 21.0-20.4  | 204.5          | 32.4- 31.7  |
| 194.8          | 16.4-15.9  | 210.5          | 23.2- 22.2  |
| 204.5          | 9.9- 9.5   |                |             |
| 210.5          | 6.48- 6.43 |                |             |

Critical pressure lies between the values quoted.

The logarithm of the pressure when plotted against the reciprocal of the absolute temperature falls on a straight line whose position is determined by the radius, the slope being common to all. In what follows it will be seen that it is of more significance to plot  $\log p/T^3$ , and this is shown in figure 1.

The different value of  $E$  found in the previous paper, when a long tube was used, may be explained by the decomposition which takes place as the

peroxide enters the tube, particularly as the inlet was a fine capillary. If a correction be applied on the basis of 0.4 sec. filling time the points relating to the temperatures 197–225° fall on a line nearly parallel to those for the other vessels.

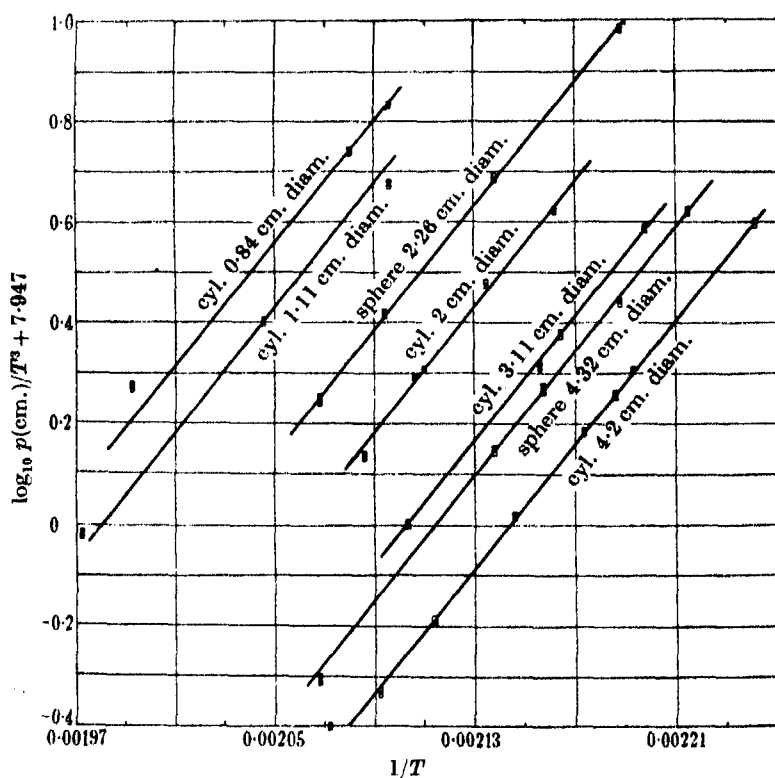


FIGURE 1

#### *Calculation of the explosion pressure*

The conditions for a thermal explosion to take place have been given in a simplified form by Semenov (1935), and by Allen and Rice (1935). The relation was obtained by equating the heat loss with the heat gain and in addition their differentials with respect to temperature. Frank-Kamenetzky (1939) used the relation  $X\nabla^2 T = -AQze^{-E/RT}$ . The sign  $\nabla^2$  is the Laplace operator, using his transformation

$$\theta = \frac{E}{RT_0^2}(T - T_0) \quad \text{and} \quad \frac{E}{RT} = \frac{E}{RT_0} - \frac{E}{RT_0^2}(T - T_0),$$

the equation for a spherical vessel becomes

$$\nabla^2\theta = \frac{1}{r^2} \frac{d}{dr} \left( r \frac{d\theta}{dr} \right) = \frac{AQze^{-E/RT_0}}{X} e^\theta \frac{E}{RT_0^2},$$

and for an infinite cylinder

$$\frac{1}{r} \frac{d}{dr} \left( r \frac{d\theta}{dr} \right) = \frac{AQze^{-E/RT_0}}{X} e^\theta \frac{E}{RT_0^2}.$$

The significance of the symbols used are as follows:  $Q$ , heat of reaction per mole;  $X$ , conductivity;  $A$ , number of moles per c.c.;  $E$ , energy of activation per mole;  $T_0$ , wall and initial temperature;  $T$ , temperature at distance  $r$ .  $A$  may be expressed as pressure,

$$A = \frac{p}{76} \frac{273}{T_0} \frac{1}{22,400}.$$

For the limiting explosive condition,  $\theta = 0$  at  $r = r_1$  (vessel radius) and  $\theta = 1$  at  $r = 0$ . By numerical integration of  $\nabla^2\theta$ , the limiting value of the product  $\left( \frac{Qze^{-E/RT_0}}{X} \frac{E}{RT_0^2} \frac{p}{76} \frac{273}{22,400} \right) r_1^2$  was found to be 3.82 for a sphere and 1.91 for an infinite cylinder, as compared with 3.32 and 2.0 found by Frank-Kamenetzky. If allowance is to be made for the decomposition which has taken place during the induction period ( $\tau$ ), a further factor  $(1 - k\tau)$  is needed, no great error being introduced by using the  $k$  corresponding to the initial temperature.

The following deductions may be made: (a) the product of the critical pressure and the square of the radius at a given temperature will be constant provided  $k$  does not vary with pressure; (b) the product  $pk/T_0^3$  is constant for a given radius, and as  $k = ze^{-E/RT_0}$  this is equivalent to

$$\log \frac{p}{T_0^3} = \frac{E}{RT_0} + \text{constant};$$

neglect of the factor  $(1 - k\tau)$  will make the line  $(\log p/(1/T^3))$  pass below the experimental points at higher temperatures.

From the curves in figure 1 the ratio between the critical pressures in the spherical vessels is 3.47, the ratio of the squares of the radii is 3.65. The results of Allen and Rice (1935) for azomethane show that for spheres having  $r_2/r_1 = 2.52$  the ratio of the products  $p_1k_1/p_2k_2$  is about 2.56. Similarly, from the paper of Campbell and Rice (1935) using the same reaction vessels, the ratio  $p_1k_1/p_2k_2$  for ethyl azide is about 2.25. Owing to lack of data it is not possible to estimate the  $k$  for the pressure used with exactitude. These authors related the critical pressure with the surface/volume ratio,

i.e. with the inverse of the radius instead of the inverse square, and explained the lack of agreement which resulted as being due to changes in the conductivity.

The slope of the lines in figure 1 leads to a value of  $E$  of 28.3 kcal. which compares well with the experimental value found by kinetic measurements 31.6 kcal. For dipropyl peroxide the corresponding figures are 34.2 from explosion data and 36.8 from kinetics. Rice and his co-workers have shown agreement for the activation energies of the azo-compounds, determined similarly.

In order to apply the equation to data obtained in cylindrical vessels it is necessary to find the value of the integral for the limiting condition. This is conveniently done by treating the cylinder as a sphere of radius  $r$  and a length of "infinite" cylinder and taking a mean as follows: if  $L$  is the length of the cylinder,  $(L - 2r)$  is the operative length of "infinite" cylinder, so  $\left(\frac{L - 2r}{L}\right) 1.92$  is the contribution from this, and  $\frac{2r}{L} 3.82$  is the contribution from the sphere; adding these, the figure for the finite cylinder is obtained. In the table below the theoretical value of the product

$$P = \frac{Qk}{X} \frac{E}{RT^3} \frac{p}{76} r^2 \frac{273}{22,400}$$

is compared with the experimental value. The latter is always lower than the former, but the ratio remains constant, showing that the treatment of a cylinder in the manner described is justified:

| Vessel                    | Sphere | Sphere | Cyl. | Cyl. | Cyl.  | Cyl.  | Cyl. |
|---------------------------|--------|--------|------|------|-------|-------|------|
| Radius, cm.               | 2.16   | 1.13   | 2.1  | 1.55 | 1.00  | 0.555 | 0.42 |
| Length, cm.               | —      | —      | 7.7  | 8.0  | 7.6   | 8.2   | 8.4  |
| Theoretical value of $P$  | 3.82   | 3.82   | 2.96 | 2.66 | 2.42  | 2.18  | 2.10 |
| Experimental value of $P$ | 2.59   | 2.85   | 2.18 | 2.24 | 1.515 | 1.55  | 1.3  |
| Ratio                     | 0.68   | 0.75   | 0.74 | 0.84 | 0.63  | 0.71  | 0.62 |

The results relating to the 1.55 cm. cylinder show a rather higher critical pressure and value of  $P$ , but in this case the peroxide had not been so completely purified.

If a value of 30,000 cal. be used for the heat of decomposition of ethyl azide and for azomethane, the value of the product  $P$  can be obtained from the data in the papers cited. It comes to 5.84 for azomethane in the 200 c.c. spherical bulb and 5.94 in the 50 c.c. spherical bulb, the corresponding figures for the azide being 4.9 and 4.0. If a lower value of  $Q$  be used, as seems to be indicated by application of Todes's formula (see p. 260), the agreement with theory will be closer.

*The heat of decomposition*

The calculation of the condition for explosion involves the heat of the slow decomposition reaction which precedes explosion. The value used by Neumann and Tutakin (1938) was obtained from the indicator diagram of the explosion which has a different heat value. Accordingly, the heat of combustion, determined in this laboratory by Dr Stathis, was used to calculate the heat of formation and the heat of decomposition.

The heat of combustion was 7150 cal./g. (liquid). This corresponds to a value of 651 kcal./mol. of gas, allowing 7.5 kcal./mol. as the latent heat of evaporation. (The value of  $L$  found by Blat, Gerber and Neumann (1939) was 7.3 kcal.) The heat of formation is then 68.5 kcal., and using the data given by Harris and Egerton (1938) in table 3 concerning the decomposition products from 17.4 mol. of peroxide which are given as 3.9 mol. HCHO, 6.9 mol.  $\text{CH}_3\text{CHO}$ , 14.2 mol.  $\text{C}_2\text{H}_5\text{OH}$ , 9.8 mol. CO, 1.1 mol.  $\text{H}_2$ , 5.9 mol.  $\text{CH}_4$ , and 3.9 mol.  $\text{C}_2\text{H}_6$ , the heat of decomposition of 1 mol. of peroxide to the corresponding fractions of a mol. of product comes to 30 kcal., which incidentally is nearly equal to the activation energy.

The heat evolved in the explosive reaction  $(\text{C}_2\text{H}_5\text{O})_2 \rightarrow 2\text{HCHO} + \text{C}_2\text{H}_6$  is much less, being only 10 kcal.

*The addition of inert gases*

The influence of added gases has been further studied, and if the conductivity of the added gas is low (e.g. nitrogen and carbon dioxide) a small diminution in the critical pressure is found to occur. At  $234^\circ$  the critical pressure was 13.9 mm. with no  $\text{N}_2$ , 12.8 mm. with 109 mm.  $\text{N}_2$ , 11.55 mm. with 200 mm.  $\text{N}_2$ , and rose to 13.3 mm. with 328 mm.  $\text{N}_2$ . This effect is similar to that noticed by Gubiansky when studying the inflammation of ether-oxygen mixtures. It may indicate a certain proportion of chains in the decomposition which leads up to explosion, or may merely be due to activation of the peroxide by nitrogen. Neumann and Tutakin (1938) state that the rate of slow decomposition is accelerated by nitrogen, but this was not found by Harris and Egerton (1938).

The conductivity of the peroxide will probably be of the same order as that of ethyl acetate (0.000057 cal./cm. deg. sec.), that of nitrogen is 0.00007, and hydrogen and helium possess very similar conductivities, about 0.0004. If mixtures of peroxide and hydrogen (or helium) follow the same law relating composition and conductivity as hold for mixtures of hydrogen and oxygen, which are given in Landolt-Bornstein's Tables, estimates of the conductivity of mixtures used may be made. In the table below the

conductivity and the ratio of the conductivities are set out, together with the ratio of the critical pressures found experimentally. A set of figures based on Allen, Campbell and Rice's results is included.

| Mixture          |                  |                  | Conductivity     | $X/X_0$ | $p/p_0$          |
|------------------|------------------|------------------|------------------|---------|------------------|
| Diethyl peroxide |                  |                  | $0.000059 = X_0$ | 1       | 1                |
| 78 %             | diethyl peroxide | 22 % $H_2$       | 0.00010          | 1.7     | 1.1, 1.2         |
| 67 %             | "                | 33 % $H_2$       | 0.00013          | 2.2     | 1.52, 1.47, 1.50 |
| 50 %             | "                | 50 % $H_2$       | 0.00018          | 3.0     | 1.5, 1.42, 1.65  |
| 20 %             | "                | 80 % $H_2$ or He | 0.00030          | 5.1     | 1.5              |
| 13 %             | "                | 87 % $H_2$       | 0.00033          | 5.6     | 2.0, 2.2         |
| 7 %              | "                | 93 % $H_2$       | 0.000365         | 6.2     | 1.93             |
| 67 %             | ethyl azide      | 33 % He          | 0.00013          | 2.2     | 1.23, 1.27, 1.30 |
| 50 %             | "                | 50 % He          | 0.00018          | 3.0     | 1.40, 1.45, 1.60 |
| 67.5 %           | azomethane       | 32.5 % He        | 0.00016          | 2.2     | 1.25             |
| 40.8 %           | "                | 59.2 % He        | 0.000215         | 3.6     | 1.58             |
| 23.7 %           | "                | 76.3 % He        | 0.000285         | 4.75    | 1.86             |

The increase in critical pressure is evidently only about half the increase in conductivity, which is not in accord with the theoretical equation. However, the question of the possibility of energy transfer arises. If the activated products of the slow reaction cannot pass on energy to the hydrogen, but only to the peroxide, then clearly the hydrogen will not have any influence. From the above results it would appear that only a third to a half of the total number of collisions between hydrogen and active products result in transfer of energy.

#### *The induction period of the explosion*

Approximate solutions of the differential equations relating the time to attain the maximum temperature with the reaction velocity have been given by Rice, Allen and Campbell (1935) and Todes (1936). The equation  $\left(\tau = \frac{(E/RT) + 2}{(E/RT)^2 k Q/CT}\right)$  obtained by Todes (1936) was applied to the explosion of diethyl peroxide by Neumann and Tutakin (1938), who concluded that the explosion was not thermal in origin because the calculated delay  $\tau$  was 0.2 sec at 210° and their experimental result was 0.4 sec. The equation applied to the present results leads to good agreement between calculated and experimental values.  $C$  is the mean molar heat capacity and was taken as 46 kcal., this being obtained by multiplying the specific heat of diethyl ether by the molecular weight of the peroxide.

The value of  $Q/C$  required to co-ordinate the calculated results for azomethane and ethyl azide with the experimental values of the explosion

delay found by Rice *et al.*, is very much lower than the value estimated from their own equation, being of the order of 300 compared with 1500.

| Temp. °C | $\tau$ (calc.) | $\tau$ (found) |
|----------|----------------|----------------|
|          | sec.           | sec.           |
| 172.5    | 2.9            | 2.4            |
| 187      | 1.0            | 1.0            |
| 189      | 0.9            | 0.7            |
| 193      | 0.66           | 0.5            |
| 210      | 0.2            | 0.2-0.1        |

The author wishes to express his thanks to Professor Egerton for having supervised and encouraged this work and also for Professor S. Chapman's advice on a mathematical question: also to the Trustees of the Beit Research Fellowships for a Fellowship which has rendered it possible to complete the work.

#### SUMMARY

1. Further measurements on the critical explosion pressure of diethyl peroxide have been made in vessels of different dimensions.
2. The conditions determining the explosion of diethyl peroxide have been shown to be in accord with those predicted by the thermal theory.
3. The increased conductivity caused by hydrogen and helium does not cause a corresponding increase in the critical pressure, which may be due to inefficient energy transfer.
4. The behaviour of azomethane and of ethyl azide is compared and shown to be similar.

#### REFERENCES

- Allen and Rice 1935 *J. Amer. Chem. Soc.* **57**, 310.  
Blat, Gerber and Neumann 1939 *Acta Phys. Chem. U.S.S.R.* **10**, 273.  
Campbell and Rice 1939 *J. Amer. Chem. Soc.* **57**, 1044.  
Frank-Kamenetzky 1939 *Acta Phys. Chem. U.S.S.R.* **10**, 365.  
Harris and Egerton 1938 *Proc. Roy. Soc. A*, **168**, 1.  
Neumann and Tutakin 1938 *Acta Phys. Chem. U.S.S.R.* **9**, 861.  
Rice, Allen and Campbell 1935 *J. Amer. Chem. Soc.* **57**, 2212.  
Semenoff 1935 *Chemical Kinetics and Chain Reactions*. Oxford University Press.  
Todes 1936 *J. Soc. Phys.-Chim. Russ.* **8**, 866.
-





delay found by Rice *et al.*, is very much lower than the value estimated from their own equation, being of the order of 300 compared with 1500.

| Temp. °C | $\tau$ (calc.)<br>sec. | $\tau$ (found)<br>sec. |
|----------|------------------------|------------------------|
| 172.5    | 2.9                    | 2.4                    |
| 187      | 1.0                    | 1.0                    |
| 189      | 0.9                    | 0.7                    |
| 193      | 0.66                   | 0.5                    |
| 210      | 0.2                    | 0.2-0.1                |

The author wishes to express his thanks to Professor Egerton for having supervised and encouraged this work and also for Professor S. Chapman's advice on a mathematical question: also to the Trustees of the Beit Research Fellowships for a Fellowship which has rendered it possible to complete the work.

#### SUMMARY

1. Further measurements on the critical explosion pressure of diethyl peroxide have been made in vessels of different dimensions.
2. The conditions determining the explosion of diethyl peroxide have been shown to be in accord with those predicted by the thermal theory.
3. The increased conductivity caused by hydrogen and helium does not cause a corresponding increase in the critical pressure, which may be due to inefficient energy transfer.
4. The behaviour of azomethane and of ethyl azide is compared and shown to be similar.

#### REFERENCES

- Allen and Rice 1935 *J. Amer. Chem. Soc.* **57**, 310.  
 Blat, Gerber and Neumann 1939 *Acta Phys. Chem. U.S.S.R.* **10**, 273.  
 Campbell and Rice 1939 *J. Amer. Chem. Soc.* **57**, 1044.  
 Frank-Kamenetzky 1939 *Acta Phys. Chem. U.S.S.R.* **10**, 365.  
 Harris and Egerton 1938 *Proc. Roy. Soc. A*, **168**, 1.  
 Neumann and Tutakin 1938 *Acta Phys. Chem. U.S.S.R.* **9**, 861.  
 Rice, Allen and Campbell 1935 *J. Amer. Chem. Soc.* **57**, 2212.  
 Semenov 1935 *Chemical Kinetics and Chain Reactions*. Oxford University Press.  
 Todes 1936 *J. Soc. Phys.-Chim. Russ.* **8**, 866.

# Relaxation methods applied to engineering problems

## VI.\* The natural frequencies of systems having restricted freedom

BY ANNE PELLEW, B.A., AND R. V. SOUTHWELL, F.R.S.

(Received 12 January 1940)

### INTRODUCTORY

1. Relaxation methods for determining characteristic numbers of *continuous* systems were described in Part IV of this series (Bradfield, Christopherson and Southwell 1939). The modes were assumed to be expressible (with sufficient accuracy) by a finite series of functions chosen to satisfy the boundary conditions, and thus in effect the system was given restricted freedom. In this way continuous systems can be brought within the scope of tabular computation.

When the freedom is thus restricted only in assumption, the fact that in reality the system is continuous means that suitably chosen series of continuous functions will satisfactorily represent the modes. But systems of restricted freedom are presented (e.g. in mechanical engineering) to which this treatment is not applicable. Thus it may be desired to calculate the free periods of torsional vibration for a system consisting of heavy masses connected by (relatively) light shafting: then usually it will not happen that consecutive masses have any systematic relation to one another, and accordingly the problem must be treated, like braced frameworks, by consideration of "joint displacements".

Such treatment of vibration problems has not hitherto received attention in this series, therefore is made the subject of the present paper. As in Part IV the normal technique of "liquidation" is modified in that the influence coefficients are altered at the end of each stage in the process, though they have constant values in any one stage; but here, since it is not desirable that liquidation should be taken far with inaccurate coefficients, upper and lower limits to the characteristic number are deduced at frequent intervals, and the work is arranged so that these limits continually approach. By this means the computer can decide whether further work is needed, having regard to the uncertainty of physical data which precludes an

\* Part V appeared in the *Philosophical Transactions*.

"exact" solution. (A criterion is available in statical problems, where computation should cease when all "residual forces" have been brought within the margin of uncertainty regarding external loads. For vibration problems, where there are no external loads, none has yet been suggested in this series.)

# GENERAL THEORY

2. In order to explain notation, etc., we start with a brief review of fundamental theory, based on the account given in an earlier paper (Southwell 1940).

In relation to a system specified by  $N$  generalized co-ordinates  $q_1, q_2, \dots, q_N$ , Lagrange's equations of motion are  $N$  of the type

$$\frac{d}{dt} \left( \frac{\partial \mathfrak{T}}{\partial \dot{q}_k} \right) - \frac{\partial \mathfrak{T}}{\partial q_k} + \frac{\partial \mathfrak{V}}{\partial q_k} = Q_k, \quad (1)$$

$\mathfrak{T}$  and  $\mathfrak{V}$  denoting the kinetic and potential energies and  $Q_k$  a generalized "component of external force". When the motion is a *small* free vibration about an equilibrium configuration, and when the vibration is "normal" in the sense that every co-ordinate fluctuates with the same frequency and phase so as to be expressible in the form

$$q_k = a_k \sin(pt + \epsilon) \quad (a_k \text{ constant}), \quad (2)$$

then we may write

$$\mathfrak{V} = V \sin^2(pt + \epsilon), \quad \mathfrak{T} = Tp^2 \cos^2(pt + \epsilon), \quad (3)$$

where  $V$  and  $T$  are homogeneous quadratic functions of the  $a$ 's, *essentially positive*. The type equation (1) reduces to

$$V_k - p^2 T_k = 0, \quad (4)$$

where (for brevity)

$$V_k, T_k \text{ stand for } \frac{\partial V}{\partial a_k}, \frac{\partial T}{\partial a_k} \text{ respectively,} \quad (5)$$

and because (by a well-known property of quadratic forms)

$$\left. \begin{aligned} 2V &= a_1 \cdot V_1 + a_2 \cdot V_2 + \dots + a_k \cdot V_k + \dots, \\ 2T &= a_1 \cdot T_1 + a_2 \cdot T_2 + \dots + a_k \cdot T_k + \dots, \end{aligned} \right\} \quad (6)$$

from the  $N$  equations of type (4) we deduce that

$$V = p^2 T. \quad (7)$$

Alternatively we can derive (7) as a consequence of the assumption (2) applied to the equation

$$\mathfrak{V} + \mathfrak{T} = \text{const.}, \quad (8)$$

which (for conservation of energy) must hold in the absence of forces doing external work on the system.\*

3. The  $N$  equations of type (4) are the conditions for a stationary value of  $p^2$  as deduced from (7). For if  $p^2 = \mathbf{V}/\mathbf{T}$  is stationary, then

$$\delta(\mathbf{V}/\mathbf{T}) = \delta\mathbf{V}/\mathbf{T} - \mathbf{V}\delta\mathbf{T}/\mathbf{T}^2 = (\delta\mathbf{V} - p^2\delta\mathbf{T})/\mathbf{T}$$

must vanish for all possible variations, therefore for any variation  $\delta a_k$  occurring singly. On this result Lord Rayleigh based his well-known "principle" whereby the gravest natural frequency may be estimated from (7) on the basis of an assumed form for the corresponding mode: An error of the first order made in regard to the mode will, by reason of the stationary property, entail an error of the second order of small quantities in regard to  $p^2$ ; and in regard to the gravest value  $p_1^2$  (which, being the smallest of the stationary values, is an absolute *minimum*) the estimate must err, if at all, on the side of *excess*.

4. With a view to treatment by relaxation methods we now replace (4) by

$$F_k = p^2 T_k - V_k, \quad (9)$$

and we think of  $F_k$  as a force which "corresponds with" the displacement  $a_k$  and comes upon an imaginary constraint controlling  $a_k$ . Then (as in earlier statical applications) the aim of the liquidation process will be to bring all such forces to zero. The "influence coefficients" (which must measure the changes in these forces resulting from displacements imposed singly) will be given by such quantities as

$$\left. \begin{aligned} (k, k) &= \frac{\partial F_k}{\partial a_k} = p^2 \frac{\partial T_k}{\partial a_k} - \frac{\partial V_k}{\partial a_k}, \\ (k, r) &= \frac{\partial F_k}{\partial a_r} = p^2 \frac{\partial T_k}{\partial a_r} - \frac{\partial V_k}{\partial a_r} = \frac{\partial F_r}{\partial a_k} = (r, k), \end{aligned} \right\} \quad (10)$$

in virtue of (5). Their expressions involve  $p^2$ , and on that account their

\* The qualification is needed, in order that external forces due to *constraints* may not be excluded.

values will require to be altered as liquidation proceeds: for the rest they involve quantities of the types

$$\left. \begin{aligned} \frac{\partial T_k}{\partial a_k} &= \frac{\partial^2 \mathbf{T}}{\partial a_k^2}, & \frac{\partial V_k}{\partial a_k} &= \frac{\partial^2 \mathbf{V}}{\partial a_k^2}, \\ \frac{\partial T_k}{\partial a_r} &= \frac{\partial^2 \mathbf{T}}{\partial a_k \cdot \partial a_r}, & \frac{\partial V_k}{\partial a_r} &= \frac{\partial^2 \mathbf{V}}{\partial a_k \cdot \partial a_r}, \end{aligned} \right\} \quad (11)$$

which, since they have fixed values, can be calculated once for all.

5. Our rule for the imposition of upper and lower limits to the gravest frequency (given in § 12 of the paper cited in § 2) is

$$p^2 - \left( \frac{F}{T} \right)_L < p_1^2 < p^2 - \frac{\sum_N [a_k \cdot F_k]}{\sum_N [a_k \cdot T_k]}, \quad (12)$$

$(F/T)_L$  being defined as the *algebraically largest value of  $F_k/T_k$  which corresponds with a positive product  $a_k \cdot T_k$* . With a view to later developments (§§ 14–16) we remark that  $p_1^2$  may be replaced by any higher frequency parameter  $p_r^2$ , provided that  $p_r^2$  is the smallest value which can be taken by  $p^2$  under the conditions imposed in computation. Strictly speaking (12) will need qualification if any “ $a \cdot T$  products” have negative values; but these (when liquidation has been carried so far that all the  $F$ ’s are small) will not occur except in the neighbourhood of nodal points, and there for *practical purposes* they may be disregarded. Otherwise the rule is not restricted, and can be applied at any stage in the relaxation process. The  $a$ ’s stand for generalized co-ordinates, so its range is very wide.

The upper limit in (12) is derived by “Rayleigh’s principle” (§ 3), according to which  $p^2$  as calculated from (7) cannot underestimate the gravest frequency. For in virtue of (6) that equation can be written as

$$0 = \sum [a_k (p^2 T_k - V_k)] = \sum [a_k \cdot F_k], \quad (13)$$

and according to (9) an addition  $\Delta p^2$  made to a trial value of  $p^2$  will alter  $F_k$  to  $(F_k + \Delta p^2 \cdot T_k)$ . The altered value will clearly satisfy (13) if

$$\Delta p^2 = -\sum [a_k \cdot F_k] / \sum [a_k \cdot T_k].$$

The lower limit is based on a less familiar theorem, also due to Lord Rayleigh, regarding the effect on the natural frequencies of a change made in the masses of a system: Except when mass is added at a nodal point (in which event the effect is *nil*), *any increase of mass will lower every one of the natural frequencies, and vice versa*. A trial solution can be made exact if appropriate changes are made to the masses, and a chosen value of  $p^2$  will

underestimate the frequency of a given system if it applies exactly to a system modified by addition of mass. Therefore the highest value which can with certainty be termed a lower limit is that value which requires, to make it exact, no change in one mass and positive additions to all the others. Translated into symbols this conclusion leads to (12).

#### DETAILS OF PROCEDURE BY THE RELAXATION METHOD. DETERMINATION OF THE GRAVEST MODE AND FREQUENCY

6. Given the forms of  $\mathbf{V}$  and  $\mathbf{T}$  as functions of the  $a$ 's, we can deduce constant values for  $\partial^2 \mathbf{V} / \partial a_r \partial a_k$ ,  $\partial^2 \mathbf{T} / \partial a_r \partial a_k$  and embody these in a table once for all. Then, starting from a guess (as good as possible) as to the form of the first mode, we can deduce the corresponding forces of types  $V_k$  and  $T_k$  and thence, using (6) and (7), a corresponding estimate of  $p_1^2$ . Inserting this value in (9) we can evaluate the forces which come initially on the constraints; inserting it in (10), from the table already constructed we can deduce starting values for the influence coefficients; and embodying these starting values in an "operations table" we can by a normal relaxation process start to liquidate the initial forces. When every force has been brought nearly to zero, the altered values of  $a_1, a_2, \dots, a_N$  will give a closer approximation to the normal mode. *We shall not have solved our problem*, because although the mode as thus modified would entail no appreciable forces on constraints if  $p^2$  had the value adopted in our calculations, it is not (in general) consistent with that value according to (7).

But now we can take advantage of the minimal property of  $p_1^2$ , which means (§3) that starting from a reasonably close assumption for the first normal mode, according to (7) we shall start with a very close approximation to  $p_1^2$  and thereafter (since we shall be working in the neighbourhood of its minimum)  $p^2$  as given by (7) will alter very slowly as the  $a$ 's are modified. Hence according to (9) the  $F$ 's will be very little affected, whether  $p^2$  is kept constant throughout the liquidation process or is altered in accordance with (7) after each operation: therefore we may conveniently work in "stages" during each of which  $p^2$  is kept constant, and alter  $p^2$  only at the end of every stage, when all residual forces have been brought (sensibly) to zero.

7. According to (10) and (11)

$$\begin{aligned} (k, k) &= \frac{\partial F_k}{\partial a_k} = p^2 \frac{\partial^2 \mathbf{T}}{\partial a_k^2} - \frac{\partial^2 \mathbf{V}}{\partial a_k^2}, \\ &= \frac{2}{a_k^3} (p^2 \mathbf{T} - \mathbf{V}), \end{aligned}$$

when  $T$  and  $V$  have values corresponding with a single displacement  $a_k$ . By Rayleigh's principle, in these circumstances  $V/T$  will have a value not less (and as a rule considerably greater) than  $p_1^2$ : consequently throughout the liquidation process, unless  $p^2$  very seriously overestimates  $p_1^2$ , all influence coefficients of the type  $(k, k)$  will have negative values, therefore any residual force can be brought (temporarily) to zero by the imposition of a "corresponding" displacement. Moreover, it has been shown in (10) that

$$(k, r) = (r, k),$$

so the influence coefficients satisfy "Maxwell relations" exactly as in a statical problem. Consequently the usual proof of convergence (Black and Southwell 1938, §I; Temple 1939) will hold in respect of any one stage of the relaxation process, during which ( $p^2$  being treated as constant) every influence coefficient has a constant value.

No modification of the normal relaxation procedure is required except this division into stages and a recalculation at the end of every stage of  $p^2$ , of the residual forces, and of the operations table.

*Numerical example: torsional vibrations of an elastic shaft*

8. In illustration of these methods we shall calculate the normal modes and frequencies for torsional vibrations of the system shown in figure 1. A light shaft of uniform torsional rigidity  $C$ , carrying six pulleys or similar inertial loads, has one end  $O$  held fixed and so can vibrate in modes which have a nodal point at that end.\*

To obviate dimensional factors, and at the same time give the solutions somewhat greater generality, at the outset we express all inertial loads as multiples of  $I_1$  and all shaft lengths as multiples of  $l$  (cf. figure 1). Then, if  $\alpha \times (1, a_2, \dots, a_6)$  are the angular displacements of  $I_1, I_2, \dots, I_6$  respectively,  $\alpha$  being proportional to  $\sin(pt + \epsilon)$ , it is easy to verify that

$$V = \frac{1}{2} \frac{C}{l} \alpha^2 \left[ 1 + \frac{(a_2 - 1)^2}{0.8} + \frac{(a_3 - a_2)^2}{1} + \frac{(a_4 - a_3)^2}{0.6} + \frac{(a_5 - a_4)^2}{1.1} + \frac{(a_6 - a_5)^2}{1.2} \right],$$

$$T = \frac{1}{2} I_1 \alpha^2 [1 + 4a_2^2 + 0.8a_3^2 + a_4^2 + 6a_5^2 + 0.8a_6^2].$$

If now we introduce a non-dimensional quantity

$$\lambda = p^2 I_1 l / C, \quad (14)$$

\* An exactly analogous problem is presented by a light tensioned string, loaded with concentrated masses which vibrate transversely. Cf. Den Hartog 1934, §30.



and substitute in (3), the dimensional factors in  $V$  and  $T$  (namely  $C\alpha^2/l$  and  $I_1\alpha^2$ ) may be suppressed provided that  $p^2$  is replaced by  $\lambda$ . Making this simplification, hereafter we shall take as expressions for  $V$  and  $T$

$$\left. \begin{aligned} 2V &= 2.25(1 + a_2^2) + 2.6a_3^2 + 2.57a_4^2 + 1.742a_5^2 + 0.83a_6^2 \\ &\quad - 2(1.25a_2 + a_2a_3 + 1.6a_3a_4 + 0.90a_4a_5 + 0.83a_5a_6), \\ 2T &= 1 + 4a_2^2 + 0.8a_3^2 + a_4^2 + 6a_5^2 + 0.8a_6^2, \end{aligned} \right\} \quad (15)$$

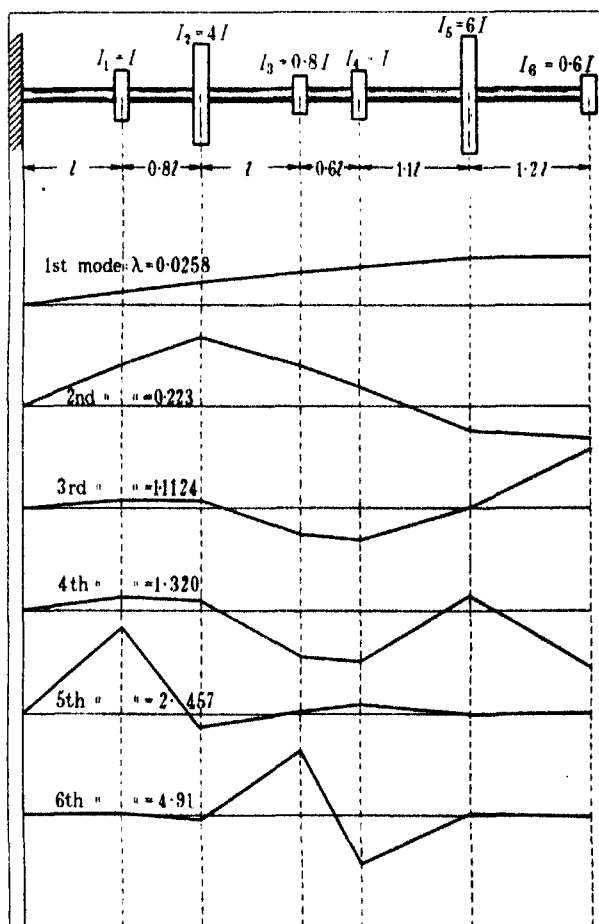


FIGURE 1

and write instead of (4), (7) and (9)

$$V_k - \lambda T_k = 0, \quad (4A)$$

$$V = \lambda T, \quad (7A)$$

$$F_k = \lambda T_k - V_k, \quad (9A)$$

$V_k, T_k$  standing as before for  $\partial V/\partial a_k, \partial T/\partial a_k$ . The  $a$ 's in (15) are purely numerical,  $a_1$  having the value 1.

9. Equation (4 A) holds for  $k = 2, 3, 4, 5, 6, a_1 (= 1)$  being now invariant. Therefore according to (15)

$$\left. \begin{aligned} 2.25a_2 - (1.25 + a_3) &= \lambda \times 4a_2, \\ 2.6a_3 - (a_2 + 1.6a_4) &= \lambda \times 0.8a_3, \\ 2.57a_4 - (1.6a_3 + 0.90a_5) &= \lambda a_4, \\ 1.742a_5 - (0.90a_4 + 0.83a_6) &= \lambda \times 6a_5, \\ 0.83(a_6 - a_5) &= \lambda \times 0.8a_6. \end{aligned} \right\} \quad (16)$$

Multiplying these equations by  $a_2, a_3, \dots, a_6$  respectively and summing, we deduce that if  $V = \lambda T$ , then

$$2.25 - 1.25a_2 = \lambda. \quad (17)$$

The same equation would have obtained from (4 A), with  $k$  made unity, if  $a_1$  had been left as a variable in (15) until after differentiation. Thus no generality is lost by this "non-dimensional" treatment.

Equations (16) and (17) may be used to verify results obtained by the Relaxation Method. Giving any value to  $\lambda$  we can deduce  $a_2$  from (17), then  $a_3$  from the first of (16),  $a_4$  from the second,  $a_5$  from the third,  $a_6$  from the fourth. The fifth of (16), unless by chance, will not be satisfied: but plotting against  $\lambda$  the ratio of its left- and right-hand sides we can use the resulting curve to estimate values of  $\lambda$  for which this ratio is unity.\* Here the ratio is found to change from a value slightly on one side of unity to a value slightly on the other side within ranges of  $\lambda$  (determined by relaxation methods in §§ 10-20) as under:

|   | Fractional range<br>of uncertainty |        |
|---|------------------------------------|--------|
| $\lambda_1 = 0.02585604 \pm 0.00000475$ | $\pm 0.018_4 \%$                   | } (18) |
| $\lambda_2 = 0.2239265 \pm 0.0000430$   | $\pm 0.019_2 \%$                   |        |
| $\lambda_3 = 1.1124143 \pm 0.0000103$   | $\pm 0.00092_8 \%$                 |        |
| $\lambda_4 = 1.3205877 \pm 0.0000547$   | $\pm 0.0041_4 \%$                  |        |
| $\lambda_5 = 2.457850 \pm 0.000142$     | $\pm 0.0057_8 \%$                  |        |
| $\lambda_6 = 4.914422 \pm 0.001613$     | $\pm 0.032_8 \%$                   |        |

Moreover, the values thus obtained for  $a_1, a_2, \dots, a_6$  confirm very satisfactorily the modes as determined in §§ 10-20. These modes are indicated in figure 1: clearly their forms are not such as could have been estimated *a priori*.

\* This is described by Den Hartog (1934, § 40) as "Holzer's method".

TABLE 1. VALUES OF  $\frac{\partial T}{\partial a_r \partial a_k}$  AND OF  $\frac{\partial V}{\partial a_r \partial a_k}$  FOR THE SYSTEM DEFINED IN FIGURE 1

| $k$   | $\frac{\partial T}{\partial a_r \partial a_k}$ |   |     |   |   |     | $\frac{\partial V}{\partial a_r \partial a_k}$ |       |      |       |       |       |
|-------|--|---|-----|---|---|-----|--|-------|------|-------|-------|-------|
|       | 1  | 2 | 3   | 4 | 5 | 6   | 1  | 2     | 3    | 4     | 5     | 6     |
| $r=1$ | 1  | — | —   | — | — | —   | 2.25   | -1.25 | —    | —     | —     | —     |
| 2     | —  | 4 | —   | — | — | —   | -1.25  | 2.25  | -1   | —     | —     | —     |
| 3     | —  | — | 0.8 | — | — | —   | —  | -1    | 2.6  | -1.6  | —     | —     |
| 4     | —  | — | —   | 1 | — | —   | —  | —     | -1.6 | 2.57  | -0.90 | —     |
| 5     | —  | — | —   | — | 6 | —   | —  | —     | —    | -0.90 | 1.742 | -0.83 |
| 6     | —  | — | —   | — | — | 0.8 | —  | —     | —    | —     | -0.83 | 0.83  |

TABLE 2

| $k$          | $T_k = \partial T / \partial a_k$ |    |     |    |     |      | $V_k = \partial V / \partial a_k$ |       |      |       |       |       |
|--------------|-----------------------------------|----|-----|----|-----|------|-----------------------------------|-------|------|-------|-------|-------|
|              | 1                                 | 2  | 3   | 4  | 5   | 6    | 1                                 | 2     | 3    | 4     | 5     | 6     |
| $a_1=1$      | 1                                 | 0  | 0   | 0  | 0   | 0    | 2.25                              | -1.25 | 0    | 0     | 0     | 0     |
| $a_2=2$      | 0                                 | 8  | 0   | 0  | 0   | 0    | -2.5                              | 4.5   | -2   | 0     | 0     | 0     |
| $a_3=3$      | 0                                 | 0  | 2.4 | 0  | 0   | 0    | 0                                 | -3    | 8    | -5    | 0     | 0     |
| $a_4=4$      | 0                                 | 0  | 0   | 4  | 0   | 0    | 0                                 | 0     | -6.6 | 10.30 | -3.63 | 0     |
| $a_5=5$      | 0                                 | 0  | 0   | 0  | 30  | 0    | 0                                 | 0     | 0    | -4.54 | 8.712 | -4.16 |
| $a_6=6$      | 0                                 | 0  | 0   | 0  | 0   | 4.8  | 0                                 | 0     | 0    | 0     | -5    | 5     |
| Total forces | 1                                 | 8  | 2.4 | 4  | 30  | 4.8  | -0.25                             | 0.25  | -0.6 | +0.75 | 0.075 | 0.83  |
| $a_k$        | 1                                 | 2  | 3   | 4  | 5   | 6    | 1                                 | 2     | 3    | 4     | 5     | 6     |
| Products     | 1                                 | 16 | 7.2 | 16 | 150 | 28.8 | -0.25                             | +0.5  | -2   | 3.03  | 0.378 | 5     |

Total =  $2T = 219$  ( $\lambda = V/T = 0.0304068$ )

Total =  $2V = 6.6596$

TABLE 3. OPERATIONS TABLE FOR THE SYSTEM DEFINED IN FIGURE 1: FIRST STAGE OF THE RELAXATION PROCESS ( $\lambda = 0.03$ )

| No. and<br>nature of operation      | $F_1$ | $F_2$ | $F_3$   | $F_4$    | $F_5$    | $F_6$  | $2\sum(F)$ |
|-------------------------------------|-------|-------|---------|----------|----------|--------|------------|
| 2 $a_1=1000$                        | 1250  | -2130 | 1000    | —        | —        | —      | 120        |
| 3 $a_2=1000$                        | —     | 1000  | -2642.6 | 1666.6   | —        | —      | 24         |
| 4 $a_3=1000$                        | —     | —     | 1666.6  | -2545.75 | 909.09   | —      | 30         |
| 5 $a_4=1000$                        | —     | —     | —       | 909.09   | -1562.42 | 833.3  | 180        |
| 6 $a_5=1000$                        | —     | —     | —       | —        | 833.3    | -809.3 | 24         |
| 1 $a_6=a_2=a_4=a_5$<br>= $a_3=1000$ | +1250 | -1130 | +24     | +30      | +180     | +24    | 378        |

# CALCULATION OF THE GRAVEST MODE AND FREQUENCY

10. Attacking the problem by relaxation methods we first construct Table 1, deriving the relevant quantities from (15) in accordance with § 4. By including columns and a line for  $k = 1, r = 1$  we can take advantage in computation of the relations (6): for all quantities of the types  $V_k, T_k$  are linear functions of the  $a$ 's without constant terms, so can be computed with the aid of Table 1 when values have been assigned to  $a_1, a_2, \dots, a_6$ ; and then, multiplying by the  $a$ 's and summing in accordance with (6), we can evaluate  $V, T$  and deduce a corresponding value of  $\lambda$  from (7 A). The computations are given tabular form in Table 2. We keep  $a_1$  unity throughout (cf. §§ 8, 9).

In order that the test of method may be stringent, we here make no attempt to guess the first mode closely. Instead, we take as starting values

$$(a_1 = 1), \quad a_2 = 2, \quad a_3 = 3, \quad a_4 = 4, \quad a_5 = 5, \quad a_6 = 6, \quad (19)$$

thus assuming a roughly uniform twist throughout the shaft. Table 2 relates to these values and deduces corresponding values of  $T, V$  and  $\lambda (= V/T)$ . We know that the value of  $\lambda$  must be too high, so we proceed on the assumption that

$$\lambda = 0.03, \quad (20)$$

and from Table 1, giving  $\lambda$  this value, we construct an operations table (Table 3) for use in the first stage of the relaxation process.

This example is intended not so much to illustrate physical aspects as to be a test of method: therefore more significant figures are retained in the tables than would ordinarily be reasonable, having regard to the uncertainty in practice of the physical data. (To facilitate checking by the reader, Tables 1-3 have been made *exact* by the retention of recurring decimals.) Correctly to 8 significant figures, according to (9 A) with  $\lambda = 0.03$  we have from the line marked "Total Forces" in Table 2

$$\left. \begin{aligned} F_1 &= 0.28, & F_2 &= -0.01, & F_3 &= 0.73866667, \\ F_4 &= -0.63757576, & F_5 &= 0.82424242, & F_6 &= -0.68933333. \end{aligned} \right\} \quad (21)$$

These values (multiplied by 1000 for convenience) we insert as "initial forces" in the first line of Table 4.

11. The relaxation table (in which operations were performed by slide-rule) is not reproduced but is summarized in Table 4: there the multiplications have been carried to 8 significant figures with the aid of a machine. It will be noticed that account is kept (in the lower columns) of forces of the type  $T_k$ : this is with a view to periodic improvement of the approximation

TABLE 4

| Line | Nature and amount of imposed displacements   | $\lambda$ | $F_1$     | $F_2$     | $F_3$     | $F_4$       | $F_5$       | $F_6$       |
|------|--|-----------|-----------|-----------|-----------|-------------|-------------|-------------|
| 1    | From (21) and Table 2, for initial displacements (19)  | 0.03      | 280.0000  | -10.0000  | 738.6667  | -637.57576  | 824.24242   | -689.33333  |
| 2    | $\Delta a_1 = -0.19$   |           | -237.5    | 404.7     | -190      | —           | —           | —           |
| 3    | $\Delta a_2 = -0.39$   |           | —         | -380      | 1030.64   | -650        | —           | —           |
| 4    | $\Delta a_3 = -0.945$  |           | —         | —         | -1575     | 2408.74091  | -859.00091  | —           |
| 5    | $\Delta a_4 = -1.220$  |           | —         | —         | —         | -1109.00091 | 1906.16758  | -1016.66667 |
| 6    | $\Delta a_5 = -1.220$  |           | —         | —         | —         | —           | -1783.33333 | 1731.97333  |
| 7    | $\Delta a_6 = -2.140$  |           | —         | —         | —         | —           | 87.97576    | 25.97333    |
| 8    | Total forces   |           | 42.50000  | 4.70000   | 4.30667   | 9.07424     | 3.780       | 3.860       |
| 9    | $\sigma_2$ (corrected)   |           | 1         | 1.81      | 2.61      | 3.055       | 3.780       | 3.860       |
| 10   | Products (19) $\times$ (8) ( $T_k \cdot \sigma_k$ )  |           | 42.50000  | 8.50700   | 11.24040  | 27.72161    | 332.54836   | 100.25707   |
| 11   | $\Delta \lambda$ as chosen for 2nd stage = -0.00413139 ( $\lambda = 0.025860794$ ; too high)                                       |           | —         | —         | —         | —           | —           | —           |
| 12   | $\Delta \lambda$ as chosen for 2nd stage = -0.004115 ( $\lambda = 0.02585$ )   | 0.02585   | —         | —         | —         | —           | —           | —           |
| 13   | Force from line 7 (repeated)   |           | 42.50000  | 4.70000   | 4.30667   | 9.07424     | 87.97576    | 25.97333    |
| 14   | $\Delta \lambda \cdot T_k = -0.00415 T_k$  |           | -4.15000  | -30.04600 | -8.66520  | -12.67825   | -94.12800   | -12.81530   |
| 15   | Corrected Residuals (sums of lines 11 and 12)  |           | 38.35000  | -25.34600 | -4.35853  | -3.60401    | -6.14624    | 13.15813    |
| 16   | $\Delta a_1 = -0.03073$  |           | -38.41250 | 65.96502  | -30.73000 | —           | —           | —           |
| 17   | $\Delta a_2 = -0.04412$  |           | —         | -41.01000 | 108.51191 | -68.35000   | —           | —           |
| 18   | $\Delta a_3 = -0.04462$  |           | —         | —         | -73.53333 | 112.50192   | -40.10909   | —           |
| 19   | $\Delta a_4 = -0.03652$  |           | —         | —         | —         | -40.56364   | 70.82841    | -37.18333   |
| 20   | Total forces   |           | -0.06250  | -0.39498  | -0.10995  | -0.01573    | -24.60000   | 23.98653    |
| 21   | $\sigma_2$ (corrected)   |           | 1         | 1.77927   | 2.56899   | 3.01088     | -0.02862    | -0.03567    |
| 22   | Products (19) $\times$ (20) ( $F_k \cdot \sigma_k$ )   |           | -0.06250  | -0.69566  | -0.28246  | -0.04736    | 3.73538     | 3.83048     |
| 23   | $\Delta \lambda$ according to (13) = $-\Sigma F_k \cdot \sigma_k / \Sigma T_k = 0.000010794$ ( $\lambda = 0.025860794$ ; too high) |           | —         | —         | —         | —           | -0.10603    | -0.13653    |

| Line | Nature and amount of imposed displacements   | $\lambda$ | $T_1$ | $T_2$     | $T_3$    | $T_4$    | $T_5$     | $T_6$     |
|------|--|-----------|-------|-----------|----------|----------|-----------|-----------|
| 1    | From (21) and Table 2, for initial displacements (19)  | 0.03      | 1000  | 8000      | 2400     | 4000     | 30000     | 4800      |
| 2    | $\Delta a_1 = -0.19$   |           | —     | -760      | —        | —        | —         | —         |
| 3    | $\Delta a_2 = -0.39$   |           | —     | —         | -312     | —        | —         | —         |
| 4    | $\Delta a_3 = -0.945$  |           | —     | —         | —        | -945     | —         | —         |
| 5    | $\Delta a_4 = -1.220$  |           | —     | —         | —        | —        | -7320     | —         |
| 6    | $\Delta a_5 = -2.140$  |           | —     | —         | —        | —        | —         | -1712     |
| 7    | Total forces   |           | 1000  | 7240      | 2088     | 3055     | 22680     | 3068      |
| 8    | $\sigma_2$ (corrected)   |           | 1     | 1.81      | 2.61     | 3.055    | 3.780     | 3.860     |
| 9    | Products (19) $\times$ (8) ( $T_k \cdot \sigma_k$ )  |           | 1000  | 13104.4   | 5449.68  | 9333.025 | 85730.4   | 11919.08  |
| 10   | $\Delta \lambda = -\Sigma T_k \cdot \sigma_k / \Sigma T_k = -0.00413139$ ( $\lambda = 0.025860794$ ; too high)                     |           | —     | —         | —        | —        | —         | —         |
| 11   | $\Delta \lambda$ as chosen for 2nd stage = -0.004115 ( $\lambda = 0.02585$ )   | 0.02585   | —     | —         | —        | —        | —         | —         |
| 12   | Force from line 7 (repeated)   |           | 1000  | 7240      | 2088     | 3055     | 22680     | 3068      |
| 13   | $\Delta \lambda \cdot T_k = -0.00415 T_k$  |           | -1000 | -7240     | -2088    | -3055    | -22680    | -3068     |
| 14   | Corrected Residuals (sums of lines 11 and 12)  |           | —     | —         | —        | —        | —         | —         |
| 15   | $\Delta a_1 = -0.03073$  |           | —     | -122.92   | —        | —        | —         | —         |
| 16   | $\Delta a_2 = -0.04412$  |           | —     | —         | -32.808  | —        | —         | —         |
| 17   | $\Delta a_3 = -0.04462$  |           | —     | —         | —        | -44.12   | —         | —         |
| 18   | $\Delta a_4 = -0.03652$  |           | —     | —         | —        | —        | -267.72   | —         |
| 19   | Total forces   |           | 1000  | 7117.08   | 2055.192 | 3010.86  | 22412.28  | 3064.384  |
| 20   | $\sigma_2$ (corrected)   |           | 1     | 1.77927   | 2.56899  | 3.01088  | 3.73538   | 3.83048   |
| 21   | Products (19) $\times$ (20) ( $T_k \cdot \sigma_k$ )   |           | 1000  | 12663.207 | 5279.766 | 9065.396 | 83718.363 | 11758.062 |
| 22   | $\Delta \lambda$ according to (13) = $-\Sigma T_k \cdot \sigma_k / \Sigma T_k = 0.000010794$ ( $\lambda = 0.025860794$ ; too high) |           | —     | —         | —        | —        | —         | —         |

of  $\lambda$ , with guidance given by upper and lower limits imposed in accordance with (12).

That rule implies that an assumed value  $\lambda$  will be too high if at any stage of the relaxation process, as in line 9 of Table 4, all such quantities as  $a_k \cdot F_k$  and  $a_k \cdot T_k$  are positive. In lines 8–10, computations which are self-explanatory in the light of (12) show that an addition  $\Delta\lambda$  of  $-0.00413139$  will leave  $\lambda$  still too high: that is to say, the required value.

$$\lambda_1 \text{ (say)} < 0.02586861. \quad (22)$$

Accordingly in the second stage of relaxation we investigate the effect of a somewhat larger alteration (namely,  $\Delta\lambda = -0.00415$ ), and take as our next trial value  $\lambda = 0.02585$ .

12. Line 13 of Table 4 gives the residual forces as altered by this change in  $\lambda$ . As was to be expected, some have had their signs reversed, others remain positive. The new values are

$$38.35, \quad -25.346, \quad -4.35853, \quad -3.60401, \quad -6.14624, \quad 13.15813, \quad (23)$$

correctly to the fifth decimal place. (As in § 11, a calculating machine was used to obtain this approximation.)

Lines 14–18 of Table 4 summarize the second stage of the relaxation process, made with an operations table similar to Table 3 but differing on account of the altered value of  $\lambda$ . This stage was stopped when all quantities of the type  $a_k F_k$  had become negative (line 19), so that (all quantities of type  $a_k T_k$  being positive) according to (12) a *positive* addition  $\Delta\lambda$  is required by the upper limit. Calculations which are given in lines 20–22 gave the required addition as

$$\Delta\lambda = 10.794 \times 10^{-6},$$

so showing that (22) can be replaced by

$$\lambda_1 < (0.02585 + 10.793 \times 10^{-6}) = 0.025860794. \quad (24)$$

13. The ratio  $F_k/T_k$  has the following values at the end of the first stage (line 7) and second stage (line 19) respectively:

| $k =$                     | 1     | 2       | 3       | 4      | 5      | 6       |
|---------------------------|-------|---------|---------|--------|--------|---------|
| Line 7: $10^{-3} \times$  | 42.5  | 0.649   | 2.063   | 2.970  | 3.879  | 8.411   |
| Line 19: $10^{-3} \times$ | -62.5 | -54.935 | -53.499 | -5.224 | -1.290 | -11.640 |

Therefore according to § 5

$$\begin{aligned} \lambda - \left( \frac{F}{T} \right)_L &= 0.03 - 0.0425, \quad \text{at the close of the first stage,} \\ &= 0.02585 - (-1.29 \times 10^{-6}) \quad \text{at the close of the second stage.} \end{aligned}$$

Combining these results with (22) and (24), we have finally, as "brackets" for  $\lambda_1$ ,

$$-0.0125 < \lambda_1 < 0.02586861 \quad (25)$$

at the end of the first stage, and

$$0.02585129 < \lambda_1 < 0.025860794 \quad (26)$$

at the end of the second.

Since  $\lambda_1$  is known *ab initio* to be positive, the lower limit in (25) is nugatory; but applied to the figures resulting from the second stage in Table 1 our rule has yielded a very close "bracket". The total range of uncertainty is  $9.5 \times 10^{-8}$ , so that by giving to  $\lambda$  the mean value

$$\frac{1}{2}(0.02586079 + 0.02585129) = 0.02585604 \quad (27)$$

we shall certainly keep the error within

$$\frac{4.75}{25,856} = 0.018_4 \%$$

This result is verified in § 9.

#### GENERAL THEORY (CONTINUED). DETERMINATION OF HIGHER MODES AND FREQUENCIES

14. When as in the preceding example  $\lambda_1$  (i.e.  $p_1^2$ ) has been bracketed between limits sufficiently close, calculation can be stopped and we are left with close estimates not only of  $p_1^2$  (to which an approximation could have been obtained by other methods based on Rayleigh's theorem) but also of the associated mode (which that theorem does not determine). On this account, making use of the Conjugate Property which is a characteristic of "normal modes", we can proceed to similar calculations of  $p_2^2$ ,  $p_3^2$ , ..., etc., and of the modes associated with those higher frequencies. This is an important merit of the relaxation procedure.

The conjugate or "orthogonal" property of normal modes (Southwell 1936, § 504) implies that equation (7) can be written as

$$p^2 = \frac{\mathbf{V}}{\mathbf{T}} = \frac{A_1^2 \mathbf{V}_1 + A_2^2 \mathbf{V}_2 + \dots + A_N^2 \mathbf{V}_N}{A_1^2 \mathbf{T}_1 + A_2^2 \mathbf{T}_2 + \dots + A_N^2 \mathbf{T}_N} \quad (28)$$

( $\mathbf{V}_1, \mathbf{V}_2, \dots, \mathbf{V}_N$  and  $\mathbf{T}_1, \mathbf{T}_2, \dots, \mathbf{T}_N$  denoting the values of  $\mathbf{V}$  and  $\mathbf{T}$  for the first, second, ...,  $N$ th normal modes) if the mode is regarded as composed of these  $N$  modes combined in the proportion  $A_1 : A_2 : \dots : A_N$ . It follows that

$$\frac{\partial p^2}{\partial A_r} = 0, \quad \text{when all the } A\text{'s are zero except } A_r,$$

so that (in accordance with §3)  $p^2$  as given by (7) has a stationary value when the mode is normal. But (28) shows further that if  $A_1$  is zero then the smallest of such stationary values is  $p_2^2$ : that is to say,  $p_2^2$  is the minimum value of  $p^2$  as given by (7) provided that the mode has no "first normal component".

15. When an assumed mode satisfies this requirement, in normal co-ordinates  $\mathbf{V}$  and  $\mathbf{T}$  will have the forms

$$\mathbf{V} = A_2^2 \mathbf{V}_2 + A_3^2 \mathbf{V}_3 + \dots, \quad \mathbf{T} = A_2^2 \mathbf{T}_2 + A_3^2 \mathbf{T}_3 + \dots,$$

and so, for the assumed mode,

$$\frac{\partial \mathbf{V}}{\partial A_1} = \frac{\partial \mathbf{T}}{\partial A_1} = 0,$$

whatever be the magnitudes of  $A_2, A_3, \dots$ , etc. This means that no work *on the whole* will be done by either the elastic or kinetic forces of the assumed mode in acting through displacements corresponding with the first normal mode ( $A_1$ ); and the Reciprocal Theorem (Southwell 1936, §12) shows that in consequence *no work would be done by either the elastic or kinetic forces of the first mode in acting through the displacements of the assumed mode*. We thus obtain a relation which must hold between the displacements in an assumed mode in order that this shall have no "first normal component"; and to modes thus restricted Rayleigh's principle (§3) can be applied with the modification that  $p_2^2$  is now the minimum value which can be assumed by  $p^2$  as calculated from (7). Clearly the argument can be extended.

16. To formulate the relation, we denote by  $(V_k)_1, (T_k)_1$  the typical elastic and kinetic force in the first mode. Then, if  $a_k$  typifies the displacement in the assumed mode, the above criterion requires that

$$\left. \begin{aligned} a_1(V_1)_1 + a_2(V_2)_1 + \dots + a_N(V_N)_1 &= 0, \\ a_1(T_1)_1 + a_2(T_2)_1 + \dots + a_N(T_N)_1 &= 0, \end{aligned} \right\} \quad (29)$$

—these relations being equivalent because the ratio  $T_k/V_k$  has the same value, by (4), for all values of  $k$ . Knowing the first mode we can give numerical values to  $(V_1), \dots$ , etc.

Since it demands that (29) be satisfied, the requirement that the assumed mode shall have no "first component" in effect reduces the order of freedom by 1; but when the requirement is satisfied, then  $p^2$  as given by (7) can in no case be less than  $p_2^2$ . Having determined  $p_2^2$  and its associated mode, we can similarly calculate  $p_3^2$ , and so on.



TABLE 5

|              |           | $T_k$ |          |          |          |           |           |
|--------------|-----------|-------|----------|----------|----------|-----------|-----------|
|              | $k =$     | 1     | 2        | 3        | 4        | 5         | 6         |
| $a_1 =$      | 1         | 1     | —        | —        | —        | —         | —         |
| $a_2 =$      | 1.284482  | —     | 5.137929 | —        | —        | —         | —         |
| $a_3 =$      | 1.140196  | —     | —        | 0.912157 | —        | —         | —         |
| $a_4 =$      | 0.499041  | —     | —        | —        | 0.499041 | —         | —         |
| $a_5 =$      | -0.419628 | —     | —        | —        | —        | -2.517769 | —         |
| $a_6 =$      | -1.495509 | —     | —        | —        | —        | —         | -1.196407 |
| Total forces |           | 1     | 5.137929 | 0.912157 | 0.499041 | -2.517769 | -1.196407 |
| $a_k$        | 1         | 1     | 1.284482 | 1.140196 | 0.499041 | -0.419628 | -1.495509 |
| Products     |           | 1     | 6.599577 | 1.040038 | 0.249042 | 1.056526  | 1.789239  |

$$\text{Total} = 2T = 11.734422 \quad (\lambda = V/T = 0.3016)$$

*Numerical example (continued): second mode and frequency*

17. We now apply these methods to the torsional system of which the fundamental frequency is given (within narrow limits) by (26) of § 13. Here the forces  $(T_1)_1, \dots, (T_N)_1$  have values given in line 19 of Table 4, consequently the second of equations (29) is

$$1 + 7.117080a_2 + 2.055192a_3 + 3.010880a_4 + 22.412280a_5 + 3.064384a_6 = 0, \quad (30)$$

on the assumption made previously (§§ 8, 10) that  $a_1$  is unity. We know that the second mode must have a node at some point in the shaft; so a suitable form is obtained by multiplying the displacements  $a_1, a_2, \dots, a_6$  of the first mode by  $1, 1 - \alpha, 1 - 2\alpha, \dots, 1 - 5\alpha$  respectively, and then choosing  $\alpha$  so that (30) is satisfied.

The resulting value of  $\alpha$  is 0.2780847, and the corresponding displacements are

$$a_1 = 1, \quad a_2 = 1.284482_2, \quad a_3 = 1.140196_4, \\ a_4 = 0.499041_0, \quad a_5 = -0.419628_1, \quad a_6 = -1.495509_4. \quad (31)$$

Table 5, constructed for these displacements in the manner of Table 2, gives for  $\lambda$  a value 0.3016 and thus suggests the assumption

$$\lambda = 0.3 \quad (32)$$

for the first stage of the relaxation process. The corresponding initial forces are obtained in the last three lines.

18. Again the relaxation table is not reproduced, and here the tabular summary (Table 6) is condensed still further. Operations effected by slide rule, and without regard to (30),\* suggested additions to the displacements

\* By waiving this requirement we greatly simplify the individual operations. In some instances lower limits were computed before the lower modes had been eliminated.

TABLE 5 continued

| $k =$  | $V_k$     |           |           |           |           |           |
|--|-----------|-----------|-----------|-----------|-----------|-----------|
|  | 1         | 2         | 3         | 4         | 5         | 6         |
| $a_1 = 1$  | 2.25      | -1.25     | —         | —         | —         | —         |
| $a_2 = 1.284482$                                     | -1.605603 | 2.890085  | -1.284482 | —         | —         | —         |
| $a_3 = 1.140196$                                     | —         | -1.140196 | 3.040523  | -1.900327 | —         | —         |
| $a_4 = 0.499041$                                     | —         | —         | -0.831735 | 1.285409  | -0.453674 | —         |
| $a_5 = -0.419628$                                    | —         | —         | —         | 0.381480  | -0.731170 | 0.349690  |
| $a_6 = -1.495509$                                    | —         | —         | —         | —         | 1.246258  | -1.246258 |
| Total forces   | 0.644397  | 0.499889  | 0.924306  | -0.233439 | 0.061414  | -0.896568 |
| $a_k$  | 1         | 1.284482  | 1.140196  | 0.499041  | -0.419628 | -1.495509 |
| Products   | 0.644397  | 0.642098  | 1.053891  | -0.116495 | -0.025771 | +1.340825 |
| Total = $2V = 3.538945$ ( $\lambda = V/T = 0.3016$ ) |           |           |           |           |           |           |
| $0.3T_k$   | 0.3       | 1.541379  | 0.273647  | 0.149712  | -0.755331 | -0.358922 |
| $-V_k$   | -0.644397 | -0.499888 | -0.924306 | 0.233439  | -0.061414 | +0.896568 |
| Sum = $F_k$  | -0.344397 | 1.041490  | -0.650659 | 0.383151  | -0.816745 | 0.537645  |

which were then modified (with the use of a machine) so that (30) was satisfied; finally their consequences were calculated (again by machine) and recorded in Table 6. The modification consisted in an addition of "first-mode displacements" as recorded in line 20 of Table 4, multiplied by a constant determined from (30). By this means advantage was taken of the calculations in lines 19-22 of the same table: thus the additions to (31) suggested by a rough liquidation were

$$\begin{aligned} \Delta a_1 &= 0, & \Delta a_2 &= 0.3, & \Delta a_3 &= -0.2, \\ \Delta a_4 &= -0.07, & \Delta a_5 &= -0.2, & \Delta a_6 &= 0.7, \end{aligned} \quad (33)$$

and accordingly  $\beta$ , the multiplying constant, could be deduced from the equation

$$\begin{aligned} 123.464817\beta + 0.3 \times 7.117080 - 0.2 \times 2.055192 - \\ - 0.07 \times 3.01088 - 0.2 \times 22.41228 + 0.7 \times 3.064384 = 0. \end{aligned}$$

The result was  $\beta = 0.006674478$ ,

and in consequence the corrections (33) were altered to

$$\begin{aligned} \Delta a_1 &= 0.006674, & \Delta a_2 &= 0.311876, & \Delta a_3 &= -0.182853, \\ \Delta a_4 &= -0.049904, & \Delta a_5 &= -0.175068, & \Delta a_6 &= 0.725566, \end{aligned} \quad (34)$$

which satisfy (30) and entail the forces shown in line 2 of Table 6. It will be observed (line 4) that  $a_1$  is no longer exactly unity: nevertheless by keeping it unity in the trial liquidation we have attained our object of avoiding a null solution.

TABLE 6. (N.B. all forces have been multiplied by  $10^6$ )

| Line    | Imposed displacements   | $\lambda$ | $F_1$    | $F_2$    | $F_3$                      | $F_4$    | $F_5$     | $F_6$     |
|---------|---|-----------|----------|----------|----------------------------|----------|-----------|-----------|
| Stage 1 |   |           |          |          |                            |          |           |           |
| 1       | Initial displacements (31)  | 0.3       | -344397  | 1041490  | -650659                    | 383151   | -816745   | 537645    |
| 2       | Displacement corrections (34)   |           | 376829   | -501980  | 672426                     | -350339  | 549192    | -576392   |
| 3       | Total forces  |           | 32432    | 539510   | 21767                      | 32812    | -267553   | -38747    |
| 4       | $a_k$ (corrected)   |           | 1.006674 | 1.596358 | 0.957343                   | 0.449137 | -0.594696 | -0.769943 |
| 5       | Products (3) $\times$ (4) ( $F_k \cdot a_k$ )   |           | 32648    | 861251   | 20839                      | 14737    | 159113    | 29833     |
| 6       | $(F/T)_L = 0.08449$ ; $\Sigma F/\Sigma T = 0.075887$ ; hence, according to (12), $0.21551 < \lambda < 0.224113$         |           |          |          | ( $\Sigma F = 1,118,422$ ) |          |           |           |
| 7       | $\Delta\lambda$ chosen for second stage = -0.077  | 0.223     |          |          |                            |          |           |           |
| 8       | Forces from Line 3 (repeated)   |           | 32432    | 539510   | 21767                      | 32812    | -267553   | -38747    |
| 9       | $\Delta\lambda \cdot T_k = -0.077T_k$   |           | -77514   | -491678  | -58972                     | -34584   | 274750    | 47428     |
| Stage 2 |   |           |          |          |                            |          |           |           |
| 10      | Corrected Residuals (sums of Lines 7 and 8)   |           | -45082   | 47832    | -37205                     | -1772    | 7197      | 8681      |
| 11      | Displacement corrections (35)   |           | 37595    | -49067   | 35922                      | -279     | -2928     | -8043     |
| 12      | Total forces  |           | -7487    | -1235    | -1283                      | -2051    | 4269      | 638       |
| 13      | $a_k$ (corrected)   | 0.2238    | 1.007154 | 1.627211 | 0.949575                   | 0.440581 | -0.602905 | -0.768106 |
| 14      | Products (11) $\times$ (12) ( $F_k \cdot a_k$ )   |           | -7541    | -2010    | -1218                      | -903     | -2574     | -490      |
| 15      | $(F/T)_L = -0.000190$ ; $\Sigma F/\Sigma T = -0.000971$ ; hence, according to (12), $0.223190 < \lambda < 0.223971$     |           |          |          | ( $\Sigma F = -14,736$ )   |          |           |           |
| 16      | $\Delta\lambda$ chosen for third stage = 0.0008   |           |          |          |                            |          |           |           |
| 17      | Forces from Line 11 (repeated)  |           | -7487    | -1235    | -1283                      | -2051    | 4269      | 638       |
| 18      | $\Delta\lambda \cdot T_k = 0.0008T_k$   |           | 806      | 5207     | 608                        | 353      | -2894     | -492      |
| Stage 3 |   |           |          |          |                            |          |           |           |
| 19      | Corrected Residuals (sums of Lines 15 and 16)   |           | -6681    | 3972     | -675                       | -1698    | 1375      | 146       |
| 20      | Displacement corrections (36)   |           | 6495     | -4515    | -150                       | 1388     | -641      | 37        |
| 21      | Total forces  |           | -186     | -543     | -825                       | -310     | 734       | 183       |
| 22      | $a_k$ (corrected)   |           | 1.004014 | 1.627319 | 0.949130                   | 0.439763 | -0.602680 | -0.767875 |
| 23      | Products (19) $\times$ (20) ( $F_k \cdot a_k$ )   |           | -186     | -884     | -783                       | -136     | -442      | -140      |
| 24      | $(F/T)_L = -0.0000835$ ; $\Sigma F/\Sigma T = -0.0001696$ ; hence, according to (12), $0.2238835 < \lambda < 0.2239696$ |           |          |          | ( $\Sigma F = -2,572$ )    |          |           |           |

TABLE 6 (continued)

| Line    | Imposed displacements   | $\lambda$                         | $T_1$    | $T_2$    | $T_3$    | $T_4$                     | $T_5$     | $T_6$     |
|---------|---|-----------------------------------|----------|----------|----------|---------------------------|-----------|-----------|
| Stage 1 |   |                                   |          |          |          |                           |           |           |
| 1       | Initial displacements (31)  | 0.3                               | 1000000  | 5137929  | 912157   | 499041                    | -2517769  | -1196407  |
| 2       | Displacement corrections (34)   |                                   | 6674     | 1247503  | -146283  | -49904                    | -1050410  | 580453    |
| 3       | Total forces  |                                   | 1006674  | 6385432  | 765874   | 449137                    | -3568178  | -616954   |
| 4       | $a_k$ (corrected)   |                                   | 1.006674 | 1.596358 | 0.957343 | 0.449137                  | -0.594696 | -0.769943 |
| 5       | Products (3) $\times$ (4) ( $T_k, a_k$ )  | 0.223                             | 1013394  | 10193434 | 733205   | 201724                    | 2121983   | 474250    |
| 6       | $(F/T)_L = 0.08449$ ; $\Sigma F/\Sigma T = 0.075887$ : hence, according to (12), $0.21551 < \lambda < 0.224113$         |                                   |          |          |          | $(\Sigma T = 14,737,989)$ |           |           |
| 7       | $\Delta\lambda$ chosen for second stage = -0.077  |                                   |          |          |          |                           |           |           |
| 8       | Forces from Line 3 (repeated)   |                                   | 1006674  | 6385432  | 765874   | 449137                    | -3568178  | -616954   |
| Stage 2 |   |                                   |          |          |          |                           |           |           |
| 9       |   |                                   | 480      | 123413   | -6214    | -8556                     | -49251    | 1470      |
| 10      | Displacement corrections (35)   | 0.2238                            | 1007154  | 6508845  | 759660   | 440581                    | -3617429  | -614484   |
| 11      | Total forces  |                                   | 1.007154 | 1.627211 | 0.949575 | 0.440581                  | -0.602905 | -0.768106 |
| 12      | $a_k$ (corrected)   |                                   | 1014359  | 10591266 | 721354   | 194112                    | 2180965   | 471989    |
| 13      | Products (11) $\times$ (12) ( $T_k, a_k$ )  |                                   |          |          |          | $(\Sigma T = 15,174,046)$ |           |           |
| 14      | $(F/T)_L = -0.000190$ ; $\Sigma F/\Sigma T = -0.000971$ : hence, according to (12), $0.223190 < \lambda < 0.223971$     | 0.2238                            |          |          |          |                           |           |           |
| 15      | $\Delta\lambda$ chosen for third stage = 0.0008   |                                   |          |          |          |                           |           |           |
| 16      | Forces from Line 11 (repeated)  |                                   | 1007154  | 6508845  | 759660   | 440581                    | -3617429  | -614484   |
| Stage 3 |   |                                   |          |          |          |                           |           |           |
| 17      |   |                                   | -3140    | 429      | -356     | -818                      | 1351      | 184       |
| 18      | Displacement corrections (36)   | 0.2238835 < $\lambda$ < 0.2239696 | 1004014  | 6509274  | 759304   | 439763                    | -3616078  | -614300   |
| 19      | Total forces  |                                   | 1.004014 | 1.627319 | 0.949130 | 0.439763                  | -0.602680 | -0.767875 |
| 20      | $a_k$ (corrected)   |                                   | 1008045  | 10592663 | 720678   | 193391                    | 2179336   | 471705    |
| 21      | Products (19) $\times$ (20) ( $T_k, a_k$ )  |                                   |          |          |          | $(\Sigma T = 15,165,819)$ |           |           |
| 22      | $(F/T)_L = -0.0000835$ ; $\Sigma F/\Sigma T = -0.0001696$ : hence, according to (12), $0.2238835 < \lambda < 0.2239696$ |                                   |          |          |          |                           |           |           |

The table is self-explanatory, except as regards the corrections applied in the different stages to the displacements. In the first stage (line 2) these are as given in (34); in the second stage (line 10) they are

$$\left. \begin{aligned} \Delta a_1 &= 0.000480, & \Delta a_2 &= 0.030853, & \Delta a_3 &= -0.007768, \\ \Delta a_4 &= -0.008556, & \Delta a_5 &= -0.008208, & \Delta a_6 &= 0.001837; \end{aligned} \right\} \quad (35)$$

and in the third stage (line 18) they are

$$\left. \begin{aligned} \Delta a_1 &= -0.003140, & \Delta a_2 &= 0.000107, & \Delta a_3 &= -0.000445, \\ \Delta a_4 &= -0.000818, & \Delta a_5 &= 0.000225, & \Delta a_6 &= 0.000231. \end{aligned} \right\} \quad (36)$$

Equation (30) is satisfied both by (35) and (36).

The progress of the approximation is indicated by the narrowing "brackets" which follow lines 6, 14 and 22. According to the last of these, giving to  $\lambda$  the mean value 0.2239265 we can be sure that the error is within

$$\frac{4.31}{22,388} = 0.019_{25} \% \quad (37)$$

and the result is verified in § 9.

#### HIGHER MODES AND FREQUENCIES

19. The procedure for determining the third and higher modes and frequencies is exactly similar. The third mode must be "orthogonal" not only to the first but also to the second: therefore its displacements must satisfy not only (30) but also the equation

$$\begin{aligned} 1.004014a_1 + 6.509274a_2 + 0.759304a_3 + 0.439763a_4 - \\ - 3.616078a_5 - 0.614300a_6 = 0, \end{aligned} \quad (38)$$

which can be based on an exactly similar argument. To obtain a starting assumption we multiply the displacements  $a_1, a_2, \dots, a_6$  in the second mode by 1,  $1 - \gamma$ ,  $1 - 2\gamma$ , ...,  $1 - 5\gamma$  respectively and then choose  $\gamma$  so that (38) is satisfied. In this way we obtain a mode having one more nodal point and containing no "second normal component": if now we correct its displacements in the manner of § 17, what results has neither a first nor a second normal component.

In the liquidation process we start as before (§ 18) by slide-rule and without satisfying (30) and (38), then with the use of a machine modify the suggested additions and record their consequences. Now, of course, a double correction is necessary: to eliminate the first normal component from a set

of displacements  $a_1, a_2, \dots, a_6$  we must add first-mode displacements multiplied by  $\beta_1$ , where

$$123.464817\beta_1 + a_1 + 7.117080a_2 + 2.055192a_3 + 3.010880a_4 + \\ + 22.412280a_5 + 3.064384a_6 = 0, \quad (39)$$

and to eliminate the second normal component we must add second-mode displacements multiplied by  $\beta_2$ , where

$$15.165819\beta_2 + 1.004014a_1 + 6.509274a_2 + 0.759304a_3 + \\ + 0.439763a_4 - 3.616078a_5 - 0.614300a_6 = 0. \quad (40)$$

20. Every new mode and frequency (except the sixth, which results *at once* when all graver components have been eliminated\*) entails a separate relaxation process and a summary of the type of Tables 4 and 6, so six tables of this kind were entailed by the problem of figure 1. The last four are not reproduced, but are briefly summarized in Tables 7-10 to show how the solutions converge. The results are verified in § 9.

We have thus determined within narrow limits of error all of the natural frequencies, together with the associated modes, of the torsional system specified in § 8.

#### TORSIONAL SYSTEMS WHICH ARE ENTIRELY UNRESTRAINED

21. That system is in one respect artificial—namely, in that the end point  $O$  of figure 1 is fixed and therefore nodal for every mode. Torsional systems usually terminate at each end with a finite mass which takes part in the vibration; there is no constraint entailing an external force, therefore every normal vibration must conform with the principle of the Conservation of Moment of Momentum. That is to say, in every vibration the total moment of momentum  $\Sigma[I_k \cdot \dot{q}_k]$  must have a constant value throughout all time, and so in a normal vibration, according to (2),

$$\Sigma[I_k \cdot a_k] = 0. \quad (41)$$

Now (41), as implying a linear relation between the  $a$ 's, will affect the computations exactly as in §§ 17-19 they were affected by (30), the condition for no "first normal component". Like (30), in effect it reduces the order of

\* In this last instance, of course, Rayleigh's principle provides the *lower* limit, and an upper limit can be found in the manner of § 5 from (12) with  $(F/T)_L$  replaced by  $(F/T)_S$ , the *smallest* value of  $F/T$ . Improvement was not found to be practicable: thus the narrow range of uncertainty as regards  $\lambda_6$  in (18) is an indication of the accuracy with which the lower modes have been computed.

TABLES 7-10. SUMMARIZED RESULTS FOR THE HIGHER MODES AND FREQUENCIES

| Limits imposed on $\lambda$ | Displacements in the corresponding mode |           |           |           |           |           |           |
|-----------------------------|---|-----------|-----------|-----------|-----------|-----------|-----------|
|                             | $a_1$                                   |           |           |           |           | $a_6$     |           |
|                             |   | $a_2$     | $a_3$     | $a_4$     | $a_5$     |           |           |
| Table 7: 3rd mode           |   |           |           |           |           |           |           |
| 1st stage                   | $0.998332 < \lambda_3 < 1.159069$       | +0.338890 | +0.203307 | -0.851204 | -1.008288 | +0.031210 | +0.750523 |
| 2nd stage                   | $1.102694 < \lambda_3 < 1.112744$       | +0.258677 | +0.232939 | -0.841638 | -1.033750 | -0.109284 | +1.754027 |
| 3rd stage                   | $1.111714 < \lambda_3 < 1.112426$       | +0.258239 | +0.235217 | -0.840769 | -1.036127 | -0.127633 | +1.884832 |
| 4th stage                   | $1.112404 < \lambda_3 < 1.112426$       | +0.258319 | +0.235147 | -0.839694 | -1.036192 | -0.128461 | +1.890370 |
| Table 8: 4th mode           |   |           |           |           |           |           |           |
| 1st stage                   | $0.907112 < \lambda_4 < 1.326799$       | +0.198410 | +0.213154 | -0.903893 | -1.098391 | +0.312674 | -1.161203 |
| 2nd stage                   | $1.320314 < \lambda_4 < 1.320656$       | +0.262771 | +0.195087 | -0.919453 | -1.005190 | +0.297671 | -1.111658 |
| 3rd stage                   | $1.320533 < \lambda_4 < 1.3206425$      | +0.262352 | +0.195103 | -0.919200 | -1.005067 | +0.297614 | -1.111429 |
| Table 9: 5th mode           |   |           |           |           |           |           |           |
| 1st stage                   | $-3.155846 < \lambda_5 < 2.673405$      | +1.068596 | -0.194316 | +0.313160 | -0.106366 | -0.000956 | +0.004064 |
| 2nd stage                   | $2.410248 < \lambda_5 < 2.458006$       | +1.347033 | -0.224312 | +0.018600 | +0.138864 | -0.010271 | +0.007597 |
| 3rd stage                   | $2.457708 < \lambda_5 < 2.457992$       | +1.346877 | -0.224125 | +0.015654 | -0.140984 | -0.010341 | +0.007615 |
| Table 10: 6th mode          |   |           |           |           |           |           |           |
|                             | $4.912809 < \lambda_6 < 4.916035$       | +0.057970 | -0.123640 | +2.078960 | -1.501980 | +0.049640 | -0.013360 |

the freedom by 1, and makes the gravest frequency take a higher value than it has when (one end being fixed) all masses can move together in the same direction. We can if we like regard the fixity of  $O$  in figure 1 as due to the attachment there of an infinite mass: then on account of this added mass  $N$  is increased from 6 to 7, but it is again reduced to 6 (as in our calculations) when we impose the momentum condition (41).\*

#### FORCED OSCILLATIONS

22. Occasionally it may be required to calculate the response of a given system to fluctuating forces specified both as to magnitude and periodicity. Then the forces which call for liquidation will be given not by (9) but by such expressions as

$$F_k = \bar{F}_k + p^2 T_k - V_k, \quad (42)$$

$\bar{F}_k$  and  $p^2$  being specified. The procedure required for liquidation will apply without change, but only one "stage" will be entailed, because  $p^2$  is known throughout.

This is on the understanding that the response is wanted only for one periodicity of the applied forces. But in fact a solution for free vibrations such as we have obtained in this paper provides material for a solution applicable to all frequencies. If  $(T_1)_1, (T_2)_1, \dots, (T_N)_1$  stand as in § 16 for the inertia forces in the first mode, and if  $p_1^2$  relates to the natural frequency in that mode, then a first-mode displacement associated with some other frequency-parameter  $p^2$  will entail forces on constraints of which

$$(F_k)_1 = p^2 (T_k)_1 - (V_k)_1$$

is typical: consequently all forces on constraints will vanish provided that for every  $k$  the external force

$$\begin{aligned} \bar{F}_k &= - (F_k)_1 = (V_k)_1 - p^2 (T_k)_1, \\ &= (p_1^2 - p^2) (T_k)_1, \end{aligned}$$

since (4) is satisfied in the first-mode displacement. This means that if for all  $k$ 's the external force

$$\bar{F}_k = A \cdot (T_k)_1 \quad (43)$$

( $A$  having any constant value), the response of the system will consist of first-mode displacements multiplied in the ratio

$$A / (p_1^2 - p^2), \quad (44)$$

\* On this aspect cf. Southwell 1940, Part II.



—a well-known result. Similar relations hold in relation to the other normal modes; so we can calculate the response to any given system of external forces, provided that we can express these by a series of the form

$$\bar{F}_k = A_1(T_k)_1 + A_2(T_k)_2 + \dots + A_N(T_k)_N \quad (45)$$

in which the  $A$ 's have values independent of  $k$ .

23. Taking advantage of the conjugate property (§ 14) it is easy to evaluate the  $A$ 's in (45). For in virtue of that property we have

$$\Sigma_N[\bar{F}_k \cdot (a_k)_r] = A_r \Sigma_N[(T_k)_r' (a_k)_r] = 2A_r \cdot T_r \quad (46)$$

simply,  $(a_k)_r$  denoting the displacement  $a_k$ , and  $T_r$  the value of  $T$ , appropriate to the  $r$ th normal mode. Thus suppose that in our torsional example

$$\bar{F}_1 = \bar{F}_2 = \bar{F}_3 = \bar{F}_4 = \bar{F}_6 = 0, \quad \bar{F}_5 = 1, \quad (47)$$

and that we want  $A_2$ . The displacements in the second mode are given in line 20, and the corresponding  $T$ -forces in line 19 of Table 6; moreover in line 22 of the same table the value of  $\Sigma_N[(T_k)_2 \cdot (a_k)_2]$ , which is  $2T_r \times 10^6$ , is recorded as 15,165,819; therefore in this instance (46) becomes

$$15 \cdot 165819 A_2 = 1 \times (-0 \cdot 002680). \quad (48)$$

The other  $A$ 's can be calculated similarly.

#### APPROXIMATE TREATMENT OF SYSTEMS WHICH INCLUDE DAMPING FORCES

24. It will be realized that this general treatment of forced oscillations is possible only for the reason that relaxation methods can determine the modes as well as the frequencies of free vibration. A further consequence is the possibility of making allowance for damping forces, *provided that these are small*.

When (as is usual) the damping forces can be derived from a "dissipation function"  $\Phi$  which is a homogeneous quadratic function of the generalized velocities,\* equation (1) is replaced by

$$\frac{d}{dt} \left( \frac{\partial \mathfrak{T}}{\partial \dot{q}_k} \right) - \frac{\partial \mathfrak{T}}{\partial q_k} + \frac{\partial \Phi}{\partial \dot{q}_k} + \frac{\partial \mathfrak{V}}{\partial q_k} = Q_k, \quad (49)$$

and if  $\Phi$  is necessarily positive then all free vibrations will come ultimately to zero. Consequently, if "normal" free vibrations (of *small* amplitude) be

\* Cf. e.g. Lamb 1920, § 96. The dissipation function was first introduced by Rayleigh (1873).

defined by the statement that every co-ordinate varies in accordance with a common time factor  $e^{\lambda t}$ , so that (2) is replaced by

$$q_k = a_k e^{\lambda t} \quad (a_k \text{ constant}), \quad (50)$$

and if (3) be now replaced by

$$\mathbf{T} = \mathbf{T} e^{2\lambda t}, \quad \Phi = \Phi e^{2\lambda t}, \quad \mathbf{V} = \mathbf{V} e^{2\lambda t}, \quad (51)$$

so that each of  $\mathbf{T}$ ,  $\Phi$ ,  $\mathbf{V}$  is a homogeneous quadratic function of the  $N$  displacements typified by  $a_k$ , then  $\lambda$  will either be real and negative or complex with negative real part. The type equation (4) is replaced by

$$\lambda^2 T_k + \lambda \Phi_k + V_k = 0, \quad (52)$$

where  $\Phi_k$  (conformably with our previous notation) stands for  $\partial \Phi / \partial a_k$ ; and because  $\lambda$  may be complex in a solution of the  $N$  equations typified by (52), we must contemplate the possibility that some or all of the  $N$  displacements of type  $a_k$ —i.e. of the  $(N-1)$  ratios of type  $a_k/a_1$ —will also be complex.

Formally the orthodox treatment of normal vibrations is not greatly altered by the inclusion of  $\Phi$ , but in practice the labour becomes prohibitive when  $N$  exceeds 3 or 4, since the order of the "frequency equation" is now raised from  $N$  to  $2N$ . In ordinary applications the damping forces are small, and on that understanding it was shown by Rayleigh (1926, § 102) that approximate solutions can be found. The main effects of damping are revealed as (i) the imposition on each normal oscillation of some finite decay factor unaccompanied by change in periodicity and (ii) a modification of each mode whereby the different co-ordinates no longer fluctuate in phase.

25. An approximate treatment of *small and positive* damping can be briefly indicated here. When by the methods of this paper all of the  $N$  normal modes and associated frequencies have been determined, we can change from the co-ordinates  $a_1, a_2, \dots, a_N$  to "normal co-ordinates"  $\phi_1, \phi_2, \dots, \phi_N$  which are the multiplying constants required to make

$$a_k = \phi_1(a_k)_1 + \phi_2(a_k)_2 + \dots + \phi_N(a_k)_N \quad (53)$$

hold for all  $k$ 's,  $(a_k)_r$  having the same significance as in § 23. Then the expressions for  $\mathbf{T}$  and  $\mathbf{V}$  can be replaced by\*

$$\left. \begin{aligned} \mathbf{T} &= \phi_1^2 \mathbf{T}_1 + \phi_2^2 \mathbf{T}_2 + \dots + \phi_N^2 \mathbf{T}_N, \\ \mathbf{V} &= \phi_1^2 \mathbf{V}_1 + \phi_2^2 \mathbf{V}_2 + \dots + \phi_N^2 \mathbf{V}_N, \end{aligned} \right\} \quad (54)$$

where

$$\mathbf{V}_r = p_r^2 \cdot \mathbf{T}_r = \mu_r \mathbf{T}_r, \quad \text{say,}$$

\* The  $\phi$ 's in this section have the same significance as the  $A$ 's in § 14, so equations (54) are compatible with (28).

all  $\mu$ 's being known from our solution.  $T_r$  and  $V_r$  (as in §14) denote the (known) values of  $T$  and  $V$  appropriate to the  $r$ th normal mode.\*

In general the corresponding expression for  $\Phi$  will involve products as well as the squares of the normal co-ordinates, but it will always be a homogeneous quadratic function: therefore in (52), *which will also hold when  $T_k, \Phi_k, V_k$  are interpreted as standing for  $\partial T/\partial \phi_k, \partial \Phi/\partial \phi_k, \partial V/\partial \phi_k$* ,  $\Phi_k$  will be a linear function of (in general) all the  $\phi$ 's. From (54) we have

$$2T_k(\lambda^2 + \mu_k)\phi_k + \lambda\Phi_k = 0, \quad (55)$$

and when  $\Phi = 0$  these  $N$  equations yield  $N$  solutions typified by

$$\lambda^2 + \mu_k = 0, \quad \phi_k \text{ unrestricted}, \quad \phi_r = 0 \quad (r \neq k), \quad (56)$$

—as we should expect. Starting with any one of these solutions we trace the effect of  $\Phi$  assumed *finite but small*.

26. When the starting solution is that in which  $\phi_k$  does not vanish, it follows from (56) that all  $\phi$ 's except  $\phi_k$  (since they vanish with  $\Phi$ ) may for a first approximation be neglected in the expression for  $\Phi_k$ . Accordingly in (55) we may write

$$\left. \begin{aligned} \Phi_k &\approx \alpha_{kk} \cdot \phi_k, \\ \text{where } \alpha_{kk} &\equiv \frac{\partial^2 \Phi}{\partial \phi_k^2}, \text{ so is small of order } \Phi. \end{aligned} \right\} \quad (57)$$

$$\text{Then (55) reduces to } \{2T_k(\lambda^2 + \mu_k) + \lambda\alpha_{kk}\}\phi_k = 0, \quad (58)$$

and for  $r \neq k$  we have to the same approximation

$$\left. \begin{aligned} 2T_r(\lambda^2 + \mu_r)\phi_r + \lambda\alpha_{kr}\phi_k &= 0, \\ \text{where } \alpha_{kr} &= \frac{\partial^2 \Phi}{\partial \phi_k \partial \phi_r}, \text{ so is small of order } \Phi. \end{aligned} \right\} \quad (59)$$

If now we postulate that  $\phi_k = 1$  in the  $k$ th mode as modified by damping,† then the solution of (58) is (to the approximation of this section)

$$\left. \begin{aligned} \lambda &= -\frac{1}{4} \frac{\alpha_{kk}}{T_k} \pm i\sqrt{\mu_k}, \\ \text{and to a like approximation we have from (59)} \\ (\mu_k - \mu_r)\phi_r &= \pm \frac{i\alpha_{kr}\sqrt{\mu_k}}{2T_r} \quad (r \neq k). \end{aligned} \right\} \quad (60)$$

\* By so defining the normal modes (in regard to amplitude) that all quantities of the type  $T_r$  have the value 1, we can simplify the expressions which follow. But the simplification is purely formal: it does not save labour in computation.

† The mode is indeterminate as regards absolute magnitude, so the postulate entails no restriction.

In real form, and with time factors now included in  $\phi_k$ ,  $\phi_r$ , the modified solution can be written as

$$\left. \begin{aligned} \phi_k &= \exp \left[ -\frac{1}{4} \frac{\alpha_{kk} t}{T_k} \right] \cos (\sqrt{\mu_k} \cdot t + \epsilon), \\ (\mu_r - \mu_k) \phi_r &= \exp \left[ -\frac{1}{4} \frac{\alpha_{kk} t}{T_k} \right] \sin (\sqrt{\mu_k} \cdot t + \epsilon) \times \frac{\alpha_{kr} \sqrt{\mu_k}}{2T_r} \quad (r \neq k), \end{aligned} \right\} \quad (61)$$

confirming both of Rayleigh's conclusions (§ 24).

Without great labour this method may be extended to obtain closer approximations (including terms of the order of  $\Phi^2$ ,  $\Phi^3$ , ..., etc.).

#### EXTENSION OF THE METHOD TO CONTINUOUS SYSTEMS

27. One further application may be noticed,—namely, to continuous systems. Reference was made in § 1 to a "relaxation" treatment of such systems (in Part IV of this series) depending on the assumption that every mode can be expressed in a finite series of selected functions. Our present investigation suggests an alternative, based on the use of approximate formulae of integration and differentiation, which by permitting *local* adjustment lets us take full advantage of the double-limit rule of § 5.

Suppose for example that we want to determine the six gravest modes and frequencies of torsional vibration for a cantilever shaft of non-uniform diameter. Let  $\bar{I} \delta x / l$  be the rotatory inertia of the slice  $\delta x$  at  $x$ ,  $l$  now denoting the length of the cantilever; let  $\alpha \sin (pt + \epsilon)$  denote the angular displacement of this slice in a "normal" free vibration (§ 2); and let  $0, \alpha_1, \dots, \alpha_6$  be the values of  $\alpha$  at sections  $0, 1, \dots, 6$  which divide  $l$  into six equal parts. Then in the notation of § 2

$$T = \frac{1}{2l} \int_0^l \alpha^2 \bar{I} dx = \frac{\alpha_1^2 I_1}{2l} \int_0^l a^2 \frac{\bar{I}}{I_1} dx, \quad (62)$$

where  $a$  stands for the ratio  $\alpha/\alpha_1$ , so that  $a_0 = 0, a_1 = 1$ .

Now the "six-strip rule" of integration (Bickley 1939, formula 1.6) shows that the definite integral can be evaluated (approximately) in terms of seven equidistant values of the integrand. We have

$$\frac{1}{l} \int_0^l a^2 \frac{\bar{I}}{I_1} dx \approx \frac{1}{840} \{41(q_0 + q_6) + 216(q_1 + q_5) + 27(q_2 + q_4) + 272q_3\}, \quad (63)$$

when

$$q = a^2 \bar{I} / I_1,$$

the lowest term in the error being  $-9l^9 \frac{d^8 q}{dx^8} / 1400 \times 6^9$ .

Again in the notation of § 2 we have

$$\mathbf{V} = \frac{1}{2} \int_0^l \bar{C} \left( \frac{d\alpha}{dx} \right)^2 dx = \frac{1}{2} \frac{C}{l} \alpha_1^2 \times l \int_0^l \frac{\bar{C}}{C} \left( \frac{da}{dx} \right)^2 dx, \quad (64)$$

$\bar{C}$  denoting the torsional rigidity at section  $x$  and  $C$  (like  $I_1$ ) being as yet unspecified; and by the "six-strip rule" we have

$$\left. \begin{aligned} l \int_0^l \frac{\bar{C}}{C} \left( \frac{da}{dx} \right)^2 dx &\approx \frac{l^2}{840} \{41(q_0 + q_6) + 216(q_1 + q_5) + 27(q_2 + q_4) + 272q_3\}, \\ \text{when} \quad q &= \frac{\bar{C}}{C} \left( \frac{da}{dx} \right)^2. \end{aligned} \right\} \quad (65)$$

Moreover with close approximation we may write

$$\left. \begin{aligned} \left( \frac{da}{dx} \right)_k^2 &= \frac{1}{2} \left\{ \left( \frac{a_{k+1} - a_k}{l/6} \right)^2 + \left( \frac{a_k - a_{k-1}}{l/6} \right)^2 \right\} \\ &= \frac{18}{l^2} \{ (a_{k+1} - a_k)^2 + (a_k - a_{k-1})^2 \}, \end{aligned} \right\} \quad (66)$$

with  $a_0 = 0$ ,  $a_1 = 1$  as before and

$$\left( \frac{da}{dx} \right)_0^2 = \frac{36}{l^2} a_1^2, \quad \left( \frac{\partial a}{\partial x} \right)_6^2 = \frac{36}{l^2} (a_6 - a_5)^2,$$

and on this understanding the right-hand side of (65)

$$\begin{aligned} &\equiv \frac{3}{140C} [(41 \times 2\bar{C}_0 + 216\bar{C}_1) + (216\bar{C}_1 + 27\bar{C}_2)(a_2 - 1)^2 \\ &\quad + (27\bar{C}_2 + 272\bar{C}_3)(a_3 - a_2)^2 + (272\bar{C}_3 + 27\bar{C}_4)(a_4 - a_3)^2 \\ &\quad + (27\bar{C}_4 + 216\bar{C}_5)(a_5 - a_4)^2 + (216\bar{C}_5 + 41 \times 2\bar{C}_6)(a_6 - a_5)^2]. \end{aligned} \quad (67)$$

We now have expressions both for  $\mathbf{T}$  and  $\mathbf{V}$  which, like those of § 8, involve only six displacements  $a_1 (= 1)$ ,  $a_2$ , ...,  $a_6$ ; and from these we can determine six normal modes and the associated frequencies, exactly as in the example treated in this paper.

28. In fact, according to (63) the expression (62) for  $\mathbf{T}$  will be identical with that of § 8 provided that\*

$$\left. \begin{aligned} a_0 = 0, a_1 = 1 &\quad (\text{as assumed for the cantilever}) \\ \text{and} \quad 840I_1(1, 4, 0.8, 1, 6, 0.8) \\ &= (216\bar{I}_1, 27\bar{I}_2, 272\bar{I}_3, 27\bar{I}_4, 216\bar{I}_5, 41\bar{I}_6). \end{aligned} \right\} \quad (68)$$

\*  $\alpha_1$  in this section is identical with  $\alpha$  in § 8.

If then we could provide similarly for elastic equivalence, the solution which has been obtained in this paper would also apply to the continuous cantilever. The calculated modes would define the angular displacements of six equidistant sections, and fair curves drawn through their plotted values would give (approximately) the six gravest modes for the cantilever.

Actually this complete equivalence (which would have only academic interest) cannot be realized for the reason that it would imply a cantilever having *negative* stiffness in some part of its length. Identity of (64) with the expression for  $V$  in § 8 would require, according to (65) and (67), that

$$\begin{aligned} \frac{140C}{3} \times \left( 1, \frac{1}{0.8}, 1, \frac{1}{0.6}, \frac{1}{1.1}, \frac{1}{1.2} \right) \\ = (82\bar{C}_0 + 216\bar{C}_1, 216\bar{C}_1 + 27\bar{C}_2, 27\bar{C}_2 + 272\bar{C}_3, \\ 272\bar{C}_3 + 27\bar{C}_4, 27\bar{C}_4 + 216\bar{C}_5, 216\bar{C}_5 + 82\bar{C}_6), \end{aligned} \quad (69)$$

and if these relations were satisfied it would follow that

$$82\bar{C}_0 + 216\bar{C}_5 = \frac{140}{3} C \left( 1 - \frac{1}{0.8} + 1 - \frac{1}{0.6} + \frac{1}{1.1} \right) = -\frac{140C}{3 \times 132}, \quad (70)$$

therefore either  $C_0$  or  $C_5$  would be negative.

#### SUMMARY

In this paper Relaxation Methods are applied to the difficult problem of determining the natural modes and frequencies of a system having restricted but considerable freedom (i.e. where the independent co-ordinates number 6 or more). A theorem published recently (Southwell 1940) is used to impose lower limits on the wanted frequency, and upper limits are calculated on the basis of "Rayleigh's principle". In the "liquidation" process these upper and lower limits converge steadily, and when they have become closely coincident both the frequency and the associated mode (which Rayleigh's principle does not determine) are given with sufficient accuracy for all practical purposes.

An example treated in detail relates to undamped torsional vibrations or (by analogy) to transverse vibrations of a tensioned and loaded string. Concluding sections indicate some immediate extensions of the method, viz. (a) to vibrating systems which are entirely unconstrained, (b) to dissipative systems in which the damping forces (as is usual in practice) are relatively small, (c) to continuous systems, for which the method is an alternative to that given in Part IV of this series.

## REFERENCES

- Biokley, W. G. 1939 *Math. Gaz.* **23**, 352-359.  
Black, A. N. and Southwell, R. V. 1938 *Proc. Roy. Soc. A*, **164**, 447-467.  
Bradfield, K. N. E., Christopherson, D. G. and Southwell, R. V. 1939 *Proc. Roy. Soc. A*, **169**, 289-317.  
Den Hartog, J. P. 1934 *Mechanical Vibrations*. New York and London: McGraw-Hill Co.  
Lamb, H. 1920 *Higher Mechanics*. Camb. Univ. Press.  
Rayleigh, Lord 1873 *Proc. Lond. Math. Soc.* **4**, 357-368; also *Collected Papers*, **1**, 170-181.  
— 1926 *Theory of Sound*, 2nd ed. Macmillan and Co.  
Southwell, R. V. 1936 *Introduction to the Theory of Elasticity*. Oxford Univ. Press.  
— 1940 *Proc. Roy. Soc. A*, **174**, 433-457.  
Temple, G. 1939 *Proc. Roy. Soc. A*, **169**, 476-500.
- 

The glide elements of body-centred cubic crystals,  
with special reference to the effect of temperature

BY E. N. DA C. ANDRADE, F.R.S. AND Y. S. CHOW, PH.D.

*Physics Laboratory, University College, London*

(Received 9 March 1940)

[Plates 2-4]

1. INTRODUCTION

In a previous paper from this laboratory (Andrade and Tsien 1937) the particular interest of body-centred cubic crystals was pointed out, and the glide elements for single crystals of sodium and potassium at atmospheric temperatures were determined, viz. glide plane (123) and glide direction [111]. Another paper (Tsien and Chow 1937) describes the determination of the glide elements for molybdenum, for which the glide direction was again [111], but the glide plane was different at different temperatures, viz. (110) at 1000° C and (112) at 300 and 20° C. Planes (123), (110) and (112) have all been given as glide planes for  $\alpha$ -iron by different workers (Taylor and Elam 1926; Gough 1928; Fahrenhorst and Schmid 1932), while for tungsten (Goucher 1924) the glide plane has been given as (112) and for  $\beta$ -brass under certain conditions (G. I. Taylor 1928) as (110). With all the

metals just enumerated the glide direction is  $[111]$ , but it appears as a general result that  $(110)$ ,  $(112)$  and  $(123)$  are all possible glide planes for the body-centred cubic crystal, the operative plane varying from metal to metal.

Since the geometry of all body-centred metals is the same, it seems probable that different plastic behaviour of the different metals in respect of the glide plane must be due to some secondary influence which has varied from metal to metal in the previous experiments. The results of Tsien and Chow for molybdenum have shown that temperature has an influence, the plane changing with this metal from  $(112)$  to  $(110)$  as the temperature is raised. It therefore appears that temperature may be the determining factor with any particular metal in the selection of the glide plane among the three which have been found possible for the body-centred structure, a fact to which attention has already been directed by one of us (Andrade 1938) in a discussion organized by the Royal Society. The present investigation was undertaken in order to investigate the glide properties of particular body-centred metals over a wide range of temperature. A general law has been found, viz. that the glide plane changes systematically from one of the three specified planes to another as the temperature is raised, the ratio of the temperature of experiment to the melting point of the metal being, at any rate as a first approximation, the parameter which determines the operative plane. Preliminary reference was made to the law in the discussion to which reference has just been made.

Evidence as to the mechanism of hardening has been found in the variation of the strain-hardening curves with temperature, and a general explanation found for the different appearance of the asterisms found with different metals. Certain generalities in the spacing of the glide planes have also been demonstrated.

## 2. PRODUCTION OF THE CRYSTALS

The metals used were sodium, potassium, and  $\alpha$ -iron. The sodium and potassium were taken from the very pure specimens used by Andrade and Tsien (1937), and the single crystals were prepared by the method described by them. The single crystals of  $\alpha$ -iron were prepared by the method of heating the wire by the passage of a current and using a moving subsidiary furnace (Andrade 1937; Tsien and Chow 1937). The iron was a particularly pure specimen, estimated 99.98 % pure iron, supplied by Messrs Hilger and drawn by Messrs Johnson and Matthey.

In the case of iron it was necessary to estimate the temperature of the wire. This cannot be done by optical methods, since the hot metal vaporizes



*in vacuo*, giving a deposit on the inside of the quartz tube, which cuts down the transmitted radiation. A method was devised which depends upon the resistivity and radiating properties of the wire: it has the advantage that it eliminates the effect of thermal conduction at the ends of the wire, which leads to cooling and so renders difficult the measurement of temperature by resistivity alone. Consider a length  $\Delta l$  of the wire sufficiently remote from the ends for conduction effects to be neglected. Then

$$\frac{\rho \Delta l}{\pi r^2} i^2 = A E \sigma T^4 = 2\pi r \Delta l E \sigma T^4,$$

where  $i$  is the current,  $r$  is the radius of the wire,  $\rho$  the electrical resistivity,  $A$  the surface area,  $E$  the emissivity of the surface,  $\sigma$  Stefan's constant, so that

$$i = \left\{ \frac{2\pi^2 r^3 E \sigma}{\rho} \right\}^{1/2} T^2.$$

This gives the temperature of the main part of the wire.

For molybdenum the necessary data for  $\rho$  and  $E$  as functions of  $T$  are given by Esper and Knoll (1936), so that, for a given  $r$ , a curve of  $i$  against  $T$  can be prepared: to transfer to any other radius  $r'$  we have only to remember that  $i$  is proportional to  $r^{1/2}$ . When the original measurements on molybdenum were carried out this method had, however, not been devised. For iron, which has not been used for filaments in high vacuum work, the data known to us at the time were scanty. A series of measurements of the resistivity at different temperatures was therefore carried out. A wire of the very pure iron to which reference has been made, 1 mm. in diameter and 60 cm. long, in the form of a hair pin, was sealed in a highly exhausted quartz tube which also contained a suitably placed thermocouple. The leads were stout copper rods, in which the ends of the iron wire were firmly gripped, and the tube was inserted in a long electric furnace, special precautions being taken to ensure that the whole wire and a length of the leads lay well within the part of the furnace where the temperature had been found to be uniform. The resistivity was calculated from the current, read on a carefully calibrated standard milliammeter, and the potential difference, measured on a potentiometer. The following readings were obtained between 20 and 1000° C.\*

\* Dr Chow had to leave hurriedly for China, owing to the outbreak of war, and took the notebook with the actual data with her. The values in the table are reconstructed from the recorded points on the curve, and are consequently not as accurate as the actual readings made. The error should not, however, exceed +0.1.

TABLE 1

| Temp.<br>° C | Resistivity in<br>microhm-cm. |
|--------------|-------------------------------|
| 100          | 16.5                          |
| 183.5        | 22.25                         |
| 316          | 32.7                          |
| 413          | 43.2                          |
| 520          | 57.5                          |
| 596          | 68.5                          |
| 680          | 82.0                          |
| 790          | 99.1                          |
| 889          | 107.0                         |
| 990          | 112.0                         |

Some time after these readings were obtained the interest for modern theory of the change of curvature in the neighbourhood of the Curie point, pointed out by Mott (1935, 1936), came to our notice. At Mott's instigation measurements on the resistivity of pure iron were carried out by H. H. Potter (1937), who, however, determined only the ratio of the resistance to the resistance at 0° C. Both Mott and Potter have overlooked measurements by Chevenard (1932), who gives the resistivity of iron up to 1050° C in the form of a curve, without any tabulated values. For comparison the results of the three experiments are given in figure 1, Potter's values being made to fit Chevenard's in the neighbourhood of 300° C. Chevenard's curve is given as a broken line.

Our absolute values agree very closely (as nearly as measurements taken from his curve admit) with Chevenard's above the Curie point, but below, while the form of his curve follows ours closely, his values are lower, by something about 2% in the mid-region. It is unfortunate that Potter gives no absolute values. It is quite clear, however, that his values in the neighbourhood of, and above, the Curie point must be considerably in excess of ours, unless the resistance of his specimen was abnormally low in the 100–600° C region. Our values and Chevenard's show a strong concavity to the temperature axis at high temperatures, as required by Mott's theory.

To estimate very roughly the temperature of that part of the wire surrounded by the subsidiary furnace, which was about 2 cm. long and 2 cm. in diameter, and subtended a solid angle of  $2\pi$  at its centre, we note that the energy radiated to the centre is about  $\frac{1}{2}\sigma T_f^4$ , where  $T_f$  is the temperature of the furnace. The temperature  $T'$  of this hottest part of the wire can then be estimated from

$$E\sigma T'^4 = E\sigma T_f^4 + \frac{1}{2}\sigma T_f^4,$$

where  $T$  is the temperature of the wire heated by the passage of the current in the absence of the furnace. This is admittedly an exceedingly rough estimate, but nothing more is required.

For preparing single crystals, iron wires of diameter 0.5, 0.7 and 1 mm. were used. The wire was polished with Hubert emery papers from no. 0 to

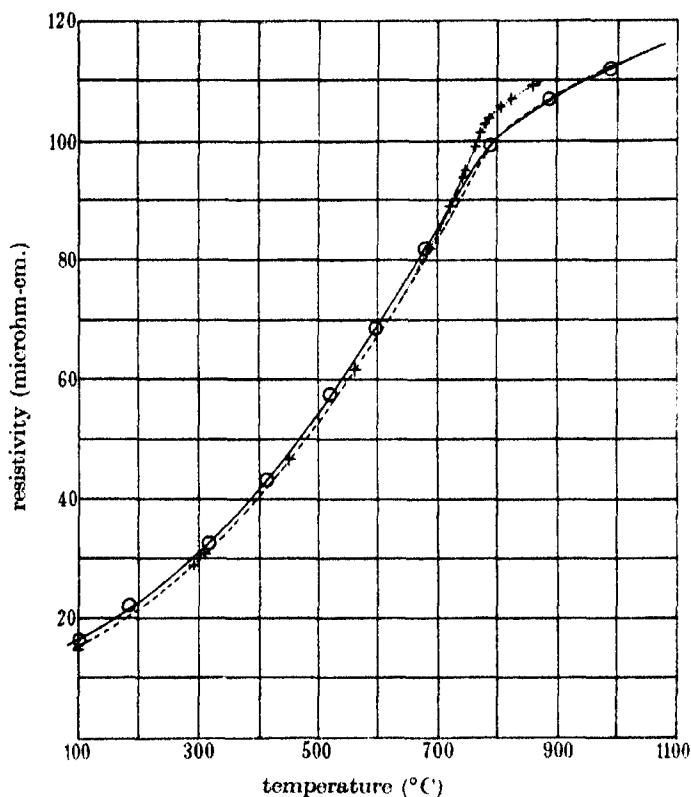


FIGURE 1

|                      |                    |
|----------------------|--------------------|
| —○— Andrade and Chow | } absolute values. |
| - - - Chevenard      |                    |
| ...+... Potter       |                    |
|                      | } relative values. |

no. 0000 successively before insertion in the heating apparatus (see figure 2, Tsien and Chow 1937), where it was maintained in a high vacuum. It was heated, by the passage of a current, to 1500° C for 10 min. or so, and then maintained at 800° C. The travelling furnace was also maintained at 800° C and travelled at 8 cm./hr., the hottest part of the wire within it being estimated as 200° above the temperature of the main part of the wire.

Crystals several cm. in length, which were successfully grown with molybdenum, were never produced with iron, but single crystals 1 cm. or so in length were regularly obtained.

The production of single crystals of sodium and potassium is easy, and has already been described elsewhere.

### 3. EXTENSION AND MEASUREMENT OF CRITICAL SHEAR STRESS

An apparatus was constructed which enabled sodium and potassium wires to be slowly extended *in vacuo*, the tensile stress being readable at any stage. It is shown in figure 2. *B* is a ring of phosphor-bronze strip, the deformation of which measures the stretching force. A smooth rod *r*, rigidly fixed to the top of the ring, moves freely within a tube *t*, which both acts as a guide and enables the deformation to be observed, the distance between the mark *u* and the sharp edge of the tube being read with a microscope. From previous calibration this distance gives the applied force. The ring is carried by a threaded rod *R*<sub>1</sub>, which is moved vertically, without rotation, by the nut *S*, supported by the glass tube *G*. The joint is made vacuum-tight by the rubber sleeve *D*.

The whole ring is contained in a flat brass box *A*, with opposite windows of stout glass parallel to the plane of the paper. To the box is attached a glass tube *G*<sub>1</sub> which carries a metal cylinder *M*, pierced by two long opposite openings, through which the chucks can be adjusted. One chuck, *H*<sub>1</sub>, is attached to the lower part of the ring by the rod *R*<sub>2</sub>, the other, *H*<sub>2</sub>, is carried by *M*. These chucks hold the wire to be extended.

*T* is a small funnel, from which a long glass tube *L* passes into the apparatus by way of a vacuum-tight joint. It serves to

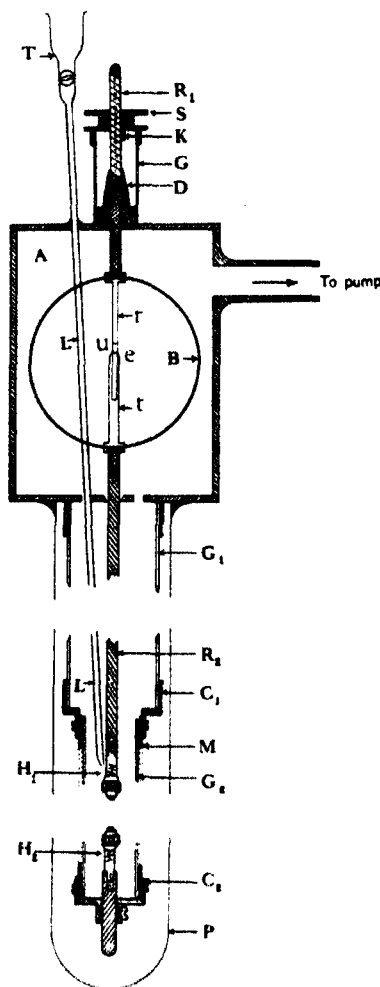


FIGURE 2

introduce oil for recoating the crystal. The glass tube  $G_2$  serves to hold the oil. A pyrex glass tube  $P$  encloses the lower part of the apparatus: the whole can be evacuated through the tube shown.

The oil tube  $L$  was necessary for the following reason. In the earlier experiments at room temperature the sodium or potassium wire was protected by a film of anhydrous apiezon L grease, but at liquid air temperature this grease becomes a hard solid layer which is stronger than the crystal itself. In the present experiments a mixture of 50 % apiezon L and 50 % apiezon oil was used, which is thick enough to form a permanent layer at room temperature, but flows very freely at 50° C. The sodium crystal was made to pass from the protecting glass tube in which it was made into this mixture. The crystal, protected by its layer of grease, was fixed in the chucks, and the apparatus evacuated. The tube  $P$  was then surrounded by water at 50° C, with the result that the grease ran off, leaving a bright surface. It was found advisable to fill the lower part of  $P$  with metal filings, to make good thermal contact with the metal frame and lower chuck.

After the stressing had been carried out, apiezon oil was introduced by  $L$ , and the oil frozen by surrounding the tube with solid  $\text{CO}_2$ . Air was then admitted, and the crystal, protected by a coat of frozen oil, removed, and plunged into apiezon L at 50° C. The oil melted and a protective layer of mixed oil and grease was formed. In spite of these precautions a certain amount of very slow oxidation usually took place, but the surface markings were always plainly visible for a considerable time.

The measurement of critical shear stress was carried out as follows. The evacuated tube was surrounded by the bath, either of liquid air or of carbon dioxide snow in alcohol, and left for some time to come into temperature equilibrium. A reading microscope with a 40 mm. objective and eyepiece, provided with a graticule of 100 divisions (1 division = 0.023 mm.), was focused on  $e$ , and the nut  $S$  slowly turned so as to move the uppermost part of the ring at a rate of about 0.5 mm./min. At the moment when the first movement of  $e$  was detected the distance between  $e$  and  $u$  was recorded, which, by the previous calibration, gives the tension at the moment of yield. After this the rotation of the nut was continued, and various values of the displacement of  $e$ , which gives the extension of the wire, and of the distance  $eu$ , which gives the tension, were taken. After a certain extension (about 2 % at atmospheric temperature, corresponding to a glide of somewhat over 3 % with our values of  $\chi$ ) the wire started to flow appreciably at constant stress, so that if the nut was left in a fixed position the mark  $e$  crept upwards and then stopped, owing to the reduction of the

tension. The stress-strain curve cannot be usefully continued past the point at which appreciable time flow sets in.

The angle  $\chi$  between the glide plane and the wire axis was measured after the crystal had been coated with wax and removed from the apparatus. From this the initial angle  $\chi_0$ —or the angle at any stage of the extension—was found by the formula

$$\frac{\sin \chi_0}{\sin \chi} = \frac{l}{l_0}.$$

The glide direction was estimated by the geometrical method previously described. Hence the critical shear stress and the resolved shear stress at any particular strain was found. The hardening curve was obtained by plotting the resolved shear stress against the glide, expressed as the relative displacement of two (parallel) glide planes unit distance apart.

#### 4. DETERMINATION OF THE GLIDE ELEMENTS

The glide planes were visible as the familiar surface markings consequent on slight extension: in all crystals used for determination they were regular and parallel. The crystal was mounted in a goniometer and arranged so that the normal to the glide planes fell in the plane containing the horizontal beam of X-rays and the axis of the crystal wire, a horizontal low-power microscope, with its axis perpendicular to the X-ray beam, being used to make the final adjustment. The glide elements were located, relative to the surface markings of the wire, by the Laue method described earlier (Andrade and Tsien 1937). The X-ray tube was, as before, a Shearer tube with copper target, a tube of quartz glass, and a 1 mm. lithium window, protected from oxidation on the outer face by a layer of grease. The method of identification of the planes was to select a number of strong Laue spots, lying on a great circle, to rotate this, by calculation, about its diameter, so as to make it a complete primitive circle, and then to compare all the spots with one of the standard stereographic projection figures for the body-centred lattice. Agreement not only in position, but in intensity, was obtained.

The plastic deformation of a single crystal is accompanied by a rotation of crystal fragments about an axis lying in the glide plane and perpendicular to the glide direction (Burgers 1931; Andrade and Tsien 1937). These rotations, which may spread over some degrees, are evidenced by the distortion of the Laue spots into the familiar asterisms, which in the case of sodium and potassium are made up of a series of discrete patches

(Andrade and Tsien 1937). One reflecting plane, however, cannot produce an asterism, viz. that normal to the axis of rotation just mentioned. If the azimuth adjustment of the crystal brings the normal to the glide plane into the plane containing the X-ray beam and the wire axis, this plane cannot form a spot. However, by rotating the wire through  $6^\circ$  or so an intense undistorted spot, near the central spot, can be obtained. This undistorted spot gives a very useful supplementary method for establishing the glide plane, especially in doubtful cases. Figure 3, plate 2, taken with a sodium crystal deformed at  $-185^\circ\text{C}$ , shows the undistorted spot, 7, ringed.

The glide direction was determined by the geometrical method described by Andrade and Tsien (1937).

### 5. SPACING OF THE GLIDE PLANES

There are certain indications that the thickness of the glide packets (spacing between the glide planes) depends upon the temperature, e.g. the case of molybdenum (Tsien and Chow 1937). The present work provided an opportunity of extending observations on this point.

Molybdenum wires were stretched at higher temperatures than those recorded by Tsien and Chow. At these high temperatures it is not possible to use the simpler method of heating the single crystal wire by the passage of a current through it, since, if this is done, any slight local thinning at once leads to increased local heating, a process which rapidly culminates in fracture at this spot. Use was therefore made of a special furnace with which a temperature of  $2000^\circ\text{C}$  could easily be reached. It consisted of a tantalum tube 11 cm. long and 5 mm. diameter, the wall thickness being 0.3 mm. This tube,  $T$ , which was mounted *in vacuo*, was heated by a heavy current drawn from special storage batteries. The method of mounting is shown in figure 4. The tube  $T$  is fitted friction-tight into two terminal copper collars,  $J_1$  and  $J_2$ , of which the upper is supported by a quartz plate  $Q_1$ , the current being led in by the brass rods  $L_1$  and  $L_2$ , which serve to support  $Q_1$  and  $Q_2$ , and a connecting strip of heavy copper. The quartz plate  $Q_2$  supports a guide which keeps  $J_2$  in line, the loose fit allowing for thermal expansion. The current is conveyed from  $J_2$  by flexible strips of heavy copper braid, shown dotted in the diagram. The whole is covered by a large bell-jar, which carries at the top a screw device for stretching the wire. The collar  $EE$ , with wires leading over pulleys to a counter-balancing weight, is for lifting the jar.

When molybdenum single crystals are stretched at  $1500^\circ\text{C}$  the glide packets are even broader than those observed at  $1000^\circ\text{C}$  by Tsien and

Chow, cf. figure 5, plate 2. At  $2000^{\circ}\text{C}$  the glide takes place on one or two planes only, separated by considerable lengths of the wire. Figure 6, plate 2, shows such an isolated glide plane as seen from the side, and

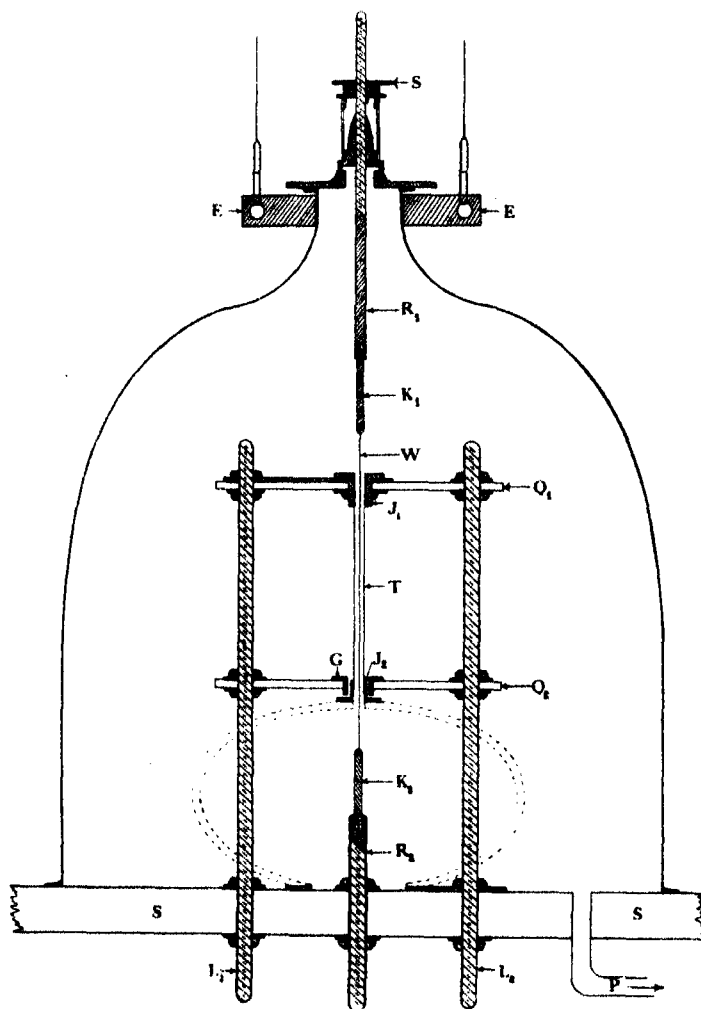


FIGURE 4

figure 7, plate 2, is a view of the same wire rotated through a right angle about its axis, taken to show the well-marked elliptical shape of the bared area, which gives evidence that the movement is really glide on one plane. Pictures of crystals extended at  $300$  and  $20^{\circ}\text{C}$  will be found in the paper by



Tsien and Chow. These experiments show clearly that for molybdenum the glide planes are very close at atmospheric temperature, and get farther and farther spaced as the temperature is raised, until at 2000° C they are separated by distances of the order of 1 cm.

With sodium and potassium crystals the spacing of the glide planes is markedly closer at low temperatures than at room temperatures, the bands produced by stretching at -182° C being exceedingly fine. When prolonged manipulation is necessary it is very difficult to avoid slight oxidation, which tends to obscure those very fine bands.

With  $\alpha$ -iron the same variation of the spacing of the bands with temperature is evident, as can be seen from figures 8 and 9, plate 2, the former being extended at 700° C and the latter at 25° C.

Boas and Schmid have found that with cadmium (1929) and zinc (1930) the glide packets are much coarser at high temperature than at atmospheric temperature. Andrade and Roscoe (1937) found with lead, it is true, only a slight increase in spacing at 100° C as compared with 15° C, but the difference in temperature is here comparatively small. It seems established then, that, as a general rule, the spacing of the glide planes increases with increasing temperature.

## 6. THE GLIDE ELEMENTS

Crystals of sodium and potassium were extended at -82 and -185° C, the glide plane being found in the manner already described. The results are given in table 2, where  $\epsilon = l/l_0$ ,  $l$  being the final length and  $l_0$  the original length;  $\chi_0$  is the angle between the glide plane and the wire axis;  $\eta$  is the angle between the glide direction and the projection of the wire axis on the glide plane. Figures 10 and 11 show the distribution of the poles of the

TABLE 2. GLIDE OF SODIUM SINGLE CRYSTAL AT LOW TEMPERATURES

| Ref. no.<br>of<br>crystal | Working<br>temp. ° C | $\epsilon$ | $\chi_0$ | Angle between glide<br>plane and |       |       | $\eta$ |
|---------------------------|----------------------|------------|----------|----------------------------------|-------|-------|--------|
|                           |                      |            |          | {110}                            | {123} | {112} |        |
| I                         | -185                 | 1.040      | 60° 55'  | 30°                              | 11°   | 0°    | 0°     |
| II                        | -185                 | 1.018      | 44° 0'   | 25°                              | 5°    | 5°    | 8°     |
| III                       | -185                 | 1.018      | 47° 10'  | 30°                              | 11°   | 0°    | 4°     |
|                           |                      |            | 65° 5'   | 29°                              | 10°   | 1°    | 1°     |
| IV                        | -185                 | 1.018      | 45° 37'  | 29°                              | 10°   | 3°    | 5°     |
| V                         | -185                 | 1.020      | 48° 46'  | 39°                              | 10°   | 6°    | 6°     |
| VI                        | -82                  | 1.019      | 53° 56'  | 6°                               | 13°   | 24°   | 8°     |
| VII                       | -82                  | 1.055      | 52° 10'  | 5°                               | 14°   | 25°   | 2°     |
| VIII                      | -82                  | 1.040      | 53° 25'  | 7°                               | 12°   | 23°   | 4°     |

glide planes at  $-82$  and  $-185^{\circ}\text{C}$  round the zone axis  $[110]$  and  $[112]$  respectively. It will be seen that the glide plane at  $-82^{\circ}\text{C}$  is  $(110)$ , and at  $-185^{\circ}\text{C}$  is  $(112)$ . These diagrams should be compared with figure 6 and figure 7, for, respectively, sodium and potassium crystals at atmospheric temperature, given in the paper by Andrade and Tsien. Tables 3 and 4 give the figures, which were not published in the earlier paper.

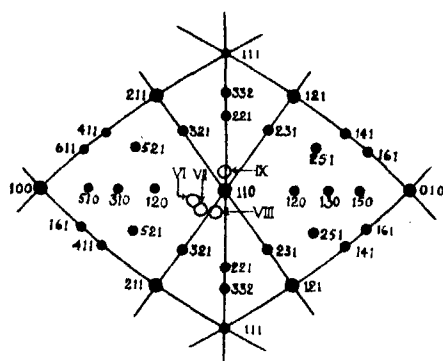


FIGURE 10

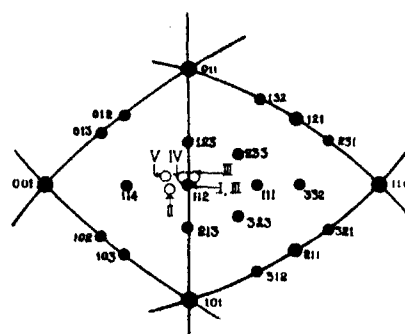


FIGURE 11

TABLE 3. GLIDE OF SODIUM SINGLE CRYSTALS AT  $25^{\circ}\text{C}$

| Ref. no.<br>of<br>crystal | $\epsilon$ | $\chi_0$         | Angle between glide<br>plane and |               |                | $\eta$        |
|---------------------------|------------|------------------|----------------------------------|---------------|----------------|---------------|
|                           |            |                  | $\{112\}$                        | $\{123\}$     | $\{110\}$      |               |
| I                         | 1.032      | $46^{\circ} 10'$ | $7^{\circ}$                      | $4.5^{\circ}$ | $23^{\circ}$   | $6^{\circ}$   |
| II                        | 1.040      | $30^{\circ} 30'$ | $35^{\circ}$                     | $8^{\circ}$   | $29^{\circ}$   | $6^{\circ}$   |
| III                       | 1.051      | $46^{\circ} 50'$ | $15^{\circ}$                     | $3^{\circ}$   | $16^{\circ}$   | $1^{\circ}$   |
| IV                        | 1.046      | $47^{\circ} 40'$ | $12^{\circ}$                     | $3^{\circ}$   | $19^{\circ}$   | $2^{\circ}$   |
| V                         | 1.036      | $57^{\circ} 10'$ | $16^{\circ}$                     | $5^{\circ}$   | $14.5^{\circ}$ | $11^{\circ}$  |
| VI                        | 1.017      | $51^{\circ} 10'$ | $11^{\circ}$                     | $4^{\circ}$   | $20^{\circ}$   | $24^{\circ}$  |
| VII                       | 1.004      | $45^{\circ} 25'$ | $12^{\circ}$                     | $4^{\circ}$   | $19^{\circ}$   | $10^{\circ}$  |
| VIII                      | 1.046      | $47^{\circ} 0'$  | $9^{\circ}$                      | $4.5^{\circ}$ | $23^{\circ}$   | $5.5^{\circ}$ |
| IX                        | 1.060      | $44^{\circ} 30'$ | $13.5^{\circ}$                   | $4^{\circ}$   | $17.5^{\circ}$ | $4^{\circ}$   |
| X                         | 1.152      | $45^{\circ} 10'$ | $13^{\circ}$                     | $4^{\circ}$   | $18^{\circ}$   | $8^{\circ}$   |

There remains the question as to how great is the preference for the glide plane selected, which may be expressed by considering the actual resolved shear stress on each plane in the glide direction, and finding how that on the plane selected differs from that on the other planes. Owing to the high symmetry of the cubic crystal the direction of pull can never lie very far from a favourable position for glide on a  $\{110\}$ ,  $\{112\}$  or  $\{123\}$  plane.

TABLE 4. GLIDE OF POTASSIUM SINGLE CRYSTALS AT 25° C

| Ref. no.<br>of<br>crystal | $\epsilon$ | $\chi_0$ | Angle between glide<br>plane and |       |       | $\eta$ |
|---------------------------|------------|----------|----------------------------------|-------|-------|--------|
|                           |            |          | {112}                            | {123} | {110} |        |
| I                         | 1.11       | 48° 30'  | 10°                              | 7°    | 24°   | 10°    |
| II                        | 1.02       | 43° 0'   | 14°                              | 3°    | 16.5° | 2°     |
| II'                       | —          | 44° 0'   | 10°                              | 6°    | 22°   | 22°    |
| III                       | 1.14       | 49° 37'  | 18°                              | 7°    | 12°   | 13°    |
| IV                        | 1.10       | 44° 0'   | 15°                              | 4°    | 15°   | 0°     |
| V                         | 1.04       | 47° 20'  | 17°                              | 5°    | 14°   | 5°     |

The resolved shear stress is proportional to  $\cos \lambda \sin \chi$ . As, for a given direction of applied tension,  $\lambda$  is fixed, the resolved shear stress on the planes will be proportional to  $\sin \chi_{110}$ ,  $\sin \chi_{123}$ ,  $\sin \chi_{112}$ . A general examination of the geometry (which would have been carried out in more detail if the work had not been interrupted) indicates that it is not possible to choose a direction such that the resolved shear stress on the most favourable plane of any class of planes is less than 0.84 of the resolved shear stress on the most favourable plane of all three classes. Thus the resolved shear stress on selected planes from the three classes are never very different.

Tables 5–7 have been prepared to show the resolved shear stress on the most favoured plane of each class, compared to that on the most favoured of all three classes taken as 100. With molybdenum at 1000° C the stress on the operative glide plane was never exceeded by that on any other plane, although it was in four cases equalled by that on another plane (differences up to 3% are certainly within experimental error). At 300° C the resolved stress was about equal on all three planes in one case, and on two planes in the other. With potassium at room temperature the stress was generally about equal on all three planes.

#### 7. CONFIRMATION OF CHANGE OF GLIDE PLANE WITH TEMPERATURE

In the experiments with body-centred crystals, then, the resolved shear stress in the glide direction on the effective glide plane was never far from the maximum resolved shear stress, so that at first it might be supposed that the crystal was merely slipping on the plane of maximum resolved shear stress. Examination of the data, however, speaks against this supposition. In the first place, there are cases where the resolved shear stress on the operative plane was definitely less than that on one of the other possible planes, e.g. with sodium at  $-185^\circ \text{C}$ , crystal II, the resolved

TABLE 5. RESOLVED SHEAR STRESSES ON PLANES FOR GLIDE OF MOLYBDENUM SINGLE CRYSTALS

| Ref. no.<br>of<br>crystal | Working<br>temp.<br>° C | $\chi_{(hkl)}$ |       |       |       | $\sin \chi_{110} : \sin \chi_{112} : \sin \chi_{113}$ |           |           |
|---------------------------|-------------------------|----------------|-------|-------|-------|---|-----------|-----------|
|                           |                         | {110}          | {123} | {112} | [111] | $S_{110}$   | $S_{112}$ | $S_{113}$ |
| I                         | 1000                    | 45°            | 40°   | 37°   | 45°   | 100   | 92        | 86        |
| II                        |                         | 43°            | 38°   | 35°   | 42°   | 100   | 90        | 84        |
| III                       |                         | 44°            | 43°   | 38°   | 44°   | 100   | 99        | 90        |
| IV                        |                         | 34°            | 33°   | 31°   | 34°   | 100   | 98        | 93        |
| V                         |                         | 39°            | 38°   | 36°   | 36°   | 100   | 97        | 94        |
| VI                        |                         | 51°            | 48°   | 45°   | 50°   | 100   | 95        | 91        |
| VII                       |                         | 40°            | 40°   | 35°   | 40°   | 100   | 100       | 89        |
| VIII                      | 300                     | —              | 37°   | 37°   | 42°   | 100   | 98        | 98        |
|                           |                         | 57°            | —     | —     | 57°   |   |           |           |
| IX                        |                         | 30°            | 34.5° | 35.5° | 35.5° | 85  | 100       | 99        |

TABLE 6. RESOLVED SHEAR STRESS ON PLANES FOR GLIDE OF POTASSIUM AT ROOM TEMPERATURE

| Ref. no.<br>of<br>crystal | $\chi_{hkl}$ |       |       |       | $\sin \chi_{110} : \sin \chi_{112} : \sin \chi_{113}$ |           |           |
|---------------------------|--------------|-------|-------|-------|---|-----------|-----------|
|                           | {110}        | {123} | {112} | [111] | $S_{110}$   | $S_{112}$ | $S_{113}$ |
| I                         | 30°          | 32°   | 32°   | 32°   | 95  | 100       | 100       |
| II                        | 38°          | 39°   | 38°   | 39°   | 99  | 100       | 99        |
| III                       | 46°          | 46°   | 44°   | 46°   | 100   | 100       | 97        |
| IV                        | 37°          | 40°   | 38°   | 40°   | 94  | 100       | 97        |
| V                         | 39°          | 39°   | 39°   | 39°   | 100   | 100       | 100       |

TABLE 7. RESOLVED SHEAR STRESS ON PLANES FOR GLIDE OF SODIUM AT LOW TEMPERATURES

| Ref. no.<br>of<br>crystal | Working<br>temp.<br>° C | $\chi_{hkl}$ |       |       |       | $\sin \chi_{110} : \sin \chi_{112} : \sin \chi_{113}$ |           |           |
|---------------------------|-------------------------|--------------|-------|-------|-------|---|-----------|-----------|
|                           |                         | {110}        | {123} | {112} | [111] | $S_{110}$   | $S_{112}$ | $S_{113}$ |
| I                         | -185                    | 48°          | 58°   | 58°   | 58°   | 87  | 100       | 100       |
| II                        |                         | —            | 39°   | 36°   | 38°   | —   | 100       | 94        |
| III                       |                         | 55°          | 62°   | 66°   | 65°   | 90  | 97        | 100       |
| IV                        |                         | —            | 46°   | 45°   | 45°   | —   | 100       | 99        |
| V                         |                         | 37°          | 40°   | 42°   | 41°   | 88  | 94        | 100       |
|                           |                         | —            | 42°   | 41°   | 42°   | —   | 100       | 99        |
| VI                        | -82                     | 36°          | 36°   | 34°   | 38°   | 100   | 100       | 95        |
| VII                       |                         | 51°          | 44°   | 42°   | 52°   | 100   | 89        | 86        |
| VIII                      |                         | 47°          | 43°   | 41°   | 47°   | 100   | 93        | 91        |
| IX                        |                         | 45°          | 45°   | 41°   | 45°   | 100   | 100       | 93        |

In connection with these tables it should be remembered that the glide plane is as follows: molybdenum at 1000° and 300°, (110) and (112) respectively; potassium at room temperature, (123); sodium at -185° and -82°, (112) and (110) respectively.

shear stress on (112) was 94 % of that on (123), which is outside experimental error. Further there are fourteen cases in which the resolved shear stress on two of the plane systems were equal to within 2 %, and in all these cases the glide plane was according to the rule put forward, to which, in all the experiments, no exception has ever been found.

It was thought that the strongest confirmation of this effect of temperature would be to take a long single crystal, cut it into three parts and stretch them at three different temperatures, selected to lie within the different ranges. Accordingly a sodium single crystal some 20 cm. long was made in a glass tube marked with a line parallel to the axis, which enabled a reference line to be made on the surface of the crystal. Three lengths of about 4 cm. each were cut from this crystal, and extended by the same amount at 20,  $-82$  and  $-185^{\circ}\text{C}$  respectively. These crystals were then examined at the same orientation, as decided by the reference mark, and it was at once clear that the glide had taken place on a different plane in each case. The glide was simple in all cases, so that the experiment was decisive. Figure 12, plate 2, shows the three specimens, viewed from the same direction in azimuth with reference to the original specimen. A certain amount of oxidation had taken place, in spite of protection, before the photographs were taken, the markings being much clearer when the visual comparison was made than they are in the figure.

#### 8. CRITICAL SHEAR STRESS

By means of the apparatus already described the critical shear stress and the hardening, as evidenced by the shear stress *v.* glide curve, was measured for sodium at 20,  $-82$  and  $-185^{\circ}\text{C}$ . The results are shown in figure 13. At  $-185^{\circ}\text{C}$  the results of two separate experiments, indicated by crosses and circles, were very concordant (curve I), but those of a third experiment (curve II) depart somewhat, although the general form of the curve is the same. Closer agreement is not usual in single crystal experiments, where slight preliminary strain may affect the hardness considerably. Curves III and IV, at  $-82^{\circ}\text{C}$ , resemble one another closely in form, and the difference of stress at a given glide, about 4 %, is small. At  $20^{\circ}\text{C}$  two experiments, indicated by circles and crosses, agreed extremely well (curve VI), but a third (curve V) gave a slightly larger shear stress at each value of the glide. The form of the curve at each temperature is well defined. The curves were not extended to higher values of the glide, since for such values a time flow began to manifest itself at room temperature.

The critical shear stress can be obtained by taking the value of resolved

shear stress at which glide begins. It has been pointed out (Andrade and Roscoe 1937) that the value of the critical shear stress depends slightly on the rate of flow that is taken to indicate the beginning of glide. In the present case it was somewhere about 1 % per min. The values obtained are as follows:

*Sodium*

| Temp.<br>° C | Critical shear stress<br>g.wt./mm. <sup>2</sup> |
|--------------|---|
| -185         | 7.1   |
| - 82         | 5.3   |
| 20           | 4.9   |

These figures show the same slight increase of critical shear stress with decrease of temperature as is evidenced by cadmium and other metals (Schmid and Boas 1935). This slow variation has been explained by Orowan (1934).

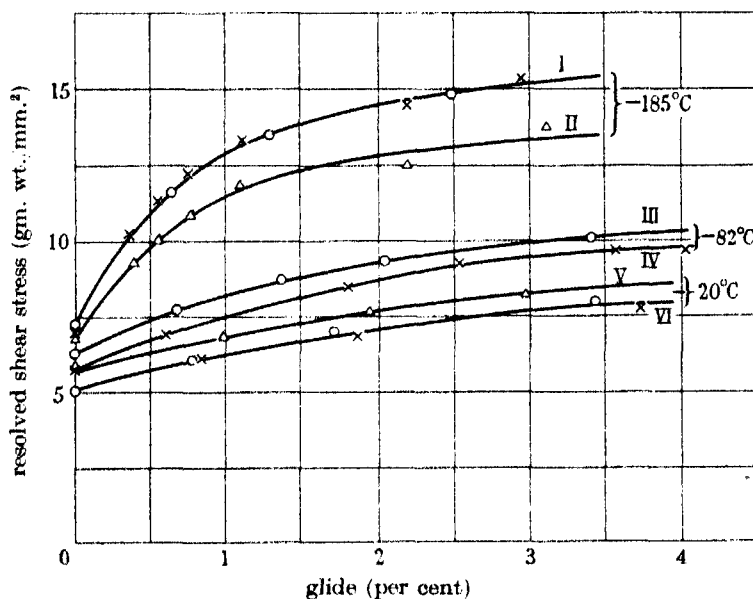


FIGURE 13

## 9. HARDENING AND CRYSTAL BREAK-UP

It has been suggested that hardening is connected with the rotation of small fragments of crystal which accompanies permanent glide (e.g. W. G. Burgers 1934; Andrade and Roscoe 1937). This rotation is evidenced by the

appearance of asterisms, which in the case of sodium consist of discrete spots. The spread of these spots in the different asterisms on the same photograph corresponds to a rotation through a fixed angular range about an axis in the glide plane and normal to the glide direction (Andrade and Tsien 1937).

Laue pictures of sodium crystals at different extensions and different temperatures were taken for comparison with the hardening curves. The results are shown in figure 14, plate 3, where the pictures in a horizontal row are for about the same percentage extension  $e$ , but different temperatures. As the angle of the glide planes was about the same in all cases, equal extension means equal glide.

To measure the range of rotation of the crystal fragments, the angle corresponding to the extreme spots in each asterism was measured on the stereoscopic projection diagram, and it was found, in agreement with Andrade and Tsien, that in a given picture all the asterisms corresponded to the same amount of rotation about the axis already specified. The range of angle  $\Delta\theta$  is given beneath each picture.

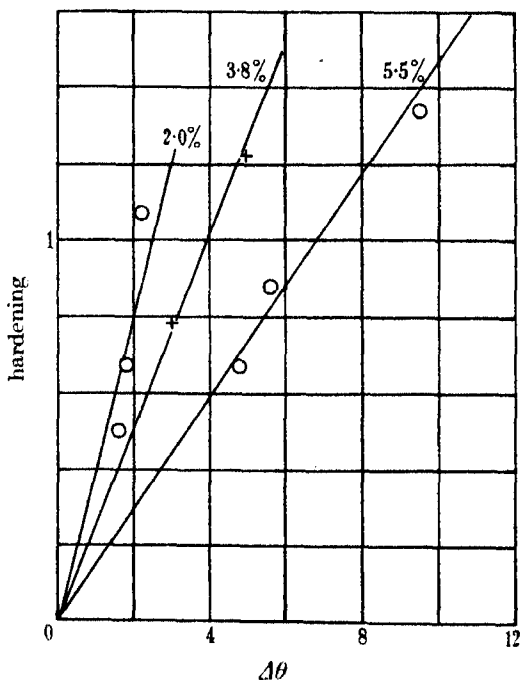


FIGURE 15. Hardening against  $\Delta\theta$  at constant extension.

It will at once be seen that, for equal extension, the range of rotation is much greater at  $-185$  than at  $-82^{\circ}\text{C}$ , and greater at  $-82$  than at  $20^{\circ}\text{C}$ . If we consider the curves of figure 13 it will be seen that at, say, a glide of 4 %, the hardening, as measured by  $(\sigma - \sigma_0)/\sigma_0$ ,  $\sigma$  being the shear stress at the given glide and  $\sigma_0$  the critical shear stress, is very much greater at  $-185$  than at  $-82^{\circ}\text{C}$ , and somewhat greater at  $-82$  than at  $20^{\circ}\text{C}$ .

Some kind of quantitative comparison can be made. From figure 13 we can find the hardening at a glide of 4 %, and plot it against  $\Delta\theta$ . To find the hardening at the other glides concerned means a large extrapolation, but as the general form of the hardening curves is known, this can be done without an error excessive for a rough comparison of the kind in hand. Figure 15 shows hardening against  $\Delta\theta$  at three different extensions, the temperature varying. It will be seen that the points lie roughly on straight lines through the origins, the comparatively large divergencies for the extension of 2 % being accounted for by the difficulty of measuring  $\Delta\theta$  accurately when it has small values. Roughly speaking, at fixed extension the hardening, different at different temperatures, is proportional to the range of rotation of the crystal fragments. This is not put forward as a precise law: what is emphasized is that hardening increases with increasing range of rotation, the extension being fixed. It is the range of rotation, and not the extension, that determines the hardening.

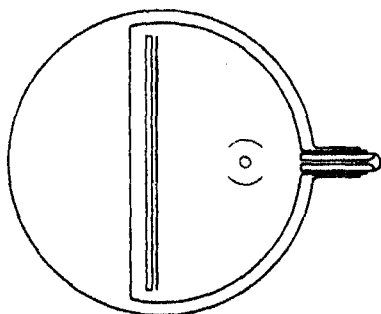
#### 10. THE CAUSE OF THE DISCRETE SPOTS IN ASTERISMS

Sodium and potassium show asterisms consisting of discrete spots, of which advantage has been taken to get an arbitrary measure of the range of rotation of the crystal fragments. Other metals exhibit asterisms in the form of a continuous smear. The fact which distinguishes the two first named metals is that, at whatever temperature they are extended, they are photographed at a temperature near (about  $70$  and  $40^{\circ}\text{C}$  respectively below) their melting-points. It appeared that the discrete spots might be due to recrystallization about certain preferential, probably highly strained, crystallites.

There are two ways in which this supposition can be verified: (a) to stretch sodium or potassium wires at a very low temperature, and photograph them at this temperature, instead of letting them warm up, in the expectation of continuous asterisms; (b) to stretch, say, an iron wire at room temperature and then raise it to a temperature near its transformation point, in the expectation of discontinuous asterisms.



To stretch and photograph, by X-rays, sodium wires at liquid-air temperature a special apparatus was made. The stretching apparatus and camera, shown in figure 16, consisted of a brass box, whose horizontal cross-section was in the shape of a *D*; it was made from a stout brass tube



Horizontal cross section of beaker and camera

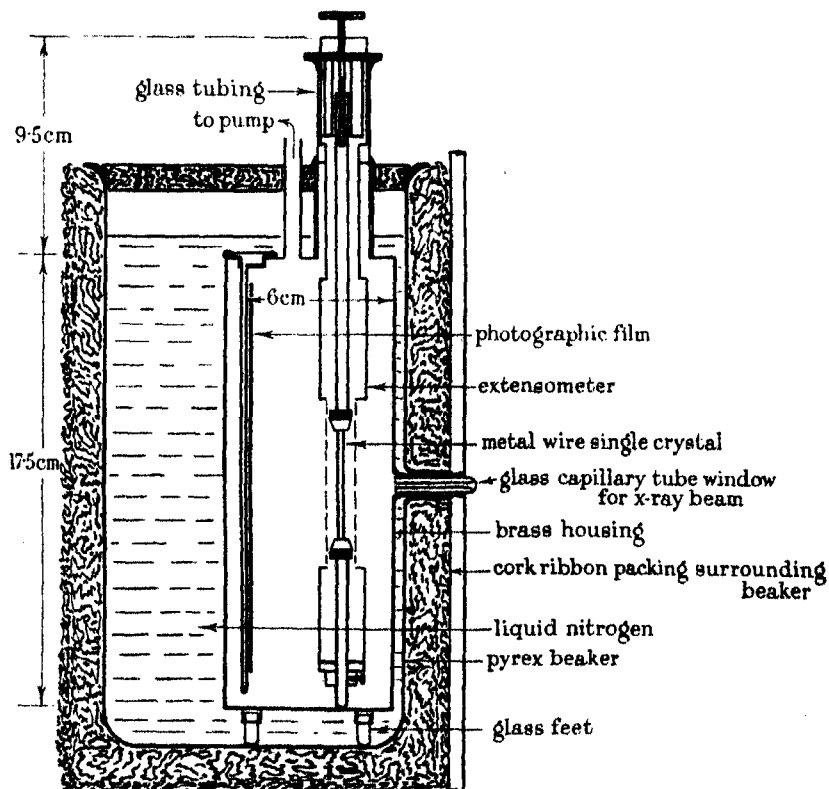


FIGURE 16

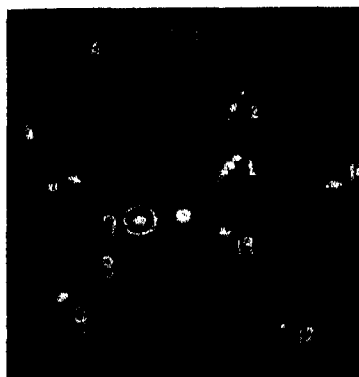


FIGURE 3



FIGURE 5



FIGURE 6



FIGURE 7



FIGURE 8

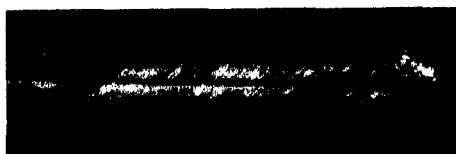


FIGURE 9

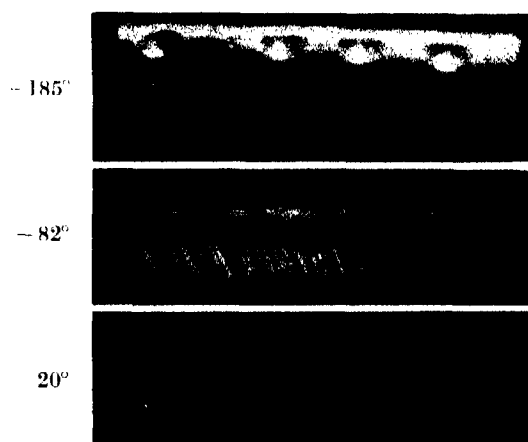


FIGURE 12

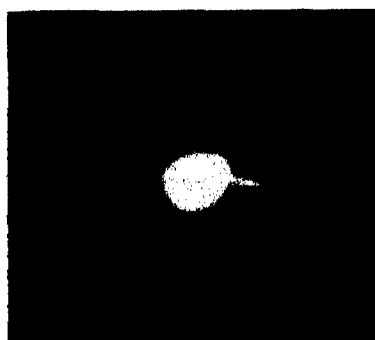


FIGURE 17

(Facing p. 308)

$-185^{\circ}\text{C}$

$-82^{\circ}\text{C}$

$20^{\circ}\text{C}$



$e = 5.5\%$ ,  $\Delta\theta = 9.5^{\circ}$

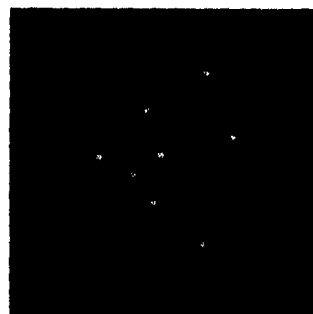
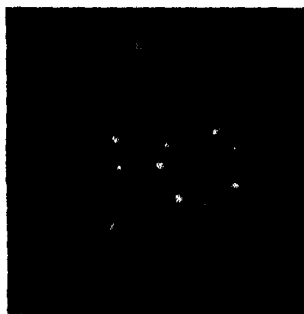
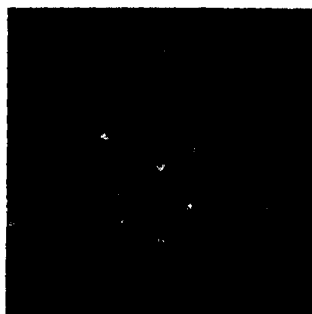
$e = 5.5\%$ ,  $\Delta\theta = 5.6^{\circ}$

$e = 5.5\%$ ,  $\Delta\theta = 4.8^{\circ}$



$e = 3.6\%$ ,  $\Delta\theta = 5^{\circ}$

$e = 4\%$ ,  $\Delta\theta = 3^{\circ}$



$e = 2\%$ ,  $\Delta\theta = 2.2^{\circ}$

$e = 2\%$ ,  $\Delta\theta = 1.8^{\circ}$

$e = 1.9\%$ ,  $\Delta\theta = 1.6^{\circ}$

FIGURE 14



FIGURE 18. Iron stretched at  $20^{\circ}\text{C}$ .

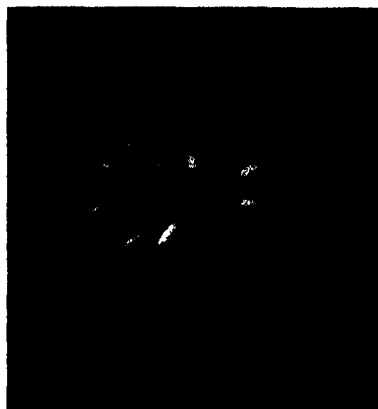


FIGURE 19. Iron stretched at  $450^{\circ}\text{C}$ .

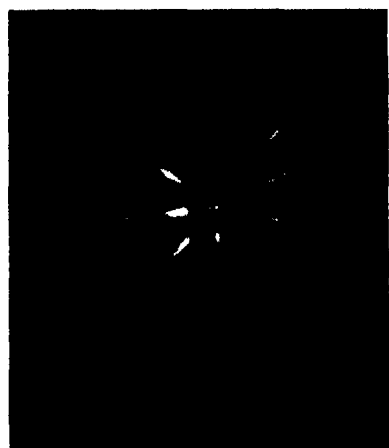


FIGURE 20. Iron at  $840^{\circ}\text{C}$   
for 2 hours.

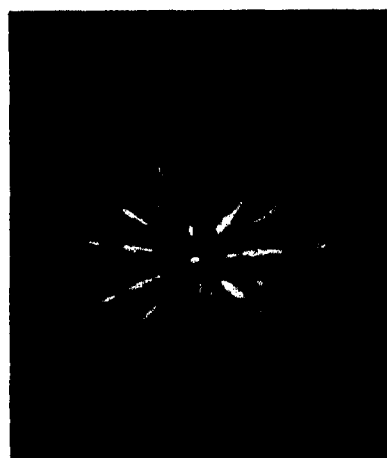


FIGURE 21. Iron at  $860^{\circ}\text{C}$   
for 4 hours.



FIGURE 22. Iron at  $700^{\circ}\text{C}$ .



FIGURE 23. Iron at  $880^{\circ}\text{C}$   
for 4 hours.



split axially, and provided with a flat back, against which the photographic film, wrapped in black paper, was held in a special holder. Opposite this was the hole for admitting the X-ray beam, consisting of a thick glass tube with a fine capillary bore, on the end of which a small very thin bulb was blown, to admit the rays. This tube was mounted in a brass holder soldered to the box. The holder for the sodium wire was a brass frame much like that used in the stretching experiments, but without the ring for measuring the tension, which was applied by a screw head, separated from the main tube by a length of glass tube, to diminish heat conduction. This frame was inserted through a hole in the top of the camera, and the whole made vacuum-tight.

The camera stood on glass feet in a glass beaker, to one side of which a short glass tube had been blown, to take the X-ray "slit" tube. The joint between the tubes was made tight with picein, so that the beaker could be filled with liquid nitrogen. The beaker stood in a box filled with a special cork ribbon preparation, which proved a very effective thermal insulator. A Dewar vessel was not used on account of the technical difficulty of blowing the tube through both walls at the required spot. Liquid nitrogen was chosen in preference to liquid air or liquid oxygen because of the danger attendant on chance contact of liquid oxygen, diluted or undiluted, with the cork preparation.

Plates were used in the first attempts to take photographs at liquid nitrogen temperature, but the effect of the extreme cold was that the emulsion split into fine ribbons. It was found, however, that films stood up to the conditions well.

The crystal, protected by a thin film of apiezon oil, was quickly fastened in the chucks, and placed in position. The apparatus was then evacuated and the liquid nitrogen introduced into the beaker, completely submerging the camera. After 20 min. the crystal was stretched and then photographed *in situ*, an exposure of about 6 hr. being necessary. Figure 17, plate 2, shows a photograph taken with a severely stretched crystal, which should be compared with the photographs of figure 14, plate 3. It will be seen that the asterisms are continuous smears, like those obtained with, for example,  $\alpha$ -iron, stretched at room temperature (cf. figure 18, plate 4).

The complementary experiment, which is an attempt to produce discrete spots where continuous asterisms are usually found, was made with  $\alpha$ -iron. Fig. 18, plate 4, is a Laue photograph of a single crystal of  $\alpha$ -iron stretched at room temperature. In the hope of producing a break up of the asterisms the crystal was kept at about 850° C, a temperature at which it still

maintains a body-centred structure. Figure 19, plate 4, shows a photograph of a crystal stretched about 5% at 450°: Figure 20, plate 4, was taken with the same crystal after it had been kept at 840° for 2 hr.; figure 21, plate 4, after a second heating at 860° for 4 hr. It will be seen that the asterisms show signs of progressive break up. There are also certain fresh spots produced by the heating, a sign of recrystallization.

In another experiment the crystal was stretched at 700° C; the asterisms showed some discontinuity (figure 22, plate 4). This crystal was reheated at 880° C for 4 hr., and cooled by gradual withdrawal from the furnace in 10 min. The Laue photograph after this reheating is shown in figure 23, plate 4. The main asterisms, marked 1, 2, 3 and 4, show break up into discrete patches, and in addition the photograph gives evidence of a large number of small crystals which were not present before. All the iron photographs were, of course, taken at room temperature.

These experiments seem to prove conclusively that the break up of the sodium asterisms into discrete spots is due to recrystallization taking place in the strained crystal at room temperature.

## 11. DISCUSSION

The following table shows the results for all the body-centred metals so far investigated, except iron, with which the findings are so far inconclusive. In the second column  $\theta = T/T_M$ , where  $T$  is the absolute temperature of the experiment ( $t^\circ\text{C}$ ),  $T_M$  the melting point of the metal. The melting-point has been selected instead of the characteristic temperature, which suggests itself, because of the comparatively large uncertainty that exists as to the value of the latter (e.g. for sodium values from 140 to 202 are given for the characteristic temperature).

| $t^\circ\text{C}$ | $\theta$ | Metal          | Glide plane | Reference         |
|-------------------|----------|----------------|-------------|-------------------|
| 20                | 0.08     | W              | (112)       | Goucher           |
| 20                | 0.10     | Mo             | (112)       | Tsien and Chow    |
| 300               | 0.20     | Mo             | (112)       | Tsien and Chow    |
| - 185             | 0.24     | Na             | (112)       | Andrade and Chow  |
| 20                | 0.26     | $\beta$ -brass | (110)       | G. I. Taylor      |
| 1000              | 0.40     | Mo             | (110)       | Tsien and Chow    |
| - 82              | 0.50     | Na             | (110)       | Andrade and Chow  |
| 20                | 0.80     | Na             | (123)       | Andrade and Tsien |
| 20                | 0.87     | K              | (123)       | Andrade and Tsien |

All the results, then, agree with the rule, put forward at the "Discussion" (Andrade 1938), that as  $\theta$  increases the glide plane changes from (112)

through (110) to (123), and that at a given value of  $\theta$ , the glide plane is the same for all body-centred metals. The glide direction is always [111].

The case of  $\alpha$ -iron is peculiar, in that all three planes have been suggested by different authors (cf. Andrade and Tsien 1937) as operative at room temperature. The outbreak of war interrupted investigations which we were carrying out on this point before any conclusive results were obtained. The value of  $\theta$  for iron at room temperature is 0.163 if  $T_M$  be taken as the melting-point of the metal, and 0.250 if  $T_M$  be taken as the temperature of transformation of the body-centred into the face-centred structure, viz. 1179° abs., so that, according to the rule, the glide plane should be (112). It is very difficult to get really pure iron, and the presence of traces of impurity may affect the choice of plane.

The question arises as to why the glide plane changes with temperature. This is perhaps to be attributed to a preferential direction of vibration of the atoms, acting in conjunction with the potential energy due to spacing. It is possibly significant that body-centred crystals are not close packed. The phenomenon may have some analogy with the change in crystal structure that takes place with temperature in the case of certain metals, as exemplified by calcium, which is cubic face-centred at room temperature and close-packed hexagonal above 450° C, or zirconium, which is close-packed hexagonal at room temperature, and body-centred cubic at 862°. This change must depend upon the way in which the free energy of the different crystalline forms varies with the temperature, which in its turn will mainly depend upon how the energy of vibration varies with the temperature. The suggestion is put forward tentatively. In any case, the experiments indicate that the rate of variation of strength with temperature is somewhat different for each of the three systems of planes.

In iron of ordinary purity it seems likely that glide can take place on all three planes at once. These planes would form hexagons, though not regular hexagons, on any plane which they traverse, and G. I. Taylor's picture of rod-like slipping can easily be explained on the basis of this threefold slip. The non-planar glide surfaces can be built up by slip, in the [111] direction, taking place on different planes in short, adjacent, parallel-sided strips.

It appears, then, that it is the glide direction that is fundamental, this being in all cubic and hexagonal crystals the most closely packed line. The choice of glide plane appears to be influenced not only by temperature but by slight deformation, Greenland (1937) having shown that, with very pure mercury, crystals which had suffered very slight preliminary strain slipped on well-defined planes, while crystals that were absolutely unstrained



slipped on irregular surfaces. The slight strain may produce preferential hardening on certain planes, but the whole question of choice of slip planes is one that requires further experimental investigation.

Turning to other aspects of the work, our results, taken with those of previous workers, go to emphasize that there is a marked contrast between the behaviour of single crystals under stress at high and at low temperatures, which may be tabulated as follows:

| Low temperature            | High temperature           |
|----------------------------|----------------------------|
| Great hardening with glide | Small hardening with glide |
| Close glide planes         | Widely-spaced glide planes |
| Large crystallite rotation | Small crystallite rotation |
| Large hardening            | Small hardening            |
| Little time flow           | Large time flow            |

We have further to note that the effect of temperature on hardening, as measured roughly by the spacing of the stress-glide curves for a given difference of temperature, is comparatively small at high and low temperatures, but greater at intermediate temperatures.

It is not intended to attempt here anything in the nature of a full discussion of the theoretical implications, but a few general suggestions are made.

The variation of the spacing of the glide planes with temperature is clearly connected with the hardening phenomena. It is generally agreed that glide sets in at some kind of flaw or dislocation, and Orowan has introduced a "notch factor"  $q$  to express the local increase of stress in the neighbourhood of a surface crack or other such imperfection. We suggest that, quite generally,  $q$  has a wide range of values for different flaws in the same material. What is required is a theory which shall take into account the fact, expressed either by a varying  $q$  or otherwise, that there must be a statistical distribution in magnitude of the local concentrations of energy involved in the system of flaws.

The hardening may be assumed to be linear with glide on, or in the neighbourhood of, any particular glide plane, but the hardening for given glide is much more marked at low temperature, owing to the spontaneous recovery which takes place at higher temperature. If, now, at high temperatures, glide starts at a few localities of large  $q$ , then, in consequence of the relatively slight hardening which is a manifestation of the temperature recovery, glide proceeds progressively on the same few planes, and the law of hardening will tend to be linear. At low temperatures, on the other hand, the glide on the initial planes leads to rapid hardening in the immediate neighbourhood, and increasing stress then initiates glide at intermediate

localities of smaller  $q$ . The number of glide planes increases with stress, and, while the exact form of the stress-glide curve depends on a number of assumptions, it is easily shown that it will depart from linearity in the direction of a parabolic law.

In many cases the law of stress against glide tends to be parabolic for metals at temperatures far below the melting point (cf. aluminium and copper at atmospheric temperature) and linear with metals near the melting point (cf. cadmium and zinc at  $200^{\circ}\text{C}$ ), but the rule is not completely general (cf. magnesium and zinc at  $-185^{\circ}\text{C}$ , where the curve appears to be concave towards the stress axis). Further systematic experiment is required, under precise conditions, with glide taking place on one set of planes only.

As regards the hardening itself, it has already been suggested by Andrade and Roscoe (1937) that the hardening round a glide plane is due to stoppage of glide by progressively rotated crystallites; the objection that hard crystallites cannot lock soft material is based on a misunderstanding of the suggestion, our contention being that unflawed material is hard, and the crystallites merely block the propagation of dislocations. If there is a fairly rapid recrystallization at high temperatures, the smaller hardening can be understood in a general way.

The approximately parabolic law of hardening at low temperature has been explained by G. I. Taylor on the basis of the propagation of dislocations arising in some manner, which has not been elaborated, within the crystal. It is an essential feature of this theory that fresh dislocations are called into play as the macroscopic strain increases, but the mechanism has not been discussed. From his assumptions, which include flaws limiting the travel of the dislocations, Taylor deduces his law of hardening, which is certainly not obeyed at higher temperatures. One formal feature of Taylor's theory is the system of flaws which stop, but do not initiate, dislocations: another is that it is purely two-dimensional. Taylor's positive and negative dislocations, however, running in opposite directions and exerting a force on one another where they tend to pass, produce a mechanism for rotating small portions of the crystal structure.

Orowan has brought clearness into the many aspects of the plastic flow of single crystals by concentrating attention on the rate of flow, rather than the strain. He combines Becker's conception of flow as due to thermal fluctuations, which raise the stress locally from time to time, with the conception of stress concentration at a flaw. His considerations explain the variation of flow with temperature and, as a particular case, give a convincing representation of the small variation of critical shear stress

with temperature, but do not explain hardening. W. G. Burgers and J. M. Burgers (1935) have combined all the previous theories and suppose that the arrest of the travel of the dislocations leads to local curvature of the glide lamellae, such as is evidenced by the asterisms discussed by them and us. Their theory does not, however, really explain what leads to the arrest.

In general, none of the present theories devotes much attention to the glide plane, better called, perhaps, since it is of finite width, the glide lamella, in which some kind of avalanche-like disturbance is clearly concentrated. This narrow region of preferential glide—or discontinuous character of the glide in space, as it may be called—is an essential feature of the process of plastic deformation in metals, as is also the discontinuous character of the glide in time, expressed in the jerky nature of the extension investigated by Klassen-Nekludowa (1929), Becker and Orowan (1932), and Schmid and Valouch (1932). A theory which undertakes to give a physical picture of what takes place should be able to connect this twofold discontinuity with the law connecting hardening and glide at low temperatures and small stresses and with the law connecting glide and time at high stresses and high temperatures.

We have had the advantage of discussing certain aspects of this work with Dr E. Orowan and of receiving comments from Professor Mott, who kindly read the paper through. To both of these gentlemen we express our grateful thanks for their interest in the work.

#### SUMMARY

The glide elements of single crystals of the body-centred cubic metal, sodium, have been determined at various temperatures. The glide direction is in all cases  $[111]$ , but the glide plane changes successively from  $(112)$  to  $(110)$  to  $(123)$  as the temperature goes from  $-185$  to  $20^{\circ}\text{C}$ . It is shown that this change of glide plane with temperature is a particular case of a general rule to which body-centred metals conform: all three planes are possible glide planes but which is operative at any particular temperature is determined by the temperature, referred to the melting-point of the particular metal as standard. The case of iron, for which all three planes seem to be operative at once, is considered separately.

The critical shear stress has been determined for sodium, and shows a small variation only over the temperature range  $-185$  to  $20^{\circ}\text{C}$ .

Experiments with sodium, iron and molybdenum go to show that the spacing of the glide planes increases markedly as the temperature is raised.

It has been found that, for equal strain, the crystallite rotations, as evidenced by the asterisms, are much greater at low temperatures, where the hardening is greater, which goes to support the view that hardening is intimately connected with the rotation of crystal fragments. The breaking up of the asterisms into discrete spots which has been found with sodium and potassium is shown to be due to recrystallization.

The general implications of the results are discussed.

#### REFERENCES

- Andrade, E. N. da C. 1937 *Proc. Roy. Soc. A*, **163**, 19.  
 — 1938 *Proc. Roy. Soc. A*, **168**, 310.  
 Andrade, E. N. da C. and Chalmers, B. 1932 *Proc. Roy. Soc. A*, **138**, 348.  
 Andrade, E. N. da C. and Roscoe, R. 1937 *Proc. Phys. Soc.* **49**, 152.  
 Andrade, E. N. da C. and Tsien, L. C. 1937 *Proc. Roy. Soc. A*, **163**, 1.  
 Becker, R. and Orowan, E. 1932 *Z. Phys.* **79**, 566.  
 Boas, W. and Schmid, E. 1929 *Z. Phys.* **57**, 575.  
 — — 1930 *Z. Phys.* **61**, 767.  
 Burgers, W. G. 1931 *Z. Phys.* **67**, 605.  
 — 1934 *International Conference on Physics*, **2**, 139.  
 Burgers, W. G. and J. M. 1935 *Trans. Roy. Acad. of Sci., Amst.*, **25**, 173.  
 Chevenard, M. P. 1932 *Revue de Nickel*, p. 55.  
 Esper, W. and Knoll, M. 1936 *Werkstoffkunde der Hochvacuumtechnik*.  
 Fahrenheit, W. and Schmid, E. 1932 *Z. Phys.* **78**, 383.  
 Gouher, F. S. 1924 *Phil. Mag.* **48**, 229, 800.  
 Gough, H. J. 1928 *Proc. Roy. Soc. A*, **118**, 498.  
 Greenland, K. M. 1937 *Proc. Roy. Soc. A*, **163**, 28.  
 Klassen-Nekludowa, M. 1929 *Z. Phys.* **55**, 555.  
 Mott, N. F. 1935 *Proc. Phys. Soc.* **47**, 571.  
 — 1936 *Proc. Roy. Soc. A*, **153**, 699 and **156**, 368.  
 Orowan, E. 1934 *Z. Phys.* **89**, 605, 614, 634.  
 Potter, H. H. 1937 *Proc. Phys. Soc.* **49**, 671.  
 Schmid, E. and Boas, W. 1935 *Kristallplastizität*, p. 153. Berlin.  
 Schmid, E. and Valouch, M. A. 1932 *Z. Phys.* **75**, 531.  
 Taylor, G. I. 1928 *Proc. Roy. Soc. A*, **118**, 1.  
 Taylor, G. I. and Elam, C. F. 1926 *Proc. Roy. Soc. A*, **112**, 337.  
 Tsien, L. C. and Chow, Y. S. 1937 *Proc. Roy. Soc. A*, **163**, 19.  
 Yamaguchi 1928 *Inst. Phys. Chem. Res., Tokio*, no. 151, p. 289.
-

# Experiments with a velocity-spectrometer for slow neutrons

By G. E. F. FERTEL, D. F. GIBBS, P. B. MOON,  
G. P. THOMSON, F.R.S., AND C. E. WYNN-WILLIAMS

(Received 14 March 1940)

The properties of slow neutrons of different velocities have been investigated mainly by methods in which their velocities are determined indirectly, for example, by way of the absorption coefficient of boron, which is believed to vary inversely with the velocity of the neutron. Direct measurements of velocity within the thermal range ( $\sim 2.5 \times 10^5$  cm./sec.) have, however, been made with velocity-selectors employing high speed rotary shutters which allow neutrons to pass for brief periods at regular intervals (Dunning, Pegram, Fink, Mitchell and Segrè 1935). If two such shutters are arranged at a distance  $l$  apart, a neutron of velocity  $v$  can pass through both shutters in succession only if the second is open at a time  $l/v$  later than the first; if the two shutters are driven at identical frequencies with a suitable difference of phase, only those neutrons whose velocities lie within certain ranges will be transmitted.

While this type of apparatus has yielded important results, its development meets with difficulties in two directions. First, no material is completely opaque to neutrons and there is always a large "background" of neutrons which have passed through a "closed" shutter. The ratio of this background to the velocity group which it is intended to isolate increases rapidly as the fraction of time for which the shutter is open decreases; the resolving power of the apparatus is therefore limited to a low figure. Secondly, the speed of rotation of the shutters is limited by the mechanical strength of the materials of which they are made, and although this represents no great difficulty when thermal velocities are to be measured, it seems likely to prevent the extension of the method to neutrons of substantially higher speeds.

The present paper describes a method which is in principle free from these limitations. A truly intermittent source of neutrons is employed and the instants at which it is active are recorded, by means of a cathode-ray oscillograph, on photographic paper. The instants of arrival of individual neutrons at a distant ionization chamber are recorded on the same photograph and their times of flight from source to detector are thus measured.

Since neutrons of all speeds are dealt with in a single experiment, this type of apparatus bears the same relation to a spectroscope that the velocity selector bears to a monochromator; as in optics, the relative merits of the two types of instrument will depend on the particular measurement contemplated.

The apparatus has been used to investigate the velocity distribution of the neutrons of thermal energies in the beam from a wax "howitzer". By comparison of this velocity distribution with that obtained when an absorber is interposed between the howitzer and the detector, the variation with velocity of the absorption coefficients of boron and cadmium have been studied.

#### THE INTERMITTENT SOURCE OF NEUTRONS

The neutrons were obtained by bombarding a target of heavy ice with about  $20\ \mu\text{A}$  of deuterons generated in a discharge tube of the Oliphant type and accelerated by a steady potential of 150–250 kV. Details of the discharge tube and accelerating system are shown in figure 1. The main accelerating voltage was obtained from an 80 kV transformer by the voltage-multiplication circuit of Cockcroft and Walton; the voltage for the discharge tube (about 25 kV) was derived from a transformer-rectifier unit whose primary was supplied by an alternator mounted on insulating pillars and driven from a motor below. This alternator also supplied, by way of transformers, the power for valve filaments and other apparatus at the high-potential end of the accelerating system. The accelerating tube was evacuated by a pair of oil diffusion pumps (Metropolitan-Vickers type O3) backed by two of the O2 type and these again by a Megavac rotary pump.

The heavy hydrogen for the discharge tube was generated by the electrolysis of acidulated heavy water in a simple automatic pressure-regulating tube, was conveyed to the top of the discharge tube at approximately

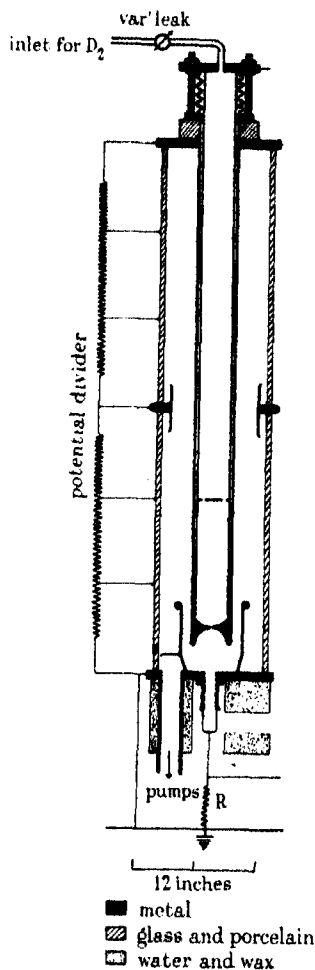


FIGURE 1. Discharge tube.

atmospheric pressure, and was there admitted through a Kaye leak which could be adjusted from below.

The voltage through the electrodes of the discharge tube was applied intermittently, the duration of each impulse being about  $5 \times 10^{-4}$  sec., and the interval between successive impulses being  $5 \times 10^{-3}$  sec. This was accomplished as follows. An intermittent beam of light was obtained by placing a lamp behind a slotted disk rotated by a motor which was synchronized to the 50-cycle A.C. mains. This intermittent light beam was focused by a lens upon the cathode of a photoelectric cell which was carried on a platform on the top of the discharge tube (see figure 2). The intermittent current from this cell was amplified by a four-stage capacity-coupled

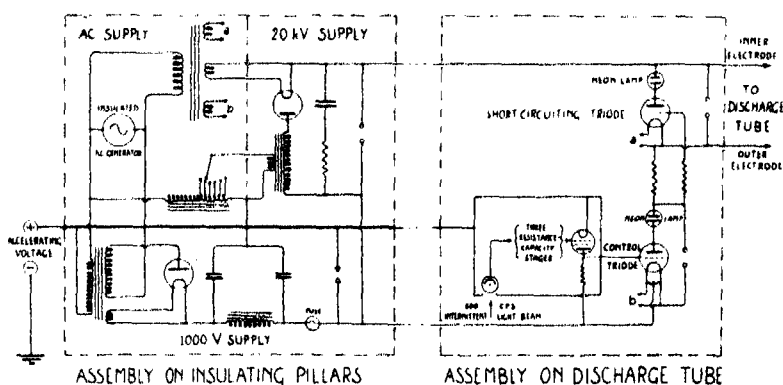


FIGURE 2. Circuit for producing intermittent pulses.

amplifier, the last stage of which delivered an impulse of 1000 V at each flash of light. These impulses were applied between the grid and cathode of a triode valve (which we shall call the control triode) in such a way that the grid was 1000 V negative with respect to the cathode except during each flash of light, when its potential rose approximately to zero. The anode and cathode of the control triode were connected in series with the discharge tube; the amplification factor of the triode was so high ( $\sim 60$ ) that with the grid at  $-1000$  V no current could pass in spite of the 25 kV applied continuously to the circuit. At each flash of light the triode became suddenly conducting and the discharge started abruptly. Owing to the capacity between the electrodes of the discharge tube, the discharge did not cease immediately when the control triode became non-conducting again. A second triode (the short-circuiting triode) was therefore connected in parallel with the discharge tube, its grid potential being controlled by the current through the control triode in such a manner that it

was conducting whenever the control triode was not conducting. A neon lamp was placed in the anode circuit of each of the triodes, and these lamps, when viewed in an oscillating mirror, showed clearly the intermittent nature of the current through them and so gave a valuable check on the working of the apparatus.

### TARGET

The target consisted of a layer of heavy ice formed inside a hollow copper cylinder insulated by a glass tube into which the copper was sealed. To form the target, a tap was opened for a short time and  $D_2O$  vapour allowed to diffuse on to the lower end of the cylinder, which was kept in liquid air. The cylinder was connected to earth by means of a resistance  $R$  (figure 1), the potential difference between the ends of which gave a measure, at every instant, of the current striking the target. By applying this potential to the deflection plates of a cathode ray oscillograph, it was verified that the target current was truly intermittent; the current was zero for about four-fifths of each cycle, and at least three-quarters of the total current was concentrated in one-tenth of the cycle.

### PASSAGE OF NEUTRONS FROM SOURCE TO DETECTOR

In order to reduce the velocities of the fast neutrons to thermal values, the target was surrounded by a "howitzer" of water tanks and paraffin wax blocks, the opening pointing towards an open window. The average time required for a fast neutron to reach thermal equilibrium is known to be of the order of  $10^{-5}$  sec. The average life of a neutron in thermal equilibrium before it either escapes or is captured by a nucleus is of the order of  $2 \times 10^{-4}$  sec., and since each pulse of deuterons lasts for about  $5 \times 10^{-4}$  sec. we may estimate the duration of each pulse of slow neutrons to be  $7 \times 10^{-4}$  sec. By placing a boron-lined ionization chamber near to the howitzer and recording the amplified impulses from the chamber on bromide paper in the same manner as is described later, we have been able to verify experimentally that the duration of the pulses of neutrons is not greater than estimated above. The interval between pulses being  $5 \times 10^{-3}$  sec., the highest resolving power which the apparatus can give is of the order of 7.

The most favourable distance between source and detector will be such that the average thermal neutron (velocity about  $2.5 \times 10^5$  cm./sec.) occupies in its flight to the detector a considerable fraction of the interval between pulses, while very few neutrons take longer than that interval.



Such very slow neutrons, of course, will be indistinguishable from fast neutrons generated by the succeeding pulse of deuterons. For a Maxwellian distribution of velocities at ordinary temperature, a distance of 5.3 m. satisfies these conditions fairly well, and this distance was accordingly chosen. With the source and the detector so widely separated, neutrons scattered from the floor and walls of the room form, under ordinary conditions, a large fraction of the total number of neutrons reaching the detector. The discharge tube was therefore placed as near as practicable (about 1.5 m.) to a window to which the howitzer pointed and the detector was hung in mid-air about 4 m. outside the building. A light sheet-iron tube, coated internally and externally with cadmium, extended from the window to the detector and served as a further protection against scattered neutrons. The geometry of the system is shown in figure 3.

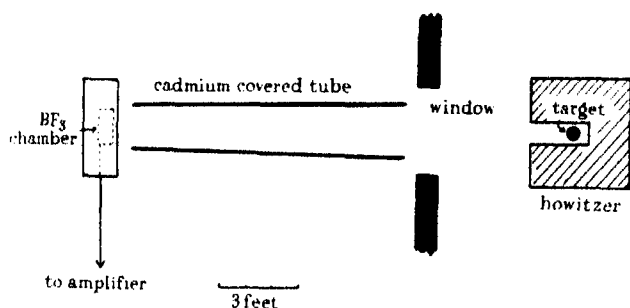


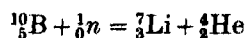
FIGURE 3. Geometry of system.

#### THE DETECTION OF THE SLOW NEUTRONS

The conditions to be satisfied by the detector are (1) that it should register the time of arrival of the neutron with as high accuracy as possible, and in any case to within  $7 \times 10^{-4}$  sec., which is the duration of the slow neutron pulses at the source, and (2) that it should be sufficiently sensitive and have a low natural count.

These conditions were realized by an ionization chamber filled with BF<sub>3</sub> gas at atmospheric pressure, coupled to a five-stage linear amplifier, the output of which was applied to a cathode-ray oscillograph. A scale drawing of the chamber is given in figure 4, which shows that the chamber is much larger than is customarily used. This was necessary to secure sufficient sensitivity, but it introduced the difficulty that the electrostatic capacity was high (about 60 cm.) and the voltage impulses due to the collection of ions were correspondingly low. In order that each impulse

should rise above the background due to shot-effect in the amplifier within a sufficiently short time, it was necessary to apply 2000 V between the electrodes. It was then possible to fix within  $2 \times 10^{-4}$  sec. the time at which each  $\alpha$ -particle from the (instantaneous) nuclear reaction



passed through the chamber. It may be pointed out that the voltage of the collecting electrode begins to change as soon as the positive and negative ions begin to separate under the electrostatic field; it is therefore the *start* of each pulse which indicates the time at which ionization took place.

The first valve of the amplifier (a Western Electric type 259 B, stabilized by a grid leak of about  $5 \times 10^8$  ohms) was mounted next to the ionization

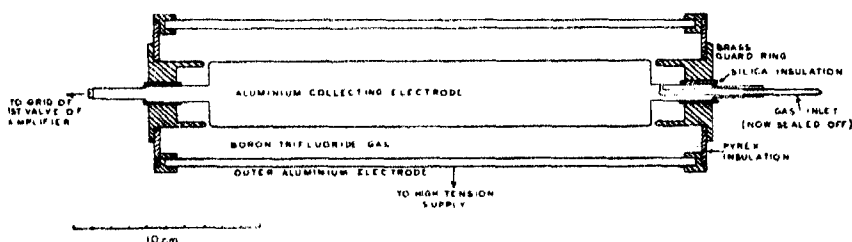


FIGURE 4

chamber, but the remainder of the amplifier was placed indoors, a low capacity shielded lead carrying the impulses from the first stage to the second. Into the second stage of the amplifier were also injected the voltage impulses which appeared across the resistance  $R$  in figure 1, so that the oscillograph stream showed a trace interrupted at intervals of  $5 \times 10^{-3}$  sec. by kinks representing the times at which the deuterons were striking the target. The same trace showed the occasional kinks representing the instants at which neutrons were detected by the  $\text{BF}_3$  chamber; the interval between the beginning of a "neutron kink" and the middle of the previous "deuteron kink" or "time mark" should give the most probable value for the time of flight of that particular neutron over a distance of 5.3 m. Since the polarity of an impulse is reversed at every stage in a resistance-capacity coupled amplifier, the deuteron and neutron kinks were in opposite directions. The oscillograph had a 25-cycle time base, synchronized to the 50-cycle mains, so that eight deuteron kinks appeared at fixed positions on each traverse of the spot. The traces were photographed on a considerably reduced scale on a moving strip of bromide

paper, the camera employed having been made in the Imperial College workshops to the design of one of us (C. E. W.-W.).

Measurements made later on the photographs, under suitable magnification, enabled the time of flight of each neutron to be recorded.

Two portions of record are shown in figure 5; the portions illustrated show eighteen neutrons and in this respect are more than ordinarily favourable, the average rate of counting being about twenty-five per minute. The natural count of the chamber was about three per minute.

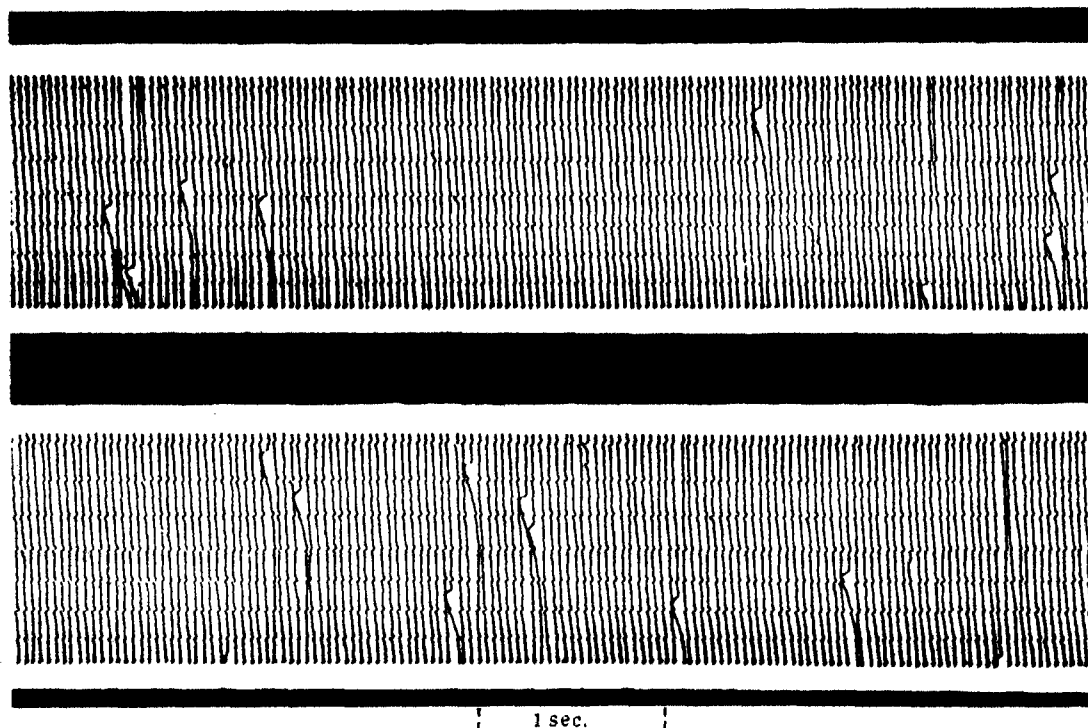


FIGURE 5

#### METHOD OF ANALYSING TRACES

It is convenient to divide the neutrons recorded on the trace into ten groups according to their times of transit. Group 0 contains those which arrived too soon for their time of transit to be measured with certainty and groups 1-9 have successively greater times of transit. In order to make the successive groups cover equal increments in the times of transit we adopted the following procedure. We projected a magnified image of

the film on to a ground glass screen. On this screen a scale was drawn consisting of eleven lines, numbered 0, 1, 2, 3, 4, 5, 6, 7, 8, 9, 0, passing through a point and making equal intercepts on the line of the image of the trace (figure 6). The screen was moved until the first line was at the middle of the first time mark and the eleventh line at the middle of the second time mark. The particle is assigned to the group 0-9 according to the number of the nearest line to the first detectable "rise" (downwards in Fig. 6) of the trace, group 0 being assigned to particles nearest to the line through the first time mark and the others in order.

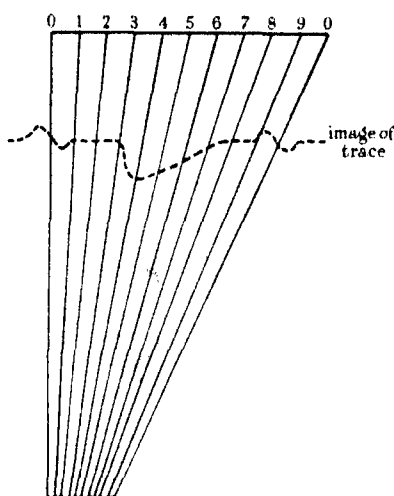


FIGURE 6

This method gives a true histogram of the velocity distribution of the neutrons, provided that the duration of the pulse of neutrons is negligible and that the middle of the time mark accurately represents the middle of the pulse. The true distribution cannot be obtained from such a histogram to an accuracy greater than that corresponding to the steps chosen. Actually the total duration of the beam of ions is known, from observations on an oscillograph operated directly from the beam, to extend over about one-fifth of the period, though the large majority of ions come within one-tenth. It follows that the results from groups 1 and 9 will be modified by the inclusion of a proportion, difficult to calculate, of fast neutrons which really belong to group 0. This effect will be relatively important in the case of group 9, containing the slowest neutrons, which we should expect to be few in number, but both groups must be regarded as suspect

and no important conclusions can be drawn from them. Group 0, which of course is also affected, is not of importance as we are not specially interested in the number of fast neutrons recorded.

A similar error is of course produced in each group; for example, a small portion of group 6 will be lost to groups 5 and 7, which conversely will give something to group 6; but here, since the numbers in successive groups vary smoothly, the effect on the final result will be small.

In order to ensure that there should be no systematic delay of the traces of either time signals or particles the impulses from both were passed through the same amplifier circuit. This procedure had the disadvantage that the circuit used to give sharply rising traces for the particles distorted the time signals into the shape shown in figure 7, the total duration of a time mark being one-quarter of the interval between successive time marks. Observation on an oscillograph directly connected to the target showed that the pulses were really quite simple in form, rising sharply to a maximum and falling almost symmetrically. The width of such a pulse, measured one-third the way up, was about one-seventh of the spacing between the pulses, while the time marks as we have seen, ranged up to one-quarter. The difference, say one-tenth, represents a drawing out of the time mark by the circuit, and half this value gives the error due to setting the line on the middle of the apparent mark instead of an ideal undistorted mark. The shapes of the time marks in the runs used have been examined, and although slight variations exist there is no systematic difference between those taken with and without the absorbers. The only effect of the error is thus to decrease slightly the velocity corresponding to a given group, the absorption coefficient for the group as found by the method discussed below being unaffected.

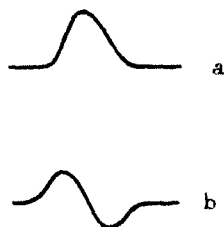


FIGURE 7

#### MEASUREMENTS OF ABSORPTION COEFFICIENTS

In order to measure the absorption coefficient of an element for neutrons of the range of velocities covered by the apparatus, an absorber must be made, large enough to cover the entrance of the cadmium coated tube, and of such thickness as to absorb about half the neutrons striking it. A series of runs is then made with the absorber in place, and the number of neutrons in any one time group is compared with the number in the same group when the absorber is absent. Another series is made with an absorber made of borax of sufficient thickness to absorb practically all those neutrons

which would normally go direct from the source to the chamber. The count with this absorber in place represents the effect of neutrons scattered from the walls and parts of the apparatus.

To allow for the fact that the intermittent source will not always be of the same strength, a standardizing experiment is made in which the intermittent source is replaced by a 100 mg. Ra + Be source placed as close as possible to the target and with the same distribution of wax around it. The particles so obtained are photographed in the usual way, though of course there are no time marks, and their number per minute is counted under three conditions: no absorber "*a*" thick boron absorber "*b*", absorber to be tested "*d*". Suppose that in the runs with the intermittent source the number of particles in a particular one "*g*" of the ten groups totals  $A_g$  for the runs without absorber,  $B_g$  for the runs with the thick boron absorber, and  $D_g$  for those with the absorber to be tested. Then with the intermittent source working with a (mean) strength of 100 mg. for one minute the number of particles recorded in group *g* which went directly from source to detector would have been

$$N_g = \frac{A_g}{\sum_g A_g} a - \frac{B_g}{\sum_g B_g} b$$

without the absorber, and

$$N'_g = \frac{D_g}{\sum_g D_g} d - \frac{B_g}{\sum_g B_g} b$$

with the absorber in place. The ratio  $N_g/N'_g$  of these quantities is therefore equal to  $e^{n\sigma}$ , where *n* is the number of absorbing nuclei per sq. cm. of the absorber and  $\sigma$  the cross-section for absorption including scattering. In forming all these quantities the natural count of the chamber is subtracted. The determination of an absorption coefficient in this way is independent of any assumption as to the relative efficiency of the detecting chamber for neutrons of different velocities. In the earlier groups a small allowance should be made for the fact that a few of the neutrons in them are really slow ones produced by the previous pulse of ions.

The "thin" boron absorber was made from a mixture of 4 parts sulphur to 1 of anhydrous borax fused together and cast into sheets. Four of these sheets were fitted together in a suitable frame to give an area of 46 × 46 cm. with a weight of 0.53 g./cm.<sup>2</sup>. The "thick" boron absorber was formed of borax packed to a thickness of about 5 cm. between tin plates. The cadmium absorber was made by plating cadmium on to sheet iron 56 × 51 cm. to a thickness of 0.0296 g./cm.<sup>2</sup>.

The results for the variation of the absorption cross-section of boron with group number (i.e. with  $1/v$ ) are shown in figure 8. One is at once struck by the marked contrast between our results and those to be expected from the  $1/v$  law, which would give a straight line through the point  $P$  (figure 8).

The principal experimental evidence in favour of the  $1/v$  law for boron is the negative result of the spinning-absorber experiment of Rasetti and others, which if our results are correct should have shown a change in the

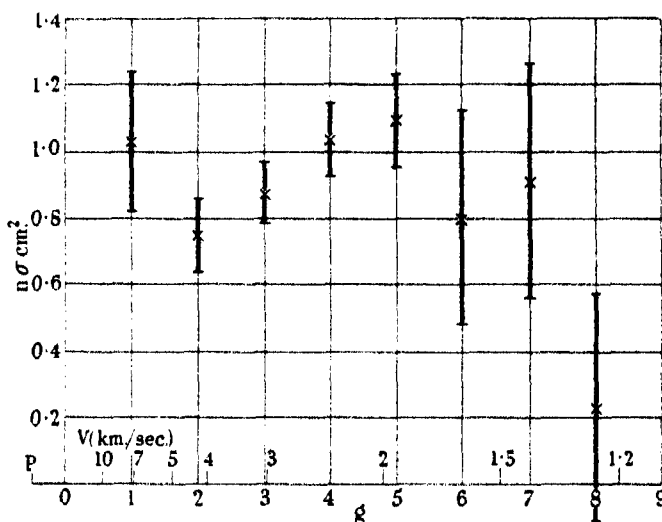


FIGURE 8. Absorption coefficients for boron absorber with  $1.26 \times 10^{21}$  atoms per cm.<sup>2</sup>.

same sense and the same order of magnitude as that which they found for cadmium. Alvarez, using an apparatus which has some similarity to ours, but working with still slower neutrons, has found an absorption coefficient greater than that for an unanalysed beam by approximately the amount which the  $1/v$  law would predict; in the region of velocity which we have studied he found what appeared to be a considerable divergence from the  $1/v$  law but ascribed it to unsuitable adjustment of his apparatus.

All our attempts to trace the divergence of our results from the  $1/v$  law to errors of experiment have failed, and as we are unable at the present time to pursue the matter experimentally we make no further comment except to give later in this paper some details of the two aspects of the work which seemed to us to offer the only possibilities of serious experi-

mental error. We refer to the measurement of the traces which, in large part we were unable to do ourselves, and some difficulties experienced with the cadmium-coated tube.

We have considered the possibility that the thin boron absorber might have been inhomogeneous (owing, for example, to imperfect mixing of the

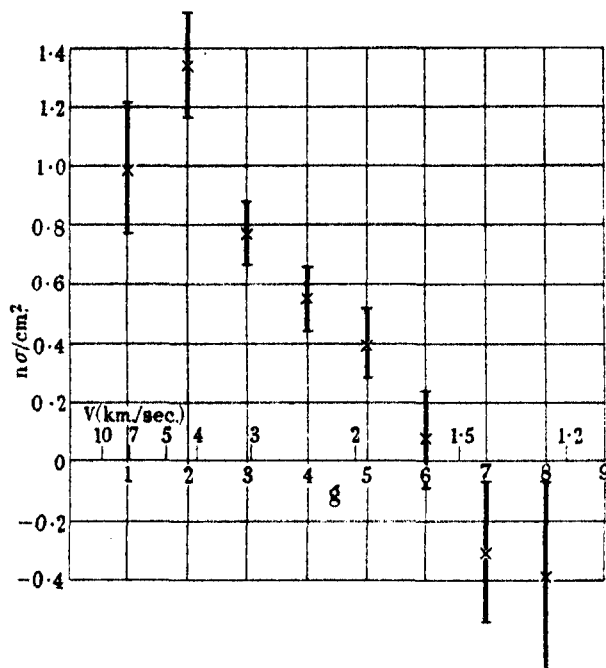


FIGURE 9. Absorption coefficients for cadmium absorber with  $1.59 \times 10^{20}$  atoms per  $\text{cm}^3$ .

borax and sulphur), and have satisfied ourselves that this was not so. Any such inhomogeneity would tend to reduce the observed absorption coefficient and to make it apparently less dependent upon the velocity of the neutrons.

The results for cadmium are shown in figure 9. Though it is perhaps surprising that the absorption coefficient should be so small for the slowest neutrons, yet our curve does not contradict any facts known to us, and it predicts a result from the spinning-absorber experiment almost identical with that found by Rassetti *et al.*



## DISTRIBUTION IN VELOCITY OF THE NEUTRONS

No further experiments are required in order to obtain the velocity distribution of those neutrons of the original beam which are registered by the  $\text{BF}_3$  chamber, for this is already given as a function of the group number  $g$  by the expression  $N_g$ . In order to convert this to the actual velocity-distribution in the beam we should require to know how the

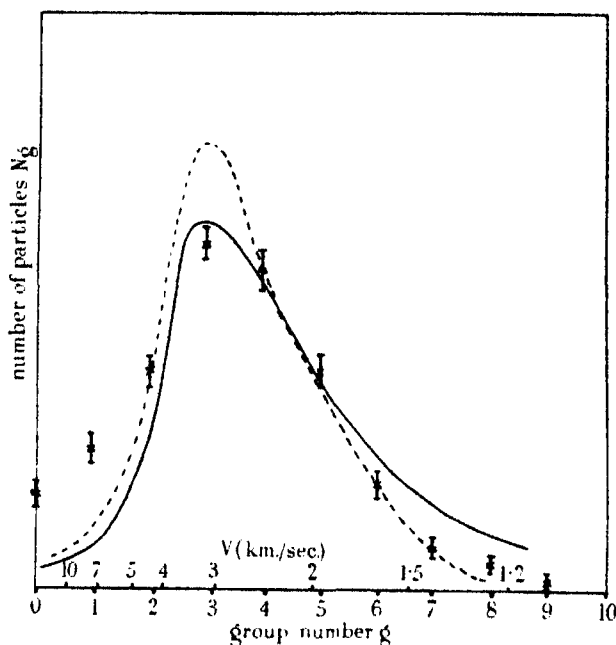


FIGURE 10. Figures X show observed distribution of neutrons among the time-groups. The vertical lines show calculated standard deviations for the experimental points. The results to be expected for a Maxwell distribution at  $290^\circ \text{K}$  are shown by the full curve if the chance of detection is proportional to  $1/V$  and by the broken curve, if the chance of detection is given by our experimental absorption measurements.

efficiency of detection depends upon the velocity. Since the fraction of the beam absorbed in the  $\text{BF}_3$  chamber was small (about 2 %) the efficiency of detection is proportional to the absorption coefficient in boron of the neutrons. In view of the discrepancy between our measurements and the " $1/v$ " law of absorption, we have preferred not to make such a conversion but simply to plot our experimental results directly and compare them with what would be expected on various suppositions.

Figure 10 shows the values of  $N_g$  experimentally obtained for each of the ten groups, the vertical lines indicating the statistical standard

deviations of these values as calculated from the numbers of particles involved. An additional scale of abscissae shows the velocities which correspond to the centres of the groups. The full curve is drawn through points which are the numbers that would be expected to fall in the various groups if the velocity distribution of the neutrons were that of molecules issuing from a small hole in an enclosure containing a gas of unit molecular weight at room temperature, it being supposed that the efficiency of detection varies inversely with the velocity. The dotted curve is drawn through points calculated from the same Maxwellian law, but on the supposition that the efficiency of detection varies with velocity according to our experimental measurements of the boron absorption coefficient. The vertical scale of each calculated curve, which is of course arbitrary, has been adjusted to give the best possible fit to the experimental points. The discrepancy at the peak of the broken curve may be explained by quite small random errors in measurement, which will make the observed peak less sharp than the calculated one, in which allowance has been made only for the finite resolving power of the apparatus itself; otherwise distinctly the better fit is obtained by the use of our experimental values of the absorption coefficient.

Too much stress should not be laid on this because the velocity distribution of the neutrons must not be expected to be exactly Maxwellian. Since the neutrons have a finite lifetime in the wax, a true Maxwellian equilibrium is not obtained in the interior, and an excess of faster neutrons must be expected. Moreover, the relation between the velocity distribution of the neutrons which escape and the velocity distribution inside will not necessarily be the same for neutrons escaping from a material surface as for molecules emerging freely from an orifice, and may vary with the angle at which the neutrons leave the surface.

#### CORRECTIONS FOR SCATTERED PARTICLES

As explained above, we allow for the neutrons which arrive at the detector by an indirect path, by taking counts with the standard source and with a thick boron absorber in the path of the direct beam. The importance of this correction depends on the absorbing powers of the cadmium coated tube which acts as a shield. At first the cadmium was applied to the tube as a paint. After the runs with and without the boron absorbers had been taken, it was found that the paint was peeling off, and a count with the standard source showed that the correction had considerably increased (about doubled). We believe, however, that much the

greater part of the loss of paint occurred after these runs, and have therefore used the corrections as determined for the tube when new. The runs with the cadmium absorber in place were made with a second tube of iron electrolytically plated with cadmium, and gave a count with the thick boron absorber slightly less than that given when the painted tube was new. The following table shows the counts per min. with the 100 mg. source after subtracting the "natural" count:

| Cadmium tube                            | Absorbers      |               |               |               |
|---|----------------|---------------|---------------|---------------|
|   | None           | Thin boron    | Thick boron   | Cadmium       |
| Original arrangement<br>(relative only) | 17.0           | $9.3 \pm 0.7$ | $3.6 \pm 0.4$ | —             |
| After loss of paint                     | $17.0 \pm 0.6$ | $9.7 \pm 0.3$ | $6.0 \pm 0.3$ | —             |
| With plated tube                        | $13.2 \pm 0.5$ | —             | $2.4 \pm 0.4$ | $9.1 \pm 0.5$ |

From these figures and the results for the boron absorber given above the cross section of boron for the slow neutron beam as a whole may be calculated. The original arrangement gives a value of  $6.7 \times 10^{-22}$  cm.<sup>2</sup>, while after the loss of paint a value of  $8.0 \times 10^{-22}$  cm.<sup>2</sup> results. The discrepancy is rather serious and we have no satisfactory explanation for it. But even if we were to make the extreme assumption that the paint fell off suddenly after the "Maxwell" runs but before the runs with the boron absorber (which is certainly wrong, and moreover the two series overlapped to some extent) the curve of absorption against group number, though less violently in contradiction with the  $1/v$  law, is still in definite disagreement with it.

In calculating the absorption curve for cadmium, we have again taken the data for the original arrangement so far as the direct beam is concerned. The value for the average cross section is  $3.0 \times 10^{-20}$  cm.<sup>2</sup>.

We should like to state that G. E. F. F., P. B. M., G. P. T. and C. E. W.-W. (1939), were responsible for the design and construction of the apparatus in substantially its final form and for the taking of a few early readings; D. F. G., G. P. T. and C. E. W.-W. have made some improvements of detail and have made the experiments here reported. We are all much indebted to Mr H. Hutchinson for technical assistance.

#### SUMMARY

A velocity spectroscope for slow neutrons has been constructed upon the principle of measuring the times of transit of individual neutrons from an intermittent source to a distant ionization chamber.

Measurements have been made of the velocity distribution of the slow neutrons from a paraffin-wax howitzer at room temperature.

By the interposition of absorbers, the absorption coefficients of boron and cadmium have been measured for neutrons of different velocities. The results for boron are inconsistent with the law of inverse velocity.

#### REFERENCES

- Dunning, Pegram, Fink, Mitchell and Segrè 1935 *Phys. Rev.* **48**, 704.  
Fertell, Moon, Thomson and Wynn-Williams 1939 *Nature, Lond.*, **142**, 829.
- 

## A magnetic study of the two-phase iron-nickel alloys

BY A. T. PICKLES AND W. SUCKSMITH, F.R.S.

*H. H. Wills Physical Laboratory, University of Bristol*

(Received 20 March 1940)

#### INTRODUCTION

The iron-rich alloys of iron and nickel resemble pure iron in that they undergo a phase change from body-centred cubic ( $\alpha$ ) structure to face-centred cubic ( $\gamma$ ) structure on heating. On cooling the alloys, however, the return to the original state takes place at a much lower temperature, and on account of this thermal hysteresis the alloys are known as irreversible.

A magnetic investigation of these alloys has been made by Peschard (1925), who measured the variation of the saturation intensity of the alloys with temperature. The change from the  $\alpha$  to the  $\gamma$  lattice is accompanied by a decrease of the saturation intensity of the alloy, since the  $\gamma$  phase is non-magnetic at the temperature of the change. Curves showing the variation of intensity with temperature are very useful in the study of these alloys, since they give visual evidence of the irreversibility.

The relation of the irreversible changes to the equilibrium phase diagram is not clearly understood. Recently, however, equilibrium diagrams of the iron-nickel system, determined by means of X-ray data, have been published by Bradley and Goldschmidt (1939) and Owen and Sully (1939).

The phase diagram given by Owen and Sully approximates more closely to that determined magnetically by the writer, but Bradley and Goldschmidt emphasize that their phase diagram is purely tentative and put forward in the hope of stimulating further experimental work. Both investigations were made after long periods of annealing to produce the equilibrium two-phase state. The purpose of the following paper is to show that measurements of the variation of the magnetic intensity with temperature can be used in the iron-nickel system to determine the equilibrium phase diagram, and to investigate the relation of the irreversible changes to equilibrium conditions.

#### EXPERIMENTAL METHOD AND PREPARATION OF SPECIMENS

The intensity measurements have been carried out by means of the magnetic balance devised by Sucksmith (1939*a*, 1939*b*) for a study of the iron-nickel-aluminium system. Through collaboration with Dr Bradley specimens of the alloys used in his X-ray investigation were available; the preparation and purity of the alloys is described in his paper (Bradley and Goldschmidt 1939).

As in the previous work with this balance, all measurements were made relative to Hilger iron of 99.96 % purity as standard, the intensity per unit mass being taken as 217.8 at 20° C (Weiss and Forrer 1929). While taking measurements the temperature of the furnace was raised or lowered continuously by means of a motor-driven rheostat. A magnetizing field of 16,000 oersted was used in all measurements. No correction for the variation of saturation intensity with field has been applied to the intensity-temperature curves, but the error is small except at temperatures in the neighbourhood of the Curie point; in the majority of these alloys, however, the magnetic intensity falls to zero as a result of a phase change which occurs below the Curie point, and the temperature at which this fall in intensity takes place was found to be unaffected by the magnetic field.

A set of twelve alloys covering the range from 3 to 35 % Ni were received from Dr Bradley who had subjected them to a preliminary heat treatment. This consisted of a lump anneal just under the melting-point, and then a further lump anneal at 550° C for 9 days. Small specimens, approximately  $1\frac{1}{2} \times 1\frac{1}{2} \times 4$  mm., were cut from these alloys, and were subjected to further annealing treatments. The annealing of the specimens was carried out either actually in the apparatus, or in external electric furnaces. When the former method was used, the temperature was maintained

constant to within  $\pm 3^\circ \text{C}$  in the course of a 16 hr. run, by the use of regulator lamps in series with the furnace winding. For the other annealing processes, large thermostatically controlled furnaces were used, in which the temperature was maintained within  $\pm 2^\circ$  for periods of the order of months. Sets of specimens of a range of nickel content were sealed in quartz or pyrex tubes and placed in these furnaces. It was calculated that the small amount of air in the protecting tubes could only produce a negligible amount of oxide on the surface of the specimens, which weighed approximately 40 mg. each. The specimens sealed in quartz did not show any sign of oxidation after annealing, while the specimens sealed in glass acquired a thin film of dark-coloured oxide which, however, did not lead to any detectable change of weight or saturation moment.

The alloys as received were partly in the two-phase state as a result of the preliminary heat treatment. In order to obtain specimens in the single-phase state it was necessary to heat them to  $1000^\circ$  for 24 hr. Specimens heated to  $850^\circ \text{C}$  for 24 hr. still remained two-phase to a small extent owing to the very slow rate at which equilibrium is attained. In view of the small size of the specimens and the sluggishness of the alloy system, the specimens were not quenched in water after annealing, but were allowed to air-cool.

#### THE MAGNETIC INTENSITY OF THE QUENCHED ALLOYS

The intensity-temperature curves of the quenched alloys have been determined by Peschard, and in the course of the present investigation his results have been confirmed. The results are briefly recapitulated here, so that the changes produced by prolonged annealing may be appreciated. On heating a specimen of an irreversible alloy, the intensity diminishes slowly in the usual manner, until a temperature  $T$  is reached, when the  $\alpha$  lattice begins to transform rapidly into the  $\gamma$  lattice. The  $\gamma$  phase is paramagnetic at these temperatures, so the intensity falls, becoming zero on the completion of the  $\gamma - \alpha$  transition at  $T'$ . On cooling, the  $\alpha$  lattice is not formed from the  $\gamma$  lattice until the temperature has fallen considerably below  $T'$ , the corresponding temperatures being  $T$  and  $T'$ . The result is a magnetization-temperature curve as in figure 1, curve A.

The usual rate of change of temperature in these measurements is  $5\text{--}10^\circ \text{C}$  per min., i.e. the cycle can be described in some 3 hr. If the temperature changes are carried out more rapidly, the shape of the cycle remains unaltered, while holding at a given temperature in the apparatus for practicable periods produces at most a small change of intensity. The

cycle appears to represent a metastable condition which is only slowly affected by annealing. A phase diagram, as in figure 2, can be constructed which describes the properties of the irreversible alloys under ordinary rates of temperature change.

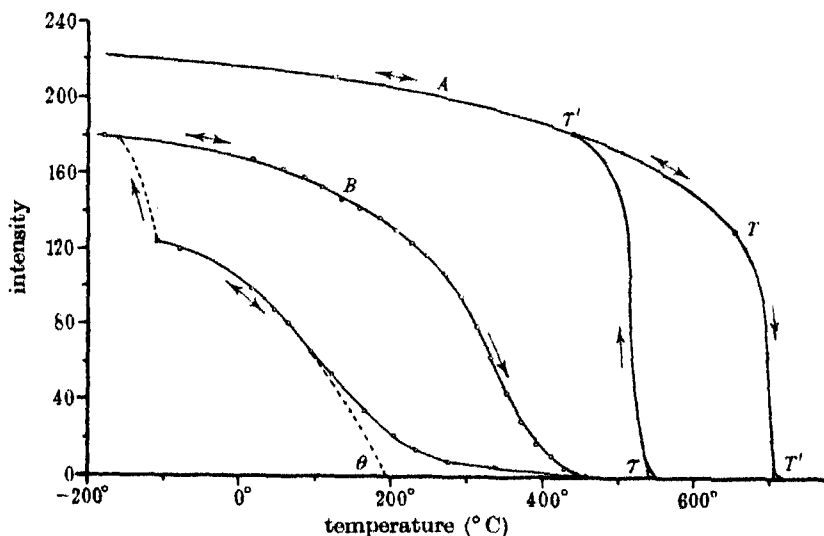


FIGURE 1. Irreversible intensity-temperature curves of 9 % and 32 % nickel-iron alloys after quenching. A, 9 % nickel alloy; B, 32 % nickel alloy after 30 hours at  $-180^{\circ}\text{C}$ .

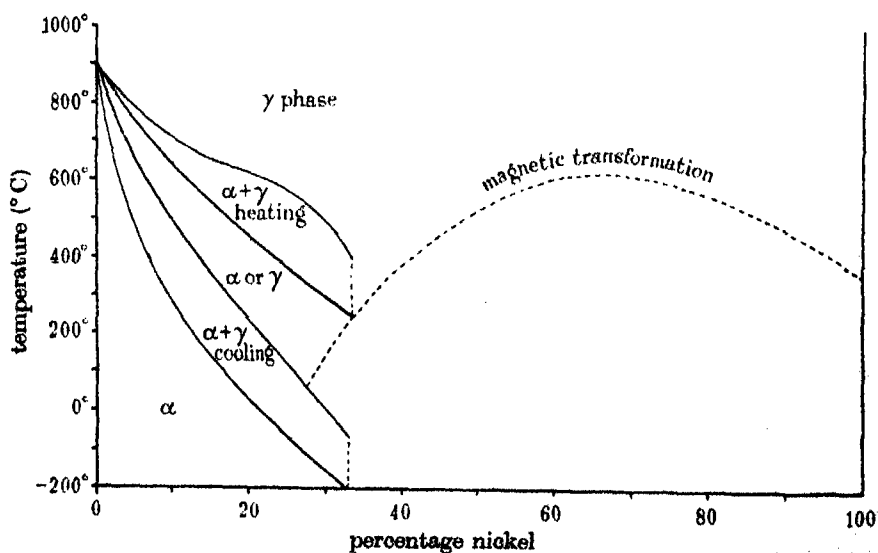


FIGURE 2. Iron-nickel practical phase diagrams (from Peschard).

As the nickel content of the alloy is increased, the hysteresis loop becomes more extended, until finally the  $\gamma$ - $\alpha$  transition takes place at room temperature. But at the same time a new phenomenon occurs; the Curie temperature of the  $\gamma$  phase rises with increasing nickel content, and finally becomes greater than the temperature at which the  $\gamma$ - $\alpha$  transition begins. Thus, on cooling the specimen from the high temperature, there is first an increase of magnetization at the Curie point of the  $\gamma$  phase, and afterwards a further increase due to the  $\gamma$ - $\alpha$  transition. This type of variation of intensity with temperature is shown in figure 1, curve *B*, for the 32 % Ni alloy. The lower branch corresponds to the  $\gamma$  structure, with a Curie point at about 190° C. This structure is stable down to solid carbon dioxide temperature, but between this and liquid air temperature it undergoes an irreversible  $\gamma$ - $\alpha$  structure change. The actual experimental points are given in this diagram to illustrate the extent to which they lie on smooth curves. Finally, in alloys of nickel content greater than 33 atomic %, it is no longer possible to produce a  $\gamma$ - $\alpha$  transition by cooling. Consequently the  $\alpha$  lattice is not formed, and the alloys remain fully reversible under ordinary rates of temperature change.

The transitions do not take place by a diffusion mechanism. The  $\alpha$  lattice of the alloys at room temperature is distorted owing to the  $\gamma$ - $\alpha$  transition. The  $\gamma$  lattice, however, represents the original high temperature condition of the alloy and is not distorted (Bradley and Goldschmidt, 1939).

#### THE EFFECT OF PROLONGED ANNEALING

If the alloys are annealed at a sufficiently high temperature to allow diffusion to take place, then the alloy segregates into an iron-rich component having an  $\alpha$  structure, and a  $\gamma$  nickel-rich component. The iron-rich component has a higher intensity and Curie temperature than the original single-phase alloy; the nickel-rich component has similarly a lower intensity and Curie temperature. The intensity-temperature curve will show the presence of both these components. Thus the annealing process produces a modification of the shape of the hysteresis cycle. This effect was first shown by Scheil (1935) by means of a dilatometer, using a 4.8 % Ni alloy annealed in the neighbourhood of 700° C.

Quenching from the annealing temperature may, however, lead to the nickel-rich component undergoing an irreversible transition into the  $\alpha$  structure. An intensity-temperature curve of such an alloy differs little from that of the single-phase alloy since the transition temperatures of the

\* In this paper, the composition of all alloys is given in atomic per cent.



two components are not widely separate. The presence of an iron-rich component is, however, shown by the increased temperature at which the magnetization finally falls to zero. If the composition of the nickel-rich phase is such that it does not undergo a  $\gamma - \alpha$  transition on cooling to room temperature, then its presence in the alloy may be recognized by X-ray measurements, or the inflexions on the intensity-temperature curve. The composition of the nickel-rich phase depends on the annealing temperature, and the unmodified  $\gamma$  component is obtained at room temperature only if the annealing is carried out at a temperature less than about 550° C.

Examination of alloys cooled to room temperature for signs of the presence of the  $\gamma$  phase is therefore only suitable for determining the equilibrium at temperatures less than 550° C. Alloys annealed at 525 and 450° C have been examined in this way.

#### THE EQUILIBRIUM AT 525° C

The room temperature intensity of specimens annealed at 525° C is given in table 1. The specimens were first annealed at 550° C for 9 days and then at 525° C for a further 9 days. Almost identical results have been obtained with further sets of specimens annealed at 525° C for 9 and 20 days respectively. It appears that some form of limit has been reached,

TABLE 1. ROOM TEMPERATURE INTENSITY OF QUENCHED AND ANNEALED SPECIMENS

| % Ni content | Intensity of quenched specimens | Intensity of specimens after annealing at 525° C |     |     |     |
|--------------|---------------------------------|--|-----|-----|-----|
|              |                                 | A  | B   | C   | D   |
| 3            | 218                             | 219  | —   | 218 | —   |
| 6            | 218                             | 219  | —   | 218 | —   |
| 7.6          | 219                             | 213  | —   | 213 | —   |
| 9            | 219                             | 211  | —   | 211 | —   |
| 13           | 214                             | 177  | 177 | 169 | 162 |
| 16           | 214                             | 162  | 156 | 126 | 120 |
| 20           | 209                             | 92   | 90  | 83  | 82  |
| 25           | 163                             | 82   | 79  | 118 | 110 |

Specimens in column A were annealed for 9 days at 525° C after preliminary heat treatment at 550° C.

Specimens in column B were annealed for 18 days at 525° C after preliminary heat treatment at 550° C.

Specimens in column C were annealed for 9 days at 525° C after quenching from 1000° C.

Specimens in column D were annealed for 18 days at 525° C after quenching from 1000° C.

after which annealing at 525° C produces little further change, but this may not represent equilibrium, since 20 day anneals on similar sets of specimens which had previously been quenched from a high temperature to eliminate the result of the preliminary heat treatment at 550° C, gave different values of intensity at room temperature. In these alloys, the time taken to reach equilibrium depends on the previous heat treatment, and it has not proved possible to obtain an equilibrium value of intensity which is entirely independent of preliminary heat treatments.

The intensities of the 3 and 6 % Ni alloys are not affected by annealing, but the 7.6 % alloy has a lower intensity. The  $\alpha$  boundary at 525° C therefore appears to lie between 6 and 7.6 % Ni.

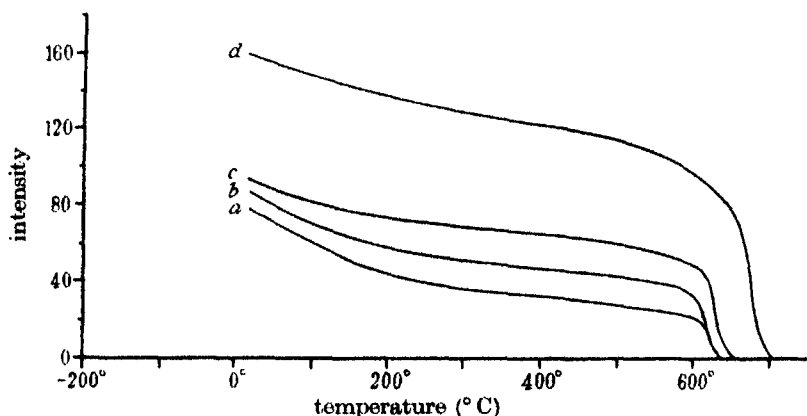


FIGURE 3. Intensity-temperature curves of alloys annealed at 525° C. *a*, 25 % nickel; *b*, 23 % nickel; *c*, 20 % nickel; *d*, 16 % nickel.

The intensity-temperature curves of the alloys containing from 12 to 26 % Ni show the Curie point of the  $\gamma$  phase as an inflexion at about 150° C, thus demonstrating the presence of the nickel-rich phase (figure 3). The presence of the iron-rich phase is shown by the increased temperature at which the magnetization finally falls to zero. The alloys 7.6 and 9 % Ni do not show the inflexion, but in these cases the amount of  $\gamma$  phase present is small, and the evidence for the existence of two phases in these specimens rests on the fall of intensity produced on annealing. The position of the  $\gamma$  boundary is fixed as lying between 26 and 29 % Ni by the fact that the 29 % alloy is not affected by annealing at 525° C. The 26 % alloy is only slightly affected, so the  $\gamma$ -phase boundary at this temperature appears to lie between 26 and 27 % Ni. This is confirmed by the fact that quenched specimens of the 26 % alloy may show an inflexion in the neighbourhood of 150° C.

If a two-phase alloy is immersed in liquid air, then the  $\gamma$  nickel-rich component undergoes an irreversible transformation into the  $\alpha$  structure, since its composition is about 26.5 % Ni. The resultant intensity-temperature curve shows an inflexion at about 540° C; this inflexion corresponds to the transition of the nickel-rich  $\alpha$  structure into the  $\gamma$  structure. The transition temperature of the 26.5 % alloy is in fact about 525° C, so the agreement between the expected and the observed value of the temperature of the inflexion is good. Figure 4 shows this inflexion in curves

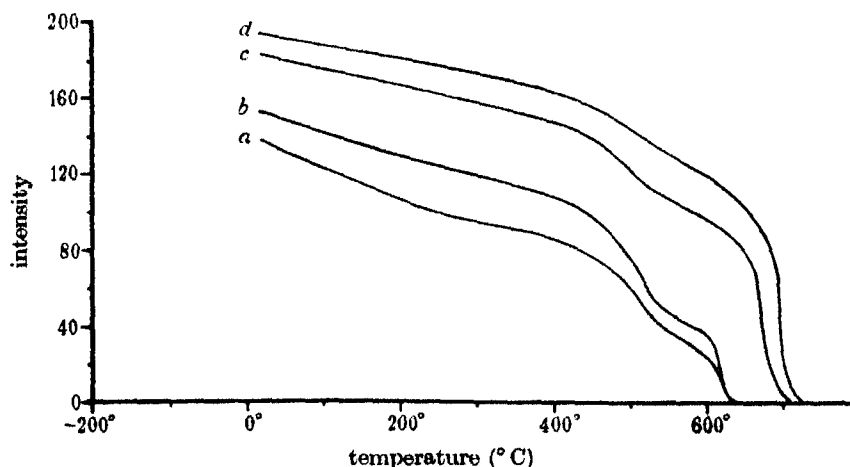


FIGURE 4. Intensity temperature curves of alloys annealed at 525° C and subsequently cooled to -180° C. *a*, 25 % nickel; *b*, 23 % nickel; *c*, 16 % nickel; *d*, 13 % nickel.

for alloys ranging in composition from 25 to 13 % Ni. The inflexion at about 200° C in the curves for the 25 and 23 % Ni alloys is due to the Curie point of some untransformed nickel-rich component. At a given temperature the completeness of the  $\gamma$ - $\alpha$  transition in an iron-nickel alloy is dependent on the physical state. An alloy containing 26.5 % Ni is normally completely transformed into the  $\alpha$  structures by cooling in liquid air, but in the highly dispersed state in which the nickel-rich component occurs in the two-phase alloy, the conversion is not so complete.

#### THE EQUILIBRIUM AT 450° C

The rate of attainment of equilibrium at 450° C is slow, but specimens annealed for 2 months at this temperature are considerably modified. If the specimens are already in the  $\alpha$  phase, formed in the quenched specimens

of the nickel-rich alloys by immersion in liquid air, then annealing at 450° C does not produce as large a fall of intensity at room temperature, as in the case of the specimens annealed at 525° C.

On the other hand, the two-phase alloys are now reversible between room temperatures and liquid air temperature. This means that the  $\gamma$  phase segregated is reversible and therefore contains more than 33 % Ni (the limit of the irreversible alloys). Other evidence on the composition of the  $\gamma$  phase at this temperature is available from the intensity-temperature curves of the annealed alloys (figure 5). These show an inflexion in

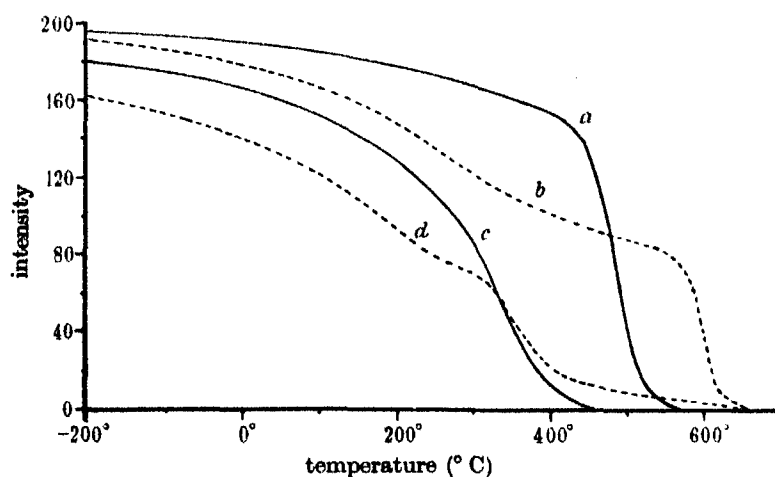


FIGURE 5. Intensity-temperature curves showing modifications produced by annealing at 450° C. *a*, 26 % nickel quenched; *b*, 26 % nickel annealed at 450° C for 8 weeks; *c*, 32 % nickel quenched; *d*, 32 % nickel annealed at 450° C for 8 weeks.

the neighbourhood of 350° C corresponding to the Curie point of an alloy containing about 35 % Ni. There are two inflexions in the curve of the 32 % Ni alloy. The first, at about 250° C, corresponds to the Curie point of the  $\gamma$  structure of the single-phase 32 % alloy. The second, at about 400° C, corresponds to the Curie point of the nickel-rich phase, but the inflexion is not well defined owing to the small amount of iron-rich phase present. Curves of the 23 and 25 % Ni alloys show a well-defined inflexion at 350° C, as in the curve of the 26 % Ni alloy. That an estimate of 35 % Ni at the limit of the two-phase region is slightly too high is shown by the fact that the 35 % alloy is not affected by the annealing treatment, while the intensity-temperature curve of the 32 % alloy shows the presence of two phases. The position of the  $\gamma$  boundary at 450° C therefore lies between 33 and 35 % Ni.

The position of the  $\alpha$  boundary is less definite since, owing to the small proportion of the  $\gamma$  phase present in the iron-rich alloys, evidence cannot be derived from the intensity-temperature curves. The room temperature intensity of two sets of specimens show a fall of intensity below the quenched value at between 7.6 and 9 % Ni, but the change is not sharp as is the case with the sets of alloys annealed at 525° C. At these low temperatures the magnetic method is not as suitable for fixing the position of the  $\alpha$  boundary as for the  $\gamma$  boundary, when the presence of two phases is immediately recognizable on the intensity-temperature curve.

#### THE PHASE BOUNDARIES AT TEMPERATURES ABOVE 525° C

Specimens annealed at temperatures above about 525° C do not show the presence of a  $\gamma$  phase on cooling to room temperature. This is not due to the two-phase field narrowing suddenly above 525° C, but depends on the fact that the composition of the nickel-rich phase at above this temperature is such that the phase undergoes the  $\gamma - \alpha$  transition on cooling, producing diffuse X-ray lines and affording no evidence of the existence of the two-phase region at the annealing temperature.

Although the presence of a  $\gamma$  nickel-rich phase cannot be detected, the presence of an iron-rich phase can be deduced from the fact that the transformation temperature of the annealed alloy is greater than that of the quenched alloy. Instead, however, of annealing sets of alloys at various temperatures above 525° C, and determining the composition at which no change was produced by annealing, specimens of quenched alloys have been annealed in the apparatus.

The behaviour of the alloys under these conditions is illustrated by an experiment carried out on a 16 % Ni alloy. The intensity-temperature curve of the quenched alloy was first determined, and the temperature  $T'$  at which the  $\alpha - \gamma$  change was completed was found to be 622° C. In order to determine  $T'$  accurately, the rate of heating was reduced to about 3°/min. over the steep part of the curve. The alloy was then cooled to room temperature and afterwards held at  $601 \pm 2^\circ$  C for 3 hr. The intensity fell from 70 to 20 units. That this did not simply represent the incomplete breakdown of the  $\alpha$  lattice into a homogeneous  $\gamma$  lattice was shown on raising the temperature by 2-3°/min., when the intensity finally fell to zero at 630° C, showing that the breakdown of the quenched alloy at this temperature involved the building up of a small amount of  $\alpha$  phase of less nickel content than 16 %.

Similar results have been obtained with other alloys. In all cases,

annealing the alloy at temperatures less than the transition temperature  $T'$  involved the production of an iron-rich phase. The temperature  $T'$ , therefore, at which the quenched alloy completes the  $\alpha-\gamma$  change is also the temperature of equilibrium between the  $\gamma$  and the  $(\alpha+\gamma)$  regions. Above this temperature the alloy is entirely in the  $\gamma$  phase; below it, an iron-rich  $\alpha$  phase is formed in addition to the  $\gamma$  phase. The  $\gamma$  boundary above 550° C has been determined therefore from a series of measurements of the temperature  $T'$  for alloys of from 3 to 23 % Ni. The results are given in table 2.  $T'$  is determined from the intensity-temperature curves by extrapolating the steep part of the curve to zero intensity.

TABLE 2. THE  $\gamma$  BOUNDARY BETWEEN 3 AND 23 % Ni

| % Ni | Transition<br>temperature<br>° C | % Ni | Transition<br>temperature<br>° C |
|------|----------------------------------|------|----------------------------------|
| 3    | 806                              | 16   | 625                              |
| 6    | 744                              | 20   | 585                              |
| 7.6  | 721                              | 23   | 572                              |
| 9    | 705                              | 25   | 540                              |
| 12   | 668                              |      |                                  |

When the nickel content of the alloy is greater than about 20 %, the temperature of completion of the  $\alpha-\gamma$  change becomes increasingly ill-defined owing to the appearance of a "tail" to the magnetization-temperature curve. Nevertheless, the  $\gamma$  boundary determined in this way joins smoothly with the boundary determined by quenching experiments at 525 and 450° C.

The determination of the  $\alpha$  boundary at these temperatures presents considerable difficulties, since the nickel content of the pure  $\alpha$  phase is small and varies only slowly with temperature. An attempt has been made to determine the temperature at which the 3 % Ni alloy enters the mixed phase region by annealing the alloy in the apparatus at a series of temperatures; in the mixed phase region such annealing leads to a fall of intensity due to the production of the  $\gamma$  phase.

Under ordinary rates of heating this alloy shows an  $\alpha-\gamma$  transition beginning at 800° C and ending at 806° C. One specimen was heated at 747° C for 10 hr., but at this temperature the magnetization-temperature curve appeared stable. Another specimen was heated at  $778 \pm 2^\circ$  for 12 hr.; in the course of this period the intensity gradually fell, showing that at this temperature the 3 % Ni alloy lies in the two-phase region. The  $\alpha$  phase boundary for this composition therefore lies between these two temperatures, and owing to its steepness there is little error in placing it at 760° C.

## THE LOW TEMPERATURE EQUILIBRIUM OF THE IRON-NICKEL ALLOYS

Sufficient data has now been accumulated to enable an equilibrium phase diagram to be drawn. This is given in figure 6. The transition temperature of pure iron has been taken as  $910^{\circ}\text{C}$ , the mean of the results of Adcock and Bristow (1935). Between  $910$  and  $550^{\circ}\text{C}$  the position of the  $\gamma$  boundary rests on observations of the transition temperature of the quenched alloys. The  $\gamma$  boundary at  $525$  and  $450^{\circ}\text{C}$  rests on annealing experiments carried out with series of alloys to determine the limits of composition of the mixed

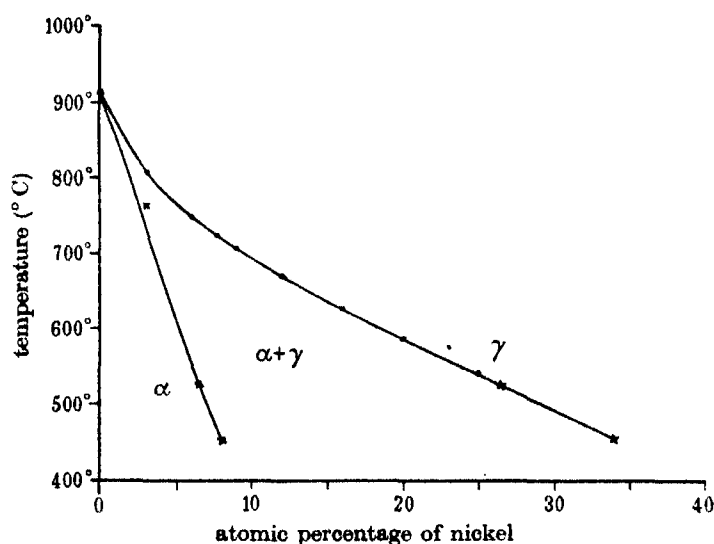


FIGURE 6. Equilibrium phase diagram of the iron-rich nickel-iron alloys.

phase region. The measurements of the variation of saturation intensity with temperature gives a convenient and accurate method of determining the  $\gamma$  boundary, but its application to the determination of the  $\alpha$  boundary cannot be considered to afford equally reliable evidence.

At temperatures below  $450^{\circ}\text{C}$ , equilibrium probably cannot be obtained except after annealing periods of the order of years, and preliminary work on the magnetization-temperature curves of alloys annealed at 400 and  $350^{\circ}\text{C}$  has not given the definite results obtained by annealing at higher temperatures.

The relation of this equilibrium phase diagram to the hysteretic diagram obtained at ordinary rates of temperature change can now be stated. The temperature  $T$  at which the  $\alpha - \gamma$  change begins to take place rapidly does not bear a direct relation to equilibrium conditions, since alloys annealed

below this temperature become two-phase. On the other hand, the temperature  $T'$  at which the  $\alpha - \gamma$  change is completed is also the temperature of equilibrium between the  $(\alpha + \gamma)$  and the  $\gamma$  regions. At lower temperatures the precise definition of  $T'$  is difficult, so its relation to equilibrium conditions is correspondingly obscure.

The temperature  $\tau$  at which the  $\gamma$  phase alloy begins to transform irreversibly on cooling does not correspond to equilibrium conditions. Alloys annealed in the  $\gamma$  phase at temperatures above  $\tau$  and less than  $T'$  begin to transform slowly into two phases. In addition, it is found that in the 29 % alloy, where  $\tau$  lies slightly below room temperature, cold work by wire-drawing the alloy initiates the  $\gamma - \alpha$  change at room temperature. Finally, the temperature  $\tau'$  at which the cycle is completed is very ill defined, and in the case of those alloys in which it lies at liquid air temperature, it is also a function of the time for which the alloy is cooled.

#### THE RATE OF ATTAINMENT OF EQUILIBRIUM

At temperatures less than 850° C diffusion processes take place very slowly in the iron-nickel alloys. Nevertheless, at 525° C, annealing for even 12 hr. leads to a considerable breakdown of the single-phase alloys. This is true, however, only if the alloy is heated to 525° C from room temperature, when it is in the distorted  $\alpha$  condition. If the alloy is first heated to 1000° C and then cooled to 525° C, remaining in the  $\gamma$  condition owing to the temperature hysteresis, an anneal of 9 days does not appear to modify the alloy, and the intensity at room temperature is only slightly lower than if the alloy had been cooled directly.

The rate of diffusion therefore is dependent on the structure as well as on the temperature. The distorted  $\alpha$  structure produced by the irreversible  $\gamma - \alpha$  change breaks up into two phases more readily than the more perfect  $\gamma$  structure which was the original state of the alloy. When the  $\gamma$  structure is annealed for a sufficiently long time at a high temperature then it too may segregate into two phases. In the case of a 6 % alloy annealed in the  $\gamma$  state for 18 hr. at 720° C, i.e. within the two-phase region of the equilibrium diagram, the intensity rose from 1 to 5 units in the course of the anneal. This increase can only be ascribed to the production of an iron-rich  $\alpha$  phase from the  $\gamma$  lattice, but the rate at which the  $\gamma$  lattice of this alloy breaks down at 720° C is only of the same order as the rate of breakdown of the distorted  $\alpha$  lattice at 525° C. In view of the exponential relation between velocity of diffusion and temperature, the extreme slowness of diffusion processes in the undistorted  $\gamma$  lattice is evident.



Owen has reported the effect of the mechanical distortion produced by filing in accelerating diffusion processes in the nickel-iron alloys at low temperatures. This factor is not operative in the  $4 \times 1\frac{1}{2}$  mm. specimens used in the present investigation.

We are indebted to Dr Bradley for his kindness in supplying the alloys used in the above investigation. One of us (A. T. P.) wishes to record his thanks to the Directors of the Electrical Research Association for a grant.

#### SUMMARY

Measurements of magnetic saturation intensity of annealed iron-nickel alloys have been used to demonstrate the existence of a two-phase field in the iron-rich part of the system. The phase boundaries have been determined at temperatures above  $450^{\circ}\text{C}$ , and the relation of the equilibrium phase diagram to the thermal hysteresis observed under normal rates of temperature change has been studied.

#### REFERENCES

- Adcock and Bristow 1935 *Proc. Roy. Soc. A*, **153**, 172.  
Bradley and Goldschmidt 1939 *J. Iron and Steel Inst.*  
Owen and Sully 1939 *Phil. Mag.* **27**, 814.  
Peschard 1925 Thesis, Strasbourg.  
Scheil 1935 *Arch. Eisenhüttenw.* **9**, 163.  
Sucksmith 1939*a* *Proc. Roy. Soc. A*, **170**, 551.  
— 1939*b* *Proc. Roy. Soc. A*, **171**, 525.  
Weiss and Forrer 1929 *Ann. Phys., Paris*, **12**, 279.
-

Determination of the Rydberg constants,  $e/m$ , and the  
fine structures of  $H_\alpha$  and  $D_\alpha$  by means of a  
reflexion echelon

BY J. W. DRINKWATER, SIR OWEN RICHARDSON, F.R.S.

AND W. EWART WILLIAMS

*King's College, London*

(Received 16 April 1940)

CORRIGENDA

In the *Note added in proof* at the end of this paper (these *Proceedings*, 174, 187) some of the values of important constants which would follow from the adoption of Birge's proposed change in the value of  $q$  are incorrect. Except in one case, where there is a printer's error, the changes are quite small; but as the quantities are believed to be determined very accurately it is important that the published values should be the right ones. The changes are:

- p. 187, bottom line, for  $9591.4_1 \pm 1.0_2$  read  $9572.7_9 \pm 1.0_2$ .
- p. 188, first line, for  $1837.7_2$  read  $1837.5_0$ .
- p. 188, second line, for 0.0084 read 0.00116.
- p. 188, third line, for  $109737.27_2$  read  $109737.27_{27}$ .
- p. 188, third line, for  $109737.26_{38}$  read  $109737.27_{154}$ .

The last rounds off to  $109737.27_2 \pm 0.020 \text{ cm.}^{-1}$ , which is the value given in the paper, on p. 178, when the Barrell and Sears correction is included.

We are glad to take this opportunity to thank Professor Birge for drawing our attention to these corrections.

# Some cases of the steady two-dimensional percolation of water through ground

BY B. DAVISON AND L. ROSENHEAD, D.Sc.

*University of Liverpool*

(Communicated by J. Proudman, F.R.S.—Received 22 August 1939)

## 1. INTRODUCTION AND SUMMARY

In this paper we examine three cases of steady two-dimensional motion of water through uniform permeable ground and obtain exact mathematical solutions of the problems which are investigated. In the cases considered the ground soaked with water is bounded by impervious surfaces, boundaries of water-basins and free surfaces. (The term “free surface” is used to denote that surface in ground-water motions which engineers call the “water table”.) Further, with the exception of the free surfaces, the boundaries are restricted to be plane. These problems do not involve seepage surfaces, but the method can, in certain cases, be applied to problems in which plane seepage surfaces occur. As we are considering only two-dimensional problems the plane surfaces are represented by straight lines in the representative plane—as for example in figure 1. In this figure  $LBCM$

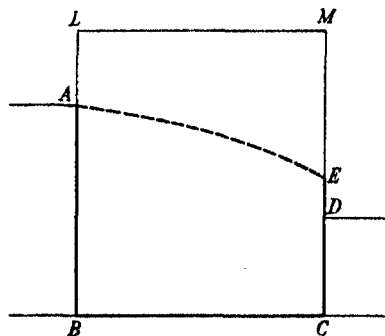


FIGURE 1

is an earth embankment.  $AB$  is the boundary of the head water-basin,  $BC$  is the impervious base of the embankment and  $CD$  is the boundary of the tail water-basin.  $AE$  is the free surface or water table, that is, the upper level of the water which is percolating through the embankment. Above

*AE* the pores between the particles of soil are filled with air. *ED* is the seepage surface, that is, the surface of the embankment through which water is steadily leaking and falling into the tail water. We assume that in the region of flow the "inertia forces" are neglected and that Darcy's law is satisfied, that is, that the frictional forces per unit volume between the water and the permeable ground are proportional to the first power of the "percolation velocity". The percolation velocity is defined as the limiting value of the ratio of discharge to area as the area tends to zero, it being understood that the discharge is measured in a direction normal to the area and that "area" includes not only the clearance between particles of soil but also the soil itself.

A general method of solution has been given by one of the authors in a previous paper (Davison 1936*a*). The present paper is a development of this work and contains, in §2, a lemma which is useful in special cases. As examples of this, three problems are discussed below.

The principal equations and symbols upon which the following work is based are given here.

*Ox* is the horizontal axis; *Oy*, directed upwards, is the vertical axis;

$\phi$  is the velocity potential;

$\psi$  is the stream function;

*W*, the complex potential, is  $\phi + i\psi$ ;

$w = dW/dz = u - iv$ ;

*u*, *v*, the components of percolation velocity are given by the equations

$$u = \frac{\partial \phi}{\partial x} = \frac{\partial \psi}{\partial y}, \quad v = \frac{\partial \phi}{\partial y} = -\frac{\partial \psi}{\partial x};$$

*p* is the average pressure at a point *x*, *y*.

The components of frictional force are defined, in agreement with Darcy's law, as  $\rho g u/k$  and  $\rho g v/k$ , where  $\rho$  is the density of the water, *g* the acceleration due to gravity and *k* is the percolation coefficient.

The equation of continuity is

$$\frac{\partial u}{\partial x} + \frac{\partial v}{\partial y} = 0. \quad (1.1)$$

The equations of motion are

$$\left. \begin{aligned} -\frac{\partial p}{\partial x} - \frac{\rho g}{k} u &= 0, \\ -\frac{\partial p}{\partial y} - \frac{\rho g}{k} v - \rho g &= 0, \end{aligned} \right\} \quad (1.2)$$

which demonstrate the existence of a velocity potential given by the equation

$$\phi = -k\left(\frac{p}{\rho g} + y\right). \quad (1.3)$$

The boundary conditions were shown (Davison 1936*a*) to be

- (i) On the surface of a water-basin,  $\phi$  is constant.
- (ii) On an impervious surface,  $\psi$  is constant.
- (iii) On a seepage surface,  $p$  is constant.
- (iv) On a free surface from which there is no evaporation,  $\psi$  is constant and  $p$  is constant.
- (v) On a free surface from which evaporation takes place,  $(\psi - \epsilon x)$  is constant and  $p$  is constant.

The quantity  $\epsilon$ , which is constant, is defined to be the volume of outer water (as, for example, rain water) which penetrates in unit time through each section of the free surface, whose projection parallel to  $Ox$  is of unit area, into the water flowing through the soil. Evaporation through the pores filled with air just above the free surface may be represented by negative values of  $\epsilon$ . In practice  $\epsilon$  is always less than  $k$ .

Taking into account the fact that the equations of the water-basin, impervious and seepage surfaces are prescribed, it is clear that two boundary conditions must be satisfied on each of the four types of boundary we have discussed. These conditions take the form

$$\left. \begin{aligned} ax + by + c\phi + d\psi &= e, \\ a'x + b'y + c'\phi + d'\psi &= e', \end{aligned} \right\} \quad (1.4)$$

where  $a, b, c, d, e, a', b', c', d', e'$  are real constants. These conditions can also be written as

$$\left. \begin{aligned} I(mz + nW) &= e, \\ I(m'z + n'W) &= e', \end{aligned} \right\} \quad (1.5)$$

where  $I$  denotes the imaginary part of the complex quantity and  $m, n, m', n'$  are constants which, in general, are complex. With these definitions it has been shown (Davison 1936*a*) that in the  $w$  plane the above boundaries all become arcs of circles or portions of straight lines, the equation of the appropriate transformed boundary being

$$I\left(\frac{m + nw}{m' + n'w}\right) = 0. \quad (1.6)$$

The problems considered below are

(I) The characteristics of ground-water motion in a broad embankment with vertical faces, due allowance being made for evaporation from the free surface or water table (see figure 2).

If  $h_1$  and  $h_2$  are the depths of the head and tail waters and  $l$  is the width of the embankment, it is shown that a seepage surface must exist if

$$(h_1 - h_2)/l > \sqrt{(-\epsilon/k)}. \quad (1.7)$$

Further, in the absence of a seepage surface, the velocity field in the embankment is determined, the shape of the free surface is found implicitly and the flux over  $AB$  and  $CD$  is shown to be  $Q_1$  and  $Q_2$  where

$$\begin{aligned} Q_1 &= \frac{k(h_1^2 - h_2^2)}{2l} + \frac{(-\epsilon)l}{2}, \\ Q_2 &= \frac{k(h_1^2 - h_2^2)}{2l} - \frac{(-\epsilon)l}{2}. \end{aligned} \quad (1.8)$$

If no evaporation takes place a seepage surface must exist. This problem has been discussed previously (Davison 1932; Hamel 1934 and 1935).

(II) The characteristics of ground-water motion in the soil outside an irrigation dyke of rectangular section, the base being horizontal and at a constant height above a plane impervious surface. Evaporation is taken into account (see figure 5).

The equation of the free surface is obtained in a form involving integrals. In addition, formulæ are derived for the quantity of fluid entering the soil in unit time and for the width, at the impervious surface, of the strip of soil irrigated by the dyke.

(III) The characteristics of ground-water motion in the soil outside a number of parallel draining tubes (see figure 9).

The equation of the free surface is obtained.

## 2. LEMMA

The lemma which we propose to prove is:

"Let  $w_0$  be a constant complex quantity satisfying the relation

$$I\left(\frac{m+nw}{m'+n'w}\right) = 0. \quad (2.1)$$

We now define an  $\Omega$ -plane by the formula

$$\Omega = \lambda + i\mu = W - w_0 z. \quad (2.2)$$

Then that part of the boundary in the  $w$ -plane which is represented by (2.1) is transformed into a straight line in the  $\Omega$ -plane."

The proof is:

We make use of the following two identities:

$$I\left(\frac{m+nw}{m'+n'w}\right) - I\left(\frac{m+nw_0}{m'+n'w_0}\right) = -I\left(\frac{mn'-m'n}{m'+n'w_0} \frac{w-w_0}{m'+n'w}\right), \quad (2.3)$$

and 
$$\frac{d(W-w_0z)}{d(m'z+n'W)} = \frac{(dW/dz) - w_0}{m' + n'(dW/dz)} = \frac{w-w_0}{m'+n'w}. \quad (2.4)$$

Hence from (2.1), (2.3) and (2.4)

$$I\left(\frac{mn'-m'n}{m'+n'w_0} \frac{d(W-w_0z)}{d(m'z+n'W)}\right) = 0, \quad (2.5)$$

or, expressed in another way,

$$\arg\left(\frac{mn'-m'n}{m'+n'w_0}\right) + \arg\frac{d(W-w_0z)}{d(m'z+n'W)} = s\pi, \quad (2.6)$$

where  $s$  is some integer. Since  $(mn'-m'n)/(m'+n'w_0)$  is a constant we have

$$\arg\frac{d(W-w_0z)}{d(m'z+n'W)} = \text{constant}. \quad (2.7)$$

Putting  $m'z+n'W = R_0 + iI_0$  and remembering that on the boundary in question  $I_0 = \text{const.}$ , the equation (2.7) can be written as

$$\arg\left(\frac{d(\lambda + i\mu)}{dR_0}\right) = \text{constant}, \quad (2.8)$$

that is 
$$\frac{d\mu/dR_0}{d\lambda/dR_0} = \text{constant}, \quad (2.9)$$

and hence the corresponding part of the boundary in the  $\Omega$ -plane is a straight line.

The converse of this lemma is also true.

In applying this lemma to the problems under consideration we see that if all the parts of the boundary in the  $w$ -plane have a point,  $w_0$  say, in common, or rather if their equations are satisfied by the same complex quantity  $w_0$ , then all the parts of the boundary in the  $\Omega$ -plane are straight

lines. The interior of the polygon so formed can then be transformed into a half-plane,  $I(\zeta) \geq 0$  say, by means of a Schwarz-Chrystoffel integral. Let the transformation so obtained be

$$\Omega = g(\zeta). \quad (2.10)$$

Let us also define an  $\omega$ -plane by the relation

$$\omega = \frac{1}{w - w_0}. \quad (2.11)$$

$\omega_0$ , the point corresponding to  $w_0$ , is at infinity. In the  $w$ -plane the boundary is composed of straight lines and circles passing through  $w_0$ . The effect of the transformation (2.11) is to transform these circles and straight lines into circles or straight lines in the  $\omega$ -plane passing through  $\omega_0$ . Since  $\omega_0$  is at infinity all the parts of the boundary in the  $\omega$ -plane are rectilinear. Hence a second Schwarz-Chrystoffel transformation,

$$\omega = h(\zeta) \quad (2.12)$$

say, transforms the region of flow into half of the  $\zeta$ -plane. From (2.10) and (2.12) we have

$$\begin{aligned} z = \int dz &= \int \frac{dz}{d(W - w_0 z)} d(W - w_0 z) \\ &= \int \frac{1}{w - w_0} d\Omega = \int \omega d\Omega = \int h(\zeta) \frac{dg(\zeta)}{d\zeta} d\zeta, \end{aligned} \quad (2.13)$$

and  $z$  is thus determined as a function of  $\zeta$ . Applying this to (2.2) we get finally

$$W = \Omega + w_0 z,$$

where  $\Omega$  can now be expressed as a function of  $z$ . This is the complex potential which gives the solution of the problem.

If, however, the boundary in the  $w$ -plane possesses two points in common,  $w_0$  and  $w_{00}$  say, as, for example, when the boundary consists of a straight line and an arc of a circle, it is possible to define two  $\Omega$ -planes,  $\Omega_1$  and  $\Omega_2$  say, by means of the relations

$$\left. \begin{aligned} \Omega_1 &= W - w_0 z, \\ \Omega_2 &= W - w_{00} z, \end{aligned} \right\} \quad (2.14)$$

in which the boundaries are all parts of straight lines. This gives rise to two independent Schwarz-Chrystoffel transformations

$$\left. \begin{aligned} \Omega_1 &= g_1(\zeta), \\ \Omega_2 &= g_2(\zeta), \end{aligned} \right\} \quad (2.15)$$



from which, without any further integration, it is possible to deduce the relation between  $z$  and  $\zeta$ , namely,

$$z = \frac{g_1(\zeta) - g_2(\zeta)}{w_{00} - w_0}, \quad (2.16)$$

and here the complex potential  $W$  can be expressed as a function of  $z$  by means of the relation

$$W = \frac{w_{00}g_1(\zeta) - w_0g_2(\zeta)}{w_{00} - w_0}. \quad (2.17)$$

The formulae (2.14), (2.15), (2.16) and (2.17) are just the formulae which will be used in the following three special problems.

### 3. PERCOLATION THROUGH A BROAD EMBANKMENT

Let us consider the ground-water motion in a broad embankment with vertical faces. The base of the embankment is horizontal and impervious. The height of the head-water is  $h_1$  and that of the tail-water  $h_2$ . The width of

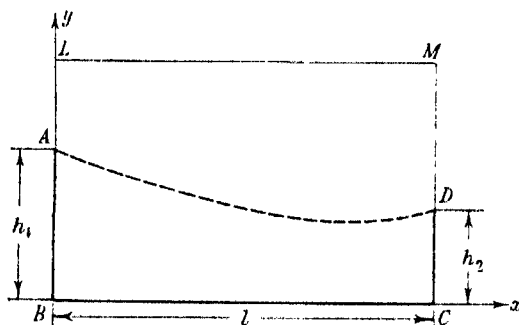


FIGURE 2.  $z$ -plane.

the embankment is  $l$ . We assume that evaporation takes place over the free surface, or water-table, and is sufficiently intense in nature to prevent the existence of a seepage surface. Let  $k$  be the percolation coefficient and  $(-\epsilon)$ , which is positive, the coefficient of evaporation, that is, the volume of fluid which evaporates in unit time from each section of the free surface whose horizontal projection is of unit area.

The boundary conditions are:

- (i) Along  $AB$  (i.e.  $x=0$ ),  $\phi$  is constant. Hence  $v = 0$ .
- (ii) Along  $BC$  (i.e.  $y=0$ ),  $\psi$  is constant. Hence  $v = 0$ .
- (iii) Along  $CD$  (i.e.  $x=l$ ),  $\phi$  is constant. Hence  $v = 0$ .
- (iv) Along  $DA$ , the pressure  $p$  is constant and also  $(\psi - \epsilon x)$  is constant.

These conditions can be expressed as follows: Along  $AB$ ,  $BC$  and  $CD$

$$I(w) = I(u - iv) = 0. \quad (3.1)$$

Along  $DA$ , the constancy of pressure can be expressed as

$$I(iW + kz) = \text{constant}, \quad (3.2)$$

and the constancy of  $(\psi - \epsilon x)$  can be written as

$$I(W - i\epsilon z) = \text{constant}. \quad (3.3)$$

Hence, according to equation (1.6),

$$I\left(\frac{w - i\epsilon}{iw + k}\right) = 0 \quad (3.4)$$

is satisfied on the free surface. This can be verified very easily as follows. The equation (3.4) is equivalent to

$$u^2 + (v + \epsilon)(v + k) = 0. \quad (3.5)$$

Along the free surface, however, the relation  $p = \text{constant}$ , or in the alternative form  $\phi + ky = \text{constant}$ , gives rise to

$$\frac{\partial \phi}{\partial x} \delta x + \left( \frac{\partial \phi}{\partial y} + k \right) \delta y = 0, \quad (3.6)$$

while the condition  $\psi - \epsilon x = \text{constant}$  can be written as

$$\left( \frac{\partial \psi}{\partial x} - \epsilon \right) \delta x + \frac{\partial \psi}{\partial y} \delta y = 0. \quad (3.7)$$

The condition (3.5) can be deduced from (3.6) and (3.7) by eliminating  $\delta y / \delta x$ .

The boundaries in the  $w$ -plane are therefore the circular arc given by (3.5), and a segment of the straight line given by (3.1). These curves intersect in the two points

$$w = \pm \sqrt{(-k\epsilon)}. \quad (3.8)$$

Hence, according to the lemma proved in § 2, the boundary of the region of flow in the  $z$ -plane corresponds to a polygon both in the  $\Omega_1$  and in the  $\Omega_2$ -planes where

$$\left. \begin{aligned} \Omega_1 &= W - z\sqrt{(-k\epsilon)} = \lambda_1 + i\mu_1, \\ \Omega_2 &= W + z\sqrt{(-k\epsilon)} = \lambda_2 + i\mu_2. \end{aligned} \right\} \quad (3.9)$$

and

Let  $B$  coincide with the origin  $O$  of the  $z$ -plane and the point  $(-kh_1, 0)$  of the  $W$ -plane. Hence, using the boundary conditions, it can be shown that

(i) in the  $W$ -plane

$$\begin{aligned} A &\equiv (-kh_1, Q_1), & B &\equiv (-kh_1, 0), \\ C &\equiv (-kh_2, 0), & D &\equiv (-kh_2, Q_1 + \epsilon l) \end{aligned}$$

and (ii) in the  $\Omega_1$ -plane

$$\left. \begin{aligned} A &\equiv (-kh_1, & Q_1 - h_1\sqrt{(-k\epsilon)}, \\ B &\equiv (-kh_1, & 0), \\ C &\equiv (-kh_2 - l\sqrt{(-k\epsilon)}, & 0), \\ D &\equiv (-kh_2 - l\sqrt{(-k\epsilon)}, & Q_1 + \epsilon l - h_2\sqrt{(-k\epsilon)}). \end{aligned} \right\} \quad (3.10)$$

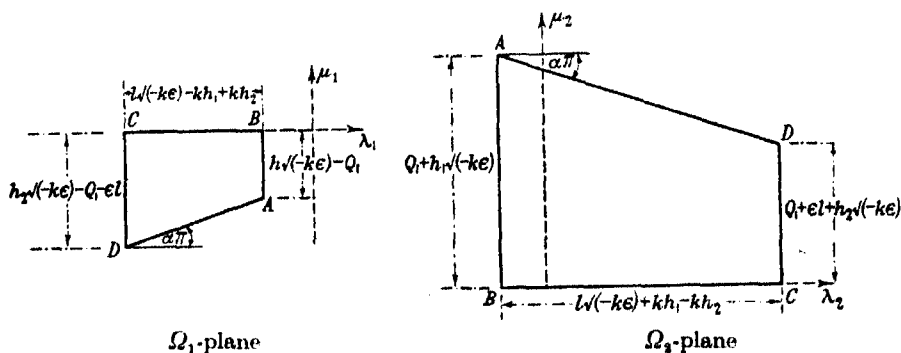


FIGURE 3

It should be noted that  $Q_1$  is the volume of fluid entering at the head-water in unit time and that  $Q_1 + \epsilon l$  is the volume of fluid leaving at the tail-water in unit time. Hence, as was to be expected,

$$Q_1 = Q_2 - \epsilon l. \quad (3.11)$$

Similarly in the  $\Omega_2$ -plane

$$\left. \begin{aligned} A &\equiv (-kh_1, & Q_1 + h_1\sqrt{(-k\epsilon)}, \\ B &\equiv (-kh_1, & 0), \\ C &\equiv (-kh_2 + l\sqrt{(-k\epsilon)}, & 0), \\ D &\equiv (-kh_2 + l\sqrt{(-k\epsilon)}, & Q_1 + \epsilon l + h_2\sqrt{(-k\epsilon)}). \end{aligned} \right\} \quad (3.12)$$

The shape of the polygons in the  $\Omega_1$ - and  $\Omega_2$ -planes are shown in figure 3. In both of them  $AD$  is inclined to the horizontal axis at an angle  $\alpha\pi$  where

$$\tan(\alpha\pi) = \frac{(h_1 - h_2)\sqrt{(-k\epsilon)} - \epsilon l}{k(h_1 - h_2) + l\sqrt{(-k\epsilon)}} = \sqrt{\left(-\frac{\epsilon}{k}\right)}. \quad (3.13)$$

The quadrilaterals  $ABCD$  in the  $\Omega_1$ - and in the  $\Omega_2$ -planes are to be transformed into a half  $\zeta$ -plane in such a way that both quadrilaterals transform into the  $\xi$ -axis of the  $\zeta$ -plane and the points corresponding to the vertices coincide,  $A$  with  $A$ ,  $B$  with  $B$ ,  $C$  with  $C$  and  $D$  with  $D$ . This implies that four conditions must be imposed. In the Schwarz-Chrystoffel transformation, however, there are only three degrees of arbitrariness. The additional condition serves to determine a relation between the various constants in the problem.

In the  $\zeta$ -plane let  $A$  correspond to  $\xi = -1/\kappa$ ,  $B$  to  $\xi = -1$ ,  $C$  to  $\xi = 1$  and  $D$  to  $\xi = 1/\kappa$  where  $\kappa$  is still to be determined and is such that  $0 < \kappa < 1$ . The conformal transformations are

$$\begin{aligned}\Omega_1 &= C_1 + C'_1 \int_0^\xi \left( \frac{1+\kappa\zeta}{1-\kappa\zeta} \right)^\alpha \frac{d\zeta}{\sqrt{(1-\zeta^2)(1-\kappa^2\zeta^2)}}, \\ \Omega_2 &= C_2 + C'_2 \int_0^\xi \left( \frac{1-\kappa\zeta}{1+\kappa\zeta} \right)^\alpha \frac{d\zeta}{\sqrt{(1-\zeta^2)(1-\kappa^2\zeta^2)}},\end{aligned}\quad (3.14)$$

where  $C_1, C'_1, C_2, C'_2$  are constants. If now  $\zeta$ , the upper limit of the integral, is given values corresponding to the points  $A, B, C$  and  $D$ , we obtain the appropriate values of  $\Omega_1$  and  $\Omega_2$  at these points. These should be equal to the values given in (3.10) and (3.12). From the relations so obtained it can be verified that

$$-\frac{C'_2}{C'_1} = \frac{l\sqrt{(-k\epsilon) + k(h_1 - h_2)}}{l\sqrt{(-k\epsilon) - k(h_1 - h_2)}} = \frac{Q_1 + h_1\sqrt{(-k\epsilon)}}{h_2\sqrt{(-k\epsilon)} - Q_1 - \epsilon l} = \frac{Q_1 + \epsilon l + h_2\sqrt{(-k\epsilon)}}{h_1\sqrt{(-k\epsilon)} - Q_1}, \quad (3.15)$$

whence it follows that

$$Q_1 + \frac{1}{2}\epsilon l = \frac{k(h_1^2 - h_2^2)}{2l}. \quad (3.16)$$

This can be written in the form

$$\frac{1}{2}(Q_1 + Q_2) = \frac{k(h_1^2 - h_2^2)}{2l}. \quad (3.17)$$

This formula is very closely related to the approximate Dupuit law which states that, neglecting the effect of evaporation,

$$Q_1 = Q_2 = \frac{k(h_1^2 - h_2^2)}{2l}. \quad (3.18)$$

An exact solution, which neglects the effect of evaporation, shows that there must be a seepage surface, in contradiction of the assumption made above, and yields a result which though not identical with Dupuit's formula, is very close to it.

It should be noted, also, that the relations between the  $\Omega_1$  and  $\Omega_2$  co-ordinates, when transformed into the  $\zeta$ -plane, provide a sufficient number of relations to determine  $\kappa$ ,  $C_1$ ,  $C'_1$ ,  $C_2$ ,  $C'_2$ . When these values have been obtained the final solution is

$$\left. \begin{aligned} z &= \frac{1}{2\sqrt{(-k\epsilon)}} \int_0^\zeta \left[ C'_2 \left( \frac{1-\kappa\zeta}{1+\kappa\zeta} \right)^a - C'_1 \left( \frac{1+\kappa\zeta}{1-\kappa\zeta} \right)^a \right] \frac{d\zeta}{\sqrt{(1-\zeta^2)(1-\kappa^2\zeta^2)}}, \\ W &= \frac{1}{2} \int_0^\zeta \left[ C'_2 \left( \frac{1-\kappa\zeta}{1+\kappa\zeta} \right)^a + C'_1 \left( \frac{1+\kappa\zeta}{1-\kappa\zeta} \right)^a \right] \frac{d\zeta}{\sqrt{(1-\zeta^2)(1-\kappa^2\zeta^2)}}, \end{aligned} \right\} \quad (3.19)$$

except for arbitrary additive constants which have the effect of shifting the origins. The equations in (3.19) can be used to determine the exact equation of the free surface.

This problem has been solved on the assumption that all the sides of the polygons in the  $\Omega_1$ - and  $\Omega_2$ -planes (cf. figure 3) are positive in magnitude. A consideration of the formulae giving these lengths, coupled with equation (3.16) shows that the necessary conditions are

$$\frac{(h_1 + h_2)}{l} > \sqrt{\left(-\frac{\epsilon}{k}\right)}, \quad (3.20)$$

and

$$\sqrt{\left(-\frac{\epsilon}{k}\right)} > \frac{h_1 - h_2}{l}. \quad (3.21)$$

If (3.20) is not satisfied the boundaries in the  $\Omega_1$ - and  $\Omega_2$ -planes become self-intersecting quadrilaterals and the analysis is invalid. This means that the geometrical assumptions with regard to the region of flow in the  $z$ -plane do not hold. In this case the region of flow splits into two disconnected parts. One part will be contiguous with the head-water and the other with the tail-water. The velocity of percolation in the head-water section will be constant and given by the relations

$$u = \sqrt{(-k\epsilon)}, \quad v = 0, \quad (3.22)$$

and that in the tail-water section by the relations

$$u = -\sqrt{(-k\epsilon)}, \quad v = 0. \quad (3.23)$$

The free surfaces of both sections will be straight lines inclined to the horizontal at an angle  $(\alpha\pi)$ . This can be proved very easily as follows. The head-water region of flow will be bounded by three surfaces: (i) a vertical water-basin surface along which  $v = 0$ , (ii) a horizontal impervious surface along which  $v$  is also zero, and (iii) a free surface which, in the  $w$ -plane, is represented by part of a circle. The boundary of the region in the  $w$ -plane is a circular arc and part of a straight line. Davison (1936 *b*) has shown that the

$x$ -velocity in the region must be positive everywhere and this is only possible when the boundary in the  $w$ -plane degenerates into the point of intersection of the arc and the straight line. This leads to the result that the velocity of percolation is constant throughout the region and is given by equation (3.22). Alternatively the result can be obtained from (3.5) by putting  $v = 0$ . The complex potential can now be obtained immediately

$$W = z\sqrt{-k\epsilon},$$

from which  $\phi = x\sqrt{-k\epsilon}$  and  $\psi = y\sqrt{-k\epsilon}$ ,

and the equation of the free surface is, from (1.3),

$$x\sqrt{-k\epsilon} + k(y - h_1) = 0. \quad (3.24)$$

This is a straight line inclined to the  $x$ -axis at an angle  $\tan^{-1}\sqrt{-\epsilon/k} = \alpha\pi$ . Similarly the free surface associated with the tail-water is also a straight line. The free surfaces cut the horizontal axis at points, inside the embankment, distant  $kh_1/\sqrt{-k\epsilon}$  and  $kh_2/\sqrt{-k\epsilon}$  from the vertical faces of the embankment. The sum of these two distances is less than  $l$ , leading to the inequality

$$\frac{h_1 + h_2}{l} < \sqrt{\left(-\frac{\epsilon}{k}\right)}.$$

If (3.21) is not satisfied the following analysis shows that a seepage surface is inevitable. We choose that value of  $1/\sqrt{(1-\zeta^2)(1-\kappa^2\zeta^2)}$  which is positive along  $BC$  ( $-1 \leq \xi \leq 1$ ) and bearing in mind that the region of flow is transformed into the upper half of the  $\zeta$ -plane we find  $1/\sqrt{(1-\zeta^2)(1-\kappa^2\zeta^2)}$  is

- (i) real negative along  $DA$  (that is  $\frac{1}{\kappa} < \xi < \infty$  and  $-\frac{1}{\kappa} > \xi > -\infty$ ),
- (ii) negative imaginary along  $AB$  (that is  $-\frac{1}{\kappa} < \xi < -1$ ),
- (iii) real positive along  $BC$  (that is  $-1 < \xi < 1$ ),
- (iv) positive imaginary along  $CD$  (that is  $1 < \xi < \frac{1}{\kappa}$ ).

Similarly,  $[(1+\kappa\zeta)/(1-\kappa\zeta)]^\alpha$  is defined to be real and positive along  $AB$ ,  $BC$  and  $CD$ . Considering the length of  $BC$  in the  $\Omega_2$ -plane we find

$$k(h_1 - h_2) + l\sqrt{-k\epsilon} = C'_2 \int_{-1}^1 \left( \frac{1-\kappa\zeta}{1+\kappa\zeta} \right)^\alpha \frac{d\zeta}{\sqrt{(1-\zeta^2)(1-\kappa^2\zeta^2)}}, \quad (3.25)$$

so that  $C'_2$  is real and positive. From (3.15) and using

$$\frac{h_1 - h_2}{l} > \sqrt{\left(-\frac{\epsilon}{k}\right)}, \quad (3.26)$$

we deduce that  $C'_1$  is real and positive. Applying this to (3.19) we find the value of  $dz$  along  $CD$  and along the free surface  $DA$ . It emerges that  $dy$  is first positive and then negative along  $CD$  and that along  $DA$  the value of  $dx$  is first positive and then negative while  $dy$  is always positive. The appropriate mathematical configuration is shown in figure 4 and this is physically impossible. The significance of this is that a seepage-surface must exist. If the inequality (3.21) is used instead of (3.26) we find that  $C'_1$  is real and negative,  $dy$  is positive along  $CD$  and  $dx$  is negative along  $DA$ , so that the configuration is as shown in figure 2.

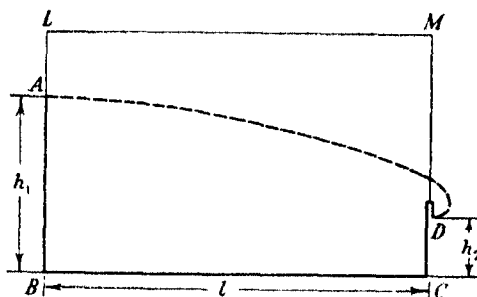


FIGURE 4.  $z$ -plane.

#### 4. PERCOLATION FROM A DYKE OF RECTANGULAR SECTION

As a second example we consider the penetration into soil of the water flowing from a dyke of rectangular section. The faces  $AF$ ,  $ED$ , of the dyke are vertical. The base  $EF$ , which is horizontal, is at a constant height  $h$  above a horizontal impervious layer. The height of the water in the dyke is  $H$ , the width is  $l$ , and the width of the irrigated strip is  $l_1$  at the impervious surface (cf. figure 5). Evaporation over the free surface is taken into account.

Along the impervious layer  $BC$  the velocity is horizontal. Along the faces  $DE$ ,  $FA$  the value of  $\phi$  is constant. We choose this constant to be zero. The velocity on  $DE$  and  $FA$  is horizontal and that on  $EF$  is vertical. The faces  $DE$  and  $FA$  and the layer  $BC$  are represented in the  $w$ -plane by parts of the line  $I(w) = 0$  while the free surface is represented, as in the previous problem, by a section of the circle

$$I\left(\frac{w - i\epsilon}{iw + k}\right) = 0.$$

The circle and straight line intersect in the points  $w = \pm \sqrt{(-k\epsilon)}$ . The bottom of the dyke, however, is represented by  $R(w) = 0$ , and this line does not pass

through the points  $w = \pm\sqrt{(-k\epsilon)}$ . This difficulty can be overcome by the following artifice. We add to the region of motion its mirror representation constructed with regard to the straight line  $EF$ . The enlarged region of motion in the  $z$ -plane is shown in figure 6. The points  $E$  and  $F$  are branch points of the Riemann surface upon which the region is situated.  $\psi$  has equal values, and  $\phi$  has equal and opposite values, at points symmetrical with respect to the line  $EF$ . In addition, the original region (see figure 5) is symmetrical with regard to the vertical line passing through the centre

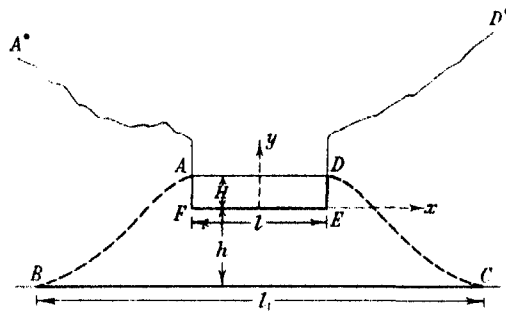


FIGURE 5.  $z$ -plane.

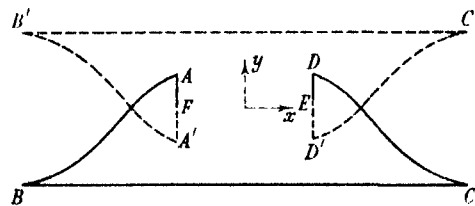


FIGURE 6. Enlarged  $z$ -plane.

of the dyke. The enlarged region, therefore (see figure 6), has two axes of symmetry, one of which is horizontal and the other vertical. The  $w$ -plane for the enlarged region is shown in figure 7. In going once round the boundary shown in figure 6 one goes twice round the boundary in figure 7. It is clear also that the values  $w = \pm\sqrt{(-k\epsilon)}$  satisfy the equations of all parts of this boundary. We can therefore invent  $\Omega_1$ - and  $\Omega_2$ -planes in accordance with the definitions of equation (3.9). The corresponding boundaries in these planes are as shown in figure 8. This can be verified very easily if consideration is paid to the fact that along  $BC$  and  $C'B'$  the value of  $w$  satisfies the inequalities

$$\sqrt{(-k\epsilon)} \geq w \geq -\sqrt{(-k\epsilon)}$$



and that as a consequence

$$\frac{d\Omega_1}{dz} = w - \sqrt{(-k\epsilon)}$$

is negative along  $BC$  and  $C'B'$ , and that along the corresponding lines in the  $\Omega_2$ -plane

$$\frac{d\Omega_2}{dz} = w + \sqrt{(-k\epsilon)}$$

is positive. The lines  $AB$ ,  $A'B'$ ,  $CD$ ,  $C'D'$  are, as in the previous problem, inclined at an angle  $\alpha\pi = \tan^{-1}\sqrt{(-\epsilon/k)}$  to the  $\lambda$ -axes.

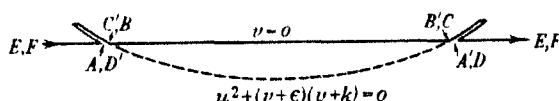


FIGURE 7.  $w$ -plane.

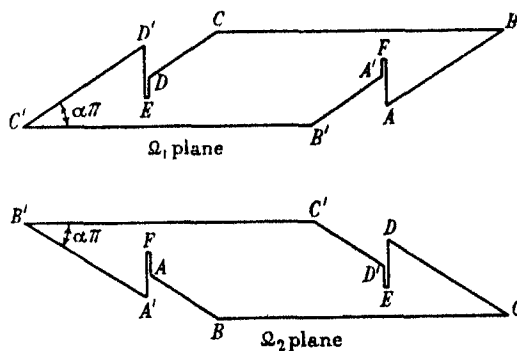


FIGURE 8

In deducing the conformal transformation it is here convenient to map the region of flow in the enlarged  $z$ -plane on the area enclosed by a circle in the auxiliary  $\zeta = \xi + i\eta$  plane. We chose this region in the  $\zeta$ -plane to be  $|\zeta| \leq 1$ . The two perpendicular axes of symmetry of figure 6 are transformed into perpendicular diameters of this circle. The points  $F$  and  $E$ , which lie at the extremities of one of these diameters, are chosen to be  $\zeta = \pm 1$  respectively. Making use of the symmetry of the system we introduce the following notation, where  $\frac{1}{2}\pi > \gamma > \beta > 0$ . We write

$$\left. \begin{aligned} \zeta_A &= e^{i\beta}, & \zeta_B &= e^{i\gamma}, & \zeta_C &= e^{i(\pi-\gamma)}, & \zeta_D &= e^{i(\pi-\beta)}, \\ \zeta_E &= e^{i\pi}, & \zeta_{D'} &= e^{i(\pi+\beta)}, & \zeta_{C'} &= e^{i(\pi+\gamma)}, & \zeta_{B'} &= e^{i(2\pi-\gamma)}, \\ \zeta_{A'} &= e^{i(2\pi-\beta)}, & \zeta_{F'} &= e^{i2\pi}. \end{aligned} \right\} \quad (4.1)$$

By making use of a proper choice of origin, in order to get rid of an additive constant in the answer, we find that the Schwarz-Chrystoffel integral leads to the equations:

$$\left. \begin{aligned} \Omega_1 &= W - z\sqrt{-k\epsilon} \\ &= D'_1 \int_1^\zeta \frac{\zeta^2 - 1}{\zeta^2 - e^{2i\gamma}} \left( \frac{\zeta^2 - e^{-2i\beta}}{\zeta^2 - e^{2i\beta}} \frac{\zeta^2 - e^{-2i\gamma}}{\zeta^2 - e^{2i\gamma}} \right)^\alpha \frac{d\zeta}{\sqrt{(\zeta^2 - e^{-2i\beta})(\zeta^2 - e^{2i\beta})}}, \\ \Omega_2 &= W + z\sqrt{-k\epsilon} \\ &= D'_2 \int_1^\zeta \frac{\zeta^2 - 1}{\zeta^2 - e^{-2i\gamma}} \left( \frac{\zeta^2 - e^{-2i\beta}}{\zeta^2 - e^{2i\beta}} \frac{\zeta^2 - e^{-2i\gamma}}{\zeta^2 - e^{2i\gamma}} \right)^\alpha \frac{d\zeta}{\sqrt{(\zeta^2 - e^{-2i\beta})(\zeta^2 - e^{2i\beta})}}. \end{aligned} \right\} \quad (4.2)$$

These expressions can be simplified by introducing the relations

$$\left. \begin{aligned} \zeta &= +\sqrt{\{(1-is)/(1+is)\}}, \\ \tan \beta &= a, \quad \tan \gamma = b. \end{aligned} \right\} \quad (4.3)$$

We then get

$$\left. \begin{aligned} \Omega_1 &= D_1 \int_0^s \frac{s}{s+b} \left( \frac{s-as+b}{s+as-b} \right)^\alpha \frac{ds}{\sqrt{(s^2+1)(s^2-a^2)}}, \\ \Omega_2 &= D_2 \int_0^s \frac{s}{s-b} \left( \frac{s+as-b}{s-as+b} \right)^\alpha \frac{ds}{\sqrt{(s^2+1)(s^2-a^2)}}. \end{aligned} \right\} \quad (4.4)$$

The transformation (4.3) maps the surface which is contained within the circle  $|\zeta| = 1$  on to the lower half planes  $I(s) \leq 0$  of the two sheets of the Riemann surface passing through  $s = \pm i$ . As we are dealing with many-valued functions we define the values of

$$\left( \frac{s-a}{s+a} \right)^\alpha, \quad \left( \frac{s+b}{s-b} \right)^\alpha, \quad \frac{1}{\sqrt{(s^2+1)}} \quad \text{and} \quad \frac{1}{\sqrt{(s^2-a^2)}}$$

to be positive along  $BC$ . With these definitions it can be shown that

$$D_1 + D_2 = 0, \quad (4.5)$$

and hence that

$$\left. \begin{aligned} W &= D_3 \sqrt{-k\epsilon} \int_0^s \left\{ \frac{s}{s+b} \left( \frac{s-as+b}{s+as-b} \right)^\alpha - \frac{s}{s-b} \left( \frac{s+as-b}{s-as+b} \right)^\alpha \right\} \frac{ds}{\sqrt{(s^2+1)(s^2-a^2)}}, \\ z &= -D_3 \int_0^s \left\{ \frac{s}{s+b} \left( \frac{s-as+b}{s+as-b} \right)^\alpha + \frac{s}{s-b} \left( \frac{s+as-b}{s-as+b} \right)^\alpha \right\} \frac{ds}{\sqrt{(s^2+1)(s^2-a^2)}}, \end{aligned} \right\} \quad (4.6)$$

where  $D_3$  is a constant.

The analysis now contains three unknown quantities  $\beta$ ,  $\gamma$ ,  $D_3$ . These can be determined from the known values of  $h$ ,  $H$  and  $l$ . The connecting equations

can be deduced from (4.6) and by using the transformation  $s = -it$ . The required relations are:

$$h = 2D_3 \int_1^\infty \left\{ t^2 \cos 2 \left[ \alpha \left( \tan^{-1} \frac{t}{a} - \tan^{-1} \frac{t}{b} \right) \right] - tb \sin 2 \left[ \alpha \left( \tan^{-1} \frac{t}{a} - \tan^{-1} \frac{t}{b} \right) \right] \right\} \\ \times \frac{dt}{(b^2 + t^2) \sqrt{(a^2 + t^2)} (t^2 - 1)}, \quad (4.7)$$

$$H = D_3 \int_{-a}^a \frac{s}{b-s} \left( \frac{a+s b-s}{a-s b+s} \right)^\alpha \frac{ds}{\sqrt{(a^2 - s^2)} (s^2 + 1)}, \quad (4.8)$$

$$l = 4D_3 \int_0^1 \left\{ t^2 \cos 2 \left[ \alpha \left( \tan^{-1} \frac{t}{a} - \tan^{-1} \frac{t}{b} \right) \right] - tb \sin 2 \left[ \alpha \left( \tan^{-1} \frac{t}{a} - \tan^{-1} \frac{t}{b} \right) \right] \right\} \\ \times \frac{dt}{(b^2 + t^2) \sqrt{(a^2 + t^2)} (1 - t^2)}. \quad (4.9)$$

After having obtained the values of  $\beta$ ,  $\gamma$  and  $D_3$  the equation

$$l_1 - l = 2D_3 \cos \alpha \pi \left\{ \int_a^b \left[ \frac{s}{b-s} \left( \frac{s+ab-s}{s-ab+s} \right)^\alpha - \frac{s}{b+s} \left( \frac{s-ab+s}{s+ab-s} \right)^\alpha \right] \right\} \frac{ds}{\sqrt{(s^2 + 1)} (s^2 - a^2)} \quad (4.10)$$

gives the value of  $l_1$ , the width at the impervious surface of the irrigated strip. When  $l_1$  is known the equation

$$Q = -\epsilon(l_1 - l) \quad (4.11)$$

gives the volume of fluid entering the soil in unit time.

## 5. THE MOTION OF WATER OUTSIDE A NUMBER OF PARALLEL DRAINING TUBES

For the third example consider a set of parallel draining tubes (or tunnels), in uniform permeable soil, stretching to infinity. The tubes will be considered as line sinks of uniform strength and of negligible cross-section. A sketch of the region of flow in a plane perpendicular to the axes of the tubes is shown in figure 9. The boundary consists only of the free surface  $C_1 C_2$ . The permeable soil is supposed to extend downwards to infinity. The tubes cut the representative plane in the points  $K_1, K_2, K_3$ , etc. For the purposes of this problem we assume that the number of tubes is finite. The method can, however, be extended to the case where the number of tubes is infinite. We assume that the tube  $K_1$  absorbs a volume  $m_1$  of water in unit time, that the tube  $K_2$  absorbs  $m_2$ , and so on. Evaporation or penetration is allowed for.

It will be seen that the problem is not mathematically determinate. When one additional piece of information is given, as for example when the co-ordinates of some point on the free surface are known, the problem can be solved. The solutions given below, therefore, involve one arbitrary parameter.

Along the free surface  $C_1C_2$  the equation (3.4) must be satisfied. The boundary in the  $w$ -plane is, therefore, an arc of a circle. In going over the free surface in the  $z$ -plane parts of this arc can be passed over several times.

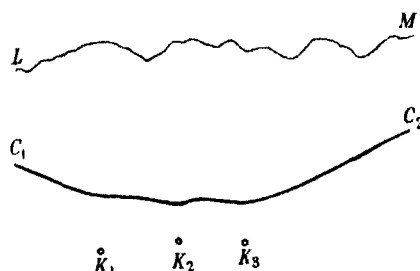


FIGURE 9.  $LM$  is the upper surface of the soil;  $C_1C_2$  is the free surface or water-table;  $K_1, K_2, K_3$  are points representing the draining tubes.

Since the boundary in the  $w$ -region consists of only parts of the same circular arc any two points on the arc may be taken as  $w_0$  and  $w_{00}$ . Two obvious points to choose are

$$w_0 = ik \quad \text{and} \quad w_{00} = i\epsilon. \quad (5.1)$$

We must construct  $\Omega_1$  and  $\Omega_2$ -planes, given by equation (2.14), which possess logarithmic singularities at those points which represent the tubes.

We transform the  $\Omega_1$ - and  $\Omega_2$ -planes into the lower half of a  $\zeta$ -plane (that is,  $I(\zeta) \leq 0$ ) so that  $z = \infty$  corresponds to  $\zeta = \infty$ . In the neighbourhood of the tube  $K_j$ , which is of strength  $m_j$ , the expansion in the  $W$ -plane must be of the form

$$W = -\frac{m_j}{2\pi} \log(\zeta - \zeta_j) + \text{terms regular in the region of } \zeta_j.$$

Similar expansions must be valid in the  $\Omega_1$ - and  $\Omega_2$ -planes in the vicinity of the corresponding points. In the  $\Omega_1$ -plane the free surface is represented by a vertical line while in the  $\Omega_2$ -plane it is represented by a horizontal line. Along the appropriate line in the  $\Omega_1$ -plane the real part of  $\Omega_1$  must be constant while along the corresponding  $\Omega_2$  line we must have that  $I(\Omega_2)$  is constant. This can be arranged by the introduction of appropriate images.

The most general solution can easily be proved to be

$$\left. \begin{aligned} \Omega_1 &= \sum_{j=1}^n -\frac{m_j}{2\pi} \log \left( \frac{\zeta - \zeta_j}{\zeta - \bar{\zeta}_j} \right) - ib\zeta, \\ \Omega_2 &= \sum_{j=1}^n -\frac{m_j}{2\pi} \log (\zeta - \zeta_j) (\zeta - \bar{\zeta}_j) + a\zeta, \end{aligned} \right\} \quad (5.2)$$

where we have neglected arbitrary additive constants, where  $a$  and  $b$  are perfectly real and where  $n$  is the number of draining tubes.

Applying equations (2.15), (2.16) and (2.17) we get

$$\left. \begin{aligned} z &= \frac{i}{\pi(k-\epsilon)} \sum_{j=1}^n m_j \log (\zeta - \bar{\zeta}_j) + \frac{b-ia}{k-\epsilon} \zeta + C_1, \\ W &= \frac{1}{2\pi} \sum_{j=1}^n m_j \left\{ \log \frac{1}{(\zeta - \zeta_j)} + \frac{k+\epsilon}{k-\epsilon} \log \frac{1}{(\zeta - \bar{\zeta}_j)} \right\} + \frac{ka+ib\epsilon}{k-\epsilon} \zeta + C_2, \end{aligned} \right\} \quad (5.3)$$

where  $C_1$  and  $C_2$  are complex constants.

We must now compare the number of unknown quantities with the number of data. The unknowns are  $a, b, R(\zeta_1), I(\zeta_1), R(\zeta_2), I(\zeta_2), \dots, R(\zeta_n), I(\zeta_n)$ , making  $(2n+2)$  in all. The number of unknowns must, however, be reduced by two for the  $\xi$  and  $\eta$  co-ordinates of the tube  $K_1$ , say, are at our disposal. The given quantities involve the velocity at infinity and  $R(z_2-z_1), I(z_2-z_1), R(z_3-z_1), I(z_3-z_1), \dots$ , etc. The geometrical data are  $(2n-2)$  in number. A knowledge of the two components of velocity at infinity adds only one piece of information, for the two components must satisfy the relation which is valid on the free surface—for the free surface is assumed to extend to infinity. We therefore have  $2n$  unknown quantities and  $(2n-1)$  data. The problem can only be solved if one additional piece of information is given. In practical application this is most likely to be the  $x$  and  $y$  co-ordinates of a point which is known to lie on the free surface.

The parameter  $b$  is not entirely at our disposal. This is due to the fact that the curve representing the free surface must be limited to the type which is not self-intersecting. If this limitation is not imposed the definition of "free surface" is meaningless in the neighbourhood of points of self-intersection. In order to avoid this the condition is that  $R(dz/d\zeta)$  must not change sign on the free surface for otherwise regions would appear in which  $dx$  would change its sign. With our choice of signs and directions this condition simply is  $R(dz/d\zeta)$  must always be positive or zero on the free surface. The mathematical form of this condition can be deduced from the first of the equations (5.3) if it is remembered that  $(k-\epsilon)$  is positive. The condition is

$$\pi b + \Sigma R \left\{ \frac{im_j}{\zeta - \bar{\zeta}_j} \right\} \geq 0. \quad (5.4)$$

To conclude this section let us consider the case of one drainage tunnel which absorbs a volume  $m$  per unit length in unit time. There is no evaporation or penetration of water and the percolation velocity at infinity is zero. Then  $\epsilon = 0$ ,  $n = 1$  and

$$\lim_{\zeta \rightarrow \infty} \left( \frac{dW}{d\zeta} \frac{dz}{d\zeta} \right) = \frac{ka + ibc}{b - ia} = 0, \quad (5.5)$$

whence  $a = 0$ . Let  $\zeta_j = \zeta_1 = -i$ . The solution (5.3) becomes

$$\left. \begin{aligned} z &= \frac{im}{\pi k} \log(\zeta - i) + \frac{b}{k} \zeta + \frac{ib}{k} - \frac{im}{\pi k} \log(-2i), \\ W &= -\frac{m}{2\pi} \log(\zeta^2 + 1). \end{aligned} \right\} \quad (5.6)$$

The constant  $C_1$  is chosen so as to make the origin of the  $z$ -plane coincide with the tunnel. The constant  $C_2$  is taken to be zero. The inequality (5.4) becomes

$$\pi b + R \left( \frac{im}{\zeta - i} \right) \geq 0 \text{ for all values of } \zeta \text{ for which } I(\zeta) = 0.$$

This condition is 
$$b \geq \frac{m}{\pi}. \quad (5.7)$$

Separating the first equation of (5.6) into real and imaginary parts, treating  $\zeta$  as real, and then eliminating  $\zeta$ , we get

$$\pi kx = \pi b \left( 4 \exp \left\{ \frac{2\pi k}{m} \left( y - \frac{b}{k} \right) \right\} - 1 \right)^{\frac{1}{2}} - m \tan^{-1} \left( 4 \exp \left\{ \frac{2\pi k}{m} \left( y - \frac{b}{k} \right) \right\} - 1 \right)^{\frac{1}{2}}. \quad (5.8)$$

$b$  is the undetermined parameter. The height of the free surface above the drainage tube increases as  $b$  is made bigger and  $m$  is left unaltered.

#### REFERENCES

- Davison, B. 1932 *Mém. Inst. Hydrol.* **6**, 11.  
 — 1936 a *Phil. Mag.* (7), **21**, 881.  
 — 1936 b *Phil. Mag.* (7), **21**, 904.  
 Hamel, G. 1934 *Z. angew. Math. Mech.* **14**, 129.  
 Hamel, G. and Günther, E. 1935 *Z. angew. Math. Mech.* **15**, 255.

# Hyperfine structure in the arc spectrum of bromine

By S. TOLANSKY AND S. A. TRIVEDI

*The University of Manchester*

*(Communicated by W. E. Curtis, F.R.S.—Received 21 November 1939)*

## INTRODUCTION

In an earlier work Tolansky (1932) reported measurements for the hyperfine structures of 18 lines of the arc spectrum of bromine. Although resolution was incomplete in every line, it was possible to prove that both the bromine isotopes 79 and 81 have the same nuclear spin,  $\frac{3}{2}$ , and have practically identical nuclear magnetic moments. In carrying out the hyperfine structure term analysis at that time, use was made of the interesting graphical method proposed by Fisher and Goudsmit (1931) and thus approximate hyperfine structure interval factors could be derived. At the time this work was done the existence of deviations from the interval rule was not suspected. Any such deviations destroy the validity of the Fisher-Goudsmit method of analysis. The frequent occurrence of nuclear electrical quadrupole moment leads one to suspect that there may be deviations from the interval rule in many spectra; hence we have undertaken a new and more complete examination of the hyperfine structures of the lines of Br I.

The measurements reported here are more extensive and more accurate than those previously given. We have measured the structures of 76 lines extending from the infra-red at 8700 Å down to 4390 Å. All the principal lines in this region have been measured and, with very few exceptions, the structures have been completely accounted for. The results obtained here are much more accurate than those given earlier for the following reasons:

- (1) The modified source is much more intense.
- (2) It is cooled, giving sharper lines.
- (3) In place of the single Fabry-Perot previously available (with one thickness of silvering) we have used various silvered Fabry-Perot interferometers, similar interferometers coated with aluminium, and a high-quality quartz Lummer plate.
- (4) The camera focal length used now is 125 cm., that of the earlier instrument being only 50 cm.
- (5) Much more rapid plates are now available, particularly in the infra-red region.

As a result of these improvements the structures in many lines have been completely resolved, and we have not only been able to determine the interval factors for 38 terms, but have also demonstrated the existence of deviation from the interval rule in at least one of them. This is almost certainly due to the existence of nuclear electrical quadrupole moment, the value of the latter being approximately the same for both isotopes.

### EXPERIMENTAL

As shown in the earlier paper by Tolansky, the Br I spectrum can be excited in bromine vapour by means of an electrodeless high-frequency discharge. High-frequency oscillations were generated by a 250 W thermionic valve designed to operate upon short wave-lengths. Care was taken in the lay-out of the circuit in order to avoid losses. The high-frequency field was applied by means of external electrodes of copper foil to a glass tube. With the type of tube used maximum intensity of emission was found when the wave-length was of the order of 15 m. With so active a material as bromine the absence of internal electrodes is an advantage. The discharge tube was part of a vacuum circulating system which had charcoal and liquid-air traps in the circuit. A continuous stream of pure bromine was circulated through the discharge tube during the exposures. This was supplied from a side limb, which contained an ample supply of the material, cooled with a mixture of solid carbon dioxide and alcohol until the vapour pressure was of the order of 1 mm. The pressure was critical and, if not correct, Br<sub>2</sub> bands appeared in the emission spectrum. The circulation of the gas was essential, for without it hydrogen lines and impurity bands rapidly appeared, due no doubt to the chemical action of the bromine upon the grease on the taps.

The portion of the discharge tube emitting the spectrum was effectively cooled by directing on to it a strong blast of air. Air cooling avoids the difficulties associated with the introduction of earthed water around a fairly unstable high-frequency discharge. The source was very brilliant, the stronger lines being photographed through the interferometers in a few seconds. With the long exposures required for the weaker lines (there are very wide ranges in intensity, and some of the weak lines have weak components) a reduction in accuracy was brought about by the faint Br<sub>2</sub> bands which came up with exposures exceeding 2 hr. The bands make a practically continuous background (only with the long exposures) and so reduce effective resolving power for the lines which are quite weak.



The high resolving power instruments used were variable gap Fabry-Perot interferometers coated by evaporation *in vacuo* either with silver or aluminium, and a 20 cm. long quartz Lummer plate by Hilger. The interferometer was in each case introduced into the parallel beam of a constant deviation glass spectrograph. This was built in this Laboratory, and as the camera focal length is 125 cm. a large dispersion results, particularly with the Lummer plate. The high resolving power attained and the narrowness of the fringes are illustrated in figure 1.

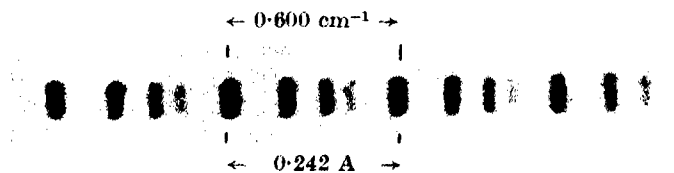


FIGURE 1. Hyperfine structure of  $\lambda$  6350. Fabry-Perot interferometer gap 8.3 mm.

#### OBSERVATIONS

The observed hyperfine structures are given in table 1. The wavelengths and allocations of the lines are taken from the exhaustive paper of Kiess and de Bruin (1930) on the analysis of the multiplets in the Br I spectrum. The structures are given in units of  $\text{cm.}^{-1} \times 10^{-3}$ , and beneath each component is the visually estimated intensity. Blends are indicated by the binding of components with a hyphen, and where the optical centre of gravity of an obvious complex has been estimated, an approximation sign is placed above this measurement. The numeral I in the last column indicates good resolution of individual components and a high order of accuracy in measurement (errors mostly of the order of  $1 \text{ cm.}^{-1} \times 10^{-3}$ ). The numeral II implies that the pattern is so intrinsically complex that resolution is unavoidably poor.

The measurements for a number of unclassified lines, and lines of the Br II spectrum are given in another table later.

#### ANALYSIS OF THE STRUCTURES

The nature of the transitions studied here is very comprehensive. Many terms are involved so frequently (for example, the deepest term occurs in ten of the transitions) that ample opportunity is afforded for checking the proposed interpretations. In very few cases only no check is available.

TABLE 1. HYPERFINE STRUCTURES IN THE LINES OF Br I.  
UNITS CM.<sup>-1</sup> × 10<sup>-3</sup>

| Wave-length | Allocation   | Structure |     |      |        | Class |
|-------------|--|-----------|-----|------|--------|-------|
|             |  | Red       |     |      | Violet |       |
| 8638.6      | 5s <sup>4</sup> P <sub>1</sub> -5p <sup>4</sup> P <sub>1</sub>                                     | 0         | 72  | 137  | 203    | II    |
|             |  | 6         | 4   | 3    | 5      |       |
| 8477.5      | 5s <sup>4</sup> P <sub>1</sub> -5p <sup>4</sup> S <sub>1</sub>                                     | Single    |     |      |        | I     |
| 8446.5      | 5s <sup>4</sup> P <sub>1</sub> -5p <sup>4</sup> D <sub>1</sub>                                     | 116       | 51  | 0    | 67     | I     |
|             |  | 3         | 2   | 5    | 1      |       |
| 8343.7      | 5s <sup>4</sup> P <sub>1</sub> -5p <sup>2</sup> P <sub>1</sub>                                     | 47        | 0   |      |        | I     |
|             |  | 3         | 5   |      |        |       |
| 8334.7      | 5s <sup>2</sup> P <sub>1</sub> -5p <sup>2</sup> P <sub>1</sub>                                     | 0         | 99  | 162  | 194    | I     |
|             |  | 9         | 7   | 5    | 3      |       |
| 8272.4      | 5s <sup>4</sup> P <sub>1</sub> -5p <sup>4</sup> D <sub>1</sub>                                     | 120       | 0   | 75   | 127    | I     |
|             |  | 1         | 10  | 8    | 6      | 5     |
| 8131.5      | 5s <sup>4</sup> P <sub>1</sub> -5p <sup>2</sup> P <sub>1</sub>                                     | Single    |     |      |        | I     |
| 7989.9      | 5s <sup>2</sup> P <sub>1</sub> -5p <sup>2</sup> D <sub>1</sub>                                     | 0         | 90  | 145  | ~164   | II    |
|             |  | 9         | 7   | 5    | 3      |       |
| 7938.6      | ( <sup>1</sup> D) 5s <sup>2</sup> D <sub>1</sub> -5p <sup>2</sup> P <sub>1</sub> ( <sup>1</sup> S) | 0         | 121 | 225  | 295    | I     |
|             |  | 6         | 4   | 2    | 2      |       |
| 7803.0      | 5s <sup>4</sup> P <sub>1</sub> -5p <sup>2</sup> D <sub>1</sub>                                     | Single    |     |      |        | I     |
| 7513.0      | 5s <sup>4</sup> P <sub>1</sub> -5p <sup>4</sup> D <sub>1</sub>                                     | 0         | 84  | 144  | 200    | I     |
|             |  | 8         | 6   | 3    | 4      | 3     |
| 7348.5      | 5s <sup>4</sup> P <sub>1</sub> -5p <sup>2</sup> D <sub>1</sub>                                     | 0         | 57  | 86   | ~99    | II    |
|             |  | 9         | 7   | 5    | 3      |       |
| 7005.2      | 5s <sup>4</sup> P <sub>1</sub> -5p <sup>2</sup> P <sub>1</sub>                                     | 0         | 65  | ~92  | ~107   | II    |
|             |  | 9         | 7   | 5    | 3      |       |
| 6631.6      | 5s <sup>4</sup> P <sub>1</sub> -5p <sup>2</sup> D <sub>1</sub>                                     | 0         | 190 | 319  | 402    | II    |
|             |  | 9         | 7   | 5    | 3      |       |
| 6582.2      | 5p <sup>4</sup> P <sub>1</sub> -4d <sup>4</sup> D <sub>1</sub>                                     | 0         | 61  | 81   | ~95    | II    |
|             |  | 9         | 7   | 5    | 3      |       |
| 6559.8      | 5s <sup>4</sup> P <sub>1</sub> -5p <sup>4</sup> S <sub>1</sub>                                     | 0         | 196 | 322  | 407    | I     |
|             |  | 9         | 7   | 5    | 3      |       |
| 6544.6      | 5p <sup>4</sup> P <sub>1</sub> -4d <sup>4</sup> D <sub>1</sub>                                     | 0         | ~44 | ~75  | ~102   | II    |
|             |  | 10        | 6   | 4    | 3      |       |
| 6410.3      | 5p <sup>4</sup> P <sub>1</sub> -4d <sup>4</sup> F <sub>1</sub>                                     | ~0        | ~59 |      |        | II    |
|             |  | 9         | 7   |      |        |       |
| 6350.7      | 5s <sup>4</sup> P <sub>1</sub> -5p <sup>2</sup> P <sub>1</sub>                                     | 0         | 203 | 342  | 427    | I     |
|             |  | 9         | 7   | 5    | 3      |       |
| 6244.3      | 5p <sup>4</sup> D <sub>1</sub> -5d <sup>4</sup> P <sub>1</sub>                                     | 166       | 0   | 154  |        | I     |
|             |  | 4         | 5   | 4    |        |       |
| 6203.0      | 5p <sup>4</sup> P <sub>1</sub> -4d <sup>4</sup> P <sub>1</sub>                                     | ~0        | ~97 | ~190 |        |       |
|             |  | 1         | 10  | 2    |        |       |
| 6177.4      | 5p <sup>4</sup> D <sub>1</sub> -5d <sup>4</sup> F <sub>1</sub>                                     | 0         | 37  | 87   |        | II    |
|             |  | 1         | 2   | 8    |        |       |
| 6148.6      | 5s <sup>4</sup> P <sub>1</sub> -5p <sup>2</sup> D <sub>1</sub>                                     | 0         | 191 | 319  | 399    | I     |
|             |  | 9         | 7   | 5    | 3      |       |

TABLE 1 (continued)

| Wave-length | Allocation                    | Structure        |              |              |               | Class |
|-------------|-------------------------------|------------------|--------------|--------------|---------------|-------|
|             |                               | Red              |              |              | Violet        |       |
| 6122.1      | 5p $^4D_1-5d \ ^4F_1$         | Single           |              |              |               | I     |
| 5940.5      | 5s $^3P_1-6p \ ^4P_1$         | 0                | 86           | 173          | 260           | I     |
|             |                               | 5                | 1            | 5            | 5             |       |
| 5852.1      | 5p $^4P_1-5d \ ^4D_1$         | Single, width 31 |              |              |               | I     |
| 5833.4      | 5p $^4P_1-5d \ ^4D_1$         | Single           |              |              |               | I     |
| 5536.4      | 5p $^4P_1-5d \ ^4P_1$         | Single, width 26 |              |              |               | I     |
| 5529.0      | 5p $^4P_1-5d \ ^4P_1$         | Single           |              |              |               | I     |
| 5466.2      | 5s $^3P_1-6p \ ^3P_1$         | 0                | 79           | 94           | 185           | I     |
|             |                               | 4                | 7            | 7            | 4             | 20    |
| 5395.5      | 5s $^3P_1-6p \ ^3P_1$         | 0                | 83           | 248          | 332           | I     |
|             |                               | 5                | 1            | 5            | 5             |       |
| 5370.3      | 5s $^3P_1-6p \ ^4P_1$         | 75               | 0            | 91           |               | II    |
|             |                               | 3                | 12           | 2            |               |       |
| 5364.2      | 5s $^3P_1-6p \ ^4D_1$         | 108              | $\tilde{31}$ | 0            |               | II    |
|             |                               | 1                | 3            | 6            |               |       |
| 5345.4      | 5s $^4P_1-6p \ ^4P_1$         | 278              | 232          | 144          | 0             | I     |
|             |                               | 1                | 3            | 5            | 7             |       |
| 5245.1      | 5s $^4P_1-6p \ ^4D_1$         | 250              | 207          | 123          | 0             | I     |
|             |                               | 1                | 3            | 5            | 7             |       |
| 5002.7      | 5s $^3P_1-6p \ ^4S_1$         | 0                | 98           |              |               | I     |
|             |                               | 5                | 3            |              |               |       |
| 4979.7      | 5s $^3P_1-6p \ ^3P_1$         | 0                | 100          | 176          | 270           | I     |
|             |                               | 4                | 3            | 9            | 2             |       |
| 4954.7      | 5s $^3P_1-6p \ ^3S_1$         | 0                | 25           | $\tilde{66}$ | 121           | II    |
|             |                               | 5                | 5            | 1            | 6             |       |
| 4921.0      | 5s $^3P_1-6p \ ^3P_1$         | 153              | 91           | 0            | 95            | I     |
|             |                               | 9                | 8            | 20           | 6             |       |
| 4834.4      | 5s $^4P_1-6p \ ^4P_1$         | 155              | 87           | 0            | 61            | I     |
|             |                               | 3                | 2            | 7            | 1             |       |
| 4807.6      | 5s $^3P_1-5p \ ^3P_1 \ (^1S)$ | 0                | 95           | 187          |               | I     |
|             |                               | 4                | 5            | 4            |               |       |
| 4785.2      | 5s $^4P_1-6p \ ^4P_1$         | 101              | — 0 —        | $\tilde{58}$ |               | II    |
|             |                               | 2                | 4            | 1            |               |       |
| 4780.3      | 5s $^4P_1-6p \ ^4D_1$         | 140              | — 100 —      | 60           | 0             | II    |
|             |                               | 3                | 2            | 4            | 5             |       |
| 4775.2      | 5s $^3P_1-5p \ ^3P_1 \ (^1S)$ | 80               | 0            | 85           |               | I     |
|             |                               | 4                | 6            | 4            |               |       |
| 4765.6      | *5s $^3P_1-7p \ ^3P_1$        | $\tilde{85}$     | 0            |              |               | II    |
|             |                               | 3                | 5            |              |               |       |
| 4752.2      | 5s $^4P_1-6p \ ^4D_1$         | 0                | 44           | 81           | 133           | II    |
|             |                               | 2                | 1            | 2            | 4             | 1     |
| 4643.5      | 5s $^4P_1-6p \ ^4D_1$         | 0                | 102          | 175          | $\tilde{199}$ | II    |
|             |                               | 9                | 7            | 5            | 3             |       |
| 4614.6      | 5s $^3P_1-6p \ ^3D_1$         | 0                | 104          | 153          | $\tilde{171}$ | II    |
|             |                               | 7                | 5            | 3            | 1             |       |

TABLE 1 (continued)

| Wave-length | Allocation   | Structure        |              |                               |                               | Class |
|-------------|--|------------------|--------------|-------------------------------|-------------------------------|-------|
|             |  | Red              |              |                               | Violet                        |       |
| 4592.2      | 5s <sup>3</sup> P <sub>1</sub> -6p <sup>4</sup> S <sub>1</sub>                   | 0                | 100          | —                             | $\tilde{65}$                  | II    |
|             |  | 7                | 5            |                               | 4                             |       |
| 4575.7      | 5s <sup>3</sup> P <sub>1</sub> -6p <sup>2</sup> D <sub>1</sub>                   | 0                | 83           |                               | $\tilde{162}$ — $\tilde{178}$ | II    |
|             |  | 7                | 5            |                               | 2 2                           |       |
| 4529.9      | 6s <sup>4</sup> P <sub>1</sub> -6p <sup>4</sup> S <sub>1</sub>                   | Single           |              |                               |                               | I     |
| 4525.6      | 5s <sup>4</sup> P <sub>1</sub> -6p <sup>4</sup> P <sub>1</sub>                   | 0                | 93           | 145                           | 187                           | I     |
|             |  | 5                | 3            | 1                             | 2                             |       |
| 4513.4      | 5s <sup>4</sup> P <sub>1</sub> -6p <sup>4</sup> P <sub>1</sub>                   | 0                | 42           | 84                            | 130                           | II    |
|             |  | 4                | 4            | 2                             | 1 3                           |       |
| 4490.4      | 5s <sup>4</sup> P <sub>1</sub> -6p <sup>2</sup> S <sub>1</sub>                   | Single, width 25 |              |                               |                               | I     |
| 4477.7      | 5s <sup>4</sup> P <sub>1</sub> -6p <sup>4</sup> D <sub>1</sub>                   | 0                | 83           | 130                           | — $\tilde{147}$               | I     |
|             |  | 9                | 7            | 5                             | 3                             |       |
| 4441.7      | 5s <sup>4</sup> P <sub>1</sub> -6p <sup>4</sup> D <sub>1</sub>                   | 0                | 73           | 123                           | 157                           | I     |
|             |  | 4                | 3            | 2                             | 1 2                           |       |
| 4425.1      | 5s <sup>4</sup> P <sub>1</sub> -6p <sup>2</sup> P <sub>1</sub>                   | 165              | 130          | 0                             | 62                            | I     |
|             |  | 7                | 7            | 20                            | 7                             |       |
| 4423.0      | 5s <sup>3</sup> P <sub>1</sub> -7p <sup>4</sup> P <sub>1</sub>                   | 0                | $\tilde{52}$ |                               |                               | II    |
|             |  | 3                | 2            |                               |                               |       |
| 4399.7      | 5s <sup>3</sup> P <sub>1</sub> -5p <sup>3</sup> P <sub>1</sub> ( <sup>1</sup> S) | 0                | —            | $\tilde{86}$                  |                               | II    |
|             |  | 3                |              | 2                             |                               |       |
| 4391.6      | *5s <sup>3</sup> P <sub>1</sub> -7p <sup>2</sup> P <sub>1</sub>                  | $\tilde{92}$ —   | 0            | —                             | $\tilde{182}$                 | II    |
|             |  | 2                | 8            |                               | 3                             |       |
| 4369.2      | 5s <sup>4</sup> P <sub>1</sub> -5p <sup>2</sup> P <sub>1</sub> ( <sup>1</sup> S) | 95               | 0            |                               |                               | I     |
|             |  | 3                | 5            |                               |                               |       |
| 4365.1      | 5s <sup>4</sup> P <sub>1</sub> -7p <sup>4</sup> P <sub>1</sub>                   | 190              | —            | $\tilde{148}$ — $\tilde{112}$ | 0                             | II    |
|             |  | 1                | 3            | 5                             | 7                             |       |

\* See discussion on anomalies.

Apart from these, the term structures derived from different lines are in excellent agreement.

Tolansky has already proved that the spins of both the bromine isotopes 79 and 81 are  $\frac{3}{2}$  and that the nuclear magnetic moments are practically identical. In no lines have we detected any isotope displacement effect other than the fact that in many the individual components appear to be broader than expected. Space prevents us from illustrating in detail the full analysis of all the lines we have studied. We have therefore selected from these a number of groups involving common terms in order to indicate the reliability of the analysis.

Consider first the group of  $\Delta J = \frac{1}{2} \rightarrow \frac{1}{2}$  transitions, the analysis for which is given in figure 2. It is clear from the diagram that the analysis in each line is highly satisfactory, any differences between the observed and

predicted positions of the components being of the order of the error of measurement.

With the aid of the structure already evaluated for  $6p^3P_1$  that of  $5s^3P_1$  can be found from the line 4921. The analysis for this and two other of the lines having  $5s^3P_1$  as a common lower term is shown in figure 3. The last

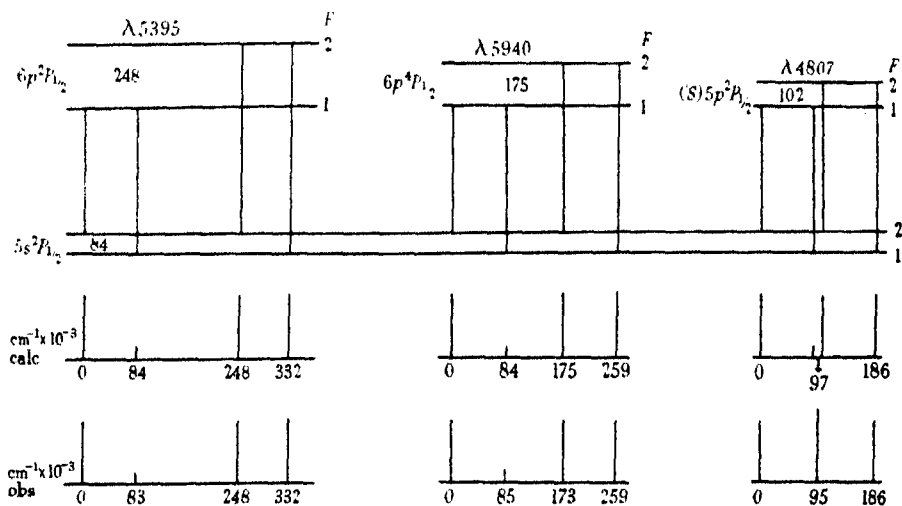


FIGURE 2

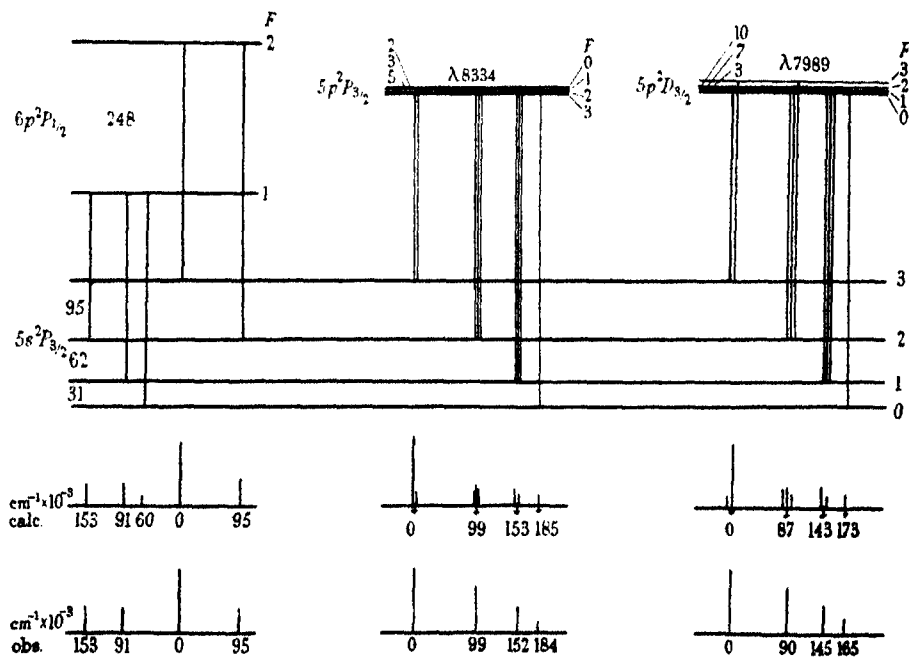


FIGURE 3

two components in the line 7989 were not fully resolved experimentally, a fact which accounts for the discrepancy in this case.

The structures derived for  $5p\ ^2P_{\frac{1}{2}}$  and  $5p\ ^2D_{\frac{3}{2}}$  are valuable for the elucidation of the patterns of lines based upon the important  $5s\ ^4P_{\frac{1}{2}}$  term. A number of striking regular quartet patterns are based upon this as lower term. It is clear from the similarity of the patterns that  $5s\ ^4P_{\frac{1}{2}}$  has a quartet structure, from which it follows that the nuclear spin for both isotopes is  $\frac{3}{2}$ . As the individual components of the quartets are sharp, there is no isotope displacement, and the nuclear magnetic moments are, as far as can be measured, identical.

Although the quartet patterns are very closely similar to each other, they are not identical, due to the fact that the structures in the upper terms, although small, differ considerably. Thus, for the four regular quartet patterns measured here, the  $\Delta F = 4-3$  separations are respectively 203, 196, 191 and 190. This fact introduced a certain difficulty in the analysis of these lines previously undertaken by Tolansky. There was at the time insufficient data to show which of these intervals most closely approaches that of the term structure. The closest fit into a Fisher-Goudsmid diagram was taken to give the term structure, since it was not at that time suspected that the interval rule might break down. It will be shown that it does actually break down for this term, the consequences being that the interval factor previously reported, although of the right order, is in error by 20 %.

Figure 4 shows the predicted and observed patterns for three of the quartet lines (the fourth is very faint and only the first two components are measured with an accuracy comparable with that of the components of the three lines illustrated). It is to be remembered that the structures of the upper  $5p\ ^2P_{\frac{1}{2}}$  and  $5p\ ^2D_{\frac{3}{2}}$  terms are already fixed. The interval rule breaks down in the lower term. This will be discussed later.

A striking feature of the hyperfine structures in the Br I spectrum is the fact that many of the  $4p^4\ np$  and  $4p^4\ nd$  configuration terms have very wide structures. This is in accord with the observations of Tolansky upon the analogous arc spectrum of iodine. Figure 5 illustrates the analysis of complex lines in which both the upper and the lower structures are large. (This is also true for the lines illustrated in figure 2.)

The structures and transitions already illustrated for 11 lines indicate clearly that there is excellent correlation between the structures derived independently from lines involving a common term, a fact proving that the interpretation is correct. It is hardly necessary to multiply the examples already given.

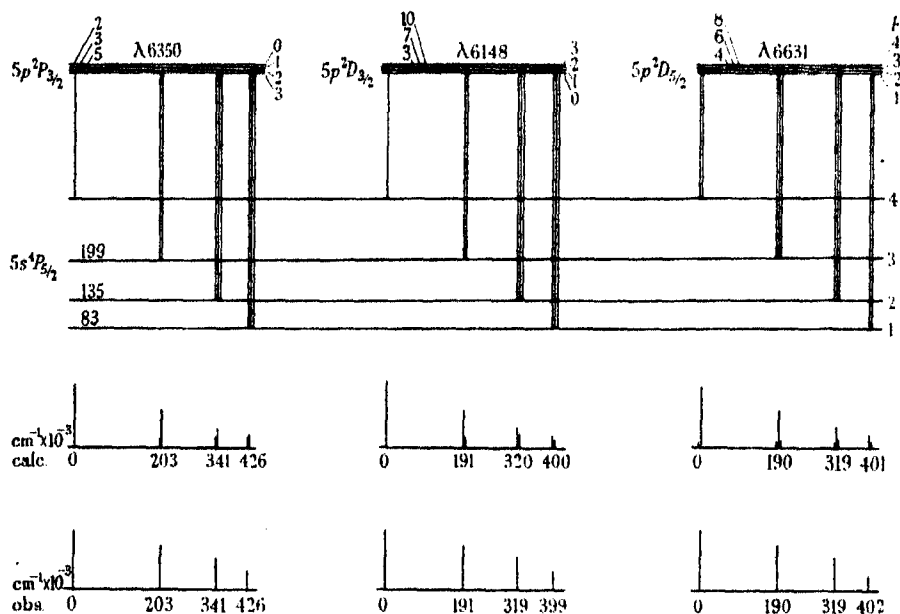


FIGURE 4

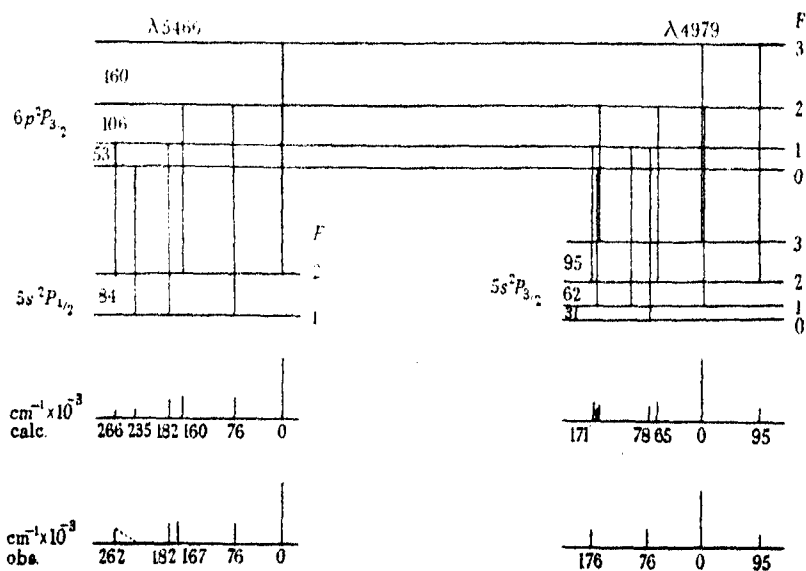


FIGURE 5

Sixty-two of the measured lines have been classified. In a limited number of quartet terms it has only been possible to establish the positions of three out of the four levels. These suffice to give a term interval factor and to show whether or not there is serious deviation from the interval rule. In some cases only two levels have been identified. We have failed entirely to account for the structure of 4643. This is given by Kiess and de Bruin as  $5s\ ^2P_1-6p\ ^4D_1$ . The three lines 7938, 4775, 4399, which have, according to Kiess and de Bruin, a common upper level  $5p\ ^2P_1\ (^1S)$ , have structures which are anomalous. We shall discuss these later.

#### INTERPRETATION

In certain cases the line patterns are so narrow and complex that it is only possible to arrive at approximate values for interval factors. Table 2 shows the term hyperfine structures which we have derived. An asterisk implies that the values given are accurate. Where the value given is only approximate, an approximation sign is given. A minus sign before the first interval implies that the whole structure is inverted, the highest  $F$  value lying deepest.

The term interval factors derived from the structures in table 2 are given in the last column. These are of interest. The normal electron configuration for Br I is  $4s^2\ 4p^5$ , and excitation leads to the configurations  $4s^2\ 4p^4\ ns$ ,  $4s^2\ 4p^4\ np$ ,  $4s^2\ 4p^4\ nd$ , etc., with terms going respectively to the series limits which are the SPD terms of the basic ion Br II.\* The  $6s$  terms involve lines so far in the infra-red that no transitions have been observed.

The frequent large interval factors in the  $4s^2\ 4p^4\ 5p$  and  $4s^2\ 4p^4\ 6p$  configurations show that the  $4p^4$  electron group couples strongly with the nucleus. This is in accord with what Tolansky has found for the corresponding  $5p^4$  electron group in iodine. With the exception of the  $^3P$  terms, there is no very great difference between corresponding  $5p$  and  $6p$  terms, from which it can be concluded that the resultant coupling factor of the  $4p^4$  group is much greater than that of either the  $5p$  or  $6p$  electron. The  $^2P$  terms exhibit an anomalous increase in going from the  $5p$  to the  $6p$  terms. This can be due to configuration interaction, but it is also possible, and indeed more likely, as it occurs in both terms of the doublet, that there is a change in the nature of the electron coupling, in moving from  $4s^2\ 4p^4\ 5p\ ^2P$  to  $4s^2\ 4p^4\ 6p\ ^2P$ .

\* It is usual, for the sake of brevity, to omit the  $4s^2\ 4p^4$  group when indicating term denominations.



TABLE 2. HYPERFINE STRUCTURES IN THE TERMS OF Br I. INTERVALS

| Configuration  | Term                          | Structure<br>cm. <sup>-1</sup> × 10 <sup>-3</sup> |      |     | Interval<br>factors<br>cm. <sup>-1</sup> × 10 <sup>-3</sup> |
|--|-------------------------------|---|------|-----|---|
|  |                               |   |      |     |   |
| 4s <sup>2</sup> 4p <sup>4</sup> 5s                   | <sup>4</sup> P <sub>1</sub> * | 199   | 135  | 83  | 47.1  |
|  | <sup>4</sup> P <sub>1</sub>   | 63  | 38   | 19  | 20  |
|  | <sup>4</sup> P <sub>1</sub> * | -6  |      |     | -3  |
|  | <sup>2</sup> P <sub>1</sub> * | 95  | 62   | 31  | 30  |
|  | <sup>2</sup> P <sub>1</sub> * | 84  |      |     | 42  |
| 4s <sup>2</sup> 4p <sup>4</sup> 5p                   | <sup>4</sup> P <sub>1</sub>   | ~96   | ~72  | ~48 | ~24   |
|  | <sup>4</sup> P <sub>1</sub> * | 127   | 86   | 43  | 43  |
|  | <sup>4</sup> D <sub>1</sub> * | 124   | 84   | 60  | 23  |
|  | <sup>4</sup> D <sub>1</sub> * | 115   | 75   | ?   | 38  |
|  | <sup>2</sup> D <sub>1</sub> * | 8   | 6    | 4   | 2   |
|  | <sup>4</sup> S <sub>1</sub>   | -3  | 2    | 1   | -1  |
|  | <sup>2</sup> P <sub>1</sub> * | 49  |      |     | 24½   |
|  | <sup>2</sup> P <sub>1</sub> * | -5  | ~3   | ~2  | -2  |
|  | <sup>2</sup> D <sub>1</sub> * | 10  | ~7   | ~3  | 3   |
|  | <sup>2</sup> D <sub>1</sub> * |   |      |     |   |
| 4s <sup>2</sup> 4p <sup>4</sup> 6p                   | <sup>4</sup> P <sub>1</sub> * | 106   | 78   | 52  | 26  |
|  | <sup>4</sup> P <sub>1</sub>   | 147   | 98   | 49  | 49  |
|  | <sup>4</sup> D <sub>1</sub> * | 116   | 88   | 65  | 22  |
|  | <sup>4</sup> P <sub>1</sub> * | 175   |      |     | 87½   |
|  | <sup>4</sup> D <sub>1</sub>   | 119   | ?    | ?   | ~30   |
|  | <sup>4</sup> D <sub>1</sub> * | 126   | 85   | 43  | 42  |
|  | <sup>2</sup> P <sub>1</sub> * | 160   | 106  | 53  | 53  |
|  | <sup>2</sup> P <sub>1</sub> * | 248   |      |     | 124   |
|  | <sup>2</sup> D <sub>1</sub>   | -11   | ~7   | ~4  | -4  |
|  | <sup>4</sup> S <sub>1</sub>   | -6  | 4    | 2   | -2  |
|  | <sup>2</sup> D <sub>1</sub>   | 12  | 8    | 4   | 3   |
|  | <sup>2</sup> S <sub>1</sub>   | 33  |      |     | 16½   |
|  | <sup>2</sup> S <sub>1</sub>   |   |      |     |   |
| 4s <sup>2</sup> 4p <sup>4</sup> 7s                   | <sup>4</sup> P <sub>1</sub>   | ~96   | ~72  | ~48 | ~24   |
| 4s <sup>2</sup> 4p <sup>4</sup> 5p ( <sup>1</sup> S) | <sup>2</sup> P <sub>1</sub> * | 102   |      |     | 51  |
| 4s <sup>2</sup> 4p <sup>4</sup> 7p                   | <sup>4</sup> P <sub>1</sub>   | ~72   | ?    | ?   | ~24   |
|  | † <sup>2</sup> P <sub>1</sub> | ~90   | ~60  | ~30 | ~30   |
| 4s <sup>2</sup> 4p <sup>4</sup> 4d                   | <sup>4</sup> D <sub>1</sub>   | ~35   | ~28  | ~21 | ~7  |
|  | <sup>4</sup> D <sub>1</sub>   | ~52   | ~39  | ~26 | ~13   |
|  | <sup>4</sup> F <sub>1</sub>   | ~60   | ?    | ?   | ~12   |
|  | <sup>4</sup> P <sub>1</sub>   | ~80   | ~60  | ?   | ~20   |
|  | <sup>4</sup> P <sub>1</sub>   |   |      |     |   |
| 4s <sup>2</sup> 4p <sup>4</sup> 5d                   | <sup>4</sup> D <sub>1</sub>   | ~50   | ?    | ?   | ~10   |
|  | <sup>4</sup> F <sub>1</sub>   | 90  | ?    | ?   | ~15   |
|  | <sup>4</sup> F <sub>1</sub>   | ~140  | ~112 | ~84 | ~28   |

† Given as <sup>4</sup>P<sub>1</sub> by Kiess and de Bruin, but as <sup>2</sup>P<sub>1</sub> by Lacroute (see later).

It has not been possible to fix the structure of 5s <sup>4</sup>P<sub>1</sub> with a high degree of accuracy or to show the existence of any deviation from the interval rule in this term. The value given here differs considerably from that given earlier. This will be discussed shortly.

## ANOMALIES IN ANALYSIS

We shall consider now four lines whose structures cannot be fitted at all into the above scheme which accounts so excellently for the remaining large number. According to Kiess and de Bruin the transitions for the three lines 7938, 4775 and 4399 are those shown in figure 6. We are quite unable to fit these lines into our analysis. If we assume that the allocations made by Kiess and de Bruin are correct, then the structures of the lower terms of 4775 and 4399 are known with certainty from other lines. It is not possible to fit in any upper term structure with  $J = \frac{3}{2}$  unless at the same time an arbitrary distortion of intensities is introduced. It is clearly possible to arrive at any pattern by suitable adjustment of both intensities and intervals simultaneously but such a procedure has very questionable significance.

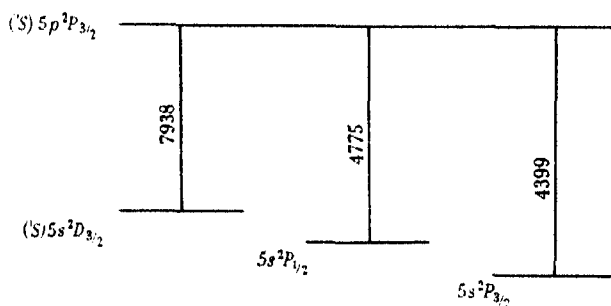


FIGURE 6

As shown in figure 7 a very good fit for these two lines results if the upper term [given as  $(S) 5p^2P_{3/2}$ ] is assumed to have a  $J$  value of  $\frac{1}{2}$  instead of  $\frac{3}{2}$ . This would mean a faulty interpretation by Kiess and de Bruin. Furthermore, the latter authors have not observed any intercombinations between this term and one with  $J$  greater than  $\frac{3}{2}$  so that our suggested alteration of the value of  $J$ , and therefore of the allocation, is in no way contradicted by the multiplet analysis.

The third line involving the doubtful term, 7938, has a remarkable structure, each of the components being very sharp indeed and almost certainly single. The impression is given that the line is a transition between terms in one of which the structure is large and in the other very small. However, both the intensities and the intervals are highly irregular. We cannot fit this line either into the proposed scheme in figure 6 or into any other scheme, nor can we invoke any possible isotope displacement effect to account for the structure. No other line involving the lower term

has been observed by us. Clearly we can justifiably assume that one of the terms is strongly perturbed, that being so the classification may easily be faulty.

The remaining line which we cannot interpret is 4643, the classification given for this by Kiess and de Bruin being  $5s\ ^4P_{\frac{1}{2}}-6p\ ^4D_{\frac{1}{2}}$ . Tolansky's earlier value for the structure of  $5s\ ^4P_{\frac{1}{2}}$  was based upon this line. The structure does not fit with the analysis made for other lines having the lower terms  $5s\ ^4P_{\frac{1}{2}}$ . On the other hand, the structure in the line is close

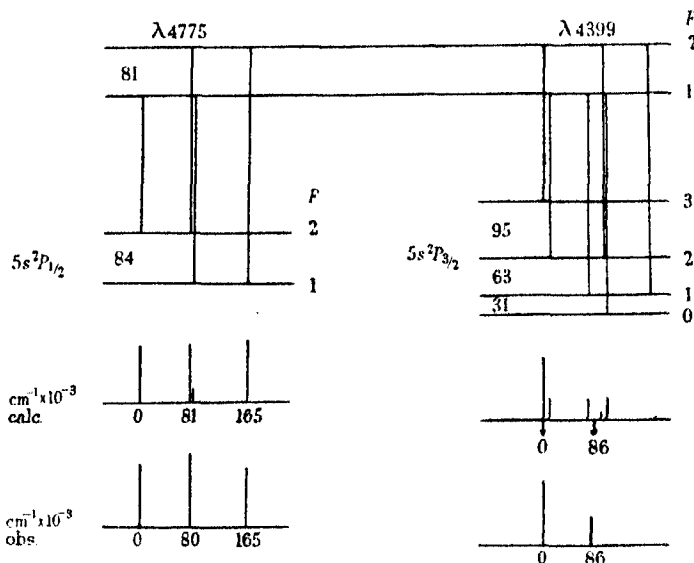


FIGURE 7

to the structure in the  $5s\ ^2P_{\frac{1}{2}}$  term. If the line is incorrectly classified, it is a transition between  $5s\ ^2P_{\frac{1}{2}}$  and an upper term, as yet not identified, the value of which will be  $6843.7\text{ cm}^{-1}$ .

Two other lines remain to be discussed for which we have not adopted the classification given by Kiess and de Bruin. It is impossible to interpret the lines 4391 and 4765, which have the same common upper term, by taking this common term to be  $7p\ ^4P_{\frac{1}{2}}$  (the interpretation given by Kiess and de Bruin). We can only obtain a fit by adopting a  $J$  value  $\frac{3}{2}$  for the upper term. This is unquestionably correct, since recently Lacroute (1935), who has made Zeeman effect observations on Br I terms, has concluded that this term is in reality  $7p\ ^2P_{\frac{1}{2}}$ . We agree with this interpretation and have adopted it in making the analysis.

UNCLASSIFIED LINES AND SPARK LINES

The structures for the following lines of Br II and for unclassified lines have also been measured. The Br II classifications are given by Lacroute (1935). The units are  $\text{cm.}^{-1} \times 10^{-3}$ .

TABLE 3

| Wave-length | Spectrum | Allocation            | Structure |     |     |        |
|-------------|----------|-----------------------|-----------|-----|-----|--------|
|             |          |                       | Red       |     |     | Violet |
| 6095.7      | —        | —                     | 0         | 104 | 204 | 277    |
|             |          |                       | 16        | 17  | 19  | 20     |
| 6064.3      | —        | —                     | 0         | 88  | 160 | 221    |
|             |          |                       | 4         | 3   | 2   | 1      |
| 5785        | —        | —                     | Single    |     |     |        |
| 5591        | —        | —                     | Single    |     |     |        |
| 5182.3      | Br II    | $5s\ ^4S_1-5p\ ^3P_2$ | 0         | 37  | 128 |        |
|             |          |                       | 1         | 2   | 3   |        |
| 4816.1      | Br II    | $5s\ ^4S_1-5p\ ^3P_1$ | 0         | 156 | 264 | 327    |
|             |          |                       | 4         | 3   | 2   | 1      |
| 4719.8      | Br II    | —                     | 0         | 127 | 220 | 273    |
|             |          |                       | 4         | 3   | 2   | 1      |
| 4412        | —        | —                     | 0         | 47  | 132 |        |
|             |          |                       | 1         | 2   | 3   |        |

We are extending our measurements upon the Br II lines and will report later on this.

DEVIATIONS FROM THE INTERVAL RULE

In dealing with deviations from the interval rule it is essential to eliminate spurious effects that can arise from inadequate resolution or only approximately correct analysis. Any such errors leading to a slight displacement in estimating the position of even a single  $F$  level will appear to indicate the existence of deviation from the interval rule. We are therefore confining our examination to the  $5s\ ^4P_1$  term, since the structure in this is large and has been evaluated with certainty from many transitions. Apart from this term the structures are also known accurately for quite a number of others, but it so happens that in all but one of these any existing deviations from the interval rule are of the same order as the error in estimating the positions of the levels. Use cannot of course be made of the many accurately determined structures of terms with  $J = \frac{1}{2}$  since these cannot exhibit deviations from the interval rule.

The distortion is shown in figure 8. The observed positions of the levels are shown by straight lines and those calculated from the interval rule by

dotted lines. The disposition of the Br I terms gives no reason for supporting that  $5s\ ^4P_4$  suffers configuration interaction which might produce distortion. The effect can therefore be attributed to the existence of nuclear electrical quadrupole moment in bromine. According to Schüller and Schmidt (1935) and Casimir (1935) the interaction energy between the angular momentum  $J$  of a non-spherically symmetrical electron configuration and the spin  $I$  of a non-spherically symmetrical nucleus does not obey the simple cosine law which leads to the interval rule. Instead the

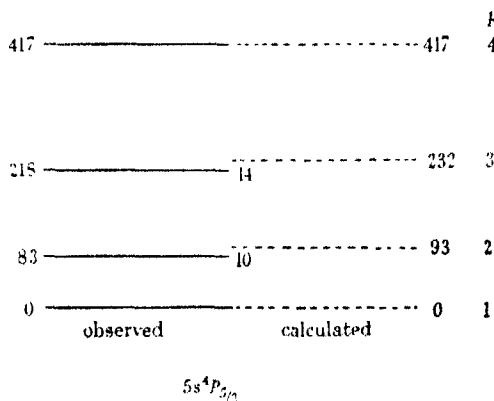


FIGURE 8

interaction law for each hyperfine structure  $F$  level of energy  $E$  is of the form

$$E = A_0 + AIJ \cos IJ + BIJ \cos^2 IJ.$$

This can be rewritten as

$$E = a_0 + \frac{1}{2}a \cdot C + b \cdot C(C+1),$$

where  $C = F(F+1) - I(I+1) - J(J+1)$  in which  $F$ ,  $J$  and  $I$  have the usual meanings. In this interaction law  $a_0$ ,  $a$  and  $b$  are constants,  $a_0$  being the displacement of the centre of gravity of the hyperfine structure pattern from the position the term would have occupied if the spin had been zero,  $a$  is the hyperfine structure interval factor which is a function of the nature of the electron configuration and is also proportional to the nuclear magnetic moment,  $b$  is a measure of the deviation from the interval rule. The quantity  $b$  is a function of the nuclear electrical quadrupole moment and, if the coupling constants of the term have been calculated, it is possible in suitable cases to derive a numerical value for the quadrupole moment from  $b$ .

The interaction formula has three constants, and since there are four levels in the term suffering distortion, a check is available upon the validity of the formula. When the calculation is made for the  $5s\ ^4P_{\frac{1}{2}}$  term, we find for  $a$ , derived from different  $F$  combinations respectively (units  $\text{cm.}^{-1} \times 10^{-3}$ )

$$\begin{aligned} a &= 47.04 \\ a &= 47.10 \end{aligned} \quad \text{mean value } a = 47.1$$

and for the quadrupole term  $b$

$$\begin{aligned} b &= 0.175 \\ b &= 0.161 \end{aligned} \quad \text{mean value } b = 0.17.$$

The check is highly satisfactory, showing that the quadratic formula is obeyed within the limits of observation. This may be taken to prove that the distortion is due to nuclear electrical quadrupole moment only. The value of  $a_0$  is  $223 \text{ cm.}^{-1} \times 10^{-3}$ . Hence  $E = 223 + \frac{1}{2} \times 47.1C + 0.17C(C+1)$ .

The term  $5p\ ^4D_{\frac{1}{2}}$  is also distorted but as this term structure has only been derived from the measurements made upon one line it is not possible to say with certainty whether the distortions are real or not, especially since the line in question is only partially resolved.

Our thanks are due to Professor P. M. S. Blackett, F.R.S. for his kind continual encouragement and to Professor D. R. Hartree, F.R.S. for very helpful discussions.

Thanks are due to the Government Grants Committee of the Royal Society with whose aid some of the necessary instruments have been acquired.

#### SUMMARY

Sixty-five classified lines of the Br I spectrum, lying in the region 8650—4350 Å have been investigated for hyperfine structure and analysed. It is confirmed that the nuclear mechanical and magnetic moments of both isotopes are the same. No isotope displacement is observed. Hyperfine structure interval factors are derived for 38 terms amongst which are 7 complete multiplet groups. From the hyperfine structure analysis it has been possible to correct some errors in the multiplet analysis.

The coupling of the  $4p^4$  electron group with the nucleus is shown to be quite large. This group therefore behaves in a manner similar to that of the corresponding  $5p^4$  group of iodine.

The  $4s^2 4p^4 5s^4 P_3$  term exhibits deviation from the interval rule, and this accurately obeys the quadratic formula for the interaction which arises when the nucleus has an electrical quadrupole moment. The interaction formula for this term is

$$E = 223 + \frac{1}{2} \times 47.1C + 0.17C(C+1) \text{ cm.}^{-1} \times 10^{-3}.$$

#### REFERENCES

- Casimir 1935 *Physica*, 7, 719.  
 Kiess and de Bruin 1930 *Bur. Stand. J. Res., Wash.*, 4, 667.  
 Lacroute 1935 *Ann. Phys., Paris*, 3, 5.  
 Schüler and Schmidt 1935 *Z. Phys.* 98, 239.  
 Tolansky 1932 *Proc. Roy. Soc. A*, 136, 585.

## Orientation of nuclear spins in metals

BY H. FRÖHLICH AND F. R. N. NABARRO

*H. H. Wills Physical Laboratory, University of Bristol*

(Communicated by N. F. Mott, F.R.S.—Received 22 February 1940)

### 1. INTRODUCTION

In recent years, temperatures down to about  $1/100$ – $1/1000$  degree absolute have been reached by means of the magnetic cooling method. This method, which was proposed by Debye and by Giauque, consists essentially of isothermal magnetization of a paramagnetic substance, followed by adiabatic demagnetization. Kürti and Simon (1935) have shown that the lowest temperatures which can be reached by this method are proportional to the interaction energy between magnetic dipoles of the substances used. Therefore, in order to reach still lower temperatures, it was proposed by these authors and by Gorter (1934) that the magnetism of atomic nuclei should be used. F. Simon (1939) has recently discussed this idea in greater detail and found that it should be possible to realize it experimentally.

The question now arises of what temperatures can be reached in this way, what times will be necessary and what will be the properties of the nuclear spins at these temperatures.\* In this paper we shall investigate these

\* Enquiries from Professor Simon on these points stimulated the present work.

questions for metals. Here, the magnetic interaction between the conduction electrons and the nuclei leads to an indirect coupling between the magnetic moments of the nuclei which for many metals is considerably larger than their direct magnetic interaction. We shall show that any metal for which this is the case becomes ferromagnetic with respect to the nuclei. The Curie temperature will be of the order  $10^{-6}$  degree or less, and the temperatures reached by the magnetic cooling method will consequently be of the same order of magnitude. The attainment of such temperatures where the nuclear spins are orientated may be of great importance in nuclear physics.

In insulators the coupling between the nuclear spins is much smaller than in metals, because here their direct magnetic interaction is only slightly influenced by the electrons. Also the times required to reach equilibrium are probably much longer. Metals are therefore the most suitable substances for investigations in the near future, and we shall confine ourselves to them.

## 2. INTERACTION BETWEEN NUCLEAR SPINS AND ELECTRONS

In order to investigate the behaviour of nuclear spins in metals we have to find the contributions to the total energy which depend on the direction of these nuclear spins. These contributions arise from two kinds of interaction. The first is the direct magnetic interaction between the nuclear spins. This contribution is *not* characteristic of metals but occurs also in insulators. We shall assume it to be small compared with the second part, which is confined to metals and represents the interaction between nuclear spins and electronic spins. As we shall see in § 6 this condition is fulfilled for most monovalent metals. We shall also restrict ourselves to monovalent metals, i.e. to Cu, Ag, Au and the alkali metals. A free atom of this kind has in the ground state one *s*-electron in an incomplete shell. The interaction between nuclear moment and electron in such an atom is well known from experimental and theoretical investigations on the hyperfine structure of spectral lines. According to a formula, first derived by Fermi (cf. Bethe 1933), the interaction energy may be written as

$$2C(\mathbf{i}, \mathbf{s}), \quad (1)$$

if the electron is in an *s*-state. Here  $\mathbf{i}$  is the angular momentum of the nucleus,  $\mathbf{s}$  is the spin operator of the electron and  $C$  is independent of  $\mathbf{i}$  and  $\mathbf{s}$  but depends on the value of the electronic wave function near the nucleus. Expression (1) has two proper values according to the two possible orientations of the electronic spin. Their separation determines the hyperfine splitting  $\epsilon$ :

$$\epsilon = C(i + \tfrac{1}{2}), \quad i \neq 0, \quad (2)$$



which has been measured for all monovalent atoms. In a given atom the hyperfine splitting of an  $s$ -state is usually much greater than the splitting of a  $p$ ,  $d$ , ... state, although for such states there is in addition the interaction with the orbital momentum. This is because the magnetic field of the nuclear spin decreases very rapidly with distance, and an  $s$ -electron comes much nearer to the nucleus than an electron with orbital angular momentum different from zero.

Now let us consider the corresponding interaction in the metallic state. Here, according to F. Bloch, the wave function of an electron spreads over the whole metal, i.e. an electron has an equal probability  $1/N$  of being near any of the  $N$  nuclei of the metal. The magnitude of the interaction mainly depends on the behaviour of the wave function very near to the nucleus, where it is approximately the same as in the free atom. Its absolute value may be slightly different, owing to the difference in the normalizations. Consequently the contribution of the  $n$ th nucleus to the interaction is

$$\frac{2\alpha}{N} C(\mathbf{l}_n, \mathbf{s}), \quad (3)$$

where  $\hbar \mathbf{l}_n$  is the angular momentum of the  $n$ th nucleus and  $\alpha$  takes account of the different normalization. Thus the total interaction is

$$\frac{2\alpha}{N} C(\Sigma \mathbf{l}_n, \mathbf{s}) = \frac{2\alpha}{N} C(\mathbf{M}, \mathbf{s}),$$

where  $\hbar \mathbf{M}$  is the total angular momentum of all nuclei in the metal. As in the free atom, an electronic state splits into two, corresponding to the two possible orientations of the electronic spin. Their separation  $\Delta E(M)$  is given by

$$\Delta E(M) = \frac{\alpha}{N} C(M + \tfrac{1}{2}), \quad M \neq 0,$$

analogous to equation (2). Here,  $\frac{1}{2}$  can be neglected since, given a certain angular momentum per unit volume,  $M$  is proportional to  $N$ . Expressing  $C$  by the hyperfine splitting  $\epsilon$  (equation (2)), we find for the splitting of an electronic state in a metal

$$\Delta E(M) = \frac{\alpha \epsilon M}{(i + \tfrac{1}{2})N}. \quad (4)$$

We thus see that, owing to the interaction between electronic and nuclear spins, an electronic state splits into two, corresponding to anti-parallel spin directions, just as happens under the influence of an external magnetic

field  $H$ , where the splitting is  $2\mu H$ ,  $\mu$  being the Bohr magneton. The interaction with an external magnetic field

$$H(M) = \alpha \epsilon M / 2\mu(i + \frac{1}{2}) N \quad (5)$$

would, therefore, give the same contribution to the total energy as does the nuclear spin electronic spin interaction, provided that we consider the action of the field on the *electronic spins* only. The total interaction energy  $U(M)$  is, therefore, given by

$$U(M) = -\frac{1}{2}\chi_p H^2(M) V, \quad (6)$$

where  $V$  is the volume and  $\chi_p$  is the *paramagnetic* susceptibility of the electrons.

If all the nuclear spins are parallel, the "effective" magnetic field  $H(M)$  is rather strong because  $s$ -electrons, as mentioned above, come very near to the nucleus. For Cu, for instance, it is about 5000 G. There exists, of course, also a diamagnetic interaction between electrons and nuclear spins. For this kind of interaction, as far as it depends on the *direction* of the nuclear spins, the effective magnetic field is much smaller than  $H(M)$ , so that the contribution to the total interaction is negligible.\*

Inserting (5) into (6) we find

$$U(M) = -\frac{1}{2}\chi_p \frac{\alpha^2 \epsilon^2 M^2 V}{\mu^2 (i + \frac{1}{2})^2 N^2}. \quad (7)$$

Assuming the electrons to behave like free electrons with an effective mass  $m^*$ ,  $\chi_p$ , first calculated by Pauli, may be written as (cf. Fröhlich 1936)

$$\chi_p = \frac{3\mu^2 n}{2\zeta}, \quad (8)$$

\* There are two diamagnetic parts: first, the diamagnetism of closed shells. Here the interaction of a nuclear spin with its own closed shell is independent of the *direction* of the spin and hence does not give a contribution to the spin-dependent interaction. The interaction with neighbouring shells is very small indeed, even compared with the direct interaction between nuclear spins which has already been neglected. In fact it is just a part of the correction which has to be made to this direct interaction because the interaction takes place in a medium with a certain magnetic susceptibility, and not *in vacuo*. In Cu the effective magnetic field is of the order of 1 G or less. There is secondly the diamagnetism of the conduction electrons (Landau diamagnetism) which even if it had to be considered would only reduce equation (6) to two-thirds of its value (cf. for example, Fröhlich 1936). But in fact for the part of the interaction which depends on the direction of the nuclear spins, the effective magnetic field should again be smaller than  $H(M)$ . For only an interaction with the orbital momentum of the electron can depend on the *direction* of nuclear spin. As mentioned above, this leads to a smaller interaction than that considered in the text.

where 
$$\zeta = \frac{\hbar^2}{2m^*} (3\pi^2 n)^{\frac{2}{3}} \quad (9)$$

is the energy region occupied by the conduction electrons, and

$$n = N/V \quad (10)$$

is the number of atoms per unit volume.

Inserting (8) and (10) into (7), we find for the interaction energy

$$U(M) = -\frac{3\alpha^2 \epsilon^2}{16} \frac{M^2}{\zeta (i + \frac{1}{2})^2 N}. \quad (11)$$

This means that the state in which all nuclear spins are parallel, i.e. in which  $M$  has its highest value, has the lowest energy.

### 3. THERMAL PROPERTIES

In order to derive the thermal properties of the metal, we calculate its free energy  $F$ , which, according to a well-known theorem is given by

$$e^{-F/kT} = \sum_{\text{nuclei}} \sum_{\text{electrons}} e^{-E_n/kT}. \quad (12)$$

Here  $E_n$  is the energy of the  $n$ th quantum state of the whole metal.  $n$  represents a whole series of indices, including the quantum numbers of all electrons and the spin directions of all nuclei. The sum has to be carried out over all states of the electrons and of the nuclear spins. Let us first carry out the sum over all electronic states for a fixed state of nuclear spins, leading to a nuclear angular momentum  $\hbar M$ . Then, according to the results of § 2, the energy states are the same as they would be if the electron spins were not in interaction with the nuclei, but instead with a magnetic field of strength  $H(M)$ , given by equation (5). Therefore

$$\sum_{\text{electrons}} e^{-E_n/kT} = e^{-F(M)/kT}, \quad (13)$$

where  $F(M)$  is the free energy of the electrons in the magnetic field  $H(M)$ , i.e. since the paramagnetic susceptibility  $\chi_p$  of the electrons does not depend on temperature (cf. equation (7))

$$F(M) = F_0 - \frac{1}{2} \chi_p H^2(M) V = F_0 + U(M). \quad (14)$$

Here  $F_0$  is the free energy of the electrons without a magnetic field.  $F_0$  depends on  $T$ , but not on  $M$ . Inserting (13) and (14) into (12) we obtain

$$e^{-(F-F_0)/kT} = \sum_{\text{nuclei}} e^{-U(M)/kT}. \quad (15)$$

Now we remark that, since according to (7)  $U(M) \sim -M^2$ ,  $F - F_0$  is identical with free energy of a ferromagnetic substance in Weiss's theory of ferromagnetism (cf. Stoner, 1934). Let  $F_{\text{ferro}}$  be the free energy according to this theory; then the total free energy becomes

$$F = F_0 + F_{\text{ferro}}. \quad (16)$$

Just as in a ferromagnetic substance, we consequently have to expect at a temperature  $\theta$  a phase transition of the second order, a so-called  $\lambda$ -point or Curie point characterized by a jump in the specific heat leading up to values of the order of the Boltzmann constant.  $\theta$  is given by the Weiss theory (cf. Stoner 1934) as (cf. equations (5) and (6))

$$k\theta = -\frac{2i(i+1)}{3} \frac{U(M)N}{M^2} = \frac{1}{12} \frac{i(i+1)}{(i+\frac{1}{2})^2} \frac{\alpha^2 \epsilon^2}{\chi_p \mu_n^2}, \quad (17)$$

or making use of the theoretical value (8) for  $\chi_p$

$$k\theta = \frac{1}{8} \frac{i(i+1)}{(i+\frac{1}{2})^2} \frac{\alpha^2 \epsilon^2}{\xi} \simeq \frac{1}{8} \frac{\alpha^2 \epsilon^2}{\xi}. \quad (18)$$

#### 4. MAGNETIC PROPERTIES

In order to derive the magnetic properties, we have to calculate the free energy in the presence of an external magnetic field  $H$ . This can be done by a method similar to that of § 3, replacing the internal field  $H(M)$  by the total field  $H + H(M)$  and adding the diamagnetic interaction and the direct interaction between  $H$  and nuclear spins. Thus we have to replace  $U(M)$  by

$$U(M, H) = -\frac{1}{2} \chi_p (H + H(M))^2 V + \frac{1}{2} \chi_d H^2 V - \mu_n \frac{MH}{i}.$$

Here  $\chi_d$  ( $> 0$ ) is the diamagnetic susceptibility. Its sign is chosen so that the total susceptibility  $\chi$  is given by

$$\chi = \chi_p - \chi_d;$$

$\mu_n$  is the magnetic moment of a nucleus.

Using equation (6) reduces the above expression to the form

$$U(M, H) = U(M) - \frac{1}{2} \chi H^2 V - \mu^* MH/i, \quad (19)$$

where

$$\mu^* = \mu_n + \chi_p H(M) i V / M. \quad (20)$$

According to expression (19) the metal shows its ordinary susceptibility  $\chi$  on which the ferromagnetism of the nuclei is superposed. The nuclear spins

behave as if they had not their magnetic moment  $\mu_n$  but an effective magnetic moment  $\mu^*$ . Its meaning can easily be understood if we consider the metal without a magnetic field at a temperature  $T < \theta$ . Then the total magnetic moment consists of that of the nuclear spins plus the contribution of the electrons, which is  $\chi_p H(M)$ .  $|\mu^* - \mu_n|/\mu_n$  is usually very small; its order of magnitude is  $10^{-2}$ .

## 5. TIME OF RELAXATION

The magnetic cooling method can only be carried out successfully if after the application of a magnetic field at the initial temperature  $T_i$  thermodynamic equilibrium is established in a reasonable time. Heitler and Teller (1936) have already considered this question. They show that a nucleus can change its spin direction when it collides with an electron, the total angular momentum being conserved. They calculate the probability  $w$  that such a transition will take place in unit time from the well-known quantum mechanical formula

$$w = 4\pi^2 |W|^2 \rho / h, \quad (21)$$

where  $W$  is the matrix element of the interaction between nuclear spin and electron.  $\rho$  is the density of states per energy interval  $dE$  of the electrons near the top of the Fermi distribution  $\zeta$ . They assume  $W \sim \epsilon$ , the hyperfine structure splitting, and find

$$w \simeq \epsilon^2 k T_i / h \zeta^2. \quad (22)$$

In the derivation of this expression it was assumed that because of the Pauli principle only electrons in an interval of the order  $kT_i$  near the top of the Fermi distribution can make transitions. This is, however, only true if  $2\mu_n H < kT_i$ ,  $H$  being the external magnetic field. If  $2\mu_n H > kT_i$ , electrons in an interval  $2\mu_n H$  will be able to make collisions in which their spin changes its direction. This is because in such a collision the nucleus (assuming  $i = \frac{1}{2}$ ) loses magnetic energy  $2\mu_n H$  which has to be taken up by the electron as kinetic energy. It should be mentioned that the electrons are assumed to be in equilibrium with the magnetic field. We then find after a simple calculation

$$w = \frac{9\pi^2 \epsilon^2 \mu_n H}{2 h \zeta^2}, \quad \mu_n H \gg kT_i. \quad (23)$$

If the condition  $\mu_n H \gg kT_i$  is no longer fulfilled,  $w$  becomes larger; for  $\mu_n H \ll kT_i$ ,  $2\mu_n H$  has to be replaced by  $kT_i$ . Our formula then becomes identical with Heitler and Teller's formula (22), apart from a numerical factor which they have not considered.

## 6. DISCUSSION

In the previous sections we found that the nuclei of a monovalent metal should become ferromagnetic at a temperature  $\theta$  given by equations (17) or (18), provided that the direct interaction between the nuclear spins is sufficiently small. This direct interaction  $U'(M)$  may be estimated as follows: Let  $H'$  be the magnetic field produced by all the nuclei except one, say the  $n$ th, whose angular momentum is  $h\mathbf{l}_n$ . Then  $\frac{\mu_n}{l_n}(\mathbf{l}_n, \mathbf{H}')$  is its energy. Thus the total interaction energy is given by

$$U'(M) = -\frac{1}{2} \frac{\mu_n}{i} (\mathbf{M}, \mathbf{H}').$$

Supposing that the Lorentz formula can be applied approximately,  $H'$  is given by

$$H' = \frac{4\pi\mu_n M}{3iV},$$

i.e. 
$$U'(M) = -\frac{2\pi\mu_n^2 M^2}{3i^2V}.$$

Thus the ratio  $\gamma$  of the two interactions, which we have assumed to be small compared to one, is, using equation (11)

$$\gamma = \frac{U'(M)}{U(M)} = \frac{32\pi \left(i + \frac{1}{2}\right)^2 \mu_n^2 n \zeta}{9 \alpha^2 \epsilon^2}. \quad (24)$$

In the following table we give the values of the Curie temperature  $\theta$  (18) for those monovalent metals for which the condition  $\gamma \ll 1$  holds. We also give in this table the nuclear spin  $i$ , the magnetic moment  $\mu_n$  in terms of the nuclear magneton  $\mu_0$ , the hyperfine structure splitting†  $\epsilon$  in  $\text{cm.}^{-1}$ , and the ratio  $f = m/m^*$  of the real to the effective electronic mass, used‡ in order to calculate  $\zeta$  according to equation (9). The factor  $\alpha$  was for Cu found to be about 1.7 according to wave functions kindly provided by Dr K. Fuchs (cf. also Fuchs 1935). For the other metals no such wave functions were available. We used  $\alpha = 1$  which for the alkali metals should be very near to the actual value, owing to their large atomic volume.

† Cf. Elliott and Wulff (1939); Jackson and Kuhn (1937, 1939); Tolanski and Forester (1938).

‡ This ratio  $f$  is taken from Fröhlich (1936), table 9, where it is calculated from the experimental susceptibilities of the metals. These  $f$ -values are rather smaller than  $f$ -values obtained in other ways, which indicates that the interaction between the metal electrons plays some role in determining the susceptibility.

|                                 | Cu 63<br>and 65 | Ag 107    | Ag 109             | Au 197 | K 39               | Rb 85 | Rb 87 | Cs 133 |
|---------------------------------|-----------------|-----------|--------------------|--------|--------------------|-------|-------|--------|
| $i$                             | 3/2             | 1/2       | 1/2                | 3/2    | 3/2                | 5/2   | 3/2   | 7/2    |
| $\mu_n/\mu_0$                   | 2.7             | 0.1       | 0.2                | 0.2    | 0.37               | 1.3   | 2.6   | 2.5    |
| $\epsilon$ in cm. <sup>-1</sup> | 0.40            | 0.04      | 0.08               | 0.22   | 0.015              | 0.10  | 0.23  | 0.31   |
| $f$                             | 0.4             | 0.5       | 0.5                | 0.55   | 0.6                | 0.65  | 0.65  | 0.9    |
| $\theta \times 10^4$ °          | 4               | $10^{-2}$ | $4 \times 10^{-2}$ | 0.4    | $4 \times 10^{-3}$ | 0.2   | 1     | 2      |
| $\gamma$                        | 0.07            | 0.04      | 0.04               | 0.00   | 0.2                | 0.03  | 0.03  | 0.01   |

This table shows that the Curie temperature for nuclear ferromagnetism is of the order of  $10^{-6}$  degree or less. The entropy which a metal has at  $T > \theta$  owing to the disorder of the nuclear spins will decrease rapidly as  $T$  becomes smaller than  $\theta$ , and the specific heat will have values of the order of the Boltzmann constant. The entropy of the electrons and of the lattice vibrations is negligibly small at such temperatures. In applying the magnetic cooling method, the number of orientated nuclear spins should, therefore, remain constant when the external field is removed. One may thus hope to reach by this method temperatures below, but of the order of magnitude of, the Curie temperature  $\theta$ .

The saturation moment of these ferromagnetic metals is of the order of 1/1000 of the magnetic moment of an ordinary ferromagnetic metal, and should, therefore, be easily detectable. In an external magnetic field  $H$  this moment is (cf. § 4) superposed by the ordinary moment  $\chi H V$  due to the ordinary magnetic susceptibility  $\chi$  of the metal. In a normally diamagnetic metal, as Cs or Cu, there exists, therefore, a field strength where the nuclear ferromagnetism and the ordinary diamagnetism just cancel. These fields are of the order of  $10^6$  G, so that under normal conditions the nuclear ferromagnetism is preponderant.

In the application of the magnetic cooling method, it is important that the time  $\tau$  which a nuclear spin requires in order to be orientated in the field shall be of a reasonable order of magnitude. This is actually the case. According to § 5,  $\tau$  is given by  $1/w$ .  $w$  decreases with increasing temperature. Its lower limit for  $T \rightarrow 0$  is given by equation (23). In a field of  $10^4$  G, this leads for Cu to an *upper limit* of about 1 sec. for  $\tau$ , an order of magnitude already derived by Heitler and Teller (1936) for a temperature of  $0.1^\circ$ .

In conclusion we should like to thank Professor F. Simon, Dr N. Kürti and Dr H. Kuhn for many interesting discussions.

## SUMMARY

In connexion with the possible use of nuclear magnetism for the magnetic cooling method, the behaviour of the nuclear spins of monovalent metals at very low temperatures is investigated theoretically. It is shown that, owing to the interaction between the nuclear spins and the conduction electrons, the nuclei of most monovalent metals should become ferromagnetic at temperatures of the order of  $10^{-6}$  degree. The Curie temperature  $\theta$  for this nuclear ferromagnetism is approximately given by

$$k\theta \sim \frac{1}{8} \frac{\epsilon^2}{\zeta}$$

where  $\epsilon$  is the hyperfine structure splitting of the free atom, and  $\zeta$  is the energy region occupied by the conduction electrons. Temperatures of this order of magnitude should be attainable by an application of the magnetic cooling method.

## REFERENCES

- Bethe, H. 1933 *Handb. d. Physik*, 2nd ed. **24/1**, 385.  
 Elliott, R. M. and Wulff, J. 1939 *Phys. Rev.* **55**, 170.  
 Fröhlich, H. 1936 *Elektronentheorie der Metalle*. Berlin.  
 Fuchs, K. 1935 *Proc. Roy. Soc. A*, **151**, 585.  
 Gorter, C. J. 1934 *Phys. Z.* **35**, 928.  
 Heitler, W. and Teller, E. 1936 *Proc. Roy. Soc. A*, **155**, 629.  
 Jackson, D. A. and Kuhn, H. 1937 *Proc. Roy. Soc. A*, **158**, 372.  
 — — 1939 *Proc. Roy. Soc. A*, **173**, 278.  
 Kürti, N. and Simon, F. 1935 *Proc. Roy. Soc. A*, **149**, 152.  
 Simon, F. 1939 *Report on the Strasbourg Conference on Magnetism*.  
 Stoner, E. C. 1934 *Magnetism and Matter*. London.  
 Tolanski, S. and Forester, G. O. 1938 *Proc. Phys. Soc.* **50**, 826.



# The determination of the lifetime of active polymeric molecules

BY T. T. JONES AND H. W. MELVILLE

*Colloid Science Laboratory, Cambridge*

(Communicated by Eric K. Rideal, F.R.S.—Received 26 February 1940)

In all homogeneous reactions the velocity is determined by the concentration of active or activated molecules which participate in the rate-determining step. If the nature and reactivity of such molecules are determined it may be said that the mechanism of the reaction is completely established. With one or two exceptions, however, this state of affairs is yet to be reached in chemical kinetics. Polymeric reactions are in this respect even in a less advanced stage of development. As with ordinary chain reactions the expression for the overall velocity contains at least three characteristic coefficients relating to the three main processes controlling the rate. By a straightforward kinetic analysis, no matter how accurate and detailed it may be, it is not possible to determine the individual values of such coefficients. In some of the photochemical reactions it has been practicable to find independently the rate of starting of polymerization or the chain length which means in effect that the ratio of the propagation and termination coefficients may be computed. But there is no way in which the individual value of either of these coefficients may be measured. It is the purpose of this paper to suggest one method how this general problem in polymerization may be approached.

In the simplest possible way the velocity of polymerization ( $R$ ) is given by the equation

$$R = \Sigma k_p(P)(M),$$

where  $P$  is the active molecule which reacts with the monomer to make the next highest polymer in the series,  $k_p$  is the corresponding velocity coefficient, and  $\Sigma$  means that all possible kinds of  $P$  molecules must be taken into account. A first approximation in the study of these reactions thus consists in determining  $\Sigma(P)$ . There are, however, no reactions which  $P$  may undergo which could be compared with the polymerization reaction itself in order that the value of  $(P)$  may be computed. Thus the method so useful when hydrogen atoms are involved, namely the measurement of the

simultaneous conversion of para-hydrogen, cannot be employed. The value of  $(P)$  may, however, be defined in another way, namely

$$\frac{d(P)}{dt} = \frac{(P)}{\tau},$$

where  $\tau$  is the mean lifetime of  $(P)$  and  $d(P)/dt$  is the rate of production. If this latter quantity can be determined then  $(P)$  may be computed if some method of measuring  $\tau$  is available.  $d(P)/dt$  is not easy to determine, but in some sufficiently simple photo-polymerizations in the gas phase its value may be calculated from the number of quanta absorbed by the system and the efficiency of the primary process in starting off polymerization. As in many photo-reactions the lifetime of the active species is too short to attempt to measure  $\tau$  directly by observing the rate of polymerization when the light or source of primary activation is suddenly removed. A method of integrating a large number of such decay periods can be devised if a rotating sector is interposed between reaction vessel and source of light. This in itself is not sufficient. But if the decrease in the value of the concentration of  $P$  is due to reaction involving two  $P$  molecules, as, for example, in the combination of free radicals, then it can easily be shown that the velocity of polymerization will depend on the sector speed. A transition between two extreme velocities (in which the ratio is  $\sqrt{2}:1$ ) occurs within a comparatively small speed interval which gives almost directly the lifetime of  $P$  (Melville 1937). This method has of course the disability that it will only work provided  $P$  disappears at a rate proportional to  $(P)^2$ . Another disadvantage of the rotating sector method is that it is confined to a comparatively limited range of measurements, *ca.*  $10^{-4}$  to  $10^{-1}$  sec. The former limit is obviously fixed by mechanical considerations but in any case such short lived molecules are rarely encountered in kinetics. The upper limit is not so seriously handicapped.

#### EXPERIMENTAL

The following method has therefore been devised to extend the technique and provide a complementary means of determining lifetimes of short-lived activated molecules. Suppose again that the active molecules disappear by mutual reaction, then, if two beams of light of equal intensity separated by a considerable distance are admitted to a reaction vessel, the velocity of the reaction when the two are switched on simultaneously will be equal to the sum of the two when each is operating separately. If, however, the beams are superimposed the rate will, in virtue of the fact that it varies with the square root of the intensity, only be  $\sqrt{2}$  times of that due to each beam

acting individually. As the distance between the beams is increased there will thus be a gradual increase in velocity to  $\sqrt{2}$  times the superimposed value. The distance at which the rate will possess an intermediate value of  $\frac{1+\sqrt{2}}{2}$  will therefore be some measure of the distance which the active poly-

mers diffuse in space, which in turn is connected with their mean lifetime.

That such an effect can actually be observed may be demonstrated most conveniently by making use of the photo-polymerization of methyl acrylate in which at pressures of the order of 50 mm. the predominant termination mechanism is by mutual combination of the active polymers. The experimental arrangement is similar to that used in previous experiments (Melville 1938). In order to get a sufficient intensity of irradiation the optical definition of the beam of light could not unfortunately be made very precise. In this reaction if narrow well-defined beams are employed the chain length becomes so long that mutual interference is observed in vessels as long as the mercury lamp itself, *ca.* 20 cm., and thus the method cannot then be used.

In front of the reaction vessel there is placed a sheet of aluminium pierced with squares of 1 cm.<sup>2</sup>, the distance of the centres apart being 1.35, 3.00 and 7.25 cm. Between the lamp and reaction vessel is a silica tube filled with acetic acid to act as a filter and cylindrical lens. Experiments were then performed by using two apertures at a time. It is difficult to obtain uniformity of output along the length of the arc, and therefore the following procedure was adopted. Runs were made with each aperture separately and then together. If  $\tau_A^{-1}$ ,  $\tau_B^{-1}$  and  $\tau_{A+B}^{-1}$  are the respective half-lives of the methyl acrylate under these conditions, then (a) if there is no interference

between the two beams  $\frac{\tau_A^{-1} + \tau_B^{-1}}{\tau_{A+B}^{-1}} = 1$ , (b) if there is complete interference

$$\frac{\tau_A^{-1} + \tau_B^{-1}}{\tau_{A+B}^{-1}} = \frac{\sqrt{\alpha + 1}}{\sqrt{(\alpha + 1)}}$$

where  $\alpha$  is defined by  $\alpha = \left(\frac{\tau_B}{\tau_A}\right)^2$ . If, however, there is not complete interference, the fraction  $Z$  observed will be given by

$$\begin{aligned} Z &= \frac{\frac{\tau_A^{-1} + \tau_B^{-1}}{\tau_{A+B}^{-1}} - 1}{\frac{\sqrt{\alpha + 1}}{\sqrt{(\alpha + 1)}} - 1} \\ &= \frac{(\tau_A^{-1} + \tau_B^{-1} - \tau_{A+B}^{-1}) \tau_{A+B} (\tau_A^2 + \tau_B^2)^{\frac{1}{2}}}{(\tau_A + \tau_B)} \end{aligned}$$

The results are given in table 1.

TABLE 1. TEMP. 20° C. PRESSURE OF METHYL ACRYLATE 43 MM.

| Distance between<br>apertures cm. | $\tau_A^*$ | $\tau_B$ | $\tau_{A+B}$ | $Z$  |
|-----------------------------------|------------|----------|--------------|------|
| 0                                 | 20         | 20       | 14.2         | 1.00 |
| 1.35                              | 20         | 16       | 13           | 1.16 |
| 3.00                              | 20         | 14       | 8.5          | 0.07 |
| 7.25                              | 20         | 15       | 8.0          | 0.00 |

\*  $\tau$  is given in min.

As will be seen from figure 1, where the percentage interference is plotted as a function of distance, there is a transition about 2.4 cm. The next problem is to consider what relationship this mid-point and therefore diffusion time bears to the mean lifetime of the active polymer.

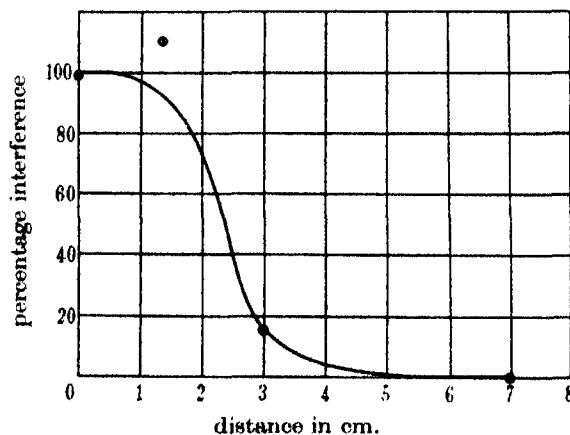


FIGURE 1. Variation of rate of polymerization with slit separation.

#### THE CORRESPONDING CASE FOR THE INTERACTION OF HYDROGEN ATOMS

The only way in which to obtain a check on this interference method is to take a system in which all the various factors are known such as diffusion coefficients, probability of combination, mean lifetime, and attempt to calculate the mean lifetime by the two independent methods. The only system which is at all suitable for this purpose concerns the production and removal of hydrogen atoms in an atmosphere of molecular hydrogen. In order to get conditions somewhat similar to those existing in photo-polymerization it will be supposed that hydrogen atoms are produced by the mercury-sensitized decomposition of hydrogen molecules. The light is supposed to enter the system in beams of which the width is considerably

smaller than the interference distance. It will also be assumed that the hydrogen atoms so generated are in thermal equilibrium with hydrogen molecules. This will not be so when the atoms are first produced, since the excitation of the mercury atom is 19 kcal. greater than the dissociation energy of hydrogen. But in any system in which a large number of binary collisions occur before the atom or radical reacts any such excess will soon be dissipated. Actually in this method to be described this factor will simply have the effect of increasing the effective width of the beams of light entering the reaction vessel.

The first question to be considered is how it is possible to construct a distribution curve of the hydrogen atom pressure spreading from a zone where the hydrogen atom pressure is assumed to be  $10^{-3}$  mm. This latter value is chosen because it is about the maximum easily obtainable by photochemical methods. It also gives atoms a reasonable chance of combining in ternary collisions. The method of obtaining the form of the distribution curve is not quite a straightforward problem in diffusion, for the atoms recombine in ternary collisions and also at the walls of the reaction vessel. The ratio of the velocity of these two reactions varies with hydrogen atom concentration, and hence it is most convenient to divide the reaction vessel into a number of finite zones and calculate what happens in each zone. In this way the necessary differential equations may be constructed. This method of finite zones is employed, since if the theory is subsequently extended to deal with polymerization in which allowance must be made for the increasing size, mass and reactivity of the active polymers, the simple mathematical solution given later for the hydrogen problem may not be applicable. In order to obtain the distribution curve of the hydrogen atom pressure the following figures were employed: Total pressure of hydrogen 760 mm. Temperature  $0^{\circ}$  C. Initial pressure of hydrogen atoms  $10^{-3}$  mm. Probability of three-body collision  $1/1000$  of a two-body collision. Number of binary collisions per sec. at N.T.P.  $1.5 \times 10^{10}$ . Diffusion coefficient for hydrogen atoms in hydrogen molecules at N.T.P. =  $1 \text{ cm.}^2/\text{sec.}$  Consider a zone  $\Delta x$  cm. thick next to the initial zone and let the pressure of hydrogen atoms be  $p_0$  ( $10^{-3}$  mm.). In travelling this distance  $\Delta x$  the time taken by the hydrogen atom is  $\Delta x^2/2D = \Delta x^2/2$  sec. In this time it has suffered  $1.5 \times 10^{10} \Delta x^2/2$  binary collisions with  $\text{H}_2$  and  $\text{H}$ . Hence with hydrogen atoms alone at a pressure  $p_0$  it has suffered  $\Delta x^2/2 \times 1.5 \times 10^{10} \times p_0/760$  collisions. The number of ternary collisions will be  $10^{-3}$  of this. However, once one ternary collision occurs the two hydrogen atoms become a hydrogen molecule, and thus the number of ternary collisions is actually the probability that two hydrogen atoms will combine in travelling the distance

$\Delta x$ . Therefore the probability of a ternary collision of two hydrogen atoms at  $p_0$  with another particle in travelling a distance  $\Delta x$  through hydrogen at 760 mm. is equal to  $\frac{\Delta x^2 p_0 \times 7.5 \times 10^9}{760 \times 10^3} = 9.9684 \Delta x^2 p_0 \times 10^3$ .

If this is the probability of a ternary collision then it is a measure of the decrease of the pressure  $p_0$  and the actual decrease is equal to

$$9.9684 \times 10^3 \Delta x^2 p_0^2.$$

Therefore after traversing the distance  $\Delta x$  the pressure of hydrogen atoms now remaining  $= p_0 - 9.9684 \times 10^3 \Delta x^2 p_0^2$ . Putting  $9.9684 \times 10^3 = K$  const. the pressure  $p_1$  at the end of distance  $\Delta x = (1 - K p_0 \Delta x^2) p_0$ . Now considering the second zone of thickness  $\Delta x$  the time required to traverse this distance is  $\frac{(2\Delta x)^2 - (\Delta x)^2}{2D} = \frac{3\Delta x^2}{2D}$ , and in general the time required to traverse the  $n$ th zone of thickness  $\Delta x$  is  $\frac{(n\Delta x)^2 - (n-1)\Delta x^2}{2D} = \frac{(2n-1)\Delta x^2}{2D}$ . The pressure in the second zone will be  $p_2$  as given above, and so the probability of a ternary collision in this zone will be  $K \cdot 3\Delta x^2 p_2^2$ , and similarly the pressure  $p_3$  at the end of this distance will be  $(1 - 3K p_2 \Delta x^2) p_2$ . In general, therefore, the pressure in any zone  $n$  will be given by  $[1 - (2n-1)K p_{n-1} \Delta x^2] p_{n-1}$ , where  $K = 9.9684 \times 10^3$ ,  $p_{n-1}$  is the pressure in the previous zone and  $\Delta x$  is the thickness of the zone, or

$$\frac{p_n - p_{n-1}}{\Delta x} = -(2n-1) K \Delta x p_{n-1}^2.$$

Since  $n\Delta x = x$ , then in the limit

$$\frac{dp}{dx} = -2Kxp^2.$$

Therefore

$$p = \frac{p_0}{1 + Kx^2 p_0}.$$

This equation is only valid provided combination occurs exclusively in the gas phase.\*

#### CORRECTION FOR WALL COMBINATION

The above calculations, however, refer to an ideal system rarely met with in practice, since the walls of the vessel afford a means of recombination, and indeed if hydrogen atoms combine exclusively at the walls then the

\* The authors thank Dr N. B. Slater for helpful discussions in connexion with these diffusion problems.

hydrogen pressure would vary as the first power of the intensity. This again is an extreme case and only observed at very low hydrogen atom and hydrogen molecule pressures. In a typical practical case where the hydrogen atom pressure is of the order of  $10^{-3}$  mm. the exponent lies between these two extremes. In a similar reaction involving deuterium atoms (Melville and Bolland 1937) the concentration was  $1.04 \times 10^{-10}$  g. mol. cm.<sup>-3</sup> or  $1.77 \times 10^{-3}$  mm., where the intensity exponent for the rate of production of deuterium atoms—as measured by the rate of an exchange reaction—was 0.64. This means that recombination of deuterium atoms took place both in the gas and at the walls of the vessel. From this it is possible to derive an expression  $P = (1-x)/x$  relating the fraction  $P$  of deuterium atoms recombining in the gas phase with the intensity exponent  $x$  indicated above. When the exponent is a half  $P = 1$ , and recombination occurs exclusively in the gaseous phase, while if the exponent rises to unity  $P = 0$ , and recombination occurs at the walls exclusively. Further, a relation may be derived between  $P$ ,  $x$  and  $(D)$  giving

$$P = \frac{1-x}{x} = \frac{2k_5(D)}{k_4 + 2k_5(D)},$$

where  $k_4$  and  $k_5$  are wall-combination and gas-combination coefficients respectively, i.e.

$$(D) = \frac{k_4(1-x)}{2k_5(2x-1)} = \frac{K(1-x)}{(2x-1)}.$$

From the practical values for  $(D)$  and  $x$  given above a value for  $K$  is obtained and so a relation between concentration of deuterium atoms and  $x$  and thus  $P$  is obtained, i.e.

$$(D) = 0.81 \times 10^{-10} (1-x)/(2x-1) \text{ g. mol. cm.}^{-3},$$

or

$$P = \frac{(D)}{1.379 \times 10^{-3} + (D)},^*$$

where  $(D)$  is expressed in mm. This equation thus gives the relation between the fraction of atoms combining in the gas phase and the pressure of deuterium atoms and therefore may be used for the present calculations with hydrogen atoms. It is seen that when the hydrogen atom pressure is high  $P$  tends to unity, that is, combination occurs mostly in the gas; while if  $(H)$  is small  $P = 0$  and recombination occurs at the walls. In the above

\* The constant in this equation is of course dependent wholly on the experimental conditions and the value taken here is merely an actual illustrative example. This, however, as will be seen later, does not alter the conclusions derived from subsequent calculations.

calculations the probability of recombination in the gaseous phase was worked out. To this probability must now be added the probability of combination at the walls. It is clear that if the probability of combination in the gas in a certain zone is  $x$  then the probability of combination at the walls in that same zone is  $\frac{(1-P)x}{P}$ , and so the total probability of combination in that zone is

$$\left(1 + \frac{1-P}{P}\right)x = \frac{x}{P}.$$

Hence the pressure in any zone is now given by

$$\left[1 - \frac{(2n-1)Kp_{n-1}\Delta x^2}{P}\right]p_{n-1} = [1 - (2n-1)K\Delta x^2(1.379 \times 10^{-3} + p_{n-1})]p_{n-1}.$$

On rearranging this equation

$$\frac{p_n - p}{\Delta x} = -2nK\Delta x(c + p_{n-1})p_{n-1} + K\Delta x(c + p_{n-1})p_{n-1},$$

where  $c = 1.379 \times 10^{-3}$  mm.

When  $\Delta x \rightarrow 0$  the second term can be neglected, and therefore putting  $n\Delta x = x$

$$\frac{dp}{dx} = -2Kx(c + p)p$$

or

$$\frac{p}{c+p} = \frac{p_0}{c+p_0} e^{-cKx^2}.$$

The value of  $p$  as a function of  $x$  is shown in table 2. In order to demonstrate the efficacy of the method of using the zone technique the results obtained by this method are also given in table 2. The procedure here consisted in finding the pressures at different distances from the origin, using zones of different thicknesses and calculating each pressure by using the value found for the pressure in the previous zone. The pressure at a given distance from the origin is then plotted against thickness of the zone and the curve so obtained extrapolated to zero zone thickness. The accuracy of the extrapolation is shown by a typical curve in figure 2 for a distance 1.5 mm. from the origin. At 3.5 mm. it can be seen that the extrapolation becomes uncertain because of the increasing differences between the pressures calculated with different zone thicknesses. This is due to the fact that the pressure for any zone thickness is obtained by using the pressure



in the previous zone and not the "true" extrapolated pressure. It is necessary therefore to use the "true" extrapolated pressure for 3.5 mm., namely,  $1.1870 \times 10^{-4}$  mm., as the previous pressure for all zones in calculating the pressure in the next zone. The pressure now is getting small and so there is no need to use  $\frac{1}{8}$  mm. zones.

TABLE 2. HYDROGEN ATOM PRESSURES AT DIFFERENT DISTANCES ( $\times 10^4$ )

| Thickness of<br>zone (mm.) ... | $\frac{1}{8}$ | $\frac{1}{4}$ | $\frac{1}{2}$ | $\frac{1}{16}$ | Extra-<br>polated<br>value<br>of ( <i>H</i> ) | Calculated<br>value<br>of ( <i>H</i> ) |
|--------------------------------|---------------|---------------|---------------|----------------|---|--|
| Distance from<br>origin        |               |               |               |                |   |  |
| 0.5                            | 9.4131        | 9.4222        | 9.4292        | 9.4329         | 9.4369  | 9.4367                                 |
| 1.0                            | 7.7966        | 7.8965        | 7.9448        | 7.9680         | 7.9903  | 7.9942                                 |
| 1.5                            | 5.7205        | 5.9687        | 6.0789        | 6.1307         | 6.1807  | 6.1804                                 |
| 2.0                            | 3.7930        | 4.1489        | 4.3047        | 4.3779         | 4.4487  | 4.4482                                 |
| 2.5                            | 2.3122        | 2.6912        | 2.8604        | 2.9407         | 3.0187  | 3.0182                                 |
| 3.0                            | 1.3018        | 1.6391        | 1.7962        | 1.8701         | 1.9416  | 1.9432                                 |
| 3.5                            | 0.6717        | 0.9363        | 1.0649        | 1.1270         | 1.1870  | 1.1917                                 |
| 4.0                            | 0.5291        | 0.6255        | 0.6599        | —              | 0.6805  | 0.6899                                 |
| 4.5                            | 0.2111        | 0.3062        | 0.3443        | —              | 0.3729  | 0.3786                                 |
| 5.0                            | 0.0769        | 0.1377        | 0.1676        | —              | 0.1977  | 0.1958                                 |
| 5.5                            | 0.0216        | 0.0564        | 0.0757        | —              | 0.0969  | 0.0952                                 |
| 6.0                            | 0.0047        | 0.0208        | 0.0316        | —              | 0.0453  | 0.0433                                 |
| 6.5                            | 0.0007        | 0.00686       | 0.0121        | —              | 0.0195  | 0.0185                                 |
| 7.0                            | 0.00006       | 0.0020        | 0.00426       | —              | 0.00781                                       | 0.00737                                |

The agreement between the figures in columns 6 and 7 is so good that the use of the zone technique is fully justified. The hydrogen atom pressure distribution curve is shown in figure 3.

#### THE INTERFERENCE BETWEEN TWO ZONES CONTAINING HYDROGEN ATOMS

The problem now is to employ this distribution curve for one slit so as to obtain the overall concentration of hydrogen atoms in a system with two slits at varying distances apart. Reverting once more to the ideal case where there is no wall recombination and an intensity exponent of 0.5, it is seen that with two slits superimposed the total hydrogen atom concentration will be  $\sqrt{2}$  times that with one slit, while when the slits are far apart it will be twice. This result is to be expected and can actually be obtained graphically employing a distribution curve for one slit in the following manner.

Let  $ABC$  (figure 4) be the distribution curve for a single slit. If now two slits are superimposed, the pressure at the origin will be  $\sqrt{2}$  times that for one slit, i.e.  $OG$ . Taking the value of the pressure  $OB$  as unity, a curve  $FGH$  can be

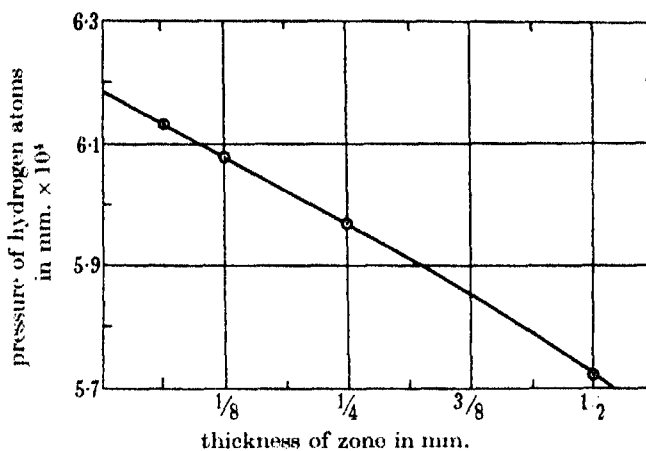


FIGURE 2. Variation of hydrogen atom pressure with zone thickness.

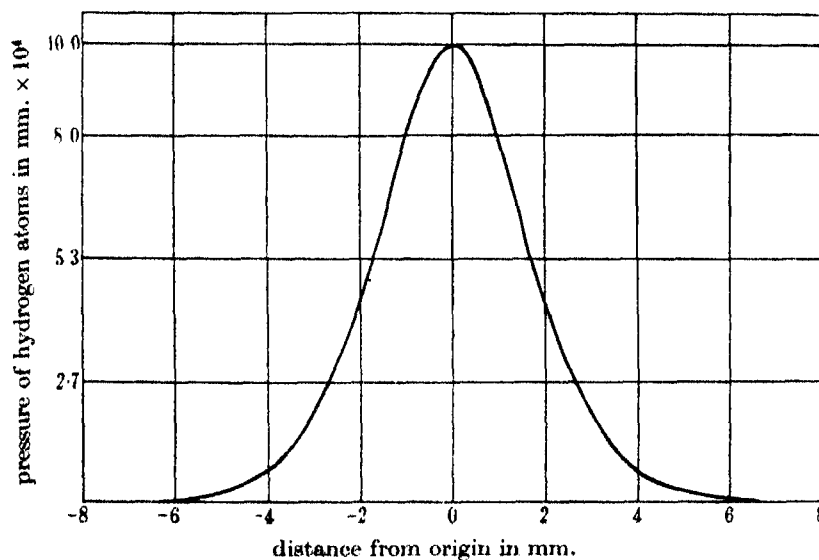


FIGURE 3. Distribution of hydrogen atom pressure as a function of distance.

constructed by doubling the ordinates of the curve  $ABC$  and taking the square root. When the slits are far apart then the ordinates of  $ABC$  are not now doubled but their square root is taken and so the curve  $DBE$  is obtained

and also a similar one at a great distance away. The total hydrogen atom concentration is represented by the area under these derived curves and, since the ratio of any ordinate of  $FGH$ , for example  $XZ$ , to the corresponding

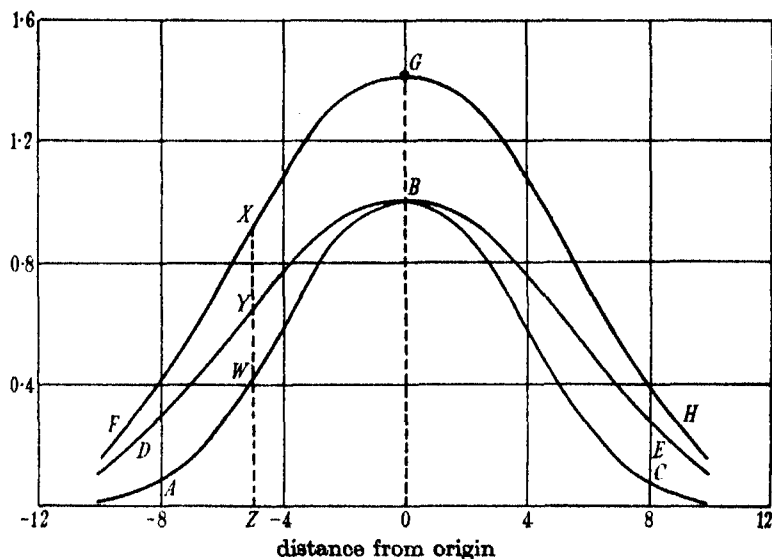


FIGURE 4. To explain formation of derived curves.

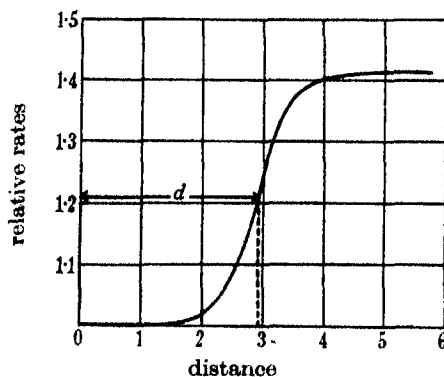


FIGURE 5. Variation of rate of reaction with slit separation.

ordinate  $YZ$  of  $DBE$  is  $\sqrt{(2WZ)}/\sqrt{(WZ)}$ , i.e.  $\sqrt{2}$ , it follows that the area under  $FGH$  (slits together) to the area under two  $DBE$  curves (slits far apart) is  $\sqrt{2}/2$  as required. What the above procedure involves is the addition of the ordinates of two superimposed  $ABC$  curves at different distances apart and then taking the square root of the result and deriving new curves

of the type *FGH* and *DBE* which are the extreme cases. The relative area under these new derived curves will then give the relative hydrogen atom concentrations and if the same procedure is adopted for different distances apart of the slits a curve like the one given in figure 5 is obtained. The distance  $d$ , where the ratio of the areas is  $(\sqrt{2} + 1)/2$ , may be taken as the distance traversed in the mean lifetime or at least it is a function of this distance. The problem is next to extend this treatment to the practical case where the exponent varies with hydrogen atom pressure and to find how the distance  $d$  as defined above is related to the same distance derived in another way to be detailed later.

The extension of the above treatment to the distribution curve already obtained consists in superimposing two such curves with their centres at different distances apart—corresponding to different distances apart of the slits—and adding the ordinates. From this new pressure the corresponding exponent could be found from a curve built up from the equation

$$(H) = 1.379 \times 10^{-3} \frac{(1-x)}{(2x-1)} \text{ mm. Hg,}$$

which connects hydrogen atom pressure and exponent. The figure found for the sum of ordinates was raised to the power of the exponent and then this new figure formed one point on the new derived curve. Many such curves were constructed (figure 6) and illustrative data for the conditions when the slits are 6 mm. apart are given in table 3. The areas under these curves are obtained by a planimeter and the ratio of these several areas to the area with the slits superimposed is plotted against the distance between the slits. The result is shown in figure 7, where the mid-point is seen to lie at a separation of 3 mm.

This distance  $x$  is related to the lifetime  $\tau$  of the hydrogen atom by the equation  $x^2 = 2D\tau$  and can be obtained in another way from the hydrogen atom distribution curve. It is therefore now necessary to see what relationship exists between these lifetimes so defined. In the normal way the mean life of the hydrogen atom is defined by the equation

$$\frac{d(H)}{dt} = \frac{(H)}{\tau},$$

where  $(H)$  is the total hydrogen atom concentration and  $d(H)/dt$  is the rate of production of atoms. This latter quantity would be equal to  $k_t(H)^2(H_2)$  if all the atoms combined in the gas.  $k_t$  has the value  $13 \times 10^{15} \text{ cm.}^6 \text{ sec.}^{-1} \text{ mol.}^{-2}$  (Steiner 1935). Hence

$$\tau = \frac{1}{k_t(H)(H_2)}.$$

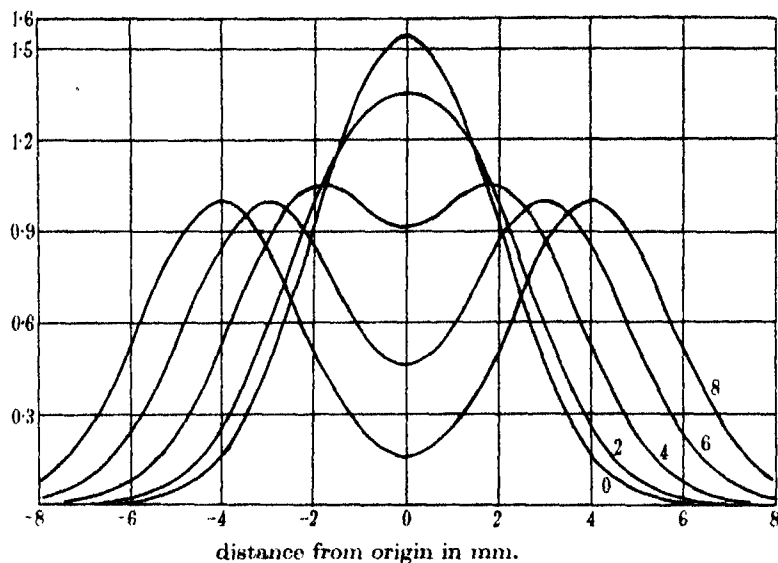


FIGURE 6. Series of derived curves as a function of separation of slits.  
Numbers on curves refer to separation of slits in mm.

TABLE 3. SLITS 6 MM. APART

| Distance<br>between<br>slits<br>mm. | Pressure due to                    |                                     | Sum    | Exponent<br>$\alpha$ | (Sum) <sup>2</sup> |
|-------------------------------------|------------------------------------|-------------------------------------|--------|----------------------|--------------------|
|                                     | First slit<br>(mm. $\times 10^3$ ) | Second slit<br>(mm. $\times 10^3$ ) |        |                      |                    |
| 0                                   | 0.1942                             | 0.1942                              | 0.3884 | 0.820                | 0.4604             |
| 0.5                                 | 0.1187                             | 0.3019                              | 0.4206 | 0.810                | 0.4958             |
| 1.0                                 | 0.0681                             | 0.4449                              | 0.5130 | 0.801                | 0.5859             |
| 1.5                                 | 0.0373                             | 0.6181                              | 0.6554 | 0.783                | 0.7185             |
| 2.0                                 | 0.0198                             | 0.7990                              | 0.8188 | 0.729                | 0.8644             |
| 2.5                                 | 0.0097                             | 0.9437                              | 0.9534 | 0.710                | 0.9668             |
| 3.0                                 | 0.0045                             | 1.0000                              | 1.0045 | 0.704                | 1.0030             |
| 3.5                                 | 0.0020                             | 0.9437                              | 0.9457 | 0.711                | 0.9610             |
| 4.0                                 | 0.0008                             | 0.7990                              | 0.7998 | 0.732                | 0.8489             |
| 4.5                                 | 0.0003                             | 0.6181                              | 0.6184 | 0.764                | 0.6931             |
| 5.0                                 | 0.0001                             | 0.4449                              | 0.4450 | 0.804                | 0.5214             |
| 5.5                                 | ---                                | 0.3019                              | 0.3019 | 0.848                | 0.3621             |
| 6.0                                 | ---                                | 0.1942                              | 0.1942 | 0.890                | 0.2325             |
| 6.5                                 | ---                                | 0.1187                              | 0.1187 | 0.927                | 0.1388             |
| 7.0                                 | ---                                | 0.0681                              | 0.0681 | 0.954                | 0.0709             |
| 7.5                                 | ---                                | 0.0373                              | 0.0373 | 0.974                | 0.0406             |
| 8.0                                 | ---                                | 0.0198                              | 0.0198 | 0.984                | 0.0209             |
| 8.5                                 | ---                                | 0.0097                              | 0.0097 | 0.994                | 0.0100             |
| 9.0                                 | ---                                | 0.0045                              | 0.0045 | 0.998                | 0.0046             |
| 9.5                                 | ---                                | 0.0020                              | 0.0020 | 0.999                | 0.0020             |
| 10.0                                | ---                                | 0.0008                              | 0.0008 | 1.0                  | 0.0008             |
| 10.5                                | ---                                | 0.0003                              | 0.0003 | 1.0                  | 0.0003             |
| 11.0                                | ---                                | 0.0001                              | 0.0001 | 1.0                  | 0.0001             |

This, however, neglects wall combination, the extent of which is dependent on  $(H)$ , and for the particular case treated here is defined by the equation

$$P = \frac{(H)}{1.379 \times 10^{-3} + (H)}.$$

To the rate of combination in the gas computed from  $k_t(H)^2(H_2)$  must therefore be added a fraction  $(1 - P)/P$  of it. This addition has to be carried out for each zone on account of the variation of hydrogen pressure. Hence

$$\begin{aligned} \frac{(H)}{\tau} &= \Sigma \left[ k_t(H)^2(H_2) + \frac{1-P}{P} k_t(H)^2(H_2) \right] \\ &= \Sigma \frac{1}{P} [k_t(H)^2(H_2)]. \end{aligned}$$

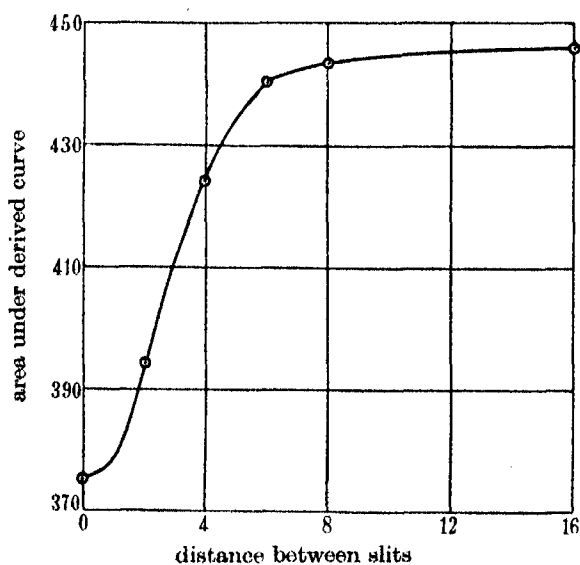


FIGURE 7. Area under derived curves of figure 6 as a function of slit separation.

The mean hydrogen atom pressure is defined by the equation

$$(\bar{H}) = \frac{\int (H) dd}{\int dd},$$

in which the variation of  $(H)$  with  $d$  is given by the distribution curve in figure 3. In order to obtain the value of  $\Sigma \frac{1}{P} [k_t(H)^2(H_2)]$  zones of thickness

of  $\frac{1}{4}$  and  $\frac{1}{2}$  mm. were taken and the mean hydrogen atom concentration in each zone taken from the distribution curve. Values for  $\frac{1}{P}[k_i(H)^2(H_2)]$  were worked out for each zone and finally multiplied by the thickness  $\Delta d$  of the zone. These values were then summated and divided by  $\Sigma \Delta d = \int dd$ . The value of  $\tau$  was then computed from the equation

$$\tau = \frac{\int (H) dd \left( \frac{\Sigma \frac{1}{P}[k_i(H)^2(H_2) \Delta d]}{\Sigma \Delta d} \right)^{-1}}{\int dd}$$

Table 4 gives the significant data for these calculations.

#### APPLICATION OF HYDROGEN ATOM CALCULATIONS TO POLYMERIZATION

The calculations concerning the methyl acrylate reaction can now be completed. With the slits 1 and 2 in operation  $1.7 \times 10^{17}$  mol. polymerize per second in a volume of 100 c.c., the number of quanta absorbed being  $3 \times 10^{15}$  per sec. But since the efficiency of the primary process is 0.3, the chain length is about 170. The average molecular weight may therefore be taken as  $85 \times 86 = 7300$ . Nothing is known about the diffusion coefficients of molecules of this size, but since the dimensions of such molecules are smaller than their mean free paths the ordinary diffusion theory will be applicable. In computing the diffusion coefficient it has been assumed that the shape of the molecule in the gas phase is spherical. The diffusion coefficient of methyl acrylate itself at 40 mm. is by analogy with molecules of similar mass and dimensions computed to be  $1.9 \text{ cm.}^2 \text{ sec.}^{-1}$ . The mean diffusion coefficient of the polymer may therefore be taken as  $(W_1/W_2)^{\frac{1}{2}}$  times this quantity, where  $W_1$  and  $W_2$  are the molecular weights of monomer and polymer respectively since the reduced mass factor in the diffusion equation is not much affected by molecular size. The diffusion coefficient of the polymer through the monomer is thus  $0.21 \text{ cm.}^2 \text{ sec.}^{-1}$ . Making use of the fact, established for hydrogen atoms, that the mean life is given by a diffusion distance of half that fixed by the mid-point in the interference curve yields a mean lifetime for the polymer of 1.8 sec. Since the chain length is 170 the average time between fruitful collisions with monomer will be  $1.1 \times 10^{-2} \text{ sec.}$  Assuming that a methyl acrylate molecule would make  $5 \times 10^8 \times 1.1 \times 10^{-2} = 5 \times 10^6$  collisions in this period then on account of its greater diameter a polymer molecule will make  $(W_2/W_1)^{\frac{1}{2}}$  or about 9 times as many collisions,

i.e.  $4.5 \times 10^7$ . The mean energy of activation for growth of the methyl acrylate molecules is 4000 cal. For a normal bimolecular reaction the collision efficiency would be  $\exp(-4000/RT)$  or  $1.5 \times 10^{-3}$ . The steric factor is thus  $1.7 \times 10^{-5}$ . Thus it will be seen that in a chain polymerization the steric factor is of a similar order of magnitude to those obtained in

TABLE 4. CALCULATION OF THE MEAN LIFE OF THE  
H ATOM FROM THE DISTRIBUTION CURVE

$k_t(\text{H}_2) 5.803 \times 10^{11} \text{ CM.}^3 \text{ SEC.}^{-1} \text{ G.MOL.}^{-1} \text{ 1 MM.} \equiv 5.874 \times 10^{-8} \text{ G.MOL./C.C.}$

| No. of zone | Thickness of zone $d$<br>mm. | Mean conc. of H<br>in zone<br>mm. | $P$      | $\frac{\Delta dk_t(\text{H}_2) (\text{H})^2}{P}$<br>$\times 10^9$ |
|-------------|------------------------------|-----------------------------------|----------|---|
| 1           | 0.25                         | $9.92 \times 10^{-4}$             | 0.4180   | 1.1775  |
| 2           | 0.25                         | $9.65 \times 10^{-4}$             | 0.4115   | 1.1324  |
| 3           | 0.25                         | $9.12 \times 10^{-4}$             | 0.398    | 1.0460  |
| 4           | 0.25                         | $8.4 \times 10^{-4}$              | 0.3786   | 0.9332  |
| 5           | 0.5                          | $7.1 \times 10^{-4}$              | 0.396    | 1.4919  |
| 6           | 0.5                          | $5.28 \times 10^{-4}$             | 0.2968   | 0.9405  |
| 7           | 0.5                          | $3.68 \times 10^{-4}$             | 0.2106   | 0.6437  |
| 8           | 0.5                          | $2.44 \times 10^{-4}$             | 0.1505   | 0.3965  |
| 9           | 0.5                          | $1.52 \times 10^{-4}$             | 0.0994   | 0.2330  |
| 10          | 0.5                          | $9.2 \times 10^{-5}$              | 0.0625   | 0.1355  |
| 11          | 0.5                          | $5.0 \times 10^{-5}$              | 0.0350   | 0.0715  |
| 12          | 0.5                          | $2.8 \times 10^{-5}$              | 0.0199   | 0.0394  |
| 13          | 0.5                          | $1.39 \times 10^{-5}$             | 0.00998  | 0.0194  |
| 14          | 0.5                          | $6.7 \times 10^{-6}$              | 0.00483  | 0.0093  |
| 15          | 0.5                          | $3.1 \times 10^{-6}$              | 0.00224  | 0.00429   |
| 16          | 0.5                          | $1.27 \times 10^{-6}$             | 0.00092  | 0.00176   |
| 17          | 0.5                          | $4.9 \times 10^{-7}$              | 0.000356 | 0.00068   |
| 18          | 0.5                          | $1.8 \times 10^{-7}$              | 0.00013  | 0.00025   |
| 19          | 0.5                          | $6.0 \times 10^{-8}$              | 0.000043 | 0.00008   |
| 20          | 0.5                          | $2.0 \times 10^{-8}$              | 0.000014 | 0.00003   |

$$\Sigma \Delta d = 9.0$$

$$\frac{\Sigma \Delta dk_t(\text{H}_2) (\text{H})^2}{P} = 8.2769$$

$$\therefore \frac{\frac{\Sigma \Delta dk_t(\text{H}_2) (\text{H})^2}{P}}{\Sigma \Delta d} = \frac{8.2769 \times 10^{-9}}{9} = 0.9197 \times 10^{-9}.$$

$$\text{Area under curve in figure 3} = \int (\text{H}) dd = 20.4 \times 10^{-4}, \int dd = 9.$$

$$\therefore (\text{H}) = 2.265 \times 10^{-4} \text{ mm. or } 1.3305 \times 10^{-11} \text{ g.mol./c.c.}$$

$$(\text{H})/\tau = \frac{\Sigma k_t(\text{H}_2) (\text{H})^2 \Delta d}{\Sigma \Delta d} = 0.9197 \times 10^{-9}.$$

$$\therefore \tau = \frac{1.3305 \times 10^{-11}}{0.9197 \times 10^{-9}} = 1.447 \times 10^{-2} \text{ sec.}$$

$$\therefore x = 1.7 \text{ mm.}$$



bimolecular association reactions (Melville 1939). Having obtained the absolute value of the mean propagation coefficient the stationary concentration of the active polymer may be computed from the equation

$$-\frac{d(M)}{dt} = k_p(P)(M) = (M) \frac{k_p}{k_t}(I)^{\frac{1}{2}}.$$

The relevant values are:

$$d(M)/dt = 2.8 \times 10^{-7} \text{ g.mol. sec.}^{-1}; \quad (M) = 2.2 \times 10^{-6} \text{ g.mol. c.c.}^{-1};$$

$$k_p = 10^9 \times \exp(-4000/RT)^* = 1.3 \times 10^6 \text{ c.c. g.mol.}^{-1} \text{ sec.}$$

Hence  $(P) = 1 \times 10^{-7} \text{ g.mol. c.c.}^{-1}$  or 2 mm.

The above-described method is not necessarily restricted to those reactions in which mutual interference occurs between active polymers. If the distribution of polymer concentration in the unilluminated zone can be measured then the mean life of the active species may be calculated. The measurement of the amount of polymer deposited is a possible method of finding the relative values of the active molecule concentration and has been tentatively employed in working out the mechanism of the mercury sensitized polymerization of acetylene (Melville 1936). At high pressures, however, this technique, and any similar one involving the measurement of the amount of dead polymer formed, fails for, on account of the exothermic character of polymerization, convection currents soon upset any regular distribution of solid polymer in space.

The authors are indebted to Professor E. K. Rideal for his continued interest in these experiments. One of them (T. T. J.) is much indebted to Messrs Bakelite, Ltd., and to the Department of Scientific and Industrial Research for maintenance grants. They also are grateful to the Chemical Society for a grant for apparatus.

#### SUMMARY

A method of determining the distance of diffusion in space of a polymer reaction is described. It depends upon the fact that in a reaction—the direct photo-polymerization of methyl acrylate—in which active molecules mutually destroy each other, this mutual interference may be demonstrated by using two sources of photo-excitation. The velocity of polymerization

\* The value of  $10^9$  in the equation is obtained from the fact that for normal reactions the  $A$ -factor as it is usually called is  $10^{14}$ .

then depends on the distance between the two sources. The exact theory of the method has been worked out for hydrogen atoms. The results obtained from this investigation are applied to the methyl acrylate reaction. This result is then further employed along with previous data to compute the absolute value of the reaction velocity coefficient between active polymer molecules and monomer.

## REFERENCES

- Melville, H. W. 1936 *Trans. Faraday Soc.* **32**, 258.  
— 1937 *Proc. Roy. Soc. A*, **163**, 511.  
— 1938 *Proc. Roy. Soc. A*, **167**, 99.  
— 1939 *Ann. Rep. Chem. Soc.* (in the Press).  
Melville, H. W. and Bolland, J. L. 1937 *Proc. Roy. Soc. A*, **160**, 384.  
Steiner, W. 1935 *Trans. Faraday Soc.* **32**, 623.
-



then depends on the distance between the two sources. The exact theory of the method has been worked out for hydrogen atoms. The results obtained from this investigation are applied to the methyl acrylate reaction. This result is then further employed along with previous data to compute the absolute value of the reaction velocity coefficient between active polymer molecules and monomer.

## REFERENCES

- Melville, H. W. 1936 *Trans. Faraday Soc.* **32**, 258.  
— 1937 *Proc. Roy. Soc. A*, **163**, 511.  
— 1938 *Proc. Roy. Soc. A*, **167**, 99.  
— 1939 *Ann. Rep. Chem. Soc.* (in the Press).  
Melville, H. W. and Bolland, J. L. 1937 *Proc. Roy. Soc. A*, **160**, 384.  
Steiner, W. 1935 *Trans. Faraday Soc.* **32**, 623.
- 

## The pressure of water waves upon a fixed obstacle

By T. H. HAVELOCK, F.R.S.

(Received 29 March 1940)

The diffraction of plane water waves by a stationary obstacle with vertical sides is examined, in particular the variation of amplitude along the sides and the average steady pressure due to the wave motion. Results similar to those in other diffraction problems are obtained for an infinite plane and for cylinders of circular or parabolic section, and approximations are made for sections of ship form. The examination was made in view of possible applications in the problem of a ship advancing through a train of waves, and the results are discussed in relation to the average additional resistance in such circumstances. It appears that the mean pressure obtained on diffraction theory from the second order terms can only account, in general, for a small proportion of the observed effect; the motions of the ship, and in particular its oscillations, are essential factors in the problem.

1. The problem to be considered is the resultant fluid pressure upon an obstacle held in position in a train of plane waves advancing over the surface of the water. In a previous paper (1937) I considered the additional resistance on a ship moving through waves, the work being restricted to the first order effect, a purely periodic force which may have an amplitude comparable with the resistance to the ship in still water; further, for the type of ship considered, the usual approximations were made and these included neglecting the effect of reflected or scattered waves as being of the

second order. One purpose of the present work is to examine that assumption; the approximate method is extended in a certain case to give the variation in amplitude of the surface oscillation along the side of the ship.

The view has been put forward recently that the mean extra resistance to a ship advancing through waves is due to the reflexion of the waves by the sides of the ship, being in fact analogous to the pressure of radiation; it has been stated, for instance, that the resultant amplitude at the bow is about one-third greater, and that at the stern one-third less, than the amplitude of the incident waves, and empirical formulae for the pressure have been constructed on that basis. The problem requires, however, a consideration of second order terms which does not appear to have been made for water waves even in simple cases. We consider total reflexion, normal or oblique, by a plane wall, and diffraction by a cylinder of circular or parabolic section, together with approximations for a section of ship form: the results are discussed in relation to the ship problem.

#### DIFFRACTION OF WATER WAVES

2. Consider a fixed cylindrical obstacle in the water, the sides vertical and extending down to an infinite depth; let  $C$  be the contour of any horizontal cross-section. We suppose plane waves of amplitude  $h$  to be travelling in the negative direction of  $Ox$ ; the origin  $O$  is in the free surface and  $Oz$  is vertically upwards. The velocity potential of the fluid motion is of the form

$$\phi = \frac{gh}{\sigma} e^{i(\sigma t + \kappa x) + \kappa z} + e^{i\sigma t + \kappa z} \phi'(x, y). \quad (1)$$

The pressure condition at the free surface is satisfied, to the usual first order terms, by  $\sigma^2 = g\kappa$ . Further, we have

$$\frac{\partial^2 \phi'}{\partial x^2} + \frac{\partial^2 \phi'}{\partial y^2} + \kappa^2 \phi' = 0, \quad (2)$$

and  $\partial\phi/\partial\nu = 0$  on the contour  $C$ . The potential may be expressed in terms of a source distribution over the surface of the cylinder, but that is, in general, merely a restatement of the problem. We are concerned meantime with an approximate solution when the contour  $C$  is of ship form; that is, we assume  $C$  to be a contour of small breadth compared with its length. We take  $Ox$  in the direction of the length and to be an axis of symmetry of the contour. The approximation is the same as that used in determining the waves produced by a moving ship. We take the source strength at any

point to be determined by the horizontal fluid velocity in the primary motion and by the gradient of the surface at the point. We then replace the obstacle by a plane distribution of sources over the vertical section by the  $zx$ -plane. The primary fluid motion in the present case is that of the plane waves. Thus, if  $(\xi, 0, -f)$  is a point on the vertical section, and if  $\partial y/\partial \xi$  is the gradient at the corresponding point on the contour, the required distribution of sources over the vertical section is of strength per unit area given by

$$-\frac{ikgh}{2\pi\sigma} \frac{\partial y}{\partial \xi} e^{i(\sigma t + \kappa \xi) - \kappa f}. \quad (3)$$

Consider now a point source  $m \cos \sigma t$  in the liquid at the point  $(0, 0, -f)$ . The velocity potential was obtained by Lamb (1922) and we use his result with a slight change of notation. The surface elevation  $\zeta$  is given by  $g\zeta = \partial \phi / \partial t$  with  $z = 0$ ; we have

$$\zeta = \frac{2i\sigma m}{g} e^{i\sigma t} \left\{ \frac{1}{(r^2 + f^2)^{\frac{1}{2}}} - i\pi \kappa e^{-\kappa f} H_0^{(2)}(\kappa r) - \frac{2\kappa}{\pi} \int_0^\infty \int_0^\infty \frac{v \sin fv + \kappa \cos fv}{\kappa^2 + v^2} e^{-vr \cosh u} du dv \right\}, \quad (4)$$

where  $r^2 = x^2 + y^2$ ,  $\kappa = \sigma^2/g$ ,  $H_0^{(2)} = J_0 - iY_0$ , and the real part of the expression is to be taken.

Let there be a vertical line source extending from the origin downwards, the source strength per unit length at depth  $f$  being  $me^{-\kappa f}$ . We substitute this value for  $m$  in (4) and integrate with respect to  $f$  from 0 to  $\infty$ . For the last term in (4) this integration gives

$$\begin{aligned} -\frac{2\kappa}{\pi} \int_0^\infty \int_0^\infty \frac{e^{-vr \cosh u}}{\kappa^2 + v^2} du dv &= -\frac{2\pi}{\kappa} \int_0^\infty \frac{K_0(vr)}{\kappa^2 + v^2} dv \\ &= -\int_0^\infty \frac{e^{-\kappa f}}{(r^2 + f^2)^{\frac{1}{2}}} df. \end{aligned} \quad (5)$$

Hence the terms in (4) which represent the local oscillations disappear from the integrated result for this particular vertical source distribution; and we obtain the simple result

$$\zeta = \frac{\pi\sigma m}{g} e^{i\sigma t} H_0^{(2)}(\kappa r) = \frac{2i\sigma m}{g} \int_0^\infty e^{i(\sigma t - \kappa r \cosh u)} du, \quad (6)$$

representing circular waves diverging from the origin. Returning to (3)

we see that the source distribution is made up of vertical line sources of this type, and we obtain for the complete surface elevation

$$\zeta = ihe^{i(\sigma t + \kappa x)} - \frac{1}{2}i\kappa h e^{i\sigma t} \int H_0^{(2)}(\kappa r) \frac{\partial y}{\partial \xi} e^{i\kappa \xi} d\kappa. \quad (7)$$

In (7), the first term represents the incident waves; further,  $r^2 = (x - \xi)^2 + y^2$ , and the integration extends over the axial length of the form. It should be noted that this result is comparatively simple because we have taken the obstacle to be of infinite draft; for a ship of finite draft there would be terms representing a local surface elevation in addition to the diverging waves from each element. Further, the result is only an approximation and assumes, in fact, that the additional surface elevation is relatively small.

3. We shall apply (7) to one case only, so as to estimate the magnitude of the effect due to the scattering of waves by a narrow ship of great draft and of form similar to those for which previous calculations of wave resistance have been made.

The model is of symmetrical form with straight sides, of total length  $2l$ , beam  $2b$ , and with a parallel middle body of length  $2a$ ; the bow and stern are equal wedges of axial length  $l - a$  and of semi-angle  $\alpha$ , where  $\tan \alpha = b/(l - a)$ . We take the origin at the centre of the axis, with the positive direction of  $Ox$  from stern to bow. Thus we have

$$\begin{aligned} \partial y / \partial \xi &= \alpha, & \text{for } -l < \xi < -a \\ &= 0, & \text{for } -a < \xi < a \\ &= -\alpha, & \text{for } a < \xi < l. \end{aligned} \quad (8)$$

From (7), the surface elevation at any point  $(x, y)$  is given by

$$\zeta = ihe^{i(\sigma t + \kappa x)} - \frac{1}{2}i\kappa h \alpha e^{i\sigma t} \int_{-l}^{-a} H_0^{(2)}(\kappa r) e^{i\kappa \xi} d\xi + \frac{1}{2}i\kappa h \alpha e^{i\sigma t} \int_a^l H_0^{(2)}(\kappa r) e^{i\kappa \xi} d\xi. \quad (9)$$

We shall use this only for the elevation along the axis  $y = 0$ , as in the corresponding calculation of wave profiles for a ship. We note that in these expressions the quantity  $r$  is essentially positive. As an example, for a point in the bow wedge, that is for  $a < x < l$ , we have

$$\begin{aligned} \zeta e^{-i\sigma t} &= ihe^{i\kappa x} - \frac{1}{2}i\kappa h \alpha \int_{-l}^{-a} H_0^{(2)}\{\kappa(x - \xi)\} e^{i\kappa \xi} d\xi \\ &\quad + \frac{1}{2}i\kappa h \alpha \int_a^x H_0^{(2)}\{\kappa(x - \xi)\} e^{i\kappa \xi} d\xi + \frac{1}{2}i\kappa h \alpha \int_x^l H_0^{(2)}\{\kappa(\xi - x)\} e^{i\kappa \xi} d\xi. \end{aligned} \quad (10)$$

These expressions may be evaluated in terms of two integrals which may be shown to have the following values:

$$\int_0^p H_0^{(2)}(u) e^{-iu} du = p e^{-ip} \{H_0^{(2)}(p) + iH_1^{(2)}(p)\} + \frac{2}{\pi}, \quad (11)$$

$$\int_0^p H_0^{(2)}(u) e^{iu} du = p e^{ip} \{H_0^{(2)}(p) - iH_1^{(2)}(p)\} - \frac{2}{\pi}. \quad (12)$$

We shall write (11) as  $L(p) + 2/\pi$ , and (12) as  $M(p) - 2/\pi$ . We also put

$$p_1 = 2\kappa l; \quad p_2 = \kappa(l+a); \quad p_3 = \kappa(l-a); \quad p_4 = 2\kappa a. \quad (13)$$

We select five points at which to make the calculations, the bow, stern, shoulders and amidships; and, in the notation indicated, we have

$$\left. \begin{aligned} \zeta(l) &= i h e^{i(\sigma t + \kappa l)} \left[ 1 - \frac{1}{2} \alpha \left\{ L(p_1) - L(p_2) - L(p_3) - \frac{2}{\pi} \right\} \right], \\ \zeta(a) &= i h e^{i(\sigma t + \kappa a)} \left[ 1 - \frac{1}{2} \alpha \left\{ L(p_2) - L(p_4) - M(p_3) + \frac{2}{\pi} \right\} \right], \\ \zeta(0) &= i h e^{i\sigma t} \left[ 1 - \frac{1}{2} \alpha \left\{ L(\frac{1}{2}p_1) - L(\frac{1}{2}p_4) - M(\frac{1}{2}p_1) + M(\frac{1}{2}p_4) \right\} \right], \\ \zeta(-a) &= i h e^{i(\sigma t - \kappa a)} \left[ 1 - \frac{1}{2} \alpha \left\{ L(p_3) - M(p_2) + M(p_4) + \frac{2}{\pi} \right\} \right], \\ \zeta(-l) &= i h e^{i(\sigma t - \kappa l)} \left[ 1 - \frac{1}{2} \alpha \left\{ M(p_3) - M(p_1) + M(p_2) - \frac{2}{\pi} \right\} \right]. \end{aligned} \right\} \quad (14)$$

We apply these results to Model No. 1144 of the National Physical Laboratory. This was a model of the given form used by Wigley (1931) in comparing calculated and observed wave profiles along the sides of the model when advancing through still water. For the present purpose we suppose the model held at rest while regular plane waves of amplitude  $h$  and wave-length  $2\pi/\kappa$  are moving past it. The dimensions of the model were

$$l = 8 \text{ ft.}; \quad a = 2.19 \text{ ft.}; \quad b = 0.75 \text{ ft.} \quad (15)$$

We calculate only one case, namely, when the wave-length is equal to the total length of the model. Thus, in the notation of (13) we have

$$p_1 = 6.28; \quad p_2 = 4.0; \quad p_3 = 2.28; \quad p_4 = 1.72. \quad (16)$$

We have also  $\alpha = 0.129$ . Using tables of Bessel functions,  $\zeta$  may be calculated from (14). We are not concerned with the phase of the total oscillation at each point, but only with its amplitude. We find the ratio of the amplitude



to that of the incident waves at the points  $x = l, a, 0, -a, -l$  to be 1.05, 1.08, 1.09, 0.99 and 0.95 respectively.

The alteration in amplitude at bow and stern would be greater for a fuller model, and especially for a bluff-ended form. Nevertheless, these approximate calculations confirm the view that for a fine model the modification caused by the reflexion of the incident waves may be treated as a second order correction. It should also be noted that these results are for a model of infinite draft; it may be presumed that the effect would be much smaller for one whose draft is small compared with the wave-length.

4. For a vertical obstacle of infinite draft, we may readily transfer results from other diffraction problems. The effect of a cylinder of elliptic section would be of special interest, but the analytical solution does not lend itself to computation when the wave-length is of the same order as the length of the axis. It is, however, worth while examining briefly two other cases from the present point of view.

Let the cylinder be circular, its water plane section being the circle  $r = a$ . For plane waves of amplitude  $h$  moving in the negative direction of  $Ox$ , the complete solution is given by

$$\phi = (gh/\sigma) e^{i\sigma t + \kappa z} \left\{ J_0(\kappa r) + 2 \sum_1^{\infty} i^n J_n(\kappa r) \cos n\theta \right\} \\ - (gh/\sigma) e^{i\sigma t + \kappa z} \left\{ b_0 H_0^{(2)}(\kappa r) + 2 \sum_1^{\infty} i^n b_n H_n^{(2)}(\kappa r) \cos n\theta \right\}, \quad (17)$$

where

$$\sigma^2 = g\kappa, \quad \text{and} \quad b_n = J_n'(\kappa a)/H_n^{(2)'}(\kappa a).$$

Putting  $r = a$  in the expression for the surface elevation, and reducing by means of relations for the Bessel functions, we obtain on the cylinder

$$\zeta = -\frac{2he^{i\sigma t}}{\pi\kappa a} \left( C_0 + 2 \sum_1^{\infty} i^n C_n \cos n\theta \right), \quad (18)$$

where

$$C_n = 1/H_n^{(2)'}(\kappa a).$$

Computation from this expression, which involves tabulation of  $J_n'^2 + Y_n'^2$ , can be carried out without much difficulty except when  $\kappa a$  is large. A detailed study might be of interest, but for the present purpose the following results suffice to show the variation of amplitude round the cylinder. The numbers in table 1 give the ratio of the amplitude at each point to the amplitude of the incident waves;  $\theta = 0^\circ$  corresponds to the bow and  $\theta = 180^\circ$  to the stern.

TABLE 1

| $\theta$<br>$\kappa a$ | 0°   | 45°  | 90°  | 135° | 180° |
|------------------------|------|------|------|------|------|
| 0.5                    | 1.44 | 1.28 | 0.97 | 0.91 | 1.00 |
| 1.0                    | 1.71 | 1.62 | 1.16 | 0.68 | 0.82 |
| 3.0                    | 1.92 | 1.75 | 1.35 | 0.82 | 0.62 |
| 5.0                    | 1.96 | 1.86 | 1.36 | 0.64 | 0.48 |

5. For the parabolic cylinder we may use the expressions given by Lamb (1906) for the diffraction of sound waves, making the necessary modifications for water waves. In this case we take the plane waves to be moving in the positive direction of  $Ox$ ; the water-plane section of the cylinder is given by

$$\kappa^2 y^2 = 4\eta_0^4 + 4\kappa\eta_0^2 x. \quad (19)$$

In the parabolic co-ordinates defined by  $\kappa(x + iy) = (\xi + i\eta)^2$ , the section of the cylinder is given by  $\eta = \eta_0$ .

The velocity potential of the motion is

$$\phi = (gh/\sigma) e^{i(\sigma t - \kappa x) + \kappa z} \left\{ 1 + C \int_{\eta}^{\infty} e^{-2i\eta^2} d\eta \right\}, \quad (20)$$

where the constant  $C$  is given by

$$2i\eta_0 \left\{ 1 + C \int_{\eta_0}^{\infty} e^{-2i\eta^2} d\eta \right\} - C e^{-2i\eta_0^2} = 0. \quad (21)$$

For the surface elevation on the cylinder, we have

$$\zeta = i h e^{i(\sigma t - \kappa x)} \left\{ 1 + C \int_{\eta_0}^{\infty} e^{-2i\eta^2} d\eta \right\}. \quad (22)$$

It follows that the amplitude of the oscillation is constant round the boundary. From (21) and (22) we find that this amplitude is  $h/p$ , where  $p$  is given by

$$p^2 = 1 + 2\pi^{\frac{1}{2}}\eta_0 \left\{ \left( \frac{1}{2} - c \right) \sin 2\eta_0^2 - \left( \frac{1}{2} - s \right) \cos 2\eta_0^2 \right\} + \pi\eta_0^2 \left\{ \left( \frac{1}{2} - c \right)^2 + \left( \frac{1}{2} - s \right)^2 \right\}, \quad (23)$$

in which  $c$  and  $s$  denote Fresnel integrals of argument  $2\eta_0\pi^{\frac{1}{2}}$ .

From (19) we have  $2\eta_0^2 = \kappa a$ , where  $a$  is the radius of curvature of the parabola at its vertex. Table 2 gives the ratio of the amplitude of the oscillation to that of the incident waves, calculated from (23) for certain values of  $\kappa a$ :

TABLE 2

| $\kappa a$ | 0.05 | 0.1  | 1.0  | 3.0  | 5.0  |
|------------|------|------|------|------|------|
| amp./h.    | 1.28 | 1.40 | 1.65 | 1.86 | 1.93 |

These may be compared with the corresponding values at  $\theta = 0$  for the circular cylinder. When  $\kappa a$  is small, we obtain from (23) the approximate value  $1 + (\pi\kappa a/2)^{\frac{1}{2}}$  for the ratio of the amplitude to that of the incident waves. We may, possibly, use this to give an upper limit for the resultant amplitude at the bow of a ship if we regard the front half of the ship as a parabola with its vertex at the bow. For instance, consider the model examined in § 3. Instead of a wedge-shaped bow, suppose it is rounded off into a parabola with its vertex at the bow and joining on to the parallel middle body at a distance of 5.81 ft. from the bow, the beam at that point being 1.5 ft. With these data, and taking the same wave-length of 16 ft., we find that  $\kappa a = 0.019$ . From the approximate formula, this gives a relative amplitude at the bow of 1.17. Comparing with the previous calculations, this seems a reasonable estimate, in spite of the various assumptions; the ratio would, of course, be greater for smaller wave-lengths.

#### THE PRESSURE OF WATER WAVES

6. For the resultant pressure upon the obstacle, the first order effect is a purely periodic force with zero mean value; this was the effect considered in the previous paper (1937) and applied to a ship among waves. To obtain a steady mean force different from zero we have to proceed to second order terms; although much work was done at one time on the pressure of vibrations, water waves do not seem to have been considered in this connexion.

We begin with plane waves, and the only general result we need is that given by Rayleigh (1915), that the usual first order expression for the velocity potential is also correct to the second order, the next term being of the third order; this was shown to be the case both for progressive waves and for stationary oscillations. There are, however, second order terms in the surface elevation.

Consider plane waves incident directly upon the plane  $x = 0$  as a fixed boundary. We take

$$\phi = (2gh/\sigma) e^{\kappa z} \cos \kappa x \sin \sigma t, \quad (24)$$

$$\zeta = 2h \cos \kappa x \cos \sigma t + 2\kappa h^2 \cos 2\kappa x \cos^2 \sigma t, \quad (25)$$

with  $\sigma^2 = g\kappa$ . We have  $\partial\phi/\partial x = 0$  at  $x = 0$ ; for the pressure we have

$$p = F(t) - g\rho z + \rho \frac{\partial\phi}{\partial t} - \frac{1}{2}\rho \left\{ \left( \frac{\partial\phi}{\partial x} \right)^2 + \left( \frac{\partial\phi}{\partial z} \right)^2 \right\}. \quad (26)$$

It may be verified that, with

$$p = -2g\rho\kappa h^2 \cos 2\sigma t - g\rho z + 2g\rho h e^{\kappa z} \cos \kappa x \cos \sigma t - 2g\rho\kappa h^2 e^{2\kappa z} \sin^2 \sigma t, \quad (27)$$

the pressure conditions at  $z = \zeta$ , given by (25), are satisfied to the second order, namely  $p = 0$  and

$$\frac{\partial p}{\partial t} - \frac{\partial \phi}{\partial x} \frac{\partial p}{\partial x} - \frac{\partial \phi}{\partial z} \frac{\partial p}{\partial z} = 0.$$

To the first order, (24) and (25) represent plane waves of amplitude  $h$  reflected at the plane  $x = 0$ . We may now evaluate the additional pressure upon this plane per unit width. We put  $x = 0$  in (27) and integrate with respect to  $z$  from  $-\infty$  to  $\zeta$ . The first order term is the periodic force  $(2g\rho h/\kappa) \cos \sigma t$ ; for the additional quadratic terms we obtain

$$-\frac{1}{2}g\rho\zeta^2 + 2g\rho h\zeta \cos \sigma t - g\rho h^2 \sin^2 \sigma t, \quad (28)$$

the second term in (28) coming from the expansion of  $e^{\kappa\zeta}$ . We put in the value of  $\zeta$  from (25), noting that we only need this to the first order; and we obtain for the additional steady force  $P$  per unit width of the plane, taking mean values,

$$P = \frac{1}{2}g\rho h^2, \quad (29)$$

where  $h$  is the amplitude of the incident waves.

It may be remarked that instead of using the fact that the second order term in the expansion of  $\phi$  is zero, it would have sufficed for the present purpose to assume  $\phi$  to be purely periodic, an assumption made by Larmor (1920) in the corresponding calculation for sound waves. It is well known that waves of finite amplitude possess linear momentum in the direction of propagation; the average amount, to second order terms, is  $\pi\rho h^2 V$  per wave length,  $V$  being the wave velocity. On the other hand, if we calculate the rate of transfer of linear momentum across a vertical plane, we obtain an average rate of  $\frac{1}{2}g\rho h^2$ ; this gives in one period one-half the average momentum in one wave-length. The average pressure  $P$  given by (29) may be regarded as due to the reversal of this flow of momentum. We notice also that  $P$  is equal to one-half the average density of energy in the standing oscillations, and this may again be connected with the fact that the group velocity for water waves is one-half the wave velocity. For plane waves of amplitude  $h$  incident upon the plane  $x = 0$  at an angle  $\alpha$  to the plane, we may take

$$\left. \begin{aligned} \phi &= (2gh/\sigma) e^{\kappa z} \cos(\kappa x \sin \alpha) \sin(\sigma t - \kappa y \cos \alpha), \\ \zeta &= 2h \cos(\kappa x \sin \alpha) \cos(\sigma t - \kappa y \cos \alpha). \end{aligned} \right\} \quad (30)$$

We obtain now, instead of (28), the quadratic terms for the additional pressure as

$$\begin{aligned} &-\frac{1}{2}g\rho\zeta^2 + 2g\rho h^2 \cos(\sigma t - \kappa y \cos \alpha) \\ &- g\rho h^2 \{\cos^2 \alpha \cos^2(\sigma t - \kappa y \cos \alpha) + \sin^2(\sigma t - \kappa y \cos \alpha)\}. \end{aligned} \quad (31)$$

Taking mean values, this gives

$$P = \frac{1}{2} g \rho h^2 \sin^2 \alpha. \quad (32)$$

7. We proceed similarly for any fixed cylinder of infinite draft with vertical sides; it is not necessary to examine the second order terms for the surface elevation, and we assume that the velocity potential is correct up to that order, or at least that any second order term is purely periodic.

Consider the solution for the circular cylinder which was given in § 4. We write it as

$$\left. \begin{aligned} \phi &= (gh/\sigma) e^{\kappa z} (L \cos \sigma t - M \sin \sigma t), \\ \zeta &= -h(L \sin \sigma t + M \cos \sigma t), \end{aligned} \right\} \quad (33)$$

where  $L, M$  are functions of  $r, \theta$  which may be obtained from (17).

At any point on the cylinder we have

$$\begin{aligned} p &= F(t) - g\rho z - g\rho h e^{\kappa z} (L \sin \sigma t + M \cos \sigma t) \\ &\quad - (\rho/2a^2) e^{2\kappa z} \{ \kappa^2 a^2 (L \cos \sigma t - M \sin \sigma t)^2 + (L' \cos \sigma t - M' \sin \sigma t)^2 \}, \end{aligned} \quad (34)$$

with  $r = a$ , and the accent denoting  $\partial/\partial\theta$ .

We integrate with respect to  $z$  from  $-\infty$  to  $\zeta$  and expand to second order terms; then for the resultant force we multiply by  $a \cos \theta d\theta$  and integrate round the circle.

It is readily seen that the first order term in the additional force is a periodic effect of amount

$$\frac{4g\rho h}{\kappa^2} \frac{J_1'(\kappa a) \sin \sigma t + Y_1' \cos \sigma t}{J_1'^2(\kappa a) + Y_1'^2(\kappa a)}. \quad (35)$$

From the quadratic terms we get, after taking mean values, the steady additional force

$$R = \frac{1}{2} g \rho h^2 a \int_0^\pi \left\{ L^2 + M^2 - \frac{1}{\kappa^2 a^2} (L'^2 + M'^2) \right\} \cos \theta d\theta, \quad (36)$$

$$\text{where} \quad L + iM = \frac{2i}{\pi \kappa a} \left( b_0 + 2 \sum_1^\infty b_n \cos n\theta \right), \quad (37)$$

and  $b_n = i^n / H_n^{(2)'}(\kappa a)$ .

We have

$$\left. \begin{aligned} \int_0^\pi (L^2 + M^2) \cos \theta d\theta &= \frac{4}{\pi \kappa^2 a^2} \sum_0^\infty (b_n b_{n+1}^* + b_n^* b_{n+1}), \\ \int_0^\pi (L'^2 + M'^2) \cos \theta d\theta &= \frac{4}{\pi \kappa^2 a^2} \sum_1^\infty n(n+1) (b_n b_{n+1}^* + b_n^* b_{n+1}), \end{aligned} \right\} \quad (38)$$

where the asterisk denotes the conjugate complex. Putting in the value of  $b_n$  and using properties of the Bessel functions, these expressions may be reduced to a simple form; we obtain finally

$$R = \frac{4g\rho h^2 a}{\pi^2 \kappa^3 a^3} \sum_0^\infty \left( 1 - \frac{n(n+1)}{\kappa^2 a^2} \right) \frac{1}{(J_n'^2 + Y_n'^2)(J_{n+1}'^2 + Y_{n+1}'^2)}, \quad (39)$$

the argument of the Bessel functions being  $\kappa a$ .

The series in (39) occurs also in an expression given by Nicholson (1912) in a similar problem for electromagnetic waves. Some values had been calculated before this reference was known, and with Nicholson's values for the series we have the results in table 3.

TABLE 3

|                            |       |       |       |       |       |
|----------------------------|-------|-------|-------|-------|-------|
| $\kappa a$                 | 0.5   | 1.0   | 2.0   | 3.0   | 5.0   |
| $R/\frac{4}{3}g\rho h^2 a$ | 0.429 | 0.998 | 0.940 | 0.950 | 0.965 |

It was shown by Nicholson that when  $\kappa a$  is large, the series approximates to the value  $\frac{1}{3}\pi^2 \kappa^3 a^3$ ; hence when the wave-length is small compared with the diameter of the cylinder, we have approximately

$$P = \frac{2}{3}g\rho h^2 a. \quad (40)$$

This agrees with the limiting value if we assume total reflexion over the front half of the cylinder and a complete shadow over the rear half, and apply to each element the expression (32) for total oblique reflexion from a plane; for we then have

$$P = \int_{-\frac{1}{2}\pi}^{\frac{1}{2}\pi} \frac{1}{2}g\rho h^2 a \cos^3 \theta d\theta = \frac{2}{3}g\rho h^2 a. \quad (41)$$

Although this limiting value is obtained theoretically as an extreme case for short waves, it is interesting to note from the preceding table that it is practically attained for comparatively long waves of wave-length even larger than the diameter. This consideration suggests using the method to give an upper limit for cylinders whose section is more like that of a ship.

8. Consider a cylinder with vertical sides, the horizontal section being of ship form and symmetrical about  $Ox$ . We assume total reflexion by the sides of the ship from the bow back to where the sides become parallel to  $Ox$ , and we assume a complete shadow aft of that point.

For the model of § 3, in which the bow is a wedge of semi-angle  $\alpha$ , we obtain for the total resistance

$$R = \frac{1}{2}g\rho h^2 B \sin^2 \alpha, \quad (42)$$

where  $B = 2b =$  beam.

In general, for any form of the front portion of the model, we have

$$R = \frac{1}{2} g \rho h^2 \int_{-b}^b \sin^2 \alpha dy = \frac{1}{2} g \rho h^2 B \overline{\sin^2 \alpha}. \quad (43)$$

In (43),  $\alpha$  is the angle the tangent to the form makes with  $Ox$ , and the bar denotes the mean value of  $\sin^2 \alpha$  with respect to the beam of the ship.

Suppose, for instance, that the section of the model is the ellipse  $x^2/a^2 + y^2/b^2 = 1$ . It is easily shown that in this case

$$\overline{\sin^2 \alpha} = \frac{b^2}{a^2 - b^2} \left\{ \frac{a^2}{b \sqrt{a^2 - b^2}} \tan^{-1} \sqrt{\frac{a^2 - b^2}{b^2}} - 1 \right\}. \quad (44)$$

This would be a full form of model. If we take  $a = 8b$ , as an average ratio of length to beam, we find from (44) that the mean value of  $\sin^2 \alpha$  is 0.17. The mean value is less for models with moderate bow angle; probably an average value would be about 0.1, with still smaller values for models with fine lines.

In a recent paper Kreitner (1939) has put forward the proposition that the extra resistance to a ship among waves is nothing else than the radiation pressure of the ocean waves. The semi-empirical formula given by Kreitner for this force upon a ship at rest in a train of waves is

$$R = g \rho h^2 B \overline{\sin \alpha}, \quad (45)$$

in the present notation, in which  $h$  is the amplitude of the incident waves; the last factor is a mean value for the angle of entrance not clearly defined. The derivation of this formula is not clear, but it appears to be based upon an estimate of the difference of resultant amplitude at bow and stern, and upon taking the mean value of the hydrostatic pressure due to the surface elevation. This latter assumption is incorrect; and further, we found in (43), that the last factor should be the mean value of  $\sin^2 \alpha$  taken across the beam. Numerically, for usual ship forms, these differences result in (43) giving about one-fifth of the value from (45).

For a certain model, a ship with full lines, the relevant data are  $B = 69.2$  ft.,  $L = 530$  ft.,  $h = 2\frac{1}{2}$  ft. If we assumed the fore half of the ship to be an ellipse and used (44), we should have 0.175 as the mean value of  $\sin^2 \alpha$ ; but this is certainly too large and we take a smaller value, say 0.12. With these values, (43) gives a force of 0.6 ton. This is, moreover, an upper limit and also assumes the ship to have vertical sides and to be of great draft. The recorded extra resistance for this ship is given as about 2.8 tons; but this was for a model advancing through the waves.

The steady pressures we have been considering will certainly be increased if the ship is itself in steady motion through the waves, but the problem

then becomes complicated and, in practice, many other factors must be taken into account. The wave resistance of the ship, as calculated for uniform motion through still water, is probably altered; moreover, the motion of the ship, and in particular its pitching and other oscillations, must have an important influence. It may well be that interactions between first order effects which in themselves are purely periodic may, through phase differences, give rise to steady additional resistances.

The calculations which have been made here refer to a model held at rest in a train of waves. The only reference to experiments of this nature appears to be in a paper by Kent and Cutland (1935). The model was No. 1255 of the National Physical Laboratory, and the dimensions were: length = 16 ft., beam = 1.92 ft., draft = 0.52 ft. For this model the mean value of  $\sin^2 \alpha$  was probably not more than 0.1. If we suppose the wave amplitude, that is half the wave height, to be 2 in. for waves, say, 5 ft. in length, then (43) gives as an upper limit a force of 0.17 lb. The experimental results were not published, no doubt because this particular experiment was only incidental to the main investigation; but it may be taken that the calculated value obtained here is of the order of one-half the measured value for waves of the given height and length. Here, again, although the model is said to be at rest, it has necessarily a certain small amount of freedom for oscillatory motion. While such motion might be expected to diminish the magnitude of the pressures we have been considering, it may also bring other effects into operation. Further experiments of this nature, with more detailed measurements, would be of great interest.

The immediate object of the present work was to examine, in cases amenable to calculation, the magnitude of the mean force obtainable on the analogy of radiation pressure. The general conclusion is that while such a force exists as a contributory cause, it is insufficient to account for the extra resistance observed in a ship advancing through waves; in those circumstances the total effect is probably the result of several factors of approximately equal importance.

#### REFERENCES

- Havelock, T. H. 1937 *Proc. Roy. Soc. A*, **161**, 299.  
Kent, J. L. and Cutland, R. S. 1935 *Trans. Instn Nav. Archit., Lond.*, **77**, 81.  
Kreitner, J. 1939 *Trans. Instn Nav. Archit., Lond.*, **81**, 203.  
Lamb, H. 1906 *Proc. Lond. Math. Soc.* **4**, 190.  
— 1922 *Proc. Lond. Math. Soc.* **21**, 359.  
Larmor, J. 1920 *Cong. Inter. Math. Strasbourg*.  
Nicholson, J. W. 1912 *Proc. Lond. Math. Soc.* **11**, 104.  
Rayleigh, Lord 1915 *Proc. Roy. Soc. A*, **91**, 345.  
Wigley, W. C. S. 1931 *Trans. N.-E. Cat Instn Engrs Shipb.* **47**, 153.
-



# An investigation of cold-worked polycrystalline alpha-iron

BY L. MULLINS, PH.D., M.SC., AND J. W. RODGERS, PH.D., M.SC.

*The University of Sheffield*

(Communicated by Sir Harold Carpenter, F.R.S.—Received 1 September  
1939—Revised 25 April 1940)

(Plate 5)

A new empirical method of approach to the mechanism of grain breakdown in metals on cold-working is described and applied in an X-ray examination of alpha-iron, cold-worked by elongation.

The individual reflexions from the grains of the metal are microphotometered along the periphery of the reflexion rings and these photometer records are analysed into the components which arise from the discrete crystal fragments of the deformed grain, a Gaussian error curve being the basis of the unit reflexion curves used in the analysis.

A survey of the many photometer records analysed showed them broadly divisible into three types, corresponding to the reflexions from the various types of actual disintegration of the metallic grain, representative curves being given.

## INTRODUCTION

The problem of the mode of grain breakdown has been studied by Gough and his co-workers, chiefly with reference to the phenomenon of fatigue. Gough and Wood (1936) have suggested that the crystal grains break down into two types of fragments which they call 'dislocated grains' and 'crystallites', the relative proportions of which depend upon the degree of cold work. The dislocated grain is composed of crystal fragments which are oriented with respect to one another over an angular range of approximately  $2^\circ$ . The crystallites are minute crystalline fragments with a wide range of orientations. In heavier degrees of deformation these are oriented almost at random, giving rise to a uniform intensity around the periphery of the reflexion ring. The present paper describes an attempt to distinguish between the various stages and types of grain breakdown, with reference to the angular displacement of the fragments only, and not with respect to the nature of the lattice disturbance produced.

The first step in the analysis of grain breakdown is the determination of the distribution of intensity in the reflexion from a single undeformed

crystal along the periphery of the reflexion ring. Neglecting minor imperfections such as secondary structure, lineage, etc., this will represent the 'unit reflexion'. The second step is to determine whether the deformed grains can be analysed into a number of these unit reflexions, corresponding to the relatively undeformed fragments or lamellae between the slip planes; and a distribution of intensity with a much wider angular range due to reflexions from the minute crystal fragments. It is however unlikely that all the larger crystal dislocations giving rise to individual reflexions will possess entirely undisturbed lattice structures. There are certain to be numbers which suffer small disturbances throughout, as would occur if the lamellae were bent during the process of slip. If this more or less uniformly distributed disturbance of the lattice structure of the fragment occurs, it will give rise to a somewhat broader curve than that corresponding to the unit reflexion. This broadening will be a measure of the deformation which has been propagated through the relatively undeformed fragment.

In all cases, the distribution of intensity is measured along the periphery of the reflexion ring. If pure monochromatic radiation were used, any change in the distribution in a radial direction would depend upon a change in the lattice parameter, which is outside the scope of this investigation. Consequently, changes of intensity in the radial direction due to rotation of the crystal fragments cannot be satisfactorily measured.

#### THE DISTRIBUTION OF INTENSITY IN THE REFLECTED X-RAY BEAM

The distribution of intensity in the spot measured along the periphery of the ring, produced on the film by reflexion from an undeformed grain (i.e. the unit reflexion) depends upon the following factors:

- (1) The divergence and width of the X-ray beam as controlled by the geometry of the camera and slit system and its position in relation to the specimen and X-ray tube.
- (2) The secondary structure of the crystals of the specimen.
- (3) The absorption of the X-rays by the specimen.

Using the same type of specimen and keeping the camera conditions constant throughout, factors 1 and 3 remain constant.

The effect of secondary structure upon the width of the spot is certainly influenced by cold deformation, heat treatment, etc. Secondary structure primarily influences the reflecting power of the crystals, and its effect upon the width of the spot is only small. On the other hand, the effect of the geometry of the beam depends upon the fact that, owing to the

finite width of the slit system, the incident beam does not consist of exactly parallel rays; consequently, the reflected beam is not completely parallel. This, together with the fact that, owing to the finite area of the irradiated surface of the specimen, the rays do not radiate from a geometrical point, combines to produce a beam of reflected radiation which, on being intercepted by the film, gives rise to a spot of finite width. It can be assumed that this width is large in comparison with that due to secondary structure. It follows, therefore, that the distribution of intensity due to any undisturbed grain should not only be constant in form, but also constant in width; in other words, the only variable in the intensity curves for different undeformed grains should be the scale of the ordinates.

It has been assumed as a first approximation that the distribution of intensity of the unit reflexion is that of the gaussian error curve of the form  $y = e^{-x^2}$ . The examination of such an intensity distribution by means of a microphotometer involves an error due to the finite width of the photometer slit; this yields an average intensity over the width of the reflexion spot examined at any position by the photometer. The average values of the gaussian error curve over this width (0.025 mm.) yield a curve of the form shown in figure 1. The most convenient method of measuring this type of curve is to take the width corresponding to half the height of the peak measured from the value of the density of the neighbouring part of the film. This density is due to X-rays scattered from various parts of the camera system plus normal chemical fog, and corresponds to the zero of the intensity of the reflected radiation.

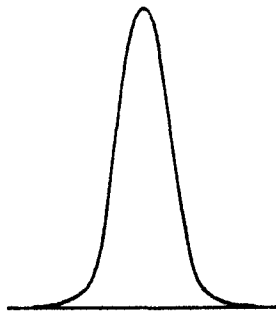


FIGURE 1

A careful preliminary survey of many undeformed reflexion spots showed that the half-width of the intensity curves had a well-defined minimum at 0.20 mm.; therefore this could be considered as the half-width of the unit reflexion. A series of gaussian curves were drawn having different maximum ordinates, but the same half-width, and these were used as component curves in the analysis of the observed intensity curves.

The analysis of the complex curves must be undertaken in two stages. In the first stage, the assumption is made that all dislocated fragments capable of producing an appreciable reflexion, give rise to one having the form of the unit reflexion. At a later stage it will be seen that this assumption is not always justified. The second stage of the analysis consists of the modification of the simple analysis of the curves.

In the first stage of the analysis, two or more unstrained fragments from the breakdown of a grain are supposed to give rise to a similar number of unit reflexions, superimposed but somewhat displaced with respect to one another along the periphery of the reflexion ring. This displacement is due to the slight amount of rotation which occurs when the fragments are formed from the parent grain. The resulting intensity curve is a summation of the separate distributions of intensity, and in the absence of any mathematical method of analysis of such curves, the empirical method of analysing the observed curves by means of the component unit reflexions must be used. This method of analysis depends chiefly upon experience and no straightforward rules can be given. The starting-point is usually an obvious peak in the observed complex curve, and a unit reflexion curve of suitable height is fitted temporarily at this point. The residual intensity curve is then drawn by subtraction and attempts are made to fit unit reflexions to this residual curve, one at a time, along the periphery of the reflexion ring. If the correct height and position for the original unit reflexion have been chosen, it should be possible to fit a second unit reflexion without a large amount of misfit. At each stage the residual intensity curve is drawn and the appropriate unit reflexions chosen. If no fit is found at any stage, it indicates that one of the previously fitted unit reflexions has the incorrect height, or has been incorrectly placed along the periphery of the reflexion ring. Accordingly a change in one or more of the curves already fitted is necessary until a suitable fit is obtained throughout the complex curve. Unfortunately, this method, apart from its tedious nature does not necessarily lead to a unique solution; the relation of the unit reflexions to the position of subsidiary peaks or shoulders give, however, a fair indication of the most probable solution.

The amount of misfit in fitting the components to the observed curves is a measure of the soundness of the method. The significance of the misfit between the built-up and observed curves is discussed in detail in a later section in the paper.

#### EXPERIMENTAL METHOD

For convenience in microphotometering the reflexion spots along the periphery of the rings, a camera, the design of which was suggested to the authors by Dr W. H. George, was constructed as shown in section in figure 2. The film was fitted around the inside of a horizontal brass cylinder, the incident X-ray beam passing along its axis and impinging on the specimen placed at the end of the film holder. The back-reflected cones of

rays were intercepted by the film, appearing as spots which lay along straight lines parallel to the long edge of the film. The density of these spots was then examined along the line by means of a Hilger microphotometer, corresponding to an examination along the periphery of the rings normally obtained in the back-reflexion method in which the plane of the film is perpendicular to the incident radiation. The density of the film at the point under consideration is given by

$$\log_{10} O_0 - \log_{10} O_1,$$

where  $O_0$  is the reading for chemically fogged unexposed film, and  $O_1$  is the reading for exposed film.

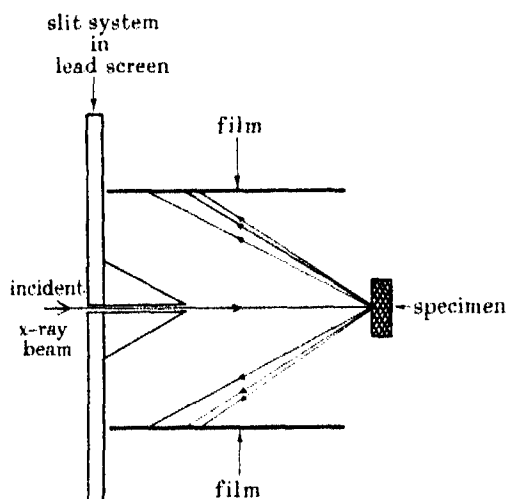


FIGURE 2

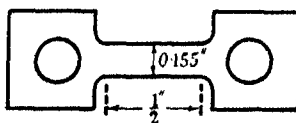


FIGURE 3

The specimens in the form of small tensile test-pieces (figure 3), were blanked out of 0.08 % carbon steel strip 0.036 in. thick. This sheet was in the fully softened condition. After a 50 % cold-rolling reduction, followed by etching in dilute nitric acid to remove the surface layers, it was annealed for 24 hr. in vacuo at 680° C to remove strain and to produce a satisfactory initial grain size. A photomicrograph revealed a grain size of about 16 grains per inch at a magnification of 100 diameters. After



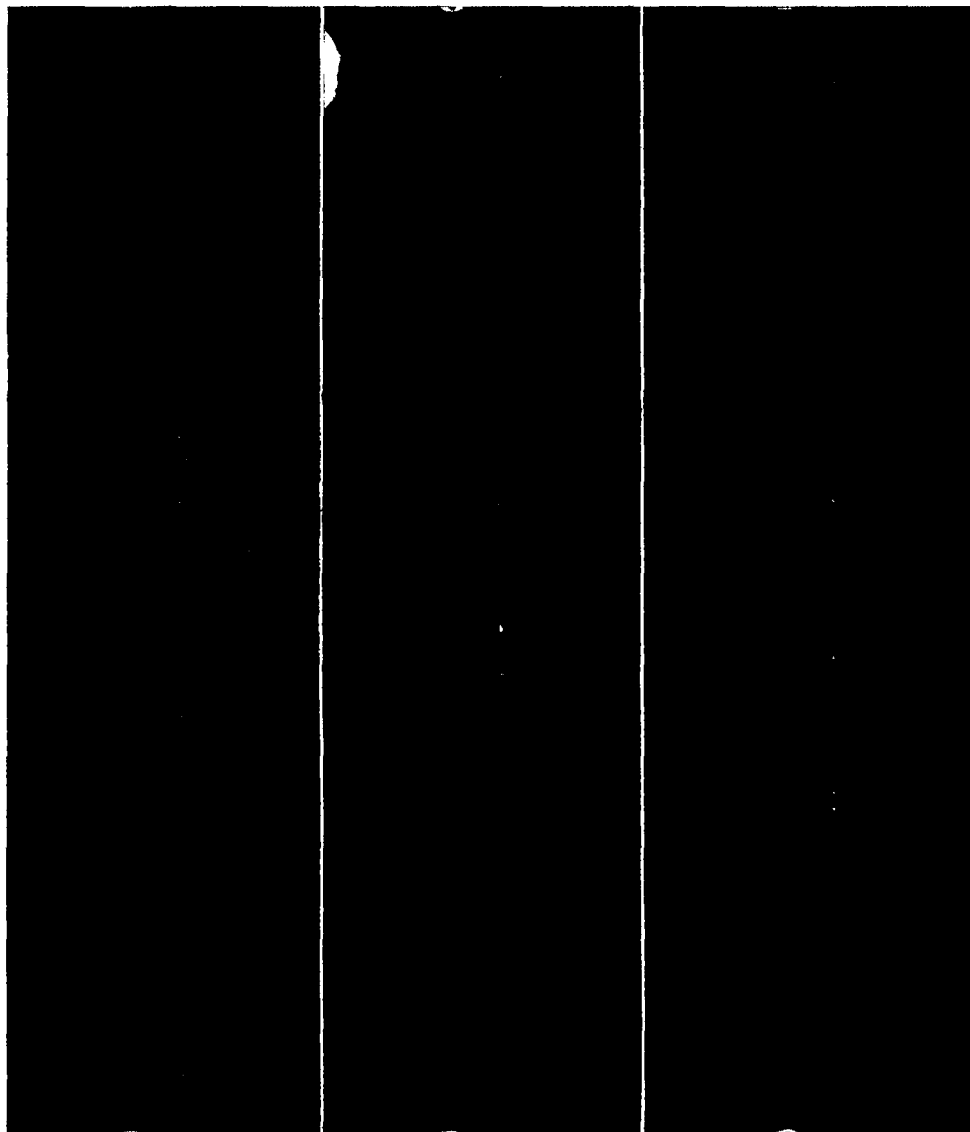


FIGURE 4

FIGURE 5

FIGURE 6

(Facing p. 427)

straining by tensile elongation in a Hounsfield Tensometer (a small hand-operated tensile testing machine) by amounts varying from less than 1% up to about 6% reduction in area, the specimens were examined by means of the X-ray camera. Figure 4 (plate 5) shows an X-ray photograph of annealed material; figures 5 and 6 (plate 5) are photographs of material strained 1.9 and 5.9% reduction respectively.

The intensity-density calibration curve for the photographic film was determined in the usual way by means of a rotating sector. An aluminium sheet was interposed in the beam to cut out much of the soft radiation which tends to upset the calibration. As the intensity-density relation is affected by the conditions of development, the latter was carefully standardized.

The X-ray exposures were so adjusted that for the majority of spots, the maximum density did not exceed that value for which the intensity-density calibration curve gave a linear relation. The densities of the spots as measured at intervals of 0.005 cm. by means of the microphotometer were thus directly proportional to the intensities of the spots on the film.

A large number of reflexion spots have been microphotometered for each degree of deformation, only a few representative examples of which have been reproduced. These curves have been drawn in the following manner: The ordinates represent intensity upon an arbitrary scale; the abscissae represent the photometer traverse distance along the periphery of the reflexion ring. The experimental curve is shown as a continuous line. The unit reflexions into which the curve has been analysed are shown composed of dashes. The dotted line (in some cases shown below on a separate base line to avoid confusion) represents the difference between the sum of the component curves and the experimental curve; this difference has been shown positive when the latter was greater than the sum of the component curves. Where it has been necessary to use a broadened component curve, as in figure 11c for instance, this has been shown as a dot and dash curve.

#### DISCUSSION OF RESULTS

An examination of the analyses of the various photometer curves indicates that their interpretation can be simplified considerably by differentiating between different types of background intensity upon which the component reflexions are superposed.

The background in some cases is of considerable breadth and of moderate intensity. It appears to have an approximately gaussian form and to have a breadth not greatly exceeding the total angular range of the various



component reflexions. This type has been termed the *coherent background*, and is occasionally observed in metal which has been subjected to small or moderate amounts of cold deformation.

Increasing degree of deformation leads to a wider distribution of reflexions along the periphery of the reflexion ring, which finally reaches a uniform intensity along its whole length at deformations greater than those described in the present investigation. This background with a wide angular range corresponds to the reflexions from the crystallites described by Gough and Wood and has been termed the *diffuse background*.

The photometer curves are roughly divisible into three types:

(1) Those showing little or no broadening; they are found to a large extent in the unworked specimens, and to a lesser extent in the worked

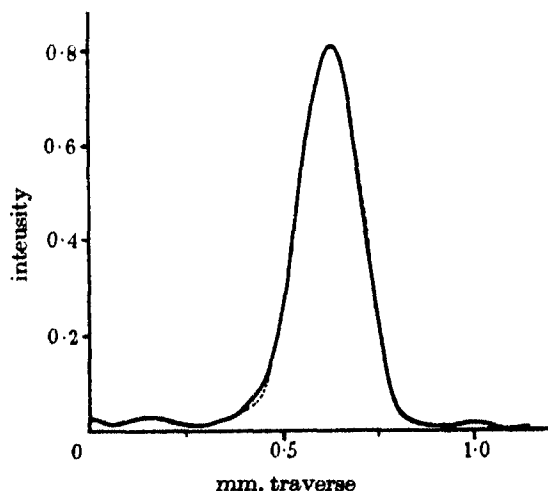


FIGURE 7

ones; the greater the deformation of the specimen, the smaller the chance of finding spots corresponding to an undistorted grain. The latter are carried as passengers in the deformation, as can be seen from the few sharply defined spots in figure 6. Such curves are fitted almost exactly by the unit reflexions. It is possible that the accuracy of the fit is limited by the errors in the photometer curve. Figure 7 is an example of this type.

(2) Curves which can be resolved into a series of unit reflexions or slightly broadened gaussian curves, displaced with respect to one another, together with negligible misfit as shown in figure 8.

(3) Curves which can be resolved into a series of component curves with a variable amount of misfit which is expressible as a background super-

posed on the component curves. Such background curves are often irregular, suggestive of errors in fitting, as shown by the dotted lines below the traverse axis in figure 9a. Others show one or two regular features, either a more or less uniform intensity along the reflexion line and comparable with the diffuse background, or a coherent background which has the appearance of a very much broadened unit reflexion. The last two types are represented by figures 10 and 9b respectively. Figure 9b is an alternative and more probable solution to figure 9a. The appearance of subsidiary shoulders to the curve suggests the existence of the coherent

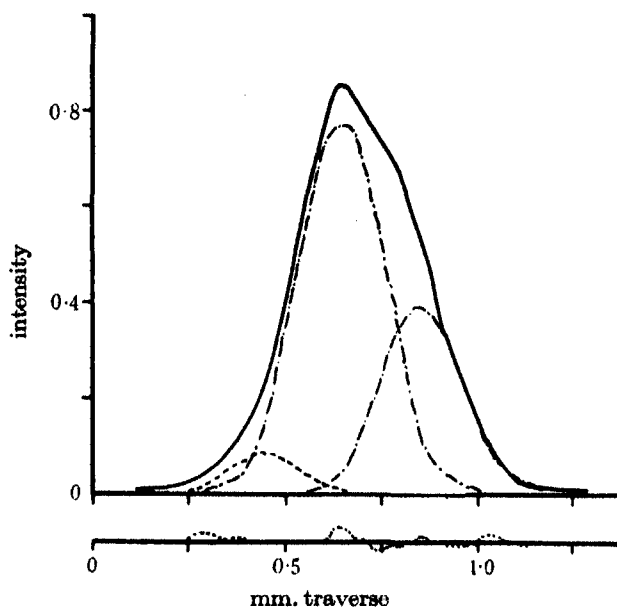


FIGURE 8

background. This has been indicated by the dotted line through the background obtained after subtracting the component curves. The second subsidiary base line shows the misfit after allowing for the coherent background. Figures 9a and 9b indicate how alternative solutions can arise, and discretion and experience must guide the choice of the most probable solution. The most complex curves generally occur in the most heavily worked specimens and are characterized by the absence of any marked peak and a width considerably greater than that due to the undistorted grain. For example, the half-width of the reflexion from an undeformed grain is 0.2 mm., while the width (the half-width of a complex curve has no particular significance) of the former type of curve is sometimes

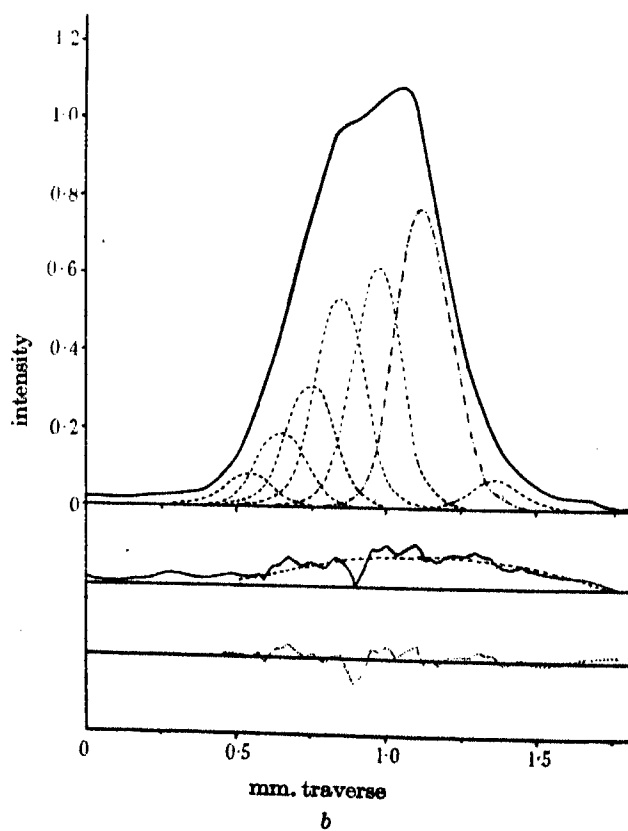
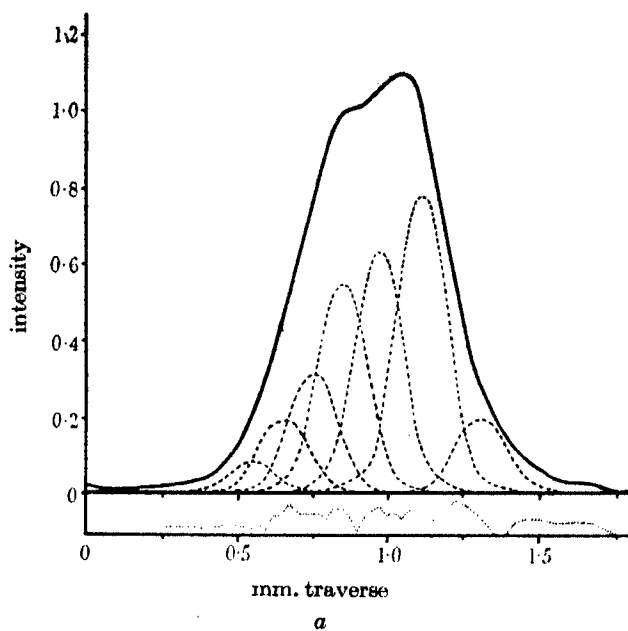


FIGURE 9

greater than 1 mm. The maximum intensity from such curves is usually only slightly greater than that of the diffuse background. The curve shown in figure 10 is of this type.

*Misfits.* So far the analysis of the curves has only been in its first stage, and any disagreement or misfit—that is to say, any intensity which owing to its distribution cannot be accounted for by the unit reflexions—has been interpreted above as a background presumably due to fragmentation into a 'powder' of minute crystals.

There is evidence that the curves, built up from unit reflexions alone, do not always leave a background of such a form as to be likely to represent the reflexions from the minute crystal fragments. Figure 11 consists of a large peak, with an obvious small reflexion to one side. Figure 11*a* is the most straightforward solution, consisting of unit reflexions of height equal to that of the observed curve, plus an irregular background. The

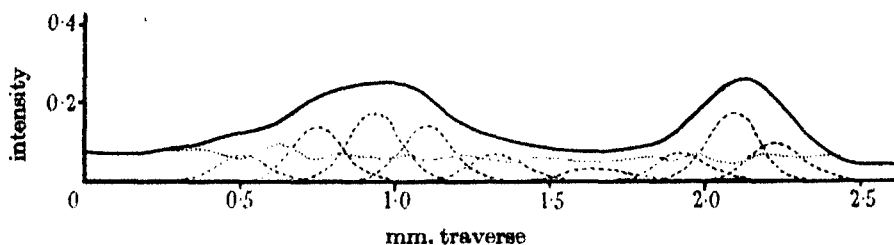


FIGURE 10

form of the background is, however, highly arbitrary, being zero in the centre of the main unit reflexion, and rising to two maxima on either side. This is a very improbable distribution for the orientations of the minute crystal fragments produced by the breakdown of the parent grain.

Since the misfit can be interpreted either as a background due to crystalline debris produced by deformation, or as evidence that the choice of component curves is at fault, an unlikely shape of misfit is more satisfactorily accounted for by the second interpretation. Figure 11*b* is an attempt to obtain a more probable background by choosing a smaller unit reflexion. The resulting background is more probable than that of figure 11*a*, in that the background could be called of the coherent type, but it is still far from representing a satisfactory distribution of intensity; and a trial shows that no series of unit reflexions will give rise to a probable solution.

It is therefore clear that the problem is not being approached in the correct manner, and the second stage of the analysis must be undertaken. Instead of attempting to analyse the curves by unit reflexions alone, a

broadened curve is used. Figure 11c shows that the observed curve is almost exactly fitted by a broadened curve of the gaussian form. The use of the broadened curve in the analysis of the photometer curves at first sight appears to introduce a considerable complication into the analysis, in that the width of the curve is variable, and consequently the choice

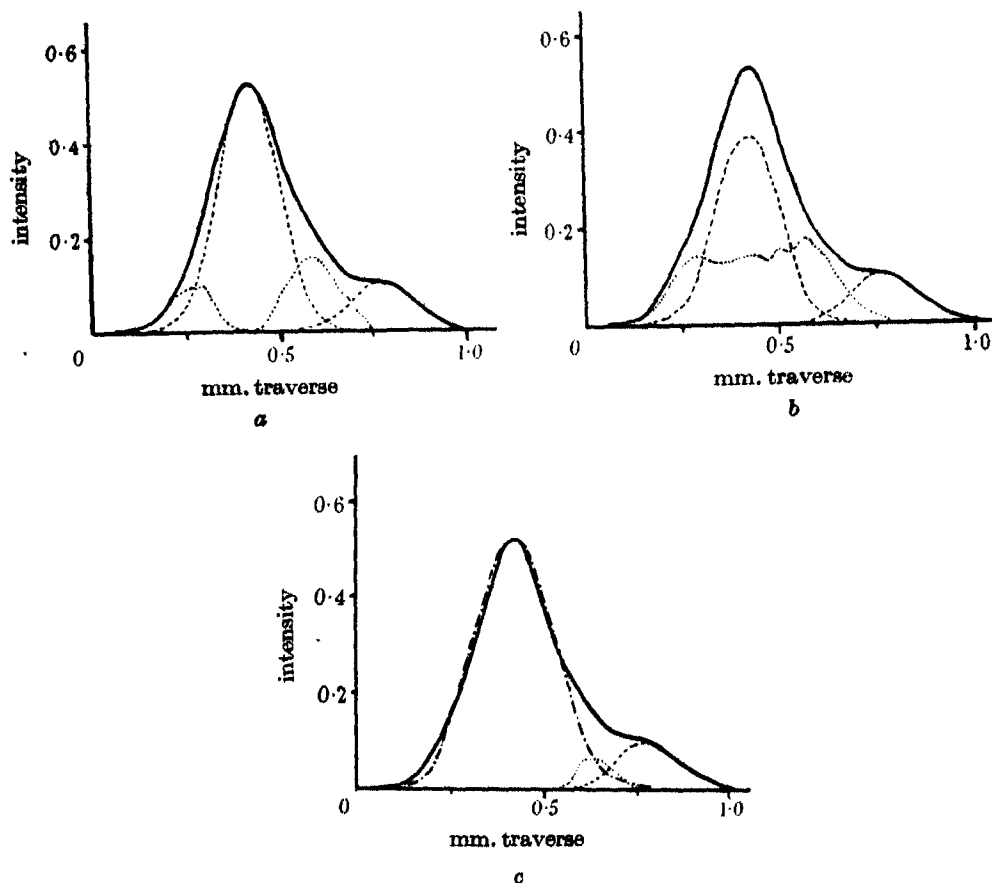


FIGURE 11

not only of suitable height but also of width would make the analysis even more ambiguous. Fortunately, the necessity for the use of a broadened curve is nearly always indicated by the shape of the misfit. Figure 10 is an example. Close examination shows it to consist of component curves, the peaks of which correspond to traces of subsidiary peaks or shoulders on the observed curve. If the component curves chosen are unit reflexions, no choice of ordinate scale is found to give a uniform background. This in

itself does not necessarily indicate that the analysis is incorrect. The form of the background is however suspicious in that there is always a minimum corresponding to the peak of each unit reflexion. A comparison with figure 11a shows that this form of background indicates that a broadened component curve should be used. The analysis of the observed curve in figure 10 has been left in its original form to show how the necessity for the use of a broadened curve in the analysis can be inferred.

### CONCLUSIONS

In order to carry out the analysis, the components of the complex photometer curves are divided into four kinds, corresponding to four types of breakdown product resulting from the deformation of crystal grains in the polycrystalline aggregate of alpha-iron:

*The unit reflexion* corresponds to a relatively large crystal fragment which retains its crystal structure undisturbed, and consequently its reflecting power unimpaired. The supposition that the distribution of intensity in this reflexion is of gaussian form is only justified by the observed distribution of intensity in the reflexion spots from undeformed grains under the particular experimental conditions used by the authors. The particular form of the unit reflexion has no fundamental significance in the method of analysis.

*The broadened reflexion* corresponds to a crystal fragment similar to the above, which however has suffered a small amount of lattice disturbance propagated almost uniformly throughout the fragment. The effect is similar to that of a mass of small crystals with a distribution of orientations over an angular range considerably smaller than that over which the individual fragments themselves are oriented in one dislocated grain. The form of many of the observed curves indicates that the distribution of orientation of these small crystals is approximately gaussian, since the use of the broadened gaussian component curve has been applied with considerable success in the analysis of the observed curves.

*The coherent background* consists of reflexions, usually of low intensity and frequently possessing an approximately gaussian distribution; it is due to minute crystal fragments which, however, do not appear to possess the large angular displacements described by Gough and Wood with reference to the crystallites. The angular range of these fragments is only of the order of the total range of the fragments of dislocation, though it usually exceeds this by a small amount, thus giving rise to subsidiary shoulders of low intensity observable in the experimental curve.

*The diffuse background* is due to the crystallites with a large angular range.

The following conclusions respecting the mode of grain breakdown can be drawn from the investigation:

(1) A small degree can cause a grain to break down into relatively large fragments with either a small degree of lattice disturbance, or no measurable disturbance at all within the individual fragments, and with the

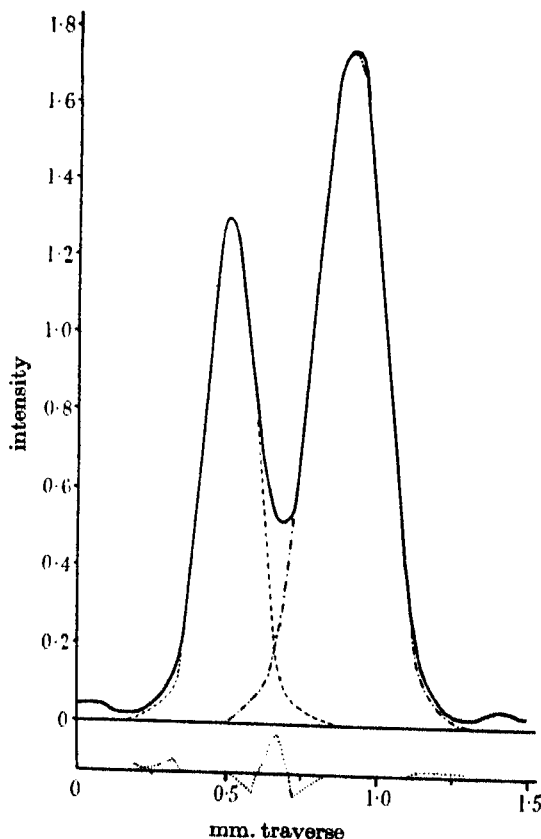


FIGURE 12

formation of a negligible amount of crystal debris (crystallites). An analysis of many experimental curves shows that within the same dislocated grain, fragments with both disturbed and undisturbed lattices may exist side by side. It very rarely occurs, however, that a grain breaks down into dislocated fragments which all possess undisturbed structures.

(2) In contrast to the mode of breakdown of large grains, small grains (those giving rise to a low integrated reflexion), on being subjected to

small degrees of deformation, are frequently deformed more or less uniformly throughout without breaking down into dislocated fragments. They give rise to the single broadened peak type of curve, which may however show small subsidiary peaks (figure 11c).

(3) Heavier deformation of larger grains causes the dislocated fragments to suffer a further degree of internal disturbance as shown by the progressive broadening of the component curves, together with a further splitting up into dislocated fragments. The maximum broadening of these component curves does not appear to be very great. There is also an increase in the relative proportion of the crystalline debris shown by the diffuse background, and this possesses increasingly wide angular displacements (figure 10).

(4) Figure 12 shows two adjacent peaks one of which is fitted exactly by a unit reflexion and therefore corresponds to an undeformed grain. The other is of even greater size and is fitted almost exactly by a broadened unit reflexion curve, indicating a small amount of uniform disturbance throughout the grain. The two reflexions are too intense to be due to fragments of the same grain and so they must be two grains close enough together to be irradiated by the narrow X-ray beam and possessing almost identical orientations. If two grains of practically the same orientation, and near enough to each other to be subjected to the same macroscopic stress system, are subjected to such different degrees of deformation, it follows that the micro-stress system must be exceedingly complex, and that it bears no simple relation to the macro-stress system.

The authors wish to express their appreciation to Professor J. H. Andrew for the help and encouragement he has accorded to them. The authors also wish to thank the Committee for Research on the Cold-Working of Steel and other Ferrous Metals, founded in 1929 by the Worshipful Company of Ironmongers, for permission to publish this paper.

#### REFERENCE

Gough, H. J. and Wood, W. A. 1936 *Proc. Roy. Soc. A*, 154, 510.

---



# The steady two-dimensional radial flow of viscous fluid between two inclined plane walls

By L. ROSENHEAD, PH.D., D.SC.

*University of Liverpool*

*(Communicated by G. I. Taylor, F.R.S.—Received 2 October 1939)*

This paper considers the steady two-dimensional radial flow of viscous fluid between plane walls which either converge or diverge. A general solution is obtained in terms of elliptic functions and the various mathematically possible types of flow are discussed.

## 1. INTRODUCTION AND SUMMARY

In this paper we consider the steady radial two-dimensional flow of viscous fluid between plane walls which either converge or diverge. The investigations on this subject were started by Jeffery (1915) and they have proved to be the starting-point for a number of researches by other authors, notably Hamel (1916), Harrison (1919), Karman (1922), Tollmien (1931), Noether (1931) and Dean (1934). These investigations deal with specialized aspects of the question and do not contain a systematic treatment of the general problem. It has been known since 1915 that a general solution is possible in terms of elliptic functions. In spite of this, however, the only case which is quoted in text-books and manuals is that which is, in effect, the degenerate case of the elliptic functions (see, for example, Goldstein 1938, p. 109).

The following investigation was started in the hope that it would lead to a clear picture of the change in flow associated with increasing Reynolds number,  $R$ . It was stimulated by the statement which is given by Goldstein (1938, p. 106). The following is a summary of the statement: For inflow the magnitude of the velocity is a maximum in the centre of the channel and diminishes uniformly to zero at the walls. With increasing Reynolds number the velocity profile always remains of this same type but becomes flatter and flatter in the middle dropping very rapidly to zero at the walls. For divergent flow with increasing Reynolds number the state of affairs is quite different. At small Reynolds numbers the magnitude of the velocity is a maximum in the middle of the channel and it decreases uniformly towards the walls. With increasing Reynolds number the flow becomes more and more concentrated in the centre of the channel until finally, at some critical value of  $R$ , regions of inflow appear on either side of the region of outflow. With

a larger outward flux than that associated with this critical value of  $R$  three solutions are possible, with the backward flow near one wall or the other, or near both walls. It seems possible that at still larger values of  $R$  the number of possible solutions also increases.

The above statement must, however, be modified in the light of the following investigation, the principal results of which are given below. At this stage it becomes necessary to define more closely what is meant by "outflow" and "inflow". In most previous investigations the Reynolds number  $R$  was defined to be of the form  $l |u_{\max.}|/\nu$ , where  $l$  was some representative length,  $\nu$  the coefficient of kinematic viscosity, and  $|u_{\max.}|$  was the maximum magnitude of the velocity in the flow. As we are now dealing with velocity profiles which contain both outflow and inflow the above definition of  $R$  cannot be used, for it makes no distinction between the Reynolds number in the case  $|u_{\max. \text{ outwards}}| = u_0$ ,  $|u_{\max. \text{ inwards}}| = u_1$ , and in the case  $|u_{\max. \text{ outwards}}| = u_1$ ,  $|u_{\max. \text{ inwards}}| = u_0$ . We therefore define the Reynolds number of the flow as  $Q/2\nu$ , where  $Q$  is the volume of fluid passing from the narrower end of the channel to the wider end, in unit time, between two planes which are at unit distance apart and are perpendicular to both the channel walls. A positive value of  $R$  will correspond to average outflow and a negative value of  $R$  to average inflow.

In the following investigation it was found advantageous, for purposes of mathematical simplicity, to use the Weierstrassian  $\wp$  function as much as possible but to transform to the Jacobian elliptic function for purposes of numerical calculation.

The principal results are as follows: For every pair of values of  $\alpha$  and  $R$  the number of mathematically possible velocity profiles of radial motion is infinite (see § 4). The profiles may or may not be symmetrical with respect to the central line of the channel. If  $\pi > \alpha > \frac{1}{2}\pi$  pure outflow is impossible, and there is a range of values of small Reynolds number in which pure inflow is impossible. The effect of increasing  $R$  in outflow is to exclude, progressively, more and more of the simpler types of flow. No such exclusion is introduced when  $|R|$  is increased in inflow. With increasing Reynolds number in pure inflow, and with small values of  $\alpha$ , the velocity profile exhibits all the well-known characteristics of boundary layers near the walls, and an approximately constant velocity across the rest of the channel. In pure outflow the flow becomes more and more concentrated in the centre of the channel as  $R$  is increased, until finally regions of inflow occur near the walls.

The analysis described below gives the mathematically possible types of flow but does not indicate which type of flow is actually assumed by the fluid. Considerations of stability would probably show that many of the

types of flow are unstable, but the present state of the theory of the stability of fluid motion does not seem to offer much hope that information will be obtained along these lines in the near future. It should be noted that in an actual experiment boundary conditions are imposed not only by the friction at the walls but also by the pressure conditions at the inlet and outlet ends of the channel. The following investigation may be considered as one which determines the proper pressure distributions over the ends which allow of steady laminar radial motion. If in an experiment the pressure distribution is not one of those obtained below, the flow may be neither steady, laminar nor radial. In normal experiments the pressure distribution over the ends approximates most closely to those required for pure inflow and outflow, so that these types are more likely to have been observed than are the other ones.

It is possible, however, to obtain a fairly plausible picture of the change of flow by the help of speculative assumptions. If we make the assumption that "If the pressure conditions over the inlet and outlet ends are not rigidly applied, that is, if the pressure profile can be assumed to be loosely self-adjusting, then the velocity profile will be that one which has the smallest number of crests and troughs", it is possible to deduce a simple systematic sequence of change. In inflow the velocity profile would always be of the symmetrical pure inflow type, and in outflow the sequence of change with increasing  $R$  is as shown in figure 4. It is assumed, also, that the non-symmetrical types, and also those which, even though they have inflow along the central line, give a positive value for  $Q$ , would not manifest themselves in experiment. This speculation can be pressed still further to provide information as to the stability of the various types of flow (see p. 467).

## 2. LIST OF SYMBOLS AND ELEMENTARY PROPERTIES OF SOME OF THE PRINCIPAL FUNCTIONS

$2\alpha$  is the angle between the walls.

$OV, OW$  are the lines of section of the walls with a representative plane which is at right angles to the line of intersection of the walls.

$OX$  is the bisector of  $OV$  and  $OW$ .

$r, \theta, h$  are the cylindrical coordinates, where  $r$  is measured from  $O$ ,  $\theta$  is measured from the central line  $OX$ , and  $h$  is measured in a direction perpendicular to the representative plane.

$r_0$  is the distance along  $OX$  of a fixed point  $O'$ .

$u, v, w$  are the velocity components in the directions of  $r, \theta, h$ . (Since the flow is radial  $v = w = 0$ .)

$\rho, \mu, \nu$  are the density, coefficient of viscosity, coefficient of kinematic viscosity, of the fluid.

$Q$  is the volume of fluid passing from the narrower end of the channel to the wider end, in unit time, between two planes which are at unit distance apart and are perpendicular to both walls. ( $Q$  may be either positive or negative.)

$$F(\theta) = ru/2\nu,$$

$$f(\theta) = -\frac{1}{3}\{F(\theta) + 1\} = \wp(\theta - \theta_0).$$

$R$  is the Reynolds number  $= Q/2\nu = \int_{-\alpha}^{\alpha} F(\theta) d\theta$ . (N.B. A positive value of

$R$  denotes average outflow and a negative one denotes average inflow.)

$a, b, \alpha_0, \theta_0$  are constants of integration ( $a, b, \alpha_0$  are real and  $\theta_0$  complex).

$p$  is the pressure in the fluid at  $r, \theta, h$ . This is equal to

$$\frac{4\mu\nu}{r^2} F(\theta) + \frac{a\mu\nu}{2r^2} + \text{constant}.$$

$\wp(\theta)$  is the Weierstrassian elliptic function defined by the equation

$$\wp'(\theta)^2 = 4\wp^3 - g_2\wp - g_3,$$

where the invariants  $g_2$  and  $g_3$  are respectively equal to  $\frac{1}{3}(4-a)$  and  $\frac{1}{27}(8-3a-3b)$ .

$e_1, e_2, e_3$  are the roots of the cubic  $4s^3 - g_2s - g_3 = 0$ . If the roots are all real, they are chosen in such a way that  $e_1 \geq e_2 \geq e_3$ . If the roots are not all real, then since  $g_2$  and  $g_3$  are real, two of the roots must be complex, and in this case they are chosen so that

$$e_1 = A + iB, \quad e_2 = -2A, \quad e_3 = A - iB,$$

where  $A$  and  $B$  are real.

$$g_2 = -4(e_2e_3 + e_3e_1 + e_1e_2) = 2(e_1^2 + e_2^2 + e_3^2).$$

$$g_3 = 4e_1e_2e_3.$$

$$H^2 = (e_2 - e_1)(e_2 - e_3) = 9A^2 + B^2 \text{ when the roots are complex.}$$

$\Delta$  is the discriminant of the cubic  $4s^3 - g_2s - g_3 = 0$ . It is equal to

$$16(e_2 - e_3)^2(e_3 - e_1)^2(e_1 - e_2)^2 = g_2^3 - 27g_3^2.$$

$\omega_1, \omega_2, \omega_3$  are the half-periods of the  $\wp$  function. If  $\Delta$  is positive, that is, if all the roots of the equation  $4s^3 - g_2s - g_3 = 0$  are real, then the real period is defined to be  $2\omega_1$  and the imaginary period is defined to be  $2\omega_2$ . If  $\Delta$  is negative, that is, if only one root is real, then the real period is defined to be  $2\omega_3$ , the other two periods being conjugate complex numbers:

$$2\omega_1 = 2(C - iD), \quad 2\omega_2 = -4C, \quad 2\omega_3 = 2(C + iD),$$

where  $C$  and  $D$  are real.

$K, E$  are the complete elliptic integrals of the first and second kinds.

$k = \sqrt{\{(e_2 - e_3)/(e_1 - e_3)\}}$  is the modulus of the elliptic integrals.

$k_1 = \sqrt{\{(e_1 - e_3)/(e_1 - e_2)\}}$  is the complementary modulus  $= \sqrt{1 - k^2}$ .

$E(u)$  is the incomplete elliptic integral of the second kind  $= \int_0^u \text{dn}^2 u \, du$ .

$Z(u)$  is the Jacobian Zeta function. It is defined by the equation

$$Z(u) = E(u) - uE/K.$$

$X = e_1 - e_3$ . When  $e_1, e_2, e_3$  are real,  $X \geq 0$ .

$\eta_1, \eta_2, \eta_3, \dots$  are the positive roots, in ascending order of magnitude, of the equation

$$\text{sn}^2(\eta\sqrt{X}) = \{(1 + k^2)X - 1\}/3k^2X.$$

They are connected by the relations

$$\begin{aligned} \eta_2 &= 2\omega_1 - \eta_1, & \eta_3 &= 2\omega_1 + \eta_1, \\ \eta_4 &= 4\omega_1 - \eta_1, & \eta_5 &= 4\omega_1 + \eta_1, \text{ etc.} \end{aligned}$$

When  $\theta_0 = \omega_3$  and  $e_1, e_2, e_3$  are real, then

$$S = 2 \int_0^{\eta_1} F(\eta) \, d\eta > 0,$$

$$T = 2 \int_{\eta_1}^{\omega_1} F(\eta) \, d\eta < 0.$$

### 3. THE EQUATIONS OF MOTION AND CONTINUITY

We are considering the steady radial motion of an incompressible viscous fluid in the region between inclined plane walls in the absence of external forces. The flow is two-dimensional, the representative plane being perpendicular to the channel walls. In this plane the co-ordinates are  $r, \theta$ , where  $r$  is the distance from  $O$ , the intersection of the walls, and  $\theta$  is measured from the central line  $OX$  (cf. figure 1). The channel walls cut the representative plane in the lines  $OV, OW$  ( $\theta = \mp \alpha$ ). The co-ordinate perpendicular to this plane is  $h$ . The flow diverges from, or converges to, the line represented by  $r = 0$ . The components of velocity in the directions of  $r, \theta, h$  are  $u, v, w$ . With the assumptions made above it can be seen that  $v = w = 0$ . The equation of continuity is

$$\frac{\partial u}{\partial r} + \frac{u}{r} = 0, \quad (3.1)$$

where  $u$  is a function of  $r$  and  $\theta$  only. This equation can only be satisfied if

$$u = 2\nu F(\theta)/r, \quad (3.2)$$

where  $F(\theta)$  is a function of  $\theta$  only. The total flux of fluid, per unit length of  $z$  axis, is  $Q$  where

$$Q = \int_{-\alpha}^{\alpha} ru d\theta = 2\nu \int_{-\alpha}^{\alpha} F(\theta) d\theta. \quad (3.3)$$

The Reynolds number of the flow,  $R$ , can be defined by the equation

$$R = Q/2\nu = \int_{-\alpha}^{\alpha} F(\theta) d\theta. \quad (3.4)$$

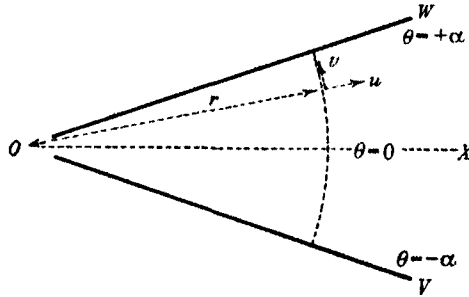


FIGURE 1

The equations of motion are

$$\rho u \frac{\partial u}{\partial r} = -\frac{\partial p}{\partial r} + \mu \left\{ \frac{\partial}{\partial r} \left( \frac{\partial u}{\partial r} + \frac{u}{r} \right) + \frac{1}{r^2} \frac{\partial^2 u}{\partial \theta^2} \right\}, \quad (3.5)$$

$$0 = -\frac{\partial p}{\partial \theta} + \frac{2\mu}{r} \frac{\partial u}{\partial \theta}. \quad (3.6)$$

Using the form of  $u$  suggested by (3.2), these become

$$-\frac{4\nu^2 F^2}{r^3} = -\frac{1}{\rho} \frac{\partial p}{\partial r} + \frac{2\nu^2 F''}{r^3}, \quad (3.7)$$

$$0 = -\frac{\partial p}{\partial \theta} + \frac{4\mu\nu F'}{r^2}, \quad (3.8)$$

where the accents denote differentiation with respect to  $\theta$ . From (3.8) we see that

$$p = \frac{4\mu\nu}{r^2} F(\theta) + p_1(r), \quad (3.9)$$

where  $p_1(r)$  is a function of  $r$  only. If this form is inserted in (3.7), we get

$$\frac{r^3}{\rho} \frac{\partial p_1}{\partial r} = \nu^2 (2F'' + 4F'^2 + 8F). \quad (3.10)$$

The left-hand side of (3.10) is a function of  $r$  and the right-hand side is a function of  $\theta$ . They are both therefore equal to a constant which, from the nature of the expressions, must be real. Putting this constant equal to  $-a\nu^2$ , we find

$$p_1 = \frac{a\mu\nu}{2r^2} + \text{const.}, \quad (3.11)$$

and 
$$2F'' + 4F'^2 + 8F + a = 0. \quad (3.12)$$

Multiplying (3.12) by  $F'$  and integrating, we obtain

$$F'^2 + \frac{4}{3}F^3 + 4F^2 + aF = \text{constant} = b, \text{ say.} \quad (3.13)$$

In this equation put  $F(\theta) = -\{3f(\theta) + 1\}, \quad (3.14)$

and (3.13) becomes  $f'(\theta)^2 = 4f^3 - g_2f - g_3, \quad (3.15)$

where 
$$\left. \begin{aligned} g_2 &= \frac{1}{3}(4-a), \\ g_3 &= \frac{1}{27}(8-3a-3b). \end{aligned} \right\} \quad (3.16)$$

From the definition of  $F(\theta)$  and from (3.12) and (3.13) it should be noted that  $a$  and  $b$ , and hence also  $g_2$  and  $g_3$ , are real. Further,  $a$  may be either positive or negative, but  $b$  must be positive, for  $u$ , and hence  $F(\theta)$  is zero at the walls and  $b$  is therefore equal to the value of  $F'(\theta)^2$  when  $\theta = \pm\alpha$ . The solution of (3.15) is

$$f(\theta) = \wp(\theta - \theta_0), \quad (3.17)$$

where  $\theta_0$  is a constant of integration which may, possibly, be complex. The solution of the problem under consideration is therefore

$$\left. \begin{aligned} u &= -\frac{2\nu}{r} \{3\wp(\theta - \theta_0) + 1\}, \\ p &= -\frac{4\mu\nu}{r^2} \{3\wp(\theta - \theta_0) + 1\} + \frac{a\mu\nu}{2r^2} + \text{constant}, \end{aligned} \right\} \quad (3.18)$$

where the invariants of the  $\wp$  function are given by (3.16). This solution is subject to the following limitations:

- (i)  $\theta_0$  must be a constant which makes  $u$  real and non-infinite for all values of  $\theta$  in the range  $\alpha \geq \theta \geq -\alpha$ .
- (ii)  $u$  must be zero at the walls, that is at  $\theta = \pm\alpha$ . Hence  $F(\theta) = 0$ , or  $f(\theta) = -\frac{1}{3}$  when  $\theta = \pm\alpha$ .

In the following investigation we assume that the walls do not actually reach the point  $r = 0$ , but fall short of it, so that the singularities which occur there are avoided.

## 4. THE VELOCITY PROFILE

Since  $f(\alpha) = f(-\alpha) = -\frac{1}{3}$ , we have

$$\wp(\alpha - \theta_0) = \wp(\alpha + \theta_0).$$

This equation can only be satisfied if

$$\alpha - \theta_0 = \pm(\alpha + \theta_0) + 2m\omega_1 + 2n\omega_3 \quad (m, n \text{ integers}),$$

and this gives

$$\left. \begin{array}{l} -\theta_0 \\ \text{or } \alpha \end{array} \right\} = m\omega_1 + n\omega_3.$$

In special cases both these possibilities may be satisfied at the same time. Since the flow depends upon  $\wp(\theta - \theta_0)$  and not upon  $\theta_0$ , there is no loss of generality in making  $\theta_0$  lie within the fundamental period parallelogram. This is equivalent to restricting  $\theta_0$  to one or other of the values  $0, \omega_1, \omega_2, \omega_3$ .  $\theta_0$  cannot be zero, for then  $u$  would be infinite at  $\theta = 0$ . Later in this section it is shown that two cases arise. In the first case,  $\omega_1$  and  $\omega_3$  are complex conjugate numbers and  $\alpha$ , being real, can only have the values  $m\omega_2$ . In the second case  $\omega_1$  is real and  $\omega_3$  is imaginary, so that here  $\alpha$  can only be put equal to  $m\omega_1$ .

These possibilities must be considered in conjunction with the fact that  $\wp(\theta - \theta_0)$  must be real for all values of  $\theta$ . The investigation must here be separated into two sections:

(I) The roots of the cubic

$$4s^3 - g_2s - g_3 = 0$$

are not all real. This corresponds to the case when the discriminant  $\Delta$  is negative. Since  $g_2$  and  $g_3$  are real, one of the roots must be real,  $e_2$  say, and the others,  $e_1$  and  $e_3$ , must be conjugate complex numbers. We put

$$e_1 = A + iB, \quad e_2 = -2A, \quad e_3 = A - iB,$$

where  $A$  and  $B$  are real. The discriminant  $\Delta$  is equal to  $-64B^2H^4$ , where

$$H = +\sqrt{(9A^2 + B^2)}.$$

$\omega_1$  and  $\omega_3$  are the roots of the equation

$$\wp(\omega_1) = e_1 \quad \text{and} \quad \wp(\omega_3) = e_3.$$



Since  $e_1$  and  $e_3$  are conjugate complex numbers and since  $g_2$  and  $g_3$  are real, one solution of these equations can be put into the form

$$\omega_1 = C - iD, \quad \omega_2 = -2C, \quad \omega_3 = C + iD,$$

where  $C$  and  $D$  are real. These values are not unique, since, for example,

$$\omega'_1 = -C - iD, \quad \omega'_2 = 2iD, \quad \omega'_3 = C - iD$$

is another set of values for which  $e_1$  and  $e_3$  are conjugate complex numbers. This second form, and other possible ones, are just alternative ways of describing the fundamental period parallelogram shown in figure 2. They introduce no feature that is not contained by the chosen values of  $\omega_1, \omega_2$  and  $\omega_3$ , and they can, therefore, be neglected. If  $0 \leq \lambda \leq 1$ , then along the lines  $ATC$  [ $z = \lambda \cdot 4C$ ],  $BT D$  [ $z = 2\omega_1 + i\lambda \cdot 4D$ ],  $s$ , which is equal to  $\wp(z)$ ,

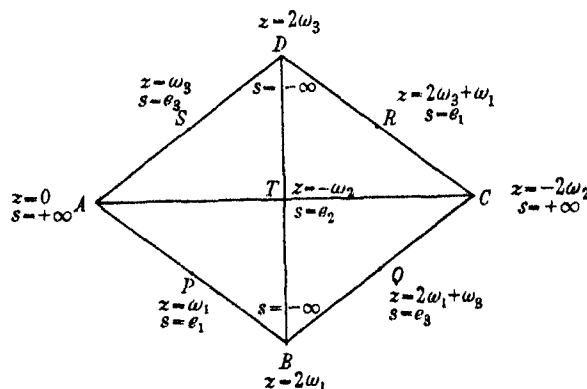


FIGURE 2.  $s = \wp(z)$ ;  $\Delta < 0$ ,  $g_1$  and  $g_3$  real.

assumes all real values from  $-\infty$  to  $+\infty$  twice over. These then are the only lines within the period parallelogram on which  $s$  assumes real values. Along  $ATC$  the variable is real so that we must here identify  $\theta_0$  with  $\omega_2$ , which is the only real half-period. Further, the range of  $\theta$  is  $\alpha \geq \theta \geq -\alpha$ , and if  $2\alpha > 4C$ , i.e.  $2\alpha > |2\omega_2|$ , the range will contain at least one point congruent with the point of zero argument, where  $\wp(z)$  is infinite. This must be avoided and hence the solution here is

$$f(\theta) = \wp(\theta - \omega_2), \quad (4.1)$$

where  $|\omega_2| > \alpha$  and where, in order to satisfy the boundary condition,  $e_2 \leq -\frac{1}{3}$ . It should be noted also that this is the only type of solution under (I), for if  $\alpha$  were to be equal to an integral multiple of  $\omega_2$  the range  $\alpha \geq \theta \geq -\alpha$

would contain at least one point at which the velocity would be infinite. The solution under (I) is therefore

$$\begin{aligned} f(\theta) = \wp(\theta - \omega_2) &= e_2 + \frac{(e_2 - e_1)(e_2 - e_3)}{\wp(\theta) - e_2} = -2A + \frac{H^2}{\wp(\theta) + 2A} \\ &= -2A + H \frac{1 - \operatorname{cn}(2\theta\sqrt{H})}{1 + \operatorname{cn}(2\theta\sqrt{H})} = -2A + H \frac{\operatorname{sn}^2(\theta\sqrt{H}) \operatorname{dn}^2(\theta\sqrt{H})}{\operatorname{cn}^2(\theta\sqrt{H})}, \end{aligned} \quad (4.2)$$

where  $k^2 = \frac{1}{2} \left( 1 + \frac{3A}{H} \right)$  and  $\omega_2 = K/\sqrt{H}$  (see Milne-Thomson 1931, pp. xi and xiv). The boundary condition is

$$\operatorname{cn}(2\alpha\sqrt{H}) = \frac{3H - (6A - 1)}{3H + (6A - 1)} \quad (4.3)$$

$$\text{or} \quad \frac{\operatorname{sn}^2(\alpha\sqrt{H}) \operatorname{dn}^2(\alpha\sqrt{H})}{\operatorname{cn}^2(\alpha\sqrt{H})} = \frac{6A - 1}{3H}. \quad (4.3a)$$

In order that this should have a solution  $6A \geq 1$ , which is the condition  $e_2 \leq -\frac{1}{3}$ .

On the central line  $f(\theta) = e_2 = -2A$  and  $F(0)$  is therefore equal to  $(6A - 1)$  which is positive. On account of the nature of  $\wp(\theta - \omega_2)$  we see that  $F(\theta)$  has a positive value on the central line and decreases monotonically towards the walls where its value is zero. The case considered under (I) always, therefore, represents outflow which is symmetrical with respect to the central line.

(II) We have discussed the case in which  $\Delta < 0$ . Let us now discuss that in which  $\Delta > 0$ . This, since  $g_2$  and  $g_3$  are real, corresponds to the case in which all the roots of the cubic

$$4s^3 - g_2s - g_3 = 0$$

are real. Let them be denoted by  $e_1, e_2, e_3$  chosen in such a way that  $e_1 > e_2 > e_3$ . (The degenerate cases, in which two or three of the roots are equal, will be discussed separately. They correspond to  $\Delta = 0$ .)

In the non-degenerate cases one of the periods,  $2\omega_1$  say, is perfectly real, and one,  $2\omega_3$  say, is perfectly imaginary (see Whittaker and Watson 1920, p. 444). The period parallelogram is then as shown in figure 3. Along the four lines  $APB$  ( $z = \lambda.2\omega_1$ ),  $ASD$  ( $z = \lambda.2\omega_3$ ),  $PTR$  ( $z = \omega_1 + \lambda.2\omega_3$ ),  $STQ$  ( $z = \omega_3 + \lambda.2\omega_1$ ), where  $0 \leq \lambda < 1$ , the Weierstrassian function  $\wp(z)$  takes all real values from  $-\infty$  to  $+\infty$  twice over, so that these are the only lines within the period parallelogram on which  $\wp(z)$  assumes real values.

We cannot identify  $\theta_0$  with  $\omega_1$ , for the argument of  $\wp(\theta - \theta_0)$  would then be represented by points on  $APB$ . Along this line  $\wp(\theta - \theta_0)$  is always

positive, and it would therefore be impossible to satisfy the boundary condition  $f(\alpha) = \wp(\alpha - \theta_0) = -\frac{1}{3}$ . Hence, since  $\alpha$  and  $\omega_1$  are real, the following possibilities arise:

(i)  $\theta_0 = \omega_3$ . The boundary condition is

$$\wp(\alpha - \omega_3) = -\frac{1}{3}. \quad (4.4)$$

In order that this condition may be satisfied it is essential that

$$e_2 \geq -\frac{1}{3} \geq e_3, \quad (4.5)$$

for the argument of  $\wp(\alpha - \omega_3)$  is a point on the line  $STQ$  of figure 3, and along this line the value of  $\wp(z)$  lies between  $e_2$  and  $e_3$ . If (4.5) is satisfied, then (4.4) may be used to determine  $\alpha$ . The number of values of  $\alpha$  satisfying (4.4) is infinite. This will be referred to later in this section.

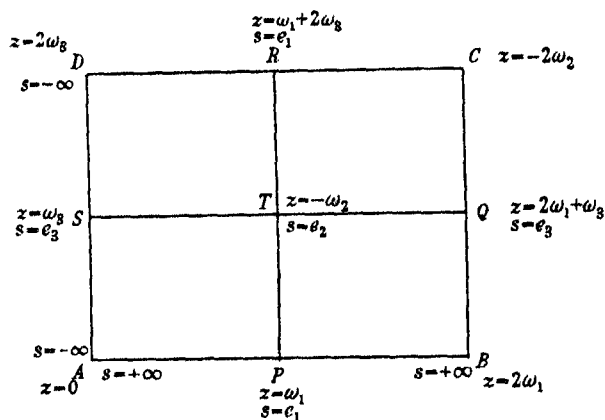


FIGURE 3.  $s = \wp(z)$ ;  $\Delta > 0$ ,  $g_1$  and  $g_3$  real.

(ii)  $\theta_0 = \omega_2$ . The boundary condition is

$$\wp(\alpha - \omega_2) = \wp((\alpha - \omega_1) - \omega_3) = -\frac{1}{3}. \quad (4.6)$$

Here again  $e_2 \geq -\frac{1}{3} \geq e_3$  and there is no unique solution of (4.6).

(iii)  $\alpha = (2n+1)\omega_1$ , where  $n$  is any positive integer. From a consideration of the values of  $\wp(\theta - \theta_0)$  in the range  $\alpha \geq \theta \geq -\alpha$  it is clear that the imaginary part of  $\theta_0$  must be equal to  $\omega_3$  and that  $e_2 \geq -\frac{1}{3} \geq e_3$ . If we put

$$\theta_0 = \alpha_0 + \omega_3, \quad (4.7)$$

where  $\alpha_0$  is real, the equation for  $\alpha_0$  becomes

$$\wp((\alpha_0 - \omega_1) - \omega_3) = -\frac{1}{3}. \quad (4.8)$$

(iv)  $\alpha = 2n\omega_1$ , where  $n$  is any positive integer. Again we see that  $\theta_0$  must be of the form suggested by (4.7) and that  $e_2 \geq -\frac{1}{3} \geq e_3$ . The equation for  $\alpha_0$  is here

$$\wp(\alpha_0 - \omega_3) = -\frac{1}{3}. \quad (4.9)$$

The obvious similarity between the boundary conditions (4.4), (4.6), (4.8) and (4.9) suggests that the four special cases are intimately connected. This is so, as the following method shows. Put

$$X = e_1 - e_3, \quad \text{and} \quad k^2 X = e_2 - e_3. \quad (4.10)$$

$X$  and  $k^2 X$  are always positive. In terms of  $k^2$  and  $X$  we have

$$e_1 = \frac{1}{3}(2 - k^2)X; \quad e_2 = \frac{1}{3}(2k^2 - 1)X; \quad e_3 = -\frac{1}{3}(1 + k^2)X; \quad \omega_1 = KX^{-1}; \quad (4.11)$$

where  $K$  is the complete elliptic integral of the first kind, and  $k$  is the modulus of the elliptic integral. The condition  $e_2 \geq -\frac{1}{3} \geq e_3$  now becomes

$$(2k^2 - 1)X \geq -1 \geq -(1 + k^2)X.$$

This condition assumes different forms according as  $k^2$  is less than or greater than  $\frac{1}{2}$ . Expressed more precisely the condition (4.5) is:

$$\left. \begin{aligned} \text{When } k^2 < \frac{1}{2}, \quad & \frac{1}{1 - 2k^2} \geq X \geq \frac{1}{1 + k^2}, \\ \text{and when } k^2 \geq \frac{1}{2}, \quad & \infty \geq X \geq \frac{1}{1 + k^2}. \end{aligned} \right\} \quad (4.12)$$

The fundamental boundary equation, that is, the one from which all the others can be obtained, is taken to be (4.4). Consider the equation

$$\begin{aligned} \wp(\eta - \omega_3) &= e_3 + (e_2 - e_3) \operatorname{sn}^2\{\eta\sqrt{(e_1 - e_3)}\} \\ &= \frac{1}{3}X \{3k^2 \operatorname{sn}^2(\eta\sqrt{X}) - 1 - k^2\} = -\frac{1}{3}. \end{aligned}$$

This can be put into the form

$$\operatorname{sn}^2(\eta\sqrt{X}) = \{(1 + k^2)X - 1\}/3k^2X. \quad (4.13)$$

The conditions laid down in (4.12) are just those which ensure that (4.13), considered as an equation for  $\eta$ , has real solutions. Let  $\eta_1, \eta_2, \eta_3, \dots$ , etc. be the positive roots of (4.13) in ascending order of magnitude. They are connected by the relations

$$\left. \begin{aligned} \eta_2 &= 2\omega_1 - \eta_1, & \eta_3 &= 2\omega_1 + \eta_1, \\ \eta_4 &= 4\omega_1 - \eta_1, & \eta_5 &= 4\omega_1 + \eta_1, \\ &\text{etc.} \end{aligned} \right\} \quad (4.14)$$

The smallest root,  $\eta_1$ , is less than  $\omega_1 (= KX^{-1})$ . After these preliminary considerations the subdivisions (i), (ii), (iii) and (iv) made above may be written as

$$(i') \quad \theta_0 = \omega_3.$$

In all cases the flow is symmetrical about the central line  $\theta = 0$  for  $\wp(\theta - \omega_3) = \wp(-\theta - \omega_3)$ . In particular the value of  $F(\theta)$  when  $\theta = 0$  is  $-(1 + 3e_3)$  which is  $\{(1 + k^2)X - 1\}$  and is therefore positive. Hence there is always outflow along the central line.

$\alpha$  can have any of the values  $\eta_1, \eta_2, \eta_3$ , etc.

If  $\alpha = \eta_1$ , the flow is pure outflow as shown in figure 4*a*.

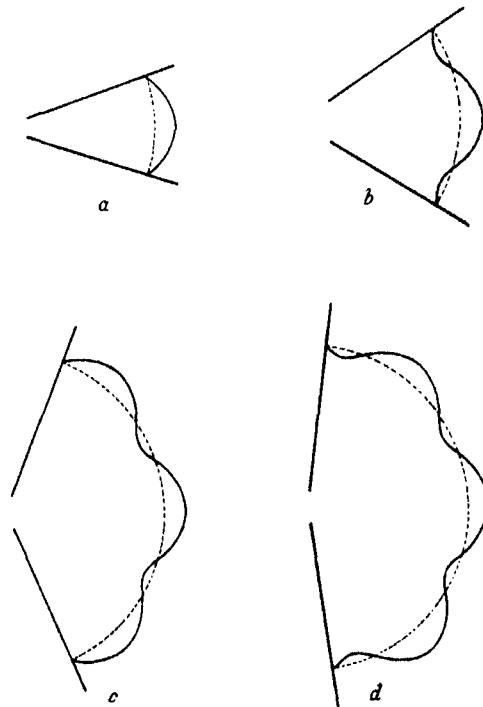


FIGURE 4. Velocity profiles corresponding to (i') of § 4.

If  $\alpha = \eta_2$ , the central outflow is bounded by regions of inflow as in figure 4*b*.

If  $\alpha = \eta_3$ , the central outflow has one region of inflow and one of outflow on either side as in figure 4*c*.

If  $\alpha = \eta_4$ , the central outflow has two regions of inflow and one of outflow on either side as in figure 4*d*.

Etc.

(ii')  $\theta_0 = \omega_2$ .

In all the cases the flow is symmetrical about the central line for  $\varphi(\theta - \omega_2) = \varphi(-\theta - \omega_2)$ . The value of  $F(0)$  is  $-(1 + 3e_2)$  which is equal to  $\{(1 - 2k^2)X - 1\}$  and is therefore negative. Hence there is always inflow along the central line.

$\alpha$  can have any of the values  $\omega_1 - \eta_1, \omega_1 + \eta_1, \omega_1 + \eta_2, \omega_1 + \eta_3, \dots$



FIGURE 5. Velocity profiles corresponding to (ii') of § 4.

If  $\alpha = \omega_1 - \eta_1$ , the flow is entirely inflow as shown in figure 5a.

If  $\alpha = \omega_1 + \eta_1$ , the central inflow is bounded on either side by a region of outflow as in figure 5b.

If  $\alpha = \omega_1 + \eta_2$ , the central inflow has one region of outflow and one of inflow on either side as in figure 5c.

If  $\alpha = \omega_1 + \eta_3$ , the central inflow has two regions of outflow and one of inflow on either side as in figure 5d.

Etc.

(iii') and (iv')  $\alpha = (2n + 1)\omega_1$  or  $\alpha = 2n\omega_1$ .

In all cases the flow is unsymmetrical with respect to the central line.

If  $\alpha = \omega_1$ , then  $\theta_0 = \alpha_0 + \omega_8$  where  $\alpha_0 = \pm(\omega_1 - \eta_1)$  and the flow is as shown in figure 6*a* or 6*a'*. There are no other types.

If  $\alpha = 2\omega_1$ , then  $\theta_0 = \alpha_0 + \omega_8$  where  $\alpha_0 = \pm\eta_1$  and the flow is as shown in figure 6*b* or 6*b'*. There are no other types.

If  $\alpha = 3\omega_1$ , then  $\theta_0 = \alpha_0 + \omega_8$  where  $\alpha_0 = \pm(\omega_1 + \eta_1)$  and the flow is as shown in figure 6*c* or 6*c'*. There are no other types.

Etc.

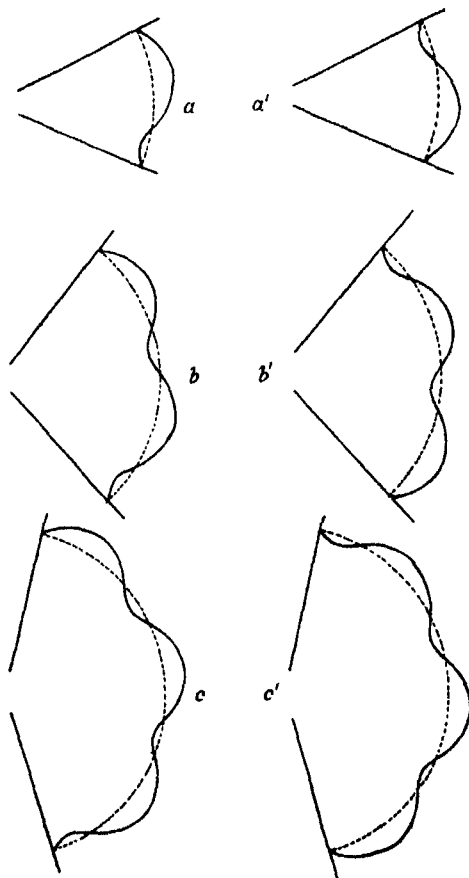


FIGURE 6. Velocity profiles corresponding to (iii') and (iv') of § 4.

##### 5. THE DEGENERATE CASES

The degenerate cases of the Weierstrassian function, when two or three roots of the fundamental cubic are equal, are of interest in that the solutions can be expressed in terms of functions which are more familiar than the

elliptic functions. In addition they provide useful pointers to the general theory. These cases correspond to  $\Delta = 0$  and can be considered under three heads.

(i)  $e_1 = e_2 = e_3$ .

Since  $e_1 + e_2 + e_3 = 0$ , the values of  $e_1, e_2, e_3$  are each zero and the equation for  $f(\theta)$  is

$$f'(\theta)^2 = 4f^3. \quad (5.1)$$

Transform this to the form involving  $F(\theta)$ , by means of the relation  $f(\theta) = -\frac{1}{3}\{F(\theta) + 1\}$  and it becomes

$$F'(\theta)^2 = -\frac{4}{3}\{F + 1\}^3. \quad (5.2)$$

This equation cannot have a physical interpretation in connexion with the present problem for it makes  $F'(\theta)^2$  negative at the walls, that is where  $F(\theta) = 0$ .

(ii)  $e_2 = e_3 = -\frac{1}{2}e_1$ , where  $e_1$  is positive.

The differential equation for  $f(\theta)$  is

$$f'(\theta)^2 = 4(f - e_1)(f + \frac{1}{2}e_1)^2, \quad (5.3)$$

and the differential equation for  $F(\theta)$  is

$$F'(\theta)^2 = -\frac{4}{3}(F + 1 + 3e_1)(F + 1 - \frac{3}{2}e_1)^2. \quad (5.4)$$

This too can have no solution capable of physical interpretation, for it makes  $F'(\theta)^2$  negative where  $F = 0$ , except in the one case where  $e_1 = \frac{2}{3}$ . The only solution then is  $F = 0$  which corresponds to no motion between the walls.

(iii)  $e_1 = e_2 = -\frac{1}{2}e_3$ , where  $e_1$  is positive.

The differential equation for  $f(\theta)$  is

$$f'(\theta)^2 = 4(f - e_1)^2(f + 2e_1), \quad (5.5)$$

and that for  $F(\theta)$  is

$$F'(\theta)^2 = \frac{4}{3}(F + 1 + 3e_1)^2(6e_1 - 1 - F). \quad (5.6)$$

As long as  $(6e_1 - 1) > 0$  this does not produce an inconsistency at points where  $F = 0$ . Put  $6e_1 - 1 = \lambda$  where  $\lambda$  is positive. Equation (5.6) becomes

$$\frac{dF}{d\theta} = \pm \frac{1}{\sqrt{3}}(2F + \lambda + 3)(\lambda - F)^{\frac{1}{2}}. \quad (5.7)$$

If we assume that  $dF/d\theta$  is positive at  $\theta = \alpha$ , we must take the positive sign in equation (5.7). This means that as  $\theta$  decreases below  $\alpha$ , the value of  $F$



decreases below its value at  $\theta = \alpha$ , which is zero. If we take the positive sign in (5.7) we are considering the case where  $F(\alpha - \epsilon)$  is negative,  $\epsilon$  being a small angle. Since  $F$  is zero at  $\theta = \pm \alpha$  there must be at least one point in the range,  $\theta = \theta'$  say, where  $dF/d\theta = 0$ . At this position  $F$  must be negative, and from (5.7) we see that at  $\theta = \theta'$  the value of  $F$  must be  $-\frac{1}{2}(\lambda + 3)$ . The solution of (5.7), however, which satisfies the boundary condition at  $\theta = \alpha$  is, however,

$$\tanh^{-1}\left(\frac{2\lambda}{3(1+\lambda)}\right)^{\frac{1}{2}} - \left(\frac{1+\lambda}{2}\right)^{\frac{1}{2}}(\theta - \alpha) = \tanh^{-1}\left(\frac{2(\lambda - F)}{3(1+\lambda)}\right)^{\frac{1}{2}}. \quad (5.8)$$

If in this we put  $F = -\frac{1}{2}(\lambda + 3)$ , we find that  $\theta' \rightarrow -\infty$  which is impossible. We are therefore compelled to take the negative sign in (5.7) and the solution is

$$\tanh^{-1}\left(\frac{2\lambda}{3(1+\lambda)}\right)^{\frac{1}{2}} + \left(\frac{1+\lambda}{2}\right)^{\frac{1}{2}}(\theta - \alpha) = \tanh^{-1}\left(\frac{2(\lambda - F)}{3(1+\lambda)}\right)^{\frac{1}{2}}. \quad (5.9)$$

From equation (5.7) it is clear that  $dF/d\theta$  is zero when  $F = \lambda$ , and in this position

$$\theta' = \alpha - \left(\frac{2}{1+\lambda}\right)^{\frac{1}{2}} \tanh^{-1}\left(\frac{2\lambda}{3(1+\lambda)}\right)^{\frac{1}{2}}.$$

By symmetry  $\theta'$  must be zero so that

$$\alpha = \left(\frac{2}{1+\lambda}\right)^{\frac{1}{2}} \tanh^{-1}\left(\frac{2\lambda}{3(1+\lambda)}\right)^{\frac{1}{2}}. \quad (5.10)$$

It should be noted also that the maximum value of  $F$  is  $\lambda$ , and this occurs at  $\theta = 0$ . If we put  $\lambda = (2H - 1)$ , where  $H > \frac{1}{2}$ , equations (5.9) and (5.10) become

$$\left. \begin{aligned} F(\theta) &= (2H - 1) - 3H \tanh^2 \theta \sqrt{H}, \\ \alpha \sqrt{H} &= \tanh^{-1}\left(\frac{2H - 1}{3H}\right). \end{aligned} \right\} \quad (5.11)$$

The equations (5.11) correspond to the case usually described in text-books and manuals (see Goldstein 1938, p. 109, equation (63)), if  $H$  is assumed to be so big that  $1/H$  can be neglected.

It can therefore be seen that the cases corresponding to positive  $\Delta$  and negative  $\Delta$  represent fundamentally different types of flow. We note that

$$27\Delta = \{(4 - a)^{\frac{1}{2}} + 8 - 3a - 3b\}\{(4 - a)^{\frac{1}{2}} - 8 + 3a + 3b\} = (4 - a)^3 - (8 - 3a - 3b)^2 \quad (5.12)$$

in terms of the constants  $a$  and  $b$  introduced in equations (3.12) and (3.13).

We note also that  $b$  must be positive as explained just after equation (3.16). Further

- (i) If  $a \geq 4$ ,  $\Delta$  is negative for all values of  $b$ .
- (ii) If  $4 > a > 3$ ,  $\begin{cases} (4-a)^{\frac{1}{2}} + 8 - 3a \text{ is negative,} \\ (4-a)^{\frac{1}{2}} - 8 + 3a \text{ is positive.} \end{cases}$
- (iii) If  $3 > a$ ,  $\begin{cases} (4-a)^{\frac{1}{2}} + 8 - 3a \text{ is positive.} \\ (4-a)^{\frac{1}{2}} - 8 + 3a \text{ is positive.} \end{cases}$

Hence  $\Delta$  is negative and the flow is always pure outflow if

$$\begin{aligned} & \text{(i)} \quad a \geq 3, \\ \text{or (ii)} \quad & 3 > a \quad \text{and} \quad 3b > 8 - 3a + (4-a)^{\frac{1}{2}}. \end{aligned} \quad (5.13)$$

In addition,  $\Delta$  is positive and the flow may be either pure inflow, or may contain regions of inflow and outflow, if

$$\text{(iii)} \quad 3 > a \quad \text{and} \quad 8 - 3a + (4-a)^{\frac{1}{2}} > 3b > 0. \quad (5.14)$$

## 6. THE CASE $\alpha = 0$

The previous analysis shows that, mathematically at any rate, the velocity profile of the two-dimensional flow between inclined plane walls may have many forms. Many of these are, most probably, unstable to slight disturbances so that they will not have been observed in experiment. It is interesting however to investigate the possibility of the existence of similar velocity profiles in the flow between plane parallel walls. The following analysis shows, however, that as  $\alpha \rightarrow 0$  the velocity profiles change and, as a limiting form, assume the parabolic shape which emerges from the well-known theoretical investigation of the flow of viscous fluid between plane parallel walls.

Let  $O'$  be a point on the line  $OX$  of figure 1, distant  $r_0$  from  $O$ . Through  $O'$  draw a line cutting  $OV$  and  $OW$  in  $V'$  and  $W'$ . We put  $O'V'$  and  $O'W'$  each equal to  $h$  and in the subsequent limiting process we keep  $O'$ ,  $V'$ ,  $W'$  fixed in space and allow  $r_0$  to tend to infinity. Introduce new variables  $x$  and  $y$  defined by the equations

$$r = r_0 + x, \quad (r_0 + x)\theta = y. \quad (6.1)$$

$x$  and  $y$  will remain finite while  $r$  and  $r_0$  tend to infinity and  $\theta$  tends to zero. Further  $u$ , the velocity, must remain finite. From (3.18) we see that

$$p = \frac{2\mu u}{r_0 + x} + \frac{a\mu v}{2(r_0 + x)^2} + C. \quad (6.2)$$

The first term tends to zero but the second and third terms are at our disposal since  $a$  and  $C$  are arbitrary. Hence

$$p \rightarrow \left( C + \frac{a\mu\nu}{2r_0^2} \right) - \frac{a\mu\nu}{2r_0^2} x + \frac{3a\mu\nu}{2r_0^4} x^2 - \dots \quad (6.3)$$

The quantity  $\left( C + \frac{a\mu\nu}{2r_0^2} \right)$  is arbitrary and may be put equal to  $p_0$ , an arbitrary constant. The expression  $(a\mu\nu/2r_0^2)$  is also arbitrary, and for any value of  $r_0$  the magnitude of  $a$  can be adjusted to make the ratio finite. Put  $(a\mu\nu/2r_0^2)$  equal to  $P$  where  $P$  is finite. Then, neglecting terms which tend to zero as  $r_0$  tends to infinity, we have

$$p = p_0 - Px. \quad (6.4)$$

If  $P$  is positive then  $a \rightarrow 2Pr_0^2/\mu\nu$ , which is very big. Hence from condition (i) of equation (5.13) the flow is pure outflow. Further, after some manipulation, it can be shown that the velocity profile tends to

$$u = u_0 \left( 1 - \frac{y^2}{h^2} \right), \quad (6.5)$$

where  $u_0 = Ph^2/2\mu$ . If  $P$  is negative, the flow remains of the same type but is reversed in direction.

If the limiting process is carried out in any other manner, the angle  $\alpha$  tends to zero in such a way that the two walls collapse and become identical. In such a limiting process all types of velocity profile mentioned previously are possible.

## 7. THE REYNOLDS NUMBER WHEN $\Delta$ IS NEGATIVE OR ZERO

The Reynolds number as defined in (3.4) is

$$R = \int_{-\alpha}^{\alpha} F(\theta) d\theta = \int_{\alpha}^{-\alpha} \{3f(\theta) + 1\} d\theta = -2\alpha + 3 \int_{\alpha}^{-\alpha} f(\theta) d\theta.$$

When  $\Delta$  is negative the flow is always pure outflow and

$$\left. \begin{aligned} f(\theta) = \wp(\theta - \omega_2) &= -2A + H \frac{\operatorname{sn}^2(\theta\sqrt{H}) \operatorname{dn}^2(\theta\sqrt{H})}{\operatorname{cn}^2(\theta\sqrt{H})}, \\ \operatorname{cn}(2\alpha\sqrt{H}) &= \frac{3H - 6A + 1}{3H + 6A - 1}, \\ \omega_2 &= K/\sqrt{H}, \\ k^2 &= \frac{1}{2}(H + 3A)/H. \end{aligned} \right\} \quad (7.1)$$

It can be shown that

$$\begin{aligned}
 \int_{\alpha}^{-\alpha} f(\theta) d\theta &= 4A\alpha - 2H^{\frac{1}{2}} \int_0^{\alpha\sqrt{H}} \frac{\operatorname{sn}^2 \eta \operatorname{dn}^2 \eta}{\operatorname{cn}^2 \eta} d\eta \\
 &= 4A\alpha - 2H^{\frac{1}{2}} \left[ \frac{\operatorname{sn} \eta \operatorname{dn} \eta}{\operatorname{cn} \eta} + \eta - 2E(\eta) \right]_0^{\alpha\sqrt{H}} \\
 &= 4A\alpha - 2\alpha H + 2H^{\frac{1}{2}} \frac{\operatorname{sn} \alpha\sqrt{H} \operatorname{dn} \alpha\sqrt{H}}{\operatorname{cn} \alpha\sqrt{H}} + 4H^{\frac{1}{2}} E(\alpha\sqrt{H}) \\
 &= 2\alpha \left[ 2A - H + 2H \frac{E}{K} \right] - \frac{2}{3}(18A - 3)^{\frac{1}{2}} + 4H^{\frac{1}{2}} Z(\alpha\sqrt{H}), \quad (7.2)
 \end{aligned}$$

where  $E(u)$  is the Jacobian elliptic integral of the second kind,  $Z(u)$  is the Jacobian zeta function defined by the relation

$$Z(u) = E(u) - \frac{E}{K}u,$$

and  $E$  and  $K$  are the complete elliptic integrals of the first and second kinds. From these formulae we therefore find

$$R = 2\alpha \left( 6A - 3H + 6H \frac{E}{K} - 1 \right) - 2(18A - 3)^{\frac{1}{2}} + 12H^{\frac{1}{2}} Z(\alpha\sqrt{H}).$$

Using the last of the relations given in (7.1), this becomes

$$R = 2\alpha \left\{ H \left( 6 \frac{E}{K} + 4k^2 - 5 \right) - 1 \right\} - 2\sqrt{3} \{ H(4k^2 - 2) - 1 \}^{\frac{1}{2}} + 12H^{\frac{1}{2}} Z(\alpha\sqrt{H}). \quad (7.3)$$

It might be noted too that  $F(0)$ , which gives a measure of the flow on the central line, is given by the relation

$$F(0) = 6A - 1 = (4k^2 - 2)H - 1. \quad (7.4)$$

The central velocity and the Reynolds number are thus expressed in terms of two parameters,  $k^2$  and  $H$ . The evaluation of the Reynolds number corresponding to any pair of values of these parameters, and of the appropriate value of  $\alpha$  given by the second of the equations in (7.1), was effected with the aid of two tables of elliptic functions published by Milne-Thomson (1931, 1932). The results of the evaluation are included in table 2.

The type of flow corresponding to the degenerate case described in (5.11) is the limiting case of (7.3) corresponding to  $\Delta = 0$ . Here  $k^2 = 1$  and

$$\left. \begin{aligned} R &= -2\alpha(H + 1) + 2\sqrt{(6H - 3)}, \\ F(0) &= 2H - 1. \end{aligned} \right\} \quad (7.5)$$

8. THE REYNOLDS NUMBER WHEN  $\Delta$  IS POSITIVE

Here again it can be shown that all the characteristics of the fluid motion can be described in terms of two parameters,  $k^2$  and  $X$ . It has been shown, however, that many different types of flow are associated with each pair of values of  $k^2$  and  $X$ . The type is determined by the value of  $\alpha$  which is chosen from the infinite set of values which are available as solutions of the boundary condition. (Physically, however, not all these values are permissible, for  $\alpha$  must be less than  $\pi$ .) The exact dependence of the type of flow upon the choice of  $\alpha$  can be seen from conditions (i'), (ii'), (iii'), (iv') of § 4. As can be seen from the diagrams of the types of flow, the two fundamental ones are those which correspond to pure outflow and to pure inflow. The associated values of the Reynolds number can be determined, and it can be seen that the Reynolds numbers of the other types of flow are sums of integral multiples of these fundamental quantities.

Referring to conditions (i') and (ii') mentioned above we see that if  $\alpha = \eta_1$  the flow is entirely outflow and that if  $\alpha = \omega_1 - \eta_1$  the flow is entirely inflow. The corresponding values of the Reynolds number are  $S$  and  $T$  where

$$S = 2 \int_0^{\eta_1} F(\eta) d\eta > 0, \quad T = 2 \int_{\eta_1}^{\omega_1} F(\eta) d\eta < 0, \quad (8.1)$$

and where  $\eta_1$  is the smallest positive root of the equation

$$\operatorname{sn}^2(\eta_1/X) = \{(1 + k^2)X - 1\}/3k^2X.$$

The other terms in equations (8.1) are defined by equations which have been derived previously but which, for purposes of convenience, are here repeated:

$$\omega_1 = KX^{-\frac{1}{2}},$$

$$\begin{aligned} F(\eta) &= -3e_3 - 3(e_2 - e_3) \operatorname{sn}^2\{\eta(e_1 - e_3)^{\frac{1}{2}}\} - 1 \\ &= 3X \operatorname{dn}^2(\eta_1/X) - (2 - k^2)X - 1. \end{aligned}$$

From these relations it can be proved that

$$\begin{aligned} S &= 6X^{\frac{1}{2}} Z(\eta_1/X) + 2\eta_1 \left\{ X \left( 3 \frac{E}{K} - 2 + k^2 \right) - 1 \right\}, \\ S + T &= 2KX^{-\frac{1}{2}} \left\{ X \left( 3 \frac{E}{K} - 2 + k^2 \right) - 1 \right\}. \end{aligned}$$

The Reynolds numbers of the various types of flow are then:

|                |               |                |                |
|----------------|---------------|----------------|----------------|
| Type figure 4a | $R = S,$      | Type figure 4c | $R = 3S + 2T,$ |
| 5a             | $R = T,$      | 5c             | $R = 2S + 3T,$ |
| 4b             | $R = S + 2T,$ | 4d             | $R = 3S + 4T,$ |
| 5b             | $R = T + 2S,$ | 5d             | $R = 4S + 3T,$ |
| etc.           |               |                |                |

|                         |                |
|-------------------------|----------------|
| Type figures 6a and 6a' | $R = S + T,$   |
| 6b and 6b'              | $R = 2S + 2T,$ |
| 6c and 6c'              | $R = 3S + 3T,$ |
| etc.                    |                |

Values of  $S$  and  $T$  are given in table 1 for different values of  $k^2$  and  $X$ . The table covers the domain  $\Delta \geq 0$  and gives the limits of  $X$  corresponding to each value of  $k^2$ . The cases  $k^2 = 1.0$  and  $k^2 = 0.0$  are critical ones and have been considered as limiting cases of  $k^2 = 1 - \epsilon$  and  $k^2 = \epsilon$  as  $\epsilon \rightarrow 0$ .

TABLE 1. VALUES OF  $k^2$  AND  $X$  WHEN  $\Delta \geq 0$

I (a)  $k^2 = 1.0$ ;  $\infty \geq X \geq 0.5$ ;  $K = \infty$ .

| $X$                | $\eta_1$                | $\omega_1$ | $S$                    | $T$       |
|--------------------|-------------------------|------------|------------------------|-----------|
| 0.500              | 0.000                   | $\infty$   | 0.000                  | $-\infty$ |
| 1.000              | 0.658                   | $\infty$   | 0.832                  | $-\infty$ |
| 1.100              | 0.666                   | $\infty$   | 0.997                  | $-\infty$ |
| 1.500              | 0.657                   | $\infty$   | 1.613                  | $-\infty$ |
| 4.000              | 0.503                   | $\infty$   | 4.136                  | $-\infty$ |
| 9.000              | 0.360                   | $\infty$   | 7.082                  | $-\infty$ |
| 16.000             | 0.277                   | $\infty$   | 9.870                  | $-\infty$ |
| 25.000             | 0.224                   | $\infty$   | 12.600                 | $-\infty$ |
| 36.000             | 0.188                   | $\infty$   | 15.278                 | $-\infty$ |
| $X \geq 100$ (say) | $1.146X^{-\frac{1}{2}}$ | $\infty$   | $2.607X^{\frac{1}{2}}$ | $-\infty$ |

I (b)  $k^2 = 1 - \epsilon$ , where  $\epsilon$  is small;  $\infty \geq X \geq 0.5(1 + \frac{1}{2}\epsilon)$ ;  $K \approx \frac{1}{2} \log_e (16/\epsilon)$ .

When  $X$  is very big

$$\begin{aligned} S &\approx 2.607X^{\frac{1}{2}}, & \eta_1 &\approx 1.146X^{-\frac{1}{2}}, \\ T &\approx \{3.393 - \log_e (16/\epsilon)\} X^{\frac{1}{2}}, & \omega_1 &\approx \{\frac{1}{2} \log (16/\epsilon)\} X^{-\frac{1}{2}}. \end{aligned}$$

I (c)  $k^2 = 0.8$ ;  $\infty \geq X \geq 0.556$ ;  $K = 2.2572$ .

| $X$                | $\eta_1$                | $\omega_1$              | $S$                    | $T$                     |
|--------------------|-------------------------|-------------------------|------------------------|-------------------------|
| 0.556              | 0.000                   | 3.030                   | 0.000                  | -4.826                  |
| 1.000              | 0.648                   | 2.257                   | 0.659                  | -3.519                  |
| 1.440              | 0.673                   | 1.881                   | 1.323                  | -3.101                  |
| 4.000              | 0.529                   | 1.129                   | 3.854                  | -2.804                  |
| 9.000              | 0.383                   | 0.752                   | 6.705                  | -2.251                  |
| 25.000             | 0.240                   | 0.451                   | 12.010                 | -4.652                  |
| 100.000            | 0.122                   | 0.226                   | 24.732                 | -8.627                  |
| $X \geq 100$ (say) | $1.230X^{-\frac{1}{2}}$ | $2.257X^{-\frac{1}{2}}$ | $2.499X^{\frac{1}{2}}$ | $-0.846X^{\frac{1}{2}}$ |

TABLE I (continued)

I (d)  $k^2 = 0.5$ ;  $\infty \geq X \geq 0.667$ ;  $K = 1.8541$ .

| $X$                | $\eta_1$      | $\omega_1$    | $S$                    | $T$    |
|--------------------|---------------|---------------|------------------------|--------|
| 0.667              | 0.000         | 2.271         | 0.000                  | -2.466 |
| 1.000              | 0.635         | 1.854         | 0.407                  | -1.573 |
| 1.690              | 0.731         | 1.426         | 2.015                  | -1.563 |
| 3.240              | 0.672         | 1.030         | 2.991                  | -0.476 |
| 9.000              | 0.490         | 0.618         | 6.472                  | -0.082 |
| $X \geq 200$ (say) | $1.854X^{-1}$ | $1.854X^{-1}$ | $2.542X^{\frac{1}{2}}$ | 0.000  |

I (e)  $k^2 = 0.4$ ;  $5 \geq X \geq 0.714$ ;  $K = 1.7775$ .

| $X$   | $\eta_1$ | $\omega_1$ | $S$   | $T$    |
|-------|----------|------------|-------|--------|
| 0.714 | 0.000    | 2.103      | 0.000 | -1.918 |
| 1.000 | 0.631    | 1.778      | 0.324 | -1.171 |
| 3.610 | 0.758    | 0.936      | 3.339 | -0.059 |
| 5.000 | 0.795    | 0.795      | 4.467 | 0.000  |

I (f)  $k^2 = 0.2$ ;  $1.667 \geq X \geq 0.833$ ;  $K = 1.6596$ .

| $X$   | $\eta_1$ | $\omega_1$ | $S$   | $T$    |
|-------|----------|------------|-------|--------|
| 0.833 | 0.000    | 1.818      | 0.000 | -0.910 |
| 1.000 | 0.623    | 1.660      | 0.161 | -0.521 |
| 1.667 | 1.286    | 1.286      | 1.250 | 0.000  |

I (g)  $k^2 = \epsilon$  (small);  $1 + 2\epsilon \geq X \geq 1 - \epsilon$ ;  $K = \frac{1}{2}\pi(1 + \frac{1}{2}\epsilon)$ .

| $X$             | $\eta_1$                                  | $\omega_1$                                | $S$                      | $T$                       |
|-----------------|---|---|--------------------------|---------------------------|
| $1 - \epsilon$  | 0.000                                     | $\frac{1}{2}\pi(1 + \frac{1}{2}\epsilon)$ | 0.000                    | $-\frac{1}{2}\pi\epsilon$ |
| 1.000           | 0.615 (app.)                              | $\frac{1}{2}\pi(1 + \frac{1}{2}\epsilon)$ | $0.800\epsilon$          | $-2.371\epsilon$          |
| $1 + 2\epsilon$ | $\frac{1}{2}\pi(1 - \frac{1}{2}\epsilon)$ | $\frac{1}{2}\pi(1 - \frac{1}{2}\epsilon)$ | $\frac{1}{2}\pi\epsilon$ | 0                         |

I (h)  $k^2 = 0$ ;  $X = 1$ ;  $K = \frac{1}{2}\pi$ .

| $X$ | $\eta_1$                       | $\omega_1$       | $S$   | $T$   |
|-----|--------------------------------|------------------|-------|-------|
| 1   | $0 \rightarrow \frac{1}{2}\pi$ | $\frac{1}{2}\pi$ | 0.000 | 0.000 |

The results of the above table were then analysed in the following way. Tables were made giving corresponding values of  $\alpha$  and  $R$  for different types of flow. Table 2 gives these values for the symmetrical outflow (cf. figure 4a). The values for symmetrical inflow (cf. figure 5a) are given in table 3. Corresponding values of  $\alpha$  and  $R$  were plotted, as shown in detail in figure 7. Each value of  $k^2$  which was considered gave rise to a curve. These curves mapped out regions in which pure outflow and pure inflow were respectively possible. From these it is clear that, corresponding to each value of  $\alpha$ , there is a range of values of  $R$  in which the type of flow considered is possible. Similar regions were mapped out for different types of flow, and the

appropriate ranges in which they are possible are shown in table 4. Some of the limits were read off from graphs and are therefore subject to error—but the general run, and the order of magnitude, of the limits are as tabulated. The limits of the ranges of the symmetrical types of flow are plotted in figure 8. Those for the non-symmetrical types are shown in figure 9. A number of deductions can be made from these figures, and, in addition, the forms of the curves give rise to a number of speculations as to the stability of the various types of flow.

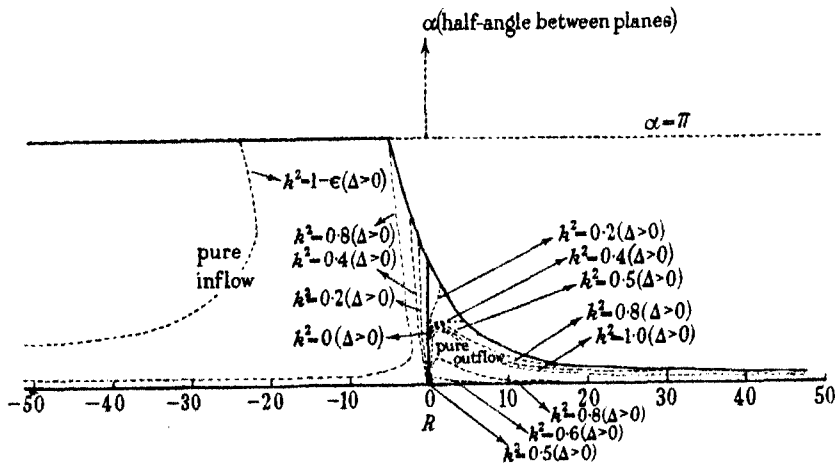


FIGURE 7. Ranges of  $R$  for pure inflow and for pure outflow.

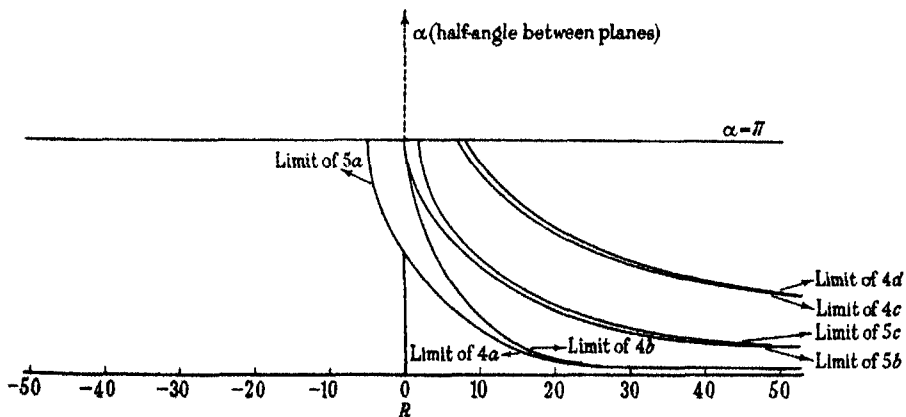


FIGURE 8. Ranges of  $R$  for different types of symmetrical flow. [Note. "Limit of 4a" should be interpreted as the "Upper limit of the Reynolds number for which flow of the type shown in figure 4a is possible." Similar interpretations should be made of the other inscriptions. All the curves tend asymptotically to zero according to the law (constant)/ $R$ .]





| $\Delta > 0$                 |          |          |  |                              |          |          |  |   |          |       |  |
|------------------------------|----------|----------|--|------------------------------|----------|----------|--|---|----------|-------|--|
| $k^2 = 0.8$                  |          |          |  | $k^2 = 0.5$                  |          |          |  | $k^2 = 0.4$                               |          |       |  |
| $X$                          | $\alpha$ | $R$      |  | $X$                          | $\alpha$ | $R$      |  | $X$                                       | $\alpha$ | $R$   |  |
| 0.556                        | 0.000    | 0.000    |  | 0.667                        | 0.000    | 0.000    |  | 0.714                                     | 0.000    | 0.000 |  |
| 1.000                        | 0.648    | 0.659    |  | 1.000                        | 0.635    | 0.407    |  | 1.000                                     | 0.631    | 0.324 |  |
| 1.440                        | 0.673    | 1.323    |  | 1.690                        | 0.731    | 2.015    |  | 3.610                                     | 0.758    | 3.339 |  |
| 4.000                        | 0.529    | 3.854    |  | 3.240                        | 0.672    | 2.991    |  | 5.000                                     | 0.795    | 4.467 |  |
| 9.000                        | 0.383    | 6.705    |  | 9.000                        | 0.490    | 6.472    |  |   |          |       |  |
| 25.000                       | 0.240    | 12.01    |  | $\infty$                     | 0.000    | $\infty$ |  |   |          |       |  |
| 100.000                      | 0.122    | 24.73    |  |                              |          |          |  |   |          |       |  |
| $\infty$                     | 0.000    | $\infty$ |  |                              |          |          |  |   |          |       |  |
| Note                         |          |          |  | Note                         |          |          |  | $k^2 = 0$                                 |          |       |  |
| When $X > 100$ (say)         |          |          |  | When $X > 200$ (say)         |          |          |  | $k^2 = \epsilon$ (small)                  |          |       |  |
| $\alpha \approx 1.230X^{-1}$ |          |          |  | $\alpha \approx 1.854X^{-1}$ |          |          |  | $X$                                       |          |       |  |
| $R \approx 2.499X^1$         |          |          |  | $R \approx 2.542X^1$         |          |          |  | $\alpha$                                  |          |       |  |
| $\alpha R \approx 3.014$     |          |          |  | $\alpha R \approx 4.713$     |          |          |  | $1 - \epsilon$                            |          |       |  |
| $R/\alpha F(0) \approx 1.13$ |          |          |  | $R/\alpha F(0) \approx 0.91$ |          |          |  | $1 - \epsilon$                            |          |       |  |
| $F(0) \approx 1.8X$          |          |          |  | $F(0) \approx 1.5X$          |          |          |  | $1 + 2\epsilon$                           |          |       |  |
|                              |          |          |  |                              |          |          |  | $0.000$                                   |          |       |  |
|                              |          |          |  |                              |          |          |  | $0.615$ (app.)                            |          |       |  |
|                              |          |          |  |                              |          |          |  | $\frac{1}{2}\pi(1 - \frac{1}{2}\epsilon)$ |          |       |  |
|                              |          |          |  |                              |          |          |  | $0.000$                                   |          |       |  |
|                              |          |          |  |                              |          |          |  | $1$                                       |          |       |  |
|                              |          |          |  |                              |          |          |  | $0 \rightarrow \frac{1}{2}\pi$            |          |       |  |
|                              |          |          |  |                              |          |          |  | $R$                                       |          |       |  |
|                              |          |          |  |                              |          |          |  | $0.000$                                   |          |       |  |



TABLE 4. RANGES OF THE REYNOLDS NUMBER IN WHICH THE VARIOUS TYPES OF FLOW ARE POSSIBLE

| $\alpha$         | Pure outflow<br>Symmetrical<br>See figure 4a |                  | Pure inflow<br>Symmetrical<br>See figure 5a |                  | Central outflow<br>with a region of<br>inflow on each side<br>Symmetrical<br>See figure 4b |                  | Central inflow<br>with a region of<br>outflow on each side<br>Symmetrical<br>See figure 5b |                  | Central outflow<br>with a region of<br>inflow and one of<br>outflow on each side<br>Symmetrical<br>See figure 4c |                  |
|------------------|--|------------------|---|------------------|--|------------------|--|------------------|--|------------------|
|                  | $R$  | $R$              | $R$   | $R$              | $R$  | $R$              | $R$  | $R$              | $R$  | $R$              |
| 0.0              | 0.0 to $+\infty$                             | 0.0 to $-\infty$ | 0.0 to $-\infty$                            | 0.0 to $+\infty$ | 0.0 to $+\infty$   | 0.0 to $+\infty$ | 0.0 to $+\infty$   | 0.0 to $+\infty$ | 0.0 to $+\infty$   | 0.0 to $+\infty$ |
| 0.1              | 0.0 47.0                                     | 0.0 $-\infty$    | 0.0 $-\infty$                               | 0.0 188          | 0.0 47   | 0.0 188          | 0.0 188  | 0.0 424          | 0.0 424  | 0.0 424          |
| 0.2              | 0.0 24.0                                     | 0.0 $-\infty$    | 0.0 $-\infty$                               | 0.0 94           | 0.0 24   | 0.0 94           | 0.0 94   | 0.0 212          | 0.0 212  | 0.0 212          |
| 0.3              | 0.0 16.5                                     | 0.0 $-\infty$    | 0.0 $-\infty$                               | 0.0 63           | 0.0 18.8   | 0.0 63           | 0.0 63   | 0.0 127          | 0.0 127  | 0.0 127          |
| 0.4              | 0.0 13.5                                     | 0.0 $-\infty$    | 0.0 $-\infty$                               | 0.0 47           | 0.0 16.5   | 0.0 47           | 0.0 47   | 0.0 106          | 0.0 106  | 0.0 106          |
| 0.5              | 0.0 11.0                                     | 0.0 $-\infty$    | 0.0 $-\infty$                               | 0.0 33           | 0.0 14.5   | 0.0 33           | 0.0 33   | 0.0 85           | 0.0 85   | 0.0 85           |
| 0.75             | 0.0 7.5                                      | 0.0 $-\infty$    | 0.0 $-\infty$                               | 0.0 23.5         | 0.0 10.5   | 0.0 23.5         | 0.0 23.5   | 0.0 66           | 0.0 66   | 0.0 66           |
| 1.00             | 0.0 4.0                                      | 0.0 $-\infty$    | 0.0 $-\infty$                               | 0.0 17.0         | 0.0 8.0  | 0.0 17.0         | 0.0 17.0   | 0.0 53           | 0.0 53   | 0.0 53           |
| $\frac{1}{2}\pi$ | 0.0 0.0                                      | 0.0 $-\infty$    | 0.0 $-\infty$                               | 0.0 9.5          | 0.0 4.0  | 0.0 9.5          | 0.0 9.5  | 0.0 29           | 0.0 29   | 0.0 29           |
| 2.00             | 0.0 0.0                                      | -2.0 $-\infty$   | -2.0 $-\infty$                              | 0.0 5.5          | 0.0 2.0  | 0.0 5.5          | 0.0 5.5  | 0.0 19           | 0.0 19   | 0.0 19           |
| 2.50             | 0.0 0.0                                      | -4.0 $-\infty$   | -4.0 $-\infty$                              | 0.0 2.5          | 0.0 1.0  | 0.0 2.5          | 0.0 2.5  | 0.0 12           | 0.0 12   | 0.0 12           |
| $\pi$            | 0.0 0.0                                      | -5.0 $-\infty$   | -5.0 $-\infty$                              | 0.0 0.0          | 0.0 0.0  | 0.0 0.0          | 0.0 0.0  | 0.0 7            | 0.0 7  | 0.0 7            |

| $\alpha$         | Central inflow<br>with a region of<br>outflow and one of<br>inflow on each side<br>Symmetrical<br>See figure 5c |                  | Central outflow<br>with two regions of<br>inflow and one of<br>outflow on each side<br>Symmetrical<br>See figure 4d |                  | Outflow and inflow<br>Non-symmetrical<br>See figure 6 (a and a') |                  | Outflow and inflow<br>Non-symmetrical<br>See figure 6 (b and b') |                  |
|------------------|---|------------------|---|------------------|--|------------------|--|------------------|
|                  | $R$   | $R$              | $R$   | $R$              | $R$  | $R$              | $R$  | $R$              |
| 0.0              | 0.0 to $+\infty$  | 0.0 to $+\infty$ | 0.0 to $+\infty$  | 0.0 to $+\infty$ | 0.0 to $+\infty$   | 0.0 to $+\infty$ | 0.0 to $+\infty$   | 0.0 to $+\infty$ |
| 0.1              | 0.0 188   | 0.0 424          | 0.0 424   | 0.0 188          | 0.0 47   | 0.0 188          | 0.0 188  | 0.0 188          |
| 0.2              | 0.0 94  | 0.0 212          | 0.0 212   | 0.0 94           | 0.0 31   | 0.0 94           | 0.0 94   | 0.0 94           |
| 0.3              | 0.0 63  | 0.0 127          | 0.0 127   | 0.0 63           | 0.0 25   | 0.0 63           | 0.0 63   | 0.0 63           |
| 0.4              | 0.0 47  | 0.0 106          | 0.0 106   | 0.0 47           | 0.0 20   | 0.0 47           | 0.0 47   | 0.0 47           |
| 0.5              | 0.0 33  | 0.0 85           | 0.0 85  | 0.0 33           | 0.0 17   | 0.0 35           | 0.0 35   | 0.0 35           |
| 0.75             | 0.0 24.5  | 0.0 66           | 0.0 66  | 0.0 24.5         | 0.0 11.5   | 0.0 27           | 0.0 27   | 0.0 27           |
| 1.00             | 0.0 18.5  | 0.0 53           | 0.0 53  | 0.0 18.5         | 0.0 7  | 0.0 22           | 0.0 22   | 0.0 22           |
| $\frac{1}{2}\pi$ | 0.0 11.5  | 0.0 29           | 0.0 29  | 0.0 11.5         | 0.0 0.5  | 0.0 14           | 0.0 14   | 0.0 14           |
| 2.00             | 0.0 7.5   | 0.0 19           | 0.0 19  | 0.0 7.5          | 0.0 1.5  | 0.0 8            | 0.0 8  | 0.0 8            |
| 2.50             | 0.0 4.5   | 0.0 12.5         | 0.0 12.5  | 0.0 4.5          | 0.0 3.5  | 0.0 4            | 0.0 4  | 0.0 4            |
| $\pi$            | 0.0 2.0   | 0.0 7.5          | 0.0 7.5   | 0.0 2.0          | 0.0 4.5  | 0.0 0            | 0.0 0  | 0.0 0            |

In order to make a rapid survey of the velocity profiles at large Reynolds numbers the characteristics of the flow can be compared with two hypothetical cases, (i) a flow in which the velocity is constant across a circular arc, centre  $O$ , spanning the walls, and (ii) a flow which is "parabolic" in form across the same arc. In this paragraph the main interest centres on "pure outflow" and on "pure inflow". The other types of flow are not without interest but it is doubtful whether they will have been observed in normal

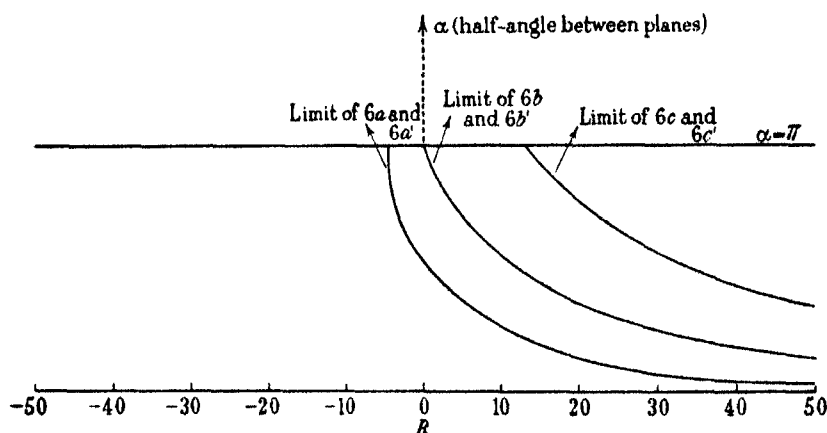


FIGURE 9. Ranges of  $R$  for different types of non-symmetrical flow.  
[Note. See legend below figure 8.]

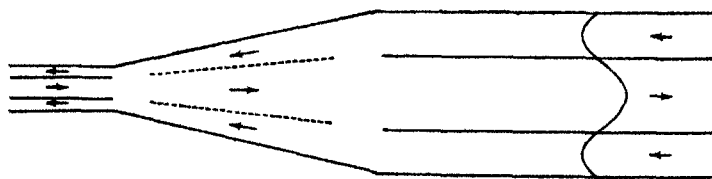


FIGURE 10

experiment. I am, however, indebted to Mr H. B. Squire, M.A., of the Royal Aircraft Establishment, Farnborough, for a suggestion that at low Reynolds numbers, at any rate, it might be possible to reproduce some of the types of flow by means of apparatus represented schematically in figure 10. By means of suitable apparatus it might be possible to obtain slow steady motion in long parallel channels between plane thin walls. At the walls the velocity would be zero. The outer walls of the set of channels could be connected to slowly converging walls and in the ensuing motion, which would be laminar at small Reynolds numbers, there would be vaguely defined layers of zero

velocity separating streams of fluid moving in opposite directions. It is probable, however, that many of these composite types of flow are unstable. This will be referred to later. Returning however to the cases of pure inflow and outflow and to the hypothetical cases mentioned above, if the velocity is constant across a span it can be shown that  $R/\alpha F(0)$  is equal to 2, and if the velocity profile is of the form

$$u = u_0 \left( 1 - \frac{\theta^2}{\alpha^2} \right),$$

the value of  $R/\alpha F(0)$  is  $1\frac{1}{2}$ . These numbers can be compared with those occurring in the notes at the feet of some of the columns in tables 2 and 3. In table 2, relating to outflow,  $\alpha R$  increases uniformly from 0 to 4.713 as  $R/\alpha F(0)$  decreases from 1.33 to 0.91, the Reynolds number being large. Hence for a constant small value of  $\alpha$ , the flow changes from the parabolic form, and becomes more and more concentrated in the centre of the channel, as  $R$  increases. As  $R$  increases still further the value of  $du/d\theta$  becomes zero at the walls and changes sign. This changes the type of flow from that shown in 4a to that in 4b. For large Reynolds number in inflow, however, the value of  $R/\alpha F(0)$  is approximately 2, suggesting a fairly constant velocity across the span dropping very rapidly to zero at the walls. As the Reynolds number is decreased the region in which the flow is approximately constant becomes smaller and finally disappears. This phenomenon has been commented on, and in greater detail, by other investigators, but not from the above point of view.

When the flow changes from the comparatively simple ones discussed in the preceding paragraph we must turn to figures 8 and 9 for a general survey. A representative example will explain the variation of flow with increasing Reynolds number. Let us consider the case  $\alpha = 0.3$  radian. When  $R = -\infty$  all types of flow are possible, except, of course, the pure outflow of type 4a. [N.B. We shall specify each type by the number of the diagram in which it occurs.] This means that the maximum and minimum velocities can be adjusted at will in any one of the types to make the total flux equal to  $2\nu$  times the required Reynolds number. This state of affairs continues right up to and including  $R = 0$ . In the range  $0 < R < 16.5$  all types of flow, except of course the pure inflow of 5a, are possible. If  $R$  increases beyond this limit, then there must be a change of type of flow *only* if the original type was that of 4a. Other types of flow would continue unchanged. Beyond  $R = 16.5$  the type 4a is not possible. Similarly beyond 18.8 all types of flow except 4a and 4b are possible. And so on! In addition, non-symmetrical types of flow are possible, and, where they occur, a mirror image of the flow with

respect to the central line gives a second possible flow, as, for example, in figures 6a and 6a'.

It can be seen quite readily that the state of affairs is extremely complicated. The above mathematical analysis only yields information as to the types of flow which are possible but gives no help on the question as to which is the type actually assumed by the flow when  $R$  and  $\alpha$  are given. It might be noted here that in a normal experiment boundary conditions are imposed not only by the friction at the walls but also by the imposed pressure conditions over the inlet and outlet ends of the channel. The above investigation may be considered as one which determines the proper pressure distributions over the ends which allow of steady laminar radial flow. If in an experiment the pressure distribution is not one of those obtained above, the flow may be neither steady, laminar nor radial. It might be noted too that the imposed pressure conditions in experiment are closer to those implied by the pure outflow and inflow than those implied by the other types, so that pure outflow and pure inflow are more likely to occur than are the other types. It is clear also, from figure 8, that if  $\alpha > \frac{1}{2}\pi$  pure outflow is quite impossible—whatever the Reynolds number may be—and that there is a range of small Reynolds number within which pure inflow is impossible.

Considerations of stability are undoubtedly the dominant ones in deciding the type of flow assumed by the fluid. On the other hand, the present state of the theory of stability of fluid does not seem to offer much hope that information will be obtained along these lines. It is possible, however, to make a fairly plausible assumption here which will have the effect of systematizing our picture of the way in which the velocity profile changes with increasing Reynolds number. The assumption is that "If the pressure conditions over the inlet and outlet ends are not rigidly applied—that is, if the pressure-profile can be assumed to be loosely self-adjusting—then the velocity-profile will be that one which has the smallest number of crests and troughs". If this assumption is accepted, and if we leave out of consideration the non-symmetrical velocity profiles and those which have inflow along the central axis and yet give a positive total flux outwards, then the sequence of changes is as follows. For inflow the velocity profile is always that of figure 5a. For outflow the velocity profile passes through the sequence of changes shown in figure 4. If these types of flow are possible for the whole range of Reynolds number, there seems to be no plausible reason why the other velocity profiles, that is, those in figures 5b, c, d, etc., and in figure 6, should ever manifest themselves, unless they can be produced by rigidly imposed pressure conditions at the ends of the channel.

This sequence of speculations can be pressed still further, and one can

surmise as to the stability of the various types of flow. If at any angle  $\alpha$  there is a rapid variation of the type of flow for a small change in the Reynolds number, it seems legitimate to suggest that the particular type of flow is unstable in the region of the Reynolds number in question. For example, when  $\alpha$  is 0.2, and  $R$  is about 24, a small increase in  $R$  produces a rapid transition from type 4a to type 4b and then to type 4c. This type of instability seems to manifest itself for all types of outflow but not for inflow.

## REFERENCES

- Dean 1934 *Phil. Mag.* (7), **18**, 759.  
Goldstein 1938 *Modern developments in fluid dynamics*. Oxford Univ. Press.  
Hamel 1916 *Jber. dtsch. MatVer.* **25**, 34.  
Harrison 1919 *Proc. Camb. Phil. Soc.* **19**, 307.  
Jeffery 1915 *Phil. Mag.* (6), **29**, 455.  
Karman 1922 *Vorträge aus dem Gebiete der Hydro- und Aero-dynamik*, p. 150. Innsbruck.  
Milne-Thomson 1931 *Die elliptischen Funktionen von Jacobi*. Berlin: Julius Springer.  
— 1932 The Zeta Function of Jacobi. *Proc. Roy. Soc. Edinb.* **52**, 236.  
Noether 1931 *Handbuch der physikalischen und technischen Mechanik*, **5**, 733.  
Tollmien 1931 *Handbuch der Experimentalphysik*, **4** (part I), 257.  
Whittaker and Watson 1920 *Modern analysis*. 3rd ed. Camb. Univ. Press.
-



# Dielectric loss in simple alkyd resins

BY D. R. PELMORE AND E. L. SIMONS

(Communicated by E. V. Appleton, F.R.S.—Received 1 February 1940)

## INTRODUCTION

The work described in this paper was suggested by the results of earlier work done in this laboratory in an endeavour to elucidate the fundamental causes of power loss in dielectrics subjected to alternating stress.

The work referred to has been described in three papers (Jackson 1935; Sillars 1938; Pelmore 1939) and refers to the dielectric characteristics of mixtures of paraffin wax with small amounts of long-chain aliphatic esters. It was shown in these papers that the observed dielectric losses can be interpreted in terms of the Debye theory of polar molecules and that the molecules probably rotate as rigid rods: this conclusion was based on a study of the effect of the chain lengths of the molecules of the polar and non-polar constituents of the system.

The last paper also described experiments in which the molecules of the polar constituent contained two polar groups: when the resolved parts of the dipole moments of these two groups transverse to the chain length were in opposing senses, no appreciable power losses resulted, but when these were in the same sense the loss characteristics were similar to those of the corresponding mono-esters. It was pointed out that this might give a clue in the search for new low loss dielectrics and that it might be possible to achieve good results by using long-chain compounds containing an even number of polar groups arranged so that half the dipole components transverse to the chain are in the opposite sense to the other half.

This paper describes the results of a preliminary investigation to find out whether these conclusions are in any way applicable to highly polymerized substances: the polymers obtained by the esterification of dibasic acids with glycols were chosen for the purpose.

## MATERIALS

The researches referred to in the introduction were made with materials whose chemical constitution and crystalline structure were known and an attempt was made to relate the observed dielectric properties to the known

facts about the physical and chemical constitution. The materials were not chosen because they had any practical possibility as dielectrics, but because they were found to be suitable for studying the effect of molecular structure on the dielectric loss and its variation with temperature and frequency.

The aim of the present work is to find out if the conclusions drawn from the earlier work are applicable to materials whose structure is more complicated. Here again the materials were chosen not because they of themselves had any practical possibilities but because it was hoped the results would be easy to interpret and that the conclusions might be applicable to a wide range of synthetic and natural materials. The repeating units in the long-chain polyesters of glycols and dibasic acids are very similar to the aliphatic esters used in the earlier work.

These polymers have been studied by Carothers and others and are found to consist of long-chain molecules of the type



The molecular weights vary with the method of preparation, but are of the order of 30,000.

The X-ray structure of such polymers has been investigated by C. S. Fuller and C. J. Frosch (1939). They found that for all the polyesters they used, except ethylene succinate, the chains were linear and had a planar zigzag structure. There are two forms of ethylene succinate and the most usual form is believed to have a helical structure. For the polyesters (containing both odd and even numbers of carbon atoms in the repeating groups) the carbon chains in drawn fibres are parallel to each other and parallel to the fibre direction. The planes containing the ends of the repeating groups are perpendicular to the chain axes in the polyesters with odd numbers of carbon atoms in the repeating units, but oblique to them in those where the repeating groups contain even numbers of carbon atoms.

For our experiments the polymers were prepared by heating the dibasic acid with a slight excess of the glycol at 160° C for 8 hr. until no more water distilled off; the excess glycol was removed by heating under a pressure of 15 mm. of mercury for 6 hr. and finally heating was continued for 4 hr. under a pressure of about 0.2 mm. The product was dissolved in chloroform dried with sodium sulphate and reprecipitated with ether.

The polymers used are given in the table in which  $x$  and  $y$  refer to the number of carbon atoms in the acid and glycol portions of the chain. The arrows in the last column of this table represent the directions of the dipole

moments of the ester groups. For example, if we write the formula of polytrimethylene succinate, we have:

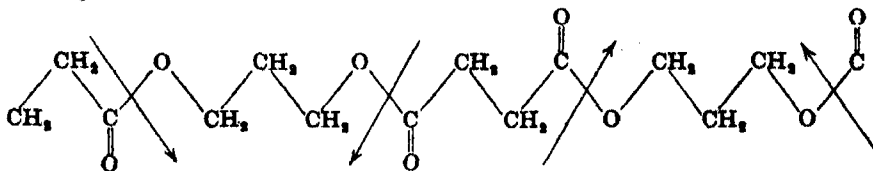


TABLE I

| No. | Polymer                    | $x$ | $y$ | Type |   |
|-----|----------------------------|-----|-----|------|---|
| 1   | Polyethylene succinate     | 4   | 2   | A    | $\nearrow \searrow \nearrow \searrow \nearrow$          |
| 2   | Polytrimethylene succinate | 4   | 3   | B    | $\searrow \nearrow \nearrow \searrow \searrow \nearrow$ |
| 3   | Polyethylene malonate      | 3   | 2   | C    | $\nearrow \searrow \searrow \nearrow$                   |
| 4   | Polytrimethylene malonate  | 3   | 3   | D    | $\nearrow \searrow \searrow \nearrow$                   |
| 5   | Polyethylene adipate       | 6   | 2   | A    | $\nearrow \searrow \searrow \nearrow \searrow \nearrow$ |

When  $x$  and  $y$  are both even, there is a regular alternation in the direction of the dipole moments with respect to the chain axis, and we should expect this type to give the least polarization. So far as the carbon chains can be considered as rigid rods, this type should give no power loss in alternating fields.

Types 2 and 3 are similar and the directions of the dipole moments transverse to the chain axes alternate in pairs: if the chains were strictly rigid these types should also give no loss.

In type 4 all the dipoles have the same direction with respect to the chain axis, and if the chain can rotate this should give the maximum polarization of the four types and the maximum power loss.

#### APPARATUS

The apparatus has been described elsewhere (Sillars 1938). The measurements were made on specimens of about 1 mm. thick, formed by the solidification of the molten resin between the condenser plates.

#### RESULTS AND DISCUSSION

Figures 1-5 give the observed values of  $\tan \delta$  for five different polymers.

In figures 2-4 (polymers type B, C and D respectively), it can be seen that the curves of  $\tan \delta$  and temperature show a well-defined maximum.  $\tan \delta$ , however, does not fall to zero at high and low temperatures as it did

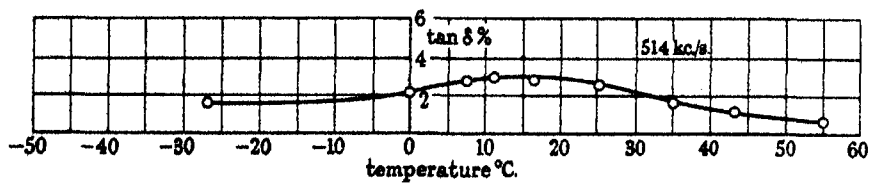


FIGURE 1. Polyethylene succinate.

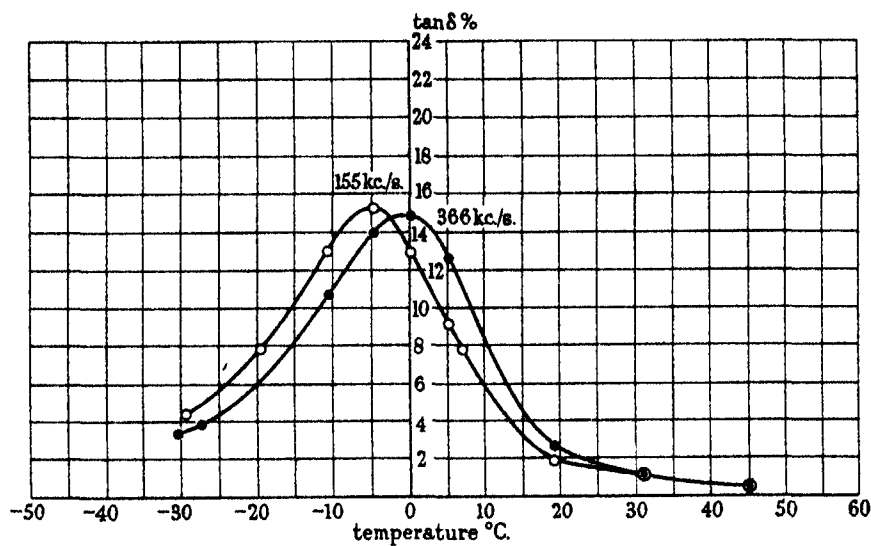


FIGURE 2. Polytrimethylene succinate.

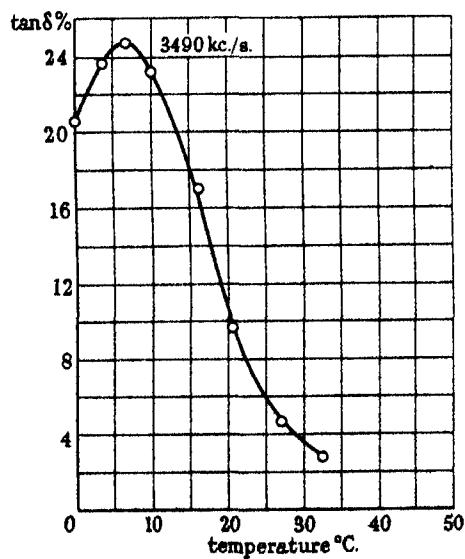


FIGURE 3. Polyethylene malonate.

in the simple paraffin ester systems; this is probably due to moisture or to impurities. Thus the curve for 165 kc./sec. in figure 4 falls to only 3% at high temperatures and this is almost certainly due to residual moisture. (Note: Garton (1939) has published recently the results of an investigation of the dielectric properties of a chemically pure glycol phthalate resin. For this pure resin there was a similar sharp maximum in the curves of  $\tan \delta$

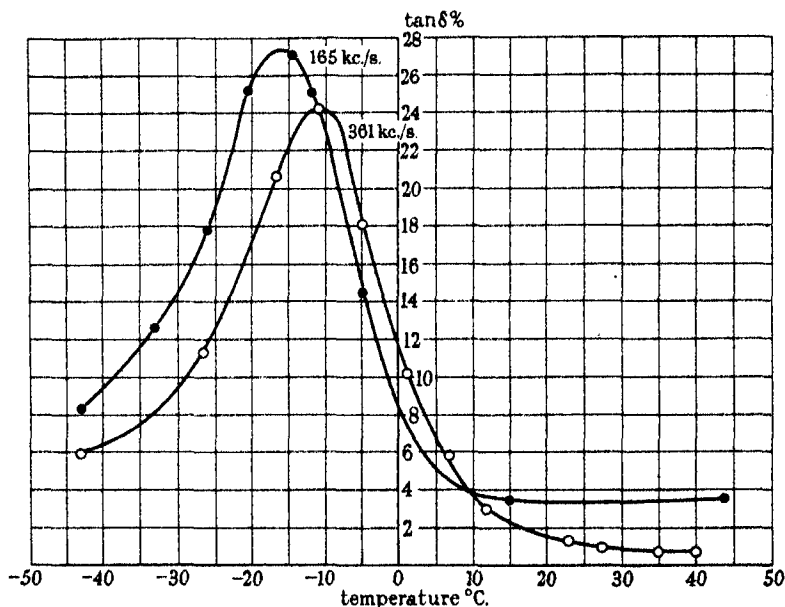


FIGURE 4. Polytrimethylene malonate.

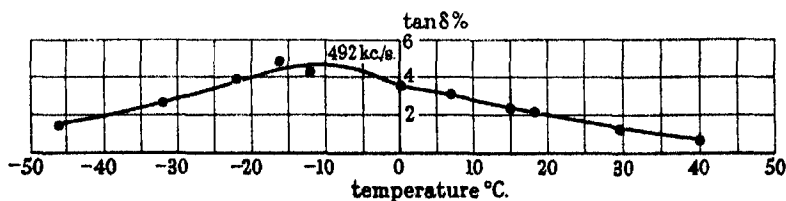


FIGURE 5. Polyethylene adipate.

plotted against temperature and the values of  $\tan \delta$  at temperatures remote from the maximum were below  $\frac{1}{2}$  %.)

Figures 1 and 5 show that for polyethylene succinate and polyethylene adipate, both of type A (see table 1) the curves are quite different from those for the other three types: the maximum value of  $\tan \delta$  is very much less and the curves are much broader. In view of the uncertainty about the structure of polyethylene succinate not much can be inferred from figure 1,

but figures 1 and 5 are nevertheless similar to each other and different from the others. It has been pointed out that if the molecular chains behaved as rigid rods, then polymers of the type A, B or C should give no loss, but this is contrary to experience. There are three alternatives:

- (1) The chains are not rigid.
- (2) The observed loss is due to other causes than the rotation of polar groups.
- (3) The observed loss is due to the end groups or to the presence of polymers of low molecular weight.

It is true that the loss in polymers of type A, as illustrated by figures 1 and 5, is insensitive to temperature and the general behaviour is very reminiscent of many commercial dielectrics. It may well be that the neutralization of the dipoles is substantially complete in this type, and that the residual loss is due almost entirely to non-polar effects. The fact that types B and C give sharp maxima of  $\tan \delta$  shows that if this loss is due to polar molecules the chains certainly do not behave as rigid rods.

It is interesting to notice that, in spite of their high molecular weight, the relaxation times in these polymers are of the same order as those found for spermaceti: we must conclude, therefore, that the relaxation in this case is not governed by the chain length as it was in the other systems, but that the loss is due to a certain flexibility in the chains.

It is seen, however, that type A is quite different from types B, C, D, and the difference is probably due to the fact that the orientation of any one group in line with the electric field is hindered by a torque in the opposite sense due to both neighbouring groups.

It is hoped that this preliminary work will lead to a more detailed investigation with a wider range of substances and an investigation of the effect of the molecular weights on the dielectric properties of such polymers.

The work was carried out in the Engineering Laboratory, Oxford, under the direction of Dr E. B. Moullin. The authors are indebted to Dr Moullin for his help and interest in the work and to the Department of Scientific and Industrial Research for grants enabling the work to be carried out.

#### REFERENCES

- Fuller, C. S. and Frosch, C. J. 1939 *J. Phys. Chem.* 7, 323.  
Garton, C. G., n.d. *Brit. Elect. Allied Industr. Res. Ass.*, Report L/A/T 195.  
Jackson, W. 1935 *Proc. Roy. Soc. A*, 150, 197.  
Pelmore, D. R. 1939 *Proc. Roy. Soc. A*, 172, 502.  
Sillars, R. W. 1938 *Proc. Roy. Soc. A*, 169, 66.

# Thermal transpiration of a dissociating gas

BY B. N. SRIVASTAVA, D.Sc.

*Lecturer in Physics, Allahabad University*

(Communicated by M. N. Saha, F.R.S.—Received 9 February 1940)

In this paper the thermal transpiration of a dissociating gas has been investigated theoretically for two chambers maintained at different temperatures and communicating with each other through a narrow opening. It has been shown that the condition of thermodynamical equilibrium and the usual transpiration relation for each constituent cannot both be satisfied simultaneously. In § 2 the problem has been treated rigorously from the viewpoint of a steady state. Expressions have been worked out showing how the law of mass action suffers modification in this case. Expressions have also been deduced for the atomic and molecular concentrations in the two chambers and the modified transpiration relation is stated. In § 3 an approximate solution of the problem has been given which is based on the assumption of thermodynamical equilibrium in each chamber. Expressions have been deduced for the absolute magnitude as well as the ratio of the atomic or molecular concentrations in the two chambers in the general case and some limiting cases. Finally, the relative merits and demerits of both the treatments have been clearly set forth.

The phenomenon of thermal transpiration or thermo-molecular pressure for a non-dissociating gas was experimentally investigated by Osborne Reynolds and can be easily explained from the kinetic theory of matter. It would be interesting to find what would happen if the gas undergoes appreciable dissociation at the temperatures prevailing in the two chambers. The problem does not appear to have been investigated so far either theoretically or experimentally. It is, however, of considerable practical importance, and the author's attention was drawn to it in connexion with his experiments on the dissociation of alkali halides (Srivastava 1938, 1939). It will therefore be discussed theoretically in this paper.

## § 1

The ordinary expression for a non-dissociating gas using Boltzmann's statistics will first be deduced. Let the two chambers be maintained at temperatures  $T$  and  $T'$  and their respective volumes be  $V$  and  $V'$ . Suppose,

in the steady state, the molecular concentrations are  $n$  and  $n'$ . The equality of flux yields

$$\frac{1}{4}n\sqrt{\frac{8kT}{m\pi}} = \frac{1}{4}n'\sqrt{\frac{8kT'}{m\pi}},$$

or

$$n\sqrt{T} = n'\sqrt{T'}. \quad (1)$$

Further

$$Vn + V'n' = M/m, \quad (2)$$

where  $M$  is the total mass of the gas. From equations (1) and (2) we get

$$n = \frac{M/m}{V + V'\sqrt{(T/T')}}; \quad n' = \frac{(M/m)\sqrt{(T/T')}}{V + V'\sqrt{(T/T')}}. \quad (3)$$

Thus the quantities  $n$  and  $n'$  depend upon  $M$ ,  $V$ ,  $V'$ , etc., but their ratio depends only on  $T$  and  $T'$  as given by equation (1).

Let us see what happens when the gas is assumed to be capable of dissociation. Consider a gas consisting of molecules of the type  $X_2$ . Each chamber will then contain  $X_2$  molecules and  $X$  atoms, which will have to be in chemical equilibrium with each other and also in mechanical equilibrium with the other chamber. It can be readily seen that under these circumstances the concentrations  $n_1, n_2, n'_1, n'_2$  ( $n_1$  referring to the atom,  $n_2$  to the molecule) cannot simultaneously satisfy the condition of chemical or thermodynamical equilibrium (i.e. law of reaction isochore), and also the condition that in the steady state the net flux is zero for each constituent. For if both the conditions were satisfied we should have

$$n_1^2 = Kn_2, \quad (4)$$

$$n_1'^2 = K'n_2', \quad (5)$$

and

$$n_1\sqrt{T} = n_1'\sqrt{T'}, \quad (6)$$

$$n_2\sqrt{T} = n_2'\sqrt{T'}. \quad (7)$$

From equations (6) and (7) we get

$$\frac{n_1}{n_2} = \frac{n_1'}{n_2'}, \quad (8)$$

and from equations (4) and (5) we have

$$\begin{aligned} \frac{K}{K'} &= \frac{n_1^2 n_2'}{n_2 n_1'^2} = \frac{n_1}{n_1'} \quad \text{from equation (8)} \\ &= \sqrt{\frac{T'}{T}} \quad \text{from equation (6)}. \end{aligned}$$



This evidently shows that both the conditions for equilibrium can be satisfied only when  $K$  varies as  $T^{-1}$ . Experimentally and theoretically we know that  $K$  generally varies exponentially with  $T$ , and hence the condition  $K/K' = \sqrt{(T'/T)}$  cannot be satisfied in practice and therefore the equations (4)–(7) cannot all hold.

The question arises: How are the equations modified? Rigorously speaking, none of the equations (4)–(7) should hold. Equations (6) and (7) must be replaced by a single equation representing the equality of flux of mass (atomic as well as molecular) of each component (here only one) in both directions. This gives for the mass of type  $X$  the condition

$$\frac{1}{4}n_1m\sqrt{\frac{8kT}{m\pi}} + \frac{1}{4}n_22m\sqrt{\frac{8kT}{2m\pi}} = \frac{1}{4}n'_1m\sqrt{\frac{8kT'}{m\pi}} + \frac{1}{4}n'_22m\sqrt{\frac{8kT'}{2m\pi}}, \quad (9)$$

$$\text{or} \quad (n_1 + n_2\sqrt{2})\sqrt{T} - (n'_1 + n'_2\sqrt{2})\sqrt{T'} = 0, \quad (10)$$

since the mass of the molecule is double that of the atom. Since equations (6) and (7) representing the equality of flux of each constituent do not now hold, it follows that there will be a net flux of the constituents in one direction or the other. From equation (9) it is evident that if there is a net flux of one constituent in one direction there will be a net flux of the other constituent in the other direction, i.e. for one chamber there will be a continuous loss of one constituent and gain of the other in the steady state by effusion alone. Strictly speaking, therefore, it is not a case of true thermodynamic equilibrium and the law of reaction isochore will not be obeyed. It is merely a case of steady state where the processes of chemical reaction and molecular effusion so balance each other that the atomic and molecular concentrations assume fixed values which do not vary with time. This method of treatment is adopted in § 2.

## § 2

As shown above, there is a net loss of one constituent, say atom, and gain of the other constituent, say molecule, in one chamber by effusion. This must be balanced in the steady state by a shifting of the equilibrium, so that there is an excess of atoms formed in the chamber equal to the amount of net loss by effusion and a deficit of molecules equal to the amount of net gain of the latter. For the sake of simplicity we shall assume that the excess number of molecules entering and atoms escaping by thermal effusion is so small that there is only a slight departure from thermodynamical equilibrium, and hence the reaction velocities are given by those prevailing under thermodynamical equilibrium.

Let  $\nu$ 's denote the concentrations for the same temperature and the same total pressure under the condition of thermodynamical equilibrium. Then the  $\nu$ 's will be given by the law of reaction isochore and we must have

$$n_1 + n_2 = \nu_1 + \nu_2;$$

$$\text{or} \quad n_1 = \nu_1 + \sigma; \quad n_2 = \nu_2 - \sigma. \quad (11)$$

$$\text{Similarly} \quad n'_1 = \nu'_1 + \sigma'; \quad n'_2 = \nu'_2 - \sigma'. \quad (12)$$

From our assumption that the reaction velocities are the same as under thermodynamical equilibrium it follows that the excess rate of recombination of atoms over their rate of formation per unit volume at a given temperature will be proportional to  $\sigma$  if  $\sigma$  is small. Following Dirac (1924) we can write it as  $H\sigma$ , where  $H$  is a constant for any given temperature and is a measure of the velocities of dissociation and recombination. If  $T > T'$  then, since for higher temperature a greater dissociation is to be expected, it can be readily seen that there will be a net effusion of atoms from  $T$  to  $T'$  and of molecules in the opposite direction. Hence the net gain of atoms in chamber  $T'$  by effusion must be equal to the excess rate of recombination of atoms in chamber  $T'$ . Hence

$$H\sigma'V' = S\left(\frac{1}{4}n_1\sqrt{\frac{8kT}{m\pi}} - \frac{1}{4}n'_1\sqrt{\frac{8kT'}{m\pi}}\right),$$

$$\text{or} \quad H\sigma'V' = \frac{S}{4}\left(\frac{8k}{m\pi}\right)^{\frac{1}{2}}(n_1\sqrt{T} - n'_1\sqrt{T'}), \quad (13)$$

where  $S$  is the area of the effusion hole.

Similarly we shall get an equation for the excess of molecules in chamber  $T$ . We get

$$L\sigma V = \frac{S}{4}\left(\frac{8k}{2m\pi}\right)^{\frac{1}{2}}(n'_2\sqrt{T'} - n_2\sqrt{T}). \quad (14)$$

$$\text{Van't Hoff's isochore gives} \quad \nu_1^2/\nu_2 = K, \quad (15)$$

$$\nu_1'^2/\nu_2' = K'. \quad (16)$$

$$\text{Or} \quad (n_1 - \sigma)^2 = K(n_2 + \sigma), \quad (17)$$

$$\text{and} \quad (n'_1 - \sigma')^2 = K'(n'_2 + \sigma'). \quad (18)$$

Further, the restraint on the system yields the condition

$$V(n_1 + 2n_2) + V'(n'_1 + 2n'_2) = M/m. \quad (19)$$

Equations (10), (13), (14), (17), (18), (19) give a complete solution of the

problem, as there are six equations to determine the six unknowns  $\sigma$ ,  $\sigma'$ ,  $n_1$ ,  $n_2$ ,  $n'_1$ ,  $n'_2$ .

From equations (13) and (14)

$$n_1 \sqrt{T} - n'_1 \sqrt{T'} = H\sigma' V' \frac{4}{S} \sqrt{\frac{m\pi}{8k}} = A\sigma' \quad (20)$$

$$\text{and} \quad \sqrt{2} (n'_2 \sqrt{T'} - n_2 \sqrt{T}) = L\sigma V \frac{8}{S} \sqrt{\frac{m\pi}{8k}} = B\sigma. \quad (21)$$

Hence, with the help of equation (10), we obtain

$$A\sigma' - B\sigma = 0,$$

$$\text{or} \quad \sigma' = (B/A)\sigma. \quad (22)$$

Substituting in equation (18) for  $\sigma'$  from (22) and assuming  $\sigma$  and  $\sigma'$  to be so small that  $\sigma^2$  and  $\sigma'^2$  can be neglected in comparison to  $n_1^2$  and  $n_1'^2$ , we get from equations (17) and (18)

$$n_1^2 - 2\sigma n_1 = K(n_2 + \sigma)$$

$$\text{and} \quad n_1'^2 - \frac{2B}{A} \sigma n'_1 = K' \left( n'_2 + \frac{B}{A} \sigma \right).$$

Substituting for  $\sigma$  from equation (21) we get

$$(\sqrt{2}/B) [n'_2 \sqrt{T'} - n_2 \sqrt{T}] (K + 2n_1) = n_1^2 - Kn_2, \quad (23)$$

$$(\sqrt{2}/A) [n'_2 \sqrt{T'} - n_2 \sqrt{T}] (K' + 2n'_1) = n_1'^2 - K'n'_2. \quad (24)$$

Equations (23) and (24) have to be combined with (10) and (19) to solve the four unknowns  $n_1$ ,  $n_2$ ,  $n'_1$ ,  $n'_2$ . From equations (23) and (24) we get by division

$$\frac{A}{B} \frac{K + 2n_1}{K' + 2n'_1} = \frac{n_1^2 - Kn_2}{n_1'^2 - K'n'_2}. \quad (25)$$

Again, from equations (10) and (19) we get, on eliminating  $n_1$ , the result

$$n_2 = C + Dn'_1 + En'_2, \quad (26)$$

where

$$C = \frac{M}{mV(2-\sqrt{2})}, \quad D = -\frac{1}{2-\sqrt{2}} \left( \frac{V'}{V} + \sqrt{\frac{T'}{T}} \right),$$

$$E = -\frac{1}{\sqrt{2}-1} \left( \sqrt{2} \frac{V'}{V} + \sqrt{\frac{T'}{T}} \right).$$

Equation (24), with the help of (26), yields

$$n_1'^2 - K'n'_2 = \frac{\sqrt{2}}{A} [n'_2 \sqrt{T'} - (C + Dn'_1 + En'_2) \sqrt{T}] (K' + 2n'_1). \quad (27)$$

This gives a relation between  $n'_1$  and  $n'_2$  which is very complicated, involving in addition to  $K'$  the various other quantities  $S$ ,  $H$ ,  $V$ ,  $L$ ,  $V'$ , etc. The simple mass law relation  $n'_1{}^2 - K'n'_2 = 0$  is thus not obeyed here. Similarly, a relation between  $n_1$  and  $n_2$  can be deduced which will also be very complicated.

Again from equations (19) and (26) we have

$$n_1 = F + Gn'_1 + Jn'_2, \quad (28)$$

where

$$F = -\frac{M}{mV(\sqrt{2}-1)}, \quad G = \frac{1}{\sqrt{2}-1} \left[ \frac{V'}{V} + \sqrt{\frac{2T'}{T}} \right], \quad J = \frac{2}{\sqrt{2}-1} \left[ \frac{V'}{V} + \sqrt{\frac{T'}{T}} \right].$$

Substituting for  $n_1$  and  $n_2$  from equations (28) and (26) in (25) we get

$$\frac{AK + 2F + 2Gn'_1 + 2Jn'_2}{B} \frac{(F + Gn'_1 + Jn'_2)^2 - K(C + Dn'_1 + En'_2)}{n'_1{}^2 - K'n'_2} = \frac{(F + Gn'_1 + Jn'_2)^2 - K(C + Dn'_1 + En'_2)}{n'_1{}^2 - K'n'_2}. \quad (29)$$

This gives yet another relation between  $n'_1$  and  $n'_2$ . Equations (27) and (29) can be combined to give  $n'_1$  and  $n'_2$  separately and then from equations (28) and (26)  $n_1$  and  $n_2$  can be determined. The problem can thus be completely solved. The relations (27) and (29) are very complicated algebraically. Any actual case, however, can be easily solved by substituting numerical values.

To solve equations (27) and (29) let us multiply them together. We get

$$\begin{aligned} (\sqrt{2}/B) [K + 2F + 2Gn'_1 + 2Jn'_2] [n'_2\sqrt{T'} - (C + Dn'_1 + En'_2)\sqrt{T}] \\ = (F + Gn'_1 + Jn'_2)^2 - K(C + Dn'_1 + En'_2), \end{aligned}$$

which can be written in the form

$$a_1 n'_1{}^2 + a_2 n'_1 + a_3 = 0,$$

where  $a_1$ ,  $a_2$ ,  $a_3$  can be expressed explicitly in terms of  $n'_2$  and the known quantities  $K$ ,  $B$ ,  $F$ ,  $G$ , etc. Hence

$$n'_1 = \frac{1}{2a_1} [-a_2 \pm (a_2^2 - 4a_1a_3)^{\frac{1}{2}}]. \quad (30)$$

Substituting this value of  $n'_1$  in equation (27) we get an equation in  $n'_2$  only, which can be solved.

We have seen above how far the mass action condition is modified. Let us now see how far the transpiration equilibrium conditions are altered. From equation (10) we have

$$\sqrt{\frac{T}{T'}} = \frac{n'_1 + n'_2\sqrt{2}}{n_1 + n_2\sqrt{2}}, \quad (31)$$

while in the ordinary case without dissociation or association the equilibrium condition is  $\sqrt{(T/T')} = n'_2/n_2$  or  $\sqrt{(T/T')} = n'_1/n_1$ . To get the actual relation between  $n_2$  and  $n'_2$  we have to substitute in equation (31) the value of  $n'_1$  in terms of  $n'_2$  from (30) and of  $n_1$  from an analogous relation in terms of  $n_2$ . In a similar way we can obtain the relation connecting  $n_1$  and  $n'_1$ . These relations are thus seen to be very complicated, in this case involving all the constants  $K, K', S, H, V, L$ , etc. Hence the relation between  $p$  and  $p'$  would also involve all these constants and be very complicated.

### § 3

The rigorous solution of the problem given in § 2 involves the reaction velocities at the two temperatures which are generally not known. Hence for practical purposes this method is not of much use. It is therefore worth while to obtain an approximate solution which may not involve these reaction velocities. For this purpose we can assume that the two chambers are in local thermodynamic equilibrium, and upon this superpose the condition of net flux of mass of each component being zero.

From the assumption of local thermodynamical equilibrium it follows that equations (4) and (5) must be assumed to hold. Combining these equations with (10) and (19) we get the four unknowns,  $n_1, n_2, n'_1, n'_2$ , and hence the problem is completely solved.

Equation (31), with the help of (4) and (5), yields

$$\sqrt{\frac{T}{T'}} = \left\{ n'_1 + \frac{n_1'^2}{K'} \sqrt{2} \right\} / \left\{ n_1 + \frac{n_1^2}{K} \sqrt{2} \right\}, \quad (32)$$

or

$$\sqrt{\frac{T}{T'}} = \frac{\sqrt{(K'n'_2) + n'_2 \sqrt{2}}}{\sqrt{(Kn_2) + n_2 \sqrt{2}}}. \quad (33)$$

Equations (32) and (33) respectively give relations between the atomic and the molecular concentrations in the two chambers. Putting  $\sqrt{(T/T')} = R$  and  $n_1/n'_1 = x$  we have

$$x^2 R \left( 1 + \frac{n_1}{K} \sqrt{2} \right) - x - \frac{n_1}{K'} \sqrt{2} = 0, \quad (34)$$

whence

$$x = \frac{n_1}{n'_1} = \frac{1 \pm \left\{ 1 + 4 \sqrt{2} \frac{n_1}{K'} \left( 1 + \frac{n_1}{K} \sqrt{2} \right) \sqrt{\frac{T}{T'}} \right\}^{\frac{1}{2}}}{2 \left( 1 + \frac{n_1}{K} \sqrt{2} \right) \sqrt{\frac{T}{T'}}}. \quad (35)$$

Evidently the negative sign before the radical cannot hold, for then  $x$  would become negative. Thus  $x$  is given by equation (35) with the positive sign

and is seen to depend not only on  $\sqrt{(T/T')}$  as in the ordinary case but also on  $n_1$ , i.e. on  $M, V_1, V_2, K, K'$ , etc. Similarly, we can obtain an expression for  $y = n_2/n'_2$  with the help of equation (33). Thus in the general case the results are complicated. We shall now consider some particular cases.

For temperatures at which there is very little dissociation, i.e.  $K$  and  $K'$  are extremely small, equations (32) and (33) respectively yield

$$\sqrt{\frac{T}{T'}} = \frac{n'_1{}^2 K}{n_1^2 K'}, \quad \sqrt{\frac{T}{T'}} = \frac{n'_2}{n_2},$$

to a rough approximation. Thus in this case the molecular concentrations are related in the usual way, but the atomic concentration ratio is modified and is given by

$$\frac{n'_1}{n_1} = \left(\frac{K'}{K}\right)^{\frac{1}{2}} \left(\frac{T}{T'}\right)^{\frac{1}{2}}.$$

The pressure ratios are given by

$$\frac{p'_1}{p_1} = \left(\frac{K'}{K}\right)^{\frac{1}{2}} \left(\frac{T}{T'}\right)^{\frac{1}{2}}; \quad \frac{p'_2}{p_2} = \sqrt{\frac{T'}{T}}.$$

It is thus seen that in this case the total pressure as well as the partial pressure of the molecule roughly obey the usual transpiration relation but the partial pressures of the atom do not.

Another particular case worthy of notice is that when there is nearly complete dissociation, i.e.  $K$  and  $K'$  are very large. For this case we get from equations (32) and (33) the approximate relations

$$\sqrt{\frac{T}{T'}} = \frac{n'_1}{n_1}, \quad \frac{T}{T'} = \frac{K' n'_2}{K n_2}.$$

Here the atoms satisfy the usual relation, but the molecular relation is modified.

It now only remains to find the actual values of the quantities  $n_1, n'_1, n_2, n'_2$ . After substituting for  $n_2$  and  $n'_2$  from equations (4) and (5) in (10) and (19) and eliminating  $n_1^2$  we get

$$n_1 = C_1 n_1'^2 + C_2 n'_1 + C_3, \quad (36)$$

where  $C_1, C_2, C_3$  are given by

$$C_1 = \frac{1}{\sqrt{2-1}} \frac{2}{K'} \left[ \sqrt{\frac{T'}{T}} + \frac{V'}{V} \right], \quad C_2 = \frac{1}{\sqrt{2-1}} \left[ \sqrt{\frac{2T'}{T}} + \frac{V'}{V} \right], \quad C_3 = -\frac{1}{\sqrt{2-1}} \frac{M}{mV}.$$

Substituting for  $n_1$  from equation (36) in (32) we get

$$b_0 n_1'^4 + 4b_1 n_1'^3 + 6b_2 n_1'^2 + 4b_3 n_1' + b_4 = 0, \quad (37)$$

where 
$$b_0 = \frac{C_1^2 \sqrt{2}}{K}; \quad 4b_1 = 2\sqrt{2} \frac{C_1 C_2}{K};$$

$$6b_2 = C_1 + \frac{C_2^2 \sqrt{2}}{K} + \frac{C_1 C_3}{K} 2\sqrt{2} - \frac{1}{K'} \sqrt{\frac{2T'}{T}};$$

$$4b_3 = C_2 + \frac{2\sqrt{2}}{K} C_2 C_3 - \sqrt{\frac{T'}{T}}; \quad b_4 = C_3 + \frac{C_3^2}{K} \sqrt{2}.$$

Using any one of the standard methods for solving the quartic, equation (37) gives four values for  $n_1'$ . Knowing  $n_1'$  in this manner equation (5) gives  $n_2'$  and (36) gives  $n_1$ . Then equation (4) gives  $n_2$ . Hence all the quantities can be determined and the equilibrium state fully calculated. The condition that all the  $n$ 's are positive and real will be found sufficient to determine uniquely the value of all these quantities out of the several sets of values given by equation (37).

We have so far considered a gas dissociating into two similar atoms. For a molecule dissociating into two dissimilar atoms such as  $XY \rightleftharpoons X + Y$ , we have the six quantities  $n_1, n_2, n_{12}, n_1', n_2', n_{12}'$  to be determined, i.e. two more than in the previous case. This can be done because we get two additional equations, one for the flux and another for the total mass of the other component. Again, if the atoms are capable of association to form  $X_2, Y_2$  also, we have four more quantities  $n_{X_2}, n_{X_2}', n_{Y_2}, n_{Y_2}'$  which can be determined with the help of the four additional relations expressing the law of reaction isochore for the dissociation of  $X_2$  and  $Y_2$  in the two chambers.

We shall now compare the treatments adopted in §§ 2 and 3. From the definition of  $A$  and  $B$  as given by equations (20) and (21) it is evident that for very small opening and large reaction velocity  $1/A$  and  $1/B$  will be extremely small and thus the left-hand side of equations (23) and (24) will be much smaller than either of the terms on the right-hand side. In the extreme case of  $H \rightarrow \infty$  or  $S \rightarrow 0$  but not actually zero, these terms will be vanishingly small and equations (23) and (24) will be practically identical with (4) and (5) though never rigorously so. Equations (4) and (5) are, however, very useful approximations of (23) and (24) for the case when the ratio (effusion rate/reaction velocity) is small. For large values of this ratio the treatment of § 3 will be quite erroneous. The results of § 2 are always applicable and approximate to those of § 3 when this ratio tends to zero.

In conclusion it is a pleasure to record my sincere thanks to Professor

M. N. Saha, D.Sc., F.R.S., for his kind interest in the work and to Dr D. S. Kothari of Delhi University for opportunities of discussion.

#### REFERENCES

- Dirac, P. A. M. 1924 *Proc. Camb. Phil. Soc.* **22**, 132.  
Srivastava, B. N. 1938 *Proc. Nat. Inst. Sci. India*, **4**, 365.  
— 1939 *Proc. Nat. Inst. Sci. India*, **5**, 313.
- 

## Radiative processes involving fast mesons§

By F. BOOTH, B.A., *Clare College, Cambridge*

AND

A. H. WILSON, *Trinity College, Cambridge*

(Communicated by R. H. Fowler, F.R.S.—Received 19 March 1940)

The general theory of the interaction of mesons with an electromagnetic field is developed, starting from Kemmer's matrix formulation of the meson equations. The general theory is applied to the scattering of light by mesons, the emission of radiation by mesons during collisions and the production of pairs of mesons. A brief discussion of the experimental results on the energy losses of "heavy electrons" in cosmic rays is given, and it is shown that the experiments are consistent with the view that the heavy electrons have spin 1 and that the theory of the interaction of mesons with an electromagnetic field is probably valid for energies considerably greater than the rest energy of a meson.

#### INTRODUCTION

1.1. A meson passing through matter can lose energy in four different ways: by absorption and re-emission by nuclei, by ordinary collisions with electrons and nuclei, by emission of  $\gamma$ -rays during a collision with a nucleus, and by the creation of pairs of electrons or mesons. The first process, which does not occur for electrons, has been considered by Bhabha (1939) and, in the non-relativistic limit, by Heitler (1938). The second process has been

§ We use the word meson to denote a particle with spin 1 (in units of  $\hbar$ ). Such particles are usually supposed to be the same as the heavy electrons (of mass about 200 times the electron mass) found in cosmic rays, but the identification is by no means certain.



calculated by Massey and Corben (1939), taking into account the effect of retardation. The third process, in which a  $\gamma$ -ray is emitted and the meson deflected either by the specific nuclear field or by the Coulomb field of a nucleus, has not so far been treated. For electrons of very high energy, the emission of  $\gamma$ -rays is the most important means of energy loss. It is therefore of considerable interest to carry out the corresponding calculations for mesons, both on account of the intrinsic interest of the problem and because of its application to cosmic rays. In the present paper we discuss this and related problems, neglecting the specific nuclear interaction.

The problem of the radiation loss is one of those in which the interest is mainly confined to the case of very high energies, but unfortunately the relativistic theory of the meson is extremely complicated. In the usual wave formulation of the meson theory, the spin bears a close analogy to the polarization of a light wave, except that the spin of the meson can have a component along the direction of motion, whereas light waves are essentially transverse, the longitudinal part of an electromagnetic field being purely static. It is customary to choose the three independent eigenstates of polarization of a meson so that two polarizations are transverse, and the other longitudinal, to the linear momentum vector. This choice is especially convenient when the velocity of the meson is small, since, in collision problems, transitions between the longitudinal and transverse states cannot then take place directly. For high energies, however, transitions occur in which the direction of polarization changes; but, since the direction of polarization is unobservable, it is necessary to sum or average over the polarizations in order to obtain a physically significant result. A similar situation occurs in the electron theory where it is necessary to sum over the two possible directions of the spin (and, in intermediate states, over the two possible values of the energy for a given momentum). However, electron theory is intrinsically less complicated than meson theory, and special methods have been evolved to effect the summations. In the wave formulation of the meson theory a similar procedure is impossible since the quantization can only be carried out after the independent states of polarization have been arbitrarily fixed, but Kemmer (1939) has recently given an alternative development of the theory, which emphasises the particle rather than the wave properties of the meson. In this formulation, certain  $\beta$  matrices occur which are analogous to the  $\alpha$  matrices of the electron theory, and which enable us to sum over the polarizations. Owing to the  $\beta$  matrices being singular, the procedure is nothing like so simple as for the electron theory, but it is nevertheless much simpler and more elegant than the straightforward methods of the wave theory. This is particularly true for

problems, such as those discussed in the present paper, which do not involve the specific nuclear reaction. One of us (F. B.), began, at the suggestion of Dr H. J. Bhabha, to calculate by the wave theory the cross-section for the radiative collision of a meson with a nucleus; the calculation was very complicated, and was abandoned when Kemmer's more powerful method became available. The two theories are, of course, completely equivalent, but the use of the  $\beta$  matrices ensures that the results are obtained in the simplest closed form possible.

In the electron theory, the second quantization can formally be dispensed with, by considering the creation of a pair of electrons to be equivalent to the transition of an electron from a state of negative energy to a state of positive energy. This formal procedure is not possible for mesons, since we should have to consider transitions in which charge is not conserved. Further, mesons obey Einstein-Bose statistics, and the concept of the states with say negative charge being occupied by an infinity of (unobservable) mesons is quite meaningless.

The first method which we used for obtaining the cross-section for the radiative collision of a meson with a nucleus was the direct calculation of the differential cross-section for the scattering of the meson and the emission of the  $\gamma$ -ray into arbitrary solid angles. The resulting formula was extremely complicated. Further, it is almost impossible to carry out experiments to determine this differential cross-section, and it is only when the cross-section is integrated over all angles of scattering of the meson and of emission of the light quantum that we obtain a result which is of physical interest. Now the order of magnitude of the integrated cross-section can be obtained indirectly by the method of impact parameters with considerably less labour (Williams 1935); in addition the loss in accuracy is more than counterbalanced by the gain in clarity. We therefore decided to adopt the simpler indirect method, and in this paper we do not propose to reproduce the unwieldy calculations of the direct method.

Owing to the  $\beta$  matrices being singular and therefore not possessing inverses, a somewhat complicated technique is required. This, and the relevant general theory, is given in § 2. In § 3 we calculate the cross-section for the scattering of unpolarized light by a meson which is initially at rest. This rather lengthy expression, which is valid for all energies, has probably no physical importance in itself, but it can be used, as we do in § 4, to obtain the radiation loss during the collision of a meson with a fixed nucleus. In § 5 we treat the related problem of the production of meson pairs, and in § 6 we give a critical discussion of our results.

In most discussions it has hitherto been assumed that, on account of the

large mass of the meson, the radiation loss from mesons would be about 40,000 times smaller than from electrons. This naïve argument, which receives some support from the fact that the formula for the radiation loss is practically the same for particles with zero spin as for electrons, turns out to be unfounded. Our calculations show that, if the present meson theory is valid for high energies, the energy loss from mesons due to radiation varies as  $E_0^2$ , where  $E_0$  is the energy of the meson; the energy loss for electrons, on the other hand, only varies as  $E_0$ . The fact that the cross-section increases with increasing energy is one of the outstanding characteristics of the meson theory, and it has led some authors to express the view that the theory is only valid when the kinetic energy of a meson is small compared with its rest energy. The occurrence of large cross-sections is due in part to the meson field being a charged, and therefore non-classical, field, and in part to the highly singular nature of the interaction of mesons with the other elementary particles. In our problem only the second of these complications is relevant, but it renders an exact theory impossible. However, the history of the quantum theory has shown that physical theories are often valid far beyond the limits within which they can be proved to be consistent, and that the limits of applicability of a theory are most clearly shown by the discussion of its consequences.

The nature of the heavy electrons found in cosmic rays is by no means certain. The only really direct evidence that they are the same as the charged mesons introduced to explain the nuclear forces is that the masses of two particles are approximately the same. However, if we assume the identity of the two particles, the theory of the specific nuclear interaction is very unsatisfactory, since the calculated cross-section for the scattering of mesons by protons due to this interaction is much greater than the total observed cross-section, even for comparatively small velocities. A somewhat simpler test of the theory is provided by the Coulomb scattering of mesons by nuclei, and by the radiation emitted during collisions. At present the experiments do not extend to sufficiently high energies for this test to be applied rigorously, and, although the results are not in contradiction with the theory, they cannot be said to confirm it. On the other hand, the occurrence of bursts consisting of a large number of particles might find an explanation in the ordinary cascade theory if the large cross-sections predicted by the theory really do exist.

## GENERAL THEORY §

2.1. In the wave formulation we have a four-vector  $U_\mu$  describing the meson field. In Kemmer's particle formulation  $U_\mu$  and the six-vector  $G_{\mu\nu}$  ( $\mu, \nu = 1, 2, 3, 4$ ), which is the curl of  $U_\mu$ , are combined into a wave function  $\psi$ , which has ten components forming a column matrix, and which, in the absence of external fields, satisfies the equation

$$\frac{\partial}{\partial x_\mu} \beta_\mu \psi + \kappa \psi = 0, \quad (1)$$

where  $\kappa = mc/\hbar$ ,  $m$  being the mass of the meson. The coordinates  $x_1, x_2, x_3$  are space coordinates, and  $x_4 = ict$ ; the  $\beta_\mu$  ( $\mu = 1, 2, 3, 4$ ) are  $10 \times 10$  Hermitian matrices satisfying the commutation relations (Petiau 1936; Duffin 1938)

$$\beta_\mu \beta_\nu \beta_\rho + \beta_\rho \beta_\nu \beta_\mu = \beta_\mu \delta_{\nu\rho} + \beta_\rho \delta_{\mu\nu}. \quad (2)$$

The conjugate complex row-matrix  $\psi^\dagger$  satisfies the equation||

$$\frac{\partial \psi^\dagger}{\partial x_k} \beta_k - \frac{\partial \psi^\dagger}{\partial x_4} \beta_4 + \kappa \psi^\dagger = 0, \quad (3)$$

since  $x_4$  is the imaginary time. It is more convenient to use instead of  $\psi^\dagger$  the quantity

$$\hat{\psi} = i\psi^\dagger \eta_4, \quad (4)$$

where

$$\eta_\mu = 2\beta_\mu^2 - 1. \quad (5)$$

By using the relations

$$\eta_\mu \beta_\nu + \beta_\nu \eta_\mu = 2\beta_\nu \delta_{\mu\nu}, \quad (6)$$

the summation convention not being used in this equation, we see that  $\hat{\psi}$  satisfies the equation

$$\frac{\partial \hat{\psi}}{\partial x_\mu} \beta_\mu - \kappa \hat{\psi} = 0. \quad (7)$$

§ Since the  $\beta$  formalism is as yet unfamiliar, we summarize and extend the results of Kemmer's paper. We are greatly indebted to Dr Kemmer not only for allowing us to see his paper in manuscript but also for extensive discussions concerning the best way of applying the general theory to special problems. In particular, the task of evaluating the spurs given in equations (63)–(73) was carried out by Dr Kemmer and Dr G. J. Kynch of the Imperial College.

|| Unless otherwise stated, we use Greek suffixes to denote 1, 2, 3, 4 or 1, 2, ..., 10 and Latin suffixes to denote 1, 2, 3 or 1, 2, ..., 6; the summation convention is used, but  $\beta_\mu^2$  (not summed) is to be distinguished from  $\beta_\mu \beta_\mu$  (summed). Note that in order to conform to the usual custom we modify Kemmer's notation and use a dagger to denote the Hermitian conjugate. This entails using a new symbol to denote  $i\psi^\dagger \eta_4$  (equation (4)) and we have chosen  $\hat{\psi}$  for this new symbol which replaces Kemmer's  $\psi^\dagger$ .

2.2. The second order equation satisfied by each component of  $\psi$  can be deduced as follows. If we multiply (1) by  $\beta_\rho \beta_\nu \partial/\partial x_\rho$  and use the commutation rules (2), we obtain

$$\kappa \frac{\partial}{\partial x_\rho} \beta_\rho \beta_\nu \psi = -\frac{1}{2} \frac{\partial^2}{\partial x_\rho \partial x_\mu} (\beta_\rho \beta_\nu \beta_\mu + \beta_\mu \beta_\nu \beta_\rho) \psi = -\frac{\partial^2}{\partial x_\nu \partial x_\mu} \beta_\mu \psi = \kappa \frac{\partial \psi}{\partial x_\nu}.$$

Hence 
$$\frac{\partial \psi}{\partial x_\mu} = \frac{\partial}{\partial x_\nu} \beta_\nu \beta_\mu \psi. \quad (8)$$

If we now operate on (8) with  $\partial/\partial x_\mu$  and apply (1) twice to the right-hand side, we immediately deduce that

$$\frac{\partial^2 \psi}{\partial x_\mu \partial x_\mu} = \kappa^2 \psi. \quad (9)$$

There are, therefore, solutions of (1) of the form

$$\psi = u e^{\mp i E t / \hbar + i \mathbf{p} \cdot \mathbf{r} / \hbar}, \quad (10)$$

where  $u$  is a ten-component column matrix, and where

$$E = c \sqrt{(m^2 c^2 + p^2)}. \quad (11)$$

So far, the theory is similar to the relativistic electron theory, but at this point we meet characteristic differences. First, since  $\beta_\mu^3 = \beta_\mu$  and  $\beta_\mu \beta_\nu \beta_\rho = 0$  when  $\mu = \rho \neq \nu$ , the  $\beta$ 's are singular matrices (actually of rank six), the eigenvalues being 1 (threefold),  $-1$  (threefold) and 0 (fourfold). Hence, for given  $\mathbf{p}$ , there are only six linearly independent solutions (10); we denote the corresponding  $u$ 's by  $u_k(\mathbf{p})$  ( $k=1, 2, \dots, 6$ ). Secondly, the energy density is positive definite (see equation (13)), so that the energy of all six states is the same; they differ, however, as regards charge. The current density four-vector is in fact  $s_\mu = e \hat{\psi} \beta_\mu \psi$ , and the charge density is

$$s_0 = i^{-1} s_4 = e \psi^\dagger \beta_4 \psi.$$

The eigenvalues of  $s_0$  are therefore  $\pm e$ .

2.3. In the wave theory, the six independent solutions, three for each sign of the charge, are taken to be transverse and longitudinal to the direction of motion. If we take a representation in which  $\beta_4$  is diagonal, the first three diagonal elements being 1, the next three being  $-1$  and the last four being zero, these solutions are as shown in table 1.

This particular choice of solutions, besides being not relativistically invariant, is not necessary or particularly convenient here, and instead

we choose the solutions so as to simplify the expressions for the charge and energy densities. The symmetrized energy-momentum tensor  $\Theta_{\mu\nu}$  is given by

$$\Theta_{\mu\nu} = imc^2[\hat{\psi}(\beta_\mu\beta_\nu + \beta_\nu\beta_\mu)\psi - \delta_{\mu\nu}\hat{\psi}\psi]. \quad (12)$$

Hence the energy density is

$$\Theta_{00} = -\Theta_{44} = -imc^2\hat{\psi}\eta_4\psi = mc^2\psi^\dagger\psi, \quad (13)$$

since  $\eta_4^2 = 1$ . Now, for given  $\mathbf{p}$ , the most general solution of (1) is of the form

$$\psi = \sum_{k=1}^6 a_k(t) u_k(\mathbf{p}) e^{i\mathbf{p}\cdot\mathbf{r}/\hbar}.$$

TABLE 1. THE LONGITUDINAL AND TRANSVERSE WAVE FUNCTIONS

The polarizations are as follows:  $k = 1$ , longitudinal polarization;  $k = 2$ , transverse polarization perpendicular to the  $z$  axis;  $k = 3$ , transverse polarization in the  $p, z$  plane. The solutions with  $k = 1, 2, 3$  have positive charge; the solutions with  $k = 4, 5, 6$  have negative charge and are obtained from the expressions above by replacing  $E$  by  $-E$  except in the normalizing factor  $(E\mu)^\dagger$ , where  $\mu = mc^2$ .

|          | $k = 1$                                    | $k = 2$   | $k = 3$   |
|----------|--|---|---|
| $u_1$    | $\frac{(E + \mu) p_x}{2(E\mu)^\dagger p}$  | $\frac{(E + \mu) p_y}{2(E\mu)^\dagger (p_x^2 + p_y^2)^\dagger}$     | $\frac{(E + \mu) p_x p_z}{2(E\mu)^\dagger p(p_x^2 + p_y^2)^\dagger}$          |
| $u_2$    | $\frac{(E + \mu) p_y}{2(E\mu)^\dagger p}$  | $-\frac{(E + \mu) p_x}{2(E\mu)^\dagger (p_x^2 + p_y^2)^\dagger}$    | $\frac{(E + \mu) p_y p_z}{2(E\mu)^\dagger p(p_x^2 + p_y^2)^\dagger}$          |
| $u_3$    | $\frac{(E + \mu) p_z}{2(E\mu)^\dagger p}$  | 0   | $-\frac{(E + \mu) (p_x^2 + p_y^2)}{2(E\mu)^\dagger p(p_x^2 + p_y^2)^\dagger}$ |
| $u_4$    | $\frac{(-E + \mu) p_x}{2(E\mu)^\dagger p}$ | $-\frac{(-E + \mu) p_y}{2(E\mu)^\dagger (p_x^2 + p_y^2)^\dagger}$   | $-\frac{(-E + \mu) p_x p_z}{2(E\mu)^\dagger p(p_x^2 + p_y^2)^\dagger}$        |
| $u_5$    | $\frac{(-E + \mu) p_y}{2(E\mu)^\dagger p}$ | $\frac{(-E + \mu) p_x}{2(E\mu)^\dagger (p_x^2 + p_y^2)^\dagger}$    | $-\frac{(-E + \mu) p_y p_z}{2(E\mu)^\dagger p(p_x^2 + p_y^2)^\dagger}$        |
| $u_6$    | $\frac{(-E + \mu) p_z}{2(E\mu)^\dagger p}$ | 0   | $\frac{(-E + \mu) (p_x^2 + p_y^2)}{2(E\mu)^\dagger p(p_x^2 + p_y^2)^\dagger}$ |
| $u_7$    | 0  | $\frac{cp_x p_z}{(2E\mu)^\dagger (p_x^2 + p_y^2)^\dagger}$          | $\frac{cpp_y}{(2E\mu)^\dagger (p_x^2 + p_y^2)^\dagger}$                       |
| $u_8$    | 0  | $\frac{cp_y p_z}{(2E\mu)^\dagger (p_x^2 + p_y^2)^\dagger}$          | $-\frac{cpp_x}{(2E\mu)^\dagger (p_x^2 + p_y^2)^\dagger}$                      |
| $u_9$    | 0  | $-\frac{c(p_x^2 + p_y^2)}{(2E\mu)^\dagger (p_x^2 + p_y^2)^\dagger}$ | 0   |
| $u_{10}$ | $\frac{icp}{(2E\mu)^\dagger}$              | 0   | 0   |

Then, by a linear transformation  $u_k = u'_l T_{lk}$  of the  $u$ 's, we can reduce both the quadratic forms  $mc^2 \psi^\dagger \psi$  and  $e \psi^\dagger \beta_4 \psi$  to the diagonal form, since the first is positive definite. With this choice of the  $u$ 's and taking  $k=1, 2, 3$  to refer to the eigenvalue 1 of  $\beta_4$  while  $k=4, 5, 6$  refer to the eigenvalue  $-1$ , we have

$$mc^2 \psi^\dagger \psi = E \sum_{k=1}^6 a_k^* a_k, \quad (14)$$

and 
$$e \psi^\dagger \beta_4 \psi = e \sum_{k=1}^3 a_k^* a_k - e \sum_{k=4}^6 a_k^* a_k. \quad (15)$$

This is equivalent to making the  $u$ 's satisfy the following normalizing and orthogonality conditions:

$$mc^2 \sum_{\rho=1}^{10} u_{\rho,k}^* u_{\rho,l} = E \delta_{kl}, \quad (16)$$

$$\sum_{\rho,\sigma=1}^{10} u_{\rho,k}^* (\beta_4)_{\rho\sigma} u_{\sigma,l} = \rho_{kl}, \quad (17)$$

where  $\rho_{kl}$  is the diagonal matrix which is equal to 1 for  $k=l=1, 2, 3$  and is equal to  $-1$  for  $k=l=4, 5, 6$ . If we represent the  $u$ 's by a matrix  $U = (u_{\rho,k})$  with ten rows and six columns, the above relations can be written in the forms

$$mc^2 U^\dagger U = EI, \quad (18)$$

and 
$$U^\dagger \beta_4 U = P, \quad (19)$$

where  $I$  is the  $6 \times 6$  unit matrix and where  $P = (\rho_{kl})$ .

As in the electron theory, there is an inverse orthogonality condition, but it is more subtle here owing to the  $\beta$ 's being singular. It is clear that there is no inverse relation corresponding to (18), since  $U$  is not a square matrix, but in (17) and (19) we can discard  $u_\rho$  ( $\rho=7, 8, 9, 10$ ), since these are associated with zero eigenvalues of  $\beta_4$ . We can therefore treat  $\beta_4$  as a  $6 \times 6$  non-singular matrix with the two threefold eigenvalues  $\pm 1$ . Then  $\beta_4^2 = I$  and  $P^2 = I$ . With this convention we have  $PU^\dagger \beta_4 U = I$ , which implies  $PU^\dagger \beta_4 = U^{-1}$ , and hence  $PU^\dagger = U^{-1} \beta_4$ , since the  $6 \times 6$  matrix  $U$  is non-singular, the  $u$ 's being linearly independent. Hence, multiplying on the left by  $U$ , we have the inverse orthogonality relation

$$UPU^\dagger = \beta_4, \quad (20)$$

that is, 
$$\sum_{k,l=1}^6 u_{\rho,k} \rho_{kl} u_{\sigma,l}^* = (\beta_4)_{\rho\sigma} \quad (\rho, \sigma = 1, 2, \dots, 6). \quad (21)$$

Since the zero eigenvalues of  $\beta_4$  are associated with  $\rho, \sigma = 7, \dots, 10$ , we can omit the restriction on  $\rho$  and  $\sigma$  by writing (21) in the form

$$\sum_{k,l=1}^6 (\beta_4^2 u_k)_\rho \rho_{kl} (u_l \beta_4^2)_\sigma^* = (\beta_4)_{\rho\sigma}, \quad (22)$$

where  $u_l$  is the transposed of  $u_l$ , and we generally use the relation in this form.

2.31. Of the solutions (10), those with  $-E$  in the exponential factor refer to mesons with positive charge while those with  $E$  refer to mesons with negative charge. To prove this we use the fact (Kemmer 1939 equation (15)) that the energy-momentum vector can be taken as

$$p_\mu = \frac{1}{i} \int \hat{\psi} \beta_4 \frac{\hbar}{i} \frac{\partial \psi}{\partial x_\mu} dx_1 dx_2 dx_3. \quad (23)$$

Hence the three dimensional momentum vector is given by

$$\bar{\mathbf{p}} = \mathbf{p} \int \psi^\dagger \beta_4 \psi dx_1 dx_2 dx_3. \quad (24)$$

By (15), this gives  $\bar{\mathbf{p}} = \mathbf{p}$  for  $k = 1, 2, 3$  and  $\bar{\mathbf{p}} = -\mathbf{p}$  for  $k = 4, 5, 6$ . Now (10) represents a wave with momentum  $\mathbf{p}$  or  $-\mathbf{p}$  according as the minus sign or plus sign in front of  $E$  is taken. Hence solutions of the form

$$\psi = u_k^+(\mathbf{p}) e^{-iEt/\hbar + i\mathbf{p} \cdot \mathbf{r}/\hbar} \quad (25)$$

represent positive mesons with momentum  $\mathbf{p}$ , while solutions of the form

$$\psi = u_k^-(\mathbf{p}) e^{iEt/\hbar + i\mathbf{p} \cdot \mathbf{r}/\hbar} \quad (26)$$

represent negative mesons with momentum  $-\mathbf{p}$ . The equations satisfied by  $u_k^+(\mathbf{p})$  and  $u_k^-(\mathbf{p})$  are

$$(-E\beta_4 + ic\mathbf{p} \cdot \boldsymbol{\beta} + mc^2) u_k^+(\mathbf{p}) = 0, \quad (27)$$

$$\text{and} \quad (E\beta_4 + ic\mathbf{p} \cdot \boldsymbol{\beta} + mc^2) u_k^-(\mathbf{p}) = 0, \quad (28)$$

where  $\boldsymbol{\beta}$  is the vector with components  $\beta_1, \beta_2, \beta_3$ .

2.4. *The second quantization.* One of the chief complications in the theory is that the four components of  $\psi$  associated with the zero eigenvalues of  $\beta_4$  must not be quantized independently of the other six, since these four components can be expressed in terms of the remainder by the equation

$$(1 - \beta_4^2) \kappa \psi + \frac{\partial}{\partial x_k} \beta_k \beta_4^2 \psi = 0, \quad (29)$$



which is obtained by multiplying (1) by  $1 - \beta_4^2$ . This equation is independent of the time, and can be regarded as a supplementary condition which enables us to eliminate the unwanted components.

The equations of motion (1) and (2) can be derived by the variation principle from the invariant Lagrangian function

$$L = i\hbar c \hat{\psi} \beta_\mu \frac{\partial \psi}{\partial x_\mu} + imc^2 \hat{\psi} \psi. \quad (30)$$

Writing  $\beta_4 = \beta_4^2$ , we can define the momentum  $p_\rho$  corresponding to any component of  $\psi$  for which  $\beta_4 \psi$  is not zero either by

$$p_\rho = \frac{\partial L}{\partial(\beta_4 \hat{\psi} / \partial t)_\rho} = \hbar(\hat{\psi} \beta_4^2)_\rho, \quad (31)$$

or by

$$p_\rho = \frac{\partial L}{\partial(\beta_4^2 \hat{\psi} / \partial t)_\rho} = \hbar(\hat{\psi} \beta_4)_\rho.$$

The commutation relations are therefore

$$i[\{\hat{\psi}(\mathbf{r}) \beta_4^2\}_\rho, \{\beta_4 \psi(\mathbf{r}')\}_\sigma] = i[\{\hat{\psi}(\mathbf{r}) \beta_4\}_\rho, \{\beta_4^2 \psi(\mathbf{r}')\}_\sigma] \\ = \delta_{\rho\sigma} \delta(\mathbf{r} - \mathbf{r}') \quad (\rho, \sigma = 1, \dots, 6), \quad (32)$$

where  $[A, B] = AB - BA$ .

We now suppose that the wave function  $\psi$  of any system is expressed in the form§

$$\psi = \frac{1}{h^{\frac{1}{2}}} \sum_{k=1}^3 \int \{a_k(\mathbf{p}, t) u_k^+(\mathbf{p}) + b_k(\mathbf{p}, t)^* u_k^-(\mathbf{p})\} e^{i\mathbf{p} \cdot \mathbf{r} / \hbar} d\mathbf{p}, \quad (33)$$

where  $a_k, b_k$  are  $q$ -numbers, and  $u_k^+, u_k^-$  are column matrices with  $c$ -number components which are chosen so as to satisfy (16), (17), (27) and (28). The quantities  $a_k(\mathbf{p}), b_k(\mathbf{p})$  satisfy the commutation relations

$$[a_k(\mathbf{p}), a_l(\mathbf{p}')^*] = [b_k(\mathbf{p}), b_l(\mathbf{p}')^*] = \delta_{kl} \delta(\mathbf{p} - \mathbf{p}'), \\ [a_k(\mathbf{p}), b_l(\mathbf{p}')] = [a_k(\mathbf{p})^*, b_l(\mathbf{p}')^*] = 0. \quad (34)$$

The formal proof of the relations (34) is as follows. We have, by (17) and by the Fourier integral theorem,

$$a_k(\mathbf{p}) = \frac{1}{h^{\frac{1}{2}}} \int u_k^+(\mathbf{p})^\dagger \beta_4 \psi e^{-i\mathbf{p} \cdot \mathbf{r} / \hbar} d\mathbf{r}. \quad (35)$$

§ When we distinguish the  $u$ 's by the superscripts  $+$  and  $-$ , it is convenient to take  $k$  to run from 1 to 3 for both  $u_k^+$  and  $u_k^-$ , whereas when the superscripts are omitted we take  $k$  to run from 1 to 6. Thus  $\sum_{k=1}^3 (u_k^+ + u_k^-)$  is equivalent to  $\sum_{k=1}^6 u_k$ . We use  $\int d\mathbf{p}, \int d\mathbf{r}, \dots$  to denote  $\int dp_1 dp_2 dp_3, \int dx_1 dx_2 dx_3, \dots$

Hence we have

$$[a_k(\mathbf{p}), a_l(\mathbf{p}')^*] = \frac{1}{\hbar^3} \iint \sum_{\rho, \sigma} u_{\rho, k}^+(\mathbf{p})^* u_{\sigma, l}^+(\mathbf{p}') [\{\beta_4 \psi(\mathbf{r})\}_\rho, \{\psi(\mathbf{r}')^\dagger \beta_4\}_\sigma] e^{-i(\mathbf{p} \cdot \mathbf{r} - \mathbf{p}' \cdot \mathbf{r}')/\hbar} d\mathbf{r} d\mathbf{r}' \quad (36)$$

on rearranging the terms and using the fact that all the elements  $u_{\rho, k}$  are  $c$ -numbers. Now  $\{\psi(\mathbf{r}')^\dagger \beta_4\}_\sigma = \{\psi(\mathbf{r}')^\dagger \beta_4^2\}_\tau (\beta_4)_{\tau\sigma}$  and hence, by (32), §

$$[\{\beta_4 \psi(\mathbf{r})\}_\rho, \{\psi(\mathbf{r}')^\dagger \beta_4\}_\sigma] = (\beta_4)_{\rho\sigma} \delta(\mathbf{r} - \mathbf{r}'). \quad (37)$$

Therefore (36) becomes

$$[a_k(\mathbf{p}), a_l(\mathbf{p}')^*] = \frac{1}{\hbar^3} \int \sum_{\rho, \sigma} u_{\rho, k}^+(\mathbf{p})^* (\beta_4)_{\rho\sigma} u_{\sigma, l}^+(\mathbf{p}') e^{-i(\mathbf{p} \cdot \mathbf{p}')/\hbar} d\mathbf{r} = \delta_{kl} \delta(\mathbf{p} - \mathbf{p}') \quad (38)$$

by (17).|| The proof of the second of the equations (34) is similar, the only difference being that we now have  $\sum u_{\rho, k}^-(\mathbf{p})^* (\beta_4)_{\rho\sigma} u_{\sigma, l}^-(\mathbf{p}) = -\delta_{kl}$ ; the minus sign here compensates the minus sign which arises because the expression (33) for  $\psi$  contains  $b^*$  and not  $b$ . The remaining relations present no difficulty.

It is also easy to show that the commutation rules (34) imply the commutation rules (32). We have, by (33) and (34),

$$[\{\beta_4 \psi(\mathbf{r})\}_\rho, \{\psi(\mathbf{r}')^\dagger \beta_4^2\}_\sigma] = \frac{1}{\hbar^3} \int \sum_{k, l=1}^6 (\beta_4 u_k)_\rho \rho_{kl} (u_l^\dagger \beta_4^2)_\sigma e^{i\mathbf{p} \cdot (\mathbf{r} - \mathbf{r}')/\hbar} d\mathbf{p}. \quad (39)$$

In order to apply (22) we write

$$\begin{aligned} \sum_{k, l=1}^6 (\beta_4 u_k)_\rho \rho_{kl} (u_l^\dagger \beta_4^2)_\sigma &= \sum_{k, l=1}^6 (\beta_4)_{\rho\tau} (\beta_4^2 u_k)_\tau \rho_{kl} (u_l^\dagger \beta_4^2)_\sigma \\ &= (\beta_4)_{\rho\tau} (\beta_4)_{\tau\sigma} = \delta_{\rho\sigma} \quad (\rho, \sigma = 1, \dots, 6). \end{aligned}$$

Equation (39) then gives

$$[\{\beta_4 \psi(\mathbf{r})\}_\rho, \{\psi(\mathbf{r}')^\dagger \beta_4^2\}_\sigma] = \delta_{\rho\sigma} \delta(\mathbf{r} - \mathbf{r}') \quad (\rho, \sigma = 1, \dots, 6), \quad (40)$$

which is the same as (32).

**2.5. Electromagnetic interaction.** In the present formulation it is a simple matter to introduce the interaction of the mesons with electromagnetic

§ This form of the commutation rule has certain advantages, in that  $\psi$  and  $\psi^\dagger$  are treated symmetrically, and, since  $\beta_4$  occurs on both sides of the equation, the relation is valid for  $\rho, \sigma = 1, \dots, 10$  and not merely for  $\rho, \sigma = 1, \dots, 6$ .

|| We can define the  $\delta$  function by  $\frac{1}{\hbar^3} \int e^{i\mathbf{p} \cdot \mathbf{r}/\hbar} d\mathbf{r} = \delta(\mathbf{p})$ .

fields; since the equations of motion are derivable from an invariant Lagrangian function, we have merely to replace  $\partial/\partial x_\mu$  by  $\partial/\partial x_\mu - ie\phi_\mu/\hbar c$ , where  $\phi_\mu$  is the four-potential of the field. The nuclear interaction is, however, much more complicated. The reason for this is that the formalism applies equally to particles with zero spin, and that any interaction, such as electromagnetic interaction, which is of the same form for particles with spin 0 and spin 1 can be introduced without using the explicit representations of the  $\beta$ 's. The form of the nuclear interaction, however, depends upon the vector character of the components of  $\psi$  for space rotations only, and the explicit representations of  $\psi$  and the  $\beta$ 's cannot be avoided. In the present paper we do not consider the nuclear interaction; the extension of the theory to include the nuclear interaction is given in another paper (A. H. Wilson 1940).

Our starting point is the symmetrical energy tensor (12) which, like the current density  $s_\mu$ , is the same whether electromagnetic fields are present or not. In order to eliminate the components of  $\psi$  which are not directly quantized we apply (29) in the generalized form (Kemmer 1939, equation (73))

$$\psi = \left[ 1 - \frac{i}{mc} \left( \mathbf{p} - \frac{e}{c} \mathbf{A} \right) \cdot \boldsymbol{\beta} \right] \beta_4^2 \psi, \quad \hat{\psi} = \hat{\psi} \beta_4^2 \left[ 1 - \frac{i}{mc} \left( \mathbf{p} - \frac{e}{c} \mathbf{A} \right) \cdot \boldsymbol{\beta} \right], \quad (41)$$

where  $\mathbf{A}$  is the vector potential.

When there are no fields present we have

$$\begin{aligned} \Theta_{00} &= mc^2 \psi^\dagger \psi = -imc^2 \hat{\psi} \eta_4 \psi \\ &= -imc^2 \hat{\psi} \beta_4^2 \left( 1 - i \frac{\mathbf{p} \cdot \boldsymbol{\beta}}{mc} \right) \eta_4 \left( 1 - i \frac{\mathbf{p} \cdot \boldsymbol{\beta}}{mc} \right) \beta_4^2 \psi \\ &= mc^2 \psi^\dagger \beta_4^2 \left[ 1 + \frac{(\mathbf{p} \cdot \boldsymbol{\beta})^2}{m^2 c^2} \right] \beta_4^2 \psi. \end{aligned} \quad (42)$$

The last line is obtained from the preceding by using the fact (equation (6)) that  $\eta_4$  anticommutes with  $\mathbf{p} \cdot \boldsymbol{\beta}$ , and that  $\eta_4 \beta_4 = \beta_4 \eta_4 = \beta_4$ . When the vector potential  $\mathbf{A}$  is not zero, the Hamiltonian is

$$\bar{H} = \int \Theta_{00} d\mathbf{r} = \bar{H}_0 + \bar{H}_1 + \bar{H}_2, \quad (43)$$

where  $\bar{H}_0$ ,  $\bar{H}_1$  and  $\bar{H}_2$  are of zero, first and second order in  $\mathbf{A}$ .

$\bar{H}_0$  is the integral of (42). We transform the integrand back into the form  $mc^2\psi^\dagger\psi$ , substitute the expression (33) for  $\psi$  and use the normalizing relations (16). We obtain

$$\bar{H}_0 = \sum_{k=1}^3 \int E(\mathbf{p}) \{a_k(\mathbf{p})^* a_k(\mathbf{p}) + b_k(\mathbf{p}) b_k(\mathbf{p})^*\} d\mathbf{p}. \quad (44)$$

We now suppose that the vector potential, which is real, is expanded as a Fourier integral (see e.g. Heitler 1936, p. 92):

$$\mathbf{A} = \frac{\sqrt{(4\pi c^2)}}{h^{\frac{1}{2}}} \int \mathbf{e}_{\mathbf{k}} [q_{\mathbf{k}} e^{i\mathbf{k} \cdot \mathbf{r}/\hbar} + q_{\mathbf{k}}^* e^{-i\mathbf{k} \cdot \mathbf{r}/\hbar}] d\mathbf{k}, \quad (45)$$

where  $\mathbf{e}_{\mathbf{k}}$  is a real unit vector in the direction of polarization of the Fourier component  $\mathbf{k}$ . We then have§

$$\begin{aligned} \bar{H}_1 = & -\frac{e}{mc} \sqrt{\frac{4\pi c^2}{h^3}} \sum_{k,l=1}^3 \iint [a_l(\mathbf{p}')^* u_l^+(\mathbf{p}')^\dagger + b_l(\mathbf{p}') u_l^-(\mathbf{p}')^\dagger] \beta_3^2 \\ & \times [q_{\mathbf{p}-\mathbf{p}'} \{(\boldsymbol{\beta} \cdot \mathbf{e}_{\mathbf{p}-\mathbf{p}'})(\mathbf{p} \cdot \boldsymbol{\beta}) + (\mathbf{p}' \cdot \boldsymbol{\beta})(\boldsymbol{\beta} \cdot \mathbf{e}_{\mathbf{p}-\mathbf{p}'})\} \\ & + q_{\mathbf{p}-\mathbf{p}'}^* \{(\boldsymbol{\beta} \cdot \mathbf{e}_{\mathbf{p}-\mathbf{p}'}) (\mathbf{p} \cdot \boldsymbol{\beta}) + (\mathbf{p}' \cdot \boldsymbol{\beta})(\boldsymbol{\beta} \cdot \mathbf{e}_{\mathbf{p}-\mathbf{p}'})\}] \\ & \times \beta_3^2 [a_k(\mathbf{p}) u_k^+(\mathbf{p}) + b_k(\mathbf{p})^* u_k^-(\mathbf{p})] d\mathbf{p} d\mathbf{p}'. \end{aligned} \quad (46)$$

Further,

$$\begin{aligned} \bar{H}_2 = & \frac{4\pi e^2}{m\hbar^3} \sum_{k,l=1}^3 \iiint [a_l(\mathbf{p}')^* u_l^+(\mathbf{p}')^\dagger + b_l(\mathbf{p}') u_l^-(\mathbf{p}')^\dagger] \beta_3^2 \\ & \times (\boldsymbol{\beta} \cdot \mathbf{e}_{\mathbf{k}})(\boldsymbol{\beta} \cdot \mathbf{e}_{\mathbf{k}}) [q_{\mathbf{k}} q_{\mathbf{k}'} \delta(\mathbf{p} - \mathbf{p}' + \mathbf{k} + \mathbf{k}') + q_{\mathbf{k}} q_{\mathbf{k}'}^* \delta(\mathbf{p} - \mathbf{p}' + \mathbf{k} - \mathbf{k}') \\ & + q_{\mathbf{k}}^* q_{\mathbf{k}'} \delta(\mathbf{p} - \mathbf{p}' - \mathbf{k} + \mathbf{k}') + q_{\mathbf{k}}^* q_{\mathbf{k}'}^* \delta(\mathbf{p} - \mathbf{p}' - \mathbf{k} - \mathbf{k}')] \\ & \times \beta_3^2 [a_k(\mathbf{p}) u_k^+(\mathbf{p}) + b_k(\mathbf{p})^* u_k^-(\mathbf{p})] d\mathbf{p} d\mathbf{p}' d\mathbf{k} d\mathbf{k}'. \end{aligned} \quad (47)$$

The occurrence of the term  $\bar{H}_2$  is to be particularly noticed. It gives rise to transitions in which two light quanta are concerned. Such a term does not occur in the relativistic electron theory, but, curiously enough, occurs in the non-relativistic theory.

We have still to introduce the interaction associated with the scalar

§ Note that in  $\psi^\dagger \beta_3^2 [(\mathbf{p} \cdot \boldsymbol{\beta})(\mathbf{A} \cdot \boldsymbol{\beta}) + (\mathbf{A} \cdot \boldsymbol{\beta})(\mathbf{p} \cdot \boldsymbol{\beta})] \beta_3^2 \psi$  we can let both  $\mathbf{p}$ 's operate forwards on  $\psi$  or we can let the first  $\mathbf{p}$  operate backwards on  $\psi^\dagger$  (remembering that then  $\mathbf{p} = i\hbar \text{grad}$ ) and let the second  $\mathbf{p}$  operate forwards on  $\psi$ . Both methods give the same result.

potential  $\phi$ . To do this we have to add the zero term (Heisenberg and Pauli 1930, p. 179)

$$\int \phi \left( \rho - \frac{1}{4\pi} \operatorname{div} \mathcal{E} \right) d\mathbf{r}. \quad (48)$$

The first term of this gives

$$\begin{aligned} \bar{H}_3 &= e \int \phi \psi^\dagger \beta_4 \psi d\mathbf{r} \\ &= \frac{e}{\hbar^3} \sum_{k,l=1}^3 \iint [a_l(\mathbf{p}')^* u_l^+(\mathbf{p}')^\dagger + b_l(\mathbf{p}') u_l^-(\mathbf{p}')^\dagger] \beta_4 \\ &\quad \times [a_k(\mathbf{p}) u_k^+(\mathbf{p}) + b_k(\mathbf{p})^* u_k^-(\mathbf{p})] \phi(\mathbf{p} - \mathbf{p}') d\mathbf{p} d\mathbf{p}', \end{aligned} \quad (49)$$

where

$$\phi(\mathbf{p} - \mathbf{p}') = \int \phi e^{i(\mathbf{p} - \mathbf{p}') \cdot \mathbf{r}/\hbar} d\mathbf{r}. \quad (50)$$

The second term is added to the Hamiltonian

$$\frac{1}{8\pi} \int (\mathcal{E}^2 + \mathcal{H}^2) d\mathbf{r} \quad (51)$$

of the electromagnetic field.

2.51. An alternative deduction of the Hamiltonian which automatically introduces the term (48) is obtained by means of the Lagrangian function. If we write  $\phi_i = A_i$  ( $i = 1, 2, 3$ ) and  $\phi_4 = i\phi$ , then the electromagnetic field strengths are

$$F_{\alpha\beta} = \frac{\partial \phi_\beta}{\partial x_\alpha} - \frac{\partial \phi_\alpha}{\partial x_\beta}, \quad (52)$$

and the Lagrangian of the electromagnetic field is

$$\frac{1}{8\pi} (\mathcal{E}^2 - \mathcal{H}^2) = -\frac{1}{16\pi} F_{\alpha\beta} F_{\alpha\beta}. \quad (53)$$

The Lagrangian of the mesons is given by (30) with  $\partial/\partial x_\mu$  replaced by  $\partial/\partial x_\mu - ie\phi_\mu/\hbar c$ . Hence the total Lagrangian is

$$L = i\hbar c \hat{\psi} \beta_\mu \frac{\partial \psi}{\partial x_\mu} + e \hat{\psi} \beta_\mu \phi_\mu \psi + imc^2 \hat{\psi} \psi - \frac{1}{16\pi} F_{\alpha\beta} F_{\alpha\beta}. \quad (54)$$

The Hamiltonian is  $\int H dr$ , where (see e.g. Heisenberg and Pauli 1929, p. 24, 1930, p. 176)

$$\begin{aligned} H &= \frac{\partial L}{\partial(\beta_4 \partial \psi / \partial x_4)} \beta_4 \frac{\partial \psi}{\partial x_4} + \frac{\partial L}{\partial(\partial \phi_k / \partial x_4)} \frac{\partial \phi_k}{\partial x_4} - L \\ &= -i\hbar c \hat{\psi} \beta_k \frac{\partial \psi}{\partial x_k} - e \hat{\psi} \beta_\mu \phi_\mu \psi - imc^2 \hat{\psi} \psi \\ &\quad - \frac{1}{4\pi} F_{4k} \frac{\partial \phi_4}{\partial x_k} - \frac{1}{8\pi} F_{4k} F_{4k} + \frac{1}{16\pi} F_{ik} F_{ik}. \end{aligned} \quad (55)$$

We transform the part of this depending on  $\psi$  by using the relations (41), and we can simplify the resulting expressions considerably by using the fact that any expression of the form  $\beta_4(\mathbf{a} \cdot \boldsymbol{\beta})\beta_4$  is zero (equation (57)). The part of  $H$  which depends only on the electromagnetic field differs from  $(\mathcal{E}^2 + \mathcal{H}^2)/(8\pi) - \phi \operatorname{div} \mathcal{E}/(4\pi)$  by a divergence. Since the Hamiltonian  $\bar{H}$  is  $\int H dr$ , the divergence is irrelevant and we finally obtain

$$\begin{aligned} \bar{H} = \int \left[ mc^2 \psi^\dagger \beta_4^2 \left( 1 + \frac{\{\boldsymbol{\beta} \cdot (\mathbf{p} - e\mathbf{A}/c)\}^2}{m^2 c^2} \right) \beta_4^2 \psi + e \phi \psi^\dagger \beta_4 \psi \right. \\ \left. - \frac{1}{4\pi} \phi \operatorname{div} \mathcal{E} + \frac{1}{8\pi} (\mathcal{E}^2 + \mathcal{H}^2) \right] dr, \end{aligned} \quad (56)$$

which is the expression obtained in the preceding section by means of the energy-momentum tensor. The presence of the term  $-\phi \operatorname{div} \mathcal{E}/4\pi$  ensures that, when we express the Hamiltonian of the electromagnetic field in terms of the  $q_k$  and the corresponding amplitudes of the longitudinal waves, the resulting expression is a sum of squares. We can, if we wish, eliminate the longitudinal part of the field in the usual way, and replace it by the Coulomb interaction, but this is unnecessary for our purpose. We always neglect the interaction between the mesons in intermediate states, and the only electrostatic force which we ever consider is the force on a meson due to a given external field.

**2.6. Spur and other relations.** In order to simplify the calculations, we always sum or average the expressions which occur over all possible polarizations of the mesons. This procedure results in the final expressions being obtained in the form of spurs, exactly as in the electron case. For the electron the evaluation of the spurs presents no great difficulty, but the present theory is so much more complex that it is necessary to make every possible simplification before inserting the values of the spurs. The following

relations, which can be readily deduced from the commutation rules (2), are some of the most useful in reducing the formulae:

$$\beta_4(\mathbf{a} \cdot \boldsymbol{\beta}) \beta_4 = 0, \quad (\mathbf{a} \cdot \boldsymbol{\beta}) \beta_4 (\mathbf{a} \cdot \boldsymbol{\beta}) = 0; \quad (57)$$

$$(\mathbf{a} \cdot \boldsymbol{\beta})(\mathbf{b} \cdot \boldsymbol{\beta}) \beta_4 + \beta_4 (\mathbf{b} \cdot \boldsymbol{\beta})(\mathbf{a} \cdot \boldsymbol{\beta}) = \beta_4 (\mathbf{a} \cdot \mathbf{b}), \quad (\mathbf{a} \cdot \boldsymbol{\beta})(\mathbf{b} \cdot \boldsymbol{\beta}) \beta_4^2 = \beta_4^2 (\mathbf{a} \cdot \boldsymbol{\beta})(\mathbf{b} \cdot \boldsymbol{\beta}); \quad (58)$$

$$\left. \begin{aligned} (\mathbf{a} \cdot \boldsymbol{\beta})^2 (\mathbf{b} \cdot \boldsymbol{\beta}) + (\mathbf{b} \cdot \boldsymbol{\beta})(\mathbf{a} \cdot \boldsymbol{\beta})^2 &= (\mathbf{a} \cdot \mathbf{b})(\mathbf{a} \cdot \boldsymbol{\beta}) + a^2 (\mathbf{b} \cdot \boldsymbol{\beta}), \\ (\mathbf{a} \cdot \boldsymbol{\beta})(\mathbf{b} \cdot \boldsymbol{\beta})(\mathbf{a} \cdot \boldsymbol{\beta}) &= (\mathbf{a} \cdot \mathbf{b})(\mathbf{a} \cdot \boldsymbol{\beta}), \quad (\mathbf{a} \cdot \boldsymbol{\beta})^3 = a^2 (\mathbf{a} \cdot \boldsymbol{\beta}); \end{aligned} \right\} \quad (59)$$

$$(\mathbf{a} \cdot \boldsymbol{\beta})^2 (\mathbf{b} \cdot \boldsymbol{\beta})^2 = (\mathbf{b} \cdot \boldsymbol{\beta})^2 (\mathbf{a} \cdot \boldsymbol{\beta})^2 + (\mathbf{a} \cdot \mathbf{b}) [(\mathbf{a} \cdot \boldsymbol{\beta})(\mathbf{b} \cdot \boldsymbol{\beta}) - (\mathbf{b} \cdot \boldsymbol{\beta})(\mathbf{a} \cdot \boldsymbol{\beta})]; \quad (60)$$

$$\left. \begin{aligned} (\mathbf{a} \cdot \boldsymbol{\beta})(\mathbf{b} \cdot \boldsymbol{\beta})^3 (\mathbf{a} \cdot \boldsymbol{\beta})^2 &= a^2 (\mathbf{a} \cdot \boldsymbol{\beta})(\mathbf{b} \cdot \boldsymbol{\beta})^2 - (\mathbf{a} \cdot \mathbf{b})(\mathbf{a} \cdot \boldsymbol{\beta})^2 (\mathbf{b} \cdot \boldsymbol{\beta}) + (\mathbf{a} \cdot \mathbf{b})^2 (\mathbf{a} \cdot \boldsymbol{\beta}), \\ (\mathbf{a} \cdot \boldsymbol{\beta})^2 (\mathbf{b} \cdot \boldsymbol{\beta})^2 (\mathbf{a} \cdot \boldsymbol{\beta}) &= a^2 (\mathbf{b} \cdot \boldsymbol{\beta})^2 (\mathbf{a} \cdot \boldsymbol{\beta}) - (\mathbf{a} \cdot \mathbf{b})(\mathbf{b} \cdot \boldsymbol{\beta})(\mathbf{a} \cdot \boldsymbol{\beta})^2 + (\mathbf{a} \cdot \mathbf{b})^2 (\mathbf{a} \cdot \boldsymbol{\beta}); \end{aligned} \right\} \quad (61)$$

$$\left. \begin{aligned} (\mathbf{a} \cdot \boldsymbol{\beta})^2 (\mathbf{b} \cdot \boldsymbol{\beta})^2 (\mathbf{a} \cdot \boldsymbol{\beta})^2 &= a^2 (\mathbf{b} \cdot \boldsymbol{\beta})^2 (\mathbf{a} \cdot \boldsymbol{\beta})^2 + (\mathbf{a} \cdot \mathbf{b})^2 (\mathbf{a} \cdot \boldsymbol{\beta})^2 - a^2 (\mathbf{a} \cdot \mathbf{b})(\mathbf{b} \cdot \boldsymbol{\beta})(\mathbf{a} \cdot \boldsymbol{\beta}) \\ &= a^2 (\mathbf{a} \cdot \boldsymbol{\beta})^2 (\mathbf{b} \cdot \boldsymbol{\beta})^2 + (\mathbf{a} \cdot \mathbf{b})^2 (\mathbf{a} \cdot \boldsymbol{\beta})^2 - a^2 (\mathbf{a} \cdot \mathbf{b})(\mathbf{a} \cdot \boldsymbol{\beta})(\mathbf{b} \cdot \boldsymbol{\beta}). \end{aligned} \right\} \quad (62)$$

The whole of the theory so far developed applies not only to mesons but (with verbal alterations) to the spinless particles discussed by Pauli and Weisskopf (1934). Kemmer has shown that there are only two inequivalent non-trivial representations of the  $\beta$ 's, the  $10 \times 10$  matrices envisaged here, and  $5 \times 5$  matrices which give rise to Pauli and Weisskopf's equations in which there occur one scalar wave function and its four-dimensional gradient. These two cases only differ in that the spurs are different. To calculate these we must use the explicit representations of the  $\beta$ 's given by Kemmer, or rather the spurs of all the independent products of the  $\beta$ 's. These somewhat tedious calculations have been carried out by Kemmer and Kynch for spurs involving up to products of ten  $\beta$ 's (for the  $10 \times 10$  matrices). Their results are as follows. § The spur of any quantity which contains an odd power of  $\beta_4$  or an odd number of  $(\mathbf{a} \cdot \boldsymbol{\beta})$ 's is zero in both representations. Also, by (57) and (58), any quantity which has an odd number of  $(\mathbf{a} \cdot \boldsymbol{\beta})$ 's between two  $\beta_4$ 's is zero.

#### Particles with spin 0

$$\left. \begin{aligned} \text{spur } I &= 5, \quad \text{spur } \beta_\mu^2 = 2, \quad \text{spur } \beta_\mu^2 \beta_\nu^2 = 1, \\ \text{spur } \beta_\mu^2 \beta_\nu^2 \beta_\rho^2 &= 1, \quad \text{spur } \beta_\mu^2 \beta_\nu^2 \beta_\rho^2 \beta_\sigma^2 = 1 \quad (\mu \neq \nu \neq \rho \neq \sigma). \end{aligned} \right\} \quad (63)$$

$$\text{spur } \beta_4^2 (\mathbf{a}_1 \cdot \boldsymbol{\beta}) \dots (\mathbf{a}_{2n} \cdot \boldsymbol{\beta}) = (\mathbf{a}_1 \cdot \mathbf{a}_2) (\mathbf{a}_3 \cdot \mathbf{a}_4) \dots (\mathbf{a}_{2n-1} \cdot \mathbf{a}_{2n}). \quad (64)$$

$$\text{spur } \beta_4 (\mathbf{a}_1 \cdot \boldsymbol{\beta}) \dots (\mathbf{a}_{2n} \cdot \boldsymbol{\beta}) \beta_4 \dots (\mathbf{a}_{2n} \cdot \boldsymbol{\beta}) = 0. \quad (65)$$

§ We use the symbol  $(m \cdot n)$  to denote the scalar product  $\mathbf{a}_m \cdot \mathbf{a}_n$ .

## Particles with spin 1

$$\left. \begin{aligned} \text{spur } I = 10, \quad \text{spur } \beta_\mu^2 = 6, \quad \text{spur } \beta_\mu^2 \beta_\nu^2 = 3, \\ \text{spur } \beta_\mu^2 \beta_\nu^2 \beta_\rho^2 = 1, \quad \text{spur } \beta_\mu^2 \beta_\nu^2 \beta_\rho^2 \beta_\sigma^2 = 0 \quad (\mu \neq \nu \neq \rho \neq \sigma). \end{aligned} \right\} \quad (66)$$

$$\text{spur } \beta_4^2(\mathbf{a}_1 \cdot \boldsymbol{\beta})(\mathbf{a}_2 \cdot \boldsymbol{\beta}) = 3(1.2). \quad (67)$$

$$\text{spur } \beta_4^2(\mathbf{a}_1 \cdot \boldsymbol{\beta})(\mathbf{a}_2 \cdot \boldsymbol{\beta})(\mathbf{a}_3 \cdot \boldsymbol{\beta})(\mathbf{a}_4 \cdot \boldsymbol{\beta}) = (1.2)(3.4) + 2(1.4)(2.3). \quad (68)$$

$$\text{spur } \beta_4(\mathbf{a}_1 \cdot \boldsymbol{\beta})(\mathbf{a}_2 \cdot \boldsymbol{\beta})\beta_4(\mathbf{a}_3 \cdot \boldsymbol{\beta})(\mathbf{a}_4 \cdot \boldsymbol{\beta}) = 2(1.2)(3.4) - 2(1.3)(2.4). \quad (69)$$

$$\begin{aligned} \text{spur } \beta_4^2(\mathbf{a}_1 \cdot \boldsymbol{\beta}) \dots (\mathbf{a}_6 \cdot \boldsymbol{\beta}) &= (1.2)(4.5)(3.6) + (3.4)(6.1)(5.2) \\ &+ (5.6)(2.3)(1.4) - (1.4)(2.5)(3.6) + (6.1)(2.3)(4.5). \end{aligned} \quad (70)$$

$$\begin{aligned} \text{spur } \beta_4^2(\mathbf{a}_1 \cdot \boldsymbol{\beta})(\mathbf{a}_2 \cdot \boldsymbol{\beta})\beta_4(\mathbf{a}_3 \cdot \boldsymbol{\beta})(\mathbf{a}_4 \cdot \boldsymbol{\beta})\beta_4(\mathbf{a}_5 \cdot \boldsymbol{\beta})(\mathbf{a}_6 \cdot \boldsymbol{\beta}) \\ = (6.1)(3.4)(2.5) + (1.3)(4.6)(2.5) + (5.6)(1.2)(3.4) \\ - (6.1)(2.4)(3.5) - (5.6)(1.3)(2.4) - (1.2)(4.6)(3.5). \end{aligned} \quad (71)$$

$$\begin{aligned} \text{spur } \beta_4^2(\mathbf{a}_1 \cdot \boldsymbol{\beta}) \dots (\mathbf{a}_8 \cdot \boldsymbol{\beta}) \\ = (1.6)(2.5)(3.8)(4.7) + (2.3)(1.4)(8.5)(7.6) + (4.5)(3.6)(2.7)(1.8) \\ + \sum_{\substack{4 \text{ cyclical} \\ \text{permutations}}} (1.2)(8.3)(4.5)(6.7) - \sum_{\substack{4 \text{ cyclical} \\ \text{permutations}}} (2.3)(1.6)(8.5)(4.7). \end{aligned} \quad (72)$$

$$\begin{aligned} \text{spur } \beta_4^2(\mathbf{a}_1 \cdot \boldsymbol{\beta}) \dots (\mathbf{a}_{10} \cdot \boldsymbol{\beta}) \\ = (2.3)(4.5)(6.7)(8.9)(10.1) - 2(2.5)(4.7)(6.9)(8.1)(10.3) \\ - 2(1.4)(3.6)(5.8)(7.10)(9.2) + (1.6)(2.7)(3.8)(4.9)(5.10) \\ - \sum_{\substack{5 \text{ cyclical} \\ \text{permutations}}} (1.2)(3.8)(4.9)(5.10)(6.7) + \sum_{\substack{5 \text{ cyclical} \\ \text{permutations}}} (10.1)(2.3)(4.9)(5.6)(7.8) \\ - \sum_{\substack{5 \text{ cyclical} \\ \text{permutations}}} (8.1)(2.5)(4.9)(3.6)(7.10) + \sum_{\substack{10 \text{ cyclical} \\ \text{permutations}}} (1.4)(10.3)(9.2)(5.8)(6.7) \\ + \sum_{\substack{10 \text{ cyclical} \\ \text{permutations}}} (3.6)(5.8)(7.10)(1.2)(4.9) - \sum_{\substack{10 \text{ cyclical} \\ \text{permutations}}} (1.4)(10.3)(9.2)(5.6)(7.8). \end{aligned} \quad (73)$$

The four and five cyclical permutations in (72) and (73) are obtained by omitting every alternate permutation.

## THE COMPTON EFFECT

3.1. The effect is exactly the same as for electrons; a light quantum with momentum  $\mathbf{k}_0$  is scattered by a (positive or negative) meson of momentum



$\mathbf{p}_0$ , the final momentum of the light quantum being  $\mathbf{k}$  and that of the meson being  $\mathbf{p}$ . Since both energy and momentum are conserved in the process, we have

$$E(\mathbf{p}) + ck - E(\mathbf{p}_0) - ck_0 = c(m^2c^2 + p^2)^{1/2} + ck - c(m^2c^2 + p_0^2)^{1/2} - ck_0, \quad (74)$$

and

$$\mathbf{p} + \mathbf{k} - \mathbf{p}_0 - \mathbf{k}_0 = 0. \quad (75)$$

The calculations are very similar to the corresponding calculations for electrons, and we follow the exposition of the latter given in Heitler's book (1936).

The scattering is a two quantum effect, one quantum being absorbed and the other emitted. The process can therefore take place either directly, through the interaction energy  $H_2$ , or by means of double transitions caused by the interaction energy  $H_1$ . (In the relativistic electron theory only the double transitions are possible.) The cross-section for scattering is then  $1/c$  times the transition probability per unit time. The differential cross-section for the light quantum to be scattered into  $d\mathbf{k}$  is, with the normalization which we have adopted,

$$\frac{4\pi^2\hbar^2}{c} |(i|H|f)|^2 \frac{d\mathbf{k}}{dE_f}, \quad (76)$$

$$\text{where} \quad (i|H|f) = \sum_n \frac{(i|H_1|n)(n|H_1|f)}{E_i - E_n} + (i|H_2|f), \quad (77)$$

the letters  $i$ ,  $n$  and  $f$  denoting the initial, intermediate and final states.

**3.2. Matrix elements.** We suppose for definiteness that we are considering the scattering of light by a positive meson. Since we ultimately either sum or average over the different polarizations of the meson, we generally omit the suffixes  $k$  which refer to the polarizations; this will also prevent the suffix from being confused with the momentum  $\mathbf{k}$  of the light quantum.

The matrix elements of  $a$ ,  $a^*$ ,  $b$ ,  $b^*$ ,  $q$ ,  $q^*$  are all matrix elements of the simple harmonic oscillator, and (cf. Heitler 1936, p. 92) we have

$$(0|a|1) = 1, \quad (1|a|0) = 0, \quad (0|a^*|1) = 0, \quad (1|a^*|0) = 1, \quad (78)$$

$$(0|b|1) = 1, \quad (1|b|0) = 0, \quad (0|b^*|1) = 0, \quad (1|b^*|0) = 1, \quad (79)$$

$$(0|q_{\mathbf{k}}|1) = \sqrt{\frac{\hbar^2}{2ck}}, \quad (1|q_{\mathbf{k}}|0) = 0, \quad (0|q_{\mathbf{k}}^*|1) = 0, \quad (1|q_{\mathbf{k}}^*|0) = \sqrt{\frac{\hbar^2}{2ck}}, \quad (80)$$

The numbers 0 and 1 refer to the numbers of particles present of the respective kinds, including light quanta. Thus  $a, b, q$  only have non-zero matrix elements when a particle is emitted, and  $a^*, b^*, q^*$  have non-zero matrix elements when a particle is absorbed.

We have the following set of transitions to consider. We first give the transition and then the corresponding matrix element; we write  $\mathbf{e}_0$  and  $\mathbf{e}$  for the polarization vectors of the incident and scattered quanta.

1. The light quantum  $\mathbf{k}_0$  and the meson  $u^+(\mathbf{p}_0)$  are absorbed, and the meson  $u^+(\mathbf{p}_0 + \mathbf{k}_0)$  is emitted.

$$(i | H_1 | n_1) = -\frac{e}{mc} \sqrt{\frac{c}{2\pi\hbar k_0}} \times u^+(\mathbf{p}_0)^\dagger \beta_4^2 [(\mathbf{e}_0 \cdot \boldsymbol{\beta}) \{(\mathbf{p}_0 + \mathbf{k}_0) \cdot \boldsymbol{\beta}\} + (\mathbf{p}_0 \cdot \boldsymbol{\beta}) (\mathbf{e}_0 \cdot \boldsymbol{\beta})] \beta_4^2 u^+(\mathbf{p}_0 + \mathbf{k}_0). \quad (81)$$

The meson  $u^+(\mathbf{p}_0 + \mathbf{k}_0)$  is then absorbed; the meson  $u^+(\mathbf{p}_0 + \mathbf{k}_0 - \mathbf{k})$  and the light quantum  $\mathbf{k}$  are emitted.

$$(n_1 | H_1 | f) = -\frac{e}{mc} \sqrt{\frac{c}{2\pi\hbar k}} \times u^+(\mathbf{p}_0 + \mathbf{k}_0)^\dagger \beta_4^2 [(\mathbf{e} \cdot \boldsymbol{\beta}) \{(\mathbf{p}_0 + \mathbf{k}_0 - \mathbf{k}) \cdot \boldsymbol{\beta}\} + \{(\mathbf{p}_0 + \mathbf{k}_0) \cdot \boldsymbol{\beta}\} (\mathbf{e} \cdot \boldsymbol{\beta})] \beta_4^2 u^+(\mathbf{p}_0 + \mathbf{k}_0 - \mathbf{k}). \quad (82)$$

2. The light quantum  $\mathbf{k}$  is emitted and a pair of mesons  $u^+(\mathbf{p}_0 + \mathbf{k}_0 - \mathbf{k})$  and  $u^-(\mathbf{p}_0 + \mathbf{k}_0)$  are created. §

$$(i | H_1 | n_2) = -\frac{e}{mc} \sqrt{\frac{c}{2\pi\hbar k}} \times u^-(\mathbf{p}_0 + \mathbf{k}_0)^\dagger \beta_4^2 [(\mathbf{e} \cdot \boldsymbol{\beta}) \{(\mathbf{p}_0 + \mathbf{k}_0 - \mathbf{k}) \cdot \boldsymbol{\beta}\} + \{(\mathbf{p}_0 + \mathbf{k}_0) \cdot \boldsymbol{\beta}\} (\mathbf{e} \cdot \boldsymbol{\beta})] \beta_4^2 u^+(\mathbf{p}_0 + \mathbf{k}_0 - \mathbf{k}). \quad (83)$$

The pair of mesons  $u^+(\mathbf{p}_0)$  and  $u^-(\mathbf{p}_0 + \mathbf{k}_0)$  are then annihilated, and the light quantum  $\mathbf{k}_0$  is absorbed.

$$(n_2 | H_1 | f) = -\frac{e}{mc} \sqrt{\frac{c}{2\pi\hbar k_0}} \times u^+(\mathbf{p}_0)^\dagger \beta_4^2 [(\mathbf{e}_0 \cdot \boldsymbol{\beta}) \{(\mathbf{p}_0 + \mathbf{k}_0) \cdot \boldsymbol{\beta}\} + (\mathbf{p}_0 \cdot \boldsymbol{\beta}) (\mathbf{e}_0 \cdot \boldsymbol{\beta})] \beta_4^2 u^-(\mathbf{p}_0 + \mathbf{k}_0). \quad (84)$$

3. The light quantum  $\mathbf{k}_0$  is absorbed, and the pair of mesons  $u^+(\mathbf{p}_0 + \mathbf{k}_0 - \mathbf{k})$  and  $u^-(\mathbf{p}_0 - \mathbf{k})$  are created.

$$(i | H_1 | n_3) = -\frac{e}{mc} \sqrt{\frac{c}{2\pi\hbar k_0}} \times u^-(\mathbf{p}_0 - \mathbf{k})^\dagger \beta_4^2 [(\mathbf{e}_0 \cdot \boldsymbol{\beta}) \{(\mathbf{p}_0 + \mathbf{k}_0 - \mathbf{k}) \cdot \boldsymbol{\beta}\} + \{(\mathbf{p}_0 - \mathbf{k}) \cdot \boldsymbol{\beta}\} (\mathbf{e}_0 \cdot \boldsymbol{\beta})] \beta_4^2 u^+(\mathbf{p}_0 + \mathbf{k}_0 - \mathbf{k}). \quad (85)$$

§ Note that  $u^-(\mathbf{p})$  has momentum  $-\mathbf{p}$ .

The light quantum  $\mathbf{k}$  is then emitted, and the pair of mesons  $u^+(\mathbf{p}_0)$  and  $u^-(\mathbf{p}_0 - \mathbf{k})$  are annihilated.

$$(n_3 | H_1 | f) = -\frac{e}{mc} \sqrt{\frac{c}{2\pi\hbar k}} \times u^+(\mathbf{p}_0)^\dagger \beta_4^2 [(\mathbf{e} \cdot \boldsymbol{\beta}) \{(\mathbf{p}_0 - \mathbf{k}) \cdot \boldsymbol{\beta}\} + (\mathbf{p}_0 \cdot \boldsymbol{\beta}) (\mathbf{e} \cdot \boldsymbol{\beta})] \beta_4^2 u^-(\mathbf{p}_0 - \mathbf{k}). \quad (86)$$

4. The meson  $u^+(\mathbf{p}_0)$  is absorbed; the meson  $u^+(\mathbf{p}_0 - \mathbf{k})$  and the light quantum  $\mathbf{k}$  are emitted.

$$(i | H_1 | n_4) = -\frac{e}{mc} \sqrt{\frac{c}{2\pi\hbar k}} \times u^+(\mathbf{p}_0)^\dagger \beta_4^2 [(\mathbf{e} \cdot \boldsymbol{\beta}) \{(\mathbf{p}_0 - \mathbf{k}) \cdot \boldsymbol{\beta}\} + (\mathbf{p}_0 \cdot \boldsymbol{\beta}) (\mathbf{e} \cdot \boldsymbol{\beta})] \beta_4^2 u^+(\mathbf{p}_0 - \mathbf{k}). \quad (87)$$

The meson  $u^+(\mathbf{p}_0 - \mathbf{k})$  and the light quantum  $\mathbf{k}_0$  are then absorbed, and the meson  $u^+(\mathbf{p}_0 + \mathbf{k}_0 - \mathbf{k})$  is emitted.

$$(n_4 | H_1 | f) = -\frac{e}{mc} \sqrt{\frac{c}{2\pi\hbar k_0}} \times u^+(\mathbf{p}_0 - \mathbf{k})^\dagger \beta_4^2 [(\mathbf{e}_0 \cdot \boldsymbol{\beta}) \{(\mathbf{p}_0 + \mathbf{k}_0 - \mathbf{k}) \cdot \boldsymbol{\beta}\} + \{(\mathbf{p}_0 - \mathbf{k}) \cdot \boldsymbol{\beta}\} (\mathbf{e}_0 \cdot \boldsymbol{\beta})] \beta_4^2 u^+(\mathbf{p}_0 + \mathbf{k}_0 - \mathbf{k}). \quad (88)$$

5. The meson  $u^+(\mathbf{p}_0)$  and the light quantum  $\mathbf{k}_0$  are absorbed, and the meson  $u^+(\mathbf{p}_0 + \mathbf{k}_0 - \mathbf{k})$  and the light quantum  $\mathbf{k}$  are emitted.

$$(i | H_2 | f) = \frac{e^2}{2\pi m \hbar c} \sqrt{\frac{1}{k k_0}} \times u^+(\mathbf{p}_0)^\dagger \beta_4^2 [(\mathbf{e} \cdot \boldsymbol{\beta}) (\mathbf{e}_0 \cdot \boldsymbol{\beta}) + (\mathbf{e}_0 \cdot \boldsymbol{\beta}) (\mathbf{e} \cdot \boldsymbol{\beta})] \beta_4^2 u^+(\mathbf{p}_0 + \mathbf{k}_0 - \mathbf{k}). \quad (89)$$

In order to simplify the algebra we take  $\mathbf{p}_0 = 0$ . This is the important case, and there is no loss of generality since any other case can be obtained from this by a Lorentz transformation. With this choice of  $\mathbf{p}_0$ , the energy differences  $E_i - E_n$  are given by

$$E_i - E_{n_1} = mc^2 + ck_0 - E(\mathbf{k}_0), \quad (90)$$

$$E_i - E_{n_2} = -ck - E(\mathbf{k}_0 - \mathbf{k}) - E(\mathbf{k}_0) = -(mc^2 + ck_0) - E(\mathbf{k}_0), \quad (91)$$

$$E_i - E_{n_3} = ck_0 - E(\mathbf{k}_0 - \mathbf{k}) - E(\mathbf{k}) = -(mc^2 - ck) - E(\mathbf{k}), \quad (92)$$

$$E_i - E_{n_4} = mc^2 - ck - E(\mathbf{k}). \quad (93)$$

The alternative expressions in (91) and (92) are obtained by using (74).

3.3. *Summation over the intermediate states.* The summation in (77) has to be extended over the three different polarizations which the meson can

have in the intermediate states. We take the intermediate states 1 and 2 together, and then

$$\sum_{n=1}^2 \frac{(i | H_1 | n) (n | H_1 | f)}{E_i - E_n} = \frac{e^2}{2\pi m^2 \hbar c} \sqrt{\frac{1}{k k_0}} \sum_{l=1}^3 \left[ \frac{u^+(0)^\dagger \beta_4^2 A \beta_4^2 u_l^+(\mathbf{k}_0) u_l^+(\mathbf{k}_0)^\dagger \beta_4^2 B \beta_4^2 u^+(\mathbf{k}_0 - \mathbf{k})}{mc^2 + ck_0 - E(\mathbf{k}_0)} - \frac{u^+(0)^\dagger \beta_4^2 A \beta_4^2 u_l^-(\mathbf{k}_0) u_l^-(\mathbf{k}_0)^\dagger \beta_4^2 B \beta_4^2 u^+(\mathbf{k}_0 - \mathbf{k})}{mc^2 + ck_0 + E(\mathbf{k}_0)} \right], \quad (94)$$

$$\text{where } A = (\mathbf{e}_0 \cdot \boldsymbol{\beta}) (\mathbf{k}_0 \cdot \boldsymbol{\beta}), \quad B = (\mathbf{e} \cdot \boldsymbol{\beta}) \{(\mathbf{k}_0 - \mathbf{k}) \cdot \boldsymbol{\beta}\} + (\mathbf{k}_0 \cdot \boldsymbol{\beta}) (\mathbf{e} \cdot \boldsymbol{\beta}). \quad (95)$$

If we multiply the first expression in the square brackets by  $mc^2 + ck_0 + E(\mathbf{k}_0)$  and the second by  $mc^2 + ck_0 - E(\mathbf{k}_0)$ , we obtain as part of the result the expression

$$(mc^2 + ck_0) \sum_{l=1}^6 \beta_4^2 u_l(\mathbf{k}_0) \rho_{ll} u_l(\mathbf{k}_0)^\dagger \beta_4^2 + E(\mathbf{k}_0) \sum_{l=1}^3 \beta_4^2 [u_l^+(\mathbf{k}_0) u_l^+(\mathbf{k}_0)^\dagger + u_l^-(\mathbf{k}_0) u_l^-(\mathbf{k}_0)^\dagger] \beta_4^2. \quad (96)$$

The first term of this can be immediately summed by using the inverse orthogonality relation (22), and it gives  $(mc^2 + ck_0) \beta_4$ . The second term is not of the form required for applying the inverse orthogonality relation; it can, however, be transformed into that form. We have, by (27) and (41),

$$\begin{aligned} E(\mathbf{p}) \beta_4 u_l^+(\mathbf{p}) &= \beta_4^2 E(\mathbf{p}) \beta_4 u_l^+(\mathbf{p}) = \beta_4^2 (mc^2 + i\mathbf{c} \cdot \mathbf{p} \cdot \boldsymbol{\beta}) u_l^+(\mathbf{p}) \\ &= \beta_4^2 (mc^2 + i\mathbf{c} \cdot \mathbf{p} \cdot \boldsymbol{\beta}) \left( 1 - i \frac{\mathbf{p} \cdot \boldsymbol{\beta}}{mc} \right) \beta_4^2 u_l^+(\mathbf{p}) \\ &= mc^2 \beta_4^2 \left[ 1 + \frac{(\mathbf{p} \cdot \boldsymbol{\beta})^2}{m^2 c^2} \right] \beta_4^2 u_l^+(\mathbf{p}). \end{aligned} \quad (97)$$

Similarly we have

$$E(\mathbf{p}) \beta_4 u_l^-(\mathbf{p}) = -mc^2 \beta_4^2 \left[ 1 + \frac{(\mathbf{p} \cdot \boldsymbol{\beta})^2}{m^2 c^2} \right] \beta_4^2 u_l^-(\mathbf{p}). \quad (98)$$

By these two relations, the second term of (96) is transformed into the required form, and on summation it gives

$$mc^2 \beta_4 \left[ 1 + \frac{(\mathbf{p} \cdot \boldsymbol{\beta})^2}{m^2 c^2} \right] \beta_4.$$

$$\text{Also, we have} \quad (mc^2 + ck_0)^2 - E(\mathbf{k}_0)^2 = 2mc^2 k_0, \quad (99)$$

and hence (94) becomes

$$I = \frac{e^2}{4\pi m^3 \hbar c^4 k_0} \sqrt{\frac{1}{kk_0}} \times u^+(0)^\dagger \beta_4^2 A \beta_4 \left[ (mc^2 + ck_0) \beta_4 + mc^2 + \frac{(\mathbf{k}_0 \cdot \boldsymbol{\beta})^2}{m} \right] \beta_4 B \beta_4^2 u^+(\mathbf{k}_0 - \mathbf{k}). \quad (100)$$

By a similar process we can show that the summation over the intermediate states 3 and 4 gives

$$II = \frac{e^2}{4\pi m^3 \hbar c^4 k} \sqrt{\frac{1}{kk_0}} \times u^+(0)^\dagger \beta_4^2 C \beta_4 \left[ (mc^2 - ck) \beta_4 + mc^2 + \frac{(\mathbf{k} \cdot \boldsymbol{\beta})^2}{m} \right] \beta_4 D \beta_4^2 u^+(\mathbf{k}_0 - \mathbf{k}), \quad (101)$$

$$\text{where } C = (\mathbf{e} \cdot \boldsymbol{\beta})(\mathbf{k} \cdot \boldsymbol{\beta}), \quad D = (\mathbf{e}_0 \cdot \boldsymbol{\beta})\{(\mathbf{k}_0 - \mathbf{k}) \cdot \boldsymbol{\beta}\} - (\mathbf{k} \cdot \boldsymbol{\beta})(\mathbf{e}_0 \cdot \boldsymbol{\beta}), \quad (102)$$

and we have used the fact that

$$(mc^2 - ck)^2 - E(\mathbf{k})^2 = -2mc^2 k. \quad (103)$$

The expression  $II$  is obtained from  $I$  by replacing  $\mathbf{e}$ ,  $\mathbf{e}_0$ ,  $\mathbf{k}$  and  $\mathbf{k}_0$  by  $\mathbf{e}_0$ ,  $\mathbf{e}$ ,  $-\mathbf{k}_0$  and  $-\mathbf{k}$ . We denote the remaining part  $(i | H_2 | f)$  of  $(i | H | f)$  by  $III$ .

3.31. *Summation and averaging over the initial and final states.* We now take the square of the matrix element  $(i | H | f)$ , and we have

$$|(i | H | f)|^2 = I^* I + II^* II + III^* III + I^* II + II^* I + I^* III + III^* I + II^* III + III^* II. \quad (104)$$

Now  $I^* I$  is proportional to

$$u^+(\mathbf{k}_0 - \mathbf{k})^\dagger \beta_4^2 B^\dagger \beta_4 \left[ (mc^2 + ck_0) \beta_4 + mc^2 + \frac{(\mathbf{k}_0 \cdot \boldsymbol{\beta})^2}{m} \right] \beta_4 A^\dagger \beta_4^2 u^+(0) \times u^+(0)^\dagger \beta_4^2 A \beta_4 \left[ (mc^2 + ck_0) \beta_4 + mc^2 + \frac{(\mathbf{k}_0 \cdot \boldsymbol{\beta})^2}{m} \right] \beta_4 B \beta_4^2 u^+(\mathbf{k}_0 - \mathbf{k}), \quad (105)$$

where  $A^\dagger$  and  $B^\dagger$  are the Hermitian conjugates of  $A$  and  $B$ . (Since  $\mathbf{p} \cdot \boldsymbol{\beta}$  is Hermitian,  $A$  and  $A^\dagger$  only differ in the order of the factors.) To average over the initial state we sum over the three polarizations and divide by 3; the wave functions of the initial state then occur in the form

$$\sum_{i=1}^3 \beta_4^2 u_i^+(0) u_i^+(0)^\dagger \beta_4^2. \quad (106)$$

In order to carry out this summation we introduce annihilation operators just as in the electron theory. By (27) and (41) we have

$$\beta_4 u^+(\mathbf{p}) = \frac{1}{2E} [E\beta_4 + ic\mathbf{p} \cdot \boldsymbol{\beta} + mc^2] u^+(\mathbf{p}) = \frac{1}{2E} \left[ E\beta_4 + mc^2 + \frac{(\mathbf{p} \cdot \boldsymbol{\beta})^2}{m} \right] \beta_4^2 u^+(\mathbf{p}).$$

$$\begin{aligned} \text{Thus} \quad & \left. \begin{aligned} \frac{1}{2E} \left[ E\beta_4 + mc^2 + \frac{(\mathbf{p} \cdot \boldsymbol{\beta})^2}{m} \right] \beta_4^2 u^+(\mathbf{p}) &= \beta_4 u^+(\mathbf{p}), \\ \frac{1}{2E} \left[ E\beta_4 + mc^2 + \frac{(\mathbf{p} \cdot \boldsymbol{\beta})^2}{m} \right] \beta_4^2 u^-(\mathbf{p}) &= 0, \end{aligned} \right\} \\ \text{and} \quad & \left. \begin{aligned} \frac{1}{2E} \left[ -E\beta_4 + mc^2 + \frac{(\mathbf{p} \cdot \boldsymbol{\beta})^2}{m} \right] \beta_4^2 u^+(\mathbf{p}) &= 0, \\ \frac{1}{2E} \left[ -E\beta_4 + mc^2 + \frac{(\mathbf{p} \cdot \boldsymbol{\beta})^2}{m} \right] \beta_4^2 u^-(\mathbf{p}) &= \beta_4 u^-(\mathbf{p}). \end{aligned} \right\} \end{aligned} \quad (107)$$

Since  $E(0) = mc^2$ , (106) can be written in the form

$$\frac{1}{2mc^2} \sum_{l=1}^6 \beta_4 (mc^2 \beta_4 + mc^2) \beta_4^2 u_l(0) \rho_{ll} u_l(0)^\dagger \beta_4^2, \quad (108)$$

the terms with  $l=4, 5, 6$  being zero. We can now apply (22); then (108) becomes

$$\frac{1}{2} (\beta_4 + \beta_4^2). \quad (109)$$

We can apply the same method to the sum over the polarizations in the final state. After we have introduced the annihilation operators we are left with an expression of the form

$$\sum_{l=1}^6 u_l(\mathbf{k}_0 - \mathbf{k})^\dagger \beta_4^2 Q \beta_4^2 u_l(\mathbf{k}_0 - \mathbf{k}) \rho_{ll} = \sum_{l=1}^6 \sum_{\rho, \sigma} (u_l^\dagger \beta_4^2)_\rho Q_{\rho\sigma} (\beta_4^2 u_l)_\sigma \rho_{ll}. \quad (110)$$

By (22), this reduces to

$$\sum_{\rho, \sigma} Q_{\rho\sigma} (\beta_4)_{\sigma\rho} = \text{spur } Q \beta_4 = \text{spur } \beta_4 Q. \quad (111)$$

We therefore have finally, putting  $\mathbf{p} = \mathbf{k}_0 - \mathbf{k}$ ,

$$\begin{aligned} I^* I &= \frac{e^4}{192\pi^2 m^8 \hbar^2 c^8} \frac{1}{kk_0^3 E(\mathbf{p})} \\ &\times \text{spur } \beta_4 [(\mathbf{p} \cdot \boldsymbol{\beta})(\mathbf{e} \cdot \boldsymbol{\beta}) + (\mathbf{e} \cdot \boldsymbol{\beta})(\mathbf{k}_0 \cdot \boldsymbol{\beta})] \beta_4 \left[ (mc^2 + ck_0) \beta_4 + mc^2 + \frac{(\mathbf{k}_0 \cdot \boldsymbol{\beta})^2}{m} \right] \\ &\times \beta_4 (\mathbf{k}_0 \cdot \boldsymbol{\beta})(\mathbf{e}_0 \cdot \boldsymbol{\beta}) (\beta_4 + \beta_4^2) (\mathbf{e}_0 \cdot \boldsymbol{\beta})(\mathbf{k}_0 \cdot \boldsymbol{\beta}) \beta_4 \left[ (mc^2 + ck_0) \beta_4 + mc^2 + \frac{(\mathbf{k}_0 \cdot \boldsymbol{\beta})^2}{m} \right] \\ &\times \beta_4 [(\mathbf{e} \cdot \boldsymbol{\beta})(\mathbf{p} \cdot \boldsymbol{\beta}) + (\mathbf{k}_0 \cdot \boldsymbol{\beta})(\mathbf{e} \cdot \boldsymbol{\beta})] \beta_4 \left[ E(\mathbf{p}) \beta_4 + mc^2 + \frac{(\mathbf{p} \cdot \boldsymbol{\beta})^2}{m} \right]. \end{aligned} \quad (112)$$

Of the remaining expressions there are only three, namely  $I^*II$ ,  $III^*III$  and  $I^*III$ , which need to be worked out in detail; the others can readily be deduced from these. The results are as follows.

$$\begin{aligned}
 I^*II &= \frac{e^4}{192\pi^2 m^3 h^2 c^3} \frac{1}{k^2 k_0^2 E(\mathbf{p})} \\
 &\times \text{spur } \beta_4 [(\mathbf{p} \cdot \boldsymbol{\beta})(\mathbf{e} \cdot \boldsymbol{\beta}) + (\mathbf{e} \cdot \boldsymbol{\beta})(\mathbf{k}_0 \cdot \boldsymbol{\beta})] \beta_4 \left[ (mc^2 + ck_0) \beta_4 + mc^2 + \frac{(\mathbf{k}_0 \cdot \boldsymbol{\beta})^2}{m} \right] \\
 &\times \beta_4 (\mathbf{k}_0 \cdot \boldsymbol{\beta})(\mathbf{e}_0 \cdot \boldsymbol{\beta})(\beta_4 + \beta_4^2)(\mathbf{e} \cdot \boldsymbol{\beta})(\mathbf{k} \cdot \boldsymbol{\beta}) \beta_4 \left[ (mc^2 - ck) \beta_4 + mc^2 + \frac{(\mathbf{k} \cdot \boldsymbol{\beta})^2}{m} \right] \\
 &\times \beta_4 [(\mathbf{e}_0 \cdot \boldsymbol{\beta})(\mathbf{p} \cdot \boldsymbol{\beta}) - (\mathbf{k} \cdot \boldsymbol{\beta})(\mathbf{e}_0 \cdot \boldsymbol{\beta})] \beta_4 \left[ E(\mathbf{p}) \beta_4 + mc^2 + \frac{(\mathbf{p} \cdot \boldsymbol{\beta})^2}{m} \right]. \quad (113)
 \end{aligned}$$

$$\begin{aligned}
 III^*III &= \frac{e^4}{48\pi^2 m^2 h^2 c^2} \frac{1}{kk_0 E(\mathbf{p})} \\
 &\times \text{spur } \beta_4 [(\mathbf{e} \cdot \boldsymbol{\beta})(\mathbf{e}_0 \cdot \boldsymbol{\beta}) + (\mathbf{e}_0 \cdot \boldsymbol{\beta})(\mathbf{e} \cdot \boldsymbol{\beta})] (\beta_4 + \beta_4^2) [(\mathbf{e} \cdot \boldsymbol{\beta})(\mathbf{e}_0 \cdot \boldsymbol{\beta}) + (\mathbf{e}_0 \cdot \boldsymbol{\beta})(\mathbf{e} \cdot \boldsymbol{\beta})] \\
 &\times \beta_4 \left[ E(\mathbf{p}) \beta_4 + mc^2 + \frac{(\mathbf{p} \cdot \boldsymbol{\beta})^2}{m} \right]. \quad (114)
 \end{aligned}$$

$$\begin{aligned}
 I^*III &= \frac{e^4}{96\pi^2 m^4 h^2 c^5} \frac{1}{kk_0^2 E(\mathbf{p})} \\
 &\times \text{spur } \beta_4 [(\mathbf{p} \cdot \boldsymbol{\beta})(\mathbf{e} \cdot \boldsymbol{\beta}) + (\mathbf{e} \cdot \boldsymbol{\beta})(\mathbf{k}_0 \cdot \boldsymbol{\beta})] \beta_4 \left[ (mc^2 + ck_0) \beta_4 + mc^2 + \frac{(\mathbf{k}_0 \cdot \boldsymbol{\beta})^2}{m} \right] \\
 &\times \beta_4 (\mathbf{k}_0 \cdot \boldsymbol{\beta})(\mathbf{e}_0 \cdot \boldsymbol{\beta})(\beta_4 + \beta_4^2) [(\mathbf{e} \cdot \boldsymbol{\beta})(\mathbf{e}_0 \cdot \boldsymbol{\beta}) + (\mathbf{e}_0 \cdot \boldsymbol{\beta})(\mathbf{e} \cdot \boldsymbol{\beta})] \\
 &\times \beta_4 \left[ E(\mathbf{p}) \beta_4 + mc^2 + \frac{(\mathbf{p} \cdot \boldsymbol{\beta})^2}{m} \right]. \quad (115)
 \end{aligned}$$

3.4. *Evaluation of the spurs.* For particles with zero spin the theory is extremely simple. The spur relations (65) and (66) show that of the expressions (112) to (115) only (114) is not zero, and that the spur in this expression reduces at once to  $4mc^2(\mathbf{e} \cdot \mathbf{e}_0)^2$ .

In order to find the cross-section we must know  $d\mathbf{k}/dE_\gamma$ . Now, from (74) and (75), we have

$$k = \frac{mck_0}{mc + k_0(1 - \cos \theta)}, \quad (116)$$

where  $\theta$  is the angle between  $\mathbf{k}$  and  $\mathbf{k}_0$ . Also  $d\mathbf{k}/dE_\gamma = d\Omega k^2 dk/dE_\gamma$ , where  $d\Omega$  is an element of solid angle in the direction of  $\mathbf{k}$ , and

$$E_\gamma = E(\mathbf{p}) + ck = ck + c\sqrt{(m^2c^2 + k_0^2 - 2kk_0 \cos \theta + k^2)}.$$

Hence, by (74) and (116),

$$\begin{aligned}\frac{dk}{dE_f} &= \frac{1}{c} \frac{E(\mathbf{p})}{E(\mathbf{p}) + c(k - k_0 \cos \theta)} = \frac{1}{c} \frac{E(\mathbf{p})}{mc^2 + ck_0(1 - \cos \theta)} \\ &= \frac{E(\mathbf{p}) k}{mc^3 k_0}.\end{aligned}\quad (117)$$

Collecting the results together and substituting them in (76), we find that the scattering cross-section is §

$$d\Omega \left( \frac{e^2}{mc^2} \right)^2 \frac{k^2}{k_0^2} (\mathbf{e} \cdot \mathbf{e}_0)^2. \quad (118)$$

This formula is very similar to, but somewhat simpler than, the Klein-Nishina formula for the scattering of light by free electrons. It is probable that this formula has no application to physical problems, and we do not discuss it further. It can be used to obtain the radiation loss from spinless particles, if such exist, but the formulae in this case are easily obtained directly.

3.41. The evaluation of the spurs for particles with spin 1 is very troublesome, and the algebra is so long that we can only indicate the method of procedure and give the final result. We consider first  $I^*I$ . The most systematic method is to arrange the various spurs according to the number of  $\beta$ 's, excluding  $\beta_4$ , which they contain. Thus the highest spur in  $I^*I$  contains fourteen  $\beta$ 's, but this vanishes on account of the relation  $(\mathbf{k}_0 \cdot \boldsymbol{\beta}) \beta_4(\mathbf{k}_0 \cdot \boldsymbol{\beta}) = 0$ . The highest non-vanishing spur contains ten  $\beta$ 's; it is

$$mc^4 \text{spur } \beta_4(\mathbf{p} \cdot \boldsymbol{\beta})^2 \beta_4(\mathbf{e} \cdot \boldsymbol{\beta}) (\mathbf{k}_0 \cdot \boldsymbol{\beta})^2 (\mathbf{e}_0 \cdot \boldsymbol{\beta})^2 (\mathbf{k}_0 \cdot \boldsymbol{\beta})^2 (\mathbf{e} \cdot \boldsymbol{\beta}), \quad (119)$$

which, by (58), is transformed into

$$mc^4 \text{spur } \beta_4^2 [\mathbf{p}^2 - (\mathbf{p} \cdot \boldsymbol{\beta})^2] (\mathbf{e} \cdot \boldsymbol{\beta}) (\mathbf{k}_0 \cdot \boldsymbol{\beta})^2 (\mathbf{e}_0 \cdot \boldsymbol{\beta})^2 (\mathbf{k}_0 \cdot \boldsymbol{\beta})^2 (\mathbf{e} \cdot \boldsymbol{\beta}). \quad (120)$$

This can now be evaluated directly, but the algebra can be considerably reduced if we apply the transformation (62) to the terms  $(\mathbf{k}_0 \cdot \boldsymbol{\beta})^2 (\mathbf{e}_0 \cdot \boldsymbol{\beta})^2 (\mathbf{k}_0 \cdot \boldsymbol{\beta})^2$ , and note that  $\mathbf{e}_0 \cdot \mathbf{k}_0 = 0$ . The ten-spur then becomes

$$\begin{aligned}k_0^3 mc^4 \text{spur } [\mathbf{p}^2 \beta_4^2 (\mathbf{e} \cdot \boldsymbol{\beta}) (\mathbf{k}_0 \cdot \boldsymbol{\beta})^2 (\mathbf{e}_0 \cdot \boldsymbol{\beta})^2 (\mathbf{e} \cdot \boldsymbol{\beta}) \\ - \beta_4^2 (\mathbf{p} \cdot \boldsymbol{\beta})^2 (\mathbf{e} \cdot \boldsymbol{\beta}) (\mathbf{k}_0 \cdot \boldsymbol{\beta})^2 (\mathbf{e}_0 \cdot \boldsymbol{\beta})^2 (\mathbf{e} \cdot \boldsymbol{\beta})],\end{aligned}\quad (121)$$

and the evaluation of this by (70) and (72) is quite easy. The only other spur

§ Note that when we are dealing with particles of zero spin a factor  $\frac{1}{2}$  must be omitted from equations (112)–(115). The  $\frac{1}{2}$  arises because of the averaging over the three polarizations of the incident meson; for spinless particles this averaging is unnecessary since there is only one polarization.



is an eight-spur, but this gives more trouble, since it has to be split up into six parts, only some of which can be reduced to spurs of lower order.

The expression  $I^*II$  is distinctly more complicated than  $I^*I$ . Again the highest non-vanishing spur contains ten  $\beta$ 's, but it cannot be so easily reduced to spurs of lower order. It is

$$\begin{aligned} mc^4 \text{spur } \beta_4(\mathbf{p} \cdot \boldsymbol{\beta})^2 \beta_4(\mathbf{e} \cdot \boldsymbol{\beta}) (\mathbf{k}_0 \cdot \boldsymbol{\beta})^2 (\mathbf{e}_0 \cdot \boldsymbol{\beta}) (\beta_4 + \beta_4^2) (\mathbf{e} \cdot \boldsymbol{\beta}) (\mathbf{k} \cdot \boldsymbol{\beta})^2 (\mathbf{e}_0 \cdot \boldsymbol{\beta}) \\ = mc^4 \text{spur } [\mathbf{p}^2 \beta_4^2 (\mathbf{e} \cdot \boldsymbol{\beta}) (\mathbf{k}_0 \cdot \boldsymbol{\beta})^2 (\mathbf{e}_0 \cdot \boldsymbol{\beta}) (\mathbf{e} \cdot \boldsymbol{\beta}) (\mathbf{k} \cdot \boldsymbol{\beta})^2 (\mathbf{e}_0 \cdot \boldsymbol{\beta}) \\ - \beta_4^2 (\mathbf{p} \cdot \boldsymbol{\beta})^2 (\mathbf{e} \cdot \boldsymbol{\beta}) (\mathbf{k}_0 \cdot \boldsymbol{\beta})^2 (\mathbf{e}_0 \cdot \boldsymbol{\beta}) (\mathbf{e} \cdot \boldsymbol{\beta}) (\mathbf{k} \cdot \boldsymbol{\beta})^2 (\mathbf{e}_0 \cdot \boldsymbol{\beta})]. \end{aligned}$$

If we wish to reduce the second term in the square brackets, we first interchange the order of  $\mathbf{e} \cdot \boldsymbol{\beta}$  and  $(\mathbf{k}_0 \cdot \boldsymbol{\beta})^2$  by using the first of the relations (59); the number of  $\beta$ 's is then reduced by two on account of the relation  $(\mathbf{e} \cdot \boldsymbol{\beta}) (\mathbf{e}_0 \cdot \boldsymbol{\beta}) (\mathbf{e} \cdot \boldsymbol{\beta}) = (\mathbf{e} \cdot \mathbf{e}_0) (\mathbf{e} \cdot \boldsymbol{\beta})$ . This term finally becomes

$$\begin{aligned} mc^4 \text{spur } [(\mathbf{e} \cdot \mathbf{e}_0) \beta_4^2 (\mathbf{p} \cdot \boldsymbol{\beta})^2 (\mathbf{k}_0 \cdot \boldsymbol{\beta})^2 (\mathbf{e} \cdot \boldsymbol{\beta}) (\mathbf{k} \cdot \boldsymbol{\beta})^2 (\mathbf{e}_0 \cdot \boldsymbol{\beta}) \\ - (\mathbf{e} \cdot \mathbf{k}_0) \beta_4^2 (\mathbf{p} \cdot \boldsymbol{\beta})^2 (\mathbf{k}_0 \cdot \boldsymbol{\beta}) (\mathbf{e}_0 \cdot \boldsymbol{\beta}) (\mathbf{e} \cdot \boldsymbol{\beta}) (\mathbf{k} \cdot \boldsymbol{\beta})^2 (\mathbf{e}_0 \cdot \boldsymbol{\beta}) \\ - (\mathbf{e} \cdot \mathbf{e}_0) k_0^2 \beta_4^2 (\mathbf{p} \cdot \boldsymbol{\beta})^2 (\mathbf{e} \cdot \boldsymbol{\beta}) (\mathbf{k} \cdot \boldsymbol{\beta})^2 (\mathbf{e}_0 \cdot \boldsymbol{\beta})], \end{aligned} \quad (122)$$

which is then evaluated directly without difficulty. There are also seven spurs, each of which contains eight  $\beta$ 's. The remaining spurs  $I^*III$  and  $III^*III$  are much simpler and consist of eight-spurs, six-spurs and four-spurs.

The expression for the cross-section is still very complicated, but it simplifies considerably when averaged over the polarizations of the light quanta. It seems unlikely that the formula for the scattering of polarized light by mesons will ever be required, and so we restrict the discussion to unpolarized light. We have actually to sum over the two independent polarizations of the scattered light and average over those of the incident light. If we denote this operation by a bar, the following results are required:

$$\left. \begin{aligned} \overline{f(\mathbf{k}, \mathbf{k}_0)} &= 2f(\mathbf{k}, \mathbf{k}_0), & \overline{(\mathbf{e} \cdot \mathbf{e}_0)^2} &= \frac{1}{2}(1 + \cos^2 \theta), \\ \overline{(\mathbf{e} \cdot \mathbf{k}_0)^2} &= k_0^2 \sin^2 \theta, & \overline{(\mathbf{e}_0 \cdot \mathbf{k})^2} &= \mathbf{k}^2 \sin^2 \theta, \\ \overline{(\mathbf{e}_0 \cdot \mathbf{k}) (\mathbf{e} \cdot \mathbf{k}_0) (\mathbf{e} \cdot \mathbf{e}_0)} &= -\frac{1}{2} k k_0 \cos \theta \sin^2 \theta, & \overline{(\mathbf{e}_0 \cdot \mathbf{k})^2 (\mathbf{e} \cdot \mathbf{k}_0)^2} &= \frac{1}{2} k^2 k_0^2 \sin^4 \theta. \end{aligned} \right\} \quad (123)$$

All these (except the first, which is obvious) are readily proved by repeated application of the formula (see e.g. Heitler 1936, p. 101)

$$\sum_{\text{polarizations}} (\mathbf{a} \cdot \mathbf{e}) (\mathbf{b} \cdot \mathbf{e}) = \mathbf{a} \cdot \mathbf{b} - \frac{(\mathbf{a} \cdot \mathbf{k}) (\mathbf{b} \cdot \mathbf{k})}{k^2}. \quad (124)$$

The final result is that the cross-section for the scattering of unpolarized light into the solid angle  $d\Omega$  is

$$\begin{aligned}
 d\Omega \left( \frac{e^2}{mc^2} \right)^2 \frac{k^2}{k_0^2} & \left[ \frac{1}{2} (1 + \cos^2 \theta) + \frac{k_0 - k}{6mc} (\cos^2 \theta - 2 \cos \theta - 3) \right. \\
 & + \frac{1}{96(mc)^2} \{ k k_0 (124 - 32 \cos \theta - 36 \cos^2 \theta + 16 \cos^3 \theta) \\
 & \quad + (k^2 + k_0^2) (5 - 40 \cos \theta + \cos^2 \theta) \} \\
 & + \frac{k_0 - k}{48(mc)^3} \{ k k_0 (7 + 6 \cos \theta - 9 \cos^2 \theta + 4 \cos^3 \theta) - 3(k^2 + k_0^2) (1 + \cos^2 \theta) \} \\
 & + \frac{k k_0}{48(mc)^4} \{ k k_0 (5 - 11 \cos \theta + 3 \cos^2 \theta - \cos^3 \theta + 4 \cos^4 \theta) \\
 & \quad \left. + 3(k^2 + k_0^2) (1 - \cos \theta + \cos^2 \theta - \cos^3 \theta) \} \right]. \quad (125)
 \end{aligned}$$

The total cross-section is obtained from (125) by integrating over the angles. The integration is elementary but very tedious. When  $k_0 \gg mc$  the result is

$$\frac{\pi}{3} \left( \frac{e^2}{mc^2} \right)^2 \left( \frac{k_0}{mc} \right)^2. \quad (126)$$

#### THE RADIATION LOSS FROM MESONS

4. Provided that we merely wish to know the order of magnitude of the effect, and regard factors of order unity as being irrelevant, we can calculate the radiation emitted by a very fast meson in the following way. Let the meson move with velocity  $v_0 \sim c$  and energy  $E_0$  past a nucleus of charge  $Ze$ , the nucleus being so heavy that it can be considered to be fixed. We consider the system in the frame of reference in which the meson is (initially) at rest and the nucleus moves past it with velocity  $v_0$ . In this frame the Coulomb field of the nucleus is very much contracted along the direction of motion, and, at not too small distances from the nucleus, the field can be considered to consist of light quanta whose direction of propagation is parallel to the direction of motion of the nucleus. At distance  $r$  from the nucleus, the intensity  $I_\nu$  of these quanta per unit frequency range per unit area is given approximately by (v. Weizsäcker 1934, equation (21))

$$\begin{aligned}
 I_\nu &= \frac{2 Z^2 e^2}{\pi c r^2} \left( \nu < \frac{E_0}{2\pi m c r} \right), \\
 I_\nu &= 0 \quad \left( \nu > \frac{E_0}{2\pi m c r} \right).
 \end{aligned} \quad (127)$$

There are various approximations involved in replacing the moving Coulomb field by light quanta and in cutting off the frequency spectrum abruptly. The errors introduced are at most of the order of  $mc^2/E_0$ .

We consider the light quanta to be scattered by the meson, and we have to pick out those light quanta which after being scattered have a given energy  $\epsilon E_0$  ( $0 < \epsilon \leq 1$ ) in the original frame of reference in which the nucleus is at rest. In the moving frame, let  $\mathbf{k}_0$  and  $\mathbf{k}$  be the momenta of the incident and scattered light quanta, and let  $\theta$  be the angle between  $\mathbf{k}_0$  and  $\mathbf{k}$ . Since the velocity  $v_0$  is parallel to  $\mathbf{k}_0$ , the energy of the scattered quantum in the original frame is §

$$\epsilon E_0 = ck \frac{1 - v_0 \cos \theta / c}{\sqrt{1 - v_0^2/c^2}} = ck \left( 1 - \frac{v_0}{c} \cos \theta \right) \frac{E_0}{mc^2} \sim k(1 - \cos \theta) \frac{E_0}{mc}, \quad (128)$$

since  $E_0 = mc^2(1 - v_0^2/c^2)^{-1/2}$  and since  $v_0 \sim c$ . Now, by (116),  $k_0$  is given by

$$k_0 = \frac{mck}{mc - k(1 - \cos \theta)},$$

and, hence by (128), we have

$$\left. \begin{aligned} k &= \frac{mce}{1 - \cos \theta}, \quad k_0 = \frac{mce}{1 - \epsilon} \frac{1}{1 - \cos \theta} = \frac{k}{1 - \epsilon}, \\ \text{and also} \quad k_0 - k &= \frac{mce^2}{1 - \epsilon} \frac{1}{1 - \cos \theta} = \frac{kk_0}{mc} (1 - \cos \theta). \end{aligned} \right\} \quad (129)$$

Now let  $f(k_0, k, \cos \theta) I(k_0) dk_0 d\Omega$  be the energy of the light quanta scattered into the solid angle  $d\Omega$  by a meson at rest when the incident intensity is  $I(k_0) dk_0$ . Since  $I_\nu d\nu = I(k_0) dk_0$  and  $k_0 = h\nu/c$ , we have

$$I(k_0) = \frac{2 Z^2 e^2}{\pi \hbar r^2} \left( k_0 < \frac{\hbar E_0}{r mc^2} \right); \quad (130)$$

$$\text{also (129) gives} \quad dk_0 = \frac{mc d\epsilon}{(1 - \epsilon)^2} \frac{1}{1 - \cos \theta}, \quad (131)$$

the angle  $\theta$  being constant, since for the moment we are considering the scattering into a given solid angle. When we transform back to the system in which the nucleus is at rest, the energy of the scattered quanta must be multiplied by the factor  $(1 - \cos \theta) E_0/mc^2$  (equation (128)), and to obtain the cross-section we must divide by the scattered energy  $\epsilon E_0$ . Finally, we

§ See v. Weizsäcker (1934) for the formulae which follow. Our calculations differ from his in several details, so that it is insufficient to quote his final result.

must integrate over  $r$  and over the solid angle, and the cross-section for the emission of a quantum with energy lying between  $\epsilon E_0$  and  $(\epsilon + d\epsilon) E_0$  is

$$\phi(\epsilon) d\epsilon = \frac{d\epsilon}{\epsilon} \int 2\pi r dr \int f(k_0, k, \cos \theta) I(k_0) \times \frac{mc/E_0}{(1-\epsilon)^2} \frac{1}{1-\cos \theta} \frac{E_0}{mc^2} (1-\cos \theta) 2\pi d \cos \theta, \quad (132)$$

where  $k$  and  $k_0$  are given in terms of  $E_0$ ,  $\epsilon$  and  $\cos \theta$  by (129). Now, since  $E_0$  and  $\epsilon$  are given quantities, there corresponds just one value of  $k_0$  to a given value of  $\cos \theta$ , and the integration over  $\theta$  is equivalent to integration over the momenta of the incident light quanta. Further, since there is a maximum value of  $k_0$ , the range of integration is restricted to

$$-1 \leq \cos \theta \leq 1 - \frac{rmc mc^2}{\hbar} \frac{\epsilon}{E_0} \frac{1}{1-\epsilon} = 1 - \eta, \quad \text{and} \quad r \leq \frac{2\hbar E_0}{mc mc^2} \frac{1-\epsilon}{\epsilon}. \quad (133)$$

It has been shown by v. Weizsäcker that the lower limit for  $r$  must be taken to be the Compton wave-length  $\lambda = \hbar/mc$ . This is, however, not a rigorous mathematical deduction from the exact theory, but is based upon the behaviour of a wave packet of linear dimensions  $\lambda$ . The interaction energy in the present theory is more singular than in the electron theory, and there is perhaps less justification for taking the lower limit to be  $\lambda$ ; but any other choice for the lower limit would not alter the theory essentially unless the lower limit were to increase with  $E_0$ , and this can certainly be ruled out.

4.1. In our present problem,  $f(k_0, k, \cos \theta) d\Omega$  is given by (125) multiplied by  $k/k_0$ . When we substitute for  $k$  and  $k_0$  from (129), the terms involving  $(1-\cos \theta)^{-4}$  and  $(1-\cos \theta)^{-3}$  vanish. Then, since  $\eta$  is very small, we can use the approximate formula (with  $n=0, 1, \dots$ )

$$\int_{-1}^{1-\eta} \frac{\cos^n \theta}{(1-\cos \theta)^2} d \cos \theta \sim \int_{-1}^{1-\eta} \frac{d \cos \theta}{(1-\cos \theta)^2} \sim \frac{1}{\eta}, \quad (134)$$

and we find that (132) becomes

$$\phi(\epsilon) d\epsilon = \frac{1}{12} \frac{Z^2 e^2}{\hbar c} \left( \frac{e^2}{mc^2} \right)^2 \frac{E_0}{mc^2} (2 - 2\epsilon + 7\epsilon^2) d\epsilon \int_{\lambda}^R \frac{\lambda dr}{r^2}. \quad (135)$$

The upper limit  $R$  in the integral with respect to  $r$  depends upon the behaviour of the electrostatic field of the nucleus at large distances. For a pure Coulomb field,  $R$  is determined by (133), but for the more physically correct model of a screened field,  $R$  is approximately  $a_0 Z^{-1}$ , where  $a_0$  is Bohr's radius of the hydrogen atom. In either case the error in extending

the integration to infinity is negligible; it is certainly less than the errors inherent in the present method of solution. We therefore have finally

$$\phi(\epsilon) d\epsilon = \frac{1}{12} \frac{Z^2 e^2}{\hbar c} \left( \frac{e^2}{mc^2} \right)^2 \frac{E_0}{mc^2} (2 - 2\epsilon + 7\epsilon^2) d\epsilon \quad (136)$$

$$= \frac{1}{12} \frac{Z^2 e^2}{\hbar c} \left( \frac{e^2}{mc^2} \right)^2 \frac{E_0}{mc^2} \frac{7E_0^2 - 12E_0 E + 7E^2}{E_0^2} d\epsilon, \quad (137)$$

where  $E = E_0(1 - \epsilon)$  is the final energy of the meson.

The average energy loss per collision is

$$\int_0^1 \epsilon E_0 \phi(\epsilon) d\epsilon = \frac{25}{144} \frac{Z^2 e^2}{\hbar c} \left( \frac{e^2}{mc^2} \right)^2 \frac{E_0^3}{mc^2}. \quad (138)$$

Formula (137) is similar to the corresponding formula for electrons but differs from it in detail. The most important point is the occurrence of the factor  $E_0/mc^2$ . Thus, whereas the cross-section for the emission of a  $\gamma$ -ray by an electron tends to a constant value as the energy of the electron increases (so long as screening is taken into account), the cross-section for the emission of a  $\gamma$ -ray by a meson increases with the energy of the meson. We discuss this in more detail in § 6. Another point of difference is that it is immaterial here whether we take screening into account or not; large impact parameters contribute negligibly to the radiation loss. For electrons, on the other hand, the integral with respect to  $r$  corresponding to the integral in (135) is  $\int_{\lambda}^R \frac{dr}{r}$ , and the choice of the upper limit is very important.

It should further be noted that (136) is not correct for small  $\epsilon$ . The method we have used gives  $\phi(\epsilon)$  expanded in inverse powers of  $E_0/mc^2$ , and it so happens that the term which contains the highest power of  $E_0/mc^2$  is not the one which contains the lowest power of  $\epsilon$ . To obtain the correct expression when  $\epsilon$  is small we consider  $E_0$  to have a fixed large value, and we find the dominant term as  $\epsilon$  tends to zero. We split the range of integration with respect to  $\cos \theta$  in (132) into the two parts  $(-1, 1 - \epsilon)$  and  $(1 - \epsilon, 1 - \eta)$ . The relations (129) show that in the first range  $k_0$  is less than  $mc/(1 - \epsilon)$ ; therefore if  $\epsilon$  is small we can use the non-relativistic form of (125), i.e. the Thomson formula, in this range, while we use the exact expression in the range  $(1 - \epsilon, 1 - \eta)$ . Now the integration over the first range gives a term containing  $d\epsilon/\epsilon$ , which is the dominant term for small  $\epsilon$ . Evaluating this, we find that

$$\phi(\epsilon) d\epsilon = \frac{16}{3} \frac{Z^2 e^2}{\hbar c} \left( \frac{e^2}{mc^2} \right)^2 \frac{d\epsilon}{\epsilon} \int_{\lambda}^R \frac{dr}{r}, \quad (\epsilon \ll 1).$$

This same term occurs in the expression for the energy loss from electrons. Its presence does not greatly affect the validity of (138), since small values of  $\epsilon$  contribute little to the total energy loss. Of course, no reliance can be placed on the numerical factors which occur in (137) and (138); the formulae are only correct as to order of magnitude. In particular the variation with  $Z$  for large  $Z$  is almost certainly incorrect, not only because  $Z/137$  is not small, but also because the radii of the heavier nuclei are of the same order as  $\lambda$ .

It should be noted that the radiation loss is mainly determined by the scattering of quanta of energy much greater than  $mc^2$ , whereas for electrons the high energy quanta have a negligible effect. The radiation loss from mesons therefore provides a test of the validity of the theory for high energies.

#### THE PRODUCTION OF MESON PAIRS

5. The cross-section for the production of a pair of mesons by the absorption of a  $\gamma$ -ray in the presence of a nucleus can easily be obtained from the formula for the emission of a  $\gamma$ -ray by a meson. Just as for the electron (see e.g. Heitler 1936, p. 195) we have merely to replace  $E_0$  and  $E$  in equation (137) by  $E_-$  and  $-E_+$ , where  $E_+$ ,  $E_-$  are the energies of the pair of mesons, and to multiply by

$$\frac{c^2 p_-^2 dE_+}{(E_+ + E_-)^2 E_- dc}.$$

This is easily shown by writing down the matrix elements for pair production and comparing them with the matrix elements for the emission of a  $\gamma$ -ray. It is not necessary to evaluate the spurs. We obtain for the differential cross-section in the extreme relativistic case the expression

$$\phi(E_+) dE_+ = \frac{1}{12} \frac{Z^2 e^2}{\hbar c} \left( \frac{e^2}{mc^2} \right)^2 \frac{7E_+^2 + 12E_+ E_- + 7E_-^2}{mc^2 (E_+ + E_-)^2} dE_+. \quad (139)$$

If  $h\nu = E_+ + E_-$  is the energy of the  $\gamma$ -ray which produces the pairs, the total cross-section, which determines the number of pairs produced, is

$$\int_0^{h\nu} \phi(E_+) dE_+ = \frac{5}{9} \frac{Z^2 e^2}{\hbar c} \left( \frac{e^2}{mc^2} \right)^2 \frac{h\nu}{mc^2}. \quad (140)$$

5.1. The probability of a meson pair being produced by a fast charged particle can also readily be found; we have merely to analyse the field of the moving particle into light quanta and apply formula (139). Let the energy and charge of the particle be  $E_0$  and  $Z_1 e$ . Then the intensity of the

light quanta is given by (127), and hence the total number  $N_\nu d\nu$  of light quanta with energies lying in the range  $h d\nu$  is

$$\begin{aligned} N_\nu d\nu &= d\nu \int_{\lambda}^{E_0/(2\pi mc\nu)} \frac{2}{\pi} \frac{Z_1^2 e^2}{c r^2 h\nu} 2\pi r dr \\ &= \frac{2}{\pi} \frac{Z_1^2 e^2}{\hbar c} \log \frac{E_0}{h\nu} \frac{d\nu}{\nu}, \end{aligned} \quad (141)$$

the effective lower limit for  $r$  being the Compton wave-length  $\lambda$  as before. If we put  $h\nu = E_+ + E_-$  and multiply by (139), we obtain as the differential cross-section for the process in which a pair of mesons is produced with energies lying in  $dE_+, dE_-$ ,

$$\frac{Z^2 Z_1^2}{6\pi} \left( \frac{e^2}{\hbar c} \right)^2 \left( \frac{e^2}{mc^2} \right)^2 \frac{7E_+^2 + 12E_+ E_- + 7E_-^2}{mc^2(E_+ + E_-)^3} \log \frac{E_0}{E_+ + E_-} dE_+ dE_- \quad (142)$$

The total cross-section is

$$\frac{10}{9\pi} \left( \frac{Z Z_1 e^2}{\hbar c} \right)^2 \left( \frac{e^2}{mc^2} \right)^2 \frac{E_0}{mc^2} \quad (143)$$

By comparing (140) and (143) we see that the probability of a pair of mesons being produced by a charged particle is  $2Z_1^2/(137\pi)$  times the probability of a pair being produced by a  $\gamma$ -ray of the same energy. We can therefore neglect pair production by charged particles.

### DISCUSSION

The meson theory, as at present formulated, cannot be regarded as satisfactory; the infinities which occur in the electron theory appear in the meson theory in an even more objectionable form, and in addition there are a number of fresh difficulties. One of the new characteristic features of the theory is the appearance of terms proportional to  $1/r^3$  in the potential energy, terms of this type occurring in the interaction of protons with neutrons, and of mesons with a Coulomb field. When the potential energy has a singularity of such a high order, eigenfunctions no longer exist, but on the other hand the use of the Born approximation gives a unique result for the scattering problem. This can only mean that the approximate method 'cuts off' the singularity in some way, but the exact manner in which this happens is obscure. It seems fairly certain that this 'cut off' must take place at a radius which decreases as the energy of the particles increases; thus the effect of the  $1/r^3$  terms is most pronounced at high energies, and this results in the cross-section increasing with increasing

energy. In the problem of the interaction of a meson with a Coulomb field the  $1/r^3$  terms tend to zero as the velocity of the meson tends to zero, but for any non-zero value of the velocity these terms occur, and the scattering problem has strictly no solution. However, the use of the Born approximation gives the same result for small velocities as we should obtain by neglecting the  $1/r^3$  terms altogether. We cannot therefore dismiss the solution given by the Born approximation as meaningless, nor does it seem possible to set a limit to the validity of the theory except by arguments based on the possible existence of a 'shortest length'. Such arguments are of very doubtful value.

The often expressed view that the meson theory is correct for small energies but invalid for high energies is an inconsistent one. It would certainly be a correct viewpoint to maintain that the meson theory is valid when the velocity of the meson is zero, but this is quite trivial, and to maintain that the theory is satisfactory only for small velocities is equivalent to saying that the  $1/r^3$  terms are unimportant because they occur with small coefficients. The only consistent attitude to take up is either to reject the theory completely or to accept it provisionally and investigate the limits of its validity. In order to carry through the latter programme, which we believe to be the correct one, it is necessary to include relativistic effects, since otherwise we revert to the Schrödinger theory. The only criterion for judging the success or otherwise of the meson theory is therefore provided by the discussion of the relativistic effects.

The 'heavy electrons' found in cosmic-rays are usually identified with mesons, but there is as yet no really convincing evidence that these cosmic ray particles have spin 1 rather than spin 0 or  $\frac{1}{2}$ . The main reason for making the identification is that thereby the number of elementary particles required is kept as small as possible. If our present ideas concerning nuclear forces are in any way correct, we require charged particles with a mass about 200 times the electron mass which are capable of being absorbed and emitted by protons and neutrons. The spin of these particles must be either 0 or 1, and if the spin is taken to be 0 the calculated nuclear forces turn out to have the wrong sign; we therefore assume the spin to be 1. However, the calculated scattering of mesons by protons deduced from the magnitude of the nuclear forces is much too large to be reconcilable with the observed scattering; at about  $10^9$  eV the observed cross-section (due to both the nuclear and the Coulomb forces) is of the order of  $10^{-28}$  cm.<sup>2</sup> (J. G. Wilson 1940), while that calculated by Heitler (1938) is of the order of  $10^{-26}$  cm.<sup>2</sup>. In order to remove the discrepancy we should have to introduce far-reaching modifications into the theory of the nuclear interaction. It would, however,



be difficult to introduce important modifications into the theory of the Coulomb-scattering and of the radiation loss without giving up the present theory entirely.

For small velocities the interaction of charged particles with an electromagnetic field is independent of the spin of the particles, and the scattering at low energies therefore gives no evidence as to the value of the spin. The spin can, however, be determined in principle from the angular variation of the elastic scattering at high energies, or, more easily, from the total energy loss in inelastic collisions. Now it is just for high energies that the results of the meson theory are most doubtful, and if the observed energy loss does not agree with the theoretical value we may only conclude either that the theory is invalid at high energies or that the cosmic ray 'heavy electrons' do not have spin 1. Only if the observations confirm the theory can we be certain of the identity of the particles. We show below that what little experimental evidence exists is in favour of the heavy electrons being mesons and of the validity of the theory of the interaction of mesons with an electromagnetic field.

The data collected by Blackett (1937) show that the energy loss of the penetrating component of the cosmic-rays increases rapidly with the energy for energies greater than about  $10^{10}$  eV, and that this energy loss is considerably greater than that due to ionization (as calculated from Bloch's formula). This extra energy loss cannot be due to radiation if the 'heavy electrons' which constitute the penetrating component have spin 0 or  $\frac{1}{2}$ , but the energy loss can be accounted for qualitatively if we assume that the 'heavy electrons' are mesons with spin 1.

In the first place the calculations of Massey and Corben (1939) show that for a collision between a meson and an electron there is a spin-dependent term in the cross-section which only becomes appreciable at high energies. The cross-section for an energy loss  $\epsilon E_0$  when a meson of energy  $E_0$  and mass  $m$  collides with an electron of mass  $m_e$  at rest is of the order of  $1 + m_e E_0 / (3m^2 c^2)$  times the corresponding cross-section for the collision of the two particles with masses  $m$  and  $m_e$  and spin  $\frac{1}{2}$ . When the above ratio is appreciably greater than 1, that is, when  $E_0$  is greater than about  $10^{10}$  to  $10^{11}$  eV, the energy transfer in close collisions will be increased and the ionization loss will be greater than that given by Bloch's formula. § This agrees qualitatively with Blackett's conclusions, but a detailed comparison is out of the question on account of the great uncertainty in the experimental results.

§ These estimates of the energies at which spin effects become important are based on the assumption that  $m = 200m_e$ ; they are very sensitive to the value of  $m$  chosen.

Secondly, the energy loss due to radiation becomes comparable with that due to ionization for energies of the order of  $10^{11}$  eV. According to (138), the radiation loss per cm. of water is about  $5 \times 10^5$  eV for  $E_0 = 10^{11}$  eV and about  $5 \times 10^7$  eV for  $E_0 = 10^{13}$  eV, while the ionization loss given by Bloch's formula is about  $1.5 \times 10^6$  eV. It therefore seems probable that the initial increase in the energy loss at about  $10^{10}$  eV is due to the extra ionization loss, while for somewhat higher energies, for which no measurements exist, the radiation loss is dominant.

Some further support for the validity of the theory at high energies can be obtained indirectly from the occurrence of cosmic-ray showers consisting of a large number of particles. It has been realized for some time that showers associated with the penetrating component of the cosmic-rays can be reasonably well explained by assuming that the cosmic-ray particles 'knock-on' atomic electrons in close collisions and that the electrons then produce showers by the ordinary cascade process. The frequency of production of small and of moderately large showers is in good agreement with the accepted theory of the process (see e.g. Lovell 1939), but the observed number of showers consisting of 100 to 1000 particles is appreciably greater than the calculated number (Carmichael and Chou 1939). Recently, Bhabha, Carmichael and Chou (1939) have suggested that this discrepancy can be removed by adopting Massey and Corben's expression for the cross-section for the collisions of a meson with an electron. If this expression is valid for high energies, there is a large probability that the electron will receive a considerable amount of energy and be capable of producing a large shower. Bhabha, Carmichael and Chou show that the modified theory gives much better agreement with the experiments than does the old theory. We have, however, shown above that, for the greatest part of the energy range for which the spin-correction term is important, the radiation loss is more important than the ionization loss; therefore the extra probability that a knock-on electron will be produced is less important than the probability that a  $\gamma$ -ray will be produced. Thus the occurrence of large showers would seem to depend mainly on the very energetic  $\gamma$ -rays emitted by the mesons, and there is the possibility that the theory will now give too many large showers. However, the calculations are not very reliable and involve an extrapolation of the energy spectrum of the incident mesons which may well not be justified. (Blackett's deduction of the energy spectrum assumes that there are no large energy losses such as are predicted by our calculations.)

A further consequence of the theory may be mentioned. The method by which mesons are produced in the atmosphere is by no means clear. The

obvious processes are those in which a proton or a neutron emits a meson either under the action of a  $\gamma$ -ray or during a collision. These involve the specific nuclear interaction and the theory of them is therefore suspect. Another process is the direct production of meson pairs by a  $\gamma$ -ray (§ 5), the  $\gamma$ -ray itself being probably a secondary produced by the incoming cosmic-rays near the top of the atmosphere. Now, for most of the  $\gamma$ -rays which occur in cosmic-rays, the production of a pair of electrons is more probable than the production of a pair of mesons, the total cross-section for the production of a pair of electrons being (Heitler 1936, p. 200)

$$\frac{Z^2}{137} \left( \frac{c^2}{m_e c^2} \right)^2 \left[ \frac{28}{9} \log \frac{183}{Z^2} - \frac{2}{27} \right], \quad (144)$$

when screening is taken into account. However, by comparing (140) and (144) we see that for energies greater than about  $10^{14}$  eV the production of a pair of mesons is the more probable process, and even for considerably smaller energies the production of meson pairs is by no means negligible. It seems probable that cosmic-ray particles exist with energies of the order of  $10^{14}$  eV, and if they do we should expect to find cascade showers containing a preponderance of mesons high up in the atmosphere, but this mechanism cannot produce the large number of mesons observed at sea level and must be comparatively unimportant.

One of us (F. B.) is indebted to the Department of Scientific and Industrial Research and to Clare College, Cambridge, for research grants.

#### REFERENCES

- Bhabha, H. J. 1938 *Proc. Roy. Soc. A*, **166**, 501.  
 Bhabha, H. J., Carmichael, H. and Chou, C. N. 1939 *Proc. Indian Acad. Sci. A*, **10**, 221.  
 Blackett, P. M. S. 1937 *Proc. Roy. Soc. A*, **159**, 19.  
 Carmichael, H. and Chou, C. N. 1939 *Nature, Lond.*, **144**, 325.  
 Duffin, R. J. 1938 *Phys. Rev.* **54**, 1114.  
 Heisenberg, W. and Pauli, W. 1929 *Z. Phys.* **56**, 1.  
 — — 1930 *Z. Phys.* **59**, 169.  
 Heitler, W. 1936 *Quantum theory of radiation*. Oxford.  
 — 1938 *Proc. Roy. Soc. A*, **166**, 529.  
 Kemmer, N. 1939 *Proc. Roy. Soc. A*, **173**, 91.  
 Lovell, A. C. 1939 *Proc. Roy. Soc. A*, **172**, 568.  
 Massey, H. S. W. and Corben, H. C. 1939 *Proc. Camb. Phil. Soc.* **35**, 463.  
 Pauli, W. and Weisskopf, V. 1934 *Helv. Phys. Acta*, **7**, 709.  
 Petiau, G. 1936 Thèse, Paris.  
 v. Weizsäcker, C. F. 1934 *Z. Phys.* **88**, 612.  
 Williams, E. J. 1935 *K. Danske Vidensk. Selsk. Skr., Math.-fys. Medd.*, **13**, no. 4.  
 Wilson, A. H. 1940 *Proc. Camb. Phil. Soc.* **36**, 386.  
 Wilson, J. G. 1940 *Proc. Roy. Soc. A*, **174**, 73.
-

# The strains produced by precipitation in alloys

By F. R. N. NABARRO

*H. H. Wills Physical Laboratory, University of Bristol*

*(Communicated by N. F. Mott, F.R.S.—Received 15 April 1940)*

If the process of diffusion in metals results simply in the interchange of pairs of atoms large strains must be set up when a new phase precipitates in an alloy. The strain energy involved is calculated for particles of precipitate of various shapes, and is found to be least if the precipitate forms thin plates. The shape of the particle actually formed is influenced by this energy, by the degree of supersaturation of the solid solution, and by surface effects; the calculated shape is shown to agree reasonably well with that observed experimentally.

## 1. INTRODUCTION

A preliminary account of some calculations of the strains produced by precipitation in alloys has already been given. (Mott and Nabarro (1940) referred to as I in the present paper, and Nabarro (1940) referred to as II.) In this paper the relation there assumed for the dependence of the strain energy of a particle on its shape is developed, and the relation of the theory to the experimental results is more fully discussed. It is found that the strain energy is large, and if the lattice of the precipitate remains continuous with that of the matrix the energy can only be reduced by a factor of the order of five by changes in the shape of the precipitated particles. If the lattice of the precipitate breaks away from that of the matrix, so that the stress in the inclusion is a simple hydrostatic pressure, the strain energy tends to zero if the particles of precipitate take the form of thin sheets. The dynamics of the precipitation, on the other hand, encourages the formation of spherical particles, as does the surface energy of the precipitate, and from a consideration of these factors a formula is deduced which represents the shape of the particles at any stage of their growth. The calculations of strain energy are contained in § 2, and the results obtained are applied in § 3.

## 2. CALCULATION OF STRAIN ENERGIES

The application of the theory of elasticity to a study of internal strains is subject to three limitations. The elastic equations are usually intractable unless the medium is isotropic, and even in the case of metals whose lattice

has cubic symmetry the condition of isotropy is usually not even approximately fulfilled. Then the scale of the internal strains is often small, so that the strain is only constant over a region of a few atoms, and the elastic equations of a continuous medium cannot properly be applied. Lastly, the strains themselves are large, perhaps as great as 10 %, so that Hooke's law must break down and it seems likely that in consequence the elastic energies actually involved will be smaller than those calculated. These large strains are larger than the technical breakdown strain, but there is ample evidence that mechanical breakdown is a structure-sensitive property dependent for its initiation on a few sensitive spots, and it seems plausible that internal strains should be limited only by the theoretical breakdown strain, which is much greater than that observed experimentally. Quinney and Taylor (1937) have shown that an energy of 0.5–1 cal./g. can be stored in a metal by cold work, and this is greater than the energy of the metal stretched homogeneously to its breaking point, so that there is direct evidence that very large internal strains can exist in a metal. For example, the tensile strength of copper is certainly less than 30 kg./mm.<sup>2</sup> and its Young's modulus is 10,400 kg./mm.<sup>2</sup>, so that it cannot acquire an energy of more than 0.01 cal./g. by homogeneous extension without breaking, while Quinney and Taylor have observed the release of 0.5 cal./g. on annealing a twisted copper wire.

Strains may be produced in a metal by cold work, by such agencies as thermal expansion and magnetostriction, and by precipitation in alloys. The nature of the strains in a cold-worked metal is not easy to determine, although experimental evidence has been collected by Wood (1935), Brindley (1940) and others, and certain possible types of strain have been discussed theoretically by J. M. Burgers (1940). An alternative model of these strains has recently been put forward by W. L. Bragg (1940), but they seem to be of so complicated a nature that their influence on the properties of the metal is difficult to discuss in detail. The same is true of thermal and magnetostrictive strains, although Kersten (1935) and Dillinger and Bozorth (1935) have shown how magnetostrictive strains fix an upper limit to the initial permeability of the metal. It is the strains due to the precipitation of a new phase in an alloy which seem most likely to lend themselves to detailed analysis, because if the new phase is present only in small quantities the strained region round each particle of precipitate is separated from its neighbours by a region of the lattice which is almost free from strain. Each particle can be considered separately as a nucleus of strain in an infinite unstrained medium, and the type of strain produced can be visualized much more readily than the random interacting strains due to cold work.

According to the dislocation theory of slip in metals developed by G. I. Taylor and others, the strength of a precipitation-hardened alloy is proportional to some mean value of the shear produced in the lattice of the matrix by the presence of particles of inclusion. This shear can only be calculated when the shape of the particles of precipitate is known, and the particles must have a tendency to precipitate in such forms that the energy of the shear is as small as possible. The energy of a flat sheet of precipitate which has not broken away has been calculated in II. The discussion of § 3.1 shows that a particle which has broken away produces the same external strain as it would do if it were fluid, and in §§ 2.1-2.4 the strain energy due to an inclusion of compressed fluid is calculated for inclusions of certain specially simple shapes. These results are exhibited graphically and a smooth curve through them (figure 2) is taken to represent the dependence of the strain energy on the shape of the particle in the case of precipitates which have broken away.

2.1. The simplest type of inclusion which gives rise to internal strains is a sphere of unstrained radius  $(1 + \delta)r_0$  inserted in a spherical hole of radius  $r_0$  in the matrix. The nature of the strain in this case has been discussed in I: the total elastic energy of a sphere of volume  $V = \frac{4}{3}\pi r_0^3$  and bulk modulus  $K$  in a matrix of rigidity  $\mu$  is

$$6\mu V\delta^2 \left/ \left( 1 + \frac{4\mu}{3K} \right) \right. . \quad (1)$$

2.2. The case of a cylindrical inclusion may be treated similarly. The displacement at distance  $r$  from the axis must be of the form  $\alpha r + \beta r_0^2 r^{-1}$ . When the inclusion is incompressible a displacement  $\frac{3}{2}\delta r_0^2 r^{-1}$  increases a volume  $V$  in the inclusion by  $3\delta V$  with an expenditure of energy equal to  $\frac{9}{2}\mu V\delta^2$ .

2.3. An infinite block of material contains an almost spherical cavity bounded by the surface

$$r = r_0\{1 + \epsilon P_\nu(\cos \theta)\}. \quad (2)$$

It is subject to a displacement which is the gradient of a potential

$$U = \kappa r_0^3 \left\{ \frac{1}{r} + k \frac{r_0^\nu}{r^{\nu+1}} \epsilon P_\nu \right\}. \quad (3)$$

Then (Love 1927) it is in equilibrium under the action of forces acting on the internal surface only.

Expressions for the strains are given by Love, but his non-diagonal components are twice the tensor components used here, and denoted by  $e_{ij}$ .

The components of stress  $p_{ij}$  are given by

$$p_{ij} = 2\mu e_{ij} + \lambda \delta_{ij} e_{kk}, \quad (4)$$

where the repeated index implies a summation and  $\lambda$  and  $\mu$  are the usual elastic constants as defined by Love. In this case  $e_{kk} = 0$ , and at the surface where  $r$  is given by (2) the displacements and strains reduce to

$$u_r = -\kappa r_0 \{1 + (k\nu + 1 - 2) \epsilon P_\nu\} + O[\epsilon^2]$$

$$u_\theta = -\kappa r_0 k \epsilon P'_\nu \sin \theta + O[\epsilon^2]$$

$$u_\phi = 0$$

$$e_{rr} = \kappa \{2 + (k\nu + 1 \over \nu + 2 - 6) \epsilon P_\nu\} + O[\epsilon^2]$$

$$e_{\theta\theta} = -\kappa + O[\epsilon]$$

$$e_{\phi\phi} = -\kappa + O[\epsilon]$$

$$e_{\theta\phi} = 0$$

$$e_{\phi r} = 0$$

$$e_{r\theta} = \kappa \over{\nu + 2} k \epsilon P'_\nu \sin \theta + O[\epsilon^2].$$

The direction cosines of the normal to the surface are

$$g_r = 1 + O[\epsilon^2], \quad g_\theta = -\epsilon P'_\nu \sin \theta + O[\epsilon^2], \quad g_\phi = 0, \quad (5)$$

while the surface element is

$$dS = r_0^2 (1 + 2\epsilon P_\nu) \sin \theta d\theta d\phi + O[\epsilon^2]. \quad (6)$$

The elastic energy of the matrix is equal to the work done by the surface forces, which is

$$-\frac{1}{2} \iint p_{ij} g_i u_j dS = 8\pi\mu r_0^3 \kappa^2 + O[\epsilon^2]. \quad (7)$$

The normal pressure is  $p_{ij} g_i g_j = 2\mu e_{rr} + O[\epsilon^2]$ ,

and this is independent of  $\theta$  as far as quantities of the order of  $\epsilon$  if

$$k\nu + 1 \over \nu + 2 = 6.$$

The original volume is

$$V = \frac{1}{3} \iint r^3 \sin \theta d\theta d\phi = \frac{4}{3} \pi r_0^3 + O[\epsilon^2]. \quad (8)$$

The change in volume is

$$\Delta V = \iint u_r r^2 \sin \theta d\theta d\phi = -4\pi\kappa r_0^3 + O[\epsilon^2]. \quad (9)$$

If, as in §§ 2.1 and 2.2,  $\Delta V = 3\delta V$ , then  $\kappa = -\delta$  and the energy is

$$6\mu V \delta^2 + O[\epsilon^2].$$

2.4. The nature of the strain around a disk-shaped cavity containing a fluid under pressure is a subject which will be of considerable interest in the later discussion. Unfortunately, only an approximate solution has been obtained. An arbitrary displacement is considered, and although this does not correspond to a uniform hydrostatic pressure inside the cavity it is used to obtain an approximate value of the energy required to enlarge the cavity.

It is possible to obtain upper and lower limits for this energy. In the first place we shall prove the general theorem that a given increase in the volume of the cavity is obtained with the least expenditure of energy by the application of a uniform hydrostatic pressure alone. \* The arbitrary displacement is then considered, and the forces on the boundary which cause it are found to be of two kinds, a normal pressure and a tangential traction. The normal pressure is constant over most of the surface, and it is shown that the work done by the pressure on those parts of the surface where the pressure differs appreciably from this value is small compared with the total work. The displacements due to the normal and tangential forces cannot be separated analytically, but it is shown that the tangential forces are clearly of a kind to increase the volume of the cavity. Now by the general theorem the whole work done in the displacement is an upper limit for the work which would be done in producing the same increase of volume by hydrostatic pressure alone. But the work done by the normal forces alone produces a greater increase in volume than would be produced by a hydrostatic pressure doing the same amount of work. For suppose that the hydrostatic pressure is proportional to  $p$ , while the tangential forces are proportional to  $t$ , so that the energy can be expressed in the form  $2W = ap^2 + 2bpt + ct^2$ . Now  $a$  and  $c$  are necessarily positive, and since both  $p$  and  $t$  increase the volume the value of  $b$  must also be positive in this case. The co-ordinate corresponding to  $p$ , the increase in volume, is  $P = ap + bt$ . The work done by the pressure is  $\frac{1}{2}Pp = \frac{1}{2}(ap^2 + bpt)$ . If this work had been done in the absence of  $t$  the internal pressure would have risen to  $p' = [(ap^2 + bpt)/a]^{\frac{1}{2}}$ , leading to an increase in volume  $P' = [a(ap^2 + bpt)]^{\frac{1}{2}}$ . Thus  $P^2 - P'^2 = abpt + b^2t^2$ , which is positive, and so the work done by the normal forces only represents a lower limit to the work required to produce the actual increase in volume.

We shall now prove the general theorem quoted above. Suppose the cavity is enlarged by the application of arbitrary surface forces. Fill the enlarged cavity with an incompressible fluid, and release the surface forces. If the system is in equilibrium, the forces reduce to a uniform pressure. If not, the system moves to another state where the cavity has the same volume, while the incompressible fluid necessarily has the same (zero) elastic potential

\* This was pointed out to me by Professor Mott.



energy. But the system as a whole has gained kinetic energy, so that the original enlargement of the hole cannot have been conducted with the least possible expenditure of work.

The arbitrary displacement which will be considered is obtained as follows. The gravitational potential of an ellipsoid of semi-axes  $a, b, c$  at external points is (Thomson and Tait 1883)

$$U = -\kappa abc \int_q^\infty \left(1 - \Sigma \frac{x^2}{a^2 + u}\right) \frac{du}{\Pi(a^2 + u)^{\frac{1}{2}}}, \quad (10)$$

where  $q$  is the greatest root in  $\theta$  of

$$\Sigma \frac{x^2}{a^2 + \theta} = 1. \quad (11)$$

The direction cosines of the normal to the ellipsoid at a point on its surface are

$$g_{nx} = \frac{x}{a^2} \left( \Sigma \frac{x^2}{a^4} \right)^{-\frac{1}{2}}, \text{ etc.} \quad (12)$$

Since  $U$  is a potential function, its gradient represents an elastic displacement which is in equilibrium under the action of forces at the surface of the ellipsoid  $\theta = 0$  alone. The components of displacement are

$$u_x = \frac{\partial U}{\partial x} = 4\kappa abc A^2 x, \text{ etc.}, \quad (13)$$

and the tensor components of strain are

$$\begin{aligned} e_{xx} &= \frac{\partial^2 U}{\partial x^2} = 4\kappa abc A^2 - 4\kappa \frac{x^2}{a^4} \left( \Sigma \frac{x^2}{a^4} \right)^{-\frac{1}{2}} \\ e_{yz} &= \frac{\partial^2 U}{\partial y \partial z} = -4\kappa \frac{yz}{b^2 c^2} \left( \Sigma \frac{x^2}{a^4} \right)^{-\frac{1}{2}}, \text{ etc.}, \end{aligned} \quad (14)$$

where

$$A^2 = \frac{1}{2} \int_0^\infty \frac{1}{a^2 + u} \frac{du}{\Pi(a^2 + u)^{\frac{1}{2}}}, \text{ etc.} \quad (15)$$

The normal displacement of a point on the surface  $\theta = q = 0$  is  $u_n = g_{nx} u_x$ , and the normal strain is  $e_{nn} = g_{ny} g_{nz} e_{yz}$ . The dilatation represented by the sum  $e_{kk}$  vanishes, and so from (4) the components of stress are given by  $p_{ij} = 2\mu e_{ij}$  and the normal stress is

$$p_{nn} = -8\kappa\mu \left[ 1 - abc \left( \Sigma \frac{x^2}{a^4} \right)^{-\frac{1}{2}} \Sigma \frac{x^2}{a^4} A^2 \right].$$

The work done by the normal stress is

$$W_1 = -\frac{1}{2} \iint p_{nn} u_n dS. \quad (16)$$

These general formulae will now be applied to the special case of an oblate spheroid  $a = b > c$ . A suitable co-ordinate system is provided by the transformation

$$x = at \cos \theta \cos \phi, \quad y = at \cos \theta \sin \phi, \quad z = ct \sin \theta. \quad (17)$$

The energy given by (16) can now be evaluated. The increase in volume is

$$\Delta V = \iint u_n dS = \frac{1}{3} \pi \kappa a^2 c. \quad (18)$$

The volume is  $V = \frac{4}{3} \pi a^2 c$ , and in the previous notation  $\Delta V = 3\delta V$ , so  $\kappa = 3\delta/4$ . In the case  $c = a$  the substitution of this in (16) leads to the expression  $6\mu V \delta^2$  already obtained for the work required to enlarge a sphere. When  $c < a$  the energy may be expanded as a powerseries in  $c/a$ . The first term is of order  $a^2 c$ , which is the volume of the inclusion, but its coefficient vanishes, and the expansion is of the form

$$W_1 = \frac{9}{2} \pi \frac{c}{a} \mu V \delta^2 + O[c^3]. \quad (19)$$

When  $a \gg c$ , the normal pressure  $p_{nn}$  is given by

$$p_{nn} \sim \frac{\frac{1}{2} \pi a c + c^2 \cot^2 \theta + O[c^3]}{a^2 + c^2 \cot^2 \theta}. \quad (20)$$

Since  $a \gg c$ , this remains nearly constant when  $\sin \theta > (c/a)^{1/2}$ , and it changes value again when  $\sin \theta = c/a$ . The only appreciable contribution to the integral (16) for  $W_1$  comes from the region where the pressure is constant. For in this region  $|\sin \theta| > (c/a)^{1/2}$  the expression (20) is of order  $\frac{1}{2} \pi c/a$ , while  $(A^2 \cos^2 \theta + C^2 \sin^2 \theta) \sim \sin^2 \theta/a^2 c$  and the range of integration is almost  $-\frac{1}{2} \pi$  to  $\frac{1}{2} \pi$ , so that the integral with respect to  $\theta$  is of order  $\pi/3a^3$ . In the region  $|\sin \theta| < (c/a)^{1/2}$  the expression (20)  $\leq 1$ , while

$$(A^2 \cos^2 \theta + C^2 \sin^2 \theta) < 2/a^3$$

and the range of integration is  $-(c/a)^{1/2}$  to  $(c/a)^{1/2}$ , so that the contribution of this part of the range to the integral is of order  $4(c/a)^{1/2}/a^3$ , which is small compared with the whole integral.

The total work done by all the surface forces is

$$W_2 = -\frac{1}{2} \iint p_{ij} u_i g_{nj} dS.$$

For a spheroid this becomes

$$W_2 = 64\pi\kappa^2 a^4 c^2 \mu \left[ \frac{2}{3} A^2 + \frac{1}{3} C^2 - a^2 c \left( \frac{2}{3} A^4 + \frac{1}{3} C^4 \right) \right]. \quad (21)$$

When  $a = c$  this again reduces to  $6\mu V \delta^2$ , but when  $c < a$  it can be expanded in the form

$$W_2 = 9\pi \frac{c}{a} \mu V \delta^2 + O[c^3]. \quad (22)$$

It only remains to be shown that the tangential stresses produce an increase in volume. There are two principal tangents, the one which is also tangent to a circle of latitude, whose direction cosines are

$$\left. \begin{aligned} g_{lx} &= -\sin \phi = -y(x^2 + y^2)^{-\frac{1}{2}}, \\ g_{ly} &= \cos \phi = x(x^2 + y^2)^{-\frac{1}{2}}, \\ g_{lz} &= 0, \end{aligned} \right\} \quad (23)$$

and the meridional tangent whose direction cosines are

$$\left. \begin{aligned} g_{mx} &= -\frac{xz}{c^2} \left( \sum \frac{x^2}{a^4} \right)^{-\frac{1}{2}} (x^2 + y^2)^{-\frac{1}{2}}, \\ g_{my} &= -\frac{yz}{c^2} \left( \sum \frac{x^2}{a^4} \right)^{-\frac{1}{2}} (x^2 + y^2)^{-\frac{1}{2}}, \\ g_{mz} &= \frac{x^2 + y^2}{a^2} \left( \sum \frac{x^2}{a^4} \right)^{-\frac{1}{2}} (x^2 + y^2)^{-\frac{1}{2}}. \end{aligned} \right\} \quad (24)$$

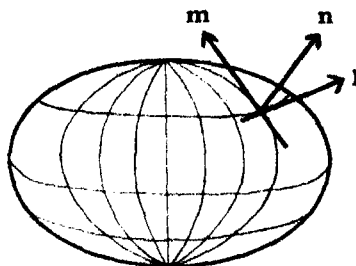


FIGURE 1. The principal directions  $l, m, n$  on a spheroid.

From a simple calculation or from the symmetry of the problem it follows that the strain  $e_{ln}$  and so the corresponding stress  $p_{ln}$  vanish. The meridional stress is

$$\begin{aligned} p_{mn} &= 2\mu e_{mn} = 2\mu e_{ij} g_{mi} g_{nj} \\ &= 8\kappa\mu(C^2 - A^2) \frac{(x^2 + y^2)^{\frac{1}{2}} z}{c \sum x^2 / a^4}. \end{aligned} \quad (25)$$

This vanishes, as it should, for a sphere where  $c = a$  and  $C = A$ . But when  $c < a$  this expression has the sign of  $(x^2 + y^2)^{\frac{1}{2}} z$ , so that the stress on the surface is always directed from the pole to the equator. The stress is proportional to  $\sin \theta \cos \theta / (a^2 \sin^2 \theta + c^2 \cos^2 \theta)$ . The angle  $\chi$  between  $\mathbf{m}$  and the  $z$  axis is given by  $c \tan \chi = -a \tan \theta$ , and as long as  $\theta > c/a$  the tangential stress represents a force roughly parallel to the equatorial plane, and tending to enlarge the cavity. When  $\theta > (c/a)^{\frac{1}{2}}$  the stress is of order  $1/a^2$ , and acts over an area of order  $a^2$ . The resultant force vanishes, and the stress can thus be represented by two "dipoles" each formed by forces of the order unity separated by a distance of the order of  $a$ , so that the strength of the dipoles is of order  $a$ . When  $(c/a)^{\frac{1}{2}} > \theta > (c/a)$  the stress is of order  $1/a^2 c$  and acts over an area of order  $ac$ , so that the dipole strength is of order  $a$  again. When  $\theta < c/a$  the tangential stress has a considerable component parallel to the axis and tending to reduce the volume. The stress is of order  $1/c^2$  and acts over an area of order  $c^2$ . But while the resultant component of force again vanishes, for this axial component the force on each element is balanced, not by the force which is its image in the axis and so is a distance of the order  $a$  away, but by the force on the element which is its image in the equatorial plane and so is a distance of the order  $c^2/a$  away. Thus the forces tending to reduce the volume form a dipole spread along the equator, the strength of which is only of order  $c^2/a$ , and produce deformations which are only appreciable in the equatorial belt. That is to say, the stresses tending to reduce the volume are confined to the equatorial belt. They are large, but as they act only over a small area they represent forces of the same order as those tending to increase the volume. Since, moreover, each force is balanced by an opposite force only a short distance away they produce only local deformations which cannot appreciably reduce the volume.

It has thus been shown that the tangential forces produce an increase in the volume of the cavity, and so it is established that the values  $W_1$  and  $W_2$  given by (19) and (22) do represent lower and upper limits for the least work required to increase the volume of an oblate spheroid. It seems likely that the work done by the traction will be rather ineffective in increasing the volume, so that probably the true value lies considerably nearer to  $W_1$  than to  $W_2$ .

2.5. A further case which will be considered is that of the disturbance caused by inserting into a cavity in the matrix a body of the same shape but of the wrong size, and of the same rigidity. The natural volume of the hole is  $V$ , while that of the inclusion is  $V(1 + 3\delta)$ . The elastic equations are satisfied if the displacement in the matrix is given by  $u_x = \gamma \frac{\partial U}{\partial x}$ , etc., and that in the

inclusion by  $u_x = \gamma \frac{\partial U}{\partial x} + \delta x$ , etc., where  $U$  is the gravitational potential of the inclusion and  $\gamma$  is a suitable constant. The energy in this case is given by (1) whatever the shape of the hole.\*

### 3. THE INFLUENCE OF THE STRAIN ON THE PROCESS OF PRECIPITATION

The energies associated with these internal strains are large, of the order of the chemical heats of solution of one metal in another. For whatever may be the nature of the precipitation process there can be little doubt that it is primarily one of diffusion, and while the mechanism of diffusion is in its turn not yet fully understood it seems certain that diffusion simply results in the interchange of pairs of atoms occupying definite lattice sites. If an island of one metal is formed by diffusion in a matrix of the same crystal structure but having an atomic spacing smaller by  $\delta$ , it behaves as a strained inclusion whose elastic energy is given by a formula of the type (1). The value of  $\delta$  is in many cases of the order 3–4 %, while the elastic constants of a pure metal are of the order  $10^{12}$  dynes/cm.<sup>2</sup>. The energy is thus of the order  $4 \times 10^9$  ergs/cm.<sup>3</sup> of precipitate, or taking the density of the metal as 5, the energy is 20 cal./g. of precipitate. In the case of silver precipitating from copper,  $\delta$  has the unusually high value of 12 %, so that the energy may be of the order of 100 cal./g. Unless these large energies were released the process of precipitation would be impossible, for it would involve an increase in the energy of the system and a decrease in its entropy, so that the free energy would necessarily increase.

3.1. If precipitation takes place solely at the crystal boundaries or if the original crystal lattice breaks up into crystallites, these strains are not produced, for the lattice of the precipitate is free to expand, and there is ample evidence (e.g. Ageew, Hansen and Sachs 1930; Cohen 1936) that both of these methods of releasing the strain are effective. But there is also evidence (e.g. Derge, Kommel and Mehl 1937; Calvet, Jacquet and Guinier 1939) that particles of precipitate are formed within single crystals, which remain apparently continuous. In the latter case it is possible that the strain has been released by some recrystallization of the matrix in the neighbourhood of the inclusions, for it is well known that strain will induce recrystallization at temperatures considerably lower than those at which it can occur in the unstrained metal (Burgers 1934).

If, as Wagner suggests (Wagner and Schottky 1930), the mechanism of

\* This result is due to Mr M. M. Crum.

diffusion is provided by the empty lattice sites which must always arise in a metal in thermodynamical equilibrium, it would be possible for the strain around a particle of silver in copper to be released by the migration of the holes in the copper to the boundaries of the silver inclusion. Since these holes can only be formed at the surface of a crystal, and the number originally present is extremely small, such an explanation of over-ageing and softening would require that a large crystal softened much more slowly than a small. There does not seem to be explicit evidence against such a relation, but it seems to be generally agreed that crystal size is in fact not an important factor in determining the rate of softening.

It is commonly stated that the strain is relieved by the agglomeration of the precipitate into large particles. However, all the formulæ obtained in § 2 show that the energy of an isolated inclusion of given shape is proportional to its volume, so that in a dilute solution where the particles of precipitate are separated by distances large compared with their size the total strain energy associated with particles of a definite form depends only on the total volume of the precipitate and not on the volumes of the individual particles. For spherical particles of radius  $r_0$  separated by distances  $r$  the mean minimum strain which in Taylor's theory determines the strength is  $\epsilon r_0^3 r^{-3}$ , where  $\epsilon$  is given in I as a constant depending only on the properties of the two phases concerned. But  $r_0^3 r^{-3}$  is simply the volume concentration of the precipitated phase, and so the hardness is independent of the size of the individual particles if their total volume remains constant. General dimensional considerations show that this must also be true for particles of any definite shape. This statement is apparently incompatible with the existence of precipitation hardening in the usual sense, and provides an example of the limitations of the theory, which obviously loses all quantitative value if an attempt is made to apply it to the solid solution in which the included particles are single atoms. The principal factor which reduces the hardness of the solid solution below that of the precipitation-hardened alloy into which it may be converted is probably that a dislocation is not seriously impeded by an adverse strain spread over a region small compared with its own "wave-length". Such a small obstacle may be surmounted in two ways, either by the dislocation breaking and reforming on the far side, or by thermal fluctuations momentarily reducing the adverse strain. The recent calculation of Peierls (1940) that the wave-length of a dislocation is only a few atomic distances shows that the detailed consideration of these effects is likely to be somewhat difficult.

Provided the precipitated particle does not break away from the matrix its energy can only be reduced to a limited extent by changes of shape. For

the particular case in which the inclusion has the same rigidity as the matrix Crum's calculation in § 2.5 shows that the strain energy is entirely independent of the shape, and it is reasonable to infer that as long as the rigidity of the inclusion remains comparable with that of the matrix its energy will not depend greatly on its shape.

W. L. Bragg has pointed out that a precipitate of flat sheets is likely to have a smaller strain energy than almost any other because the faces of the sheets are nearly free to expand, and that in an anisotropic material this lowering of energy will be particularly effective if the sheets are formed in a plane in which the lattice of the precipitate is easily stretched. It is interesting to estimate how great this reduction of strain energy would be in some particular case if the precipitate did *not* break away from the lattice. Silver precipitates from copper in sheets lying in the  $\{100\}$  planes of the copper. If the precipitate has not broken away these must also be  $\{100\}$  planes of the silver, and the calculation of II shows that in this case the energy is reduced by a factor less than 6.

It seems, then, that the strain can only be effectively released by allowing the precipitate to break away; that is to say, by allowing its lattice to become discontinuous with that of the matrix. In the further growth of the particle there need no longer be 1 : 1 correspondence between the points of the lattice of the particle and the lattice points of that part of the matrix which originally occupied the same space. The total number of atoms in the particle must, however, be equal to the number of missing points in the matrix lattice, for the interchange of atoms still takes place by simple diffusion in the main bulk of the matrix. This in fact means that the particle recrystallizes in such a way that the shear strain in it vanishes, and only a uniform compression remains; for example, the walls of a disk-shaped cavity bulge outwards owing to the increased volume of the atoms lying within it, and the inclusion recrystallizes so that atoms are removed from the compressed regions near the rim and replaced in the less strained central regions. That this internal recrystallization should occur at rather low temperatures is not surprising, for a particle of precipitate provides just the type of strained region which appears to act as a nucleus of recrystallization.

For any type of precipitate the misfit between the particle and the cavity which it occupies is accommodated partly by the deformation of the matrix and partly by that of the particle. For an inclusion which is effectively fluid the relative accommodations can easily be calculated. For suppose  $W_0$  is the energy when the whole volume misfit  $3\delta$  is taken up by compressing the inclusion, and  $W_1$  is the energy when the whole misfit is taken up by the matrix. Let the actual compression of the inclusion be  $3x$ , so that the enlargement of

the cavity is  $3(\delta - x)$ . The total energy is  $[x^2 W_2 + (\delta - x)^2 W_4]/\delta^2$ , which has its minimum value  $W_6$ , given by

$$\frac{1}{W_6} = \frac{1}{W_2} + \frac{1}{W_4}, \quad (26)$$

when  $x = W_4 \delta / (W_2 + W_4)$ . If  $W_4 \ll W_2$  then  $x \approx 0$ ,  $W_6 \approx W_4$  and the compressibility of the inclusion is unimportant.

To see how  $W_4$  varies with the shape of the inclusion, it may be determined as a function of  $c/a$  for the spheroids with semi-axes  $a, a, c$ , which provide models of several simple figures of revolution—disks, spheres and needles. It may be written in the form

$$W_4 = 6\mu V \delta^2 E \left( \frac{c}{a} \right); \quad (27)$$

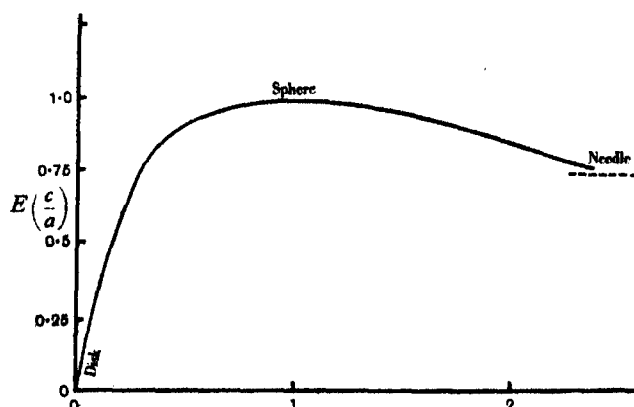


FIGURE 2. The elastic energy  $E$  of a particle of precipitate as a function of its shape.  $a$  is the equatorial diameter,  $c$  the polar diameter.

for the values of  $c/a$  for which it has been possible to calculate  $W_4$  the energy does not depend on the elastic constant  $\lambda$  of the matrix, and any possible dependence of  $W_4$  on this constant when  $c/a$  takes more general values will be neglected. When  $c/a = \infty$ , § 2.2 shows that  $E = 3/4$ . In § 2.3 put  $n = 2$ , when the cavity considered becomes a spheroid of semi-axes  $r_0(1 - \frac{1}{2}\epsilon)$ ,  $r_0(1 - \frac{1}{2}\epsilon)$ ,  $r_0(1 + \epsilon)$ , so that when  $c/a = 1 + \frac{3}{2}\epsilon + O[\epsilon^2]$  then  $E = 1 + O[\epsilon^2]$ . Finally, when  $c/a \ll 1$ , § 2.4 shows that  $W_1 < W_4 < W_2$ , and taking  $W_4 = W_1$  leads from (19) and (27) to  $E \approx \frac{2}{3}\pi c/a$ . A smooth curve through these points gives the graph of  $E(c/a)$  shown in figure 2.

The explanation of the Widmanstätten structure (Derge, Kommel and Mehl 1937) and of the laminar structures observed by Chao and Taylor (1940) and Bradley (1940) is now apparent, for provided that the precipitate or



second phase has broken away its strain energy can be reduced to any extent simply by causing the precipitate to form in sufficiently flat plates or sheets.

3.2. The breaking away of a precipitate is hindered by the same forces which cause the formation of a regular lattice. To produce the discontinuity of the lattice requires roughly the same energy as the melting of a monatomic layer of metal at the surface of the inclusion. If the latent heat of melting is  $\Lambda$  and the density is  $\rho$ , the energy of melting is  $\Lambda\rho$  cal./cm.<sup>3</sup>. The surface energy of such a discontinuity is thus  $d\Lambda J\rho$  ergs/cm.<sup>2</sup>, where  $d$  is the interatomic distance and  $J$  the mechanical equivalent of heat. For copper this is equal to 410 ergs/cm.<sup>2</sup>. This surface energy is most important for small particles of precipitate, and tends to make them spherical in shape, while the elastic energy favours an inclusion in the form of a thin sheet. It follows that there must be an equilibrium form which is the more flattened the larger the grain. Since the elastic energy is of order  $4 \times 10^9$  ergs/cm.<sup>3</sup> the tendency to form spherical grains becomes marked in the case of particles of linear dimensions less than about  $10^{-7}$  cm., a few atomic distances.

Even in grains so large that surface energy no longer has any effect there is a dynamic equilibrium form which is determined by the rate of precipitation. If the grain is in the form of a moderately thick plate, the energy required to increase its thickness may be so large as to prevent precipitation on the faces, while precipitation at the edges still occurs, so that the plate elongates. For a very thin sheet the elastic energy is negligible even if the thickness is somewhat increased, while the rate at which precipitating atoms reach the faces is far greater than the rate at which they reach the edge, so that the sheet thickens. It is clear that the differential effect of the elastic energy in promoting elongation of the plate will be most effective when the average rate of precipitation is low, and so flat sheets should be formed especially in solutions which are only slightly supersaturated.

In a mathematical treatment of the growth of a flat inclusion it is again convenient to consider it as a prolate spheroid of semi-axes  $a, a, c$ . Its surface area is

$$S = 2\pi a^2 + O[c^2 \log a/c]. \quad (28)$$

If  $a \gg c$  its elastic energy is  $W_4$ , which is equal to  $W_1$ , as given by equation (19), for  $W_2$ , the energy required to compress the inclusion into the original volume of the hole, is of order  $a^2c$  and is so large that practically all the misfit is taken up by shear in the matrix.

Suppose that when the concentration of precipitating atoms in the matrix is  $c$  their flux (number of atoms crossing unit area in either direction in unit

time) is  $cf$ , where it is assumed for simplicity that  $f$  is independent of  $c$ . The concentration (ratio of filled to total available lattice points) in the precipitate is 1. Let the heat of solution of the pure metal unstrained be  $U$ . Then in its solution the concentration is  $e^{-U/kT}$  and the flux is  $fe^{-U/kT}$ . The outward flux from a surface such that the addition of a single atom requires strain energy  $\bar{W}$  is  $fe^{(\bar{W}-U)/kT}$ . Let the "relative humidity" defined as (concentration)/(vapour pressure of unstrained metal) in the matrix be  $H$ . Then the inward flux from the matrix is  $Hfe^{-U/kT}$  and the rate of deposition is

$$fe^{-U/kT}(H - e^{-\bar{W}/kT}) = fe^{-U/kT}(s - \bar{W}/kT), \quad (29)$$

if  $\bar{W}$  is small compared with  $kT$ , and  $s$ , the "supersaturation", is  $H - 1$ .

Let the inclusion be  $2\mathcal{N}$  atoms thick and  $2\mathcal{R}$  atoms in diameter. Then  $a = d\mathcal{R}$ ,  $c = d\mathcal{N}$ , and the energy is

$$W = 2\pi d^3(3\pi\mu\delta^2\mathcal{N}^2\mathcal{R} + \Lambda J\rho\mathcal{R}^2). \quad (30)$$

The total number of atoms is  $\frac{4}{3}\pi\mathcal{N}\mathcal{R}^2$ , and so the average energy per atom required to increase the width is

$$\frac{3}{8\pi\mathcal{N}\mathcal{R}} \frac{\partial W}{\partial \mathcal{R}} = \frac{3d^3}{4} \left( 3\pi\mu\delta^2 \frac{\mathcal{N}}{\mathcal{R}} + 2\Lambda J\rho \frac{1}{\mathcal{N}} \right), \quad (31)$$

while for an increase in thickness it is

$$\frac{3}{4\pi\mathcal{R}^2} \frac{\partial W}{\partial \mathcal{N}} = \frac{3d^3}{4} 3\pi\mu\delta^2 \frac{4\mathcal{N}}{\mathcal{R}}. \quad (32)$$

So from (29)

$$\left. \begin{aligned} \frac{d\mathcal{R}}{dt} &= fe^{-U/kT} \left[ s - \frac{3d^3}{4kT} \left( 3\pi\mu\delta^2 \frac{\mathcal{N}}{\mathcal{R}} + 2\Lambda J\rho \frac{1}{\mathcal{N}} \right) \right], \\ \frac{d\mathcal{N}}{dt} &= fe^{-U/kT} \left[ s - \frac{3d^3}{4kT} 3\pi\mu\delta^2 \frac{4\mathcal{N}}{\mathcal{R}} \right]. \end{aligned} \right\} \quad (33)$$

These may be expressed in the form

$$\begin{aligned} \frac{d\mathcal{R}}{dt} &= a - b \frac{\mathcal{N}}{\mathcal{R}} - c \frac{1}{\mathcal{N}}, \\ \frac{d\mathcal{N}}{dt} &= a - 4b \frac{\mathcal{N}}{\mathcal{R}}; \end{aligned}$$

it is possible to sketch the solutions of (33) in the plane of  $\mathcal{R}$  and  $\mathcal{N}$ ,  $t$  being a parameter measured along the curves. This is done in figure 3, for arbitrary values of  $a, b, c$ , and it will be seen that the heavily drawn curve separates the

plane into two regions representing particles which can ultimately grow indefinitely and particles which ultimately vanish.

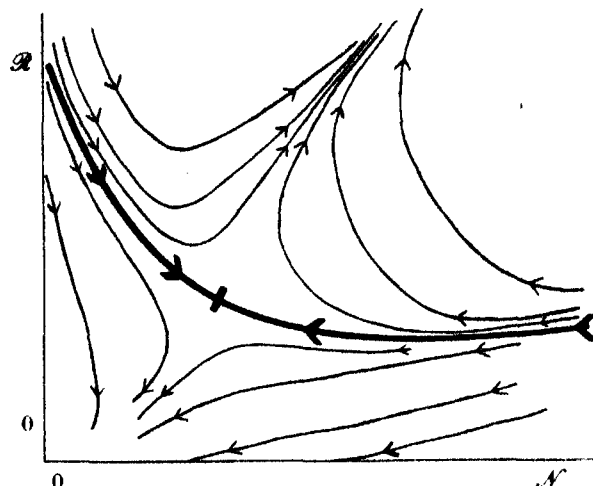


FIGURE 3. Curves showing the growth of particles of precipitate having various radii  $R$  and thicknesses  $2n$ , drawn for arbitrary values of the constants involved. The scale of  $n$  is much greater than that of  $R$ . Time is a parameter increasing along each curve in the direction marked by the arrows, and the heavily drawn curve separates the values of  $R$  and  $n$  representing particles which ultimately grow indefinitely from those representing particles which redissolve.

Even a large inclusion cannot grow unless the ratio of its breadth to its thickness is greater than  $(p-q)/2a$ , and it tends finally to grow with the constant ratio  $R/N = (p+q)/2a$ , where  $p = a + 4b$  and  $q = (a^2 + 4ab + 16b^2)^{1/2}$ . The size of particle for which surface effects are important is given by  $N \leq 2c/a$ . For such metals as copper or silver it will be sufficiently accurate to take the general values

$$d = 2.7 \times 10^{-8} \text{ cm.}, \quad \mu = 3 \times 10^{11} \text{ dynes/cm.}^2,$$

$$T = 600^\circ \text{ K.}, \quad \Delta\rho = 300 \text{ cal./cm.}^3,$$

$$\text{while } k = 1.37 \times 10^{-16} \text{ ergs/}^\circ \text{ K.}, \quad J = 4.2 \times 10^7 \text{ ergs/cal.},$$

leading to

$$a = sf e^{-U/kT}, \quad b = 510\delta^2 f e^{-U/kT}, \quad c = 4.55 f e^{-U/kT}.$$

Since  $s$  is necessarily less than unity, and in fact is usually between 3 and 15 %, while  $\delta$  is rarely as small as 1 % and may be as large as 12 %, it is clear that normally  $b \gg a$ . In this case the limiting ratio of breadth to thickness at which growth can occur is formally  $R/N = 1/4$ , which is not a flat disk.

This means that any sufficiently large flat disk will ultimately grow, although unless  $\mathcal{R}/\mathcal{N} > 4b/a \approx 2000\delta^2/s$  its thickness will at first diminish. This value  $\mathcal{R}/\mathcal{N} \approx 2000\delta^2/s$  is also the final dynamical equilibrium axial ratio for a large grain growing in a solution of supersaturation  $s$ . Surface effects are important as long as the thickness is less than  $10/s$  atoms. The final limiting form is in its order of magnitude quite a good representation of the ratio of length to breadth actually observed in the Widmanstätten structures. For example, if the atomic volumes differ by 15% and the solubility at the temperature of anneal is 5% less than the solubility at the temperature at which the alloy is prepared,  $3\delta = 0.15$  and  $s = 0.05$ , so that this expression predicts the formation of particles for which

$$\frac{\mathcal{R}}{\mathcal{N}} = \frac{2000 \times 0.05^2}{0.05} \approx 100,$$

so that the sheets are a hundred times as broad as they are thick. Experimental verification of the relation  $\mathcal{R}/\mathcal{N} \sim \delta^2/s$  would be difficult, as the effective value of  $s$  in the neighbourhood of an inclusion is not immediately available to experiment, and also there is the risk that the results may be upset by recrystallization in small regions of the matrix on the boundary of the inclusion. It is certainly true that the structures observed by Mehl (Barrett, Kaiser and Mehl 1935) in copper-silver, where  $\delta$  is large and  $s$  was small, were much finer than those formed in most other alloys.

These considerations alone in some cases explain the observed form of the age-hardening curves, particularly at low temperatures. The initial induction period is due to the difficulty of forming a nucleus of precipitation owing to the relatively large influence of surface effects. These effects have been discussed in more detail by Dehlinger (1932) and Becker (1940). (Dehlinger has also given a discussion (Dehlinger 1933) of precipitation and diffusion in which equations of the type of (33) are used.) Once precipitation has started the particles grow rapidly, and since  $s$  is fairly large they take the form of rather thick disks. This gives rise to a rapid increase in the hardness of the alloy. As the precipitation continues  $s$  decreases, and so the rate of hardening decreases. At the same time the disk can only continue to grow by taking the form of flatter disks or sheets, so causing a further reduction in the rate of hardening. Ultimately when  $s$  becomes small the increase of strain due to the slow increase in the total volume of the disks is not great enough to compensate for the decrease due to the changing shape of the disks, and a slow softening sets in. As the sheets become thinner their elastic energy becomes less important, so that the excess of vapour pressure near the face of a disk over that near the edge becomes smaller. The rate at which

the disks flatten becomes very slow, and so the softening process also becomes very slow.

This explanation is confirmed by Cohen's result (1936) that the attainment of maximum hardness and so the softening process itself during the precipitation of copper from silver in the temperature range 100–200° C have the same activation energy as the precipitation, which is undoubtedly a diffusion process. But it seems that softening is more usually due to recrystallization, for polished sections in many cases show that on long ageing the Widmanstätten sheets coagulate into globules (e.g. Calvet, Jacquet and Guinier 1939), while the breakdown of the matrix into smaller crystals is clearly shown in the X-ray photographs of Ageew, Hansen and Sachs (1930). Mehl (Barrett, Kaiser and Mehl 1935) observed in the same copper-silver system that a coarse precipitate causes the matrix crystal to break down, while the same amount of precipitate in a fine Widmanstätten structure does not induce recrystallization in the matrix, in agreement with the view adopted here that the two methods of release of strain are alternative.

3.3. These considerations apply to a large inclusion which has broken away, and show why such an inclusion retains a disk-like form as it grows. The orientation of the disk is determined by the processes forming the original nuclei of precipitation, as has been shown by Mehl and his collaborators (Derge, Kommel and Mehl 1937), Preston (1938) and Calvet, Jacquet and Guinier (1938). The latter two workers have carried out a very careful X-ray examination of single crystals of aluminium in which a precipitate of  $\text{CuAl}_2$  is forming. They find that the copper begins to segregate in regions including between 1 and 5 {100} planes of atoms, and of a breadth increasing from about ten atomic distances in the early stages of the precipitation process to a thousand atomic distances after ageing for a few hours at 200° C or a few weeks at 150° C. After prolonged ageing at 200° C the sheets have become so thick that they diffract as a three-dimensional grating, and the crystal structure and orientation of the  $\text{CuAl}_2$  phase which has precipitated can be determined. It is found that the two lattices are so orientated that the lattices of the matrix and of the inclusion fit together fairly accurately along the faces of the sheets. This result is confirmed by Mehl's work on other systems, for he finds that the precipitate usually comes out in sheets so orientated and with its own lattice in such a direction that the distributions of atoms in the plane of contact in the matrix and in the precipitate closely match.

The complete process of precipitation may be pictured as follows: Initially atoms of the precipitate segregate in an ( $lmn$ ) plane of the original

crystal, where  $(lmn)$  is determined by the condition that there exists a plane  $(\bar{l}\bar{m}\bar{n})$  in the precipitate such that the distribution of atoms in these two layers closely matches. Because of this matching the monatomic sheet of precipitate formed is not greatly stretched in its own plane, while at the same time the lattice is continuous and there is no surface energy of the kind discussed in § 3.2.\* Then this region broadens and thickens. If the atomic volume of the precipitate is greater than that of the matrix by a fraction  $3\delta$ , while the planes in contact have equal atomic spacings, the separation of these planes in the precipitate must exceed the separation of parallel planes in the matrix by  $3\delta$ , so that considerable bulging of the lattice planes in the matrix must occur. But the previous considerations on this type of strain are still valid, and even this large displacement requires little energy if the precipitate is in the form of a sufficiently thin plate. The elastic energy required to keep the two lattices in register along their plane of contact is proportional to the volume of the precipitate, while the surface energy gained thereby is proportional to the surface area of the precipitate, and ultimately becomes smaller than the elastic energy. The lattice of the precipitate breaks away completely from that of the matrix, and the further growth of the particle is governed by the considerations of § 3.2.

It is not difficult to form a rough estimate of the thickness of a sheet when it breaks away. If the misfit between the two lattices in the matched planes is  $\delta'$ , the elastic energy of unit volume is given by a formula in II and the energy of a sheet  $\pi\mathcal{N}^2$  atoms in area and  $\mathcal{N}$  atoms thick is

$$\pi\mathcal{N}^2 d^3 (c_{11} + 2c_{12}) (c_{11} - c_{12}) \delta'^2 / c_{11}.$$

The surface energy is  $\pi\mathcal{N}^2 d^3 AJ\rho$ , and these are equal when

$$\mathcal{N} = c_{11} AJ\rho / (c_{11} + 2c_{12}) (c_{11} - c_{12}) \delta'^2. \quad (34)$$

Taking the values of the constants for silver, this is roughly  $\mathcal{N} = 170/\delta'^2$ , where  $\delta''$  is the percentage misfit, so that a sheet of copper will break away from silver when it is only two atoms thick.

In a eutectic alloy two phases form from the same liquid. Elastic strain is again avoided by precipitation in sheets, but since there is no possibility of matching the precipitate lattice against that of the liquid matrix the sheets are not confined to a few preferred directions, and the typical eutectic structure of thin warped sheets is produced.

This work forms part of an investigation which is being carried out for the Department of Scientific and Industrial Research under the direction of

\* The surface energy treated by Becker is due to order-disorder forces, and is present even when the precipitate has not broken away.

Professor Mott. I should like to express my gratitude to Professor Mott for his constant advice and encouragement. I am also indebted to Dr G. H. Wannier for some valuable suggestions.

## REFERENCES

- Ageew, Hansen and Sachs 1930 *Z. Phys.* **66**, 350.  
Barrett, Kaiser and Mehl 1935 *Trans. Amer. Inst. Min. Metall. Engrs*, **117**, 39.  
Becker 1940 *Proc. Phys. Soc.* **52**, 71.  
Bradley 1940 *Proc. Phys. Soc.* **52**, 80.  
Bragg 1940 *Proc. Phys. Soc.* **52**, 105.  
Brindley 1940 *Proc. Phys. Soc.* **52**, 117.  
Burgers, J. M. 1940 *Proc. Phys. Soc.* **52**, 23.  
Burgers, W. G. 1934 *Int. Conf. Phys.* **2**.  
Calvet, Jacquet and Guinier 1938 *C.R. Acad. Sci., Paris*, **206**, 1972.  
— — — 1939 *J. Inst. Met.* **65**, 121.  
Chao and Taylor, W. H. 1940 *Proc. Roy. Soc. A*, **174**, 57.  
Cohen 1936 *Metals Tech.* **3**, T.P. 751.  
Dehlinger 1932 *Z. Phys.* **79**, 550.  
— 1933 *Z. Phys.* **83**, 832.  
Derge, Kommel and Mehl 1937 *Trans. Amer. Inst. Min. Metall. Engrs*, **124**, 367.  
Dillinger and Bozorth 1935 *Physics*, **6**, 279.  
Kersten 1935 *Z. techn. Phys.* **12**, 665.  
Love 1927 *The mathematical theory of elasticity*. Cambridge.  
Mott and Nabarro 1940 *Proc. Phys. Soc.* **52**, 86.  
Nabarro 1940 *Proc. Phys. Soc.* **52**, 90.  
Peierls 1940 *Proc. Phys. Soc.* **52**, 34.  
Preston 1938 *Phil. Mag.* **26**, 855.  
Quinney and Taylor, G. I. 1937 *Proc. Roy. Soc. A*, **163**, 157.  
Thomson and Tait 1883 *Natural Philosophy*, **1** (2).  
Wagner and Schottky 1930 *Z. phys. Chem. B*, **11**, 163.  
Wood 1935 *Phil. Mag.* **19**, 219.
-

# The combustion of aromatic and alicyclic hydrocarbons.

## V. The products of combustion of benzene and its monoalkyl derivatives

BY J. H. BURGoyNE, PH.D.

*Department of Chemical Technology, Imperial College, London*

*(Communicated by A. C. G. Egerton, Sec.R.S.—Received 25 April 1940)*

The progressive formation of products in the combustion of benzene and its monoalkyl derivatives has been studied by analytical methods, and the characteristic features of the isothermal reactions at various temperatures have been established.

A cool-flame reaction of *n*-propylbenzene has also been investigated, and by comparison with corresponding isothermal combustions, it is concluded that the propagation of cool-flames is conditioned by the accumulation of a phenylalkyl hydroperoxide.

The results are interpreted in the light of the theory of the two-stage process, and a schematic mechanism for the main combustion reaction is outlined. This comprises degradation of the side-chain (if present) and rupture of the benzene nucleus, followed by rapid degradation of the higher aliphatic aldehyde thus formed, yielding finally formaldehyde and the ultimate combustion products  $\text{CO}_2$ ,  $\text{CO}$  and  $\text{H}_2\text{O}$ .

### INTRODUCTION

In considering the combustion of benzene and its homologues at high pressures (Newitt and Burgoyne 1936) the nature of the principal products of reaction was established, and information was obtained as to their ultimate survival under specified conditions. In the present experiments, the progressive formation of these products is examined.

In the case of each of the four hydrocarbons now under consideration, slow combustion reactions above and below  $350^\circ\text{C}$  have been studied, whilst with *n*-propylbenzene the progress of a reaction in the cool-flame zone has also been investigated.

Mixtures having fuel : oxygen ratios between 1 and 0.5 were employed.

### METHODS OF PROCEDURE

In order to determine the composition of the reacting medium at any given stage in the combustion, the quartz reaction vessel was detached from the filling system, and, while still connected to the manometer,



plunged into a bath at 0° C. The equilibrium pressure was noted and a gas sample withdrawn. The condensed products in the bulb were then washed into a flask for analysis.

Previous work (Newitt and Burgoyne 1936) has indicated that the combustion products of the higher aromatic hydrocarbons attain a considerable degree of complexity. In these circumstances it is not always possible to design completely specific methods of analysis, and if the numerical results are to be justly interpreted it is necessary to have in mind the analytical processes involved. These, briefly, were as follows.

*Acids* were estimated by titration with baryta, using phenol red as indicator, whereby the interference of phenols was eliminated.

*Aldehydes* were determined by the Ripper bisulphite method, which does not apply to aromatic ketones. The aldehydes and ketones were then estimated together by a strictly comparative modification of the hydroxylamine method (allowance being made for the free acid present) and the ketones obtained by difference.

*Phenols* were estimated using the bromide-bromate reaction, it being assumed that in the case of a mixture of phenols, the average number of bromine atoms substituted by one phenol molecule is three, e.g.



To determine *alcohols*, the products were first distilled in steam from an alkaline solution, in order to separate the alcohols from acids and phenols. The distillate was then completely oxidized with alkaline potassium permanganate and the amount of oxidizing agent used was estimated iodimetrically. Due allowance having been made for the presence of aldehydes and ketones, the surplus permanganate was assumed to have been reduced by alcohols. By making some assumption as to the nature of the alcohol, the amount present could then be calculated.

*Peroxides* were estimated by iodine liberation from potassium iodide and were subdivided into three classes as follows:

- (1) Those which liberated iodine immediately from dilute neutral KI.
- (2) Those which liberated iodine with 30 min. in an atmosphere of nitrogen from a strong solution of KI acidified with acetic acid.
- (3) Those which liberated iodine in 24 hr. under the conditions obtaining in (2).

Broadly speaking, class (1) may be taken to consist of peracids, (2) of aldehyde peroxides and  $\text{H}_2\text{O}_3$ , and (3) of peroxides of the type  $\text{ROOH}$ , where  $R$  is an aryl or alkyl group. The last would also appear to some extent in (2). Previous investigators have found the peroxidic products

from hydrocarbon and aldehyde combustions to be somewhat unstable in aqueous solution. Tests were therefore carried out to ascertain how far such might be the case in the present instance. The results indicate that no rapid decomposition of the peroxides occurred after withdrawal from the reaction vessel, but that the aldehyde and alkyl peroxides disappeared on standing for several hours in darkness in an atmosphere of nitrogen: there was a corresponding small increase in the amount of aldehyde present in the solution. Peracids were found to be quite constant for a period of 24 hr. under these conditions, and the amount of acid in the products remained always constant. Nevertheless, the combustion products were invariably analysed as quickly as possible, and the peroxide estimation was commenced immediately after withdrawal from the reaction vessel.

#### EXPERIMENTAL RESULTS

In the description which follows of chemical analyses of the combustion products, the experimental results are set out in tables, accompanied by supplementary notes. Eight slow combustion reactions (1-8) are first considered, from the results of which it is possible to summarize the common features of such reactions and the effect of temperature upon them. A reaction of propylbenzene (9), in which a cool-flame is propagated, is then examined and its features are compared with the characteristics already established of corresponding isothermal combustions.

Reactions and tables are numbered to correspond.

*Reaction 1.* 225 mm. benzene + 425 mm. oxygen at 487° C.

In addition to the products included in table 1, formaldehyde, peroxides (other than peracids), ethylene, acetylene, paraffins and hydrogen were formed in small amounts. The concentration of aldehyde rose rapidly in the early stages of the reaction, and, after remaining fairly constant during the period of maximum combustion rate, fell to a very small figure in the final products. The amounts of the other intermediates mentioned were too small for accurate comparative analyses.

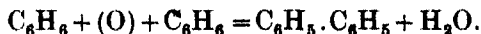
The acids appeared to be aliphatic in character and included maleic and formic acids. The only product of importance, however, other than steam and the oxides of carbon, was phenol, included under which heading are also di- and trihydric derivatives. Although hydroquinone and trihydric phenols have been detected in the combustion products of benzene during this investigation, no indication of more than a trace of these substances has ever been found.

TABLE 1. THE REACTION OF 225 MM.  $C_6H_6$  + 425 MM.  $O_2$  AT  $487^\circ C$ . TOTAL PRESSURE INCREMENT = 129.0 MM.

|                                       |        |        |       |        |
|---------------------------------------|--------|--------|-------|--------|
| Time of sampling from start in min.   | 19     | 26     | 30    | 45     |
| % pressure increment                  | 11.8   | 40.8   | 64.6  | 100    |
| % oxygen used                         | 11.1   | 40.0   | 62.7  | 100    |
| Products in mm. at $487^\circ C$ :    |        |        |       |        |
| $CO_2$                                | 12.6   | 52.4   | 57.6  | 128.8  |
| CO                                    | 29.8   | 139.6  | 203.2 | 341.1  |
| $C_6H_5OH$                            | 2.7    | 13.3   | 18.8  | 22.5   |
| Acid                                  | 0.4    | 1.1    | 2.2   | 0.4    |
| C-H-O balances                        |        |        |       |        |
| Units in initial mixture              | C 1350 | H 1350 | O 850 | C 1350 |
| Units accounted                       | 60     | 18     | 815   | 850    |
| As $H_2O$                             | —      | 42     | 21    | 625    |
| As $C_6H_6$                           | 1290   | 1290   | —     | 180    |
| Total                                 | 1350   | 1350   | 836   | 627    |
| mm. $H_2O$ at $487^\circ C$ (calc.)   | 21.2   | 96.0   | 130.9 | 445    |
| mm. $C_6H_6$ at $487^\circ C$ (calc.) | 215.0  | 179.0  | 159.8 | 725    |
|                                       |        |        | 798   | 850    |

N.B. The final products also contained: 6.4 mm.  $C_2H_4$ , 0.6 mm.  $H_2$  and 2.9 mm.  $C_2H_2$ .

Satisfactory results are obtained when carbon-hydrogen-oxygen balances are drawn up relating to the reaction. The concentration of steam calculated in the course of this process is found to follow a path similar to that of the other "final products"—carbon monoxide and carbon dioxide. The calculated volume of the products is in excess of that found by experiment, however, and the discrepancy grows as the reaction proceeds. This may be satisfactorily explained by assuming the progressive formation of polynuclear hydrocarbons through the elimination of hydrogen from molecules of benzene, in which connexion it will be recalled that evidence of the survival of diphenyl in the combustion products of benzene at high pressures has previously been obtained (Newitt and Burgoyne 1936), i.e.



Lack of reactivity (cf. Part IV) made it impossible to study the combustion of benzene below 350° C in the low-pressure apparatus employed.

*Reaction 2.* 325 mm. toluene + 325 mm. oxygen at 408° C.

As in the case of the corresponding reaction of benzene, the products contained traces of peroxides (other than peracids), ethylene, acetylene, paraffins and hydrogen. The phenols consisted principally of a dihydric derivative, although cresols were undoubtedly also present.

The products estimated by analysis (see table 2), together with steam, are not sufficient to give satisfactory carbon-hydrogen-oxygen balances. However, by assuming the formation of benzene and small amounts of polynuclear hydrocarbons such as ditolyl, this discrepancy can be largely rectified. Qualitative evidence has already been obtained of the survival of these products at high pressures (Newitt and Burgoyne 1936). Gas samples from the present (and all succeeding) reactions contained a certain amount, which increased as the combustion progressed, of an unaccounted constituent which was absorbed by concentrated sulphuric acid. This substance might be an aromatic hydrocarbon or a higher olefine, and in the present instance was undoubtedly benzene.

*Reaction 3.* 290 mm. toluene + 360 mm. oxygen at 314° C.

Although benzene does not react with oxygen at an appreciable rate under atmospheric pressure at 300–350° C, it is possible to observe the combustion of toluene and higher members of the series under these conditions. The nature of the products is little changed by lowering the reaction temperature, but peroxides (2) and (3) are now found to survive in small but appreciable quantities, and the proportion of benzoic acid is



TABLE 3. THE REACTION OF 290 MM.  $C_7H_8$  + 360 MM.  $O_2$  AT  $314^\circ C$ . TOTAL PRESSURE INCREMENT = 31.0 MM.

| Time of sampling from<br>start in min. | 12    | 17    | 29.5  | 103.5 | 160   |
|--|-------|-------|-------|-------|-------|
| % pressure increment                   | 31.0  | 47.1  | 67.8  | 95.5  | 100   |
| % $O_2$ used                           | 28.3  | 46.6  | 58.2  | 96.2  | 100   |
| Products in mm. at $314^\circ C$ :     |       |       |       |       |       |
| $CO_2$                                 | 23.3  | 36.2  | 49.2  | 86.4  | 86.4  |
| $CO$                                   | 25.3  | 41.7  | 54.9  | 86.8  | 84.0  |
| $C_6H_5COOH$                           | 7.1   | 13.5  | 14.4  | 17.5  | 18.9  |
| $C_6H_5CHO$                            | 14.5  | 17.3  | 16.8  | 12.0  | 11.2  |
| $C_6H_5CH_2OH$                         | 21.3  | 27.1  | 25.9  | 18.7  | 14.1  |
| $C_6H_5CH_2(OH)_2$                     | 11.8  | 16.8  | 18.5  | 25.8  | 25.4  |
| Peroxide (1)                           | Nil   | Nil   | Nil   | Nil   | Nil   |
| Peroxide (2)                           | 0.9   | 0.7   | 0.9   | 0.5   | 0.3   |
| Peroxide (3)                           | 0.3   | 0.2   | 0.6   | 0.2   | Nil   |
| C-H-O balances:                        |       |       |       |       |       |
| Units in initial mixture               | 2030  | 2320  | 2030  | 2320  | 2030  |
| Units accounted                        | 440   | 402   | 668   | 720   | 720   |
| As $H_2O$                              | —     | 100   | 50    | 576   | 505   |
| As $C_7H_8$                            | 1590  | 1918  | —     | 91    | 251   |
| Total                                  | 2030  | 2320  | 718   | 1294  | 1368  |
| mm. $H_2O$ at $314^\circ C$            | 50.1  | 75.9  | 90.5  | 152.0 | 125.5 |
| (calc.)                                |       |       |       |       |       |
| mm. $C_7H_8$ at $314^\circ C$          | 227.2 | 203.3 | 198.3 | 184.8 | 195.5 |
| (calc.)                                |       |       |       |       |       |

N.B. The final products also contained: 0.9 mm.  $C_2H_4$ , 1.1 mm.  $H_2$ , 0.2 mm.  $CH_4$ .

increased. No peracid is detected, however, and hydrocarbons and hydrogen are still found only in traces.

Reference to the pressure-time relationship shows that the final stages of the reaction are extremely slow, and the change from 95 to 100% occupies no less than 1 hr. Under these conditions the intermediates formed in the more rapid stages of the combustion might be expected to decompose if they were so inclined. It is seen, however, that the composition of the medium is little changed in this period, the only variations being a decline in the peroxides and a small movement through the series: alcohol  $\rightarrow$  aldehyde  $\rightarrow$  acid, which is undoubtedly brought about by slow oxygen attack. There is practically no formation of the oxides of carbon meanwhile.

As was the case in reaction 2, the carbon-hydrogen-oxygen balances indicate the progressive formation of benzene and polynuclear hydrocarbons in the course of the combustion.

*Reaction 4.* 190 mm. ethylbenzene + 210 mm. oxygen at 381° C.

In connexion with the oxidation of ethylbenzene at high pressures (Newitt and Burgoyne 1936) it was shown that while the oxygen evidently attacked the  $\alpha$ -carbon atom of the side-chain to a considerable extent, there was little indication of reaction at the  $\beta$ -atom. Thus, phenylmethylcarbinol and acetophenone were important products, and the aldehydic

TABLE 4. THE REACTION OF 190 MM.  $C_8H_{10}$  + 210 MM.  $O_2$  AT 381° C.  
TOTAL PRESSURE INCREMENT = 90.0 MM.

|  |      |      |      |      |
|--|------|------|------|------|
| Time of sampling from<br>start in min. | 1    | 4.5  | 10.5 | 40   |
| % pressure increment                   | 10.3 | 50.0 | 75.3 | 100  |
| % $O_2$ used                           | 10.8 | 47.7 | 79.4 | 100  |
| Products in mm. at 381° C:             |      |      |      |      |
| $CO_2$                                 | 6.6  | 21.6 | 29.2 | 38.7 |
| CO                                     | 7.3  | 38.5 | 66.4 | 97.5 |
| Acid                                   | 2.0  | 3.1  | 6.3  | 6.4  |
| Aldehyde                               | 7.9  | 23.4 | 29.4 | 23.0 |
| Alcohol (secondary)                    | 6.8  | 15.2 | 8.9  | 7.9  |
| Phenol                                 | 4.2  | 11.3 | 17.9 | 20.4 |

and acidic intermediates consisted almost entirely of benzaldehyde and benzoic acid, both of which, as was demonstrated, could result from the oxidation of acetophenone itself. All the reactions considered in that investigation, however, were allowed to go to completion, and in view of the known instability of the higher aromatic aldehydes and acids at high

temperatures, especially in the presence of oxidizing agents, it is not to be expected that they should ultimately survive. Nevertheless, the likelihood of the transitory formation of these substances in the more rapid stages of combustion, with which the present investigation is to some extent concerned, cannot yet be excluded.

As in the case of toluene, the phenolic constituents resulting from the combustion of ethylbenzene consist mainly of a dihydric derivative, together with lesser amounts of the ethylphenols. Negligible amounts of peroxides, ethylene, paraffins and hydrogen were also found in the products, but acetylene was not detected.

*Reaction 5.* 200 mm. ethylbenzene + 300 mm. oxygen at 314° C.

Generally speaking the intermediate combustion products of ethylbenzene show greater powers of survival at 314° C than in the high-temperature zone, notably in the case of the alcohol; and while complete figures for the ketone are not available relative to reaction 4, there are indications that this intermediate also appears in smaller amounts at the

TABLE 5. THE REACTION OF 200 MM.  $C_8H_{10}$  + 300 MM.  $O_2$  AT 314° C.  
TOTAL PRESSURE INCREMENT = 63.2 MM.

|  |        |      |      |      |
|--|--------|------|------|------|
| Time of sampling from<br>start in min. | 26     | 31.5 | 34.5 | 60   |
| % pressure increment                   | 21.8   | 50.8 | 73.0 | 100  |
| % $O_2$ used                           | 22.7   | 49.2 | 72.0 | 100  |
| Products in mm. at 314° C:             |        |      |      |      |
| $CO_2$                                 | 6.3    | 23.6 | 35.3 | 40.5 |
| CO                                     | 11.2   | 36.2 | 56.2 | 87.3 |
| Acid                                   | 1.5    | 6.2  | 10.1 | 12.7 |
| Aldehyde                               | 10.4   | 25.6 | 32.2 | 33.0 |
| Ketone                                 | 6.2    | 11.1 | 17.0 | 18.6 |
| Alcohol (secondary)                    | (99.5) | 30.3 | 33.4 | 22.9 |
| Phenol                                 | 3.9    | 13.6 | 15.9 | 23.0 |

higher temperature. Although the quantity of peroxides detected at 314° C was very small, it was a little greater than at 381° C, and the concentrations followed the same general course as in the corresponding reaction of toluene (3). Acetylene was not found in the products, however, but traces of ethylene, paraffins and hydrogen were present. The experiment in column 4 of table 5 was a "first reaction", a fact the significance of which will be discussed at a later stage.

In both reaction 4 and reaction 5, carbon-hydrogen-oxygen balances indicated the presence of lower aromatic and polynuclear hydrocarbons in



the products. In view of the evident complexity of the combustion, however, it does not seem profitable at present to speculate with the object of accurately adjusting the balances.

*Reaction 6.* 130 mm. *n*-propylbenzene + 170 mm. oxygen at 377° C.

Although experimental data relative to the combustion of propylbenzene is somewhat meagre, the evidence indicates a chemical analogy with ethylbenzene. Thus, the present investigation has shown that the alcohol formed is mainly secondary and that propiophenone is present in considerable quantity in the products. At 377° C, traces of peroxide (2), ethylene, paraffins and hydrogen were found, but acetylene was not detected.

TABLE 6. THE REACTION OF 130 MM.  $C_9H_{12}$  + 170 MM.  $O_2$  AT 377° C.  
TOTAL PRESSURE INCREMENT = 70.4 MM.

|  |      |      |      |      |      |
|--|------|------|------|------|------|
| Time of sampling from<br>start in min. | 2    | 3    | 3.5  | 8    | 23   |
| % pressure increment                   | 10.5 | 24.9 | 48.2 | 87.4 | 100  |
| % $O_2$ used                           | 3.7  | 24.5 | 50.6 | 92.8 | 100  |
| Products in mm. at 377° C:             |      |      |      |      |      |
| $CO_2$                                 | 1.4  | 6.7  | 10.9 | 17.6 | 25.6 |
| CO                                     | 4.7  | 14.8 | 34.1 | 63.0 | 75.1 |
| Acid                                   | 0.4  | 1.6  | 3.7  | 4.9  | 5.0  |
| Aldehyde                               | 6.0  | 15.0 | 21.9 | 19.3 | 21.1 |
| Ketone                                 | 2.7  | 6.0  | 12.9 | 18.3 | 14.7 |
| Alcohol (secondary)                    | 19.1 | 44.3 | 76.2 | 30.1 | 17.4 |
| Phenol                                 | 1.8  | 4.4  | 7.7  | 14.5 | 15.1 |

*Reaction 7.* 100 mm. *n*-propylbenzene + 150 mm. oxygen at 307° C.

The relationship of this reaction to the preceding appears to be normal judged by the instances already cited of toluene and ethylbenzene. In the present case, peroxides (2) and (3) were formed in appreciable amounts, and traces of ethylene, paraffins and hydrogen were also detected; but peracids and acetylene were absent from the products. The final experiment in the series (table 7, col. 4) was a "first reaction".

*Reaction 8.* 210 mm. *n*-propylbenzene + 240 mm. oxygen at 277° C.

The reactivity of propylbenzene towards oxygen made it possible to study its combustion at temperatures lower than were previously available, and the small variations between reactions 6 and 7 were found to be emphasized. Thus in the present instance the acid and ketone are seen to occupy a much more prominent place in the products than at 307° C.

TABLE 7. THE REACTION OF 100 MM.  $C_9H_{12}$  + 150 MM.  $O_2$  AT  $307^\circ C$ .  
TOTAL PRESSURE INCREMENT = 41.0 MM.

| Time of sampling from start in min. | 10   | 13.5 | 25.5 | 38   |
|-------------------------------------|------|------|------|------|
| % pressure increment                | —    | 8.0  | 84.9 | 100  |
| % $O_2$ used                        | 1.4  | 9.9  | 97.1 | 100  |
| Products in mm. at $307^\circ C$ :  |      |      |      |      |
| $CO_2$                              | 2.4  | 1.6  | 20.8 | 16.7 |
| CO                                  | 2.3  | 3.5  | 44.9 | 45.1 |
| Acid                                | 0.8  | 1.3  | 10.0 | 9.6  |
| Aldehyde                            | 1.1  | 3.5  | 21.1 | 19.3 |
| Ketone                              | 1.3  | 3.0  | 17.4 | 17.9 |
| Alcohol (secondary)                 | 18.7 | 24.6 | 6.5  | 10.3 |
| Phenol                              | 1.1  | 1.8  | 9.6  | 11.7 |
| Peroxide (1)                        | Nil  | Nil  | Nil  | Nil  |
| Peroxide (2)                        | Nil  | 0.5  | 0.7  | 0.2  |
| Peroxide (3)                        | 0.4  | 0.1  | 0.3  | Nil  |

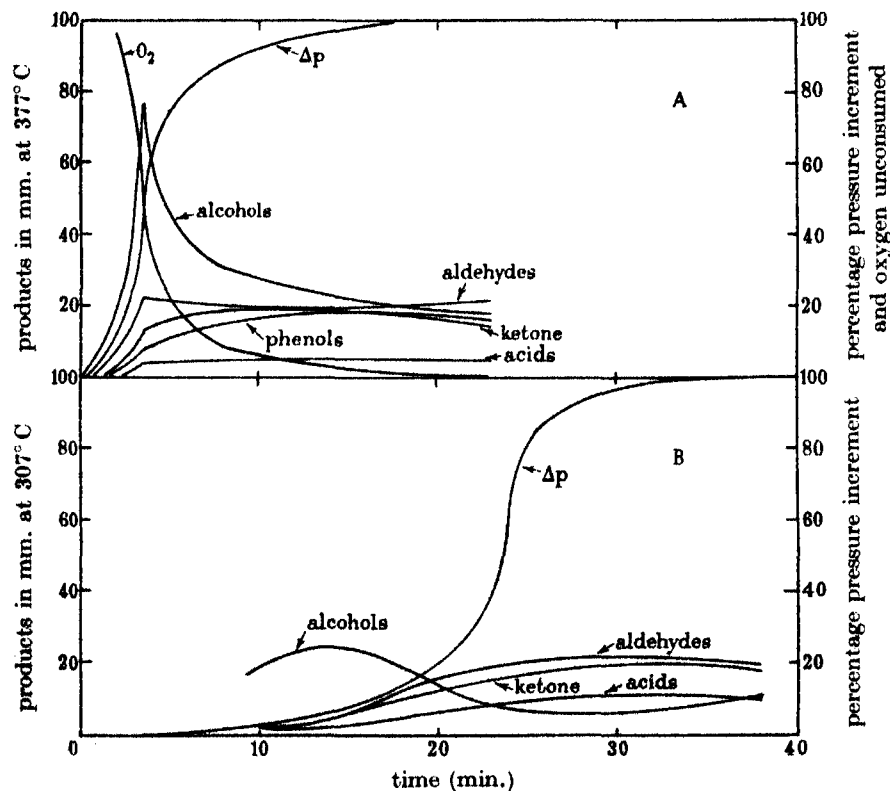


FIGURE 1A. 130 mm.  $C_9H_{12}$  + 170 mm.  $O_2$  at  $377^\circ C$ .  
FIGURE 1B. 100 mm.  $C_9H_{12}$  + 150 mm.  $O_2$  at  $307^\circ C$ .

The peroxides, too, are more in evidence, and peracids were detected for the first time in this reaction. In the latter connexion it was observed that in the main combustion period a constituent was present in the products which liberated iodine from neutral potassium iodide, not immediately, but entirely within 30 min. Thus in column 3, table 8, the 5.5 mm. of peroxide (1) indicated consists of 2.2 mm. which liberated iodine immediately and 3.3 mm. which caused slow liberation in neutral solution. At a later stage in the reaction, corresponding to an oxygen consumption of 89.7%, the figures were respectively 1.7 and 4.2 mm. In figure 2*b* the courses of these constituents are indicated separately by broken lines.

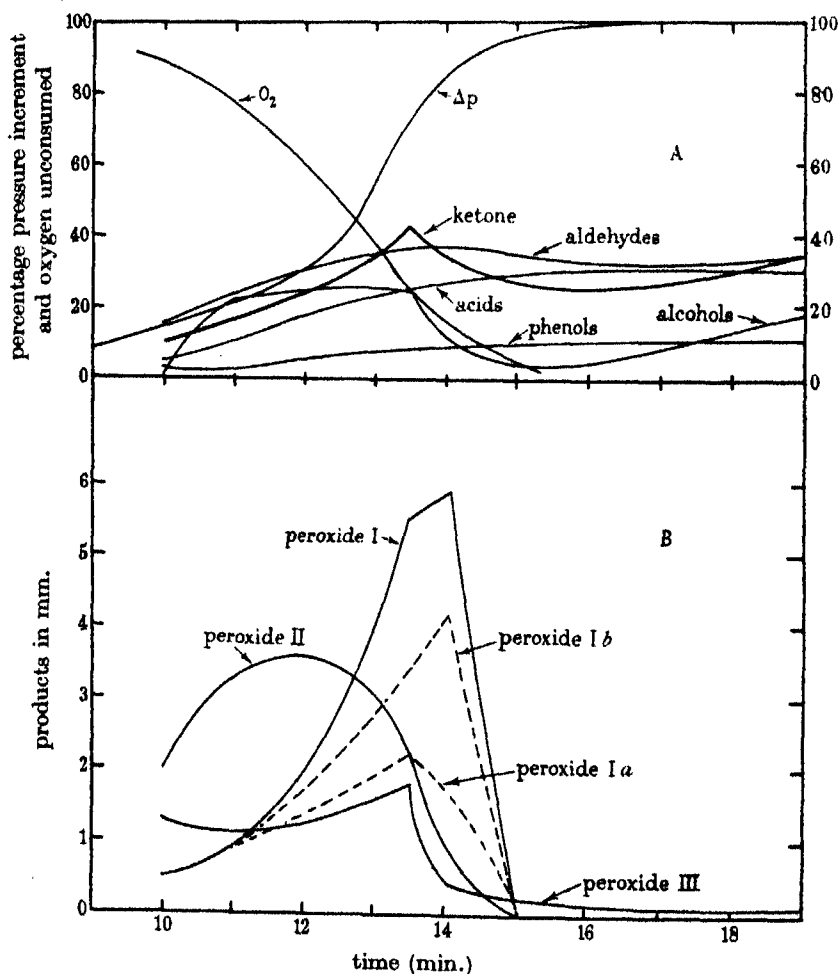


FIGURE 2. 210 mm.  $C_9H_{12}$  + 240 mm.  $O_2$  at  $277^\circ C$ . A, major products; B, peroxides.

Ethylene, acetylene, paraffins and hydrogen were present in traces in the products.

TABLE 8. THE REACTION OF 210 MM.  $C_9H_{12}$  + 240 MM.  $O_2$  AT  $277^\circ C$ .  
TOTAL PRESSURE INCREMENT = 44.0 MM.

|                                     |          |          |          |      |      |
|-------------------------------------|----------|----------|----------|------|------|
| Time of sampling from start in min. | 10       | 11       | 13.5     | 15   | 19   |
| % pressure increment                | 14.6     | 21.8     | 72.3     | 96.0 | 100  |
| % $O_2$ used                        | 10.4     | 20.9     | 72.3     | 99.8 | 100  |
| Products in mm. at $277^\circ C$ :  |          |          |          |      |      |
| $CO_2$                              | 4.9      | 9.0      | 34.1     | 45.4 | 55.9 |
| CO                                  | 4.2      | 10.0     | 39.8     | 57.4 | 62.1 |
| Acid                                | 5.6      | 9.8      | 25.8     | 29.4 | 30.3 |
| Aldehyde                            | 15.5     | 23.7     | 36.8     | 34.6 | 33.4 |
| Ketone                              | 10.1     | 15.3     | 43.2     | 26.2 | 34.1 |
| Alcohol (secondary)                 | 0.8      | 22.0     | 24.9     | 3.4  | 17.7 |
| Phenol                              | 3.0      | 2.5      | 8.6      | 10.1 | 10.7 |
| Peroxide (1)                        | 0.5      | 0.9      | 5.5      | Nil  | Nil  |
| Peroxide (2)                        | 2.0      | 3.5      | 2.2      | Nil  | Nil  |
| Peroxide (3)                        | 1.3      | 1.1      | 1.8      | 0.2  | 0.1  |
| $C_2H_4$                            | Not est. | Not est. | Not est. | 1.2  | 1.6  |
| $H_2$                               | "        | "        | "        | 0.7  | 0.5  |
| $CH_4$                              | "        | "        | "        | 1.9  | 2.2  |

*Characteristics of slow combustion reactions of benzene and its alkyl derivatives*

In order to summarize the common characteristics of the foregoing reactions it is convenient to divide them into two classes, as follows:

(1) "High-temperature reactions", taking place above  $370^\circ C$ , in which the influence of the low-temperature combustion system is not evident kinetically (cf. Part IV).

(2) "Low-temperature reactions", occurring in the region  $300$ – $320^\circ C$ , in which the kinetic characteristics of the low-temperature system attain greatest prominence.

*High-temperature reactions.* In this category are included reactions 1, 2, 4 and 6, and reference to the corresponding analytical results will show that they have several features in common. Thus the oxides of carbon, the acids and the phenols, accumulate smoothly throughout the combustion, their rate of formation being invariably proportional both to the rate of oxygen consumption and to the rate of pressure development in the reacting medium. There is no particular analogy between the acids formed in the combustion of benzene (which are aliphatic) and those

resulting from the oxidation of its alkyl derivatives (which are principally aromatic). Regarding the ketones, full data are available only in reaction 6, from which it appears that the courses of the acid and phenol concentrations are closely followed in this case, but with a tendency to decline in the later stages of the combustion.

The alcohols and aldehydes are characterized as being the least stable of the major products. Thus the alcohol concentration rises to a peak very early in the reaction after which its rate of disappearance bears an approximate relationship to the amount of oxygen remaining in the medium. The aldehyde concentration follows a somewhat similar course, but its growth and decline are less rapid and the peak is reached at the end rather than at the beginning of the period of maximum reaction velocity.

On comparing reactions 2, 4 and 6, it is seen that the initial development of the alcohol concentration becomes more marked on proceeding from toluene to propylbenzene, whilst the progression of the aldehyde remains unchanged. Both intermediates, however, occupy an increasingly prominent place in the products as the series is ascended, whilst phenolic constituents become less in evidence. Since the acid is not greatly affected meanwhile, it is clear that the effect of lengthening the hydrocarbon side-chain is to attract oxygen attack away from the nucleus. There is no evidence, however, that ring rupture is in any way diminished, for the production of the oxides of carbon proceeds with equal facility throughout the series.

Although traces of peroxide (2) are usually present, appreciable quantities of peroxides as a whole are never detected in high-temperature reactions, and there is no evidence of the occurrence of hydrogen and hydrocarbons other than in very small amounts.

*Low-temperature reactions.* This class includes reactions 3, 5 and 7, and on consulting the corresponding experimental results it is somewhat surprising to find, in view of the important kinetic differences involved, that little contrast with the high-temperature series is noticeable. Thus the courses of the oxides of carbon, acids, phenols and, generally speaking, the ketones too, are precisely similar. In other cases, however, small but significant differences are observed. Thus the alcohol concentration now attains a maximum value at an even earlier stage in the reaction, and the subsequent decline does not become rapid until the end of the main combustion period is reached. The aldehyde peak, on the other hand, is achieved somewhat later at the lower temperature, and the ensuing fall is slower.

Peroxides other than peracids are formed in appreciable amounts in reactions of this class, the peroxide (2) being generally the more prominent:

its concentration increases to a maximum value early in the reaction and thereafter falls steadily to a negligible figure. At the same time, the peroxide (3) shows two "peaks", one at the beginning and one at the end of the main combustion period.

As in the case of the high-temperature reactions, lengthening the hydrocarbon side-chain has little effect on the survival of acids, CO and CO<sub>2</sub> in the products. The alcohols and aldehydes, however, again assume an increased importance at the expense of the phenols, but in the present instance it is the aldehyde which is the more affected. The survival of peroxides, too, seems to be favoured at low temperatures by the increased size of the hydrocarbon molecule.

From a kinetic point of view, reaction 8 cannot, strictly, be included in the present class, although the progression of the products in this case shows only slight abnormalities. Thus, the ketone is seen to be somewhat stabilized and tends rather to increase than to decline in the closing stages of the combustion. An interesting feature is the appearance in the products of a certain amount of peracid, which has not previously been encountered in the present investigation: the concentration of this intermediate is seen to attain a maximum value at the end of the main reaction period.

The influence of the reaction temperature on the survival of intermediates has previously been considered in investigating reactions at high pressures. The conclusions then reached are supported by the present experiments, which indicate that a decrease in temperature generally promotes the survival of "intermediate" as contrasted with "final" products; and at very low temperatures, the appearance of acids and ketones is particularly favoured (cf. reaction 8). The ratio CO/CO<sub>2</sub> always decreases with the lowering of the reaction rate, whether by change of temperature or of pressure.

*Reaction 9.* 150 mm. *n*-propylbenzene + 200 mm. oxygen at 314° C.

In the course of this reaction a mild but well-defined cool-flame was propagated 2 min. 20 sec. after the admission of the mixture to the heated vessel. A vigorous combustion ensued without further flame formation, during which the residual oxygen was entirely consumed. The passage of the cool-flame did not cause any abnormal increase in the rate of consumption of oxygen, and apart from the transitory pressure pulse the rate of pressure development also appeared unaffected. The ratio of the final pressure increment to the initial pressure was not greater than that of a slow combustion at the same temperature.

Comparison with reaction 7 shows that the final products of combustion

are very similar, a conclusion that was also noted in the case of the methyl derivatives of benzene in Part III. It is not possible, moreover, to point to any abnormal feature in the curves of figure 3a, which depict the progression of the more prominent products during the combustion.

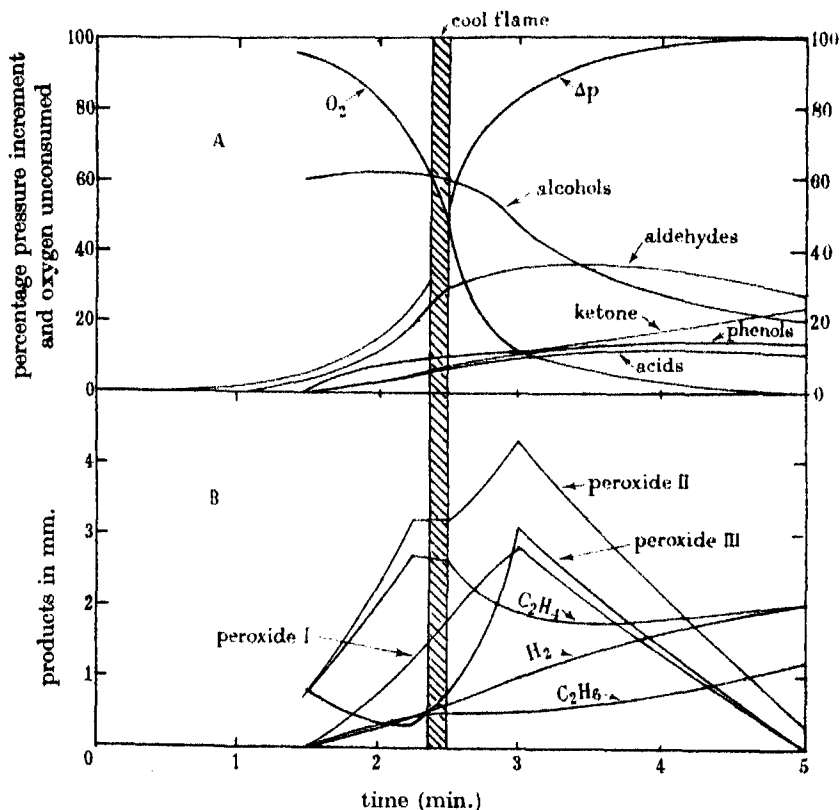


FIGURE 3. 150 mm.  $C_6H_{12}$  + 200 mm.  $O_2$  at  $314^\circ C$ . A, major products; B, peroxides.

It is only when the peroxides are considered that significant discrepancies become apparent. Thus the total survival of peroxides is considerably greater than in the corresponding isothermal reaction (7), in which peracids do not appear at all. The progression of the latter product is normal, however, judged by the results of reaction 8, the maximum concentration being attained as the rate of reaction first begins to decrease; the peroxide (3), also, shows the two maxima which have already been described as characteristic of slow combustions in the low-temperature zone. It is with the peroxide (2) that the important difference is observed, for although this intermediate normally reaches its peak early in the isothermal reaction it now continues to increase throughout the whole of

the main combustion period but with a definite "setback" during the passage of the cool-flame. It appears, therefore, that the propagation of the cool-flame is conditioned by the concentration of this intermediate, which by its disappearance causes the ignition to take place. The small amount of product concerned makes it difficult to say from the present experiments whether the peroxide is consumed by combustion or by spontaneous decomposition, though the former is the more likely.

TABLE 9. THE REACTION OF 150 MM.  $C_9H_{12}$  + 200 MM.  $O_2$  AT  $314^\circ C$ . TOTAL PRESSURE INCREMENT = 54.7 MM. COOL-FLAME PROPAGATED AFTER 3.5 MIN.

|                                     |      |          |      |      |      |
|-------------------------------------|------|----------|------|------|------|
| Time of sampling from start in min. | 1.5  | 2.25     | 2.5  | 3    | 5    |
| % pressure increment                | 5.5  | 24.0     | 52.3 | 83.0 | 100  |
| % $O_2$ used                        | 4.5  | 29.4     | 51.8 | 89.5 | 100  |
| Products in mm. at $314^\circ C$ :  |      |          |      |      |      |
| $CO_2$                              | 1.6  | 6.5      | 17.3 | 28.2 | 33.3 |
| CO                                  | 1.9  | 10.9     | 27.0 | 49.4 | 62.7 |
| Acid                                | 0.7  | 4.3      | 7.1  | 10.2 | 11.7 |
| Aldehyde                            | 3.8  | 18.9     | 29.6 | 35.5 | 27.5 |
| Ketone                              | Nil  | 9.2      | 11.4 | 14.1 | 22.7 |
| Alcohol (secondary)                 | 60.2 | 61.8     | 60.5 | 47.0 | 19.9 |
| Phenol                              | 1.7  | 4.5      | 8.0  | 11.1 | 13.2 |
| Peroxide (1)                        | Nil  | 1.2      | 1.8  | 2.8  | Nil  |
| Peroxide (2)                        | 0.8  | 3.2      | 3.2  | 4.3  | 0.3  |
| Peroxide (3)                        | 0.8  | 0.3      | 0.7  | 3.1  | Nil  |
| $C_2H_4$                            | 0.8  | 2.7      | 2.6  | 1.9  | 2.0  |
| $H_2$                               | Nil  | Not est. | 0.6  | 1.0  | 2.0  |
| $C_3H_6$                            | Nil  | „        | 0.5  | 0.5  | 1.2  |

*The influence of the history of the vessel on the reaction products*

It has already been recorded that the first combustion of a given aromatic hydrocarbon is invariably abnormal kinetically, as judged by subsequent reactions in the same vessel. It is found, too, that there is a corresponding abnormality in the survival of products under these conditions. Thus, in a "first reaction", the proportions of phenol, alcohol and aldehyde are generally slightly increased at the expense of the acid, whilst the corresponding ratio  $CO/CO_2$  tends to be erratic. As a result, the course of pressure development also becomes abnormal.

Two "first reactions" are included in the present series (see table 5, column 4 and table 7, column 4), and in both cases the figures given for alcohol, aldehyde, phenol and carbon monoxide are probably slightly too high, the concentration of acid being correspondingly diminished.



## DISCUSSION

In order to appreciate the significance of the results of the present investigation, it is important that the kinetic background of the several combustion reactions considered should be kept clearly in mind, and in table 10 the appropriate data of this character are summarized, based on the conclusions reached in Part IV. It will be observed that the "high-temperature reactions" (excepting in the case of benzene) are located on the first turning-point of the corresponding  $\log t_{20-60} - 1/T$  curve, and that the "low-temperature reactions" (excepting no. 8) are on the second turning-point. Reactions 1 and 8 are situated in regions of temperature in which the kinetics appear to be fairly regular.

TABLE 10. SUMMARY OF DATA FOR REACTIONS 1-9

| Reaction                        | ... | ... | 1        | 2        | 3        | 4           | 5           | 6           | 7           | 8           | 9           |
|---------------------------------|-----|-----|----------|----------|----------|-------------|-------------|-------------|-------------|-------------|-------------|
| Hydrocarbon                     |     |     | $C_6H_6$ | $C_7H_8$ | $C_7H_8$ | $C_8H_{10}$ | $C_8H_{10}$ | $C_9H_{12}$ | $C_9H_{12}$ | $C_9H_{12}$ | $C_9H_{12}$ |
| Temperature °C                  |     |     | 487      | 408      | 314      | 381         | 314         | 377         | 307         | 277         | 314         |
| $n$ (total concentration)       |     |     | 1.9      | 2.0      | 3.0      | 2.1         | 2.8         | 3.0         | 4.2         | 1.3         | —           |
| $n$ (oxygen concentration)      |     |     | 0.2      | 1.0      | 1.3      | 0.3         | 0.5         | 0           | 0.6         | 0.1         | —           |
| $n$ (hydrocarbon concentration) |     |     | 1.7      | 0.8      | 1.6      | 2.0         | 2.3         | 3.0         | 3.6         | 1.2         | —           |
| $E$ in kg.cal./g.mol.           |     |     | 70       | *Dec.    | *Inc.    | Dec.        | Inc.        | Dec.        | Inc.        | 58          | —           |
| Ratio $\Delta p : p$ (final)    |     |     | 0.198    | 0.123    | 0.048    | 0.225       | 0.127       | 0.235       | 0.164       | 0.098       | 0.156       |
| Ratio $CO : CO_2$ (final)       |     |     | 2.65     | 1.90     | 0.97     | 2.52        | 2.16        | 2.94        | 2.70        | 1.11        | 1.88        |
| % $CO_2$ in final products      |     |     | 17.1     | 11.0     | 12.7     | 7.8         | 7.1         | 6.8         | 5.7         | 11.2        | 8.2         |
| % $CO$ in final products        |     |     | 45.4     | 20.8     | 12.3     | 19.8        | 15.4        | 20.1        | 15.3        | 12.5        | 15.4        |

\* Decreasing and increasing.

It was shown in Part IV that a recent modification of the theory of the two-stage process, due to Belov and Neumann (1938) and to Kane (1938), is applicable to the combustion of aromatic hydrocarbons. In the light of this theory, it may be said that reaction 1 typifies the direct process  $A \rightarrow B$  in the case of benzene, and reaction 8 the two-stage process  $A \rightarrow B \rightarrow C$  in the case of propylbenzene, whilst other reactions are composed of the two together, one or the other predominating according to conditions of temperature.

It has been shown previously, and is further emphasized in table 10, that the temperature exercises a profound effect on the kinetics of combustion reactions below 400° C, but the present investigation indicates that the corresponding variations in the products are less obvious, and may be summarized as follows:

Reduction of the reaction temperature causes:

- (i) lowering of the  $\text{CO}/\text{CO}_2$  ratio, and consequently  $\Delta p/p$ ,
- (ii) an increase in the ratio of "intermediate" to "final" products,
- (iii) increased survival of peroxides, acids and perhaps ketones; together with decreased survival of alcohols and phenols,
- (iv) slower accumulation of alcohol and improved persistence; with more rapid accumulation of aldehyde.

Speaking generally, the reaction products can be divided into two classes:

(i) Stable products, which accumulate steadily throughout the reaction, at a rate which is proportional to the rate of consumption of oxygen: they comprise steam, the oxides of carbon, acids and phenols.

(ii) Unstable products, whose concentration reaches a maximum value more or less early in the reaction: these include all classes of peroxide, alcohols and aldehydes.

The position of the ketones in this scheme is not definite and they must be regarded as intermediates.

In attempting to interpret the analytical results relative to peroxidic substances a twofold difficulty is encountered. In the first place little direct information is available regarding the chemistry of aromatic peroxides, and it is necessary to assume analogy with the aliphatic series so far as side-chain derivatives are concerned. The second difficulty lies in the lack of analytical methods to distinguish the several types of peroxide one from another. The method of Clover and Houghton (1904) employed in the present work distinguishes peroxide (1) fairly well as peracidic, but the distinction between classes (2) and (3) is somewhat arbitrary. It is probable that alkyl hydroperoxides and hydrogen peroxide are the chief constituents in this section, since aldehyde peroxides are not likely to be formed in the reactions under consideration, although they may occur in the analytical solutions by the interaction of free aldehyde and hydrogen peroxide. Peroxide (2), then, may be taken to consist of  $\text{H}_2\text{O}_2$  and a certain amount of alkyl hydroperoxide, while peroxide (3) comprises the residue of the latter. Under standardized conditions, such as obtained in the present experiments, a proportionality may be tentatively assumed between peroxide (3) and the total amount of alkyl hydroperoxide. The fact that the concentration of the former class invariably shows two peaks in the course of a slow combustion suggests that two hydroperoxides, at least, are concerned. The first of these (I) may be assumed to accumulate rapidly in the early stages of the reaction and then to disappear; while the other (II) reaches its maximum concentration at the end of the main reaction period.

The hydroperoxide (I) has the characteristics of an early combustion product and probably corresponds with the initial hydrocarbon. The second substance, on the other hand, is evidently a later intermediate and is thought to correspond with the next lower member of the series. Thus, propylbenzene would yield phenylpropyl hydrogen peroxide (I) and phenylethyl hydrogen peroxide (II).

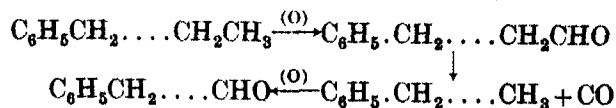
Certain peroxides, such as those of the class  $ROOR'$ , do not liberate iodine from potassium iodide without a catalyst and have not been estimated in the present investigation. Such substances, although they could scarcely result from the main combustion process, might be formed by the mutual interaction of chains.

The main combustion reaction may be assumed to involve alcohols, aldehydes, ketones, acids and phenols, since these are common to all reaction temperatures. In considering the combustion process, attention must be given separately to side-chain and nuclear reactions. The addition of an alkyl group to the benzene ring appears to facilitate oxidation by activation of the nucleus and because it is itself easily attacked. Nuclear activity must in all cases be concerned with the ultimate cleavage of the ring, and since when this occurs straight chain products must result, both nuclear and side-chain reactions resolve into an aliphatic problem.

#### *Side-chain oxidation*

The question of side-chain oxidation is subject to further subdivision according to whether reaction is at the end carbon atom remote from the nucleus or at some intermediate point. The evidence so far indicates that the higher alkyl derivatives of benzene are primarily attacked at the  $\alpha$ -carbon atom, but this is by no means conclusive owing to the instability of the higher aldehydes and acids, and the insensitivity of the appropriate analytical tests.

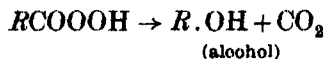
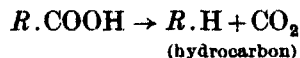
Oxidation of the end carbon atom presumably results in the formation of a primary alcohol, aldehyde and acid although, owing to the instability of the aldehydes it is possible that the reaction would not go to the acid stage. Rather would the combustion proceed by degradation thus:



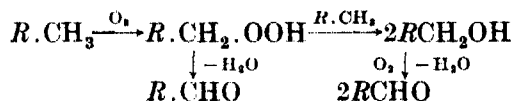
and so on, finally forming benzene.

There are other feasible mechanisms of degradation, however, which can play a part, and probably do so to varying extents. Thus, for example,

we have the decomposition of carboxylic acids and peracids forming a link with the next lower series:

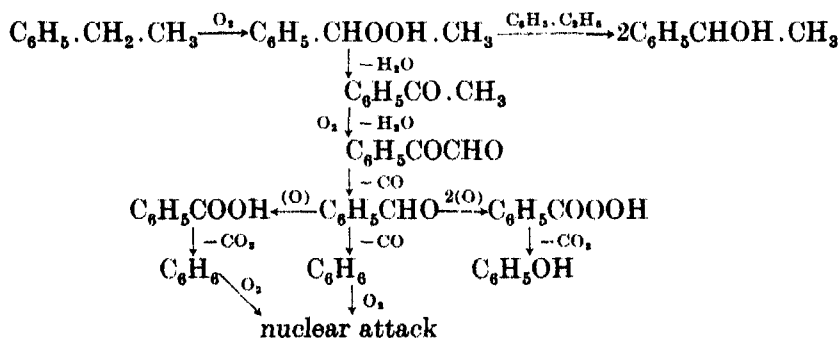


In the oxidation of toluene, the peak in the aldehyde concentration is generally attained much later than that of the alcohol, although benzaldehyde is much more readily oxidized than benzyl alcohol. Both, however, are preceded by the first maximum in the curve for peroxide (3). These results suggest the following general scheme for the formation of an aldehyde from the corresponding hydrocarbon:



In this scheme the alcohol is not in the main course of the combustion but is formed when the hydroperoxide encounters an oxidizable molecule.

Oxidation at the  $\alpha$ -carbon atom results in the formation of a secondary alcohol and a ketone, and the mechanism is likely to be analogous with that of the primary alcohol-aldehyde process, an alkyl hydroperoxide intervening. After the ketone stage is reached, the end carbon atom is probably attacked and degradation through ketonic aldehydes occurs, resulting finally in the formation of benzaldehyde, after which the reaction proceeds to benzene as before. In the case of ethylbenzene, then, we have the following scheme:



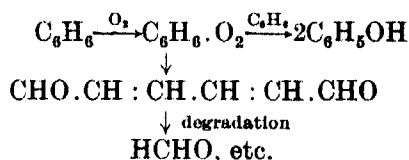
#### Nuclear oxidation

According to the process of side-chain oxidation suggested, the combustion of all aromatic hydrocarbons is resolved ultimately into an attack

on the benzene nucleus after a more or less prolonged degradation of the alkyl groups. The stability of phenolic bodies in the process of combustion, not only of benzene but also of its derivatives, is a somewhat surprising feature and suggests that these intermediates are not directly involved in ring cleavage. Their relationship to the main combustion process appears to be analogous to that of benzoic acid in side-chain oxidation.

The fact that practically no aromatic compounds other than the monohydric phenol are formed in the combustion of benzene indicates that nuclear rupture is of early occurrence, the resulting aliphatic compound being rapidly degraded as would be expected under such conditions of temperature. Consequently only small amounts of aliphatic substances survive.

It is thought that the primary oxygen attack on benzene results in the formation of an active complex which may or may not be of the nature of a peroxide. This, by encounter with a molecule capable of being oxidized, may be stabilized as phenol. Alternatively it may decompose, by ring rupture, to a higher aliphatic aldehyde, which is rapidly degraded in the oxidizing atmosphere to formaldehyde, formic acid, oxides of carbon and steam (cf. Pope, Dykstra and Edgar 1929; Newitt and Thornes 1937):



In the schemes of combustion outlined above it will be seen that in general carbon monoxide results from degradation at the aldehyde stage and carbon dioxide from the decomposition of acids and peracids. Furthermore, there seem to be no other important sources of these products, so that the ratio of CO/CO<sub>2</sub> may be taken as some indication of course of the combustion under varying conditions.

Reference to the data of table 10 shows that in the present experiments the CO/CO<sub>2</sub> ratio increases systematically in the series toluene → ethylbenzene → propylbenzene, the figure for benzene being perhaps rather higher than that for toluene under comparable conditions. This variation is seen to be due mainly to changes in the amount of carbon dioxide formed in corresponding reactions. The ratio CO/CO<sub>2</sub> is also increased by an increase in the rate of reaction, whether this be brought about by an increase of pressure or temperature, and the effect is mainly dependent upon the amount of carbon monoxide formed, except in very slow reactions

(cf. no. 8) when an unusually high concentration of carbon dioxide results. It has already been observed (see Part IV) that the ratio  $\text{CO}/\text{CO}_2$  in the low-temperature combustion region is higher than would be expected by extrapolation of the high-temperature relationship between  $\text{CO}/\text{CO}_2$  and  $t$ .

At high temperatures,  $\text{CO}/\text{CO}_2$  is upwards of 2, showing that in general the process of degradation is predominantly via the aldehydes. On decreasing the temperature, however, the course of reaction moves towards the acid stage reducing the amount of CO formed. At very low temperatures, when peracids are found in the products, the amount of  $\text{CO}_2$  formed is substantially increased by their decompositions.

In the series toluene  $\rightarrow$  ethylbenzene  $\rightarrow$  propylbenzene the average stability of the aldehydes involved decreases, with a resulting increase in the  $\text{CO}/\text{CO}_2$  ratio.

It must be emphasized that the mechanisms outlined are purely schematic and make no attempt at a detailed explanation of the processes involved, nor are they sufficiently complete for kinetic treatment. It has been shown, moreover, that some at least of the steps involved are chain reactions, though to what extent this is the case cannot be determined at present. Finally, it must be pointed out that steps involving oxidation do not necessarily require the intervention of molecular oxygen. In the presence of active oxidizing intermediates such as are indicated, this is unnecessary, and under these conditions oxidation reactions can be expected to occur which could not be brought about at the same rate by free oxygen.

Turning now from the examination of the main combustion process, let us consider the significance of the two-stage reaction  $A \rightarrow B \rightarrow C$  and the mechanism by which the active intermediate  $B$  gives rise to cool-flames.

The occurrence of an active intermediate in the low-temperature combustion of hydrocarbons has been recognized in general terms for several years, and a number of suggestions have been made as to its identity. Thus Ubbelohde (1935), on spectrographic and chemical evidence, favoured an alkyl peroxide, whilst Neumann and Aivazov (1936), as the result of analytical experiments with pentane, suggested that both aldehydes and peroxides were involved. More recently, however, Newitt and Thornes (1937) suggested in connection with propane that the propagation of a cool-flame depends upon the attainment of a critical concentration of higher aldehydes, without the intervention of peroxides. Moreover, they confirmed an observation of Pease and Munro (1934), that by coating the interior of the reaction vessel with potassium chloride, the peroxide content of the medium was much reduced without materially affecting the reaction

rate, and found, in addition, that in such circumstances cool-flames could still be propagated.

The present results, relating to a cool-flame reaction of propylbenzene (see figure 3) are comparable with the data for propane in that the total peroxide concentration reaches its peak *after* the passage of the cool-flame, and during the most rapid stage of the subsequent flameless combustion. There is no indication, however, of the accumulation of a critical amount of aldehyde prior to the propagation of the flame.

It is particularly unfortunate that one of the clearest indications of reaction 9 is connected with peroxide (2), the most complex class of intermediates. The results do point to a phenylalkyl hydroperoxide, however, as the active intermediate *B*, in which connexion attention is directed to the following experimental facts:

(1) The concentration of peroxide (2), which normally attains a maximum value in the early stages of a low-temperature slow combustion, is temporarily arrested in its ascent by the passage of the cool-flame, subsequently continuing to rise.

(2) The concentration of peroxide (2) is at a higher level in the cool-flame reaction than in a slow combustion at a lower temperature, in spite of the fact that the survival of this intermediate in isothermal reactions is shown to be favoured by a decrease in temperature.

(3) Although the early part of the curve for peroxide (3) in figure 3 is normal, the second peak is unexpectedly high as judged by reaction 8.

(4) Although the ratio  $\text{CO}/\text{CO}_2$  is normally increased slightly by an increase of initial pressure, the ratio is less in the cool-flame reaction than in a slow combustion at a similar temperature and the change is due entirely to an increase in the amount of carbon dioxide formed (see table 10).

(5) Peracids appear to have no connexion with the cool-flame process.

Although the results as a whole point to a phenylalkyl hydroperoxide as the primary cause of the cool-flame, sufficient data are not available to decide whether the process itself is one of combustion or spontaneous decomposition. In view of the small amount of intermediate involved, as shown by the analytical evidence, the fact that the passage of the cool-flame causes no appreciable increase in the rate of oxygen consumption or pressure rise can scarcely be regarded as conclusive. It would seem judicious then to defer decision on this point until the cool-flame process itself has been investigated kinetically.

According to the theory of the two-stage process, an important function of the intermediate *B* is to promote the main combustion process. A hydro-

peroxide would be entirely capable of filling the role of oxidizing agent and several appropriate branching chain mechanisms could be suggested.

The author is indebted to Dr D. M. Newitt for his close interest in this investigation, and to the Department of Scientific and Industrial Research for a grant, with the aid of which the work here described was carried out.

#### REFERENCES

- Belov and Neumann 1938 *C.R. Acad. Sci. U.R.S.S.* **18**, 333.  
Clover and Houghton 1904 *Amer. Chem. J.* **32**, 43.  
Kane 1938 *Proc. Roy. Soc. A*, **167**, 62.  
Neumann and Aivazov 1936 *Acta Physicochim.* **4**, 575.  
Newitt and Burgoyne 1936 *Proc. Roy. Soc. A*, **153**, 448.  
Newitt and Thornes 1937 *J. Chem. Soc.* pp. 1656, 1669.  
Pease and Munro 1934 *J. Amer. Chem. Soc.* **56**, 2034.  
Pope, Dykstra and Edgar 1929 *J. Amer. Chem. Soc.* **51**, 1875, 2203.  
Ubbelohde 1935 *Proc. Roy. Soc. A*, **152**, 354.
-





## INDEX TO VOLUME 175 (A)

- Alkyd resins, dielectric loss (Pelmore and Simons), 468.  
 Alloys, precipitation (Nabarro), 519.  
 Ammonia photolysis (Birse and Melville), 187.  
 Andrade, E. N. da C. and Chow, Y. S. The glide elements of body-centred cubic crystals, with special reference to the effect of temperature, 290.  
 Atomic hydrogen, reaction (Birse and Melville), 164.
- Banwell, C. J. and Farr, C. C. Further investigations of the velocity of propagation of light *in vacuo* in a transverse magnetic field, 1.  
 Barium, thermal ionization (Srivastava), 26.  
 $\beta$ -ray spectrum, radium E (Neary), 71.  
 Birse, E. A. B. and Melville, H. W. The photolysis of ammonia, 187.  
 Birse, E. A. B. and Melville, H. W. The reaction of atomic hydrogen with hydrazine, 164.  
 Booth, F. and Wilson, A. H. Radiative processes involving fast mesons, 483.  
 Bromine, hyperfine structure in the arc spectrum (Tolansky and Trivedi), 366.  
 Browne, B. C. and Bullard, E. C. Comparison of the acceleration due to gravity at the National Laboratory, Teddington and the Bureau of Standards, Washington, D.C., 110.  
 Bullard, E. C. *See* Browne and Bullard.  
 Burgoyne, J. H. The combustion of aromatic and alicyclic hydrocarbons. V. The products of combustion of benzene and its monoalkyl derivatives, 539.
- Chalmers, B. Crystal boundaries in tin, 100.  
 Chow, Y. S. *See* Andrade and Chow.  
 Cold-worked polycrystalline alpha-iron (Mullins and Rodgers), 422.  
 Combustion of aromatic and alicyclic hydrocarbons. V (Burgoyne), 539.  
 Cosmic radiation photon component and its absorption coefficient (Jánossy and Rossi), 88.  
 Crystal boundaries in tin (Chalmers), 100.
- Davison, B. and Rosenhead, L. Some cases of the steady two-dimensional percolation of water through ground, 346.  
 Decarboxylation in solution kinetics (Johnson and Moelwyn-Hughes), 118.  
 Dielectric capacity of electrolytes in mixed solvents (Mason and Shutt), 234.  
 Drinkwater, J. W., Richardson, Sir Owen and Williams, W. E. Determination of the Rydberg constants,  $e/m$ , and the fine structures of  $H_\alpha$  and  $D_\alpha$  by means of a reflexion echelon; corrigenda, 345.
- Experiments with a velocity-spectrometer for slow neutrons (Fertel, Gibbs, Moon, Thomson and Wynn-Williams), 316.
- Farr, C. C. *See* Banwell and Farr.  
 Fertel, G. E. F., Gibbs, D. F., Moon, P. B., Thomson, G. P. and Wynn-Williams, C. E. Experiments with a velocity-spectrometer for slow neutrons, 316.

- Fox, J. J. and Martin, A. E. Investigations of infra-red spectra. Determination of C-H frequencies ( $\sim 3000 \text{ cm}^{-1}$ ) in paraffins and olefins, with some observations on "polythenes", 208.
- Fröhlich, H. and Nabarro, F. R. N. Orientation of nuclear spins in metals, 382.
- Gibbs, D. F. *See* Fertel and others.
- Glide elements of body-centred cubic crystals (Andrade and Chow), 290.
- Gravity acceleration at Teddington and Washington (Browne and Bullard), 110.
- Harris, E. J. The thermal explosion of diethyl peroxide, 254.
- Havelock, T. H. The pressure of water waves upon a fixed obstacle, 409.
- Hinshelwood, C. N. *See* Smith and Hinshelwood.
- Infra-red spectra. C-H frequencies in paraffins and olefins (Fox and Martin), 208.
- Jánossy, L. and Rossi, B. On the photon component of cosmic radiation and its absorption coefficient, 88.
- Johnson, P. and Moelwyn-Hughes, E. A. The kinetics and decarboxylation in solution, 118.
- Jones, T. T. and Melville, H. W. The determination of the lifetime of active polymeric molecules, 392.
- Kannuluik, W. G. On the thermal conductivity of gases by a relative method with an application to deuterium, 36.
- Martin, A. E. *See* Fox and Martin.
- Mason, W. A. and Shutt, W. J. The dielectric capacity of electrolytes in mixed solvents: ion association in solutions of magnesium sulphate, 234.
- Melville, H. W. *See* Birse and Melville.
- Melville, H. W. *See* Jones and Melville.
- Moelwyn-Hughes, E. A. *See* Johnson and Moelwyn-Hughes.
- Moon, P. B. *See* Fertel and others.
- Mullins, L. and Rodgers, J. W. An investigation of cold-worked polycrystalline alpha iron, 422.
- Nabarro, F. R. N. The strains produced by precipitation in alloys, 519.
- Nabarro, F. R. N. *See* Fröhlich and Nabarro.
- Neary, G. J. The  $\beta$ -ray spectrum of radium E, 71.
- Nuclear spins in metals, orientation (Fröhlich and Nabarro), 382.
- Pellaw, A. and Southwell, R. V. Relaxation methods applied to engineering problems. VI. The natural frequencies of systems having restricted freedom, 262.
- Pelmore, D. R. and Simons, E. L. The behaviour of polar molecules in solid paraffin wax, 253.
- Pelmore, D. R. and Simons, E. L. Dielectric loss in simple alkyd resins, 468.
- Percolation of water through ground (Davison and Rosenhead), 346.
- Pickles, A. T. and Sucksmith, W. A magnetic study of the two-phase iron-nickel alloys, 331.
- Polar molecules in solid paraffin wax (Pelmore and Simons), 253.
- Polymeric molecules, lifetime (Jones and Melville), 392.

- Radiative processes involving fast mesons (Booth and Wilson), 483.  
Relaxation methods applied to engineering problems, VI (Pellew and Southwell), 262.  
Richardson, Sir Owen. *See* Drinkwater and others.  
Rodgers, J. W. *See* Mullins and Rodgers.  
Rosenhead, L. The steady two-dimensional radial flow of viscous fluid between two inclined plane walls, 436.  
Rosenhead, L. *See* Davison and Rosenhead.  
Rossi, B. *See* Jánossy and Rossi.  
Rydberg constants,  $e/m$ , and the fine structure of  $H_\alpha$  and  $D_\alpha$ , corrigenda (Drinkwater and others), 345.
- Shoenberg, D. Properties of superconducting colloids and emulsions, 49.  
Shutt, W. J. *See* Mason and Shutt.  
Simons, E. L. *See* Pelmore and Simons.  
Smith, R. E. and Hinshelwood, C. N. The thermal decomposition of gaseous benzaldehyde, 131.  
Southwell, R. V. *See* Pellew and Southwell.  
Srivastava, B. N. Thermal ionization of barium, 26.  
Srivastava, B. N. Thermal transpiration of a dissociating gas, 474.  
Sucksmith, W. *See* Pickles and Sucksmith.  
Superconducting colloids and emulsions (Shoenberg), 49.
- Thermal conductivity of gases with application to deuterium (Kannuluik), 36.  
Thermal decomposition of gaseous benzaldehyde (Smith and Hinshelwood), 131.  
Thermal explosion of diethyl peroxide (Harris), 254.  
Thermal transpiration of a dissociating gas (Srivastava), 474.  
Thomson, G. P. *See* Fertel and others.  
Tolansky, S. and Trivedi, S. A. Hyperfine structure in the arc spectrum of bromine, 366.  
Trivedi, S. A. *See* Tolansky and Trivedi.  
Two-phase iron-nickel alloys, magnetic study (Pickles and Sucksmith), 331.
- Velocity of propagation of light *in vacuo* in a transverse magnetic field (Banwell and Farr), 1.  
Viscous fluid, radial flow between two inclined plane walls (Rosenhead), 436.
- Water waves, pressure upon a fixed obstacle (Havelock), 409.  
Wilkes, M. V. The theory of reflexion of very long wireless waves from the ionosphere, 143.  
Williams, W. E. *See* Drinkwater and others.  
Wilson, A. H. *See* Booth and Wilson.  
Wireless waves, reflexion (Wilkes), 143.  
Wynn-Williams, C. E. *See* Fertel and others.



# ABSTRACTS

## OF PAPERS COMMUNICATED TO THE ROYAL SOCIETY OF LONDON

In accordance with a resolution of Council, summaries or abstracts of papers are to be published as soon as practicable. The publication of such abstracts in no way indicates that the papers have been accepted for publication in any fuller form. These abstracts are issued for convenience with the "Proceedings of the Royal Society of London" but do not form a part of the "Proceedings".

---

28 MARCH 1940

---

**A study of the physical and chemical properties of the insect cuticle.** By G. FRAENKEL and K. M. RUDALL. (*Communicated by Sir William Bragg, P.R.S.—Received 4 January 1940.*)

The morphological and histological changes in the cuticle during the formation of the puparium in cyclorrhophous flies are described. The pupal contraction, resulting in the barrel shape of the puparium, is brought about by muscular action. If the central nervous system is separated from the muscles, a puparium is formed retaining the shape of the larval cuticle. During the conversion of the larval cuticle into the puparium the following physical and chemical processes take place:

(a) The arrangement of the chitin crystallites changes from random orientation in planes parallel to the surface to an arrangement in the white pupa cuticle and puparium where they lie approximately parallel to the transverse axis.

(b) In the larval and white pupa cuticles the chitin crystallites can be rotated in any direction by forces of compression or extension. This freedom of rotation is lost in the hard brown puparium.

(c) The swelling power of the puparium is very considerably less than that of larval or white pupa cuticles. In the puparium it is about the same as in purified chitin itself.

(d) The dry weight of the puparium increases to about 125 % of that of the larval cuticle.

(e) There is a marked decrease in the water content of the cuticle. This dehydration is regarded as having a chemical basis.

(f) The larval cuticle contains about 60 % chitin and the puparium about 47 % chitin. During the formation of the puparium the absolute amount of chitin remains unchanged.

It is considered that the whole of the non-chitinous substance in the larval cuticle consists of protein which is comparatively water-soluble in the larval cuticle and water-insoluble in the puparium. This protein, for which the name "insectin" is proposed, shows peculiar properties. It is characterized by high solubility in hot water and after being precipitated in trichloroacetic acid it redissolves on heating.

The hardening of the puparium can be attributed to the following: the higher degree of chitin orientation; the closer packing by dehydration of the substances which form the puparium; the increasing insolubility of the protein; the loss of swelling power in the puparium; the change from a dispersed phase of chitin in protein to a condensed chitin-protein association. According to the X-ray evidence this seems to consist of a mixed crystallization of chitin and protein.

It is not necessary to postulate the existence of special incrustations, and the term "chitinization", hitherto often used for describing the process of hardening in the insect cuticle, is misleading.

---

**Relaxation methods applied to engineering problems. VI. The natural frequencies of systems having restricted freedom.** By A. PELLEW and R. V. SOUTHWELL, F.R.S. (*Received 12 January 1940.*)

In this paper relaxation methods are applied to the difficult problem of determining the natural modes and frequencies of a system having restricted but considerable freedom (i.e. where the independent co-ordinates number six or more). A theorem published recently is used to impose lower limits on the wanted frequency, and upper limits are calculated on the basis of "Rayleigh's principle". In the "liquidation" process these upper and lower limits converge steadily, and when they have become closely coincident both the frequency and the associated mode (which "Rayleigh's principle" does not determine) are given with sufficient accuracy for all practical purposes.

An example treated in detail relates to undamped torsional vibrations or (by mathematical analogy) to transverse vibrations of a tensioned string. Concluding sections indicate some immediate extensions of the method, viz. (a) to vibrating systems which are entirely unconstrained, (b) to dissipative systems in which the damping forces (as is usual in practice) are relatively small, (c) to continuous systems, for which the method is an alternative to that given in Part IV of this series.

---

**New termite intercastes.** By A. M. ADAMSON. (*Communicated by A. D. Imms, F.R.S.—Received 15 January 1940.*)

An individual of *Nasutitermes* (*Nasutitermes*) *guayanae* (Holmgren) in the Termitidae, representing the only known termite intercaste combining intimately many important features of two castes, was found in Trinidad, B.W.I., in March 1937. The head is soldier-like in most features, but has compound eyes, ocelli and some other characters of the reproductive caste. The pronotum is intermediate between

that of the soldier and the reproductive castes; the wing-buds are somewhat like those of a reproductive nymph, except that the pigmentation approaches that of an imago.

Two soldiers of *Microcerotermes arboreus* Emerson, also in the Termitidae, with wing-buds, abnormally large vestigial eyes, and with the pronotum intermediate between those of the soldier and reproductive castes, were found in an observation colony, in Trinidad, in June 1937.

Previously reported termite intercastes appear to be merely soldiers with wing-buds in a few species of the primitive Kalotermitidae and worker-soldier intercastes in *Reticulitermes* (Rhinotermitidae) and *Nasutitermes similis* Emerson and *N. myersi* Snyder (Termitidae).

The significance of termite intercastes is discussed. They support the view of Emerson and others that the worker caste arose phylogenetically from the soldier. An explanation of the origin of the intercastes, and their relation to theories of caste determination, must await further advances in the study of the latter problem.

---

**The dielectric capacity of electrolytes in mixed solvents: ion association in solutions of magnesium sulphate.** By A. W. MASON and W. J. SHUTT. (Communicated by W. C. M. Lewis, F.R.S.—Received 16 January 1940.)

Experimental details are presented for an improved "force" method to be applied to the determination of the dielectric constants of conducting liquids. Particular attention is devoted to the method of preparation and the mode of testing of a platinized surface free from electrolytic polarization and, as far as possible, electrochemically reversible.

The dielectric properties of solutions of magnesium sulphate have been measured, at low frequency (1000 cye./sec.), over a range of dielectric constant from 37 to 110. The solvents were mixtures of dioxan and water (from 0 to 50 % dioxan) and solutions of urea in water (up to 9.0 M urea).

The experimental data may be interpreted in terms of the Bjerrum theory of ion association, after due allowance has been made both for the Debye-Falkenhagen effect of relative displacement of ion and ion atmosphere, and also for the solvent dipole saturation effect postulated by Sack. Reasonably steady values for the thermodynamic association constants ( $K_a$ ) are obtained in each solvent. The values of  $K_a$  indicate that the mean diameter of the ion pairs is not a constant, independent of the dielectric constant of the solvent; the diameter apparently falls from 5.8 Å, in 50 % dioxan, to about 3.7 Å in 9 M urea.

The degree of orientation of dipoles by the ionic charges (the Sack saturation effect) increases with falling dielectric constant of the medium. Possible reasons for these results are discussed.

This work supports the view that the behaviour of electrolytes is to be interpreted solely in terms of simple Coulomb forces; it is not necessary to invoke any specific effect due to the chemical nature of the solvent.

---



**The soft X-ray spectroscopy of solids.** By H. W. B. SKINNER. (*Communicated by A. M. Tyndall, F.R.S.—Received 25 January 1940.*)

The present paper is the first of a series which aims at the determination of the level systems of substances in the solid state, in a way as far as possible analogous to the determination of the level system of an atom by spectroscopic information on substances in the gaseous state. It is shown that, by the use of soft X-ray spectra, in the region 40–500 Å, emitted from the anticathode in an X-ray tube, this object is, to a large extent, attained in the case of elements; I hope subsequently to deal with the case of chemical compounds. The general technique for obtaining such spectra, free from contamination, is described. The effect of varying the temperature of the substance has been investigated and, in the case of a metal, is shown to be directly related to the Maxwellian distribution of the conduction electrons. Thermal expansion of the substance can also be detected spectroscopically. Several general characteristics of the level system of a solid have been established directly; in particular, the fundamental difference between the systems, metals and insulators. A discussion is given of the validity of the detailed information supplied, and the conclusion is reached that it is almost entirely reliable. Thus the experimental work also provides data for a detailed analysis of the level system of a particular solid, containing only atoms of one type, in terms of the crystal structure and of any other factors which may prove to be important.

---

**The microcoulomb experiment.** By F. EHRENHAFT. (*Communicated by A. Einstein, For.Mem.R.S.—Received 25 January 1940.*)

The present paper deals with the determination of the size and charge of single submicroscopic particles, measured in a small horizontal condenser of a diameter of approximately 8 mm. using the author's method, first stated in April 1910. To obtain the highest sensitivity solid particles (spheres) were used of an order of magnitude of  $3 \times 10^{-6}$  cm. and found charges less than that of the electron. Various objections were raised against his findings; namely, that the particles investigated were not spheres, and their density was not that of the macroscopic substance, so that his findings of charges less than the electronic charge were merely imaginary. I have succeeded in precipitating and measuring a particle after having observed it in the condenser under normal, and also very high gas, pressures. The particles were shown to be perfect spheres. A new method is indicated whereby it is possible to determine the size of submicroscopic spheres by pushing together two equal-sized spheres with a micromanipulator. The two diffraction disks overlap and render it very easy to determine the actual size. It is also possible to show that the density of each individual sphere is that of the macroscopic substance, since it can be computed easily from the velocity of fall of high gas pressures (according to Stokes's law). These two results being accurately determined, the author still found charges considerably less than the electronic charge; further, the deviations cannot be accounted for by errors of observation since the deviations are too great. The reason for using a solid substance (red amorphous selenium) and not oil, a liquid,

was in the first place that liquids evaporate and therefore do not yield correct results, and secondly, that liquid spheres are not certain to preserve their sphericity when precipitated.

Thus charges less than that of the electron are to be considered as actually existing.

It has been noted that the charge, less than the electronic as carried by a single particle, is obtained without any assumption about the atomistics (quantization) of electricity or matter. All the other methods of determining the elementary charges yield only mean values, and even those result merely from the combination with certain atomic constants, namely,  $N$ , the Avogadro number, Planck's constant  $h$ , and the electronic mass  $m$ .

---

**The thermal decomposition of gaseous benzaldehyde.** By C. N. HINSHELWOOD, F.R.S. and R. E. SMITH. (*Received 27 January 1940.*)

The thermal decomposition of benzaldehyde, which takes place predominantly according to the equation  $C_6H_5CHO \rightarrow C_6H_6 + CO$ , is homogeneous, and differs from the corresponding reaction of acetaldehyde in that it is of the first order above 100 mm., and is subject to partial inhibition by nitric oxide. The residual inhibited reaction shows a pressure dependence very like that of the normal acetaldehyde reaction. The activation energy increases as the pressure decreases.

The results can be explained by assuming the superposition of a chain reaction and of a molecular reaction. The order of the uninhibited reaction and the influence of nitric oxide at different initial pressures of benzaldehyde indicate the probable mechanism of the chain part of the decomposition, which appears to involve the decomposition of the radical  $CHO$  as an essential step.

---

**Dielectric loss in simple alkyl resins.** By D. R. PELMORE and E. L. SIMONS. (*Communicated by E. V. Appleton, F.R.S.—Received 1 February 1940.*)

The paper describes the results of measurements of dielectric losses and their variation with temperature for some simple alkyl resins prepared by the condensation of  $\alpha\omega$ -dibasic acids and  $\alpha\omega$ -glycols.

The polymers are known to consist of long chains of the form



It is found that when  $x$  and  $y$  are both even, the maximum value of dielectric loss is much smaller than when one or both of them are odd. This is attributed to the fact that when  $x$  and  $y$  are both odd the components of the dipole groups transverse to the chain are all in the same direction; when one of them is odd and the other even they alternate in pairs, and when both are even the direction of the dipoles alternates so that any one dipole is situated between two others whose sense is in the opposite direction.

The work was suggested by the results of previous work using dibasic esters mixed with paraffin wax (*Proc. Roy. Soc. A*, 1939, 172, 502), in which it was found that the loss was either negligible or positive according as the number of carbon atoms between the two ester groups was even or odd.

**The behaviour of polar molecules in solid paraffin wax.** By D. R. PELMORE and E. L. SIMONS. (*Communicated by E. V. Appleton, F.R.S.—Received 1 February 1940.*)

**The thermal explosion of diethyl peroxide.** By E. J. HARRIS. (*Communicated by A. C. G. Egerton, Sec.R.S.—Received 12 February 1940.*)

The critical pressure at which the slow decomposition of diethyl peroxide gives place to explosive reaction has been measured at different temperatures and in various vessels. On the basis of the theory of thermal explosions (Semenoff, Frank-Kamenetzky) a product  $P = \frac{Qk}{X} \frac{E}{RT^2} \frac{p}{76} r^2 \frac{273}{22,400}$  is found, which for a sphere should be 3.82, when the pressure is the limiting value at which explosion just takes place. The experimental values of the product was about 70 % of this value, and similarly the use of cylindrical vessels led to a result lower in the same ratio. The plot of  $\log p/T^2$  against  $1/T$  for a given vessel falls on a line of slope  $E$ , the  $E$  approximating to that found for the unimolecular slow reaction, which is in accord with the above as  $k = ze^{-E/RT}$ . The conductivity  $X$ , if increased by addition of hydrogen or helium, does not alter  $p$  (the critical pressure) in proportion, which may be due to inefficient energy transfer. The same considerations are applied to the data of Rice *et al.* concerning azomethane and ethyl azide.

The induction period of the explosion is shown to fit Todes's formula. The heat of decomposition was calculated from the heat of combustion.

**Structural analysis of *Oenothera* complexes.** By D. G. CATCHESIDE. (*Communicated by F. T. Brooks, F.R.S.—Received 14 February 1940.*)

The fourteen end-pairing segments of *Oenothera* chromosomes have been defined in terms of their property of pairing at meiosis and the ways in which they are combined in the chromosomes of different gametic complexes. The comparison of a number of different complexes has led to the following conclusions concerning their structure in respect of the end segments of the chromosomes:

|                |     |     |     |     |      |       |       |
|----------------|-----|-----|-----|-----|------|-------|-------|
| <i>Hookeri</i> | 1.2 | 3.4 | 5.6 | 7.8 | 9.10 | 11.12 | 13.14 |
| <i>flavens</i> | 1.4 | 2.3 | 5.6 | 7.8 | 9.10 | 11.12 | 13.14 |
| <i>velans</i>  | 1.2 | 3.4 | 5.8 | 6.7 | 9.10 | 11.12 | 13.14 |

| <i>excellens</i>               | 1-2  | 3-4  | 5-6  | 7-10 | 8-9   | 11-12 | 13-14 |
|--------------------------------|------|------|------|------|-------|-------|-------|
| <i><sup>a</sup>franciscana</i> |      |      |      |      |       |       |       |
| <i><sup>a</sup>purpurata</i>   |      |      |      |      |       |       |       |
| <i><sup>a</sup>blandina</i>    | 1-2  | 3-4  | 5-6  | 7-10 | 8-13  | 9-14  | 11-12 |
| <i>blandina-A</i>              | 1-2  | 3-11 | 4-12 | 5-6  | 7-10  | 8-13  | 9-14  |
| <i>blandina-B</i>              | 1-4  | 2-3  | 5-6  | 7-10 | 8-13  | 9-14  | 11-12 |
| <i>latifrons</i>               | 1-2  | 3-4  | 5-6  | 7-10 | 11-12 | 8-14  | 9-13  |
| <i>rubricalyx-a</i>            | 1-2  | 3-4  | 5-6  | 7-14 | 8-13  | 9-10  | 11-12 |
| <i><sup>a</sup>decipiens</i>   |      |      |      |      |       |       |       |
| <i>rigens</i>                  | 1-2  | 3-4  | 5-6  | 7-12 | 8-14  | 9-10  | 11-13 |
| <i>gaudens rubens</i>          | 1-2  | 3-11 | 4-9  | 5-6  | 7-12  | 8-14  | 10-13 |
| <i>flectens</i>                | 1-4  | 2-3  | 5-7  | 6-10 | 8-9   | 11-13 | 12-14 |
| <i>albicans</i>                | 1-4  | 2-14 | 3-6  | 5-7  | 8-9   | 10-12 | 11-13 |
| <i>curvans</i>                 | 1-14 | 2-3  | 4-6  | 5-13 | 7-11  | 8-9   | 10-12 |

The value of the analysis in relation to evolutionary and genetic studies of these plants is pointed out. The three European species *Lamarckiana*, *suaveolens* and *biennis* are related in origin; each of the first two of these has a complex in common with *biennis*, but a different one in each case. The common complexes are identical in gross structure and very similar in gene content. A preliminary genetic map of *Lamarckiana* has been drawn and a complication in the origin of new alethal complexes from *Lamarckiana* laid bare.

### Nerves controlling the tone of the alimentary canal in the earthworm.

By N. MILLOTT. (Communicated by H. Graham Cannon, F.R.S.—Received 15 February 1940.)

The alimentary canal of *Lumbricus* exhibits autonomous rhythmic movements co-ordinated by nerve elements situated in its walls.

The gut is subject to indirect control by extrinsic nerves which fall into two groups, mutually antagonistic in their effects. Nerves which augment the tone of the gut muscles leave the central nervous system by the middle and posterior nerves of each segment and join a plexus of nerve elements situated in the peritoneum of the body wall from which nerves pass to enter the gut by the ventro-lateral regions of each septum. Nerves which diminish the tone of the gut leave the central nervous system by the anterior, middle, and posterior nerves of each segment and join a plexus of nerve elements situated in the muscular layer of the body wall, from which nerves arise which enter the gut via the dorso-lateral regions of each septum.

By the uses of nicotine both augmentor and inhibitor nerve pathways are shown to include nerve cells. The action of sympathicomimetic and parasympathicomimetic drugs on the gut of *Lumbricus* is discussed, and evidence is presented showing that the augmentor nerves are cholinergic, and the inhibitors possibly adrenergic. A substance with the pharmacological properties of acetyl-choline can be extracted from the tissues of the earthworm. Another substance capable of destroying acetyl-choline (choline esterase) is shown to exist in the earthworm.

The alimentary canal receives another nerve supply from the peripharyngeal commissures of the central nervous system by means of a number of fine plexiform nerve elements partially embedded in the pharyngeal musculature of either side ("pharyngeal plexus"). The anatomical relationships of these nerves are described.

The pharyngeal plexuses are shown to embody nerve elements which also exert an indirect control over the gut. Stimulation of these nerves results in diminution of the tone of all regions of the gut behind the pharynx.

The nerve supply of the gut is compared with that which is known in other annelids, and the mechanism of indirect control is compared with that existing in vertebrates.

The significance of the results in relation to recent work on chemical transmitters in invertebrates, and to the problem of the evolution of the autonomic nervous system, is discussed.

---

**Studies on the transmission of sugar-beet yellows virus by the aphid *Myzus persicae*.** By M. A. WATSON. (*Communicated by Sir John Russell F.R.S.—Received 15 February 1940.*)

The efficiency of the vector *Myzus persicae* in transmitting sugar-beet yellows virus increased greatly with increasing feeding time on the infected plants. Infection was produced on a succession of healthy plants for 1, 2, or 3 days depending on the length of the infection feeding time. The infectivity of the vectors increased with increasing feeding time on the healthy plants undergoing infection, and decreased with increasing feeding time on healthy plants prior to those on which the infection trial was made. There was no clearly defined "incubation period" of the virus in the vector, below which no insect could cause infection, but there was variation in the time between cessation of infection feeding of the aphid and the initiation of infection in the healthy plants.

The relations of this virus with its vector differ from those of the viruses already described as *non-persistent*. For the latter viruses infectivity is lost by *M. persicae* soon after cessation of infection feeding. After fasting the vectors become optimally infective almost immediately on penetrating infected tissues of the leaf. Their infectivity decreases with increasing feeding time on the infected plants, and increases only slightly with increasing feeding time on the healthy plants.

The behaviour of sugar-beet yellows virus is compared with that of curly-top virus of sugar beet, in which infectivity also persists for an indefinite period in the vector and increases with increasing feeding time on infected and healthy plants.

---

# ABSTRACTS

## OF PAPERS COMMUNICATED TO THE ROYAL SOCIETY OF LONDON

In accordance with a resolution of Council, summaries or abstracts of papers are to be published as soon as practicable. The publication of such abstracts in no way indicates that the papers have been accepted for publication in any fuller form. These abstracts are issued for convenience with the "Proceedings of the Royal Society of London" but do not form a part of the "Proceedings".

---

10 APRIL 1940

---

**The electric strength of solid dielectrics in relation to the theory of electronic breakdown.** By A. E. W. AUSTEN and S. WHITEHEAD. (*Communicated by N. F. Mott, F.R.S.—Received 19 December 1939.*)

Methods are described by which the "intrinsic" electric strength of solid dielectrics may be defined and evaluated. It is shown that the magnitudes, and the effect, temperature and thickness upon the electric strengths of certain crystals agree with Fröhlich's theory of electronic breakdown, as also does the effect of disordered structure and microstructure in similar instances. On the other hand, departures from theory occur with complex organic dielectrics and also with crystals when, with the latter, certain limits, e.g. of temperature, are exceeded. Some observations are made on the effect of temperature and electric stress upon the conductivity.

---

**Observations on the structure, development and electrical reactions of the internal ear of the shaker-1 mouse (*Mus musculus*).** By H. GRÜNEBERG, C. S. HALLPIKE and A. LEDOUX. (*Communicated by E. D. Adrian, F.R.S.—Received 2 February 1940.*)

Histological examination of the post-foetal development of the internal ear in normal and shaker mice was carried out at periods between 9 hours and 12 days after birth.

The normal process of post-foetal development appeared to pursue an identical course in both varieties and to be completed in 12 days.

Tests of hearing, measurements of the electrical response of the cochlea and histological examination of the internal ear were carried out in normal and shaker mice at

ages between 38 and 329 days. In all the shaker material deafness was found to be correlated with pathological changes confined to the scala media complex and gross reductions of the electrical response. The changes first appeared in the stria vascularis and Corti's organ and were progressive with age. Those in the spiral ganglion appeared later.

The degenerative process was thus shown to be initiated after birth in a fully differentiated organ, and comparison was made with similar results obtained by van Lennep in the Japanese waltzing mouse.

The parallel courses of the loss of the electrical response and of the degenerative changes in both the stria vascularis and in Corti's organ rendered the results indecisive as regards the relative merits of the "membrane" and "hair cell" theories of origin of the response.

A selective reduction of the response which occurred at high frequencies was correlated with some accentuation of the degenerative changes in Corti's organ at the base of the cochlea, and the resemblance of this to similar findings by Stevens, Davis and Lurie in the guinea-pig under different experimental conditions was discussed. The results were not considered to constitute a decisive contradiction of the membrane hypothesis.

No morphological abnormalities were found in the vestibular apparatus of the internal ear. It must therefore be supposed that the abnormal head movements are of extra-labyrinthine origin.

---

**On the function of chlorocruorin.** By R. F. EWER and H. MUNRO FOX, F.R.S. (*Received 17 February 1940.*)

The oxygen consumption of *Sabella* decreases soon after the concentration of dissolved oxygen in sea water falls below the value corresponding to air saturation, both at 10 and 17° C; above air saturation at 17° C there is no significant rise in oxygen consumption. The oxygen consumption of *Sabella*, whose chlorocruorin has been converted to carboxychlorocruorin, is lower than that of normal worms; this is the case at air saturation of the water and at oxygen concentrations below air saturation both at 10 and 17° C. The fall in oxygen consumption of the animals after treatment with carbon monoxide is not due to an action of the latter on cell enzymes. It follows that chlorocruorin functions as an oxygen carrier in *Sabella* at all temperatures and oxygen pressures to which the animals are subjected in nature.

---

**The structure of the cell wall in some species of the filamentous green alga *Cladophora*.** By W. T. ASTBURY and R. D. PRESTON. (*Communicated by Sir William Bragg, F.R.S.—Received 21 February 1940.*)

With a view to extending the work on *Valonia*, the cell walls of several species of *Cladophora* have been examined in detail by means of X-ray diffraction photographs and the microscope. The walls are found to consist of layers in which the cellulose chains in any one layer are inclined to those in the preceding and subsequent layers at

an angle whose average is less than  $90^\circ$ . The two sets of striations on the layers of the wall correspond closely to the directions of the cellulose chains.

Each set of chains forms a spiral round the cell, and the spirals are of opposite sign. One tends to be flat and the other steep. On the whole, the steep spiral tends to become steeper on passing from the base of the filament to the tip, and the flat spiral flatter. In any one cell of the filament, the steep spiral is steepest at the end nearer the filament tip and the flat spiral flattest. Wherever such changes in inclination occur, the angle between the chains tends to remain constant.

It is suggested that the cell elongation is the factor causing the inclination of the steeper spiral to vary, and that the behaviour of the flatter spiral is best explained by the assumption of a protoplasmic mechanism causing a periodic change in the direction of cellulose chains through a constant angle. The development of a branch cell is reviewed and is found to proceed as the above suggestions would indicate.

---

**Orientation of nuclear spins in metals.** By H. FRÖHLICH and F. R. N. NABARRO. (*Communicated by N. F. Mott, F.R.S.—Received 22 February 1940.*)

In connexion with the possible use of nuclear magnetism for the magnetic cooling method, the behaviour of the nuclear spins of monovalent metals at very low temperatures is investigated theoretically. It is shown that, owing to the interaction between the nuclear spins and the conduction electrons, the nuclei of most monovalent metals should become ferromagnetic at temperatures of the order of  $10^{-6}$  degree. The Curie temperature  $\theta$  for this nuclear ferromagnetism is approximately given by

$$k\theta \sim \frac{1}{3} \epsilon^2 / \zeta,$$

where  $\epsilon$  is the hyperfine structure splitting of the free atom, and  $\zeta$  is the energy region occupied by the conduction electrons. Temperatures of this order of magnitude should be attainable by an application of the magnetic cooling method.

---

**The determination of the lifetime of active polymeric molecules.** By T. T. JONES and H. W. MELVILLE. (*Communicated by E. K. Rideal, F.R.S.—Received 26 February 1940.*)

A method of determining the distance of diffusion in space of a polymer reaction is described. It depends upon the fact that in a reaction—the direct polymerization of methyl acrylate—in which active molecules mutually destroy each other, this mutual interference may be demonstrated by using two sources of photo excitation. The velocity of polymerization then depends on the distance between the two sources. The exact theory of the method has been worked out for hydrogen atoms. The results obtained from this investigation are applied to the methyl acrylate reaction. This result is then further employed, along with previous data, to compute the absolute value of the reaction velocity coefficient between active polymer molecules and monomer.

---



**The glide elements of body-centred cubic crystals, with special reference to the effect of temperature.** By E. N. DA C. ANDRADE, F.R.S., and Y. S. CHOW. (*Received 9 March 1940.*)

The glide elements of single crystals of the body-centred cubic metal, sodium, have been determined at various temperatures. The glide direction is in all cases  $[111]$ , but the glide plane changes successively from  $(112)$  to  $(110)$  to  $(123)$  as the temperature goes from  $-185$  to  $20^{\circ}\text{C}$ . It is shown that this change of glide plane with temperature is a particular case of a general rule to which body-centred metals conform: all three planes are possible glide planes but which is operative at any particular temperature is determined by the temperature referred to the melting point of the particular metal as standard. The case of iron, for which all three planes seem to be operative at once, is considered separately.

The critical shear stress has been determined for sodium, and shows a small variation only over the temperature range  $-185$  to  $20^{\circ}\text{C}$ .

Experiments with sodium, iron and molybdenum go to show that the spacing of the glide planes increases markedly as the temperature is raised.

It has been found that, for equal strain, the crystallite rotations, as evidenced by the asterisms, are much greater at low temperatures, where the hardening is greater, which goes to support the view that hardening is intimately connected with the rotation of crystal fragments. The breaking up of the asterisms into discrete spots which has been found with sodium and potassium is shown to be due to recrystallization.

The general implications of the results are discussed.

---

# ABSTRACTS

## OF PAPERS COMMUNICATED TO THE ROYAL SOCIETY OF LONDON

In accordance with a resolution of Council, summaries or abstracts of papers are to be published as soon as practicable. The publication of such abstracts in no way indicates that the papers have been accepted for publication in any fuller form. These abstracts are issued for convenience with the "Proceedings of the Royal Society of London" but do not form a part of the "Proceedings".

---

16 MAY 1940

---

**Thermal ionization of strontium.** By B. N. SRIVASTAVA, D.Sc. (*Communicated by M. N. Saha, F.R.S.—Received 4 March 1940.*)

In this paper the thermal ionization of strontium vapour has been experimentally investigated by an apparatus already described by the author elsewhere in his work on barium. Experiments have been carried out at various temperatures and pressures of strontium vapour, and the equilibrium concentrations of  $\text{Sr}^+$  and electrons inside the furnace have been obtained by allowing them to effuse out through a narrow opening. From these the equilibrium constant and the energy of ionization have been calculated. The results obtained agree, within the limits of experimental error, with the theory of thermal ionization and the known spectroscopic value of the ionization potential of strontium.

---

**The growth, growth energy and ageing of the chicken's heart.** By P. B. MEDAWAR. (*Communicated by E. S. Goodrich, F.R.S.—Received 7 March 1940.*)

A property referred to as the *growth energy* of the chicken's heart, and representing the resistance of freshly explanted tissues to inhibition of their growth, is described and measured. The growth energy was found to decline exponentially with time over the range 8–18 days. It is shown that the growth energy is proportional to, and therefore a measure of, the specific growth rate of the heart *in vivo*. The growth in mass of the chicken's heart can therefore be described by a mean curve, which is that of a Gompertz equation. The growth energy of tissues rises sharply during the course of cultivation, and initial embryonic age differences are smoothed out. The growth of

mesenchyme tissues is shown to be dependent upon the movement of their constituent cells. The relation between growth, movement, metabolism, and differentiation is discussed, and a theory proposed which indicates the degree of their functional dependence upon one another. The relevance of the Gompertz equation to problems of relative growth and senescence is briefly considered.

---

**Ocular interaction in its relation to measurement of brightness threshold.**

By B. H. CRAWFORD. (*Communicated by Sir John Parsons, F.R.S.—Received 11 March 1940.*)

It is found that in all cases binocular vision produces a lower threshold than monocular vision, but, under static conditions of foveal vision at all brightness levels and of parafoveal vision at very low levels, the difference is small and can be wholly explained by the fact that with two eyes there is a greater probability of the test field being seen than with one eye. For parafoveal vision under static conditions at medium and high brightnesses binocular vision gives a threshold about 30 % lower than does monocular vision. When the state of adaptation is changing—after cutting off a conditioning field of high brightness—both foveal and parafoveal retinal areas show more rapid recovery for binocular than for monocular vision. In the fovea the difference is greater in the initial stages of recovery of dark adaptation, while in the parafovea the difference is approximately constant during the whole process.

It is also found that when one eye is used for making threshold measurements it is completely unaffected by exposure of the other eye to fields of brightness up to 130 candle/ft.<sup>2</sup>.

Any subsidiary pupil diameter effects are avoided by the use of Maxwellian view of the visual field.

---

**On a green helical organism and its motion.** By L. E. R. PICKEN. (*Communicated by J. Gray, F.R.S.—Received 13 March 1940.*)

A green helical organism is described which displays a new type of movement. The helix moves by growing at the anterior end and diminishing posteriorly; it does not rotate.

Observations on the change in shape produced by dehydration show that the structure of the organism is markedly anisotropic. By analogy with other fibrous structures, it may be concluded that anisodiametric micells or molecules are orientated parallel to the long axis.

It is pointed out how the growth and activity of the organism are related to this axis.

The systematic position of the organism is discussed and its possible affinity with the Spirochaetozoa (Dobell) and Cyanophyceae considered.

---

**Experiments with a velocity spectrometer for slow neutrons.** By G. E. F. FERTEL, D. F. GIBBS, P. B. MOON, G. P. THOMSON, F.R.S. and C. E. WYNN-WILLIAMS. (*Received 14 March 1940.*)

A velocity spectroscopy for slow neutrons has been constructed upon the principle of measuring the times of transit of individual neutrons from an intermittent source to a distant ionization chamber.

Measurements have been made of the velocity distribution of the slow neutrons from a paraffin-wax howitzer at room temperature.

By the interposition of absorbers, the adsorption coefficients of boron and cadmium have been measured for neutrons of different velocities. The results for boron are inconsistent with the law of inverse velocity.

---

**Radiative processes involving fast mesons.** By F. BOOTH and A. H. WILSON. (*Communicated by R. H. Fowler, F.R.S.—Received 19 March 1940.*)

The general theory of the interaction of mesons with an electromagnetic field is developed, starting from Kemmer's matrix formulation of the meson equations. The general theory is applied to the scattering of light by mesons, the emission of radiation by mesons during collisions and the production of pairs of mesons. A brief discussion of the experimental results on the energy losses of "heavy electrons" in cosmic rays is given, and it is shown that the experiments are consistent with the view that the heavy electrons have spin 1 and that the theory of the interaction of mesons with an electromagnetic field is probably valid for energies considerably greater than the rest energy of a meson.

---

**A magnetic study of the two phase iron nickel alloys.** By A. T. PICKLES and W. SUCKSMITH, F.R.S. (*Received 20 March 1940.*)

Measurements of magnetic saturation intensity of annealed iron-nickel alloys have been used to demonstrate the existence of a two phase field in the iron-rich part of the system. The phase boundaries have been determined at temperatures above 450° C, and the relation of the equilibrium phase diagram to the thermal hysteresis observed under normal rates of temperature has been studied.

---

**Explosion waves and shock waves. VI. The disturbance produced by bursting diaphragms with compressed air.** By W. PAYMAN and W. C. F. SHEPHERD. (*Communicated by Sir Jocelyn Thorpe, F.R.S.—Received 21 March 1940.*)

Experimental verification of the theoretical relationships governing the motion of shock waves has been derived from an investigation into the development of the

disturbance set up in a uniform tube when a body of compressed gas, confined at one end by means of a copper diaphragm, is released by rupture of the diaphragm. The wave-speed camera has been used to obtain continuous Schlieren records of the passage of these effects along the tube and to analyse their properties under a variety of experimental conditions, the main variations being those caused by the use of different thicknesses of diaphragm, different lengths of compression and expansion chambers, and of different gases in these chambers.

The pressure effects released on the rupture of the diaphragm are the shock wave, a vortex formation and the expanding gases from behind the diaphragm. Schlieren snapshot (spark) photographs have been obtained showing the structure of these pressure effects when they are projected from the end of the tube into free air. The photographs show, in addition to these details, the establishment of a system of stationary sound waves.

Diagrams have been constructed based on the experimental data showing the apparent form of the wave during various phases of its progress.

---

**A mathematical analysis of the distribution in maize of *Heliothis armigera* Hübner.** By M. G. WALKER. (Communicated by W. R. Thompson, F.R.S.—Received 28 March 1940.)

The distribution among maize plants of the eggs of the American boll-worm, *Heliothis armigera* Hübner, is discussed and analysed.

The problem is considered in relation to what is known of the connexion between the state of development of maize plants and their attractiveness to ovipositing boll-worm moths. The actual frequency distribution of the eggs suggests a random as opposed to a uniform distribution, but it is shown that the conditions required for a pure mathematical random distribution cannot be satisfied. Because the maize plants differ from one another in absolute degree of attractiveness at any one time, and in relative degree of attractiveness with the passing of time, it is not true that every plant has the same chance of receiving any given egg.

It is demonstrated that a mathematical theory, which is eventually one of random distribution, but which incorporates a modification to allow for the varying degrees of attractiveness of the plants, gives a fairly good representation of the egg distribution found in the field.

Theoretical distributions to fit the data are calculated by two methods. One is a discontinuous process which is presented as only a rough approximation of what it is intended to express. The other uses the compound Poisson series of Greenwood and Yule. The continuous variation in nature both in space and time, which is the essential difficulty of the problem, is discussed.

---

# ABSTRACTS

## OF PAPERS COMMUNICATED TO THE ROYAL SOCIETY OF LONDON

In accordance with a resolution of Council, summaries or abstracts of papers are to be published as soon as practicable. The publication of such abstracts in no way indicates that the papers have been accepted for publication in any fuller form. These abstracts are issued for convenience with the "Proceedings of the Royal Society of London" but do not form a part of the "Proceedings".

---

12 JUNE 1940

---

**The wave-form of atmospherics at night.** By J. S. ELDER, D. B. HODGES, W. E. PHILLIPS, B. F. J. SCHONLAND, F.R.S. and J. W. VAN WYK.  
(Received 5 February 1940.)

The wave-form for all atmospherics received at night from sources within 2000 km. can be accurately described as a ground-pulse followed by a series of sky-pulses produced by successive reflexions between the ionosphere and the earth, 30 such reflexions being frequently recorded. The time separation between the peaks of these pulses is determined by the distance travelled and the height of the layer. The primary pulse emitted by the source is usually a single complete oscillation of period ranging from 50 to 400  $\mu$ sec. At distances greater than 500 km. the ground-pulse and the first sky-pulse merge owing to the shortness of the time-interval between them. Differences of amplitude, form and phase between pulses can arise from differences in angle of emission from the parent lightning channel.

The height of the reflecting layer can be determined within  $\pm 1$  km. It ranged from 85.5 to 90.5 km. during two winter months, with a mean of 88.0 km. The distances of the sources as found by analysis of the pulse series were corroborated by independent location with cathode-ray direction-finders. The reflexion-coefficient of the layer for the pulses of longer period exceeded 0.80. The velocity of the ground-pulse where it can be tested is within 0.7 % of that of light.

**Operator calculus in the electron theory of metals.** By K. FUCHS. (*Communicated by M. Born, F.R.S.—Received 28 March 1940.*)

An operator calculus is developed applicable to problems in the electron theory of metals. It differs from the common operator calculus of the quantum theory in the fact that the wave function is defined in a finite space (the atomic polyhedron) bounded by a finite surface. This leads to the introduction of surface operators.

The position operator  $x$  cannot be developed with respect to the proper functions of the Hamiltonian. Instead, an operator  $\xi$  is introduced, which is essentially the Fourier development of  $x$ .

Thus there are three fundamental types of operators: The differential operator  $p$ , the multiplication operator  $\xi$ , and the surface operators. It is shown that with the help of these a consistent calculus can be developed.

---

**The reversible formation of starch from glucose-1-phosphate catalysed by potato phosphorylase.** By C. S. HANES. (*Communicated by F. F. Blackman, F.R.S.—Received 29 March 1940.*)

An enzyme (phosphorylase), which catalyses the reversible conversion of starch and inorganic phosphate to glucose-1-phosphate, has been found to occur in a number of higher plants. A method is described for obtaining from potato tubers highly active preparations of phosphorylase which are free from certain enzymes which catalyse alternative reactions.

The reversibility of the transformations: starch + inorganic phosphate  $\rightleftharpoons$  glucose-1-phosphate, is shown by the fact that the reaction proceeds in either direction until the ratio of inorganic orthophosphate/glucose-1-phosphate attains a value which is not significantly altered by wide variations in the concentrations of the reactants or the enzyme. The equilibrium value of this ratio is not detectably affected by alterations in the concentration of starch but varies considerably with alterations in the concentration of hydrogen ion. This is shown to be due to the effects upon the extents of dissociation of the inorganic and esterified phosphate, the di-valent ions alone determining the equilibrium; thus the ratio  $(\text{HPO}_4)^{-}/(\text{C}_6\text{H}_{11}\text{O}_5\cdot\text{O}\cdot\text{PO}_3)^{-}$  remained approximately constant at a value of 2.2 when the pH value was varied from 5 to 7. When glucose-1-phosphate is added to the enzyme there is an initial lag in the liberation of phosphate and the formation of starch. This induction phase is abolished, and the reaction velocity greatly increased, by small additions of starch or maltose.

The preparation on a large scale of glucose-1-phosphate (in the form of the crystalline potassium salt) by allowing crude potato juice to act in starch is described.

Observations on the polysaccharide formed from pure glucose-1-phosphate under the action of purified phosphorylase indicate that it resembles closely the so-called amylo-amylose fraction of natural potato starch.

The mechanism of this reversible interconversion and its bearing on the problems of carbohydrate metabolism in the plant are considered.

---

**The effect of field size and pattern on the change of visual sensitivity with time.** By B. H. CRAWFORD, M.Sc. (*Communicated by Sir John Parsons, F.R.S.—Received 29 March 1940.*)

Results are recorded showing the effect of size of a circular conditioning field on brightness threshold measurements made at the centre of the field, firstly, with the field steadily exposed and viewed, secondly, when the conditioning field has been cut off and the eye is returning to a state of dark adaptation. Conditioning and test fields are both illuminated by white light. No field size effect is detectable over the range  $60^\circ$  diameter down to  $3^\circ$  diameter. Below  $3^\circ$ , for a steady state of adaptation, various rather complex effects of interference between the conditioning fields are shown; these are explained in terms of the effect of distant parts of the conditioning field in raising the threshold and a perceptual interference between the patterns of conditioning and test fields. For changing states of adaptation the effect of field size cancels out—except in an isolated case—if the initial conditioning field brightnesses are adjusted to give the same steady value of threshold: then, after cutting off these various conditioning fields, the decrease of brightness threshold follows the same course. However the test patch of retina be brought to a given steady state of adaptation, as measured by the brightness threshold, it will recover its dark adaptation in the same way. These considerations apply both to foveal vision and to vision in the parafovea at  $8^\circ$  from the fovea.

---

**The pressure of water waves upon a fixed obstacle.** By T. H. HAVELOCK, F.R.S. (*Received 29 March 1940.*)

The diffraction of plane water waves by a stationary obstacle with vertical sides is examined, in particular the variation of amplitude along the sides and the average steady pressure due to the wave motion. Results similar to those in other diffraction problems are obtained for an infinite plane and for cylinders of circular or parabolic section, and approximations are made for sections of ship form. The examination was made in view of possible applications in the problem of a ship advancing through a train of waves, and the results are discussed in relation to the average additional resistance in such circumstances. It appears that the mean pressure obtained on diffraction theory from the second order terms can only account, in general, for a small proportion of the observed effect; the motions of the ship, and in particular its oscillations, are essential factors in the problem.

---

**Ionic regulation of *Carcinus maenas*.** By D. A. WEBB. (*Communicated by J. Gray, F.R.S.—Received 1 April 1940.*)

Analyses have been made, with respect to the principal inorganic constituents, of the blood and urine of *Carcinus*, when living in normal sea water, diluted sea water, and sea water modified by the addition of magnesium sulphate.

The composition of the blood of individuals living in normal sea water is as follows (the concentration of each ion being expressed as a percentage of the concentration



that would be expected if the blood were in dialysis-equilibrium with the external medium): Na 110 %, K 118 %, Ca 108 %, Mg 34 %, Cl 104 %,  $\text{SO}_4$  61 %.

This ionic regulation is the resultant of the following processes: active absorption by the gills of sodium, potassium, calcium and chloride at a rate greater than that at which they are lost by diffusion; differential excretion by the antennary gland, which tends to conserve potassium and eliminate magnesium and sulphate; inward diffusion across the gills of magnesium and sulphate in accordance with the concentration gradient.

In normal conditions there is active absorption of water. In dilute media, when osmoregulation begins, this is suspended, and possibly there is a fall in the passive permeability of the gills to water. In other respects osmoregulation is brought about by an intensification of the processes responsible for ionic regulation.

The permeability of the cuticle under physiological conditions is such that it does not affect the salt and water exchange of the animal, which is controlled by the branchial epithelium.

The structure of the gills of four species of Decapoda is described and correlated with their powers of osmotic and ionic regulation.

---

#### **The anatomy of ineffective nodules and its influence on nitrogen fixation.**

By H. K. CHEN and H. G. THORNTON. (*Communicated by Sir John Russell, F.R.S.—Received 4 April 1940.*)

The anatomy and cytology of nodules produced on clover, peas and soy beans by "effective" and "ineffective" strains of *Rhizobia* were investigated, with especial reference to the changes in volume of the active infected tissue during the life of the nodule. In clover the mean volume of this active bacterial tissue is about three times as great in "effective" as in "ineffective" nodules. This is due to an early arrest of growth in nodules produced by ineffective strains. In all nodules the active bacterial tissue eventually disintegrates, but in effective clover nodules it remains without disintegration for about six times as long as in ineffective nodules.

In an experiment to test the nitrogen fixation by clover inoculated with an effective and an ineffective strain, the difference between the strains in the amounts of nitrogen fixed could be accounted for by the differences in volume and in duration of the active bacterial tissue. In peas, nodules produced by an effective strain were nearly twice the length as those produced by an ineffective strain and their bacterial tissue remained without disintegration for about twice as long. In soy beans the mean volume of bacterial tissue was 4.75 times as great in effective as in ineffective nodules and the percentage of that volume composed of infected cells was twice as great. In ineffective soy bean nodules disintegration of the bacterial tissue began when the plant was four weeks old and was practically complete by the twelfth week, at which time no disintegration could be found in effective nodules. The difference in amount of nitrogen fixed by soy-bean plants bearing each type of nodule could be accounted for wholly by the factors mentioned above.

Thus in both clover and soy-bean nodules the volume and duration of the active infected tissue are the main, if not the only, factors determining differences in nitrogen fixation, amongst the strains tested.

---

**The soft X-ray spectroscopy of solids. II. Emission-spectra from simple chemical compounds.** By H. M. O'BRYAN and H. W. B. SKINNER. (*Communicated by A. M. Tyndall, F.R.S.—Received 9 April 1940.*)

K- and L-emission bands emitted in the soft X-ray region of the spectrum by atoms in a number of chemical compounds have been investigated. The substances for which such spectra are available through the present or previous work are: fluorides, chlorides, bromides, iodides, oxides, sulphides, boron nitride and other boron compounds; and carbides. In the cases of SiC, BN and a number of oxides, spectra from both the component atoms forming the compound have been obtained.

The results are interpreted, as those for metals and element insulators have been in a previous paper, to give the characteristics of the bands of levels which exist for the valence-electrons in the normal state of the substance. In the case of the halides, data on the *p*- and *s*-levels of the negative ions are given, and it is shown that, even in this case, the crystal structure leaves its mark on the form of the bands of levels. The 2*p* bands of oxygen in the oxides are more spread-out on an energy scale, thus showing that the interaction between electrons in neighbouring atoms is considerable. The spectra of the metal ions in oxides are very complex, and an attempt is made to disentangle the factors which lead to this complication. In doing so, it is hoped that we may have thrown some light on the difficult subject of the structure of semi-polar compounds in solid form.

---

**The strains produced by precipitation in alloys.** By F. R. N. NABARRO. (*Communicated by N. F. Mott, F.R.S.—Received 15 April 1940.*)

If the process of diffusion in metals results simply in the interchange of pairs of atoms, large strains must be set up when a new phase precipitates in an alloy. The strain energy involved is calculated for particles of precipitate of various shapes, and is found to be least if the precipitate forms thin plates. The shape of the particle actually formed is influenced by this energy, by the degree of supersaturation of the solid solution, and by surface effects; the calculated shape is shown to agree reasonably well with that observed experimentally.

---

**The fine structure of phloem fibres in untreated and swollen jute.** By B. C. KUNDU and R. D. PRESTON. (*Communicated by V. H. Blackman, F.R.S.—Received 16 April 1940.*)

Studies of the optical properties of jute suggest that the wall is composed of chains of cellulose forming a single, fairly steep spiral. During growth the wall spiral becomes steeper up to the onset of wall thickening.

This fibre provides a study complementary to that of hemp. The outer layers have the least resistance to swelling and the phenomenon of "ballooning" is therefore never observed. For similar reasons transverse cracks never develop during swelling.

The results fully confirm the conclusion that swollen material cannot safely be used in determining wall structure.

---

**Plant pigments in the Galápagos Islands.** By T. W. J. TAYLOR. (*Communicated by Sir Robert Robinson, F.R.S.—Received 18 April 1940.*)

The Galápagos Islands were visited by the Lack-Venables Expedition during the winter 1938–39, and analyses were made of the anthocyanin pigments contained in the characteristic and largely endemic plants of Indefatigable Island. The methods used for anthocyanin identification under camp conditions are described. No new pigments were found, but a high proportion of the plants were found to contain nitrogenous anthocyanins. This provides powerful support for the views already put forward as to the distribution of such pigments, although slight modification of these views is needed.

---

**Isomorphous replacement and superlattice structures in the plagioclase feldspars.** By S. H. CHAO and W. H. TAYLOR. (*Communicated by W. L. Bragg, F.R.S.—Received 19 April 1940.*)

From X-ray oscillation—and rotation—photographs of a limited number of plagioclase feldspars it seems probable that the structure-type depends upon the chemical composition in the following way. From pure soda feldspar to at least 22% lime feldspar there extends an isomorphous series with the *albite* structure, based on a unit cell with linear dimensions  $8 \times 13 \times 7\text{Å}$  approximately and containing four molecules of  $\text{NaAlSi}_3\text{O}_8$  or the equivalent when  $(\text{CaAl})$  replaces  $(\text{NaSi})$ . There is probably a similar range of isomorphism, near pure lime feldspar  $\text{CaAl}_2\text{Si}_2\text{O}_8$ , with the *anorthite* structure which has axes  $8 \times 13 \times (2 \times 7)\text{Å}$ , but is of course very similar to the albite structure. The characteristic features of the photographs of the intermediate plagioclases can be explained, with the help of an optical model, in terms of a structure in which sheets with the albite structure and sheets with the anorthite structure alternate, but more experimental data are needed for the complete elucidation of the problem.

---

**The base-catalysed prototropy of substituted acetones.** By R. P. BELL and O. M. LIDWELL. (*Communicated by C. N. Hinshelwood, F.R.S.—Received 23 April 1940.*)

Kinetic measurements have been made at  $25^\circ$  on the catalysed halogenation of the following ketones: acetone, acetylacetone, monochloroacetone, monobromoacetone, *ac*, dichloroacetone and acetylacetone.

In all cases the reactions are of zero order with respect to the halogen and exhibit general basic catalysis. For the first two ketones general acid catalysis is also detectable. For each ketone the catalytic constants  $k_B$  of four carboxylate anions are related to the dissociation constants  $K_A$  of the corresponding acids by an equation of the type  $k_B = G(I/K_A)^\alpha$ , where  $G$  and  $\alpha$  are constants for a given ketone. The catalytic constants measured cover a range of about  $10^6$ .

Examination of the results (together with those of Pedersen for the bromination of acetoacetic ester and acetoacetic acid) shows that the exponent  $\alpha$  decreases steadily from 0.88 to 0.48 as the reactivity of the ketone increases.

The catalytic coefficients of the water molecule are given approximately by the equations valid for the carboxylate anions, but the hydroxyl ion is in each case a much less efficient catalyst than these equations predict.

---

**A thermodynamical theory of the tensile strength of isotropic bodies.** By F. FÜRTH. (*Communicated by M. Born, F.R.S.—Received 24 April 1940.*)

By thermodynamic considerations a new formula connecting the tensile strength of an isotropic body with its melting energy and Poisson's elastic constant is developed and found in good agreement with experiments.

---

**General bi-harmonic analysis for a plate containing circular holes.** By A. E. GREEN. (*Communicated by G. I. Taylor, F.R.S.—Received 24 April 1940.*)

A general solution is given for problems of generalized plane stress distributions in an infinite plate which contains circular holes of varying sizes in any positions, subject only to certain conditions of convergence of the solution. The method for extending the results to allow for the effect of one or two straight boundaries is indicated.

As a particular case of the general solution the problem of the stress distribution in an infinite plate under tension containing three holes in a row is discussed, and a few numerical results are given. These results are compared with experiments which were carried out by Mr P. L. Capper. The comparison is incomplete as the experiments were done for a finite plate and the influence of the edges of the plate on the numerical values of the stresses is considerable. Agreement, however, is found for the general character of some of the stresses.

---

**Smoking and tobacco pipes in New Guinea.** By A. C. HADDON, F.R.S. (*Received 25 April 1940.*)

---

**The combustion of aromatic and alicyclic hydrocarbons. V. The products of combustion of benzene and its monoalkyl derivatives.** By J. H. BURGoyNE. (*Communicated by A. C. G. Egerton, Sec. R.S.—Received 25 April 1940.*)

The progressive formation of products in the combustion of benzene and its monoalkyl derivatives has been studied by analytical methods, and the characteristic features of the isothermal reactions at various temperatures have been established.

A cool-flame reaction of *n*-propylbenzene has also been investigated, and by comparison with corresponding isothermal combustions, it is concluded that the propagation of cool-flames is conditioned by the accumulation of a phenylalkyl hydroperoxide.

The results are interpreted in the light of the theory of the two-stage process, and a schematic mechanism for the main combustion reaction is outlined. This comprises degradation of the side-chain (if present) and rupture of the benzene nucleus, followed by rapid degradation of the higher aliphatic aldehyde thus formed, yielding finally formaldehyde and the ultimate combustion products  $\text{CO}_2$ , CO and  $\text{H}_2\text{O}$ .

---

**The mechanism of the semicircular canal. A study of the responses of single-fibre preparations to angular accelerations and to rotation at constant speed.** By O. LÖWENSTEIN and A. SAND. (*Communicated by S. W. Kemp, F.R.S.—Received 3 May 1940.*)

Single-fibre discharges have been recorded from the horizontal ampulla of the isolated labyrinth of *Raja*. Responses to different speeds of angular acceleration and to rotation at constant angular velocity are described. The existence of a spontaneous rhythm of discharge which is increased by ipsilateral, and inhibited by contralateral rotation is confirmed.

During uniform angular acceleration the frequency of impulses increases or decreases gradually in a linear manner, and the rate of increase or decrease is proportional to the speed of acceleration. The threshold speed of acceleration is in the region of  $3^\circ$  per sec.<sup>2</sup>. During prolonged rotation at constant speed the frequency of discharge, having attained a maximum or minimum co-incidentally with the initial acceleration, gradually returns to the spontaneous value over a period of about 20–30 sec. These results are interpreted in terms of the physical properties of the cupula as described by Steinhausen.

The spontaneous discharge, and its excitation and inhibition by ipsilateral and contralateral rotation provide a basis for the interpretation of labyrinthine tone, and of the reflex responses to rotation in both directions of unilaterally operated animals. The sensory activity of the semicircular canal, interpreted in terms of the physical properties of the cupula, provides a framework which is adequate to account for the time relations of nystagmus and after-nystagmus.

---

# ABSTRACTS

## OF PAPERS COMMUNICATED TO THE ROYAL SOCIETY OF LONDON

In accordance with a resolution of Council, summaries or abstracts of papers are to be published as soon as practicable. The publication of such abstracts in no way indicates that the papers have been accepted for publication in any fuller form. These abstracts are issued for convenience with the "Proceedings of the Royal Society of London" but do not form a part of the "Proceedings".

---

18 JULY 1940

---

**Melting and crystal structure.** By J. W. H. OLDHAM and A. R. UB-  
BELOHDE. (*Communicated by Sir William Bragg, P.R.S.—Received*  
*27 February 1940.*)

The role of various types of lattice flaws is discussed in their bearing on melting and crystal structure. Freezing point determinations on lattices of a single molecule indicate the presence of such flaws in the crystals of polymethylene compounds. Freezing point determinations on composite lattices of ketone+paraffin and ketone+ketone emphasize the importance of the rotation of the group for melting, and indicate that lattice holes are easily formed, without marked lowering of the freezing point. Ordered composite lattices are formed when the number of holes does not exceed 12% of all the methylene groups.

The results emphasize the importance of co-operative effects in lattice flaws. In the equilibrium state of a crystal, such flaws might arise both from energy effects at 0° K, especially in metals, and from energy and entropy effects at higher temperatures. A picture of melting is suggested in which a network of co-operative flaws breaks up the crystal into a mosaic, or aggregate of crystalline micelles, and in which the solid-liquid transition is comparable with a gel-sol transition.

---

**Molecular structure and rubber-like elasticity.** By C. W. BUNN. (*Com-  
municated by Sir William Bragg, P.R.S.—Received 16 April 1940.*)

The crystal structures of  $\beta$  gutta-percha, rubber and polychloroprene have been completely determined by interpretation of X-ray diffraction photographs. The probable molecular structure of  $\alpha$  gutta-percha molecules has also been deduced.

Knowledge of the geometry of these molecules, together with certain features of the crystal structures, lead to a promising theory of the origin of rubber-like properties.

An examination of all the well-established structures of aliphatic molecules has led to the suggestion of a new stereochemical principle which appears to play a large part in determining the bond positions for successions of linked carbon atoms, just as the tetrahedral principle determines the bond positions of any one carbon atom. The principle is also obeyed in molecules containing nitrogen and oxygen atoms as well as carbon. The principle may be used (and has already been so used) to deduce the probable configurations of aliphatic molecules, and is especially valuable for chain polymers.

---

**Potential energy curves in proton transfer reactions.** By R. P. BELL and O. M. LIDWELL. (*Communicated by C. N. Hinshelwood, F.R.S.—Received 23 April 1940.*)

The potential energy curves involved in proton transfer reactions are discussed, with special reference to the base-catalysed prototropy of ketones. The assumption of covalent binding throughout is inadequate to account in detail for the relations observed between basic strength and catalytic power. Approximate calculations from first principles show that the ionic state may well be of importance in this type of reaction, and the energy curves constructed on this basis give a much more satisfactory picture of the experimental facts.

---

**The distribution of autoelectronic emission from single crystal metal points.** By M. BENJAMIN and R. O. JENKINS. (*Communicated by R. H. Fowler, F.R.S.—Received 29 April 1940.*)

The field emission patterns from metal points show an electron distribution which can be related to the crystal lattice of the metal.

Surface atoms are mobile at relatively low temperature (the actual temperature being dependent on the nature of the metal). Owing to this mobility, the point is able to assume a shape of minimum free energy determined by the surface forces. This shape is the normal equilibrium form at all temperatures in the absence of external forces. It may be a roughly spherical surface with slight flats or hollows.

If an external field is applied, the surface atoms can be made to pile up over various parts of the surface. The degree of surface modification is a function of the strength of the applied field and of the temperature. The surface then is roughly spherical with slight hollows or elevations about 25 atoms in height. The surface can be frozen into any modification by maintaining the field and reducing the point temperature so that mobility ceases.

The flash-over phenomenon in high vacuum is discussed, and an explanation offered.

The effect of small traces of gas is illustrated and it is shown that the gas film is removed at a relatively low temperature 620–670° K.

---

**The poisoning of a palladium catalyst by carbon monoxide.** By M. G. T. BURROWS and W. H. STOCKMAYER. (*Communicated by D. L. Chapman, F.R.S.—Received 29 April 1940.*)

The combination of hydrogen and oxygen on the surface of a palladium catalyst at low partial pressures at the temperature of the laboratory is completely inhibited by very small amounts of carbon monoxide. The poisoning effect is only temporary and, during the induction periods which are observed, the carbon monoxide is removed by the oxygen in the mixture of hydrogen and oxygen. After the induction period combination proceeds at the normal rate. The length of the inert periods observed increases with the amount of carbon monoxide initially added to the system, and the rate of removal of the carbon monoxide increases as its pressure decreases and becomes comparatively very great when the carbon monoxide present does not exceed the amount required to cover the surface of the metal.

The observations recorded can be explained by a development of the hypothesis of de la Rive that the catalysis of the reaction between hydrogen and oxygen and between carbon monoxide and oxygen involves the alternate oxidation of the metal and the reduction of the surface oxide by hydrogen or by carbon monoxide respectively.

---

**The reduction of ferric oxalate by isolated chloroplasts.** By R. HILL and R. SCARISBRICK. (*Communicated by Sir Frederick Hopkins, F.R.S.—Received 30 April 1940.*)

Two methods have been used to measure the activity of chloroplasts isolated from *Stellaria media*, (a) the measurement with haemoglobin of oxygen produced from ferric oxalate, (b) the measurement of the rate of reduction of methaemoglobin in the presence of atmospheric oxygen, the methaemoglobin itself being reduced by the ferrous iron produced. The chloroplasts after isolation show a progressive fall in activity, approaching zero in 3–6 hr. Four different strains of the plant were grown which showed differences in the stability of the chloroplasts after removal. The  $Q_o$ , measured as rate of oxygen production calculated on the basis of dry weight of leaf is about 20. The  $Q_o$ , measured as rate of methaemoglobin reduction generally appeared less as the reduction of methaemoglobin by ferrous iron is relatively slow. The reduction of methaemoglobin in presence of ferric potassium oxalate has been studied quantitatively from the point of view of iron, methaemoglobin, and chloroplast concentration. The effect of different light intensities on the reduction of ferric oxalate by chloroplasts is similar to the effect of varying light intensity on photosynthesis in whole plants and lies within the range of values found by different workers. This ferric oxalate reaction is inhibited by urethane. Phenyl urethane inhibits in much smaller concentrations than ethyl urethane. The effective concentrations of urethane are similar to those affecting photosynthesis.

---



**New studies on active nitrogen. I.** By LORD RAYLEIGH, F.R.S. (*Received 3 May 1940.*)

This paper examines quantitatively the behaviour of nitrogen gas emitting the after-glow, under varied conditions.

The integrated light emitted under the most favourable conditions has been measured as 3.18 candle-sec. per c.c. of nitrogen, the (rarefied) nitrogen being reckoned as at N.T.P. The number of quanta emitted is estimated as about  $1.3 \times 10^{-3}$  of the number of molecules present.

It is concluded, in agreement with Kneser, that the addition of unexcited nitrogen to glowing nitrogen increases the (instantaneous) emission. It was found that a fivefold increase of total pressure produced about a fivefold increase of brightness. These tests were carried out at very low luminous intensities, when the spontaneous decay was negligible during an experiment.

If the active gas contained in 1 l. of weakly glowing nitrogen is allowed to diffuse quickly into an additional 1 l. volume of nitrogen, so as to dilute it by half, the candle power per unit volume is reduced about 4.3-fold. This is a fair approximation with the value 4, which would be expected if the reaction were bimolecular as regards active nitrogen, and is in agreement with the conclusion which has generally been drawn from observation on the rate of decay of the luminosity in closed vessels.

The effect of compressing the glowing gas has been re-examined, using a solid piston moving in a cylinder. It is now found that with the improved arrangements the brightness varies as the inverse cube of the volume. This is the logical conclusion from, and confirmation of, the previous experiments in which the concentration of (1) the inert nitrogen, and (2) the active nitrogen, are separately varied.

A further test was to expand the glowing gas into a doubled volume which was carried out by letting it pass into a supplementary exhausted vessel. This was expected from the previous result to reduce the intensity 8 times, but in fact did not reduce it more than 7 times. The gas was therefore somewhat brighter after the expansion than had been expected. Most sources of error would have the opposite effect, and there is an outstanding discrepancy in this result.

The effect of temperature on the nitrogen after-glow is examined quantitatively, maintaining the cooler and hotter portions in pressure equilibrium. Cooling to liquid air temperature, for instance, increases the brightness some 80 times. Most, but not all, of this is due to the additional concentration. Assuming (in accordance with the compression experiment) that the brightness is as the cube of the concentration, and correcting the results to uniform concentration, it is found that over the range examined the brightness varies as  $T^{-0.44}$  when  $T$  is the absolute temperature.

The positive temperature effect on ordinary chemical reaction corresponds to something more like  $T^{+100}$ .

---

**New studies on active nitrogen. II.** By LORD RAYLEIGH, F.R.S. (*Received 3 May 1940.*)

It is shown that pieces of sheet gold, copper, silver, or platinum may be made red hot or even melted by exposing them to active nitrogen produced in a low pressure discharge. The nitrogen gives up its energy to the metal, which remains unacted on.

This phenomenon is applied to measuring the energy of active nitrogen, drawing a known quantity of gas through the activating discharge and then over the metal, and measuring the energy liberated on the latter.

The amount of energy collected from the gas was surprisingly large, and is difficult to reconcile with existing theories of the nature of active nitrogen. In some cases the energy was as high as 10 eV for every molecule of nitrogen that passed through the discharge. This quantity of energy can with difficulty be accounted for by dissociation, even if it occurred to the extent of 100 %. The energy radiated as after-glow under favourable conditions is only of the order of  $10^{-3}$  of the energy collected by the metal.

---

**Two-phase equilibrium in binary and ternary systems. II. The system methane-methylene. III. The system methane-ethane-ethylene.** By M. GUTER, D. M. NEWITT and M. RUHEMANN. (*Communicated by A. C. G. Egerton, Sec.R.S.—Received 6 May 1940.*)

The liquid-vapour equilibrium of the system methane-ethylene has been determined at five temperatures between 0 and  $-104^{\circ}$  C and over a wide range of pressures. The results are shown on pressure-composition curves and by a three dimensional pressure-temperature-composition diagram. The equilibrium of the ternary system methane-ethane-ethylene has also been determined at 0,  $-78$  and  $-104^{\circ}$  C. The relation between the phase behaviour of the two binary systems methane-ethylene and methane-ethane and that of the ternary system is discussed and illustrated by a pressure-composition diagram covering the pressure range 10–35 atm. and the whole range of compositions.

---

**Investigations on the vibration spectra of certain condensed gases at the temperature of liquid nitrogen.** By G. K. T. CONN, E. LEE, G. B. B. M. SUTHERLAND and C. K. WU. (*Communicated by R. G. W. Norrish, F.R.S.—Received 10 May 1940.*)

A description is given of experimental methods which have been developed for the investigation of infra-red and of Raman spectra at the temperature of liquid nitrogen. The infra-red spectrometer is essentially the Pfund-Barnes type but it has been found possible to dispense with the fore-prism and to separate the overlapping orders from the grating by means of filter shutters. The spectrometer is used as a monochromator so that radiation only enters the absorption cell after it has been through the diffraction train. The absorption cell has been designed so that it may be used for high as well as low temperatures. The apparatus for the Raman effect is a modification of that introduced by De Hemptinne, being especially suitable for the examination of small quantities of material.

---

**The infra-red and Raman spectra of hydrochloric and of deuteriochloric acids at liquid nitrogen temperatures.** By E. LEE, G. B. B. M. SUTHERLAND and C. K. WU. (*Communicated by R. G. W. Norrish, F.R.S.—Received 10 May 1940.*)

The infra-red absorption spectrum of solid hydrochloric acid has been obtained at the temperature of liquid nitrogen (i.e. approximately twenty degrees below its transition point) in the region of the fundamental frequency. The results obtained agree in general with the earlier observations of Hettner and disagree with those of Shearin who reported discrete rotation lines. The doublet band observed by Hettner has been resolved into two separate bands with maxima at 2701 and 2744  $\text{cm}^{-1}$  and indications of a third band were obtained. Some fine structure, very different from that reported by Shearin, was observed on each of the two bands, which were unsymmetrical in shape, being steeper on the low frequency side. The Raman spectrum was obtained at the same temperature and also showed a doublet structure in contrast to earlier observations at higher temperatures which had given only a single line. The maxima of the two Raman lines lay at 2709 and 2759  $\text{cm}^{-1}$ . The explanation of this doubling is to be sought in the manner in which the hydrochloric acid molecules associate in the solid state, since the alteration in the fundamental frequency from that found in the gaseous state shows that strong interaction must exist. The absorption due to the fundamental frequency of deuteriochloric acid was observed under the same conditions. Here three maxima were observed at 1965, 1982 and 1992  $\text{cm}^{-1}$  and indications of more structure. These results show that the association of HCl and DCl molecules in the crystal below the transition temperature can probably take place in several different ways. Such a conclusion is in agreement with the X-ray investigations which revealed a symmetry so low that the crystalline structure could not be determined.

---

**The kinetics of mutarotation in solution.** By J. C. KENDREW and E. A. MOELWYN-HUGHES. (*Communicated by R. G. W. Norrish, F.R.S.—Received 14 May 1940.*)

The kinetics of the mutarotation of representative reducing sugars from the pentose, hexose and disaccharide series have been investigated polarimetrically over wide temperature ranges in aqueous solution.

The dependence of the velocity coefficient,  $k$ , upon temperature,  $T$ , is fairly well reproduced by an equation of the form

$$\ln k = C + (J/R) \ln T - E/RT.$$

$E$ , the energy of activation at the absolute zero, is found to be some 6000 cal. greater than the apparent value afforded by the Arrhenius equation at room temperature.  $J/R$  has a value of  $-10$ , which is identified as the number of oscillators contributing to the activation.

The constants  $C$ ,  $J$  and  $E$  of this equation are discussed, with reference to various reactions, in terms of a theory of unimolecular reactions in solution.

---

**Foraminifera from the Green Ammonite Beds, Lower Lias, of Dorset.**  
By W. A. MACFADYEN. (*Communicated by W. D. Lang, F.R.S.—Received 14 May 1940.*)

This paper is a contribution to the long continued researches on the Dorset Lias by W. D. Lang, F.R.S., who collected the described material.

Some 700 mounted specimens from the Lower Lias (*davoei* zone), of the Dorset coast have been studied. They are ascribed to six families, twenty genera, and fifty-five species; of these, eleven genera and forty-five species belong to the family Lagenidae. One genus and species, *Carixia langi*, and one other species, *Lagena davoei*, are described as new, and two new names are proposed to replace invalid names.

There were studied for comparison certain of the few described English Lias faunas, some described French and German material, and a number of well preserved but undescribed faunas from various Lias horizons and different English localities. This has yielded provisional evidence of the zonal ranges of the Dorset species. Some forms of *Frondicularia* were found to provide useful horizon markers.

A tentative correlation is given of the zoning of the Lias by various authors of papers on Lias Foraminifera; there are notes on the horizons of some described Lias faunas, and a review of previous work on British Lias Foraminifera.

Study of Jurassic Foraminifera has been comparatively neglected for many years, though there is a recent German revival. Some lengthy synonymies are therefore necessary. Certain ill-known forms are discussed in detail; they were inadequately described and figured, so that they have hitherto been wrongly placed. It has thus been possible to rectify the systematic position or status of the genera *Involutina*, *Problematica*, and *Bullopore*. The appearance in the Lias of *Bolivina* and *Plectofrondicularia* is demonstrated, genera usually stated not to occur in rocks of age earlier than the Cretaceous.

Foraminifera thrived in some of the Lias clays in which their shells are well preserved. There was a rapid evolution of new types, particularly of the predominating Lagenidae. In this family there appears to be wide variation within some of the groups, where neither "species" nor even "genera" are sharply defined.

The bulk of the paper is taken up by the systematic description of the Foraminiferal fauna; all the recorded forms are figured.

---

**Inner excited states of the proton and neutron.** By W. HEITLER and S. T. MA. (*Communicated by N. F. Mott, F.R.S.—Received 14 May 1940.*)

The present meson theory exhibits a number of serious difficulties if applied to the interaction of fast mesons with nuclear particles. In order to avoid these difficulties the following hypothesis is made: Charge and spin of a proton and neutron shall be capable of assuming higher quantum states. Thus particles shall exist with approximately protonic mass and with charges  $+2e$ ,  $-e$ , etc., and also with spins  $3/2$ ,  $5/2$ , . . . . It is assumed that the lowest of these higher states have excitation energies which turn out to be of the order of magnitude of 20 MeV. The higher spin states are introduced in the way of a simple model, namely that of a rotator with half-integer

angular momentum. The theory is essentially non-relativistic with respect to the heavy particle.

The theory leads to the following results:

(i) The cross-section for scattering of mesons by a heavy particle is smaller by an order of magnitude than according to the former theory (and in qualitative agreement with experiments) and does no longer increase with energy. Thus no multiple showers are to be expected in this theory.

(ii) The anomalous magnetic moments of the proton and neutron diverge only logarithmically and, if the theory is limited to energies smaller than the rest energy of the proton, are in reasonable agreement with the experimental values.

(iii) The influence of the higher states on the nuclear potentials results in a deepening of the potentials at small distances. Even without introducing neutral mesons there is strong attractive proton-proton potential and it is discussed whether the proton-proton scattering data can be explained without this hypothetical particle.

(iv) The deviation from the Coulomb law for a proton derived from the former meson theory is much smaller in the new theory, whereas for the photo-disintegration of the deuteron the characteristic meson effects are expected to be even more marked.

The possibilities for observing the new particles are discussed. It is pointed out that it would have been unlikely had the particles been discovered in any of the experiments which have been carried out up to the present. Yet, one track published by Anderson and Neddermeyer, which cannot be due to any of the known particles, is tentatively interpreted as due to a particle with charge  $2e$  and protonic mass.

**Succinic dehydrogenase-cytochrome system of cells. Intracellular respiratory system catalysing aerobic oxidation of succinic acid.** By D. KEILIN, F.R.S. and E. F. HARTREE. (*Received 17 May 1940.*)

The succinic dehydrogenase-cytochrome system, even in the cell-free colloidal preparation, behaves like a true respiratory system of the cell, showing the high catalytic activity and being affected by all the inhibitors in the same way and to the same degree as the respiration of intact cells. The efficiency of this system depends not only on the integrity of all its components but also on that of the colloidal structure which supports them and assures their mutual accessibility. The paper deals with the properties of each of the components of the system and with the mechanism of their interactions.

**Bose-Einstein statistics and degeneracy.** By D. S. KOTHARI and B. N. SINGH. (*Communicated by M. N. Saha, F.R.S.—Received 17 May 1940.*)

The thermodynamic properties of degenerate and non-degenerate Bose-Einstein gas in the completely non-relativistic and the completely relativistic cases are derived. The relativistic degenerate case of Bose-Einstein statistics corresponds to black-body radiation. The properties and the possibility of the existence of non-degenerate radiation are discussed.

**A study of sensitized explosions. V. Some new experiments on the hydrogen-oxygen reaction sensitized by nitrogen peroxide.** By F. S. DAINTON and R. G. W. NORRISH, F.R.S. (*Received 21 May 1940.*)

The effect of pressure and temperature of reactants, of inert gases, of vessel diameter and of surface condition on the induction periods and explosion boundary of  $2\text{H}_2 + \text{O}_2$  mixtures containing nitrogen peroxide have been determined in the temperature range  $250\text{--}410^\circ\text{C}$ . The principal results may be summarized:

(a) Increase of pressure causes the separation of the upper and lower limiting concentration of sensitizer to increase from zero, to a maximum value at the inversion pressure. Above this pressure the upper limit decreases and the lower limit increases linearly with increase of pressure. The induction periods of  $\text{H}_2\text{-O}_2\text{-NO}_2$  mixtures of constant  $\text{NO}_2$  content decrease rapidly with increase of pressure, approaching a small value asymptotically.

(b) All foreign gases lengthen the induction periods and eventually quench the ignition of an explosive mixture of  $\text{H}_2\text{-O}_2\text{-NO}_2$  of constant composition. The order of efficiency of the non-reactant gases in lengthening the induction periods is  $\text{CO}_2 > \text{N}_2 > \text{A} = \text{He}$ , whereas the order of efficiency in quenching ignition is

$$\text{CO}_2 > \text{He} > \text{N}_2 > \text{A}.$$

(c) The induction period at the upper limit always exceeds the induction period at the lower limit. The reverse is true of the rates of the slow reactions in the vicinity of the limits.

(d) At constant total pressure rise of temperature causes the upper limit ( $P_u$ ) to be raised according to the equation

$$\log P_u = E/RT + \text{a constant}.$$

$E$  is 19,500 cal. at a total pressure of 75 mm. and increases with pressure to 25,600 cal. at 472 mm.

(e) At constant pressure the upper limit decreases and the lower limit increases as the reciprocal of the square of the diameter.

**A study of sensitized explosions. VI. Experimental observations on the hydrogen-oxygen reaction sensitized by nitrosyl chloride.** By F. S. DAINTON and R. G. W. NORRISH, F.R.S. (*Received 21 May 1940.*)

Small amounts of nitrosyl chloride lower the ignition temperature of  $2\text{H}_2 + \text{O}_2$  mixtures by over  $200^\circ\text{C}$ ; the efficiency in this respect of this substance being slightly greater than nitrogen peroxide. At a given temperature the ignition is confined between a lower and an upper concentration of catalyst, outside which only slow reaction occurs. Both the slow reaction and the ignition are preceded by an induction period, the length of which passes from large values through a minimum to further large values as the catalyst concentration is increased, and which, in contrast to the  $\text{H}_2\text{-O}_2\text{-NO}_2$  system, is unaffected by irradiation with light from a mercury vapour lamp.

The induction periods and limits depend on the pressure and temperature of reactants in a very similar way to the induction periods and limits of the  $\text{H}_2\text{-O}_2\text{-NO}_2$  system described in V. The similarity of the two systems extends to the effect of non-reactant gases in quenching the ignition: the quenching pressures being of the same magnitude in both systems. A difference is, however, found in that these foreign gases shorten the induction period in this system whereas they lengthen it in the  $\text{H}_2\text{-O}_2\text{-NO}_2$  system.

---

**A study of sensitized explosions. VII. A chain-thermal theory of the reaction between hydrogen and oxygen sensitized by nitrogen peroxide or nitrosyl chloride.** By F. S. DAINTON and R. G. W. NORRISH, F.R.S.  
(Received 21 May 1940.)

Both these reactions are chain processes for which the net branching factor  $\phi$  is inversely proportional to the induction period. By applying this relation to the experimental results described in V and VI, it is shown that ignition only occurs when the net branching factor attains a value determined by the sum of two quantities, one proportional to the thermal capacity and the other proportional to the thermal conductivity. It is pointed out that this ignition condition cannot be accounted for by any isothermal theory of ignition, but that it may readily be deduced from a thermal theory in which explosion is visualized as occurring only when the initial reaction rate, in a favourable volume element, is large enough to ensure that a critical temperature  $T_c$  is reached in a critical time  $t_c$ .

Theories of reaction kinetics are developed from these two systems which give  $\phi$  in terms of the experimental variables. The expressions so deduced lead to a dependence of the induction period on these variables identical with that found experimentally. The effects of vessel diameter, surface condition, temperature, and concentrations of sensitizer, reactants and foreign gases on the explosion are satisfactorily accounted for by substituting these expressions in the ignition condition of the chain thermal theory.

---

**X-ray studies of the molecular structure of myosin.** By W. T. ASTBURY, F.R.S., and S. DICKINSON. (Received 23 May 1940.)

Starting from the similarity between the X-ray diffraction patterns of muscle and myosin and those of mammalian keratin fibres, a detailed X-ray and elastic study has been carried out of strips of myosin film prepared by drying the sol.

Methods are described of orienting the myosin chain-molecules: when oriented but unstretched they are found to give an  $\alpha$ -photograph almost indistinguishable from that of unstretched keratin, and when stretched a  $\beta$ -photograph almost indistinguishable from that of stretched keratin. As with keratin, the long-range elasticity rests on a reversible intramolecular transformation, the fully extended, or  $\beta$ -, form of the molecule being again about twice as long as the folded, or  $\alpha$ -, form.

The X-ray and elastic properties of myosin are found to resemble most closely, not those of natural keratin, but those of keratin that has suffered breakdown among the cross-linkages (including disulphide bridges) of the polypeptide grid. For example, by pressing moist myosin at ordinary temperatures selective orientation is brought about analogous to what is produced in keratin only at higher temperatures. Similarly, myosin supercontracts in hot water or cold dilute alkali without the preliminary stretching treatment required by keratin.

The supercontraction of myosin has been studied quantitatively and the accompanying structural changes followed by X-rays. The results show that the effect cannot be explained as due simply to disorientation of long thin units: it must involve a further folding of the polypeptide chain system.

The hypothesis is put forward that the contraction of muscle arises from supercontraction of its myosin component. It will be shown in a subsequent paper that X-ray photographs of muscle in various states, both living and dead, are entirely consistent with this view.

The fact that myosin and keratin are similar in both molecular configuration and elastic properties is discussed in the light of recent X-ray and chemical findings, and the X-ray interpretation is given of the denaturation of myosin.

---

**Anomalous viscosity.** By A. S. C. LAWRENCE and J. R. ROBINSON.  
(Communicated by E. K. Rideal, F.R.S.—Received 25 May 1940.)

Anomalous viscosity is examined from first principles. A viscometer is described for the simultaneous measurement of viscosity and streaming birefringence; the latter property is used to give direct evidence of the nature of the orientation associated with the measured value of the viscosity under the same flow conditions. A number of sols have been examined and the results confirm the analysis. Predicted temperature effects have been confirmed. The effects of particle size, shape and concentration are considered with special reference to the conditions needed to obtain results which can be interpreted. Several related phenomena also receive explanations.

---

**The colours of the plumose anemone *Metridium senile* (L.).** By D. L. FOX and C. F. A. PANTIN, F.R.S. (Received 30 May 1940.)

The anemone *Metridium senile* occurs in a number of striking colour varieties. These are to be found side by side in nature. The colours are inherited at least during asexual reproduction and do not depend on special food. The colour varieties are founded on three systems of pigment, black granular melanin in the endoderm, brown diffuse melanin in the ectoderm and red to orange lipochrome in fat droplets in both endoderm and ectoderm. In any variety each system may be present or absent. If all are absent we have a white form, if one is present we get red, brown or grey forms, if two or more are present we get other varieties. In combinations each pigment retains the distribution it has in the corresponding simple form.

The black endodermal pigment is a true melanin. The brown ectodermal pigment is also a melanin but is less stable. Even the white variety can be shown to possess



a complete tyrosinase system when the tissues are finely ground. It is perhaps comparable to a case of dominant albinism.

The red and orange colours are due to a variety of lipochromes. The pigment of the red variety is chiefly the acidic carotenoid described by Heilbron, Jackson and Jones. It is related to astacene and we have named it "metridene". Yellow-orange anemones of the red series may contain considerable quantities of xanthophylls in addition to metridene esters. The only pigment of the white form is contained in the gonads and appears to be astacene.

Many of the carotenoids are present in too small quantities to influence the appearance of the animal. The assortment of carotenoids present is considerably different from one lot of *Metridium* to another. There is evidence that the occurrence of a variety of xanthophylls and carotene is more common in varieties which develop melanin. But there is no obvious correlation between the presence of a particular assortment of carotenoids and a particular distribution of melanin pigments. Flavins are not present in any of the colour varieties.

Coloured purine compounds are not present. The presence of significant quantities of uric acid was demonstrated and of this purine alone. It is present in the mesenteric filaments, in the yellowish excreted mucus, and granules of uric acid form white bands in the endoderm of the tentacles. In this position they contribute their whiteness to the total colour effect. Haematins do not contribute to the colour. Those that are present are derived from the ordinary intracellular respiratory systems.

The colours of the varieties are not an adaptation to the external environment as in warning coloration, etc., nor is there evidence as yet that the colour as such is of direct physiological importance to the animal. The varieties appear to illustrate Poulton's category of "non-significant colours", in which colour is a by-product of biochemical processes utilized for other purposes.

**$\beta$ -ray spectra of light elements.** By A. A. TOWNSEND. (Communicated by J. D. Cockcroft, F.R.S.—Received 30 June 1940.)

A magnetic spectrometer has been used to investigate the  $\beta$ -ray spectra of some elements of low atomic number. It is found that all the spectra follow the Fermi distribution law for a certain range from the high energy end-point; the range over which this is true is much greater if the maximum energy is large. The end-points found are:  $C^{11}$   $0.981 \pm 0.005$  MeV,  $N^{13}$   $1.218 \pm 0.004$  MeV,  $Mn^{55}$   $2.88 \pm 0.01$  and  $1.035 \pm 0.015$  MeV,  $Cu^{64}$  (positrons)  $0.649 \pm 0.004$  MeV,  $Cu^{64}$  (negatrons)  $0.574 \pm 0.004$  MeV,  $Zn^{62}$   $2.320 \pm 0.005$  MeV.

**X-ray electrons expelled from metals by silver  $K\alpha_1$  radiations.** By C. J. BIRKETT CLEWS and H. R. ROBINSON, F.R.S. (Received 3 June 1940.)

The energies of the X-ray electrons expelled from targets of gold, platinum, silver and copper by silver  $K\alpha_1$  rays have been measured in the magnetic spectrograph. The results have been combined with those of earlier measurements, and they yield a value for Planck's constant of  $6.62 \times 10^{-27}$  erg sec.





INDIAN AGRICULTURAL RESEARCH  
INSTITUTE LIBRARY  
NEW DELHI.

[illegible]

S. C. P. - 1/6/47 P. J. - 3-5-48-2900



